THÈSE

En vue de l'obtention du
DOCTORAT DE L'UNIVERSITÉ DE TOULOUSE

Délivré par l'Université Toulouse 3 - Paul Sabatier

Présentée et soutenue par

Mathilde RIGOULET

Le 12 janvier 2022

Ligands bidentes en chimie de l'or: de la stabilisation d'espèces réactives à la catalyse.

Ecole doctorale : **SDM - SCIENCES DE LA MATIERE - Toulouse**

Spécialité : **Chimie Organométallique et de Coordination**

Unité de recherche :
LHFA - Laboratoire Hétérochimie Fondamentale et Appliquée

Thèse dirigée par
Didier BOURISSOU et KARINNE MIQUEU

Jury
M. Eric CLOT, Rapporteur
M. Mats TILSET, Rapporteur
M. Louis FENSTERBANK, Examinateur
M. Didier BOURISSOU, Directeur de thèse
Mme Karinne MIQUEU, Co-directrice de thèse
M. Eric BENOIST, Président

A mes parents,

Acknowledgement/Remerciements

First of all, I would like to thank all the members of the jury. Professor Tilset and Doctor Clot for accepting to review my manuscript, Professor Fensterbank, Doctor Chaudret and Professor Benoist for being part of this jury. Many thanks to all of you for the nice discussion.

Je voudrais ensuite commencer par remercier mes directeurs de thèse. Merci Didier de m'avoir accepté au sein du laboratoire et dans l'équipe LBPB. J'ai énormément appris auprès de toi grâce aux différents échanges qu'on a eus. Tu te rendais toujours dispo quand j'en avais besoin malgré ton emploi du temps chargé. Tu nous pousses à toujours donner le meilleur de nous-même.

Merci Karinne d'avoir accepté de co-encadrer ma thèse. Je partais de presque rien en chimie théorique et tu m'as tout appris. Merci pour la confiance que tu m'as donnée. J'ai énormément apprécié toutes nos discussions qui étaient sérieuses mais toujours dans la bonne humeur. On a tellement retourné les situations qu'on était prête à répondre à toutes les questions.

Mes remerciements vont ensuite à l'équipe LBPB grâce à qui c'était un réel plaisir de venir travailler tous les jours. Je voudrais d'abord remercier Abder avec qui j'ai commencé au LHFA. Merci d'avoir répondu à toutes mes questions quand je n'étais pas sûre à mes débuts. Ta bonne humeur était communicative et nous a quand même un peu manquée par la suite. Tu as été remplacé par Gyuri, plus discret mais toujours prêt à aider. Grâce à toi, j'ai fait le marathon par équipe et c'était une sacrée expérience. Merci pour toutes les sorties "sportives" que tu organises pour le labo.

Je voudrais également remercier Ghenwa et Blanca, vous faite partie des personne les plus bienveillantes que je connaisse. Vous étiez toujours partante pour organiser des évènements d'équipe, que ce soit les pic-nic, les anniversaires ou les pots de départ, on pouvait toujours compter sur vous. Vous avez également beaucoup contribué à ma thèse, merci pour les challenges en group meeting, et pour les précieux conseils, notamment sur les présentations.

Julien, tu es le permanent avec qui j'ai le plus échangé que ce soit de chimie ou autres (série, sport, actualité…), souvent autour d'un petit café. Tu étais toujours là quand j'avais besoin de quelque chose au labo, quand j'avais des questions bêtes ou des doutes. Merci pour la précieuse aide que tu nous apportes quotidiennement, pour ta bonne humeur et pour ton rire aussi discret que le mien.

Passons ensuite aux thésards. Je vais commencer par remercier les anciens: Abdallah, Charlie et Paul qui m'ont accueilli dans la famille LBPB et m'y ont fait m'y sentir chez moi. Merci pour tous vos précieux conseils et vos blagues qui m'en ont fait voir de toutes les

couleurs (mais je sais maintenant comment on synthétise du CD_2Cl_2). Maxime était également là quand je suis arrivée. Je me souviendrai de nos longues discussions de chimie, parce que la biblio c'est nul!! Ton départ a fait un grand vide au labo, je n'avais plus personne pour me dire que je faisais n'importe quoi ou pour me lancer des défis. Saam, the best thai person ever, you are one of the kindest persons I know and your thai food was amazing (a little bit too spicy sometimes). I hope to see you soon in Thailand.

Ensuite est arrivé Cyril. Un génie avec une âme d'enfant. Tu courrais toujours partout et ça me faisait râler, mais c'est aussi ce qui faisait ton charme. Tu étais toujours partant pour parler chimie, et on apprenait plein de chose avec toi. Maryne est arrivée pour me sauver de toute cette testostérone. Merci d'avoir été là pour m'écouter (râler sur ces garçons), pour toi aussi écouter du France Gall (Résiste, prouve que tu existes) et pour tout tes bons gâteaux.

Arnaud (le seul l'unique), je me souviens encore de ton arrivée où je me disais "pourvu qu'il soit gentil, on va passer 3 ans ensemble". Et je n'ai pas été déçue, je n'aurais pas pu rêver meilleur co-thésard que toi. Toujours prêt pour mes questions stupides (desquelles on discutait pendant 2 heures), toujours de bonne humeur, prêt à aider (qu'est-ce qu'on a marché dans Toulouse pour faire les cadeaux de départ), partant pour tout. Je te souhaite vraiment le meilleur pour la suite, surtout ne change pas et je te fais signe quand je viens au Canada.

And then the new generation arrived, staring fist with David, the new gold boy. I hope you will have as much fun as I got working on this subject. I am sure you will do something great. Looking forward for your future paper and if you need any help do not hesitate to text me. Nounau (le nouveau Arnaud), tu étais tout timide quand tu es arrivé en stage puis tu t'es libéré quand tu es passé en thèse. Merci pour tes blagues nulles et pour ton soutien dans les périodes difficile de la rédaction. Continue de t'épanouir ! Marceline, la nouvelle française de l'équipe, tu es un amour. A peine arrivée que déjà tu te plies en quinze pour l'équipe (entre les cadeaux, le secret santa, les gâteaux et le week-end ski). J'ai été très contente de te croiser même si ce fut court. Je vous souhaite à tous les deux le meilleur (je suis sûre que vous allez faire une très belle thèse et vous avez la chance de pouvoir vous soutenir mutuellement) et vous savez où me joindre si vous avez besoin ou si vous passez en Allemagne. A big thanks to Liyao and Ann for their joy. Keep smiling for the following of your PhD.

J'ai également croisé beaucoup de post doc pendant ces années. Enrico, l'italien au grand cœur. Tu es arrivé peu de temps après moi et on a passé pas mal d'année ensemble. Miquel, le pur catalan, qui voulait à tout prix éviter la glove box. Omar, la force tranquille, tu es une personne hyper bienveillante, on pouvait toujours compter sur toi. Alexis, qu'est ce qu'on a pu raconter des bêtises. C'était un plaisir de partager le bureau avec toi pendant un an, on a pu parler de tout et de rien et on a bien rigolé (tout en étant bosseur bien sûr). Marte, tusen takk to the queen of gold. You were always in a good mood, ready to discuss about chemistry or trips (especially in the pyrenees), to sing « Désenchanté » or to tell a « good » pun. Felix

and Nere, you arrived at the end of my PhD, you are two lovely persons, I was sad to not spend much time with you. Hope to see all of you somewhere around the world.

I want to thanks all the intern I met: Deidrah, Janina, LookPu, Miguel, Nicolas Adet (un grand merci pour tous les fous rires qu'on a eu dans le bureau), Nicolas JB (qui est ensuite revenu chez les Kiss, nous permettant d'entendre à nouveau son rire communicatif). I especially want to thanks my intern Sara. Your stay was too short because of the covid. I really enjoy working with you (always the smile, enthousiastic for everything) and I was glad you stay in Toulouse for your PhD since I was able to see you again. I am waiting for you in Germany.

Mais le LHFA ce n'est pas que l'équipe LBPB. C'est tout d'abord des secrétaires au top. Maryse, Serah, Florence et Miguel, merci de m'avoir toujours aidé avec le sourire et de toujours vous plier en quatre quand on a besoin. Que serait le labo sans Olivier V. Toujours partant pour discuter, raconter une petite blague et toujours prêt à nous aider et à négocier. C'est aussi une équipe d'ingénieur formidable : Olivier TdB (toujours de bons conseils que ce soit pour les manips orga ou pour éteindre un feu, ça va que pour ce dernier point ça n'est pas arrivé souvent), Romaric (c'était chouette de partager le labo avec toi), Isabelle (je me souviendrai longtemps de tes « au revoir, a demain » quand je rédigeais tard le soir), Julien B. (toujours le sourire et de bonne humeur), Saloua, Mathieu, Christian. On ne peut rêver meilleur service RX que Sonia et Nathalie. Merci à toutes les 2 pour toute l'énergie que vous mettez pour nous aider à avoir nos structures (même si des fois ça prend 3 mois), toujours avec le sourire. Merci au service RMN, Caroline, Marc et Pierre, pour leur aide et leur efficacité.

Je voudrais remercier l'équipe du CAES composé principalement de l'équipe LBPB mais aussi de Nico, Marie et Sami. Qu'est ce qu'on a pu rigoler les midis, à courir après les gens pour partir à 11h30 voir 11h15 (pardon pour les oublis), à parler de tout et de rien (bon la F1 ça allait 5 min) et à finir autour d'un café.

Un merci à tous les autres membres des autres équipes (SHEN, ECOIH, SYMAC, KISS, COP). En particulier, un gros merci à Soukaina la plus belle. Merci pour ton sourire, pour les discussions qu'on a pu avoir. Merci à Julien P. pour toujours répondre à mes bêtises. Il n'y en a pas un pour rattraper l'autre. Merci à Barbara, l'ancienne future SHEN, tu n'es pas restée longtemps mais j'ai croisé une belle personne avec qui je vais garder contact. Merci à Ugo, le nouveau dinosaure du labo, tu vas voir ce que c'est. Merci à Aymeric, pour les soirées raclettes et soirées crêpes. Merci à Jean, le marseillais qu'on entendait jusqu'à l'autre bout du couloir. Merci à Louis, qui était à moitié LBPB. Tu es la personne la plus tête en l'air que je connaisse, mais tu es toujours prêt à aider et tu as un grand cœur alors on te pardonne tes bêtises (mais s'il te plait fais des efforts pour préserver Marceline). Merci à Corentin, avec qui j'ai partagé le bureau et le labo, à son arrivée au labo (qui s'est fait en 3 fois non ?). Poses-toi moins de questions et profites. Merci à toi et Valentin, pour m'avoir toujours répondu gentiment sur mes questions photochimiques.

La these, ce sont aussi toutes les personnes qui nous entourent en dehors du labo. Je voudrais remercier d'abord ma plus veille amitié, Amandine ma folle. Je me rappelle encore quand on s'est rencontré au conservatoire et 22 ans plus tard on est toujours là l'une pour l'autre. Ma Ionion, il y aurait tellement à dire, la petite blonde que tu étais a bien changé depuis notre rencontre, mais tu restes quand même toujours là même. Toujours à prendre soin de nous, à manger du chocolat, à être là pour les moments importants. Malgré nos plannings respectifs très chargés on trouve toujours du temps l'une pour l'autre. Marine, à notre rencontre en seconde, je n'aurais jamais dit que 10 ans plus tard on serait toujours amies, mais je suis très contente qu'il en soit ainsi et je sais que ce n'est que le début. On pourra toujours compter l'une sur l'autre. Vous savez à quel point vous êtes importante pour moi, et je ne vous remercierai jamais assez de faire partie de ma vie et je nous souhaite encore une très longue amitié.

Je voudrais remercier l'équipe des « bras cassés », Edo, Pauline, Jeff, Louise, Babak et Adri, pour tous les bons moments passés à Toulouse, les escapes (qu'on a tous gagné), les randos (soi-disant facile d'après Babak alors qu'il ne vient pas), les apéros dinatoires (où il y en avait toujours trop)...

Je voudrais remercier les lyonnais. D'abord mes amies de prépa, Laure et Gwendy, avec qui on a toujours gardé contact, même si ce n'est pas toujours facile de se voir. Clélia, Laureline et Louisiane, j'ai l'impression que la coloc se terminait hier et pourtant il s'en est passé des choses depuis. Merci d'être toujours présente malgré que l'on soit réparti aux quatre coins de la France (et bientôt du monde). J'espère toute vous revoir très vite. Je voudrais également remercier la bande des copains lyonnais, Tomtom, Alex et Antonin. Merci pour votre bonne humeur, pour les soirées et pour votre aide que ce soit pour les surprises à Adri ou pour les déménagements.

Je tiens à remercier l'orchestre de la Roulotte avec qui j'ai pu me changer les idées et jouer de la musique pendant ces années de thèse. Merci pour les bons moments partagés. Au plaisir de vous recroiser dans des bals ou au détour d'un concert.

Je voudrais également remercier ma famille qui est toujours présente pour les moments importants. En particulier, mes parents et mon frère qui m'ont toujours soutenu, encouragé et si j'en suis arrivée jusque-là c'est aussi grâce à eux. Merci pour votre soutien et votre amour.

Finalement, je voudrai remercier mon chéri Adrien. Tu m'as supporté tous les jours pendant cette thèse, que ce soit en personne au début ou par téléphone après et je sais que je n'ai pas tous les jours était facile. Tu m'as toujours écouté, soutenu et rendu meilleure. Merci pour tout ce que tu m'apportes.

Table of contents

General remarks

The work presented in this manuscript was carried out in the Laboratoire Hétérochimie Fondamentale et Appliquée (UMR 5069) at the Université de Toulouse III – Paul Sabatier under the supervision Dr. Didier Bourissou and Dr. Karinne Miqueu.

I.   Experimental Conditions

General Procedures
Unless otherwise stated, all reactions and manipulations were carried out under an atmosphere of dry argon using standard Schlenk techniques or in a glovebox under an inert atmosphere. Dry, oxygen-free solvents were employed.

NMR Spectroscopy
Solution ^1H, ^{13}C, ^{11}B, ^{19}F, ^{31}P, ^{15}N NMR spectra were recorded on Bruker Avance 300, 400 or 500 spectrometers at 298 K, unless otherwise stated. Chemical shifts (δ) are expressed with a positive sign, in parts per million calibrated to residual ^1H and ^{13}C solvent signals External $BF_3.OEt_2$, 85% H_3PO_4 and $CFCl_3$ were used as reference for ^{11}B, ^{31}P and ^{19}F NMR respectively. The following abbreviations and their combinations are used: br, broad; s, singlet; d, doublet; t, triplet; q, quartet; m, multiplet. The ^1H and ^{13}C resonance signals were attributed by means of J-MOD and 2D COSY, HSQC, HMBC experiments. When a mixture of diastereoisomers was obtained, selective TOCSY was used to assign the signals of each diastereoisomer.

Mass Spectroscopy
Mass spectroscopy analyses were performed using Electrospray ionization method on a Waters UPLC Xevo G2 Q TOF apparatus or chemical ionization method on a DSQ II (Thermo Fisher Scientific) spectrometer.

GC-MS Analysis
GC-MS analyses were performed on a GC Perkin Elmer Clarus 500 apparatus coupled with a MS PerkinElmer Clarus 560.

X-ray Crystallography
Crystallographic data were collected at low temperature (193(2) K) on a Bruker-AXS APEX II Quazar diffractometer equipped with a 30W air-cooled microfocus or on a Bruker-AXS PHOTON100 D8 VENTURE diffractometer, using MoK_α radiation (λ = 0.71073 Å). Phi- and omega-scans were used. An empirical absorption correction was performed with SADABS.[1] The structures were solved by direct intrinsic phasing method (SHELXT),[2] and refined using the least-squares method on F^2.[3] All H atoms on carbon atoms were refined isotropically at calculated positions using a riding model.

Melting Points
Melting points were determined with a calibrated Stuart SMP40 apparatus.

Elemental analyses
Elemental analyses were performed on a Perkin Elmer 2400 serie II apparatus (LCC, Toulouse).

---

[1] Bruker, *SADABS*, Bruker AXS Inc., Madison, Wisconsin, USA.

[2] G. M. Sheldrick *Acta Cryst*. **2015**, A71, 3–8.

[3] G. M. Sheldrick *Acta Cryst*. **2015**, C71, 3–8.

II.   Computational details

All calculations were performed using Gaussian. The gold atom was described with the relativistic electron core potential SDD and associated basis set,[4] augmented by a set of f-orbital polarization functions.[5] The 6-31G** basis set were employed for all other atoms.[6] Optimizations were carried out without any symmetry restrictions. The nature of the minima or saddle points (TS) was verified by the absence or presence of only one negative eigenvalue, respectively. The connection between transition states and the corresponding minima were performed by intrinsic reaction coordinate (IRC)[7] calculations. All stationary points involved were fully optimized. All total energies and Gibbs free energies have been zero-point energy (ZPE) and temperature corrected using unscaled density functional frequencies. All the geometrical structures were plotted with Chemcraft program.[8]

^{1}H and ^{13}C NMR chemical shifts, and coupling constants J_{PC} or J_{PF} were evaluated by employing the direct implementation of the Gauge Including Atomic Orbitals (GIAO),[9] with the IGLOII[10] basis set for all atoms except Au, using as reference the corresponding SiMe$_4$ shielding constant calculated at the same level of theory.

Natural Bond Orbital[11] (NBO) calculations were used to analyze the bonding situation of the different gold complexes. Natural Localized Molecular Orbital (NLMO) were plotted with Chemcraft program.[8]

Charge decomposition analysis (CDA) was carried out with the CDA 2.2 program developed by G. Frenking.[12]

Atoms in Molecules (QTAIM)[13] analyses were carried out using AIMAll software.[14]

Appropriate details will be given in each chapter when needed.

[4] a) D. Andrae, U. Häussermann, M. Dolg, H. Stoll, H. Preuss, *Theor. Chim. Acta* **1990**, *77*, 123; b) M. Dolg, *Modern Methods and Algorithm of Quantum Chemistry, Vol. 1* (Ed.: J. Grotendorst), John von Neuman Institute for Computing, Jülich (Germany), **2000**, 479.

[5] A. W. Ehlers, M. Biihme, S. Dapprich, A. Gobbi, A. Hijllwarth, V. Jonas, K. F. Kiihler, R. Stegmann, A. Veldkamp, G. Frenking, *Chem. Phys. Letters* **1993**, *208*, 111.

[6] P. C. Hariharan, J. A. Pople, *Theor. Chim. Acta* **1973**, *28*, 213.

[7] a) Fukui, K. *Acc. Chem. Res.* **1981**, *14*, 363. b) Hratchian, H. P.; Schlegel, H. B. *Theory and Applications of Computational Chemistry: The First 40 Years*, Elsevier: Amsterdam, **2005**, *195*.

[8] Chemcraft graphical software for visualization of quantum chemistry computations. https://www.chemcraftprog.com

[9] a) F. London, *J. Phys. Radium* **1937**, *8*, 397; b) R. McWeeny, *Phys. Rev.* **1962**, *126*, 1028; c) R. Ditchfield, *Mol. Phys.* **1974**, *27*, 789; d) K. Wolinski, J. F. Hilton, Pulay, P. *J. Am. Chem. Soc.* **1990**, *112*, 8251; e) J. R. Cheeseman, G. W. Trucks, T. A. Keith, Frisch, M. J. *J. Chem. Phys.* **1996**, *104*, 5497.

[10] W. Kutzelnigg, U. Fleischer, M. Schindler, *The IGLO-Method: Ab Initio Calculation and Interpretation of NMR Chemical Shifts and Magnetic Susceptibilities*, Springer-Verlag, Heidelberg, **1990**, *23*.

[11] a) E. Reed, L. A. Curtiss, F. Weinhold, *Chem. Rev.* **1988**, *88*, 899; b) J. P. Foster, F. Weinhold, *J. Am. Chem. Soc.* **1980**, *102*, 7211; c) A. E. Reed, F. Weinhold, *J. Chem. Phys.* **1985**, *83*, 1736.

[12] S. Dapprich, G. Frenking, *J. Phys. Chem.* **1995**, *99*, 9352.

[13] a) R. F. W. Bader, *Chem. Rev.* **1991**, *91*, 893; b) R. F. W. Bader, *Acc. Chem. Res.* **1985**, *18*, 9.

[14] AIMAll (Version 10.10.11), Todd A. Keith, **2010** (aim.tkgristmill.com).

III.   List of abbreviations

Ad	Adamantyl
AIL	Atomic Interaction Line
AIM	Atoms-In-Molecules
Ac	Acetate
Ac^F	TrifluoroAcetate
ADF	Amsterdam Density Functional
Ar	Aryl
ASM	Activation-Strain Model
BAr^F_4	Tetrakis(bis(3,5-trifluoromethyl)phenyl)borate (Ar^F: 3,5-$(CF_3)_2C_6H_3$)
BCP	Bond Critical Point
BDE	Bond Dissociation Energy
Bpy	2,2'-Bipyridine
bq	10-iodoben([h]quinolone)
CAAC	Cyclic(Alkyl)(Amino)Carbene
CDA	Charge Decomposition Analysis
CFL	Compact Fluorescent Light
Cp	Cyclopentadiene
CT	Charge Transfer
DCB	1,2-dichlorobenzene
DCE	1,2-dichloroethane
DCM	Dichloromethane
DMA	DiMethylAurate
DMAP	4-Dimethylaminopyridine
DMF	Dimethylformamide
DMSO	Dimethylsulfoxide
DFT	Density Functional Theory
Dipp	2,6-diisopropylphenyl
DPCb	DiPhosphineCarborane
DPEPhos	Bis[(2-diphenylphosphino)phenyl] ether
dppm	Bis(diphenylphosphanyl)methane
EDA	Energy Decomposition Analysis
eq.	Equivalent
ESI	ElectroSpray Ionization
ESP	ElectroStatic Potential
Flu	Flurorene
FXR	Farnesoid X receptor
GC	Gas Chromatography
HOFO	Highest Occupied Fragment Orbital
HOMO	Highest Occupied Molecular Orbital
hq	8-hydroxyquinoline

| IBA | 1-hydroxy-3-oxobenziodoxole |
IR(PD)	InfraRed (PhotoDissociation)
IRC	Intrinsic Reaction Coordinate
IS	Internal Standard
LUFO	Lowest Unoccupied Fragment Orbital
LUMO	Lowest Unoccupied Molecular Orbital
Me	Methyl
Mes	Mesityl
MeDalPhos	Di(1-adamantyl)-2-dimethylaminophenylphosphine
MorDalPhos	Di(1-adamantyl)-2-morpholinophenylphosphine
MS	Mass spectroscopy
Nbe	Norbornene
NBO	Natural Bond Orbital
NHC	N-Heterocyclic Carbene
NLMO	Natural Localized Molecular Orbitals
NMR	Nuclear Magnetic Resonance
NOCV	Natural Orbital for the Chemical Valence
NPA	Natural Population Analysis
Nu	Nucleophile
OTf	Trifluoromethanesulfonate
PES	Potential Energy Surface
Ph	Phenyl
Phen	1,10-Phenanthroline
Ppy	PhenylPyridine
rt	room temperature
Selectfluor	1-chloromethyl-4-fluoro-1,4-diazoniabicyclo[2.2.2]octanebis(tetrafluoroborate)
SET	Single Electron Transfer
S_N	Nucleophilic Substitution
STO	Slater-Type Orbital
TDTT	5-(Trifluoromethyl)dibenzothiophenium trifluoromethanesulfonate
Tf	Triflate
TFE	TetraFluoroEthylene
TMB	1,3,5-trimethoxybenzene
Tpy	2-(p-tolyl)pyridine
Ts	Tosyl
TS	Transition State
UV-Vis	Ultra-Violet Visible
TSA	Toluenesulfonic acid
vs	*versus*
WBI	Wiberg Bond Index
XRD	X-Ray Diffraction
ZORA	Zero-Order Regular Approximation

IV. List of gold complexes
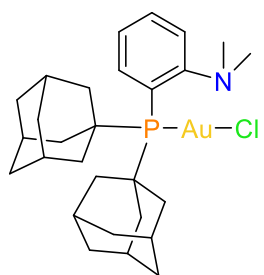
1
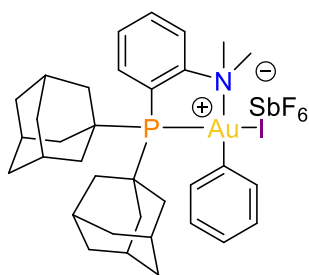
2
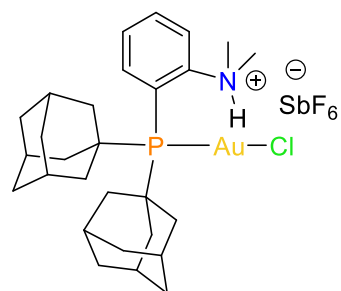
3
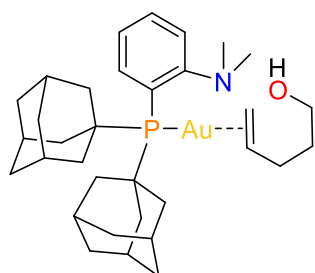
4
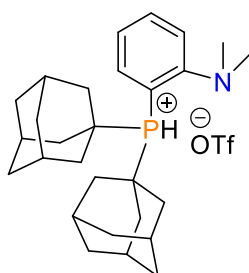
5
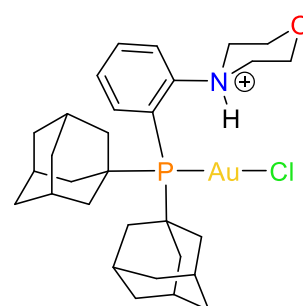
6
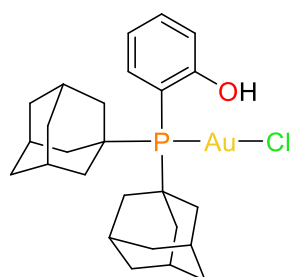
7
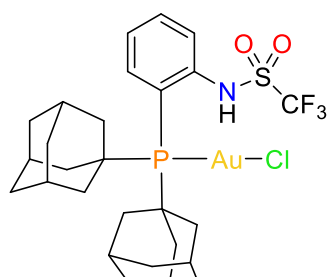
8

9

10

11

12

13

14

15

16

= BH

17

= BH   R = OMe, Ph, CF$_3$

18-R

= BH

19

= BH
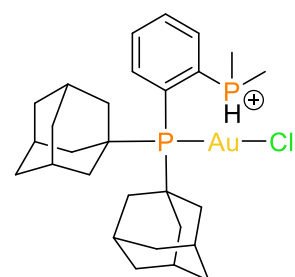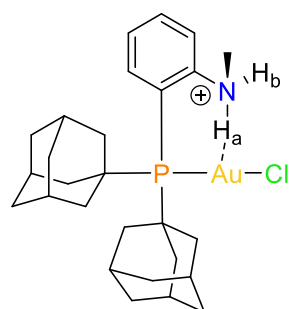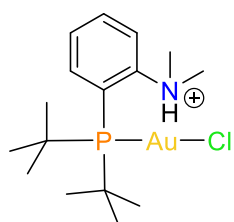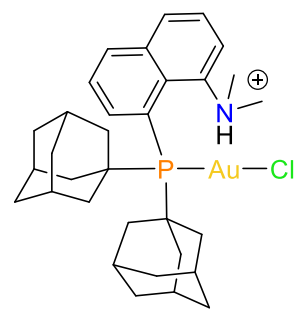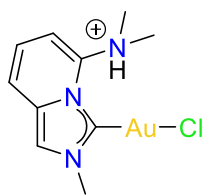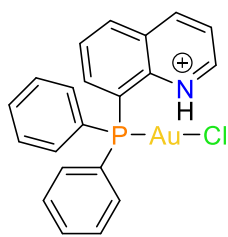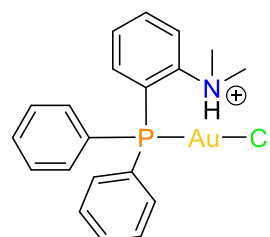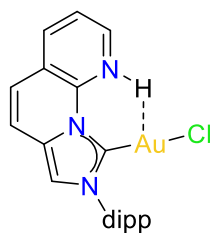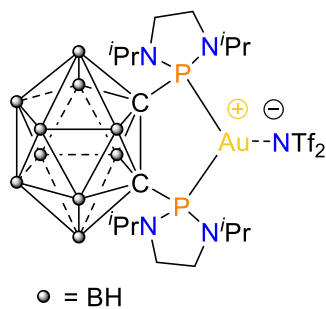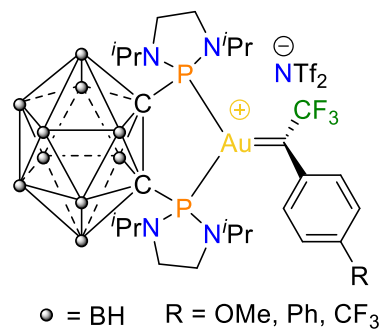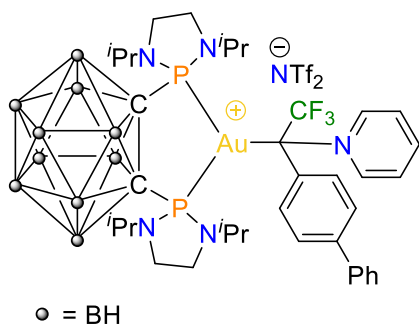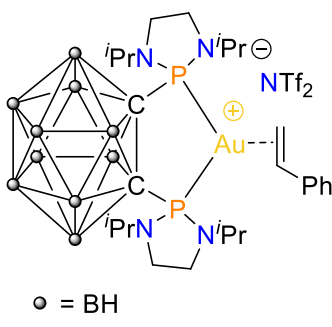
20

Chapter 1

General introduction

Gold is not only nice to wear as jewels, but it is also a peculiar metal in the periodic table. Contrary to the other metals, its study and use in chemistry is quite recent. Indeed, first reports using gold as catalyst were published in the 70s.[1]

It is the apparent inertness of gold that led to the discovery of one of the earliest examples of homogeneous gold catalysis. Gold being considered as the least active metallic material, it was used for the fabrication of flow reactors. Nevertheless, when studying the cycloreversion of diademane, Meijere and co-workers discovered in 1976 different reactivities from a glass reactor than a gold reactor.[2] The first one led to triquinacene product whereas gold catalyzed the formation of snoutene (Scheme I-1). Following this discovery, they showed that the same rearrangement can be catalyzed by (dicyclopentadiene)AuCl in solution at room temperature.

Scheme I-1: Cycloreversion of diademane with or without gold.

Since this pioneering work, gold catalysis started to be explored, notably towards the nucleophilic addition on multiple CC bonds.[3–6] However, gold catalysts were quickly reduced to inactive metallic gold, and so, only low turnovers were achieved. For this reason, gold was considered in 1995 to be "catalytically dead, in contrast to its neighbor elements on the periodic table".[7]

A real breakthrough occurred in 1998 when Teles and co-workers reported a very efficient class of gold(I) catalyst [L-Au]+ (where L is a phosphine, a phosphite or an arsine) for the addition of alcohols to alkynes, under mild conditions, with turnover numbers of up to 10^5 moles of product per mole of catalyst (Scheme I-2).[8] The nature of the ligand and counter anion were carefully studied to find a fine balance between reactivity and stability.

L = phosphine, phosphite or arsine
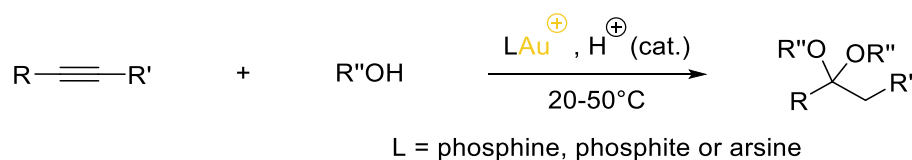
Scheme I-2: Additions of alcohol to alkyne in the presence of gold catalyst.

Inspired by this work, the carbophilic properties of gold were largely explored to develop new gold-catalyzed reactions for the synthesis of complex and highly functionalized molecules.[9–11] Often, linear gold(I) complexes LAuX were employed with L being a N-

heterocyclic carbene (NHC) or a phosphine ligand and X an anionic ligand that can be exchanged with an unsaturated substrate.[12,13] Gold(III) complexes were also used, but the difficulty to synthesize stable gold(III) species mainly limited the chemists to inorganic gold(III) salts.[14] From a mechanistic point of view, it is unclear what is the active species. Indeed, Au^{III} can be first reduced to Au^I and Au^I can then undergo a dismutation to Au^0 and Au^{III}. In all cases, it is supposed that, once the active species formed, the oxidation state of gold remains unchanged throughout the process.

To extend gold chemistry well beyond π-activation, the design of appropriate ligands, notably bidentate ligands was needed. The second coordination site of the ligand modifies the properties of gold, emulates and controls its reactivity. Thanks to bifunctional ligands, elementary reactions have been evidenced, opening new avenues to Au^I/Au^{III} catalysis. Moreover, some intermediates were isolated, characterized and analyzed by experimental and computational methods, allowing to gain mechanistic insights. The effect of the bidentate ligands was thoroughly analyzed highlighting the key factor governing the reactivity of gold complexes and further expanding its scope.[15,16]

I.   Bidentate ligands for elementary steps in gold chemistry

1. Oxidative addition

Oxidative addition is the entry point to many catalytic transformations. In striking contrast to other transition metals, this elementary reaction remained for a long time elusive in gold chemistry. The reluctance of gold(I) complexes to undergo oxidative addition was generally attributed to the really high redox potential of the Au^I/Au^{III} couple (1.41 V) compared to that of the isoelectronic Pt^0/Pt^{II} couple (1.18 V).[17] Nevertheless, more recent studies have shown that structural features play a major role. On the one hand, the strong destabilizing effect of the deformation energy of the linear L-Au-L complex disfavors kinetically the oxidative addition step.[18] On the other hand, using cationic gold(I) complexes featuring monodentate ligands (L-Au+), the activation barrier for the oxidative addition is accessible, but the generated three-coordinate Au^{III} species are highly unstable.[19,20]

To favor the oxidative addition and obtain stable gold(III) compounds, a strategy based on chelation assistance was envisioned by our group. Using an aryl-halides bearing a phosphine ligand, that upon coordination of gold, placed the metal center in close proximity to the reactive bond, the oxidative addition of C-X (X = I or Br) bonds has been achieved (Scheme I-3, top).[21] The bifunctional character and the rigidity of the (P,C) ligand stabilized the obtained

gold(III) in the form of cyclometalated complexes. The chelating ligand are known to modify the redox potentials, thus providing stability against reductive elimination. [22–24]
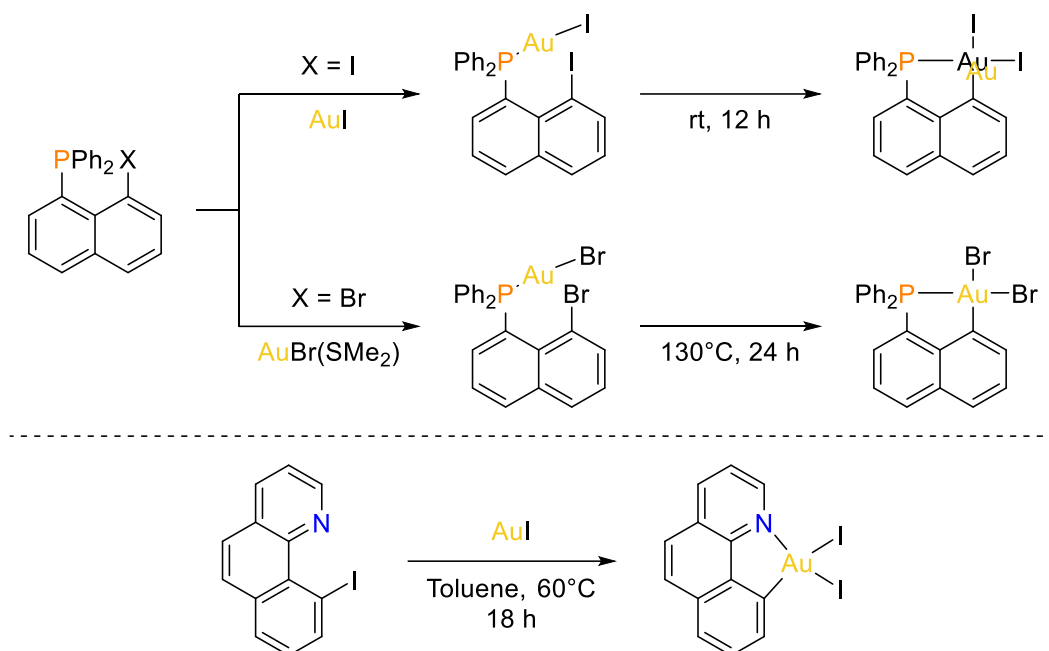
Scheme I-3: Intramolecular oxidative addition by chelating assistance. Top: Coordination of the 8-halonaphtyl phosphines to gold(I) followed by C_{sp^2}-X oxidative addition. Bottom: Synthesis of 10-iodobenzo[h]quinolone gold (III) complex.

Inspired by this strategy, Ribas' group performed the oxidative addition of a C-I bond using the 10-iodobenzo[h]quinolone, (C,N)bq ligand (Scheme I-3, bottom) and access stable (N,C) cyclometalated gold(III) complex. The reaction conditions are slightly harsher compared to the (P,C) ligand.[25]

The chelation-assisted strategy cannot be applied to achieve intermolecular oxidative addition. As mentioned before, one issue is the linear coordination of gold. To circumvent it, a strategy based on bidentate ligands featuring a small bite angle has proven to be efficient. In addition to preorganize the AuL_2 fragment to accommodate the square planar geometry of the oxidative addition product, the bidentate ligand noticeably modifies its electronic properties. As illustrated in Figure I-1, from model monophosphine to the bent chelate diphosphine cationic gold(I) complexes, the HOMO is very much raised in energy and changes from d_{z^2} to d_{xz} in symmetry increasing back-donation to the σ^* orbital of an incoming substrate and thereby favoring the oxidative addition.
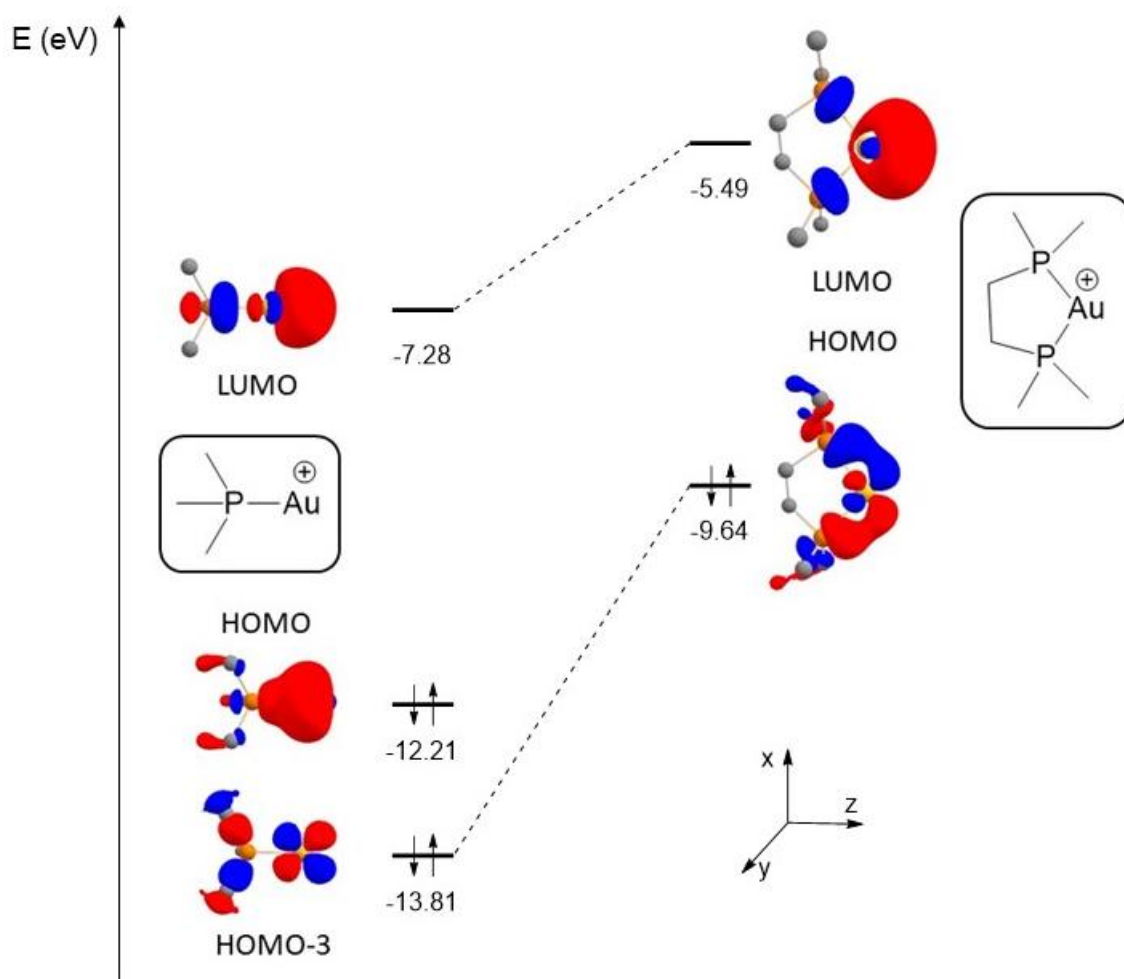
Figure I-1: Plot and positions (in eV) of the main molecular orbitals (LUMO and occupied d_{z^2} and d_{xz} orbitals) of model gold(I) complexes bearing monodentate (left) and bidentate (right) phosphine ligand calculated at the B3PW91/SDD+f(Au),6-31G**(other atoms) level of theory.

Employing the carborane diphosphine ligands (DPCb) that chelate gold(I) with PAuP angles between 90° and 100°, our group performed the oxidative addition to gold of different aryl iodides and strained C-C bonds (Scheme I-4).[26,27] Surprisingly, the electron rich substrates react faster than the electron poor ones which is opposite to that usually encountered for Pd^0 complexes.[28]

According to DFT calculations (B3PW91/SDD+f(Au),6-31G**(other atoms)), the activation barrier is lower for bent cationic gold complexes than for L_2Au^+ fragments with 2 monodentate ligands coordinated in a linear manner ($\Delta E^{\neq}$ = 10.3 kcal/mol and $\Delta G^{\neq}$ = 10.7 kcal/mol *vs* $\Delta E^{\neq}$ = 14.4 kcal/mol and $\Delta G^{\neq}$ = 27.6 kcal/mol for $(Me_3P)_2Au^+$). The role of the bending was confirmed using activation-strain model (ASM)[29,30] of reactivity: thanks to preorganization, the distortion ($\Delta E^{\#}_{strain}$) of the $(DPCb)Au^+$ fragment requires only 6.3 kcal/mol whereas 24.4 kcal/mol are needed for the $(Me_3P)_2Au^+$ fragment.[26] Moreover, for the DPCb ligand, the interaction energy ($\Delta E^{\#}_{int}$) between the distorted fragments is relatively large (−34.8 kcal/mol), resulting in a small activation barrier.

14
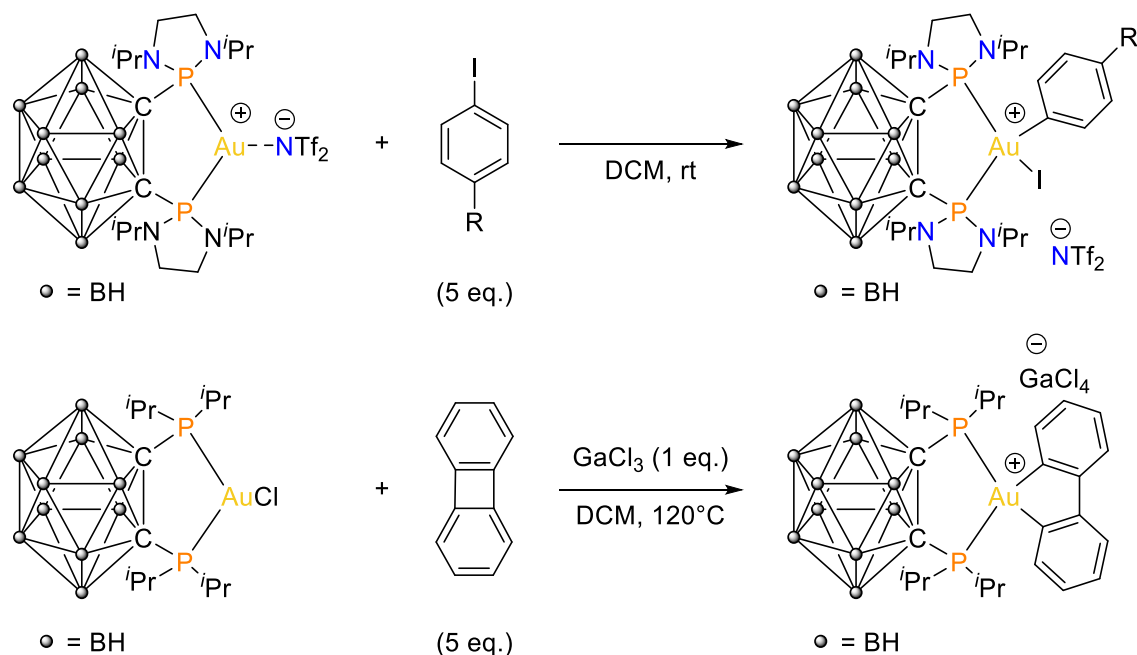
Scheme I-4: Oxidative addition of aryl iodide (top) and strained C-C bond (bottom) to bent (P,P) gold(I) complexes.

The same strategy was applied by Russel's group using 2,2'-bipyridyl ligands that chelate the gold(I) atoms with NAuN angles of 75°.[31] In this case, the presence of ethylene makes the oxidative addition to gold reversible (Scheme I-5), but removal of free ethylene from the reaction mixture drives the equilibrium to the gold(III) complex. The oxidative addition at gold for a broad scope of aryl iodides was performed. Once again, electron-rich compounds react faster than electron-poor ones.[32] With this (N,N) ligand, Russell went one step further than our group and achieved the whole synthetic sequence towards cross coupling (oxidative addition, transmetalation and reductive elimination), but didn't manage to render the overall three-step process catalytic.
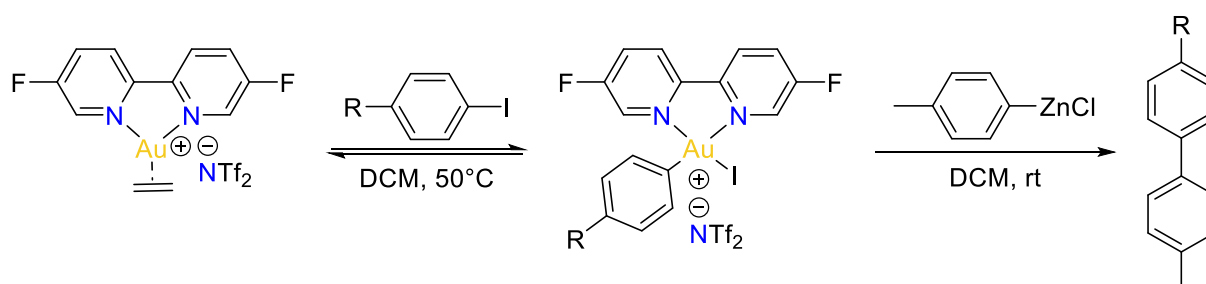
Scheme I-5: Reversible oxidative addition of aryl iodides to bent bipyridyl gold(I) complex and cross-coupling reactions with an organozinc reagent.

The "bending" strategy is limited by the strong preference of gold(I) for two-coordinate linear geometry, considerably restricting ligand modulation. To find a balance between reactivity of the gold(I) center and stability of the gold(III) species, the use of hemilabile ligands was envisioned. Bertrand and co-workers showed, employing a cyclic (alkyl)(amino)carbene (CAAC) bearing a pendant imine moiety, that the oxidative addition of biphenylene was

possible and led to stable gold(III) complex.[33] The imine arm does not coordinate the soft gold(I) (AuN distance > 3.39 Å) but binds to the hard gold(III) center (AuN distance = 2.246(3) Å) stabilizing the new complex (Scheme I-6).
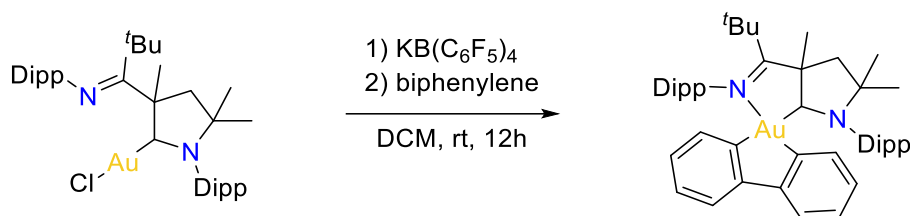
Scheme I-6: Oxidative addition of biphenylene to gold with the hemilabile CAAC ligand.

The same strategy was employed using the commercially available MeDalPhos (P,N) ligand. Our group performed the oxidative addition of biphenylene, aryl iodides and bromides to gold (Scheme I-7).[34]
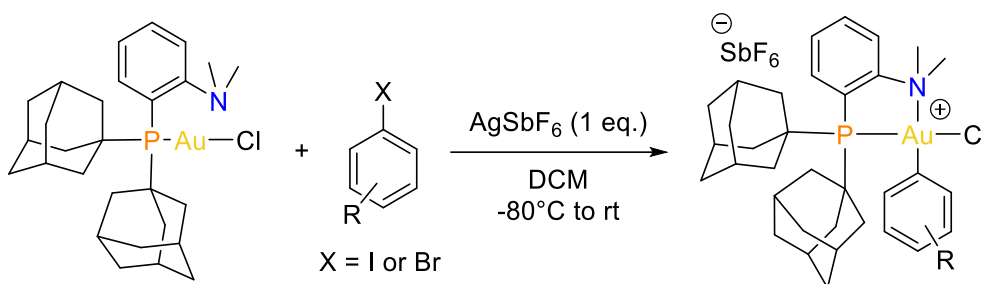
Scheme I-7: Oxidative addition of aryl iodides and bromides to gold using the hemilabile MeDalPhos (P,N) ligand.

The impact of the nitrogen arm was confirmed computationally. The reaction profiles for oxidative addition at gold with the MeDalPhos ligand or with a related ligand devoid of NMe_2 were compared. In both cases, the reaction is kinetically feasible, but the activation barrier for the ligand without NMe_2 is about one and a half as large ($\Delta G^{\#} = 11.2$ kcal/mol *vs* 17.0 kcal/mol). Moreover, the reaction with MeDalPhos gold complex is thermodynamically favored, whereas it was unfavored with the other gold complex ($\Delta G = -5.9$ kcal/mol *vs* $\Delta G = 11.2$ kcal/mol) due to the formation of a 3-coordinate Au^{III} species (Figure I-2).
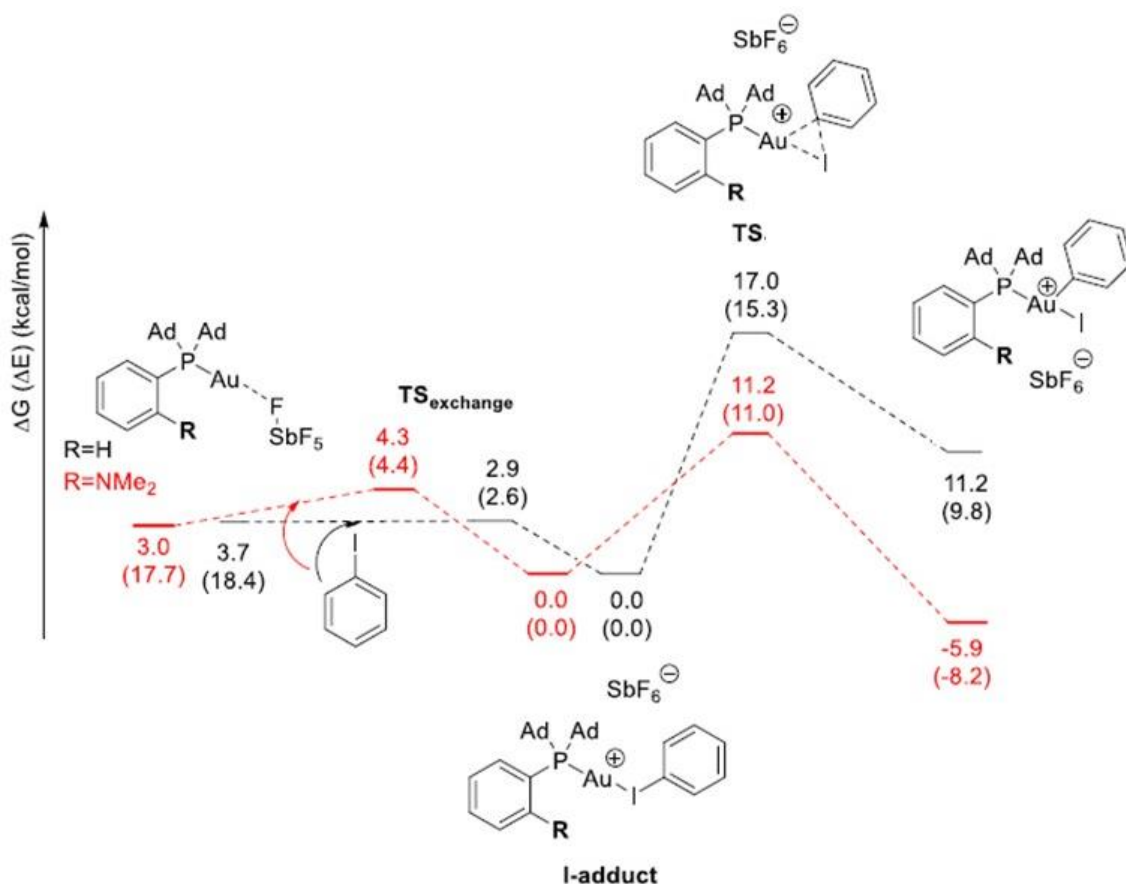
Figure I-2: Energy profiles for the oxidative addition of iodobenzene to the MeDalPhos gold(I) complex (in red) and to the model complex devoid of NMe₂ group (in black) computed at the SMD(DCM)-B97D/SDD+f(Au),SDD(I,Sb),6-31G** (other atoms) level of theory. Electronic energy (ΔE) including ZPE correction into brackets and Gibbs free energy (ΔG) in kcal/mol.

This comparison highlights the double role of the (P,N) ligand: 1) it lowers the activation barrier and 2) it stabilizes the gold(III) complex by coordination of the nitrogen atom. The (P,N) gold complex displays the same preference toward electron rich-iodoarenes than the (P,P) or (N,N) gold complexes, suggesting it is a general feature of gold. To get insight of this unique behavior, the structure of the transition state associated to the oxidative addition was analyzed for the (P,N) gold complex. Charge analysis reveals an electron transfer from iodobenzene to gold and natural bond orbital (NBO) as well as charge-decomposition analyses (CDA, d/b ratio) indicate that donor-acceptor interactions from iodobenzene to gold largely prevails over the one from gold to iodobenzene. This is in contrast with palladium for which the charge transfer is opposite (electron transfer from palladium to iodobenzene) and the PhI → Pd and Pd → PhI interactions are much more balanced. The difference of behavior between gold and palladium probably comes from the higher electrophilicity of the gold center and the important back-donation from palladium.[35] To confirm these results and further analyze the different chemical behavior of gold and palldium, the NOCV (Natural Orbital for the Chemical Valence) extension of the EDA (Energy Decomposition Analysis) approach was also used. The primary orbital interaction was found to be associated with substrate to metal donation for gold and metal to substrate back-donation for palladium (Figure I-3).

$$\Delta E_{orb}(\rho) = -22.9 \qquad\qquad \Delta E_{orb}(\rho) = -59.4$$
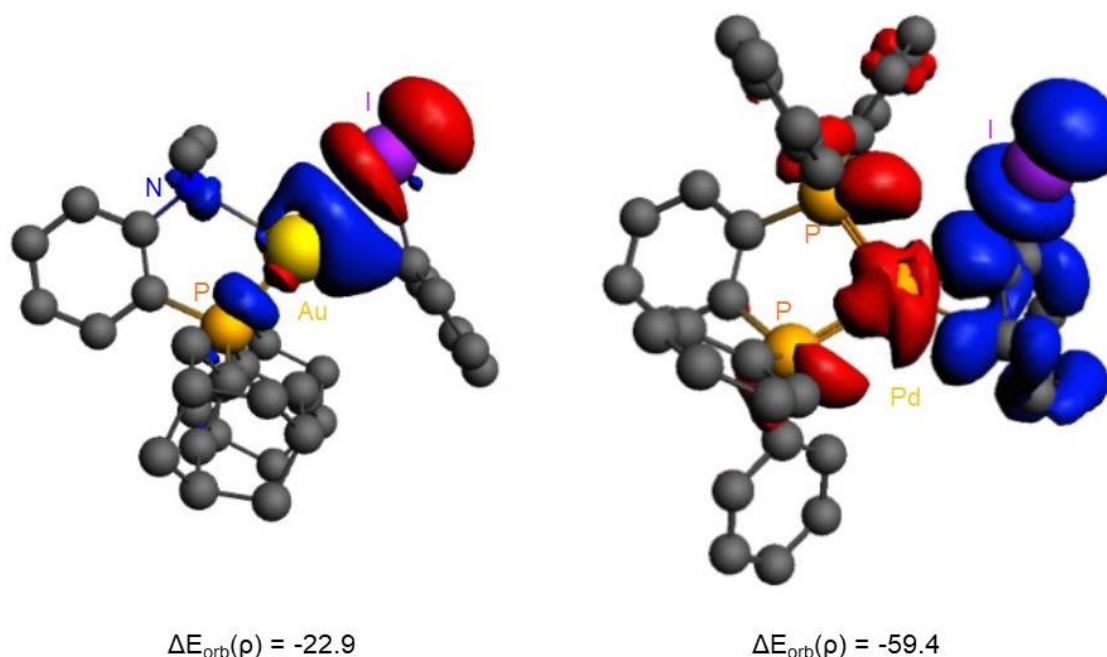
Figure I-3: Contour plot of the NOCV deformation density $\Delta\rho_{orb}$ and the associated stabilizing energy ($\Delta E_{orb}(\rho)$, in kcal/mol) for the predominant orbital interaction between PhI and the Au/Pd metal fragments. The charge flow is red → blue ($\Delta\rho < 0$ in red and $\Delta\rho > 0$ in blue). Analysis performed at ZORA-BP86-D3/TZ2P level of theory. The contour value for density is 0.001 a.u.

Our group wanted to go beyond this elementary step and showcased a Au^I/Au^{III} redox cycle. Gold(III) salts were recognized early on to readily perform C_{sp}^2-H bond activation,[36] but gold was overlooked in the C-H functionalization field. Indeed, the reluctance of gold to commute between Au^I and Au^{III} limits is use for cross-coupling reactions. To achieve the Au^I/Au^{III} redox cycle, strong external oxidants (mostly hypervalent iodine(III) reagents and F^+ surrogates)[37–39] or strong electrophiles such as diazonium salts (oxidizing gold under photochemical conditions),[40–43] were used. These strategies present the advantage to proceed under mild conditions and with selectivities complementary to palladium-catalyzed processes, but several functional groups are incompatible (notably electron rich compounds).

The (P,N) gold(I) complex achieving the oxidative addition of large scope of haloaryls (bearing electron-withdrawing or electron-donating groups) under mild conditions and gold(III) having great potential for C_{sp}^2-H bond activation, our group studied the reactivity of the (P,N)AuCl complex for direct arylation process. The transformation was first assessed under stoichiometric conditions. The reaction of the (P,N) gold(III) aryl complex with 1 equivalent of 1,3,5-trimetoxybenzene (TMB) in presence of $AgSbF_6$ afforded the desired biaryl product. In addition, the cross-coupling reaction between iodoarene and TMB was performed under catalytic conditions showing that the Au^I/Au^{III} catalytic cycle involving a C_{sp}^2-I oxidative addition, C_{sp}^2-H bond activation at gold and reductive elimination is feasible.[34] Then, the more challenging C3-arylation of indoles was developed[35] and the approach was further extended to C-N coupling (Scheme I-8).[44,45]
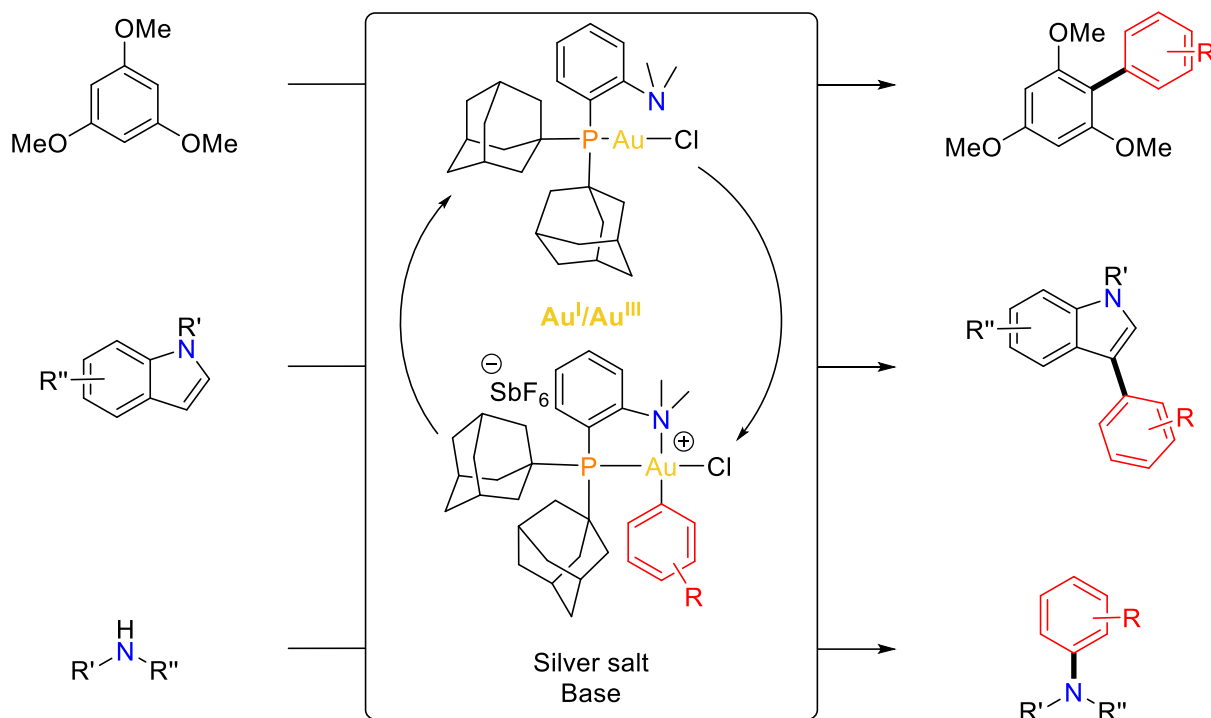
Scheme I-8: Au^I/Au^III cross-coupling catalysis enabled by MeDalPhos ligand.

Thanks to rational ligand design, the oxidative addition at gold was unlocked and gold-catalyzed cross-coupling reactions were developed without using external oxidants or strong electrophiles substrates.

2. Migratory insertion: inner-sphere *vs* outer-sphere mechanism

Migratory insertion, another elementary step in organometallic chemistry, is at the basis of many important catalytic processes involving the functionalization or coupling of unsaturated substrates (such as olefins or alkynes). Owing to their unsaturated character (d^8 configuration), gold(III) are promising candidates for migratory insertion. Two mechanisms can be envisioned. Firstly, the outer-sphere mechanism consisting in a nucleophilic attack on the π-complex *anti* to gold (Scheme I-9, top). Secondly, the inner-sphere one with *syn*-insertion of the π-substrate into a Au-nucleophile bond (Scheme I-9, bottom).
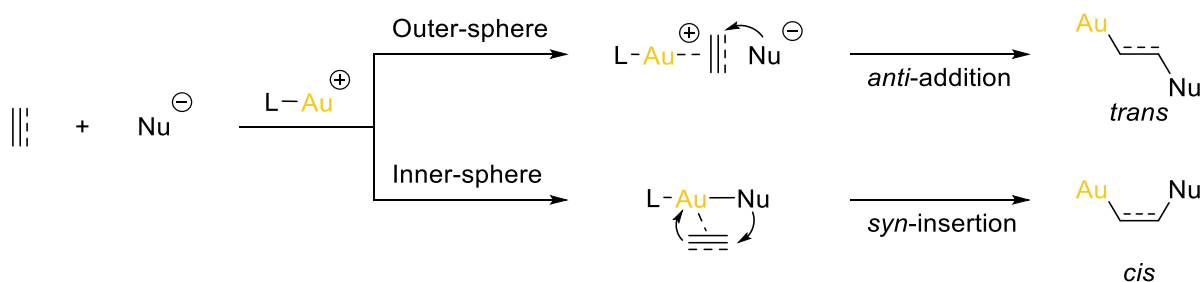
Scheme I-9: Schematic representation of the outer- and inner-sphere mechanisms for the gold catalyzed addition of nucleophiles to π-substrates.

The investigation of ethylene insertion into Au-OAc^F was carried out by Tilset and co-workers with the cyclometalated (C,N) tolypyridine (tpy) gold complex.[46] Deuterium labelling studies and DFT calculations revealed that the insertion product arises from external nucleophilic attack by the Ac^{F}O$^-$ anion on coordinated ethylene (Scheme I-10, top). Reactions with internal alkenes and other nucleophiles (like MeOH) confirmed the *anti*-addition process (Scheme I-10, middle).[47] If acetylene is employed instead of ethylene, a double insertion process operates, still by outer-sphere mechanism.[48] The gold(III) divinyl complex was not observed since protolytic cleavage of the Au-vinyl bond *trans* to tpy-C occurred rapidly (Scheme I-10, bottom), but its involvement in the catalytic cycle was authenticated by deuterium labelling and DFT calculations.
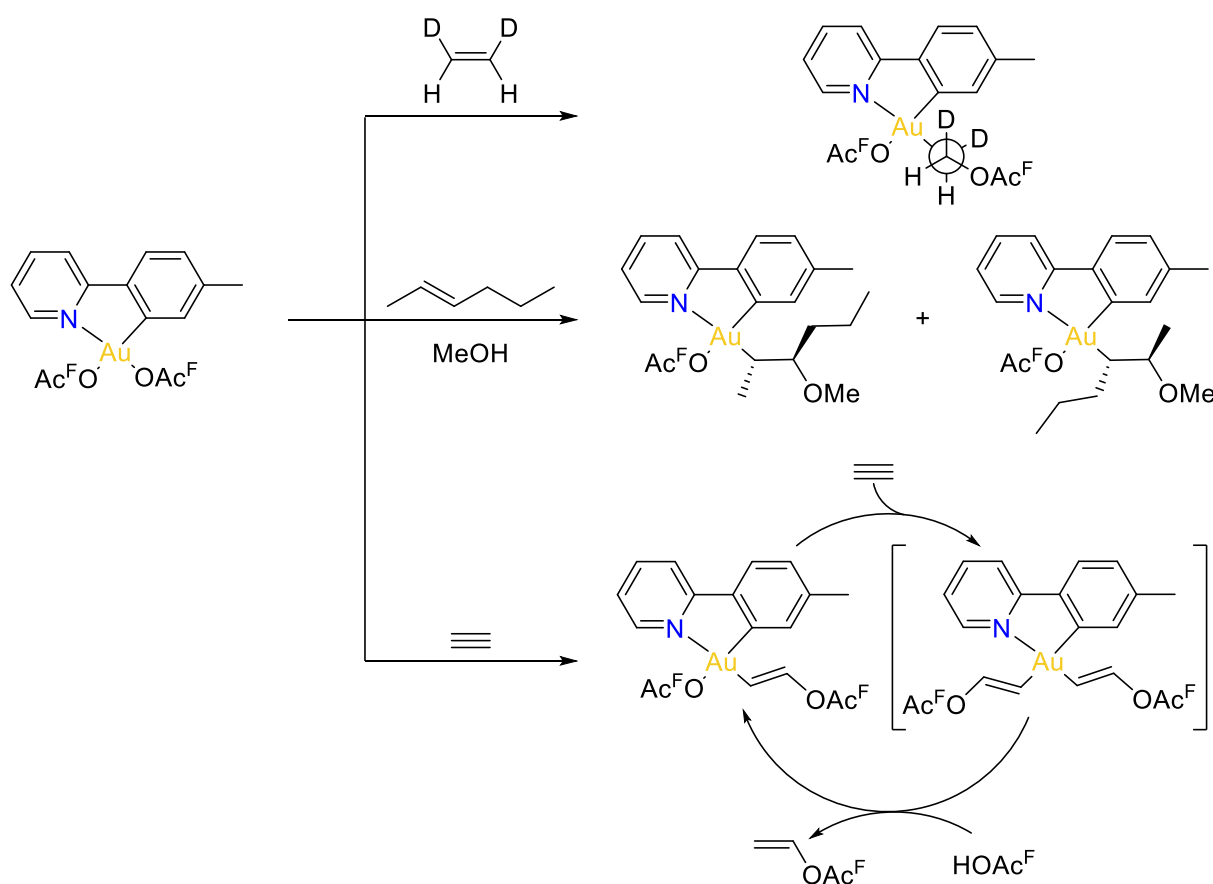
Scheme I-10: Reaction of (C,N)Au(OAc^F)$_2$ with π-substrates.

The first example of olefin migratory insertion into Au-C bonds was described by our group in 2015 with the (P,C) cyclometalated gold(III) complexes previously obtained by oxidative addition. After methylation of gold, the reactivity of the new (P,C) gold(III) dimethyl complex towards norbornene (nbe) was investigated in the presence of B(C$_6$F$_5$)$_3$. Norbornene was found to readily insert twice into the Au-C$_{sp}$^{3} bond in a *syn* manner, consistent with a coordination-insertion process (Scheme I-11, top).[49] The sequence of coordination and

migratory insertion has also been confirmed by DFT calculations and low temperature NMR monitoring.[50]
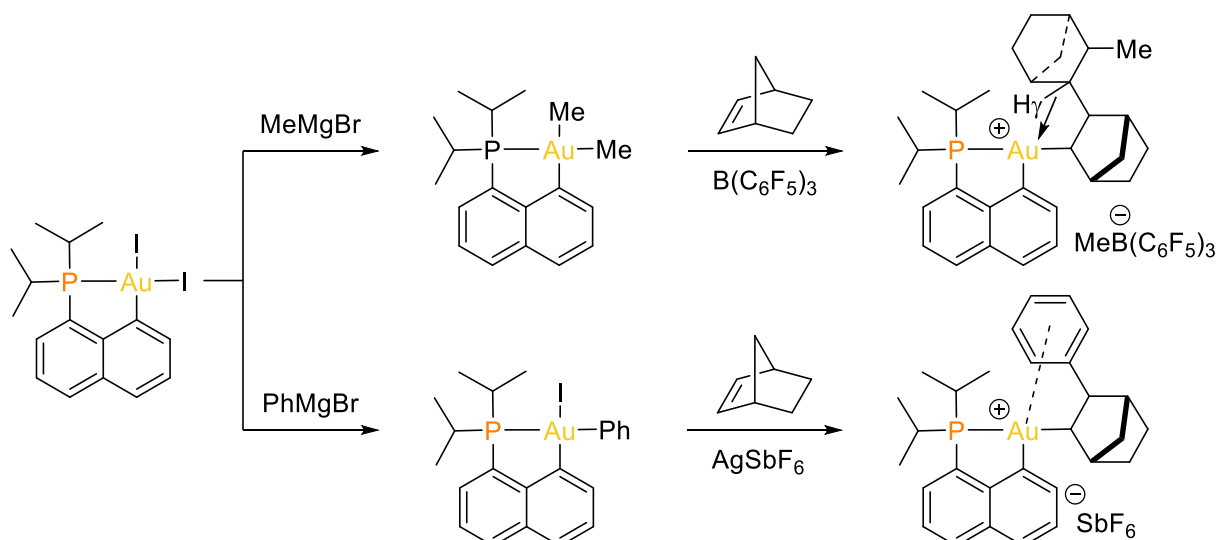
Scheme I-11: Formation of gold(III) norbornyl complex resulting from syn insertion of norbornene into Au-C bonds.

Later on, using the same (P,C) gold(III) dimethyl complex, the migratory insertion of ethylene into Au-C and Au-H bonds was evidenced, but no complex resulting from insertion was isolated due to fast β-hydride elimination.[51] When switching from methyl to phenyl substituent, migratory insertion into the Au-C_{sp}^2 bond was observed for ethylene (still followed by β-H elimination) and for norbornene (but only one molecule insert, Scheme I-11, bottom). The ensuing Au^{III} cationic complexes are stabilized by π-arene coordination.[52]

To precise the influence of the ancillary ligand, a similar reaction was performed with the (N,C)bq gold(III) phenyl complex.[53] Contrary to the (P,C) gold complex, ethylene inserts twice into Au-C bond without β-hydride elimination (Scheme I-12). The difference in reactivity between the two ligands is due to the electronic dissymmetry of the coordination sphere at gold induced by the (N,C) ligand. Indeed, because of the weak donor character of nitrogen compared to phosphorus, the energetic gap between the two reactive sites at gold are very different. The LUMO, corresponding to the vacant orbital at gold in *trans* position to the N or P atoms, and the LUMO+1, being the vacant orbital at gold in *trans* position to aryl, are close in energy for the (P,C) ligand, but the difference is more important for the (N,C) one.
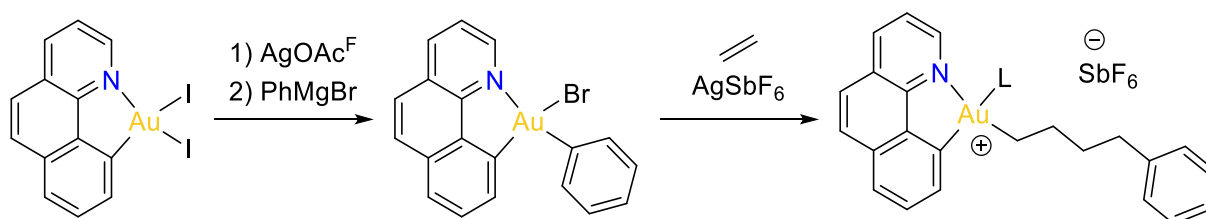
Scheme I-12: Migratory insertion of ethylene into Au-C bond with the cyclometalated (C,N)bq gold(III) complex.

Depending on the bidentate ligand employed, very different reactivities are observed. With the (C,N)tpy gold complex, insertion of ethylene into Au-O bond occurred *via* an outer-sphere mechanism. With the (C,N)bq or (P,C) gold complexes, the ethylene insertion into Au-C bonds proceed *via* inner-sphere mechanisms, but with different outcomes: either the ethylene inserts twice (with (C,N)bq) or the insertion is followed by β-hydride elimination (with (P,C)). Each time, the nature of the mechanism has been authenticated by D-labelling experiments and DFT calculations.

II. Bidentate ligands for the isolation of reactive intermediates in gold chemistry
1. Gold π-complexes with alkenes

As seen in the first part, gold is a good activator of π-bonds and so the isolation of gold π-complexes has received great attention over the last few years. Most of the known gold π-complexes are cationic dicoordinate gold(I) complexes of the type [LAu(ene)]+ with L being an NHC or a phosphine.[54] Tricoordinate species have also been reported with bidentate ligands and present unique features, as briefly reviewed hereafter.

The first cationic tricoordinate gold(I) olefin complexes was synthesized, characterized and analyzed computationally by Cinellu et al. in 2004-2006 using different bipyridine ligand.[55,56] When binuclear gold(III) μ,μ-dioxo compounds were reacted with various olefins, the gold(I) π-complexes of the type [(bpy)Au(ene)]+ were obtained (Scheme I-13). For most of these compounds, the ^{1}H NMR signals of the olefin are sharp and high-field shifted with respect to the free alkenes ($\Delta\delta^1$H = 0.8-2.2 ppm). For comparison, the changes observed upon coordination of olefins to gold(I) centers ligated to NHCs or phosphines were only minor ($\Delta\delta^1$H < 0.1 ppm). Moreover, in the solid-state structures, the gold-carbon distances were found to be slightly shorter in [(bpy)Au(ene)]+ than in linear gold(I)-alkene complexes and the C-C bond lengths of the coordinated olefin were elongated (> 0.03 Å) compared to free olefin. All these data suggest that the bidentate bipyridyl ligand increases the Au → alkene back-donation which was confirmed by DFT calculations. NBO analysis (population of $\pi_{C=C}$ and $\pi^*_{C=C}$, C-C Wiberg bond indexes (WBI)), Bond dissociation Energies (BDE) indicate indeed significant π-back-donation from gold.
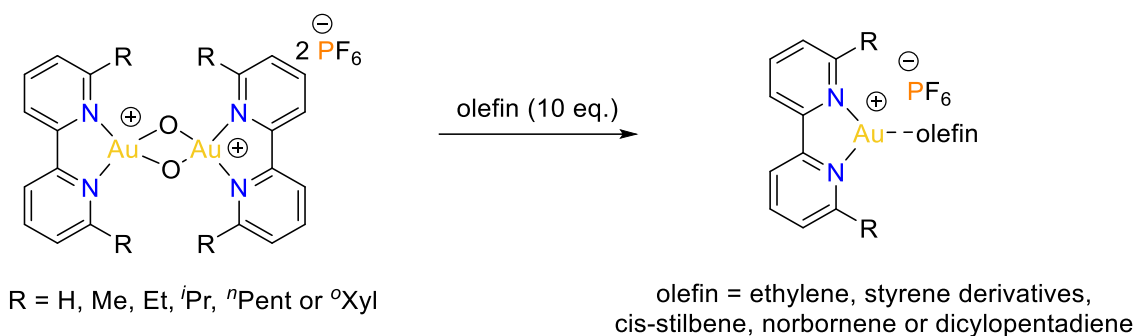
Scheme I-13: Synthesis of the tricoordinate [(bpy)Au(ene)]+ π-complexes.

Following this work, other gold(I)-olefin complexes bearing (N,N) ligands have been synthesized (Scheme I-14).
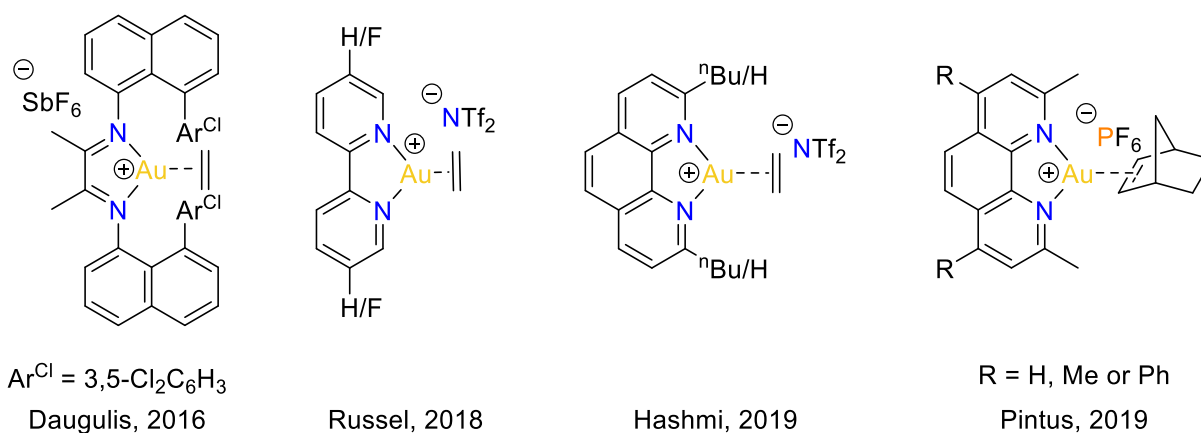
Scheme I-14: Representative examples of cationic gold(I)-olefin complexes with (N,N) bidentate ligands.

In 2016, Daugulis et al. reported a stable complex featuring an hindered α-diimine ligand.[57] In 2018, the group of Russel prepared a cationic [(bpy)Au(C_2H_4)]+ complex.[31] In 2019, the Hashmi's[58] and Pintus'[59] groups synthesized similar [(phen)Au(olefin)]+ complexes with ethylene or norbornene. For all these complexes, X-Ray analyses showed elongated C=C bond and ^{1}H NMR signals are upfield shifted compared to free olefins, in line with enhanced π-back-donation induced by the chelating ligand.

Not only (N,N) bidentate ligands stabilize gold π-complex, but also (P,P) ones. Indeed, our group studied the behavior of [(DPCb)Au]+ towards styrene and ethylene (Scheme I-15).[60,61] In both cases, the alkene is tightly coordinated to the gold(I) center, as shown by the noticeable upfield shifts of the vinylic signals in the ^{1}H and ^{13}C NMR spectra, as well as the elongation of the C=C bond by XRD. Alkenes coordinate in the same plane as the (P,P) ligand maximizing the overlap between the HOMO of the gold fragment and the LUMO of the alkene. Coordination of electron rich olefins led to oligomerization and π-complexes with electron poor olefins were detected but not isolated due to decomposition.
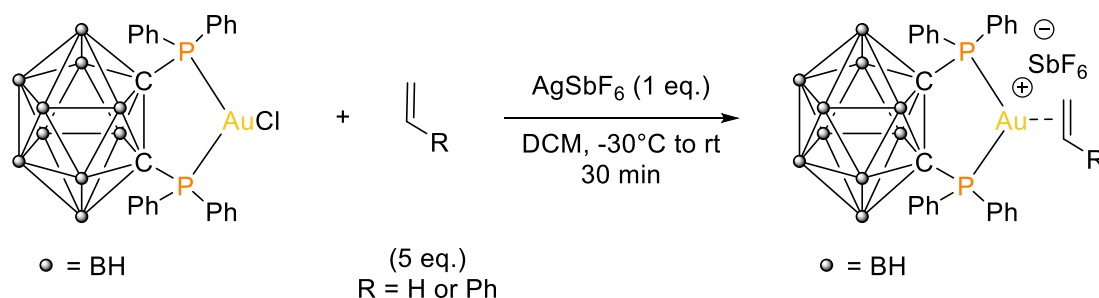
Scheme I-15: Synthesis of the (P,P) gold(I) alkene complexes.

With the aim to find a unique ligand that accommodates the π-coordination of a wide range of olefins at gold, our group looked at the behavior of the (P,N) ligand.[60,61] Studying different π-complexes with electron poor or electron rich olefins, they showed the adaptative character of the (P,N) ligand. Whatever the olefin, it coordinates to gold as indicated by the appearance of new vinylic signals in ^{1}H NMR spectrum. Moreover, a downfield shift of the N(CH$_3$)$_2$ signal is observed meaning that the nitrogen atom coordinates to the Au^I center. The poorer the olefin, the more important is the downfield shift (Table I-1).

Geometrical parameters						
Δ(C=C)^a	0.055	0.065	0.068	0.075	0.082	0.087
Au-N	2.688	2.456	2.457	2.360	2.333	2.269
Spectroscopic data						
δ^1H (H$_{NMe2}$)	2.74	3.09	3.01	3.14	3.25	3.44
	2.71	2.82	2.98		3.07	3.33
NBO Analysis						
WBI(Au-N)	0.048	0.085	0.093	0.125	0.138	0.167
LP(Au) → π*$_{C=C}$^{b}	23.0	36.7	38.9	45.1	45.1	48.9
LP(N) → Au^b	10.8	20.0	22.0	32.4	34.0	44.0
CDA analysis						
d(CC → Au)^c	0.411	0.416	0.529	0.477	0.485	0.399
b(Au → CC)^c	0.146	0.211	0.230	0.262	0.274	0.323
d/b	2.82	1.97	2.30	1.82	1.77	1.24
AIM analysis						
ρ_{AuN}^{d}	0.035	0.054	0.053	0.064	0.068	0.078

Table I-1: Key geometric distances (in Å), spectroscopic data (NMR) and NBO, CDA and AIM analyses for the π-alkene (P,N) gold(I) complexes. ^{a}Difference between C=C bond length in the gold complex and in the free alkene ^{b}Stabilizing energy $\Delta E(2)$ at 2nd order perturbation theory in kcal/mol. ^{c}Donation term (d) and back-donation term (b). ^{d}Density in e.bohr^{-3}.

Similarly to other π-complexes, XRD showed that the alkene sits in the [(P,N)Au]$^+$ coordination plane, and that the C=C bond is elongated compared to the free olefin. Moreover, the Au-N bond reduces from electron rich olefins to electron poor ones. The strength of the

Au-N interaction allows the (P,N) ligand to accommodate the electronic demand at gold. This statement was confirmed by DFT calculations, CDA, NBO and AIM analyses: the stabilizing energy $\Delta E(2)$ of the $Au \rightarrow \pi^*_{C=C}$ donor-acceptor interaction found at the second order perturbation level in NBO (back-donation from gold) as well as the $N \rightarrow Au$ interaction, the value of the WBI(Au-N) and the density ρ_{AuN} increase when the electronic demand is more important (Table I-1). In addition, the ratio donation/back-donation (CDA) decreases.

Thanks to the use of bidentate ligands, gold(I) π-complexes were stabilized, and the isolation of gold(I) ethylene complexes was possible. The change induced by the chelating ligand on the symmetry of the HOMO of gold increases the back-donation and stabilizes such species. To accommodate the electronic demand, the hemilabile MeDalPhos ligand proved to be the most versatile ligand thanks to the adaptive behavior of the pendant amine. To go beyond this overview of cationic gold(I)-olefin complexes, please refer to the recent review article published by the group on this topic.[62]

Concerning gold(III), examples of π-alkene complexes are scarce.[24] With bidentate ligands only two compounds are described. Our group, taking advantage of (P,C) cyclometallation, fully characterized the (P,C)Au(nbe) complex by multinuclear NMR spectroscopy at -90°C (Scheme I-16, left).[50] Above this temperature, norbornene insertion into the Au-Me bond occurs. The ^1H NMR spectrum shows two sets of resonances for norbornene corresponding to the bound and free olefin. The 2D HMQC ^1H-^{31}P spectrum displays a correlation between the olefinic proton of norbornene and the phosphorus at gold, confirming the coordination. The bonding situation was investigated by NBO analysis: weak back-donation from Au to $\pi^*_{C=C}$ was found at the second-order perturbation level ($\Delta E(2) = 8.6$ kcal/mol), much weaker than in gold(I) complexes or for other group 10 metals.
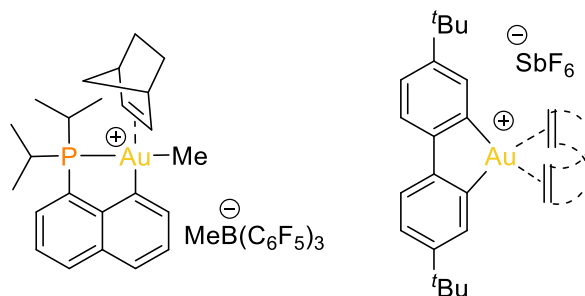
Scheme I-16: Gold(III) π-alkene complexes bearing bidentate ligand

The second example, more thermally stable, was described by Bochmann et al. with a biphenyl ligand and dienes (Scheme I-16, right).[63] Attempts to generate [(C,C)Au]⁺ complexes of ethylene or non-chelating 1-alkenes failed. To probe the influence of the (C,C) ligand, they performed some DFT calculations and showed that the greater stability of (C,C)Au(diene)

complexes comes from the increased negative charge on the (C,C) ligand leading to a more electron accepting ligand center.

2. The gold-hydrogen bonds

Bonds involving metal and hydrogen atoms can be separated into 3 main categories:[64]
(i) the covalent one, M-H, as observed in metal-hydride complexes
(ii) the agostic interaction, M ← H-C, a 3-center-2-electron interaction (3c-2e), and
(iii) hydrogen bond, M → H-X, a 3-center-4-electron interaction (3c-4e).

The metal-hydride complexes are well-established as key intermediates in numerous catalyzed reactions. Indeed, they result from β-H elimination or can undergo insertion or reductive elimination processes. Nevertheless, the characterization of such complexes with gold has proven to be a challenging field.[64] This situation has changed recently with the new arsenal of ligands available. Several stable hydride gold complexes arise from tridentate ligands, but some examples with (C,C) bidentate ligands were described by Bochmann's group (Scheme I-17).[24,65] The (C,C) chelate ligand imparts a remarkable stability toward reductive elimination, and suppresses H-C coupling.

$Ar^{tBu} = 4\text{-}^tBuC_6H_4$ $X = Cl, H, C_6F_5$ L = DMAP, PMe$_3$,
PTol$_3$ or PPh$_3$
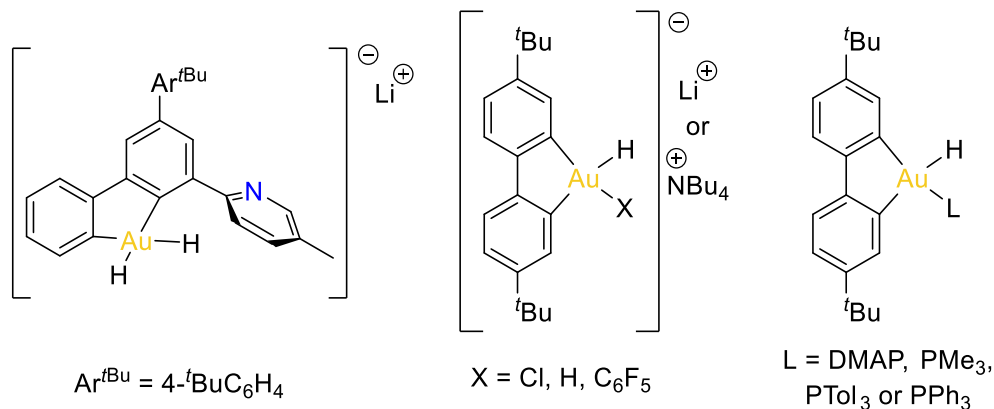
Scheme I-17: (C,C)-ligated gold(III) hydrides.

The second bonding involving M and H atoms is the agostic interaction. Reaction intermediates displaying such an interaction play a crucial role for β-H elimination and in the reverse process, the insertion of olefins into M-H bonds. They may control the stereochemistry.[66] In this M ← H-C interaction, the metal acts as a Lewis acid and receives electron density from a C-H bond. Characteristics of the agostic interaction are a reduced J_{CH} coupling constant (50-100 Hz compared to 135 Hz for classical C-H bonds) and MHC angles of 120° or less.

The only gold complex presenting an agostic interaction was isolated and characterized thanks to the use of a chelate (P,C) ligand. As mentioned earlier, the reaction between [(P,C)AuMe]$^+$ and norbornene led to double insertion of norbornene into the Au-C bond (Scheme I-11, top). Spectroscopic characterizations combined with computational studies revealed that the resulting complex presented an agostic interaction.[67] Indeed, a $^1J_{CH}$ coupling constant of 97 Hz was measured for the C-H bond in γ-position to the gold center thanks to a 2D J-resolved ^{13}C NMR experiments. Moreover, a correlation between the H_γ proton and the phosphorus was observed in 2D HMQC ^{1}H-^{31}P spectrum. The bonding situation was further assessed computationally. The geometry optimization showed a close contact (2.042 Å) between Au and H_γ, an elongated CH_γ bond (1.15 *vs* 1.08-1.10 Å) and a $AuH_\gamma C$ bond angle of 114.5°, coherent with an agostic interaction to gold. NBO calculations identified a $\sigma_{CH} \rightarrow \sigma^*_{AuCnaphthyl}$ donor-acceptor interaction at the second order perturbation level with a stabilizing energy ΔE(2) of 18.6 kcal/mol. Moreover, a bond critical point (BCP) was found between Au and H_γ with an electron density ρ_{AuH} of 0.048 e.bohr^{-3} and a Laplacien $\nabla^2\rho_{AuH}$ of 0.14 e.bohr^{-5}, typical value for agostic interaction (Figure I-4).
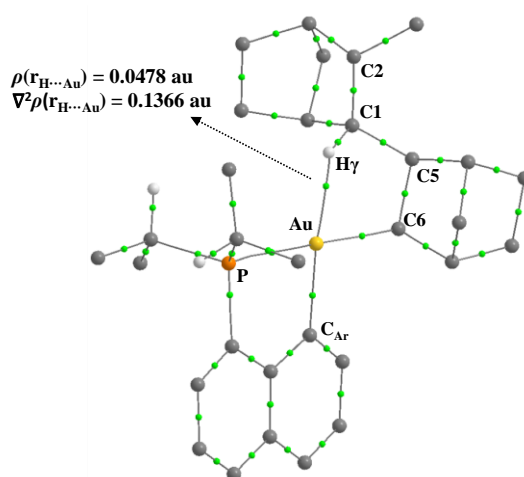
Figure I-4: Atoms-in-molecules (AIM) molecular graph showing the C-H···Au BCP (green dots) and its main electron density properties. Hydrogen atoms have been omitted for clarity except H_γ and $H_{isopropyl}$.

The last category is the hydrogen bond, M → H-X where metal acts as a Lewis base. Despite a lot of close contacts between Au and H atoms in molecular gold complexes, no evidence for complexes presenting such hydrogen bonding have been unambiguously authenticated (for more details, refer to chapter 3).[64]

3. Gold carbene complexes

The first gold carbene was synthesized by Fischer in 1981 by transfer of the carbene ligand from tungsten complexes.[68] 20 years later, carbene complexes were postulated as intermediate in the gold(I)-catalyzed cyclization of enynes.[69] Since then, there was a growing interest for the isolation and characterization of such species. To stabilize such highly reactive species, either π-conjugation with heteroatoms was employed[70] or the carbene moiety was incorporated into an aromatic cycloheptatrienylidene framework (Scheme I-18).[71] With these strategies, only a little Au → $C_{carbene}$ back-donation is observed and the electron deficient carbene is stabilized by π-delocalization. Another possibility is to use bulky ancillary ligands resulting in very strong steric shielding of the gold carbenoid motif (Scheme I-18, right).[72]

Fürstner, 2014   Widenhoefer, 2014   Straub, 2014
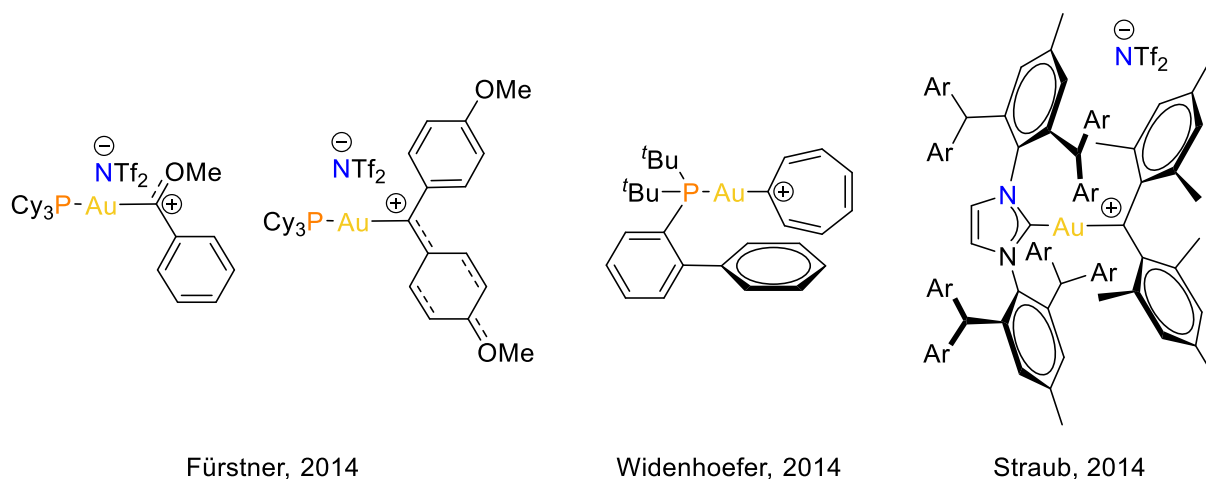
Scheme I-18: The different strategies used to stabilize highly reactive gold carbene complexes.

The first gold carbene complex stabilized by the gold fragment rather than the carbene substituents was synthesized by our group using the (P,P) ligand. As mentioned before (Figure I-1), the bent ligand impacts the frontier orbitals of gold and raises the occupied d_{xz} orbital in energy, thereby enhancing π-back-donation. The gold(I) carbene complex $[(P,P)Au(CPh_2)]^+$ was obtained by mixing $[(P,P)AuNTf_2]$ and diphenyldiazomethane at low temperature (Scheme I-19). The formation of the carbene was confirmed by the observation of a downfield signal in the ^{13}C NMR spectrum (δ 316.2 ppm).[73] The carbene center is planar and perpendicular to the $[(P,P)Au]^+$ coordination plane, which minimizes steric repulsions and enables optimal overlapping between the occupied $d_{xz}(Au)$ orbital and the vacant $2p^{\pi}(C)$ orbital at the carbene center. DFT calculations (B3PW91/SDD+f(Au), 6-31G**(other atoms)) identified this bonding interaction in the HOMO of $[(P,P)Au(CPh_2)]^+$ and an NLMO accounting for the $d_{xz}(Au) \rightarrow 2p^{\pi}(C)$ interaction was found by NBO analysis. Moreover, the absence of charge transfer from carbene to gold as well as the CDA analysis (weak d/b ratio) supported this back-donation.
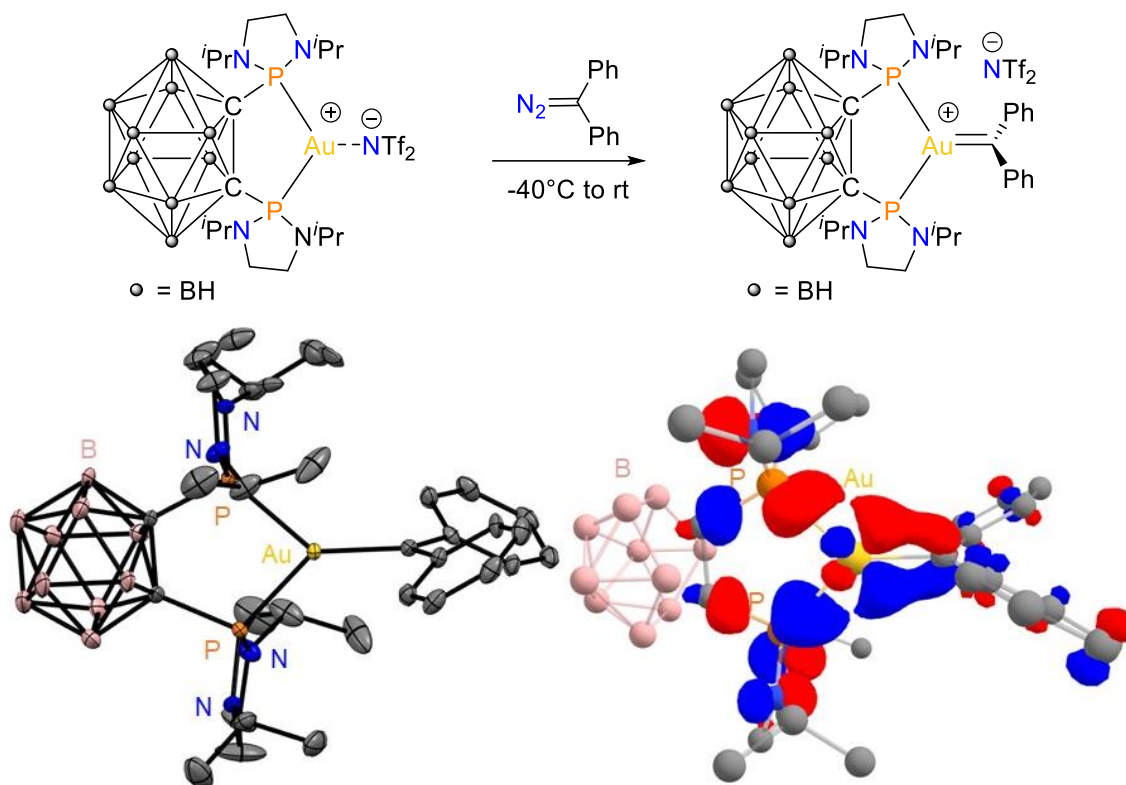
Scheme I-19: Synthesis of the (P,P) gold carbene complex, XRD structure and HOMO plot (cutoff: 0.04).

α-Oxo gold carbenes can be generated in the same way, *via* metal-catalyzed decomposition of α-diazo ketone or by an alternative strategy being the intermolecular oxidation of alkynes. For many years, all of the reactions developed relied on rapid trapping of the gold carbene either *via* facile intramolecular processes or by the reaction solvent.[74–77] To temper the high electrophilicity of α-oxo gold carbenes and permit their trapping in an intermolecular reaction, Zhang and co-workers used the hemilabile (P,N) ligand and reported the synthesis of 2,4-disubstituted oxazoles[78] and α-carboxymethyl ketones (Scheme I-20).[79] Based on DFT calculations, it was proposed that the formation of a tricoordinate gold species reduced the electrophilicity of the carbene center. However, even with this ligand, the α-oxo gold carbene complex has resisted isolation and spectroscopic characterization.
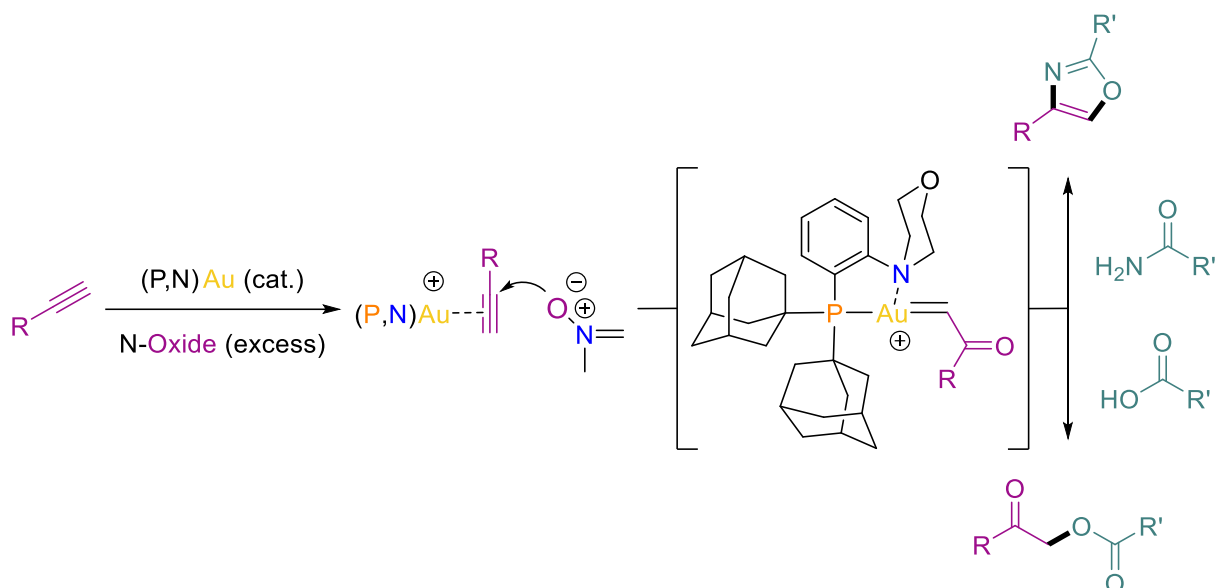
Scheme I-20: Intermolecular trapping of α-oxo gold carbene generated by intermolecular oxidation of alkyne.

The unprecedented enhanced π-back-donation at gold induced by the (P,P) ligand prompted our group to study tricoordinate α-oxo gold carbene complexes. By reacting the [(P,P)AuNTf$_2$] with an α-diazo ester, the first α-oxo gold carbene was characterized by multinuclear NMR and XRD at low temperature (Scheme I-21).[80] Characteristic data are the downfield signal observed in the ^{13}C NMR spectrum (δ 283.4 ppm) and the short Au-C bond (1.961(2) Å). As the diphenyl gold carbene, the HOMO of the complex mainly corresponds to the bonding combinations of the vacant 2p$^\pi$(C) orbital of the carbene center and the occupied d$_{xz}$ orbital at gold. The LUMO, which correspond to the antibonding interaction, is mainly developed at the C center, in line with Fischer-type carbene complex. NBO analysis indicated the push-pull nature of the α-oxo carbene with two donor-acceptor interactions: π$_{C=C}$(Ph) → 2p$^\pi$(C) and n$_C^\sigma$ → π$^*_{C=O}$ and revealed significant d$_{xz}$(Au) → 2p$^\pi$(C) back-donation (ΔE(2) = 18.2 kcal/mol), which is also apparent in the significant contribution of the 2p$^\pi$(C) orbital (12.1%) in the corresponding NLMO. This α-oxo gold carbene reacts with styrene to give the cyclopropanation product, inserts into the B-H bond of Ph$_3$P → BH$_3$ or in the O-H bond of phenol, showing that it is a mimic of the transient species.

HOMO   LUMO
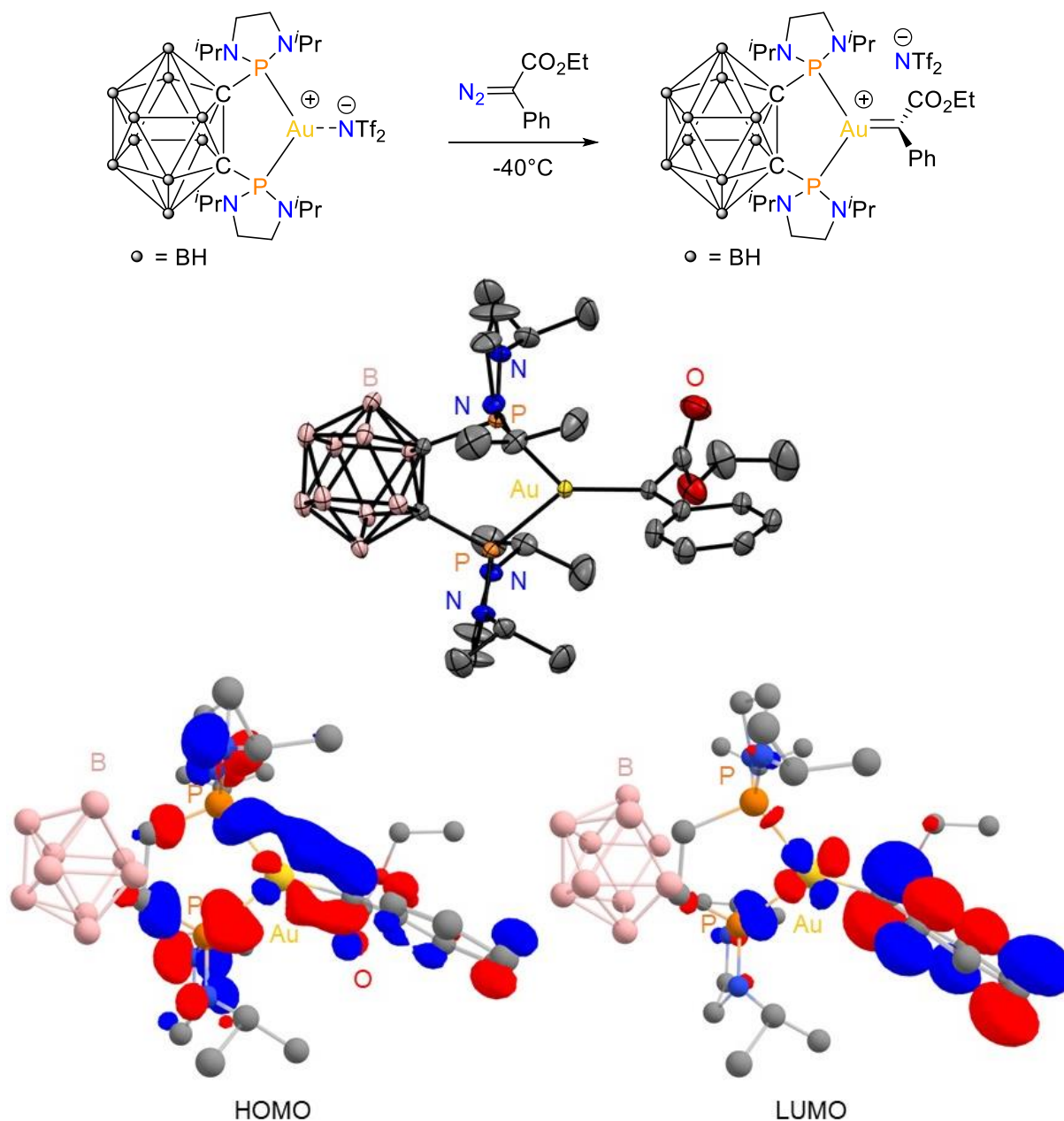
Scheme I-21: Synthesis of the (P,P) α-oxo gold carbene complex, XRD structure and HOMO and LUMO plots (cutoff: 0.04).

The influence of the ligand on the stability and reactivity of the α-oxo gold carbene was also assessed computationally.[80] Charge transfer (as estimated by the NBO charges) indicates small transfer of electron density from the $[(P,P)Au]^+$ fragment to the carbene moiety ($CT_{carbene \rightarrow gold}$ = -0.07 e) whereas a significant one is observed from the carbene to the $[(P,N)Au]^+$ fragment ($CT_{carbene \rightarrow gold}$ = 0.80 e). CDA provides a donation/back-donation (d/b) ratio of 1.76 for the (P,P) gold complex but 2.16 for the (P,N) gold one, explaining the higher stability of (P,P) α-oxo gold carbene. Moreover, the LUMO is 0.3 eV lower in energy for the (P,N) gold carbene compared to the (P,P) gold complex, explaining the higher electrophilicity of the (P,N) α-oxo gold carbene.

For gold(III), the first example of a carbene complex was also isolated thanks to the use of bidentate ligands. It was synthesized by reacting the (P,C)AuI$_2$ complex with a Ph$_2$P=S-substituted geminal dianion. The nature of the rather long Au-C$_{carbene}$ bond (2.120(3) Å) was analyzed by DFT calculations. The HOMO of the complex has π-symmetry and features the antibonding combination of the 2p$^\pi$(C) orbital of the carbene center and the d$_{xz}$ at gold, consistent with a four-electron, two-orbital interaction. This orbital being mainly developed at the C center, a nucleophilic character was predicted and confirmed experimentally showing that this new species is a Schrock-type carbene. Consistently, the (P,C) gold(III) carbene reacts with electrophiles such as phenylisothiocyanate or carbon disulfide by C=C coupling (Scheme I-22).[81]
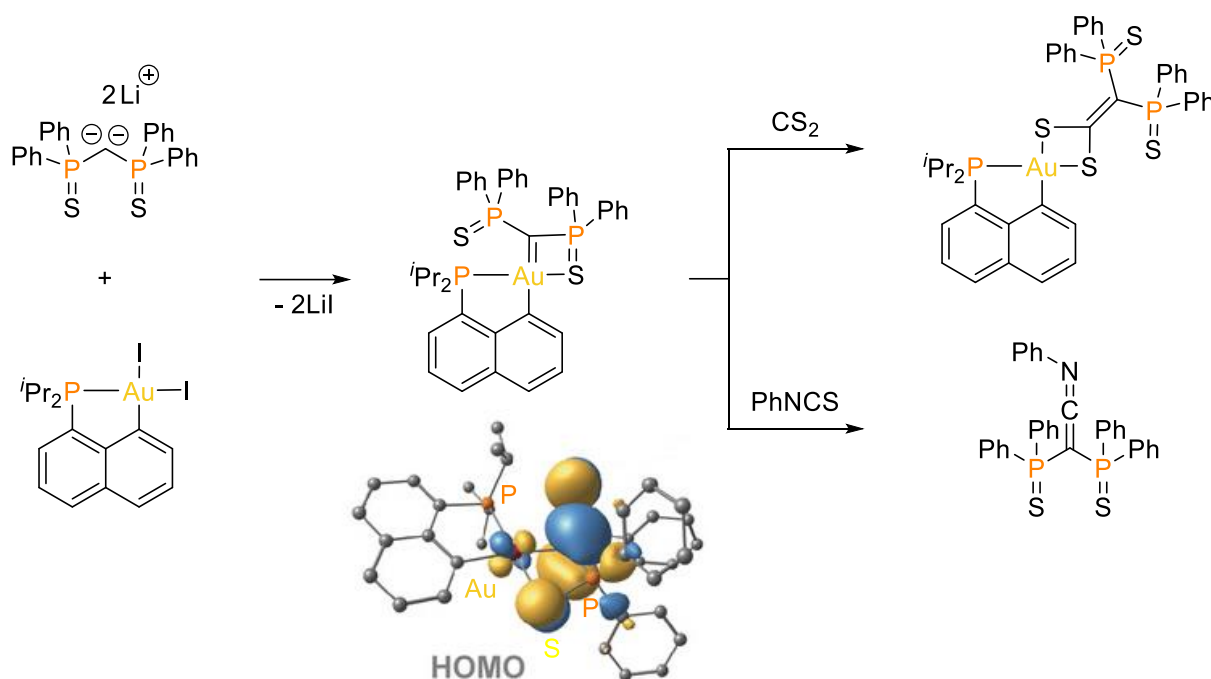
Scheme I-22: Synthesis and reactivity of (P,C)Au^{III} carbene complex.

III.　　Comparison of bidentate ligands

Thanks to the use of chelating (P,C), (N,C) or (C,C) ligands, stable well-defined gold(III) cyclometalated complexes were obtained. New reactivities of gold in this oxidation state (migratory insertion or π-activation) were substantiated and original bonding situations were observed (π-complexes, agostic interactions, hydride complexes and Schrock-type carbene).

(P,N), (P,P) and (N,N) ligands present similar behavior (they all allow oxidative addition at gold, and stabilize π-complexes), but with different characteristics. The (P,N) ligand is an hemilabile ligand with a strong P-Au bond and an N atom adapting its coordination to the electronic demand at gold. The (P,P) and (N,N) ligands are bidentate ligands that enforce gold to escape its linear coordination and the new bent geometry is symmetric.

With the (P,N) ligand, the combination of soft and hard coordination sites is ideal to cycle between Au^{I} and Au^{III} allowing to perform cross-coupling reaction in a catalytic manner, which was not achieved with the bidentate (P,P) and (N,N) ligands.

Concerning the stabilization of π-complexes, two behaviors are observed. The bent ligands (P,P) and (N,N) enhance back-donation at gold favoring the π-interaction whereas the hemilabile (P,N) ligand adapts the coordination of the N atoms with the electronic demand of the olefins. The enhanced back-donation at gold bringing by the (P,P) ligand also allows to stabilize highly reactive species like α-oxo gold carbenes (no experimental test or theoretical calculations have been reported for the (N,N) ligand). For the (P,N) ligand, these species were just postulated as intermediates in catalytic reactions involving the (P,N)AuCl complex.

Finally for a practical aspect, the (P,N) ligand is easily accessible since it is commercially available or can be prepared by C-P coupling from aniline derivatives, whereas the (N,N) ligand needs 2-3-step synthesis and the (P,P) one, 5 steps. For the structural modulation, both side of the (P,N) ligand can be modified electronically and sterically, allowing a large variety of complexes. For the (P,P) ligand, the carborane tether cannot be modified to keep the bent angle, making it unique to chelate gold, but the electronic and steric properties can be modified by playing on phosphorus substituents. For the (N,N) ligand, the electronic can be modified by adding substituents on the aryl ring and some steric hindrance can be added on the *o*-position to N. In this latter case, the modifications are more remote, so probably have less impact.

This comparison, summarized in Table I-2, has guided for the choice of ligands in our experimental work.
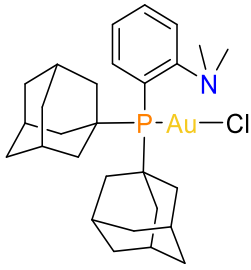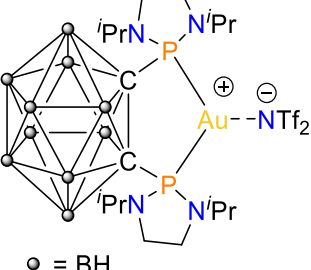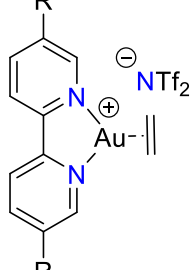
Coordination	Hemilabile	Bidentate	Bidentate
Oxidative addition	Ar-I, Ar-Br and C-C bonds	Ar-I and C-C bonds	Ar-I bonds Reversible
Coupling reactions	Catalytic	✗	Stoichiometric
Stabilization of π-complexes	Electron-rich/poor olefins	Electron-unbiased olefins	Electron-unbiased olefins
Carbene — **Isolation**	✗	✓	?[a]
Carbene — **Catalysis**	✓	✓	?[a]
Accessibility	Commercially available	5-step synthesis	2-3 step synthesis
Modulation	Steric and electronic P & N atoms	Steric and electronic P atoms	Electronic Phenyl rings (remote position)

Table I-2: Comparison between (N,N), (P,P) and (P,N) bidentate ligands. [a]No experimental test or theoretical calculations have been reported.

IV. Research objectives and thesis outline

As demonstrated in this chapter, bidentate ligands strongly impact the properties of gold in terms of bonding and chemical behavior. Taking advantage of these "tailor-made" ligands, the aim of my PhD was to extend further the reactivity of gold and to increase the variety of accessible complexes. The synthesis and characterization of original complexes and the development of new reactivities were accompanied by theoretical studies for the understanding of the electronic properties and the investigation of mechanisms.

Recently, the faculty of the hemilabile (P,N) ligand to promote oxidative addition of aryl iodides at gold has been demonstrated and was used to undertake Au^I/Au^{III} catalysis. Moreover, gold complexes are extremely powerful in activating π-bonds. Aiming at developing further Au^I/Au^{III} catalysis, we wondered about the possibility to merge oxidative addition of aryl iodides and π-activation of alkenes. In this respect, the oxy- and amino-arylation reactions of alkenes represent very nice examples of gold redox catalysis under oxidative and photoredox conditions. As reported in chapter 2, in the presence of a silver salt and a base, the MeDalPhosAuCl complex was found to efficiently catalyze these transformations and to display a complementary behavior to other gold catalysts.

The overview of all types of bonds involving gold and hydrogen atoms showed the absence of complexes presenting hydrogen bonding to gold (3-center-4-electron interaction).[64] Taking advantage of hemilabile (P,N) ligands that position a basic N atom in close proximity to the gold, the first complexes presenting hydrogen bonding to gold were synthesized. The nature of the interaction was unambiguously authenticated by NMR and IR spectroscopies and further analyzed by a computational approach as will be discussed in chapter 3.

Chelating (P,P) ligands allow to stabilize α-oxo gold carbene complexes thanks to enhanced back-donation from gold. We wondered if this ligand can also help to stabilize α-CF_3 carbene complexes that have been postulated in many metal-catalyzed reactions but never isolated. This method proved fruitful and enabled us to synthesize and characterize the first α-CF_3 gold carbene complexes. The $Au=C_{carbene}$ bonding situation was carefully analyzed computationally and its reactivity was explored in chapter 4.
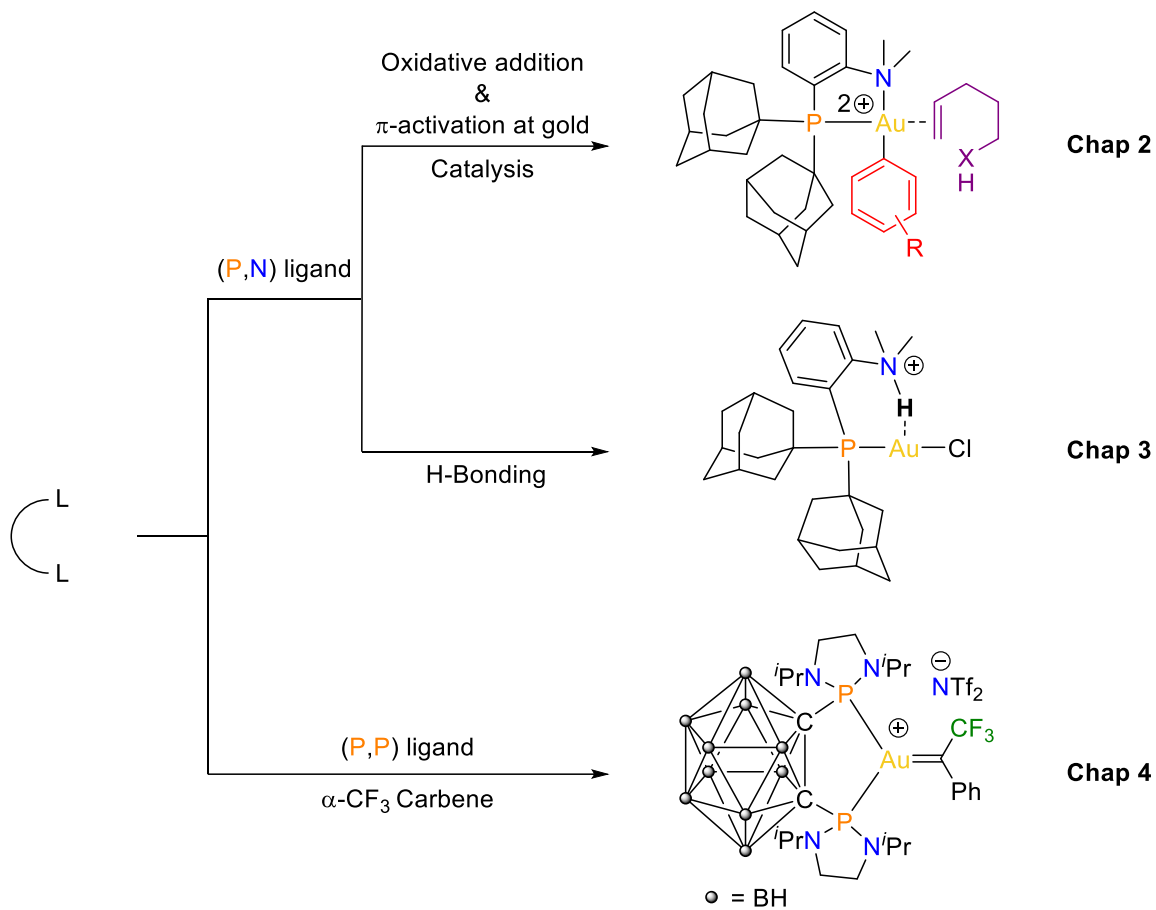
Figure I-5: Research objectives and PhD outline.

V. References

[1] G. C. Bond, *Gold Bull.* **1972**, *5*, 11–13.

[2] L.-U. Meyer, A. de Meijere, *Tetrahedron Lett.* **1976**, *17*, 497–500.

[3] Y. Fukuda, K. Utimoto, *J. Org. Chem.* **1991**, *56*, 3729–3731.

[4] R. O. C. Norman, W. J. E. Parr, C. B. Thomas, *J. Chem. Soc. Perkin 1* **1976**, 1983–1987.

[5] K. Uchimoto, Y. Fukuda, K. Utimoto, H. Nozaki, *HETEROCYCLES* **1987**, *25*, 297.

[6] Yoshihiko. Ito, Masaya. Sawamura, Tamio. Hayashi, *J. Am. Chem. Soc.* **1986**, *108*, 6405–6406.

[7] H. Schmidbaur, *Naturwiss Rundsch* **1995**, *48*, 443–451.

[8] J. H. Teles, S. Brode, M. Chabanas, *Angew. Chem. Int. Ed.* **1998**, *37*, 1415–1418.

[9] N. D. Shapiro, F. D. Toste, *Synlett* **2010**, *2010*, 675–691.

[10] A. S. K. Hashmi, *Gold Bull.* **2004**, *37*, 51–65.

[11] A. S. K. Hashmi, L. Schwarz, J.-H. Choi, T. M. Frost, *Angew. Chem. Int. Ed.* **2000**, *39*, 2285–2288.

[12] R. Dorel, A. M. Echavarren, *Chem. Rev.* **2015**, *115*, 9028–9072.

[13] C. Obradors, A. M. Echavarren, *Chem. Commun.* **2014**, *50*, 16–28.

[14] H. Schmidbaur, A. Schier, *Arab. J. Sci. Eng.* **2012**, *37*, 1187–1225.

[15] M. Joost, A. Amgoune, D. Bourissou, *Angew. Chem. Int. Ed.* **2015**, *54*, 15022–15045.

[16] R. T. Mertens, S. G. Awuah, in *Catal. Met. Complexes Nanomater. Fundam. Appl.*, American Chemical Society, **2019**, pp. 19–55.

[17] S. G. Bratsch, *J. Phys. Chem. Ref. Data* **1989**, *18*, 1–21.

[18] I. Fernández, L. P. Wolters, F. M. Bickelhaupt, *J. Comput. Chem.* **2014**, *35*, 2140–2145.

[19] P. S. D. Robinson, G. N. Khairallah, G. da Silva, H. Lioe, R. A. J. O'Hair, *Angew. Chem. Int. Ed.* **2012**, *51*, 3812–3817.

[20] M. Joost, P. Gualco, Y. Coppel, K. Miqueu, C. E. Kefalidis, L. Maron, A. Amgoune, D. Bourissou, *Angew. Chem. Int. Ed.* **2014**, *53*, 747–751.

[21] J. Guenther, S. Mallet-Ladeira, L. Estévez, K. Miqueu, A. Amgoune, D. Bourissou, *J. Am. Chem. Soc.* **2014**, *136*, 1778–1781.

[22] R. Kumar, C. Nevado, *Angew. Chem. Int. Ed.* **2017**, *56*, 1994–2015.

[23] W. Henderson, in *Adv. Organomet. Chem.* (Eds.: R. West, A.F. Hill), Academic Press, **2006**, pp. 207–265.

[24] L. Rocchigiani, M. Bochmann, *Chem. Rev.* **2021**, *121*, 8364–8451.

[25] J. Serra, T. Parella, X. Ribas, *Chem. Sci.* **2017**, *8*, 946–952.

[26] M. Joost, A. Zeineddine, L. Estévez, S. Mallet−Ladeira, K. Miqueu, A. Amgoune, D. Bourissou, *J. Am. Chem. Soc.* **2014**, *136*, 14654–14657.

[27] M. Joost, L. Estévez, K. Miqueu, A. Amgoune, D. Bourissou, *Angew. Chem. Int. Ed.* **2015**, *54*, 5236–5240.

[28] K. C. Lam, T. B. Marder, Z. Lin, *Organometallics* **2007**, *26*, 758–760.

[29] W.-J. van Zeist, F. M. Bickelhaupt, *Org. Biomol. Chem.* **2010**, *8*, 3118–3127.

[30] I. Fernández, F. M. Bickelhaupt, *Chem. Soc. Rev.* **2014**, *43*, 4953–4967.

[31] M. J. Harper, C. J. Arthur, J. Crosby, E. J. Emmett, R. L. Falconer, A. J. Fensham-Smith, P. J. Gates, T. Leman, J. E. McGrady, J. F. Bower, C. A. Russell, *J. Am. Chem. Soc.* **2018**, *140*, 4440–4445.

[32] J. A. Cadge, J. F. Bower, C. A. Russell, *Angew. Chem. Int. Ed.* **2021**, *60*, 24976–24983.

[33] J. Chu, D. Munz, R. Jazzar, M. Melaimi, G. Bertrand, *J. Am. Chem. Soc.* **2016**, *138*, 7884–7887.

[34] A. Zeineddine, L. Estévez, S. Mallet-Ladeira, K. Miqueu, A. Amgoune, D. Bourissou, *Nat. Commun.* **2017**, *8*, 565.

[35] J. Rodriguez, A. Zeineddine, E. D. S. Carrizo, K. Miqueu, N. Saffon-Merceron, A. Amgoune, D. Bourissou, *Chem. Sci.* **2019**, *10*, 7183–7192.

[36] M. S. Kharasch, H. S. Isbell, *J. Am. Chem. Soc.* **1931**, *53*, 3053–3059.

[37] L. T. Ball, G. C. Lloyd-Jones, C. A. Russell, *Science* **2012**, *337*, 1644–1648.

[38] X. C. Cambeiro, N. Ahlsten, I. Larrosa, *J. Am. Chem. Soc.* **2015**, *137*, 15636–15639.

[39] M. Hofer, A. Genoux, R. Kumar, C. Nevado, *Angew. Chem. Int. Ed.* **2017**, *56*, 1021–1025.

[40] V. Gauchot, A.-L. Lee, *Chem. Commun.* **2016**, *52*, 10163–10166.

[41] R. Cai, M. Lu, E. Y. Aguilera, Y. Xi, N. G. Akhmedov, J. L. Petersen, H. Chen, X. Shi, *Angew Chem Int Ed* **2015**, *54*, 8772–8776.

[42] V. Gauchot, D. R. Sutherland, A.-L. Lee, *Chem. Sci.* **2017**, *8*, 2885–2889.

[43] S. Witzel, J. Xie, M. Rudolph, A. S. K. Hashmi, *Adv. Synth. Catal.* **2017**, *359*, 1522–1528.

[44] J. Rodriguez, N. Adet, N. Saffon-Merceron, D. Bourissou, *Chem. Commun.* **2019**, *56*, 94–97.

[45] M. O. Akram, A. Das, I. Chakrabarty, N. T. Patil, *Org. Lett.* **2019**, *21*, 8101–8105.

[46] E. Langseth, A. Nova, E. Aa. Tråseth, F. Rise, S. Øien, R. H. Heyn, M. Tilset, *J Am Chem Soc* **2014**, *136*, 10104–10115.

[47] M. S. M. Holmsen, F. S. Ihlefeldt, S. Øien-Ødegaard, E. Langseth, Y. Wencke, R. H. Heyn, M. Tilset, *Organometallics* **2018**, *37*, 1937–1947.

[48] M. S. M. Holmsen, A. Nova, D. Balcells, E. Langseth, S. Øien-Ødegaard, R. H. Heyn, M. Tilset, G. Laurenczy, *ACS Catal.* **2017**, *7*, 5023–5034.

[49] F. Rekhroukh, R. Brousses, A. Amgoune, D. Bourissou, *Angew. Chem. Int. Ed.* **2015**, *54*, 1266–1269.

[50] F. Rekhroukh, L. Estévez, C. Bijani, K. Miqueu, A. Amgoune, D. Bourissou, *Organometallics* **2016**, *35*, 995–1001.

[51] F. Rekhroukh, L. Estévez, S. Mallet-Ladeira, K. Miqueu, A. Amgoune, D. Bourissou, *J Am Chem Soc* **2016**, *138*, 11920–11929.

[52] F. Rekhroukh, C. Blons, L. Estévez, S. Mallet-Ladeira, K. Miqueu, A. Amgoune, D. Bourissou, *Chem. Sci.* **2017**, *8*, 4539–4545.

[53] J. Serra, P. Font, E. D. S. Carrizo, S. Mallet-Ladeira, S. Massou, T. Parella, K. Miqueu, A. Amgoune, X. Ribas, D. Bourissou, *Chem. Sci.* **2018**, *9*, 3932–3940.

[54] D. Zuccaccia, L. Belpassi, F. Tarantelli, A. Macchioni, *J. Am. Chem. Soc.* **2009**, *131*, 3170–3171.

[55] M. A. Cinellu, G. Minghetti, S. Stoccoro, A. Zucca, M. Manassero, *Chem. Commun.* **2004**, 1618–1619.

[56] M. A. Cinellu, G. Minghetti, F. Cocco, S. Stoccoro, A. Zucca, M. Manassero, M. Arca, *Dalton Trans.* **2006**, 5703–5716.

[57] K. Klimovica, K. Kirschbaum, O. Daugulis, *Organometallics* **2016**, *35*, 2938–2943.

[58] Y. Yang, P. Antoni, M. Zimmer, K. Sekine, F. F. Mulks, L. Hu, L. Zhang, M. Rudolph, F. Rominger, A. S. K. Hashmi, *Angew. Chem. Int. Ed.* **2019**, *58*, 5129–5133.

[59] M. A. Cinellu, M. Arca, F. Ortu, S. Stoccoro, A. Zucca, A. Pintus, L. Maiore, *Eur. J. Inorg. Chem.* **2019**, *2019*, 4784–4795.

[60] M. Navarro, A. Toledo, M. Joost, A. Amgoune, S. Mallet-Ladeira, D. Bourissou, *Chem. Commun.* **2019**, *55*, 7974–7977.

[61] M. Navarro, A. Toledo, S. Mallet-Ladeira, E. D. S. Carrizo, K. Miqueu, D. Bourissou, *Chem. Sci.* **2020**, *11*, 2750–2758.

[62] M. Navarro, D. Bourissou, in *Adv. Organomet. Chem.* (Ed.: P.J. Pérez), Academic Press, **2021**, pp. 101–144.

[63] I. Chambrier, L. Rocchigiani, D. L. Hughes, P. M. H. Budzelaar, M. Bochmann, *Chem. – Eur. J.* **2018**, *24*, 11467–11474.

[64] H. Schmidbaur, H. G. Raubenheimer, L. Dobrzańska, *Chem. Soc. Rev.* **2013**, *43*, 345–380.

[65] L. Rocchigiani, J. Fernandez-Cestau, I. Chambrier, P. Hrobárik, M. Bochmann, *J. Am. Chem. Soc.* **2018**, *140*, 8287–8302.

[66] M. Brookhart, M. L. H. Green, G. Parkin, *Proc. Natl. Acad. Sci.* **2007**, *104*, 6908–6914.

[67] F. Rekhroukh, L. Estévez, C. Bijani, K. Miqueu, A. Amgoune, D. Bourissou, *Angew. Chem. Int. Ed.* **2016**, *55*, 3414–3418.

[68] R. Aumann, E. O. Fischer, *Chem. Ber.* **1981**, *114*, 1853–1857.

[69] C. Nieto-Oberhuber, M. P. Muñoz, E. Buñuel, C. Nevado, D. J. Cárdenas, A. M. Echavarren, *Angew. Chem. Int. Ed.* **2004**, *43*, 2402–2406.

[70]G. Seidel, A. Fürstner, *Angew. Chem. Int. Ed.* **2014**, *53*, 4807–4811.

[71]R. J. Harris, R. A. Widenhoefer, *Angew. Chem. Int. Ed.* **2014**, *53*, 9369–9371.

[72]M. W. Hussong, F. Rominger, P. Krämer, B. F. Straub, *Angew. Chem. Int. Ed.* **2014**, *53*, 9372–9375.

[73]M. Joost, L. Estévez, S. Mallet-Ladeira, K. Miqueu, A. Amgoune, D. Bourissou, *Angew. Chem. Int. Ed.* **2014**, *53*, 14512–14516.

[74]W. He, C. Li, L. Zhang, *J. Am. Chem. Soc.* **2011**, *133*, 8482–8485.

[75]P. de Frémont, E. D. Stevens, M. R. Fructos, M. M. Díaz-Requejo, P. J. Pérez, S. P. Nolan, *Chem. Commun.* **2006**, 2045–2047.

[76]M. R. Fructos, T. R. Belderrain, P. de Frémont, N. M. Scott, S. P. Nolan, M. M. Díaz-Requejo, P. J. Pérez, *Angew. Chem. Int. Ed.* **2005**, *44*, 5284–5288.

[77]W. He, L. Xie, Y. Xu, J. Xiang, L. Zhang, *Org. Biomol. Chem.* **2012**, *10*, 3168–3171.

[78]Y. Luo, K. Ji, Y. Li, L. Zhang, *J. Am. Chem. Soc.* **2012**, *134*, 17412–17415.

[79]K. Ji, Y. Zhao, L. Zhang, *Angew. Chem. Int. Ed.* **2013**, *52*, 6508–6512.

[80]A. Zeineddine, F. Rekhroukh, E. D. Sosa Carrizo, S. Mallet-Ladeira, K. Miqueu, A. Amgoune, D. Bourissou, *Angew. Chem. Int. Ed.* **2018**, *57*, 1306–1310.

[81]A. Pujol, M. Lafage, F. Rekhroukh, N. Saffon-Merceron, A. Amgoune, D. Bourissou, N. Nebra, M. Fustier-Boutignon, N. Mézailles, *Angew. Chem. Int. Ed.* **2017**, *56*, 12264–12267.

Chapter 2

Merging redox behavior and π-activation at gold: towards catalytic hetero-arylation of alkenes

I.   Gold catalysis for hetero-arylation of alkenes

Alkene 1,2-difunctionalization, the selective addition of two functional groups across a C=C double bond in a single transformation, represents a class of reactions with significant synthetic potential. It allows the construction of complex molecular frameworks from easily accessible starting materials. The oxy- and amino-carbofunctionalization of γ-hydroxy or γ-aminoalkenes represent a reliable and efficient method for the synthesis of substituted tetrahydrofurans or pyrrolidines. Palladium-catalyzed oxy-/amino-arylation reactions have gained special attention due to its ability to undergo the classical oxidative addition/migratory insertion steps. The rare *syn*-insertion of the alkene into the Pd-O bond provides tetrahydrofuran products having the two substituents in *cis*-position[1–4] (Scheme II-1, Cycle I).
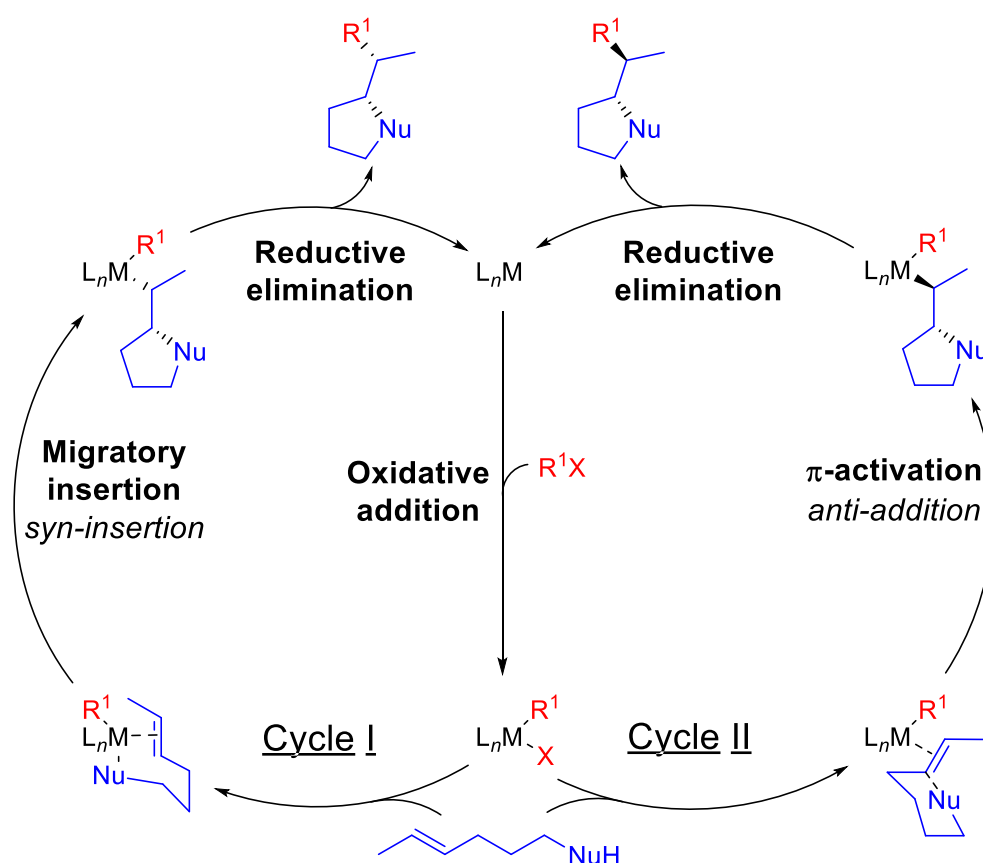
Scheme II-1: Proposed mechanisms for 1,2-difunctionalization of alkenes: cycle I corresponds to migratory insertion (inner-sphere mechanism), cycle II corresponds to π-activation (outer-sphere mechanism).

As mentioned in the introduction, gold complexes are very efficient to activate π-multiple bonds, making them catalysts of choice for selective functionalization of C=C double bonds. For gold, the multiple bond activation can proceed *via* an outer-sphere mechanism (Scheme II-1, cycle II) offering a distinct reactivity profile when compared to other transition metals and allowing to form the 1,2-difunctionalization product with the incoming groups in *anti*-position to each other.

As for the cross-coupling reaction, the inherent reluctance of gold to commute between Au^I and Au^{III} oxidation states and thus offer the desired reaction, has been overcome using strong sacrificial oxidants or a dual gold/photoredox approach as will be discussed in the following.

1. Use of external oxidant

The first example of gold-catalyzed C_{sp}^2-C_{sp}^3 coupling in an intermolecular oxidative cross-coupling manner was disclosed at the same time by Zhang[5] and Toste.[6] They developed carbo-heterofunctionalization of terminal alkenes *via* oxidative gold catalysis in the presence of aryl boronic acids and Selectfluor as strong oxidant (Scheme II-2).

A: Ph₃PAuCl (5 mol%)
Selectfluor (2 eq.)
MeCN, 60°C, 2-8h

B: dppm(AuBr)₂ (3 mol%)
Selectfluor (1.5 eq.)
MeCN, 25-40°C, 12h

ArB(OH)₂ (2 eq.)

Y = O, NTs
n= 1, 2
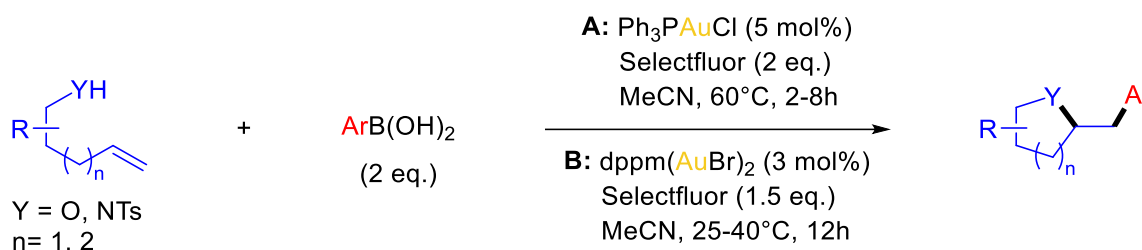
Scheme II-2: Gold-catalyzed homogeneous oxidative carbo-heterofunctionalization of alkenes (A: Zhang's conditions, B: Toste's conditions).

These conditions can be applied to a large variety of substrates. On the alkyl part, substituted 4-penten-1-ols, including secondary and tertiary alcohols are tolerated, on the nucleophilic part, alcohols, tosylamides and carboxylic acids give access to various tetrahydrofurans, pyrrolidines and γ-lactones in good to excellent yields albeit without much diastereoselectivity (1:1 dr ratios in most cases, 1.8:1 at best). However, the presence of substituents on the double bond prevents the formation of the desired product. Concerning the variety of phenyl boronic acids, the reaction is limited to weakly activated or deactivated benzene rings, with tolerance of steric hindrance. Electron-rich compounds are incompatible with Selectfluor due to competing oxidation of the boronic acid.[7]

A detailed study based on DFT calculations and experimental observations was performed by Goddard and Toste to elucidate the mechanism of the gold-catalyzed hetero-arylation.[8] First of all, they looked at the cyclization step: does it occur at Au^I or Au^{III}? No reaction was observed mixing alkenyl tosylamides and neutral phosphine gold(I) halide (equation 1, Scheme II-3). In presence of phenyl boronic acid and Selectfluor, the alkylgold(I) complex failed to produce the pyrrolidine product (equation 2, Scheme II-3). These two experiments suggest that oxidation precedes amino-auration.

Then they focus on the transmetalation step. Firstly, when mixing Ph₃PAuCl and phenyl boronic acid (equation 3, Scheme II-3), no formation of Ph₃PAuPh was detected, as judged by ^{31}P NMR spectroscopy, even after several hours or at high temperature (60°C). Secondly, in the absence of phenyl boronic acid, no reactivity was observed between preformed Ph₃PAuPh and alkenyl tosylamides in presence of Selectfluor (equation 4, Scheme II-3). Finally, addition of 4-MeC₆H₄B(OH)₂ to the previous reaction led to recovery of the reactivity with the major product being the one with the 4-MeC₆H₅ aryl coming from the boronic acid (equation 5, Scheme II-3). These three control experiments argue against a pathway involving direct transmetalation. These observations were investigated computationally:[1] transmetalation to gold(III) fluoride species exhibits high energy (> 80 kcal/mol) suggesting that this step is not operative in the catalytic cycle of hetero-arylation.
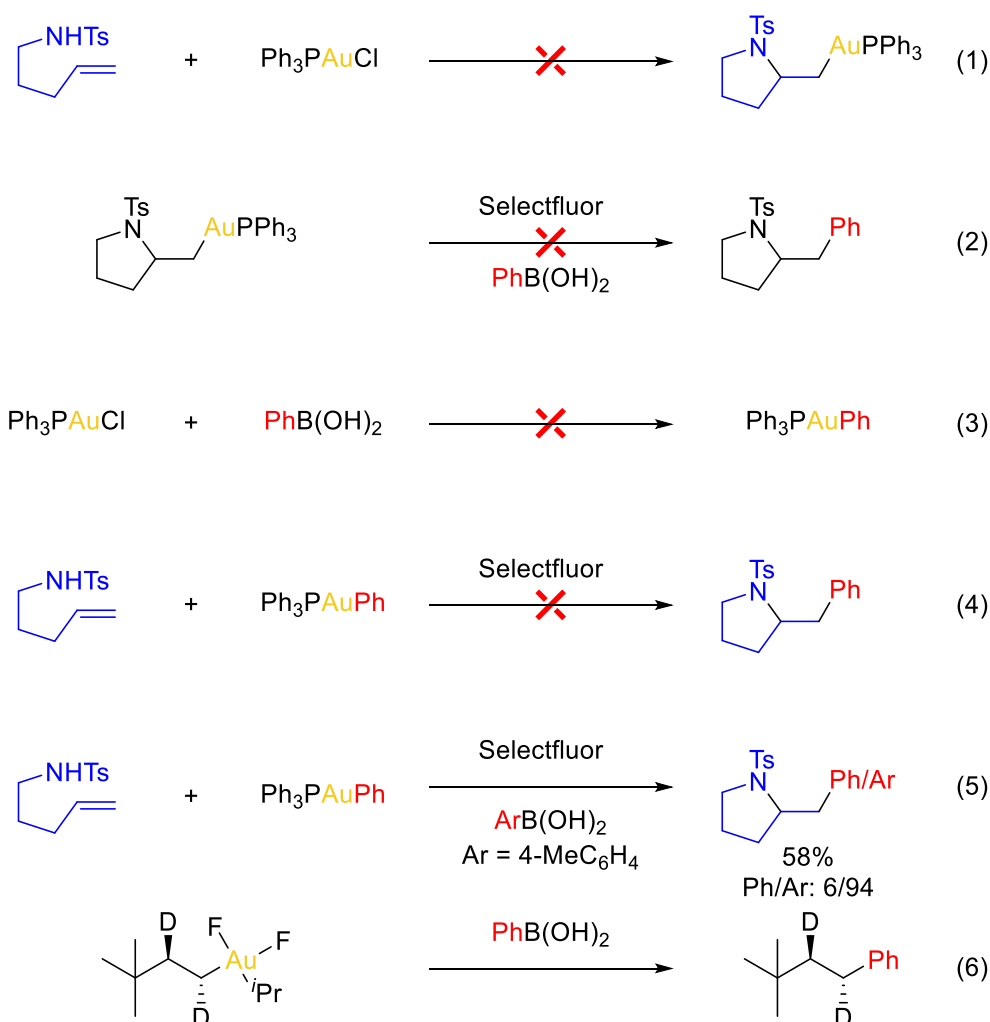
Scheme II-3: Key mechanistic clues for hetero-arylation reaction with external strong oxidant.

The absence of transmetalation implies that formation of the C-C bond by reductive elimination from phenylgold(III) is unlikely. Instead, Toste's group proposed a bimolecular

---

[1] Optimization and thermo of the reaction at M06/LACV3P**++(2f) level of theory

reductive elimination thanks to the interaction of the boronic acid with alkylgold(III) fluoride. The aryl group at boron is directly transferred and coupled to the carbon atom at gold *via* a five-centered transition state, with the fluor and boron atoms acting as tether (Scheme II-4). Concerted reductive elimination with formation of both C-C and B-F bonds effectively achieving regeneration of the catalyst and product demetallation in one step. The formation of the strong B-F bond provides the thermodynamic driving force of this step.
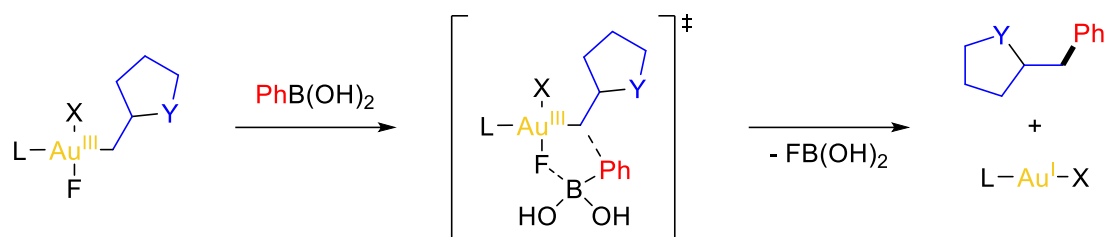
Scheme II-4: Bimolecular reductive elimination via five-centered transition state.

The reaction of alkenyl tosylamides stereoselectively labeled with deuterium at the unsubstituted end of the C=C double bond (*cis* or *trans*) revealed that the overall catalytic hetero-arylation reaction give access to the product of *anti*-addition of the nucleophile and the phenyl group to the C=C double bond (Scheme II-5). At this stage, two mechanisms can be envisioned: either *anti*-oxy-/amino-auration followed by C-C bond formation with stereochemical retention or initial *syn*-oxy-/amino-auration with inversion of the stereochemistry during the reductive elimination. To gain further insight, Toste synthesized the *neo*-hexyl-d_2 gold(III) fluoride complex and made it react with phenyl boronic acid (equation 6, Scheme II-3). The reaction proceeded with full retention of stereochemistry, confirming the *anti*-hetero-auration.
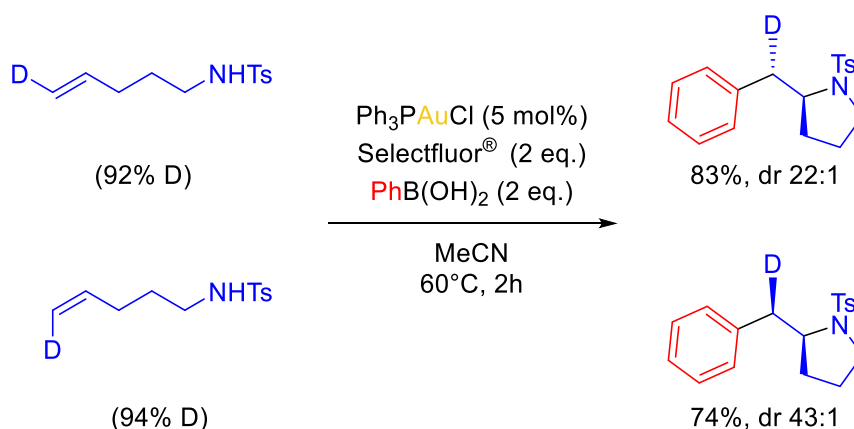
Scheme II-5: Gold-catalyzed amino-arylation of deuterated aminoalkenes in presence of Selectfluor.

In summary, the proposed mechanism for gold-catalyzed hetero-arylation reactions in presence of strong oxidant is composed of the three following steps (Scheme II-6): 1) oxidation

of gold(I) by Selectfluor 2) activation of the alkene followed by nucleophilic *anti*-addition, and 3) bimolecular reductive elimination with retention of stereochemistry.
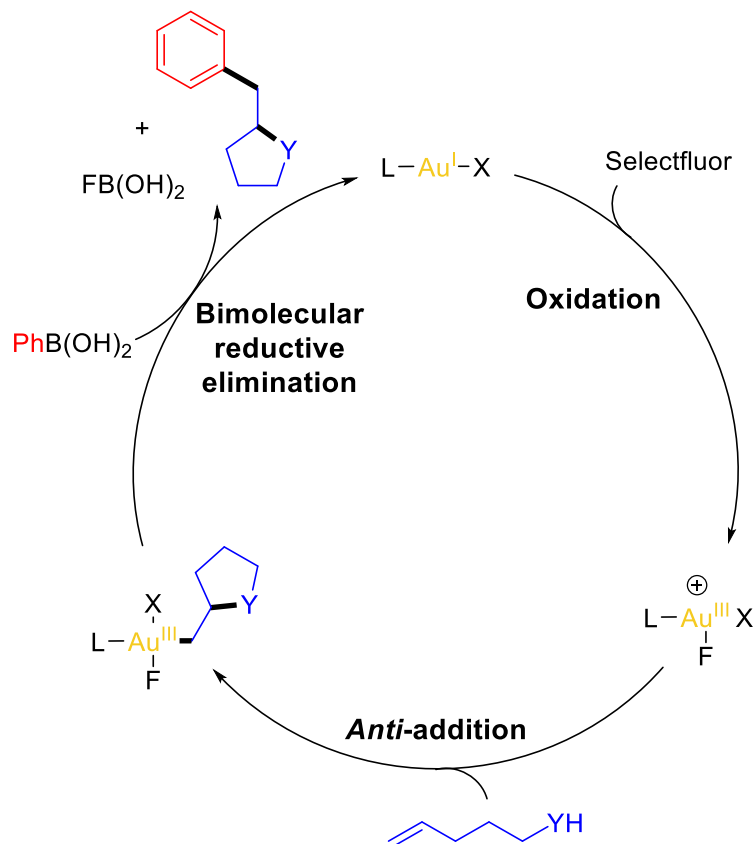
Scheme II-6: Mechanism for gold-catalyzed hetero-arylation of alkenes in presence of Selectfluor.

Toste also described the three-component gold-catalyzed oxidative oxy-arylation of alkenes with alcohols, carboxylic acids or water as nucleophiles (Scheme II-7).[9] Using water allows the formation of alcohols directly *via* hydroxy-arylation, circumventing the requirement for protective groups. The scope can be extended to arylsilane as nucleophile partner avoiding the homocoupling byproduct observed with boronic acid and allowing the use of moderately electron-rich coupling partners.[10,11]
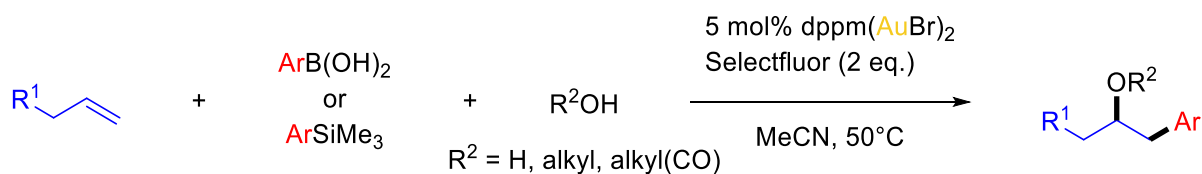
Scheme II-7 : Three-component gold-catalyzed oxy-arylation.

This Selectfluor-based methodology is limited to terminal olefins with substrates not too nucleophilic. Indeed, Selectfluor is an electrophilic fluorinating agent and direct flurorination can be competitive for styrene derivatives or *gem*-disubstituted olefins. To circumvent this issue, Russell thought to use iodine(III) as external oxidant and showed that the combination of IBA and *p*-TSA was efficient to allow the oxy-arylation of these species as well as internal olefins.[12] One drawback is the scope of *O*-nucleophiles restricted to methanol. The 1,2-difunctionalization was extended to ethylene by changing the external oxidant to IBA-OTf and worked for a broad scope of aryl silanes and alcohols (not limited to methanol in this case).[13]

2. Dual photoredox/gold catalysis

An alternative to superstoichiometric amount of sacrificial strong oxidants is the use of a dual catalysis between gold and a photoredox agent. Glorius and co-workers reported the efficiency of this strategy for the intramolecular oxy- and amino-arylation of alkenes with aryl diazonium salts[14] (Scheme II-8).
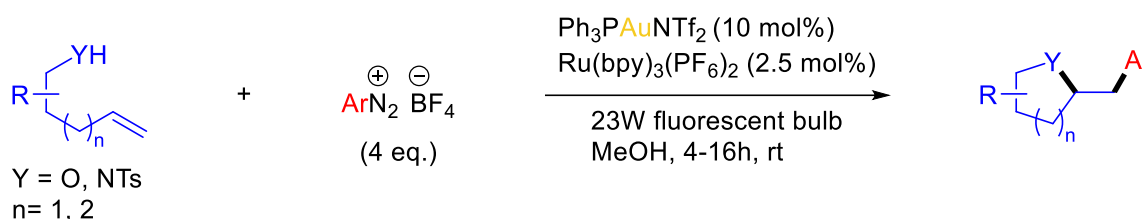
Scheme II-8: Gold-catalyzed homogeneous oxidative carbohetero-functionalization of alkenes via dual gold/photoredox catalytic system.

Aryl diazonium salts bearing an electron-withdrawing substituent were the most efficient coupling partners, electron-neutral groups were also tolerated but no reaction was described with electron-donating groups. Noteworthy, chloro or bromo aryl diazonium salts also reacted successfully, opening the way for further functionalization. The reaction tolerates all substitutions on the alkyl tether, even on the alkene itself. In contrast to the reaction with Selectfluor, internal alkenes were also suitable substrates and only the 5-*exo*-trig cyclization was detected with high diastereoselectivity (> 25:1) for the *anti*-addition product. The reaction with deuterated alkenes proceeded also in a diastereoselective manner consistent with *trans* addition across the C=C double bond (Scheme II-9).

According to this result, the following mechanism was postulated by Glorius: the cationic gold(I) catalyst initially reacts with the alkenol and promotes cyclization by outer-sphere mechanism, then the aryl radical (generated upon ruthenium-catalyzed photoredox decomposition of the diazonium salt) adds to gold and oxidation by single electron transfer

(SET) to Au^{III} occurs. The oxy-arylation product is released by reductive elimination at a 3-coordinate gold center.
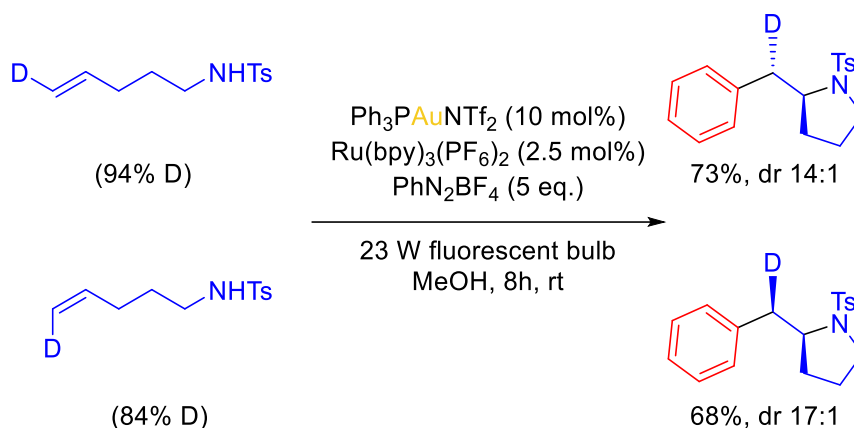
Scheme II-9: Amino-arylation of deuterated substrates under gold/photoredox dual catalysis.

In a similar gold and photoredox ruthenium-catalyzed arylative ring expansion, Toste and co-workers suggested a different mechanism:[15] the reaction begins with the radical addition and SET to generate the cationic arylgold(III) intermediate subsequently reacting with the alkene to induce the cyclization. As before, the product is released by reductive elimination.

To discriminate between these two pathways, Yu's group performed DFT calculations.[16] For the cyclization-oxidation mechanism postulated by Glorius, the energy barrier of the cyclization step is 28.5 kcal/mol, whereas, for the oxidation-cyclization one proposed by Toste, it is only 7.5 kcal/mol.[2] The difference is in accordance with the high electrophilic character of gold(III) reducing the LUMO energy of the alkene group and so facilitating the nucleophilic attack. For the most favorable mechanism, the overall pathway is achievable at room temperature with a maximum reaching for the reductive elimination step with a transition state at 16.5 kcal/mol.

Combining experimental observations and DFT calculations, the more plausible mechanism is the following one (Scheme II-10): 1) oxidation of Au^{I} to Au^{III} by radical addition of aryl and SET promoted by the ruthenium co-catalyst 2) activation of the alkene followed by nucleophilic *anti*-addition, and 3) reductive elimination at a 3-center gold(III) to release the product and regenerate the catalyst.

---

[2] Optimization performed at SMD(Methanol)-B3LYP/LanL2dz(Au, Ru)/6-31G*(other atoms) level of theory and energy calculated at SMD(Methanol)-M06/ LanL2dz(Au, Ru)/6-31G(d)(other atoms)// SMD(Methanol)-B3LYP/LanL2dz(Au, Ru)/6-31G*(other atoms) level of theory.
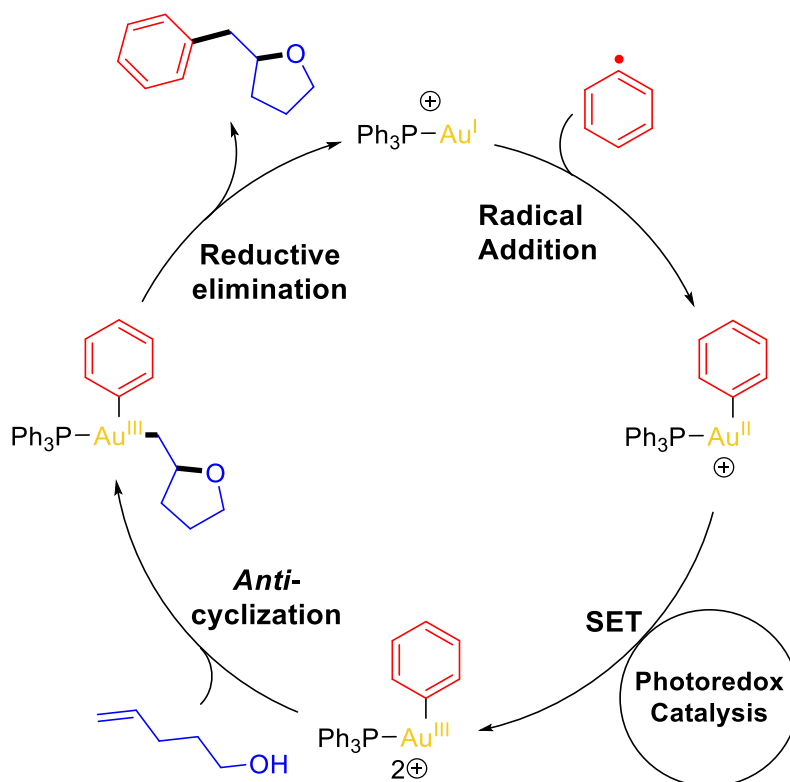
Scheme II-10: Mechanism of the visible light-mediated gold-catalyzed oxy-arylation of alkenes.

Instead of using a photoredox co-catalyst requiring strict reaction conditions (degassed solvent and inert atmosphere), a base such as Na_2CO_3 can induce diazonium decomposition under light to produce aryl radicals and promote gold(I) oxidation. This method worked well for both oxy- and amino-arylation and the scope can be extended to 7-membered ring product or carboxylic acids as nucleophile.[17]

The dual photoredox and gold catalysis strategy was applied to the trimolecular oxy-arylation reaction.[18] By mixing 1-octene and phenyl diazonium salt in the previously optimized conditions (with methanol as solvent), Glorius and co-workers were able to obtain the desired arylated ether product in 90% NMR yield. To improve the attractiveness of the process, they changed the transition metal-based photocatalyst to fluorescein, an organic dye being less expensive and less toxic, and obtained the product in a similar yield (88% NMR yield). The reaction is efficient for a selection of different terminal alkenes and aryl diazonium salt (except the electron-donating ones), but is limited to methanol as nucleophile.
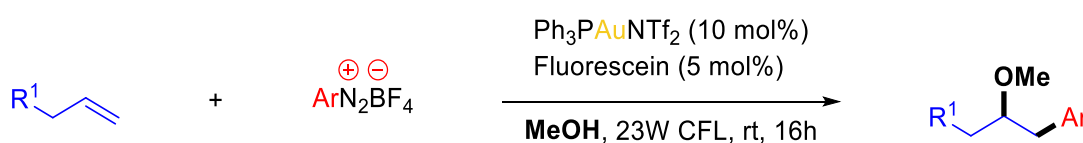
Scheme II-11: Gold/fluorescein-catalyzed three-component oxy-arylation of alkenes with aryldiazonium salts.

This overview of gold-catalyzed hetero-arylation of alkenes shows the merits and limitations of the different strategies. The oxy- and amino-arylation of alkenes can be achieved for a large scope of substrates under mild conditions (often the reaction proceed at room temperature, if heating is necessary, it doesn't exceed 70°C). Nevertheless, either the reaction required a stoichiometric amount of sacrificial oxidant or a highly reactive aryl diazonium salt. Moreover, none of the strategies is compatible with electron-donating substituents on the aryl part.

Having substantiated that oxidative addition of simple aryl halides to gold(I) occurs readily with the (MeDalPhos) ligand, we wondered about the possibility to merge this elementary step and π-activation of alkenes at gold, studying the oxy- and amino-arylation reactions. During the course of our investigations, Patil reported related work in which oxidative addition of aryl iodide and π-activation of aryl alkenes were combined to achieve the 1,2-diarylation reaction (Scheme II-12).[19]

a) 1,2-diarylation
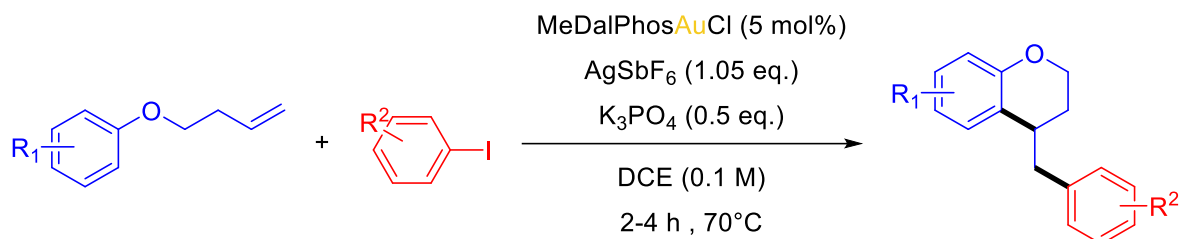
b) 1,2-oxy-/amino-arylation (this work)
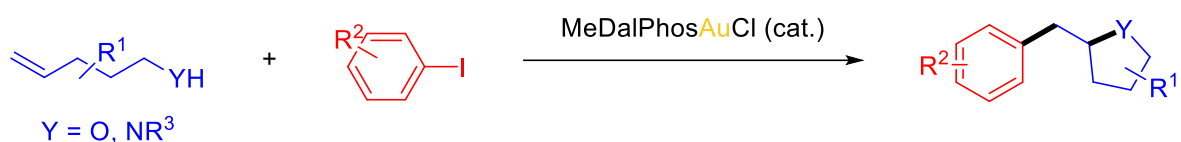
Scheme II-12: Ligand-enabled gold-catalyzed 1,2-difunctionalization of alkenes.

II. Stoichiometric reaction: feasibility of the hetero-arylation reaction and first mechanistic insight

The first question to tackle is the compatibility between the involved functional groups and the oxidative addition step. The oxidative addition of iodobenzene to (MeDalPhos)AuCl/AgSbF$_6$ is instantaneous and quantitative and give access to the aryl gold(III) complex **2** displaying a diagnostic ^{31}P{^{1}H} NMR signal at δ 74.4 ppm. In the presence of 1 equivalent of 1-octene, two signals are observed in the ^{31}P{^{1}H} NMR spectrum: a major one at δ 74.4 ppm corresponding to complex **2** while the minor one at δ 57.9 ppm is associated with the π-complex (MeDalPhos)Au(1-octene)$^+$ (Figure II-1 bottom) according to the chemical shift observed in ^{1}H NMR for the vinylic protons.[20,21] NMR monitoring reveals slow conversion of the π-complex into the oxidative addition product (90% of complex **2** after 4 days), demonstrating that alkenes slow down but do not prevent the reaction of aryl iodides (Figure II-1).
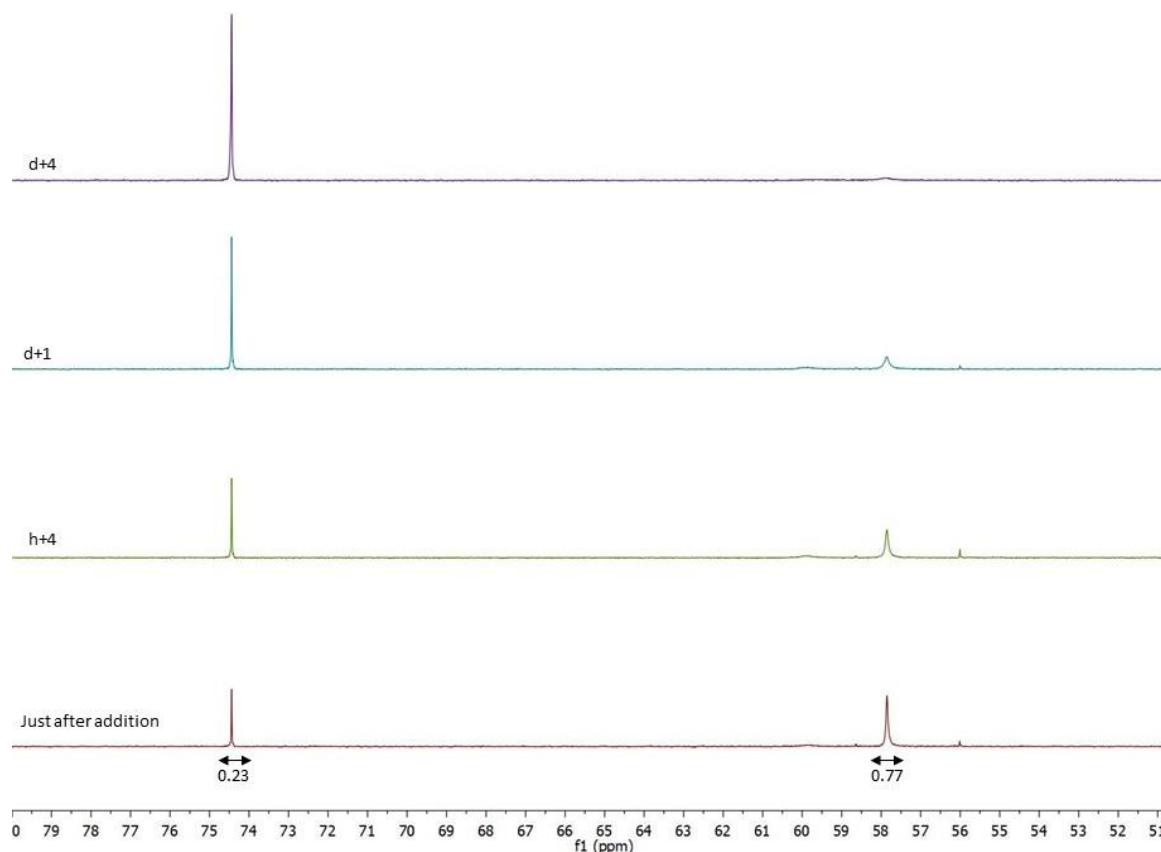
*Figure II-1: ^{31}P{^{1}H} spectra for the oxidative addition of iodobenzene to complex **1** in the presence of 1-octene. Integrals are mentioned for the first spectrum.*

The same experiment was performed with 1 equivalent of styrene and only one peak was observed at δ 57.3 ppm in the typical zone of (MeDalPhos)Au^I species without any evolution towards a gold(III) complex. Thus, styrene derivatives were not used for further reactions.

Then the feasibility of the oxidative addition in presence of nucleophiles was studied. In the presence of 1-pentanol or *N*-tosyl methylamine, iodobenzene reacts rapidly despite the formation of new (MeDalPhos)Au^I species right after mixing (at δ 59.9 ppm for 1-pentanol and δ 64.3 ppm for *N*-tosyl methylamine) and the oxidative addition is complete within 2 hours at room temperature (Figure II-2).
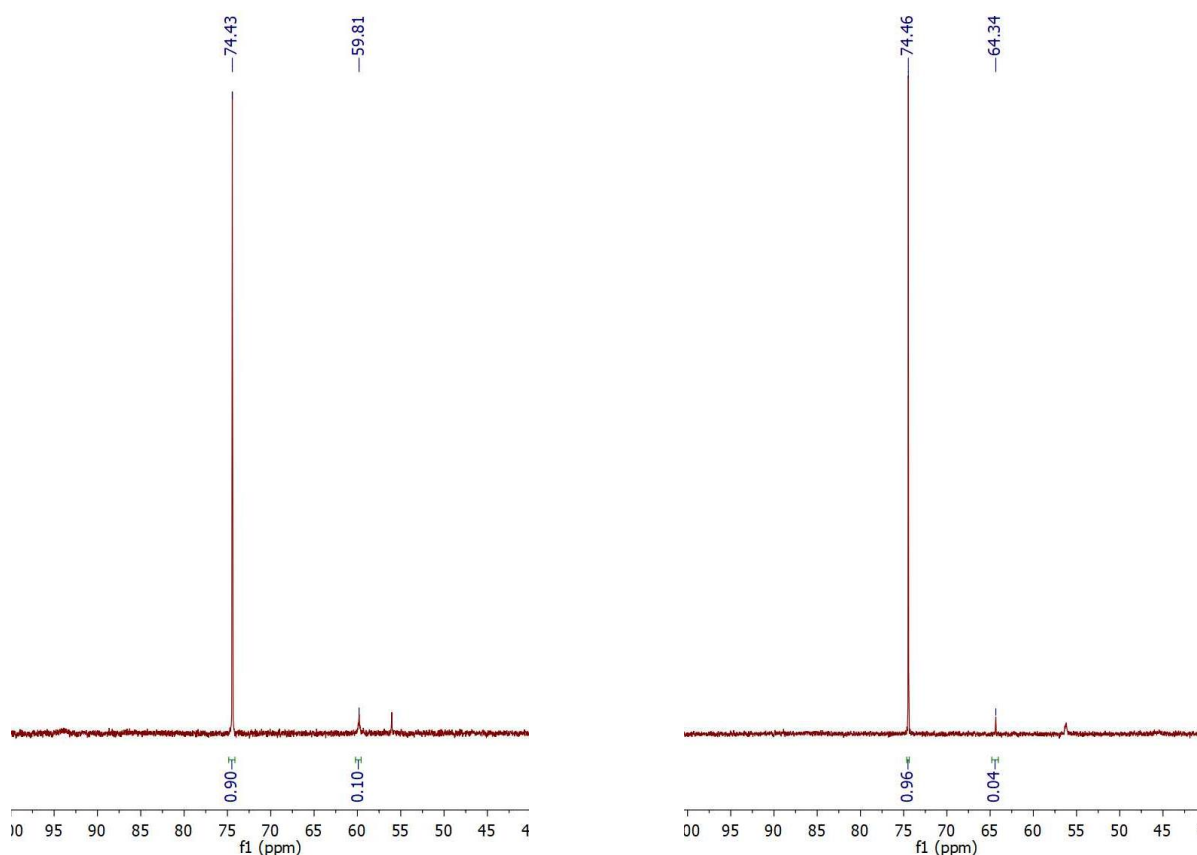
*Figure II-2: $^{31}P\{^1H\}$ spectra for the oxidative addition of iodobenzene to complex **1** in the presence of 1-pentanol (left) or N-tosyl methylamine (right).*

In the presence of allyl thiol, no oxidative addition was observed and a new peak appeared at δ 18.4 ppm characterizing gold decomposition. Therefore, thiols were not suitable substrate for hetero-arylation reactions.

Then the ability of gold complex **2** to activate C=C double bonds and promote nucleophilic addition was investigated using 4-penten-1-ol as model (Scheme II-13). The treatment of gold complex **2** with 1 equivalent of alkenol leads to the progressive formation of 2-benzyltetrahydrofuran (the oxy-arylation product) as deduced from GC-MS and ^1H NMR (87% yield after 2 days at room temperature). The monitoring of the reaction by $^{31}P\{^1H\}$ NMR showed

the quantitative disappearance of the signal of complex **2** at δ 74.4 ppm in favor of a new species at δ 45.6 ppm in the region of gold(I) complexes which was authenticated at the (MeDalPhos)H$^+$AuCl/SbF$_6^-$ and will be studied in details in chapter 3.
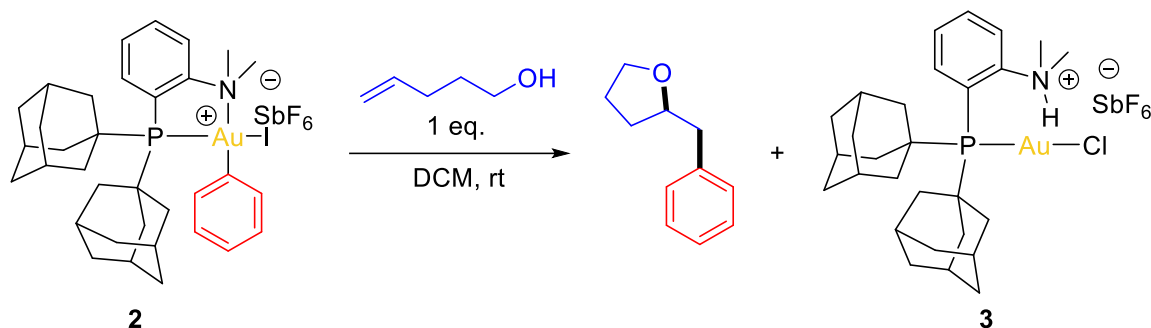
*Scheme II-13: Stoichiometric oxy-arylation upon reaction of the gold(III) complex **2** with 4-penten-1-ol.*

Encouragingly for the intended catalytic development, the reaction proceeded equally well sequentially and in one step (Scheme II-14).
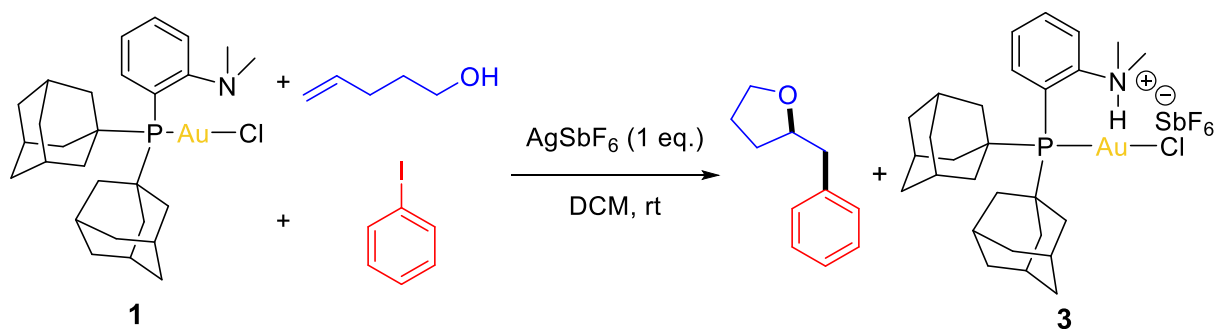
*Scheme II-14: Oxy-arylation of alkene with complex **1**/AgSbF$_6$.*

Monitoring the reaction by ^{31}P{^{1}H} NMR, the emergence and then the disappearance of the peak at δ 74.4 ppm, corresponding to the gold(III) species, was observed. This suggests the formation of the gold(III)-aryl complex **2** as an intermediate of the reaction (Figure II-3:) and supports a 2-electron redox pathway for the hetero-arylation reaction.

Of note, addition of a second equivalent of AgSbF$_6$, to abstract the iodide from **2** and generate a more electrophilic gold(III) species, afforded the desired product in 5 hours instead of 2 days.

At this stage, a screening of bases was performed in order to envision a catalytic cycle and prevent the formation of complex **3**. No reaction was observed with organic bases such as 2,6-lutine or *N, N*-diisopropylethylamine, probably due to the coordination of N to Au^I or Au^{III} complexes. The only base showing promising results for the catalytic reaction was K$_3$PO$_4$ (Cs$_2$CO$_3$ and K$_2$CO$_3$ were also tested) since the oxidative addition was observed, the desired

product was formed and complex **1** was regenerated. This result suggested that catalytic turnover may be achievable.
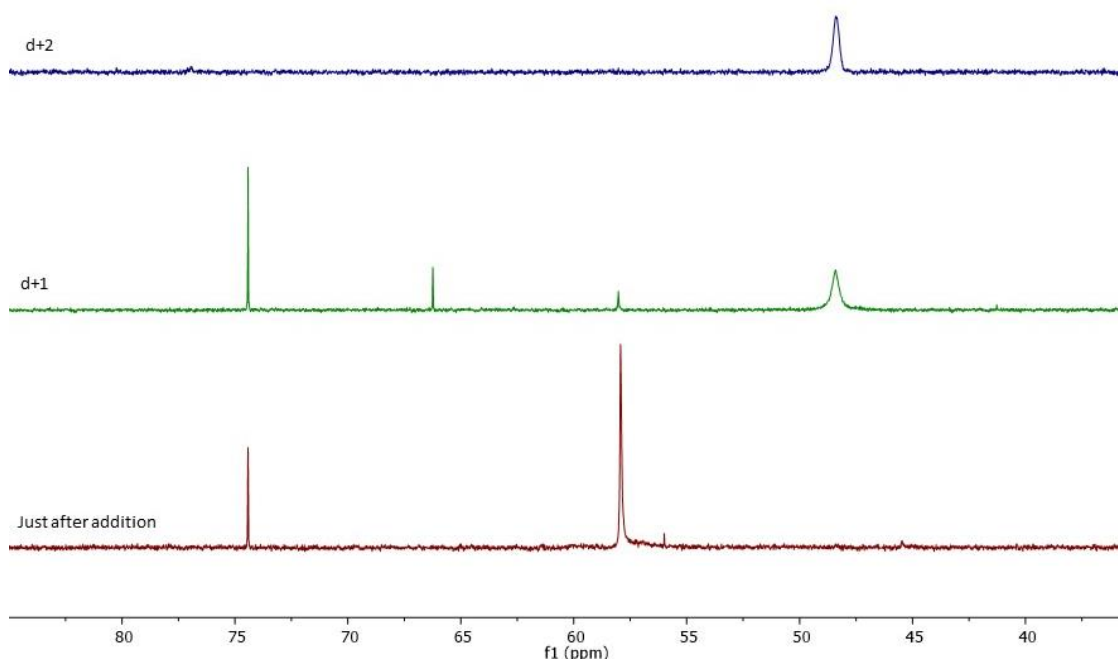
Figure II-3: $^{31}P\{^{1}H\}$ spectra monitoring the hetero-arylation reaction between iodobenzene and 4-penten-1-ol with complex 1/AgSbF$_6$.

III.   Catalytic reaction of hetero-arylation

1. Screening of conditions

The feasibility of the catalytic transformation was demonstrated using 10 mol% of the gold complex **1**, 1.1 equivalent of silver hexafluoroantimonate and 1 equivalent of K$_3$PO$_4$. In dichloromethane, the oxy-arylation product was obtained in 82% yield after 4 hours at room temperature (Table II-1, entry 1). At this point, some control experiments were set up: 1) the reaction without gold complex gave no desired product (Table II-1, entry 2) confirming the role of gold as catalyst, 2) the reaction with only 10 mol% of AgSbF$_6$ (Table II-1, entry 3) did not provide any oxy-arylation compound showing the necessity of more than 1 equivalent of halide scavenger.

Based on this promising result, the reaction parameters (solvent, additive, halide scavenger, ratio of substrates) were varied (Table II-1).

Concerning the solvent, dichloromethane or dichloroethane gave the same results (Table II-1, entry 1 and 4). Heating the reaction at 50°C in dichlorobenzene gave 63% yield of product after 2 hours (Table II-1, entry 5), without further evolution. For comparison, at room

temperature, after 2 hours, 49% of product was observed, but the reaction kept going to achieve higher yield. As expected, the reaction rate at room temperature is slower but the reaction can proceed longer and better yield can be obtained. The gold catalyst may decompose at higher temperature. Then, the influence of several additives reported to improve some gold catalyzed reactions were tested (MeOH, CHCl$_3$, DMF or DMSO), but none gave better results (Table II-1, entry 6-9). Whereas the addition of methanol was reported to enhance the reactivity of complex **1** in direct arylation of arenes,[22] it decreased the yield of the hetero-arylation reaction, probably due to a competition between the nucleophile and methanol.

An increased amount of base resulted in a lower yield (Table II-1, entry 10). Also, the ratio of the coupling partners was varied (excess of iodobenzene or 4-penten-1-ol) but showed no improvement (Table II-1, entry 11 and 12). Even a decrease is observed with an excess of 4-penten-1-ol probably due to the coordination of the alkene at gold limiting the feasibility of the reaction.

Entry	Solvent	Iodobenzene:4-penten-1-ol	Ag salt	Yield (%)[a]
1	DCM	1:1	AgSbF$_6$	82
2[b]	DCM	1:1	AgSbF$_6$	0
3[c]	DCM	1:1	AgSbF$_6$	0
4	DCE	1:1	AgSbF$_6$	80
5[d]	DCB	1:1	AgSbF$_6$	63
6	DCM/MeOH (50:1)	1:1	AgSbF$_6$	15
7	DCM/CHCl$_3$ (50:1)	1:1	AgSbF$_6$	40
8	DCM/DMF (50:1)	1:1	AgSbF$_6$	0
9	DCM/DMSO (50:1)	1:1	AgSbF$_6$	0
10[e]	DCM	1:1	AgSbF$_6$	54
11	DCM	1:5	AgSbF$_6$	31
12	DCM	5:1	AgSbF$_6$	77
13	DCM	1:1	AgOTf	11
14	DCM	1:1	AgNTf$_2$	32

*Table II-1 : Optimization of the catalytic conditions (solvent, base, halide scavenger, temperature, alkene/iodobenzene equivalents). [a]GC-MS yield after 4 h of reaction, with 10 mol% of complex **1**, 1.1 eq of halide scavenger and 0.1 M concentration in limiting substrate, using n-dodecane as internal standard. [b]Without gold complex **1**. [c]10 mol% of AgSbF$_6$. [d]Reaction performed at 50°C, GC-MS yield after 2h [e]2 eq. of K$_3$PO$_4$.*

The halide scavenger and notably the effect of the counter ion was studied (Table II-1, entry 13 and 14): OTf and NTf$_2$ coordinate more strongly to gold than SbF$_6$, slowing down the reaction by preventing the coordination of the substrates (olefin or aryl halide), and consequently decreasing the yield of the reaction.

As a conclusion, the following optimized conditions were determined: K$_3$PO$_4$ (1 eq.), DCM, 25°C, AgSbF$_6$ (1.1 eq.), 1:1 iodobenzene/4-penten-1-ol.

Then, the catalytic loading was reduced to 5 mol% of complex **1** (1.05 of AgSbF$_6$) resulting in a decrease of the yield from 82% to 57%. This issue can be circumvented by playing on the concentration (Table II-2).

Entry	Concentration in substrate (M)	Yield (%)[a]
1	0.1	57
2	0.2	75
4	0.4	80
5	0.6	60
6	0.8	40
7	1	41

Table II-2: Optimization of the catalytic conditions (concentration). [a]Yield determined by ^1H NMR using dibenzyl ether as internal standard after overnight.

Indeed, increasing the concentration to 0.4 M allowed to achieve a yield of 80%. Further increase lead to poorer yield probably due to the heterogeneous mixture because of silver salt and inorganic base.

For the scope of the reaction, the following optimized conditions were used: K$_3$PO$_4$ (1 eq.), DCM, 25°C, 1:1 iodobenzene/4-penten-1-ol, 0.4 M, AgSbF$_6$ (1.05 eq.), 5 mol% (P,N)AuCl.

2. Scope of the reaction

The results discussed in this section have been obtained in collaboration with Dr. Olivier Thillaye du Boullay.

First the scope of aryl iodides was assessed (Scheme II-15). The oxy-arylation of 4-penten-1-ol proceeds well with diverse iodobenzenes (with an average yield of 90% over 10 substrates) as well as 2-iodonaphtalene (83% yield). It tolerates electron-withdrawing groups (*p*-COCH$_3$, *p*-NO$_2$) as well as *ortho*-substituents (*o*-OCH$_3$, *o*-Ph). The reaction actually performs best with electron-rich substrates, as illustrated by the high-yield preparation (>95%) of the tetrahydrofuran products **Ig-j**. Successful incorporation of protected catechol and trihydroxyphenyl moieties (products **Ih,i**) is particularly noteworthy, these two motifs being present in a number of biologically active compounds.[23,24] Thanks to this unique ability to react with electron-rich iodobenzenes, the (P,N) gold(I) complex displays in the oxy-arylation of 4-penten-1-ol a reactivity profile complementary to that observed under photoredox and oxidative conditions, for which electron-rich substrates were found to be problematic due to competitive side-reactions. To note, no sign of *O*-arylation – a possible side-reaction previously observed with electron-poor aryl bromides under palladium catalysis[2] – was detected.
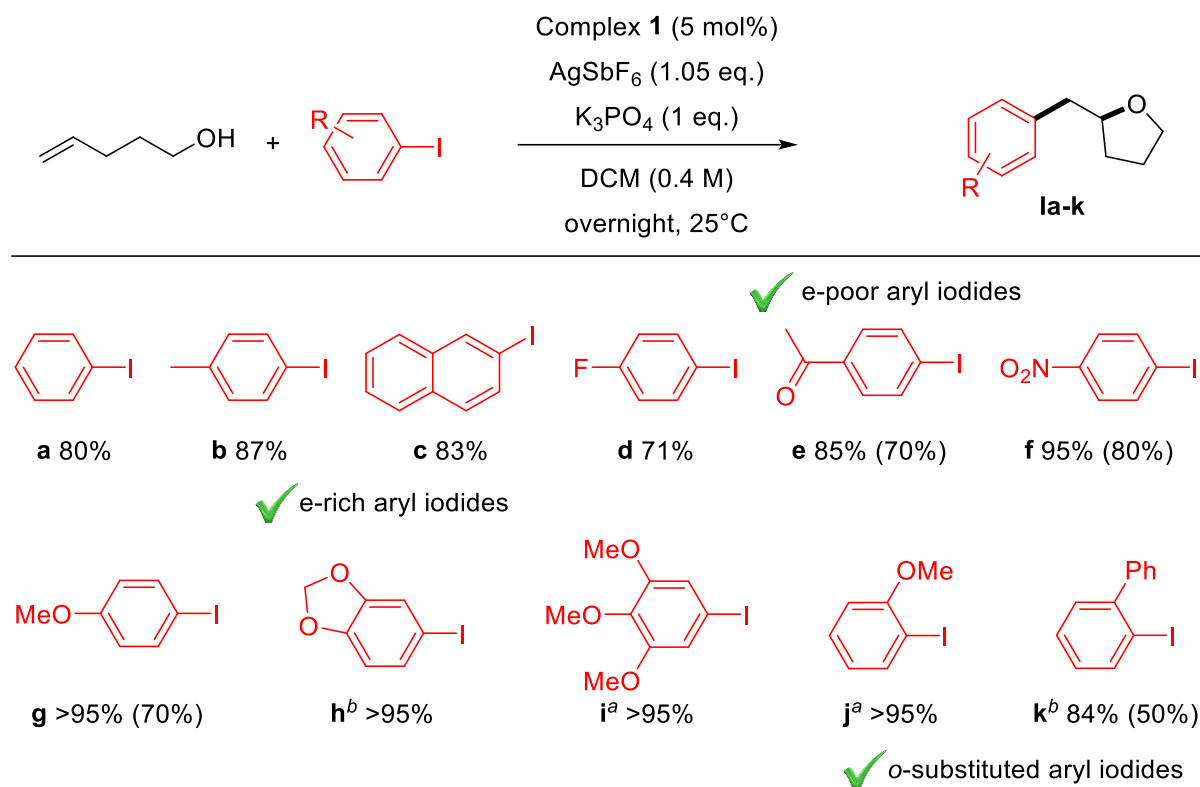
Scheme II-15: Gold-catalyzed oxy-arylation, scope of aryl iodides. Yields determined using ^1H NMR with dibenzyl ether as internal standard (isolated yields). [a]35°C. [b]35°C, 10 mol% Au.

Then the scope of alkenols was explored (Scheme II-16). The oxy-arylation tolerates aryl and alkyl substitution on all positions of the tether between the alkene and the alcohol groups (product **IIa-f**). Tetrahydrofurans fused with cyclohexane and benzene rings (products **IIg,h**) can also be readily and efficiently obtained. For the 3-substitued substrates, a good diastereoselectivity was observed (up to 6.1:1 for 2,3-disubstituted tetrahydrofuran **IIc**). This contrasts with the gold catalysis operating under photoredox or oxidative conditions (1:1 dr ratios in most cases, 2.8:1 at best).[5,14,17] The steric crowding induced at gold by the chelating (P,N) ligand may explain this high diastereoselectivity.

Double oxy-arylation of tetrafunctional substrates is possible too, giving straightforward access to spirocyclic products such as **IIi**. *Gem*-disubstituted alkenols are suitable substrates, enabling the formation of quaternary centers (product **IIj**), although it requires gentle heating (35°C) and the associated yield is lower. In all cases, the cyclization is fully regioselective and proceeds exclusively in a 5-*exo* fashion.

Remarkably, lengthening the tether to obtain more challenging > 5-membered cycles is also possible. Cyclizations proceed smoothly at 35°C with 5-hexen-1-ol as well as 6-hepten-1-ol to give the corresponding pyran and oxepane products **IIk,l** and **IIm**, respectively, in high yields.

Complex **1** (5 mol%)
AgSbF$_6$ (1.05 eq.)
K$_3$PO$_4$ (1 eq.)
DCM (0.4 M)
overnight, 25°C

IIa R = Me 80% (77%)
IIb R = Ph 87% (80%)

IIc 79% (78%)
dr 6.1:1

IId 85%
dr 1.2:1

IIe 83% (81%)
dr 1.5:1

IIf[a] 70%

IIg 95%
dr 1.7:1

IIh 95%

IIi[b] 86% (42%)

IIj[a] 50%

IIk[a] R = H >95% (66%)
IIl[a] R = Me >95% (84%)

IIm[b] 83% (50%)

IIn[b] 57%, dr >20:1

IIp[b] 64%, dr >20:1

E:Z 88:12

IIo[b] >95%, dr >20:1

IIq[b] 19%, dr >20:1
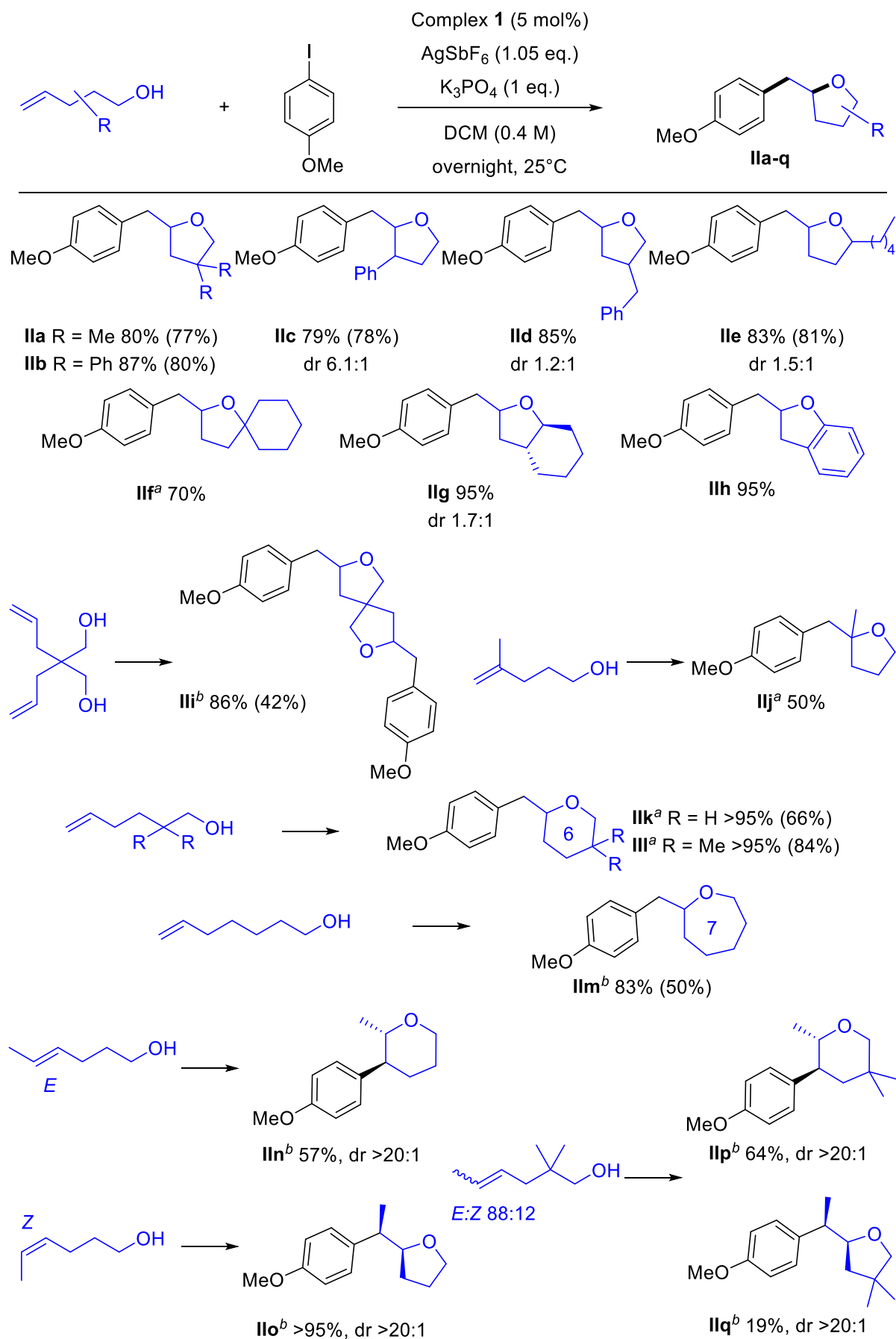
Scheme II-16: Gold-catalyzed oxy-arylation, scope of alkenols. Yields determined by ¹H NMR with dibenzyl ether as internal standard (isolated yields). [a]35°C. [b]35°C, 10 mol% Au.

Internal alkenols are also suitable substrates, as substantiated by the oxy-arylation of 4-hexen-1-ols. Both the *E* and *Z* isomers react and, in each case, a single product resulting from *trans* addition (**IIn** and **IIo**, respectively) is obtained. Most remarkable is the complete change in regioselectivity between the two isomers. The more reactive *Z* substrate undergoes the "normal" 5-*exo* cyclization, whereas the *E* substrate reacts *via* a 6-*endo* process to give a pyran ring (the structures were unequivocally attributed based on ^{1}H-^{13}C HSQC/HMBC NMR experiments and comparison with known related compounds). To assess the generality of this phenomenon, a *Z/E* mixture of *gem*-dimethyl-substituted substrates was tested. Again, the *Z* isomer was found to exclusively undergo 6-*endo* cyclization while the *E* isomer reacted *via* the classical 5-*exo* pathway, resulting in a mixture of pyran **IIp** and tetrahydrofuran **IIq**. The behavior of the (P,N) gold complex markedly contrasts with that observed by Glorius et al., combining gold and photoredox catalysis. Here, 5-*exo* cyclization occurred whatever the stereochemistry of the internal alkenol used as substrate.[14]

To the best of our knowledge, a complete switch in regioselectivity, as observed with the (P,N) gold complex is very unusual and has not been observed under Pd catalysis.[1,2,25–27] The product selectivity of gold-catalyzed transformation can be affected by many factors, notably by the substrates. Few divergent synthesis *via* substrate control has been described for gold catalysis.[28,29] Modified backbone or change of substituents on substrates, influencing the electronic and steric properties, lead to change in selectivity. Nevertheless, no divergent synthesis with variation of the stereochemistry of substrates has been described.

In order to demonstrate the robustness and synthetic practicability of the oxy-arylation, the reaction between 4-penten-1-ol and 4-iodoanisole as substrates was performed on a 5 mmol scale (instead of 0.4 mmol). In this case, the catalytic loading of gold complex was reduced to 2.5 mol% without noticeable decrease in the yield of the obtained tetrahydrofuran **Ib**. Moreover, the reaction does not require drastic precautions. It proceeds with similar efficiency operating under air, using reaction-grade solvents and reagents as received (without specific drying).

The oxidative addition/π-activation sequence proceed also well for amino-arylation reactions increasing the catalytic loading to 10 mol% and slightly raising the temperature to 35°C (Scheme II-17). Again, it tolerates electron-withdrawing (*p*-COCH$_3$ **IIIa**), neutral (H **IIIb**) and electron-rich groups (*p*-OMe **IIIc**) for which it performs best. Alkenes featuring an *N*-tosyl amine as well as *N*-tosyl amide moiety in γ-position are readily converted into the corresponding arylated-pyrrolidines **IIIc-f** and pyrrolidones **IIIg,h**: substituents are tolerated on all the positions of the tether, and strong Thorpe-Ingold effect is not needed for the cyclization

to proceed well. In addition, high diastereoselectivity (dr 10.1:1) was observed for the formation of the *trans*-2,3-disubstituted pyrrolidine **IIIe** starting from *N*-tosyl 3-phenyl hex-4-enylamine.
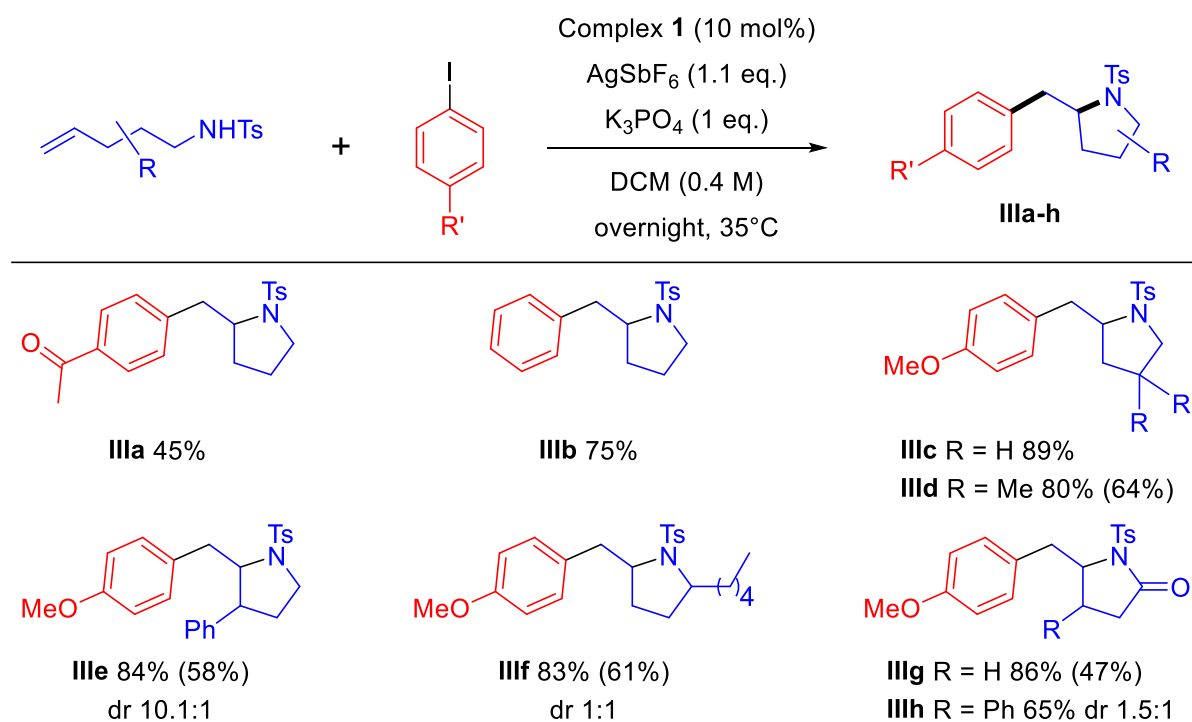
Scheme II-17: *Gold-catalyzed amino-arylation, scope of aryl iodides and aminoalkenes. Yields determined by ^1H NMR with dibenzyl ether as internal standard (isolated yields).*

To showcase the interest of the transformation, the synthesis of an analogue of anisomycin was envisioned. Anisomycin is an antibiotic known to inhibit protein synthesis in eukaryotes. Various routes have been developed to access anisomycin and analogues – the formation of the pyrrolidine ring and the introduction of the anisol group requiring multi-steps.[30] To the best of our knowledge, no reported synthesis relies on amino-arylation although it may give rapid access to the anisomycin framework from substituted γ-amino-alkenes, readily accessible from natural sugars[31,32] (Scheme II-18).

Stating from D-ribose, it was chemically transformed into **6b** by acetalization and subsequent iodination. Then, despite many attempts, no direct reductive amination to produce amine **6d** directly from **6b** was observed. Thus, **6b** was converted to alcohol **6c** *via* Boord elimination and reduction of the formed aldehyde. The direct synthesis of **6e** by classical mesylation followed by S$_N$2 substitution with tosylamides was unfortunately not completed, increasing the number of steps needed to achieve the desired substrate. The primary amine **6d** was finally obtained by Mitsunobu reaction and Gabriel synthesis. Tosylation proceeded well to obtain the desired substrate **6e**. The last step involved the amino-arylation catalyzed by gold: with 10 mol% of gold at 35°C, the product was obtained with 36% isolated yield with a moderate diastereoselectivity (1.5:1). This first result was encouraging, but further optimization

would be needed to achieve better yield and to make this strategy synthetically useful. Given the difficulties faced during the synthesis of the starting substrate and for lack of time, we decided to study only the proof of concept for the synthesis of anisomycin by gold-catalyzed amino-arylation.
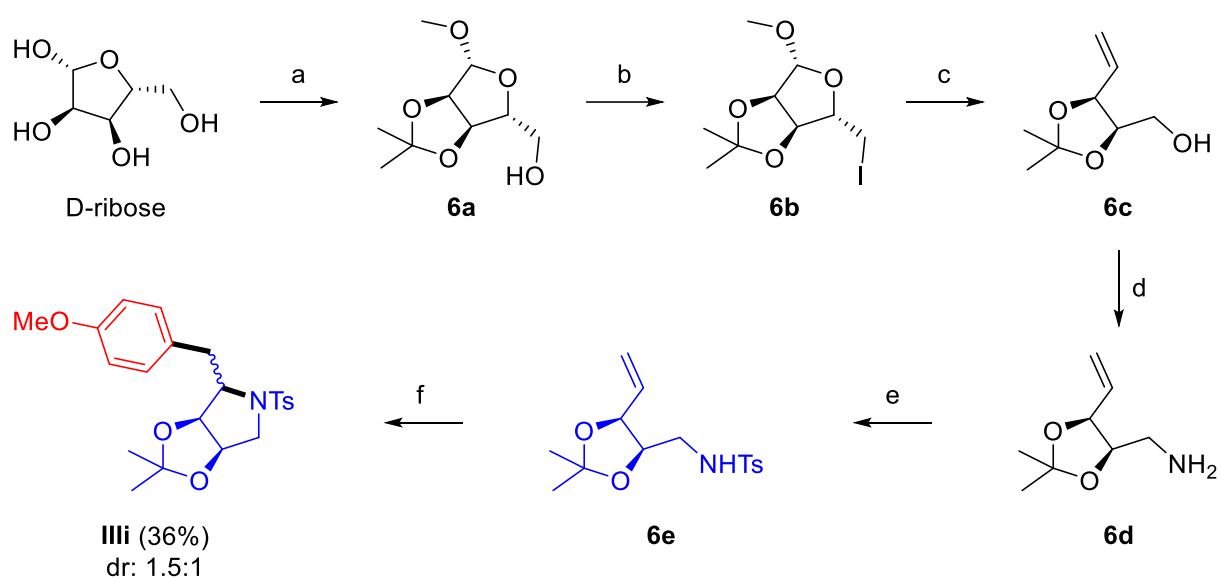
Scheme II-18 : Synthesis of anisomycin from natural sugars. Reagents and conditions: [a]H₂SO₄, MeOH/Acetone, 40°C. [b]I₂, PPh₃, Imidazole, THF. [c]1/ Zn 2/ NaBH₄, EtOH. [d]1/ PPh₃, DIAD, Phthalimide, THF 2/ NH₂NH₂.H₂O, MeOH. [e]TsCl, Et₃N, DCM. [f]gold catalyzed amino-arylation reaction.

IV.   Mechanistic study

1. Experimental observations

From a mechanistic viewpoint, several pathways are conceivable for such reactions, as mentioned for the hetero-arylation of alkenes under oxidant or photoredox conditions. With the (MeDalPhos)AuCl complex, the oxy- and amino-arylation reactions are proposed to proceed *via* Au^I/Au^{III} catalytic cycles. It should start by oxidative addition of the aryl iodide to gold, based on the faculty of the (P,N) ligand to promote this step even in the presence of alkenes, alcohols and amines.

To confirm that no cyclization occurred at gold(I) prior to the oxidative addition, a reaction between complex **1** and 4-penten-1-ol in the presence of silver hexafluoroantimonate was performed (Scheme II-19). Only the π-complex was formed as suggested by NMR and comparison with analogous (P,N) gold π-complexes.[20]

To favor the cyclization, five equivalents of a base were added on the π-complex **4**. With K₃PO₄, no change was observed, whereas with Et₃N, the olefin was released and the N coordinated to gold (according to the low field shift of the CH₂ and CH₃ signals at 3.23 and 1.46 ppm respectively), confirming that no cyclization occurred at gold(I).
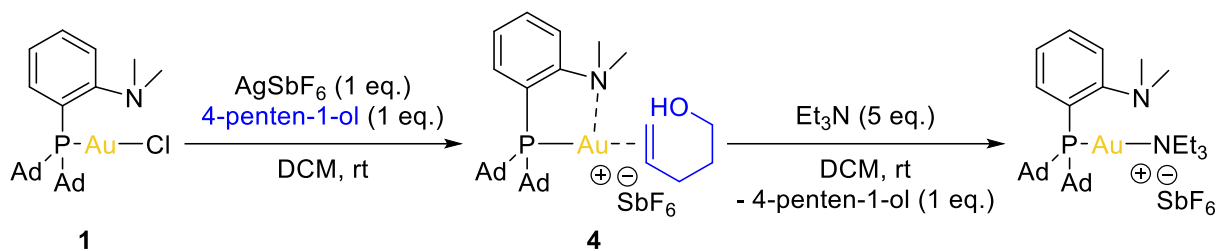
*Scheme II-19 : Control reaction between complex **1** and 4-penten-1-ol in presence of AgSbF₆.*

It is also noteworthy that exactly the same catalytic results were obtained in the oxy-arylation of 4-penten-1-ol using the MeDalPhos gold(I) complex or the corresponding gold(III) complex **2'** deriving from oxidative addition of 4-iodoanisole (Scheme II-20), going in favor of a Au^I/Au^{III} catalytic cycle.
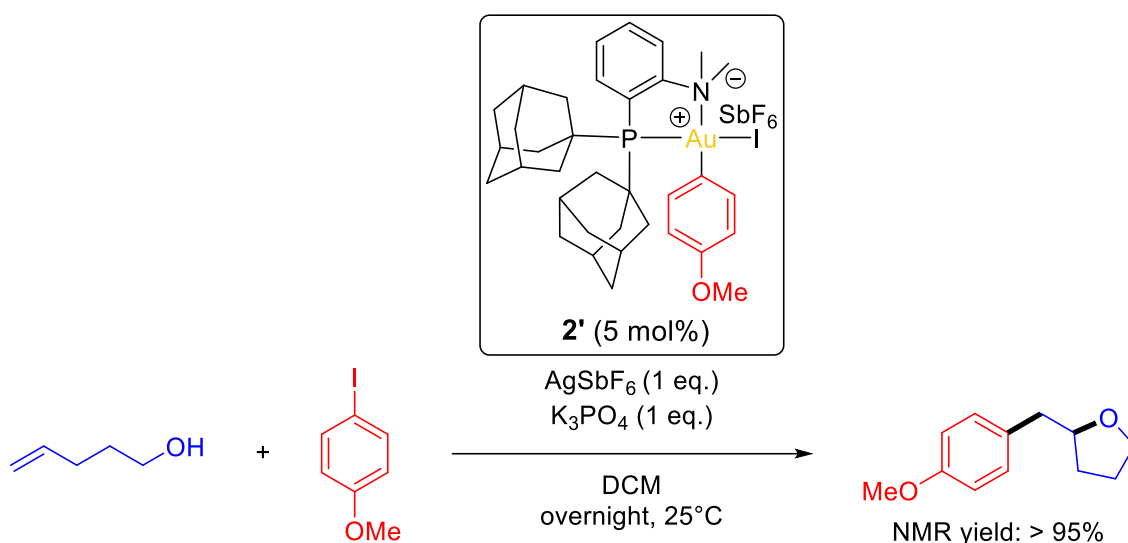
*Scheme II-20: Gold(III) complex **2'** catalyzed oxy-arylation of alkene.*

Most probably, the oxy- and amino-arylation reactions catalyzed by the (MeDalPhos)AuCl complex start by the oxidative addition of aryl iodide to gold. Then η^2-coordination of the alkene to gold(III) would promote either migratory insertion or outer-sphere attack of the O/N-nucleophile. The latest is the most consistent with the *trans* addition across the C=C double bond apparent from the stereochemistry of the tetrahydrofuran and tetrahydropyran products **IIn-q** (Scheme II-16). Reactions of D-labeled *N*-tosyl pent-4-enyl amines leading to pyrrolidines **IIIj,k** also support *trans* addition as the main route for the amino-arylation reaction. As shown in Scheme II-21, from sulfonamide (*E*)-d, no deuterium loss was detected, and moreover good diastereoselectivity was observed. Similarly, with (*Z*)-d, no deuterium loss and the other diastereoisomer was formed selectively. The relative stereochemistries were established on the basis of conformation analysis and ^{1}H-^{1}H coupling constants in comparison with Zhang's studies.[5] Of note, small amounts of the *cis* addition products were detected. The amino-arylation reaction with deuterated substrates was followed over time by ^{1}H NMR to see if some double bond isomerization occurred during the reaction,

explaining the lack of total stereoselectivity. The shift and broadening induced by π-coordination and the overlap of signals from the *Z* and *E* alkenes prevent the clear analysis of isomerization. It cannot be ruled out that some migratory insertion pathway may compete with the outer-sphere nucleophilic attack and contribute to a small extent with such substrates.

(E)-d
(98% D)

IIIj 73%, dr 4:1

(Z)-d
(97% D)

IIIk 78%, dr 4:1
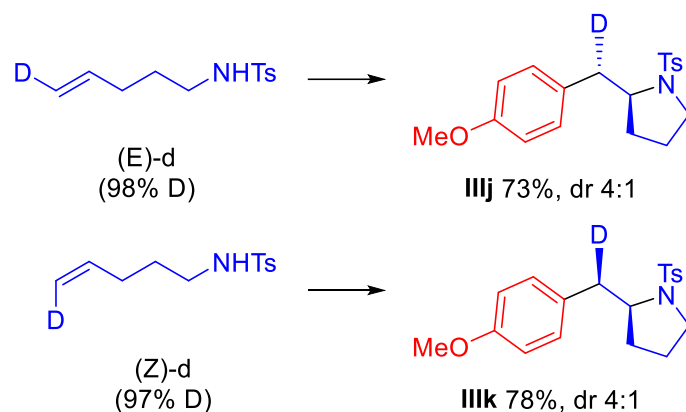
Scheme II-21 : Deuterium labelling studies for gold-catalyzed amino-arylation reaction.

As a conclusion, with the (MeDalPhos)AuCl complex, the oxy- and amino-arylation reactions are proposed to proceed *via* Au^I/Au^{III} catalytic cycles as depicted in Scheme II-22:

reductive elimination

Au(I)

π complex

oxidative addition

Au(III)

π activation

trans addition
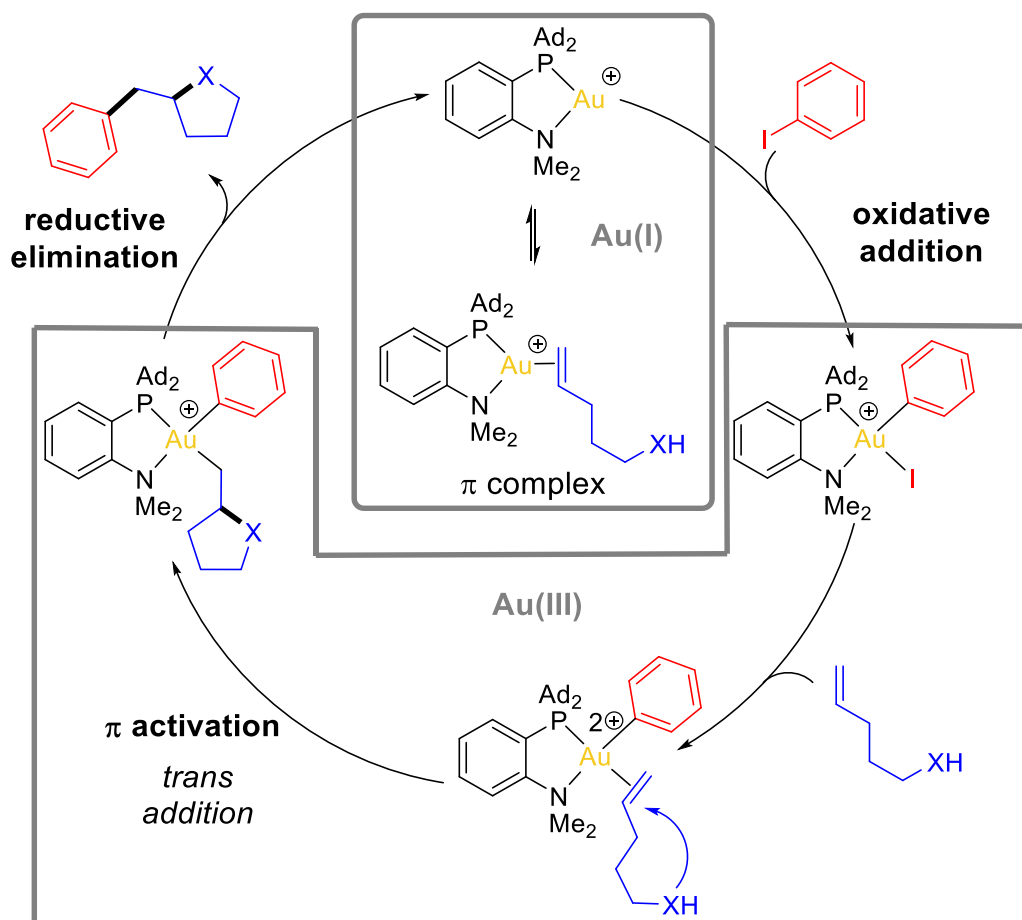
Scheme II-22 : Proposed catalytic cycle for the oxy-/amino-arylation reactions with the (MeDalPhos)AuCl complex.

The [(MeDalPhos)Au$^+$] active species is in equilibrium with the corresponding π-alkene complex. The catalytic cycle starts with the oxidative addition of the aryl iodide to gold, then η^2-coordination of the alkene to gold(III) would promote cyclization by nucleophilic addition of the pendant alcohol or amine. Finally, reductive elimination at gold would induce the C_{sp}^2-C_{sp}^3 coupling and regenerate the active species [(MeDalPhos)Au$^+$].

2. DFT calculations

The results are presented here as a draft of a mechanistic paper to be submitted soon.

The use of gold catalysis for the 1,2-difunctionalization of C-C multiple bonds has emerged as a hot research topic,[33] notably due to its complementarity compared to other transition metals in terms of chemo- and regioselectivity. Moreover, there have been numerous recent reports of the use of the (MeDalPhos)AuCl complex in transition metal-catalyzed reactions.[19,22,34–36] To better understand the mechanism and try to rationalize the rare switch of regioselectivity observed for internal *Z/E*-alkenes, I performed a computational study.

Based on the experimental mechanistic study described above, only the outer-sphere mechanism was considered theoretically. Calculations were performed at the SMD(DCM)B3PW91-D3(BJ)/SDD+f(Au), 6-31+G** (other atoms)//B3PW91/ SDD+f(Au), 6-31G** (other atoms) level of theory on the real cationic systems. Indeed, it has been previously shown that the weakly coordinating SbF_6^- counter-anion does not play a key role in the process. Its displacement by iodobenzene proceeds with a very low activation barrier and oxidative addition to gold occurs easily with an activation barrier higher than that of SbF_6^-/iodobenzene exchange ($\Delta G^{\#}$ = 11.2 kcal/mol in gas phase[22]; 10.8 kcal/mol at our level of theory). Moreover, the resulting gold(III) complex, displays a discrete ion pair structure. From this oxidative addition product, a second equivalent of $AgSbF_6$ can readily abstract iodide to give an ion pair complex $(P,N)Au^{2+}$-Ph/$2SbF_6^-$.

In this work, we theoretically explored the structure of this dicationic Au^{III} complex and its reaction with three different alkenes featuring a pendant alcohol: a terminal alkenol (4-penten-1-ol) and two internal ones (*Z/E*-4-hexen-1-ol). In addition to a detailed description of the mechanism, we aimed to address: i) does the DFT calculations support the postulated mechanism? ii) what are the key intermediates in the process (their geometrical and electronic features)? iii) how to explain and rationalize the unusual switch in regioselectivity observed for *Z/E*-internal alkenols (5-*exo vs* 6-*endo*)?

2.1 Reaction between (P,N)Au^{2+}-Ph and 4- penten-1-ol

Herein, the energy profile of the reaction between (P,N)Au^{2+}-Ph and 4-penten-1-ol was examined by DFT calculations to get more insights into the formation of the single 5-*exo* derivative. For the catalyst (P,N)Au^{2+}-Ph, two *minima* were located on the potential energy surface (PES), one with the phenyl ring *trans* to nitrogen (**2**) and another one with the phenyl ring *trans* to phosphorus (**2bis**). We found that **2** is more stable than **2bis** by 29.6 kcal/mol (Figure II-4). This result is consistent with the X-ray structures of the (P,N)Au^{III}(Ar)X complexes, where the aryl group was systematically found to be in *trans* position of the nitrogen atom. After the abstraction of the halogen, this configuration is still the favored one. Considering the high energy difference between **2** and **2bis**, only **2** was subsequently considered for the mechanistic studies.
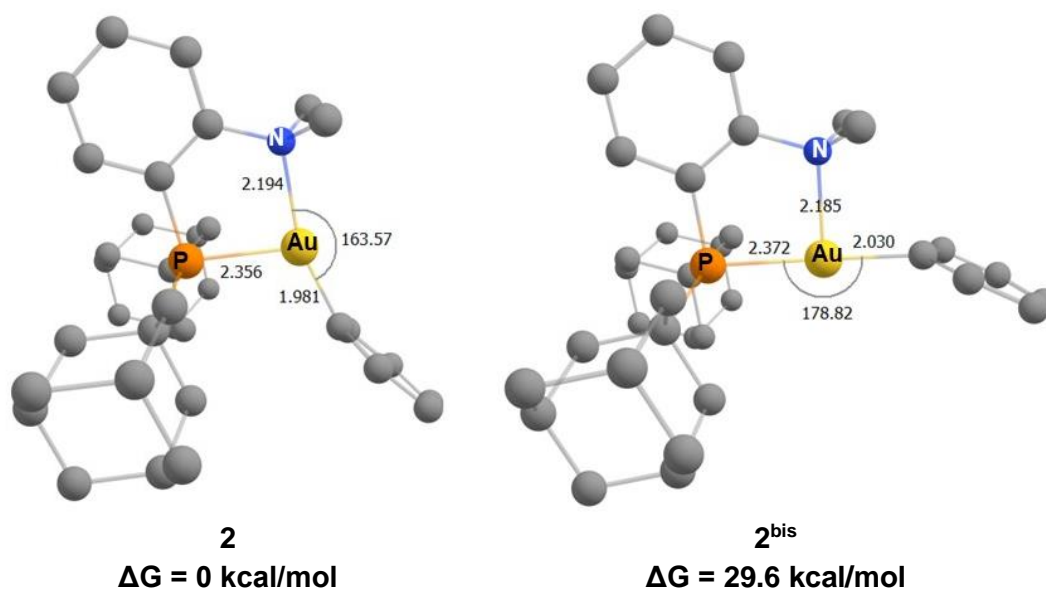
2	**2bis**
ΔG = 0 kcal/mol	**ΔG = 29.6 kcal/mol**
	This isomer has been located by imposing the PAuC$_{Ar}$ angle at 178.82°

*Figure II-4: Geometrical structures (distances in Å and bond angles in °) of the two isomers **2** and **2bis** of the (P,N)Au^{2+}-Ph complex computed at B3PW91/SDD+f(Au), 6-31G** (other atoms) level of theory. Relative stability (ΔG) in kcal/mol calculated at SMD (DCM)-B3PW91-D3(BJ)/SDD+f(Au),6-31+G**//B3PW91/SDD+f(Au), 6-31G** (other atoms) level.*

In the presence of the 4-penten-1-ol, 2 coordination modes with the gold complex **2** were identified (Figure II-5). The first isomer is the η^2-coordination of the double bond of 4-penten-1-ol to the gold fragment of **2**, *trans* to phosphorus, yielding a π-complex (**4**) *via* an interaction between the π$_{C=C}$ orbital of the alkenol and the σ*$_{AuP}$ orbital of complex **2.** This π-intermediate is slightly lower in energy than the free reactants (ΔG = -4.5 kcal/mol). Upon coordination, the Au···N bond is slightly elongated (2.267 *vs* 2.194 Å in complex **2**) but the nitrogen atom keeps interacting with the gold atom. The optimized geometry also reveals a highly asymmetric coordination of the alkenol, with an Au-C$_t$ distance 0.73 Å much shorter than

the Au-C$_i$ one (2.261 Å *vs* 2.992 Å).[3] The second isomer corresponds to the O-coordination (**4°**), where oxygen bonds to the metal center. It is lower in energy than the π-complex **4** by 5.3 kcal/mol, in agreement with the strong oxophilic character of Au^{III}. However, from the O-coordinated complex **4°**, no transition state (TS) associated to the insertion of the alkene into the Au-O bond was found on the PES. Thus, despite the competition of the two coordination modes, the π-intermediate can only be the starting point for the mechanism.

4
ΔG = 0 kcal/mol

4°
ΔG = -5.3 kcal/mol

4$_Z$

4$_E$
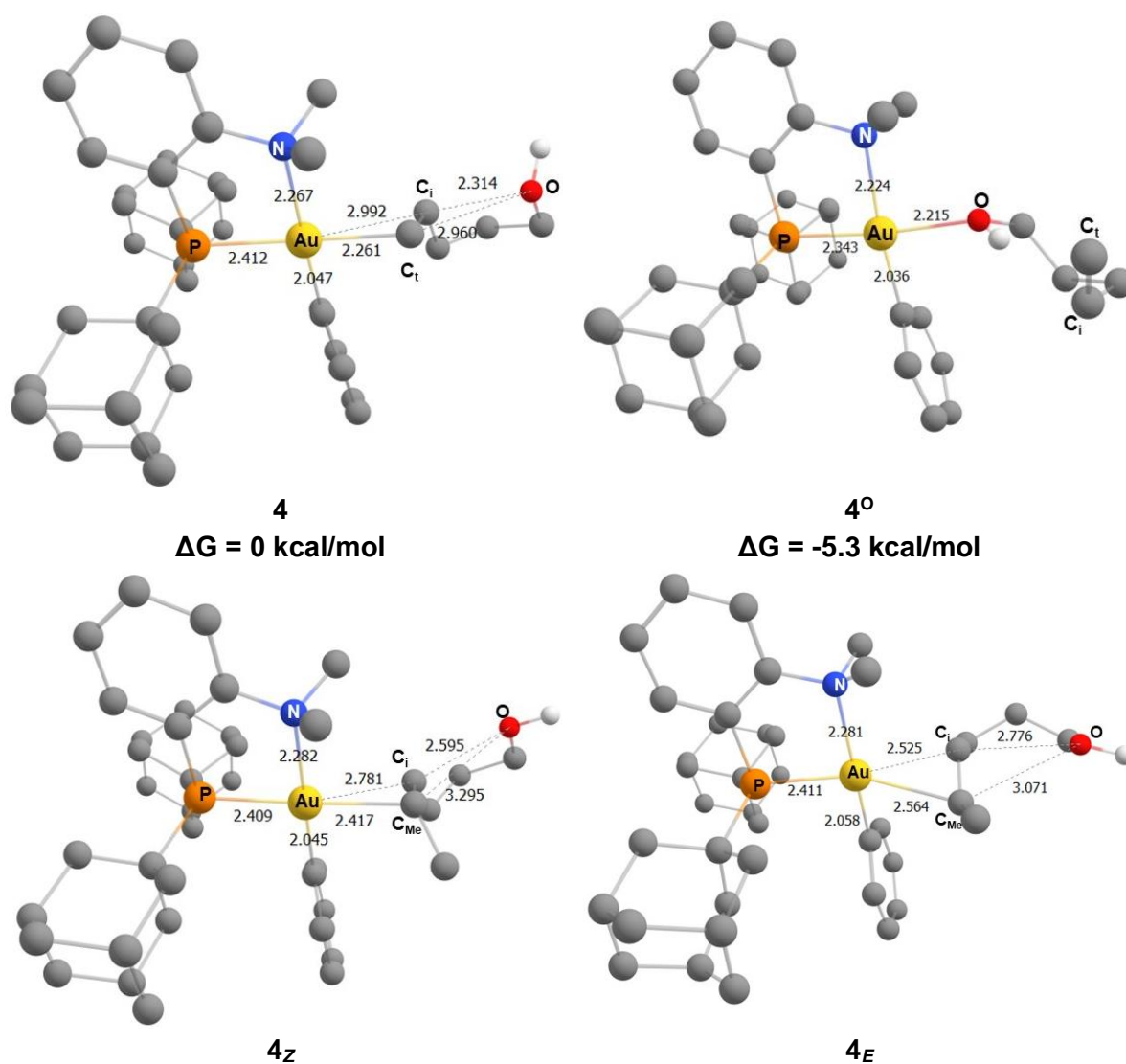
*Figure II-5: Main geometrical parameters (distances in Å) for the π-complexes **4**, **4$_Z$** and **4$_E$** associated to the oxo-phenylation cyclization with the 3 alkenols and for the O-coordination of 4-penten-1-ol (**4°**), computed at B3PW91/SDD+f(Au), 6-31G** (other atoms) level of theory. Relative stability (ΔG) for **4** and **4°** in kcal/mol calculated at SMD (DCM)-B3PW91-D3(BJ)/SDD+f(Au),6-31+G**//B3PW91/SDD+f(Au), 6-31G** (other atoms) level.*

---

[3] In the alkenol, C$_t$ and C$_i$ atoms refer respectively to terminal (CH$_2$) or internal carbon linked to the alkyl chain. This nomenclature will be subsequently adopted for the 4-hexen-1-ols, changing C$_t$ by C$_{Me}$. C$_i$ will always refer to the carbon linked to the alkyl chain.

Nucleophilic addition of the pendant alcohol can occur on the C_t atom (terminal CH_2) of the double bond or the C_i atom (internal carbon linked to the alkyl chain) through a 5 or 6-membered ring transition state (**TS1$_{OH}$**), giving respectively the O-protonated intermediates **Int$_{OH5}$** and **Int$_{OH6}$** (Figure II-6). Our DFT calculations predicted that the activation barrier for the 5-*exo* cyclization is very low (**TS1$_{OH5}$**, $\Delta G^{\#}$ = 2.7 kcal/mol) and considerably smaller than that for the 6-*endo* cyclization (**TS1$_{OH6}$**, $\Delta G^{\#}$ = 11.8 kcal/mol). As a result, the nucleophilic addition to the C_i atom proceeds easily and is clearly kinetically favored, in line with experimental observations. Closer inspection of the geometric features of **TS1$_{OH}$** also revealed some differences. Of note, the formation of the C_i-O bond is more advanced in **TS1$_{OH5}$** than that of the C_t-O bond in **TS1$_{OH6}$** (1.878 Å for **TS1$_{OH5}$** *vs* 1.639 Å for **Int$_{OH5}$** and 2.043 Å for **TS1$_{OH6}$** *vs* 1.568 Å for **Int$_{OH6}$**, see the geometrical data in Figure SII-1 & Figure SII-2, SI p.66-102). Thus, the transition state is later for the 5-*exo* (**TS1$_{OH5}$**, O-attack to C_i) than the 6-*endo* (**TS1$_{OH6}$**, O-attack to C_t) cyclization.

After the cyclization step and by considering the experimental conditions (presence of a base), we examined the abstraction of H^+ from **Int$_{OH}$** by K_3PO_4 affording the deprotonated intermediates **Int$_O$**.[37] After removal of K^+/K_2HPO_4, intermediates **Int$_{O5/6}$** are easily generated (Figure II-6). This deprotonation step is highly exergonic (ΔG = -39.0 to -40.6 kcal/mol). From **Int$_{O5}$**, the reductive elimination was then considered. An accessible activation barrier associated to the C_{sp}^2-C_{sp}^3 coupling is computed at $\Delta G^{\#}$ = 17.9 kcal/mol, affording the benzyltetrahydrofuran derivative, in line with the mild conditions (RT) under which the reaction occurs experimentally. This reductive elimination step is the rate determining step of the process. It is exergonic by 24.7 kcal/mol, leading to a π-adduct, where 2-benzyltetrahydrofuran is interacting with the gold fragment. Then, release of the product regenerates the active species. Examination of the structure of the corresponding 3-center transition state **TS2$_{O5}$** indicates a concerted cleavage of Au-C_{Ar} and Au-C_t bonds, with two slightly dissymmetric Au···C distances at 2.109 and 2.304 Å respectively, formation of C_{Ar}-C_t bond (2.043 Å) and an acute CAuC bond angle at 56.03°. The Au···N distance increases to 2.618 Å (compared to 2.279 Å in **Int$_{O5}$**), which somewhat reduces the coordination number at gold and thereby facilitates the reductive elimination, as previously demonstrated with simple phosphine ligands.[38,39] The transition state **TS2$_{O6}$**, computed from **Int$_{O6}$**, was found higher in energy than **TS2$_{O5}$** by 7 kcal/mol. However, starting from the intermediates **Int$_{O5/6}$**, the activation barriers for the two C_{sp}^2-C_{sp}^3 couplings are quite similar. The energy barrier is 17.9 kcal/mol for **TS2$_{O5}$** and 17.2 kcal/mol for **TS2$_{O6}$**, which clearly indicates that the reductive elimination step is irrelevant for the regioselectivity of the reaction. Overall, the formation of the 2-benzyltetrahydrofuran is strongly exergonic (ΔG = -68.0 kcal/mol). It is more stable than the 6-membered product, 3-phenylpyrane, by 2.0 kcal/mol. To note, K_3PO_4 facilitates the reductive elimination step through

the formation of a non-protonated intermediate **Int$_O$**. Indeed, reductive elimination from **Int$_{OH}$** was found more demanding energetically (Figure SII-4, SI p.104, ΔG$^\#$ = 25.8-32.4 kcal/mol).

*Figure II-6: Energy profiles (ΔG in kcal/mol) for the oxy-arylation reaction involving (P,N)Au^{2+}-Ph gold complex **2** and 4-penten-1-ol computed at SMD(DCM)-B3PW91-D3(BJ)/SDD+f(Au), 6-31+G**(other atoms)//B3PW91/SDD+f(Au), 6-31G** (other atoms) level of theory and in the presence of K$_3$PO$_4$. Formation of 5-exo (black) and 6-endo (blue) products. The K$_3$PO$_4$, K$_2$HPO$_4$ and K$^+$ molecules are included in order to ensure the correct energetic balance in all the reaction steps.*

Thus, DFT calculations support the postulated mechanism and rationalize the unique formation of the 5-*exo* cyclization product upon reaction of (P,N)Au^{2+}-Ph **2** with 4-penten-1-ol. On the basis of these calculations, it can be proposed that the reaction of 4-penten-1-ol with (P,N)Au^{2+}-Ph (**2**) proceeds preferentially through the 3 following steps: *i*) formation of a π-complex (**4**) resulting from coordination of the alkenol to gold, *ii*) nucleophilic addition of the alcohol to the C$_i$ atom (5-*exo* cyclization) of the double bond of **4** and formation of the dicationic intermediate **Int$_{OH5}$** which is easily deprotonated by K$_3$PO$_4$ to afford **Int$_{O5}$** and *iii*) C$_{sp}^2$-C$_{sp}^3$ reductive elimination, affording the benzyltetrahydrofuran (5-*exo* derivative, **P$_{O5}$**). By comparing the energy profiles, the regioselective discriminating step of the process turns to be

the cyclization. The 5-*exo* cyclization proceeds with a very low activation barrier (2.7 kcal/mol), smaller than the one for 6-*endo* cyclization (11.8 kcal/mol), in nice agreement with the preferential formation of the 5-*exo* derivative. Then, it is assumed that the rate determining step of the process, the reductive elimination, proceeds from the deprotonated intermediate **Int$_{O5}$** with an accessible activation barrier ($\Delta G^{\#} < 20$ kcal/mol) under the classical experimental conditions. All these data highlight that the mechanistic details associated to the intramolecular cyclization step seem to be correlated to the regioselectivity.

2.2 Reaction between (P,N)Au^{2+}-Ph and internal alkenols

In the experiments, it was shown that internal alkenols also undergo the oxy-arylation reaction and a very unusual switch in regioselectivity was observed. Both the *E* and *Z* isomers of 4-hexen-1-ol react and a single product resulting from *trans* addition was obtained in each case. The *Z* substrate undergoes 5-*exo* cyclization to produce the tetrahydrofuran derivative, whereas the *E* substrate reacts *via* a 6-*endo* process to give a pyran ring (Scheme II-16). From DFT calculations, a particular attention was gained analyzing the key differences between the energy profiles in order to understand this switch in regioselectivity.

First, we explored the mechanism involving the *Z*-substrate, where only the 5-*exo* product is obtained. The energy profile is depicted in Figure II-7. The reaction is proposed to take place in a similar way to that previously described for 4-penten-1-ol. The oxy-arylation reaction involves a common π-intermediate **4$_Z$** for the two intramolecular attacks of the hydroxy group on C$_{Me}$ or C$_i$ atoms. The optimized geometry of **4$_Z$** indicates that the *Z*-4-hexen-1-ol is coordinated to gold more symmetrically than the 4-penten-1-ol, with an Au-C$_{Me}$ distance only 0.364 Å shorter than the Au-C$_i$ one (2.417 Å *vs* 2.781 Å, Figure II-5). The π-coordination is also exergonic ($\Delta G = -5.3$ kcal/mol) and slightly more favored than that of the terminal alkenol. Substitution of the double bond in the terminal position by a methyl group modifies the activation barrier of the cyclization step but this latter always proceeds with a low barrier ($\Delta G^{\#} < 10$ kcal/mol). The barrier of the 5-*exo* process is the most affected by this substitution. It increases by 4.3 kcal/mol compared to that of 4-penten-1-ol ($\Delta G^{\#} = 7.0$ kcal/mol *vs* 2.7 kcal/mol for terminal alkene) and becomes close to that of the 6-*endo* cyclization ($\Delta G^{\#} = 9.0$ kcal/mol). However, the transition state **TS1$_{OH5Z}$** remains lower in energy than **TS1$_{OH6Z}$** but the difference is only 2.0 kcal/mol instead of 9.1 kcal/mol, as computed for 4-penten-1-ol. A closer look at the geometrical features of the transition states associated to the 5-*exo* cyclization for the two alkenols reveals the shortest C···O bond for the TS involving the *Z*-internal alkenol (1.852 Å *vs* 1.878 Å) and a more important shortening of the Au-C$_{t/Me}$ bond compared to the associated π-complex, respectively **4$_Z$** and **4** (Δ(Au-C) = 0.201 *vs* 0.072 Å), indicating a later TS for the *Z*-4-hexen-1-ol. Once again, the two intermediates **Int$_{OHZ}$** are easily deprotonated by K$_3$PO$_4$ to give

Int$_{OZ}$ in a strongly exergonic transformation (ΔG = -36.9 and -38.8 kcal/mol). The reductive elimination step is minimally affected by the presence of a methyl substituent. The computed activation barriers (ΔG$^#$ = 15.2 and 16.3 kcal/mol, respectively from **Int$_{O5Z}$** and **Int$_{O6Z}$**), are slightly lower than those previously described for the terminal alkene (ΔΔG$^#$ = 2.7 and 0.9 kcal/mol from respectively **Int$_{O5Z}$** and **Int$_{O6Z}$**) and differ from quasi the same amount (1.1 kcal/mol for the *Z* alkene and 0.9 kcal/mol for the terminal one). This step is calculated to be exergonic by 29.2-30.5 kcal/mol.

According to our computational study and in line with experimental data, the formation of the 5-*exo* derivative is kinetically privileged. This favorable pathway involves the lowest activation barriers for both the cyclization and the reductive elimination steps (ΔG$^#$ = 7.0 and 15.2 kcal/mol respectively *vs* 9.0 and 16.3 kcal/mol for the 6-*endo* reaction).
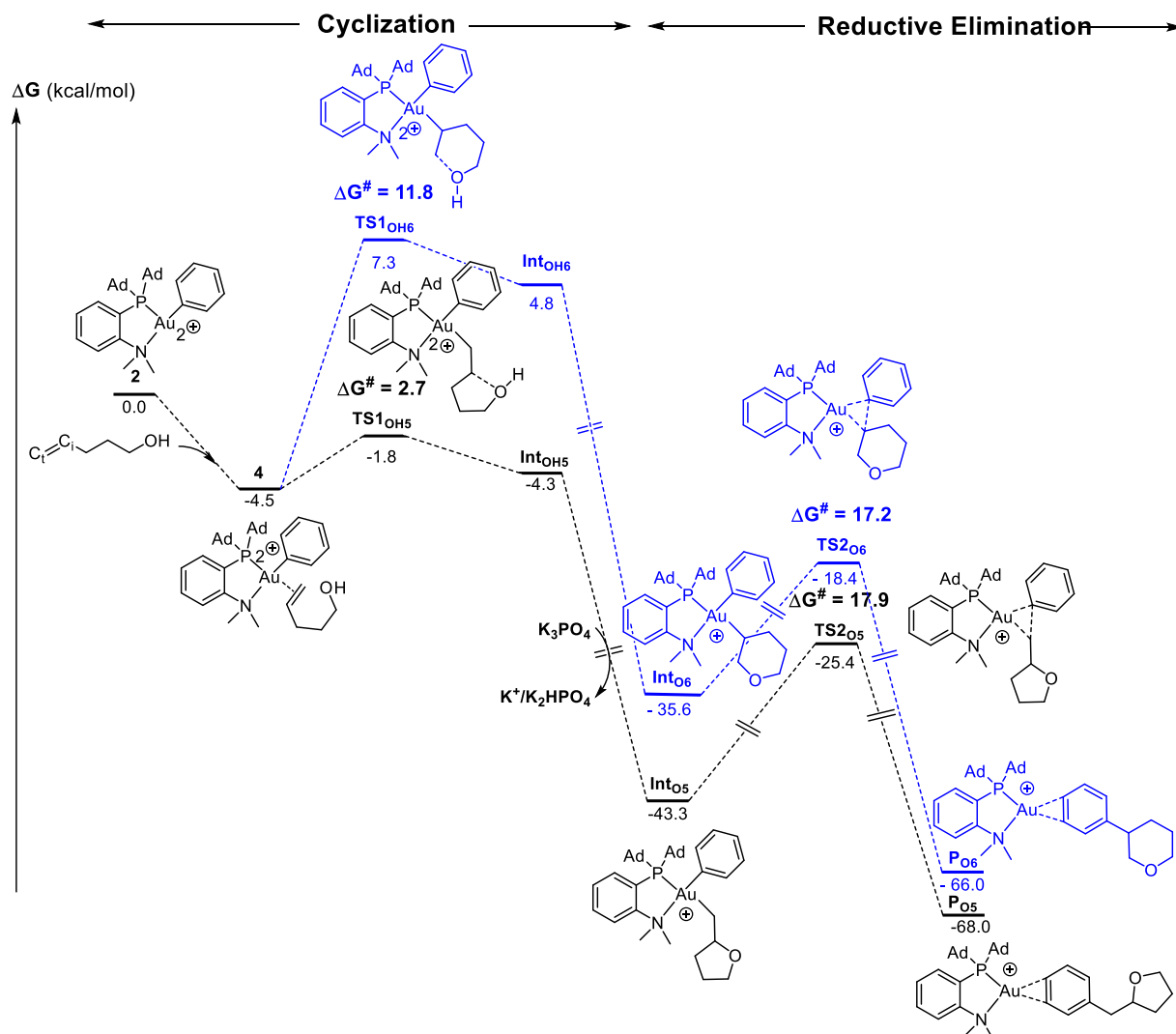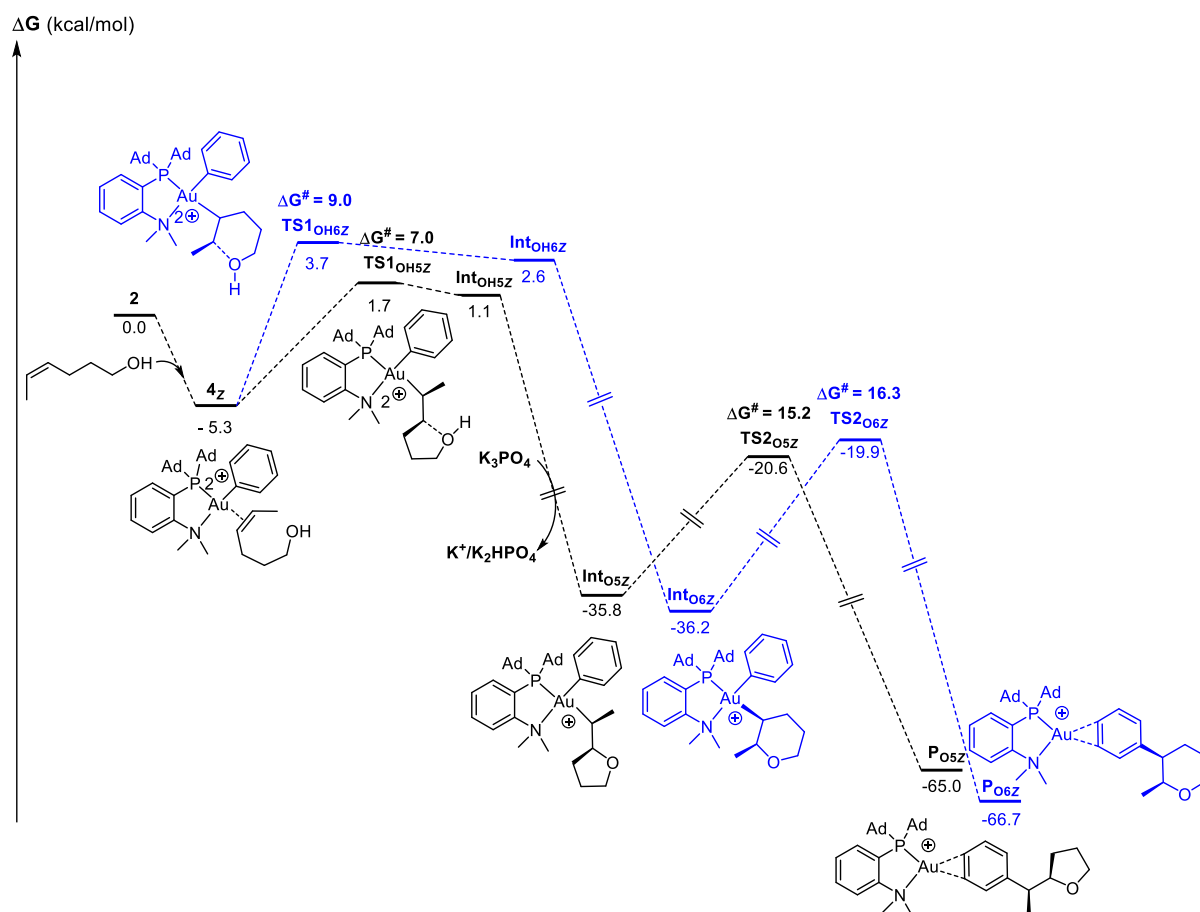

*Figure II-7: Energy profile (ΔG in kcal/mol) for the oxy-arylation reaction involving (P,N)Au^{2+}-Ph gold complex **2** and Z-4-hexen-1-ol computed at SMD(DCM)-B3PW91-D3(BJ)/SDD+f(Au), 6-31+G**(other atoms)//B3PW91/SDD+f(Au), 6-31G** (other atoms) level of theory and in the presence of K$_3$PO$_4$. Formation of 5-exo (black) and 6-endo (blue) products. The K$_3$PO$_4$, K$_2$HPO$_4$ and K$^+$ molecules are included in order to ensure the correct energetic balance in all the reaction steps.*

The reaction with the *E*-alkenol was also considered. Interestingly, the computed energy profiles for the cyclization step reveal noticeable differences (Figure II-8). The structure of the π-complex (**4$_E$**) mainly differs by the coordination of the alkene *E* to the metal center. In **4$_E$**, the alkenol is coordinated in a symmetric fashion (Au-C = 2.525-2.564 Å, C$_i$···O = 2.776 Å,

$C_{Me}\cdots O$ = 3.071 Å, Figure II-5). This π-complex is downhill in energy by 6.2 kcal/mol. Different from the reaction with the terminal alkenol or the *Z*-4-hexen-1-ol, the transition state of the 6-*endo* cyclization is 8.7 kcal/mol lower in energy than the 5-*exo* cyclization ($\Delta G^{\#}$ = 5.5 kcal/mol *vs* 14.2 kcal/mol, respectively). This is in line with experimental results where the exclusive formation of the 6-*endo* product was observed. Analysis of the geometrical features of **TS1$_{OH6E}$** reveals that the C$\cdots$O distance (2.335 Å) is elongated by 0.3 Å compared to those of the terminal and *Z*-alkenol (2.012-2.043 Å), suggesting an earlier transition state.
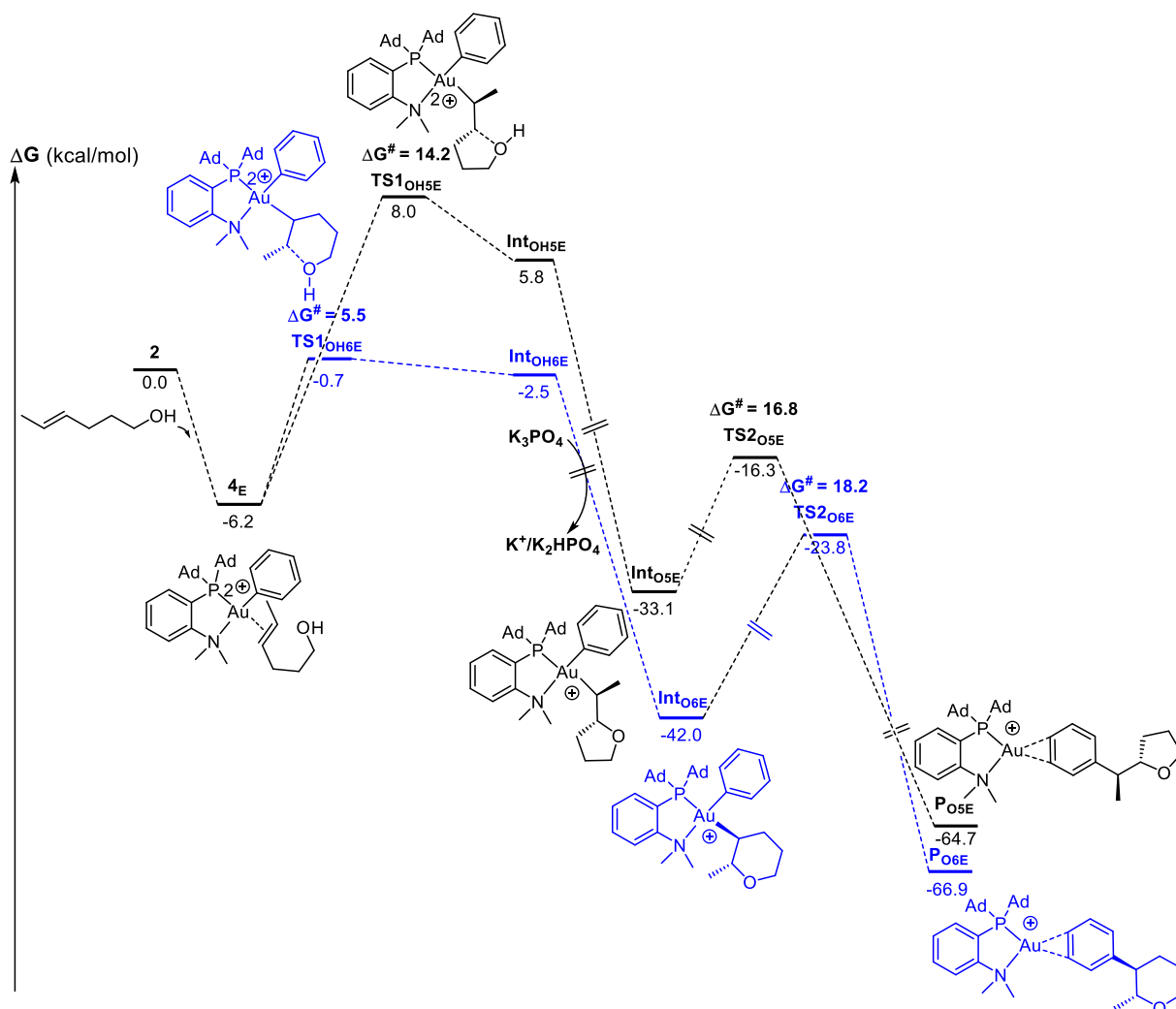
Figure II-8: Energy profile (ΔG in kcal/mol) for the oxy-arylation reaction involving (P,N)Au²⁺-Ph gold complex and E-4-hexen-1-ol computed at SMD(DCM)-B3PW91-D3(BJ)/SDD+f(Au), 6-31+G**(other atoms)//B3PW91/SDD+f(Au), 6-31G** (other atoms) level of theory and in the presence of K₃PO₄. Formation of 5-exo (black) and 6-endo (blue) products. The K₃PO₄, K₂HPO₄ and K⁺ molecules are included in order to ensure the correct energetic balance in all the reaction steps.

As previously observed, the activation barriers for the reductive elimination are relatively close for the two processes ($\Delta G^{\#}$ = 18.2 and 17.9 kcal/mol, respectively for 6-*endo* and 5-*exo*) and relatively similar to that found for the terminal alkenol, corroborating the weak impact of the alkenol on this step. Thus, these calculations show that the profile for the 6-*endo* process is downhill in energy compared to that of the 5-*exo* process, consistent with the

experimental results and the formation of the *6-endo* product. In light of these results, the switch of regioselectivity seems to be mainly correlated to the inversion of stability of the two cyclization transition states, thus suggesting the key role of the nucleophilic addition of O to the π-coordinated alkene cyclization step on this oxy-arylation reaction.

2.3 Electronic structure of the π-complexes

In order to clarify the origin of the switch of regioselectivity, we performed a detailed analysis of the cyclization step. Particular attention was given to the π-complexes. Indeed, previous theoretical studies suggested that the coordination mode of the π-CC bonds can guide the regioselectivity of nucleophilic attack. More specifically, G. Ujaque, A Lledos and I. Fernandez evidenced that the regioselectivity of the anti-Markovnikov hydroamination of alkenes catalyzed by gold(I) or [Rh(DPEPhos)]⁺ complexes can be related to the geometrical parameters of the reactant π-complex and the contribution of the p orbital from the terminal C atom *vs* the internal C atom. It has been found that the degree of η^2 to η^1 slippage is directly related to the regioselectivity (Scheme II-23).[40,41]

η^2 coordination η^1 coordination
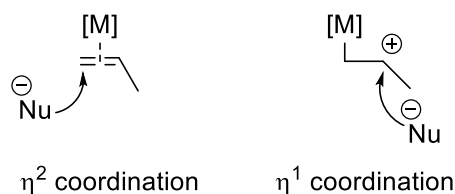
Scheme II-23: η^2 and η^1 coordination of alkene to metal.

Thus, the geometrical structures (Figure II-5) and the electronic properties (Figure II-9) of the π-complexes (**4**, **4**$_{ZIE}$) resulting from coordination of alkenol on initial gold complex **2** were analyzed. The coordination of the terminal alkene to gold is strongly asymmetric with an AuC$_t$ bond of 2.261 Å and an AuC$_i$ bond of 2.992 Å (Δ(Au-C) = 0.731 Å) indicating a η^1-like coordination mode. For the *Z*-4-hexen-1-ol, the difference between the two Au-C distances is smaller with an elongation of AuC$_{Me}$ bond to 2.417 Å and a decrease of AuC$_i$ one to 2.781 Å (Δ(Au-C) = 0.364 Å). Finally for *E*-4-hexen-1-ol, the coordination is quasi symmetric, with AuC$_{Me}$ and AuC$_i$ bonds of 2.564 Å and 2.525 Å, respectively (Δ(Au-C) = 0.039 Å), indicating a η^2-coordination mode. In addition, for all the π-complexes, the oxygen atom is always closer to C$_i$ atom, responsible of 5-*exo* cyclization than to C$_{t/Me}$ atom. However, the difference between the two bonds C$_{t/Me}$-O and C$_i$-O is larger for the terminal and *Z*-internal alkenols (Δ(O···C) = 0.646-0.700 Å) and decreases for the *E*-terminal alkenol (Δ(O···C) = 0.295 Å).

These differences in the coordination mode (slippage from η^1 to η^2-coordination) are supported by the shape of the orbital relevant to the cyclization step *i.e.* the LUMO, as

assessed specifically by an orbital composition analysis. We mainly focused on the analysis of the contribution of the $C_{t/Me}$ atom (terminal or carbon connected to the Me) and C_i atom (internal carbon) (Figure II-9 and Figure SII-6) orbital, which are the two atoms that can be involved in the nucleophilic attack. This LUMO mainly corresponds to the interaction between the σ^*_{AuP} orbital of the gold fragment and the $\pi_{Ct/Me=Ci}$ orbital of the alkenol. The calculated relative percentages of the two carbon atoms involved in the $\pi_{Ct/Me=Ci}$ orbital show a major contribution of the C_i atom, the carbon involved in the 5-*exo* cyclization, for 4-penten-1-ol (85.5% C_i, 14.5% C_t) and *Z*-4-hexen-1-ol (81.0% C_i, 19.0% C_{Me}). In contrast, for *E*-4-hexen-1-ol, where the 6-*endo* cyclization occurs, the two contributions are relatively similar (46.3% C_i, 53.7% C_{Me}) and the participation of C_{Me} becomes the most important.

Terminal alkene (4)

C$_i$: 85.5%
q$_i$ = 0.05

C$_t$: 14.5%
q$_t$ = - 0.73

Z-alkene (4$_Z$)

C$_i$: 81.0%
q$_i$ = - 0.04

C$_{Me}$: 19.0%
q$_{Me}$ = - 0.37

E-alkene (4$_E$)

C$_i$: 46.3%
q$_i$ = - 0.25

C$_{Me}$: 53.7%
q$_{Me}$ = - 0.17
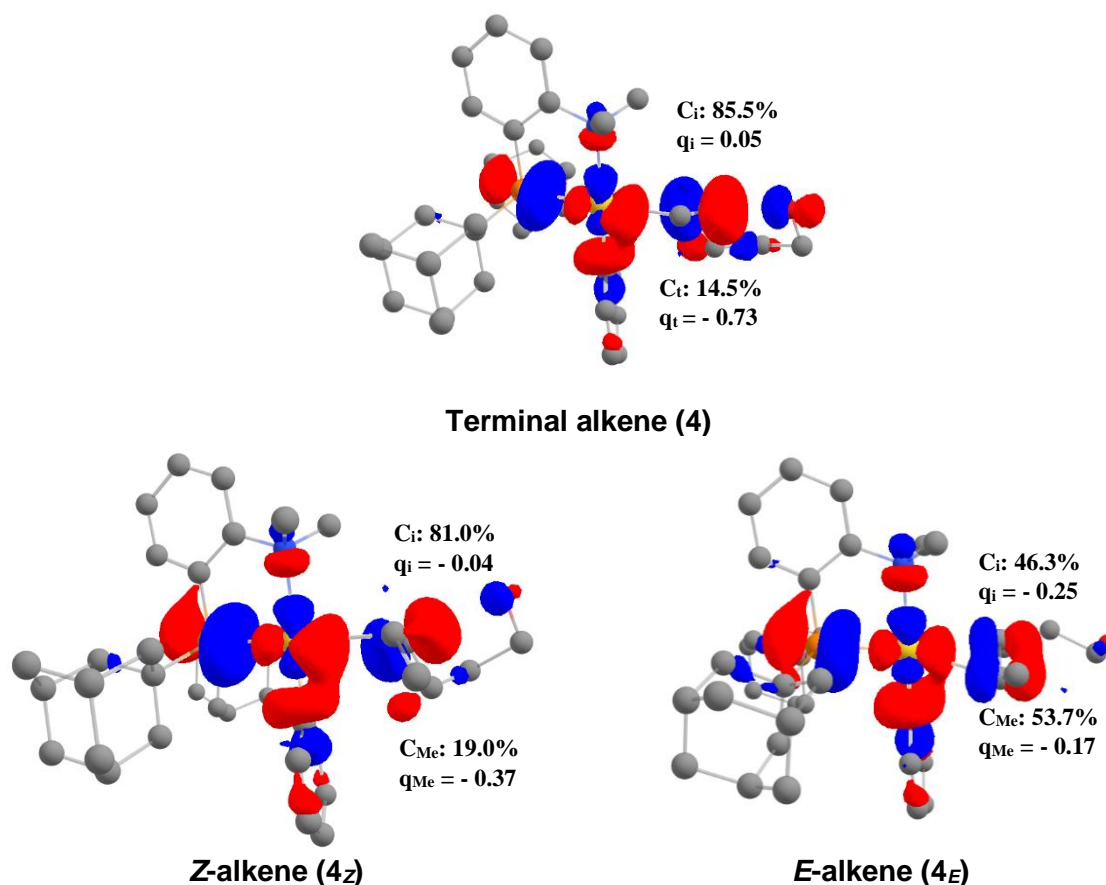
Figure II-9: Plot of the LUMO (cutoff :0.04) for the π-complexes 4 and $4_{Z/E}$ associated to the oxy-arylation cyclization with the 3 alkenols. Relative participation of $C_{t/Me}$ and C_i atoms (in %) in the $\pi_{Ct/Me=Ci}$ orbital. NPA charges (q).

The NBO charges of the $C_{t/Me}$ and C_i carbon atoms also reveal some correlation with the privileged cyclization mode (Figure II-9). For 4-penten-1-ol, the C_i atom is positively charged, whereas the C_t atom is negatively charged, in line with the favored nucleophilic attack of O to C_i. For the *Z*-alkenol, the charge of the C_i atom remains higher than that of C_{Me}, but the difference between the two is reduced (Δq = 0.41 *vs* 0.78 e⁻ for terminal alkene). For the *E*-alkenol, the difference is even more reduced (Δq = 0.08 e⁻) in line with the symmetry of the

coordination, but most remarkably, the C_{Me} atom bears the highest charge in this case, in line with the 6-*endo* cyclization. Of note, no correlation was found by the Ujaque's group between the charge of the C atoms and the regioselectivity in the Rh-promoted hydroamination reaction, suggesting orbital control prevailed.[41]

On the basis of these results, the unusual switch of regioselectivity can be correlated to the geometry and the electronics of the π-complexes. Orbital and charge effects go in the same direction to drive the nucleophilic attack of O to $C_{t/Me}$ or C_i. The origin of the switch of regioselectivity observed for the *E*-internal alkenol is likely the symmetric coordination of the double bond at gold, involving a large coefficient on the C_{Me} atom in the LUMO of **4$_E$** and a reversal of charge between the C_i and C_{Me} atoms.

2.4 DFT calculations for oxy-vinylation reaction

During the course of the theoretical investigation, other members of the group found that the MeDalPhos gold complex was also efficient in promoting the hetero-vinylation of alkenols. The postulated mechanism was similar to the one for the heteroarylation (oxidative addition, π-activation and reductive elimination). As for the hetero-arylation, a switch of regioselectivity was observed for the 4-hexen-1-ols. Indeed, experimental results have shown the unique formation of the 5-*exo* product at 80°C with 4-penten-1-ol and *Z*-4-hexen-1-ol and a mixture of tetrahydrofuran/tetrahydropyran with *E*-4-hexen-1-ol (Scheme II-24).[42] To strengthen the previous theoretical work, confirm the key role of the π-intermediates and the trend observed for the relation between the coordination mode of the alkene, and the regioselectivity, the hetero-vinylation reaction was investigated computationally.
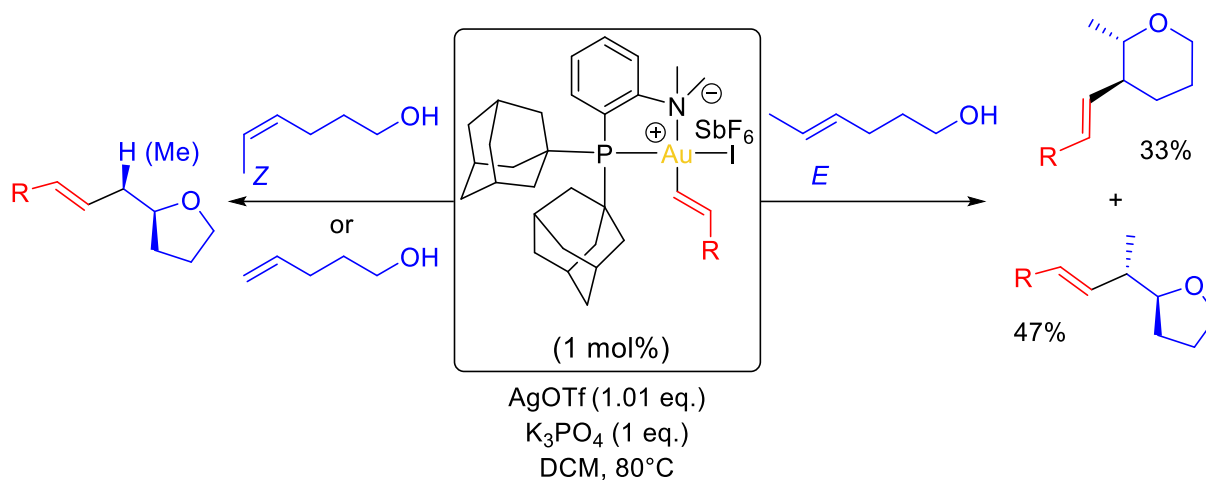
Scheme II-24: Switch in regioselectivity for oxy-vinylation reaction with the (MeDalPhos)Au²⁺-vinyl complex and Z/E-4-hexen-1-ol.

Based on the previous theoretical results on hetero-arylation reaction, efforts were focused on the gold-catalyzed oxy-cyclization step and on the analyses of the π-complexes to rationalize the regioselectivity observed with the vinyl substituent on the gold center. Since the X-ray structure of the vinyl (P,N)gold(III)(vinyl)I complex showed the *trans* relationship between the vinyl group and the nitrogen atom, and according to the results obtained for [(P,N)Au-Ph]²⁺, only the coordination of the alkenol *trans* to phosphorus (after iodide abstraction) was analyzed theoretically.

The (P,N)Au²⁺-vinyl catalyst being unsymmetric contrary to the (P,N)Au²⁺-aryl one, different orientations had to be considered (Figure SII-7, SI p.106) upon coordination of the alkenol at gold. To simplify the discussion, only the favored one will be presented, which corresponds to the less sterically hindered, meaning the one where the CH_2 or the Me group are on the same side as the vinyl moiety. In this case, the π-complex **4v** is slightly downhill in energy (ΔG = -3.7 kcal/mol ; Figure II-11). In **4v**, the two Au-C bonds are dissymmetric (Au-C_t = 2.243 and Au-C_i = 2.966 Å: Δ(Au-C) = 0.723 Å *vs* 0.731 Å for oxy-arylation), the LUMO involves a strongly dissymmetric $\pi_{C_t=C_i}$ orbital with an important coefficient at C_i (86.2% C_i, 13.8% C_t) and the charge of C_i is higher than that of the C_{Me} (Δq = 0.78 e⁻), in line with the unique formation of the 5-*exo* product (Figure II-10 & Figure SII-10 SI p.108).

4v

4v$_z$

4v$_E$

4'v$_E$
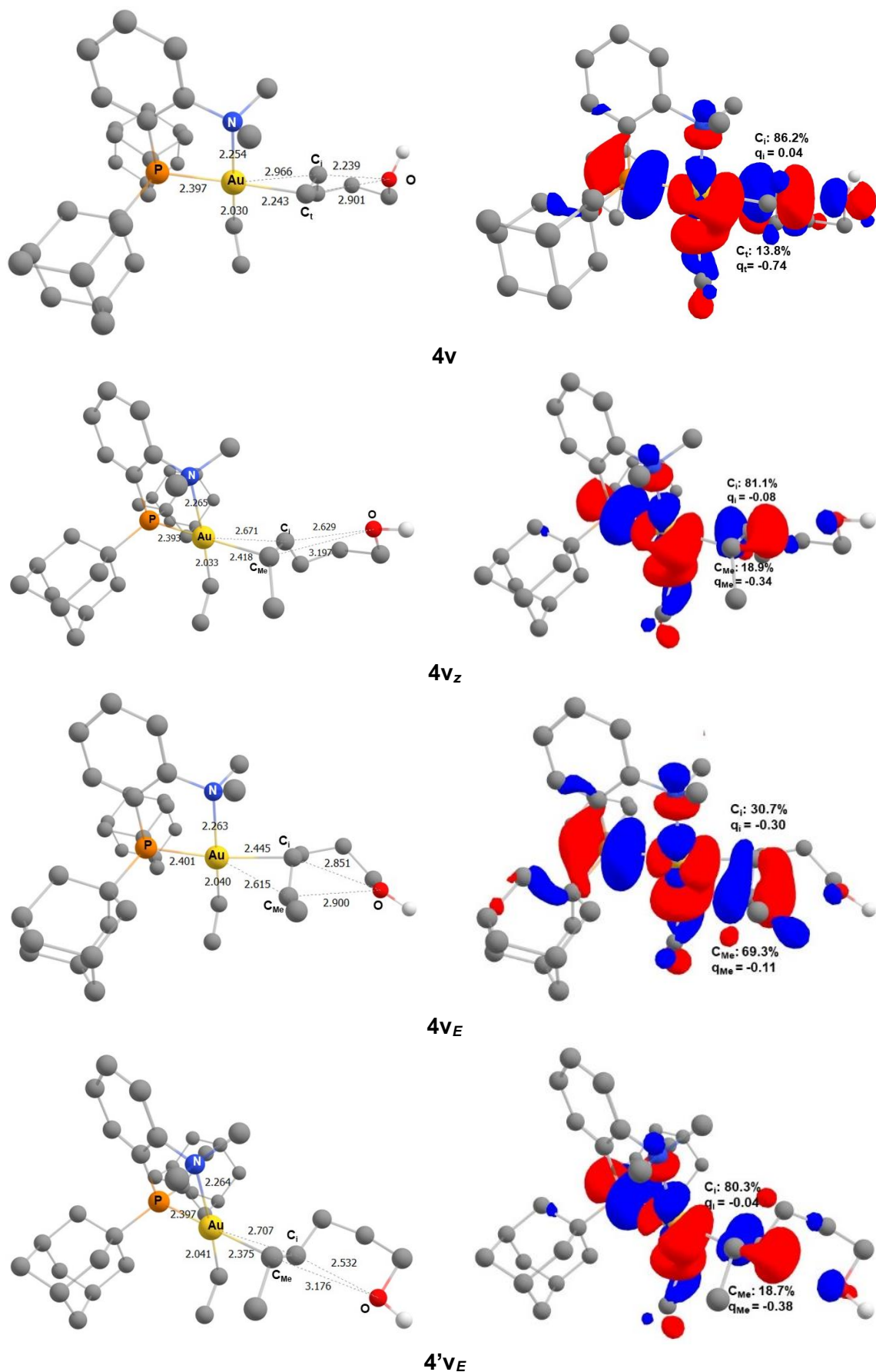
Figure II-10: Main geometrical parameters (distances in Å, left) and plot of the LUMO (cutoff :0.04, right) for the π-complex
***4v**, associated to the oxy-vinylation cyclization. Relative participation of $C_{t/Me}$ and C_i atoms (in %) in the $\pi_{Ct/Me=Ci}$ orbital.*

77

This result is corroborated by the calculation of the energy profiles. As previously observed for the oxy-arylation reaction, the energy difference between the two activation barriers of the nucleophilic attack of 4-penten-1-ol on C_t or C_i atoms of the double bond is important ($\Delta\Delta G^{\#}$ = 9.0 kcal/mol) and in favor of the formation of the 5-*exo* product (Figure II-11). For the attack on C_i (5-*exo*), the activation barrier is slightly lower than that for the aryl ligand on Au (2.1 *vs* 2.7 kcal/mol) leading to **Intv$_{OH5}$**. The associated transition state **TS1v$_{OH5}$** presents the longest C···O distance (1.965 Å *vs* 1.878 Å), indicating an earlier TS. The intermediate **Intv$_{O5}$** is then formed through an exergonic deprotonation process from **Intv$_{OH5}$**.
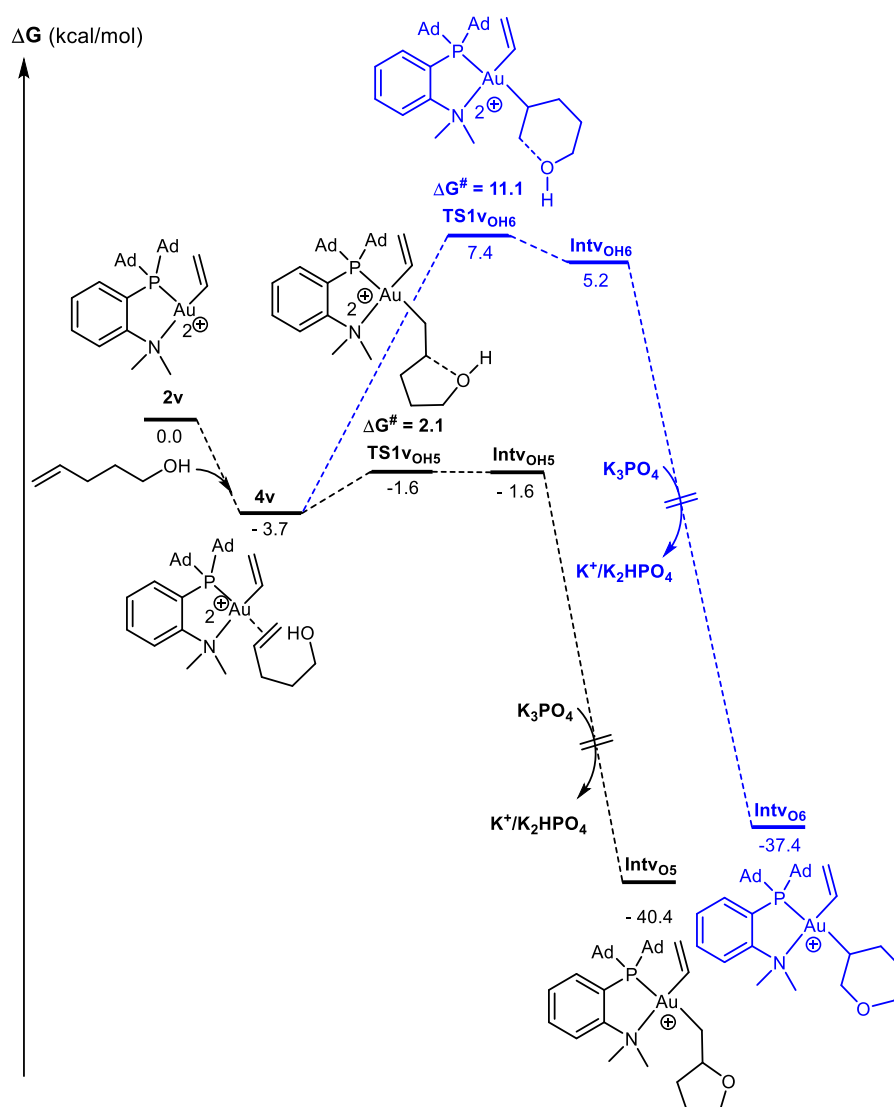
*Figure II-11: Energy profiles (ΔG in kcal/mol) for the cyclization step of the oxy-vinylation reaction involving (P,N)Au^{2+}-vinyl gold complex **2v** and 4-penten-1-ol computed at SMD(DCM)-B3PW91-D3(BJ)/SDD+f(Au, 6-31+G**(other atoms)// B3PW91/SDD+f(Au), 6-31G** (other atoms) level of theory. Formation of 5-exo (black) and 6-endo (blue) products.*

As readily seen in Figure II-12, left, the energy profile for the oxy-vinylation cyclization of *Z*-4-hexen-1-ol is also found to be very similar to that of the oxy-arylation reaction. The cyclization step occurs more easily through the carbon atom responsible of the 5-membered ring cyclization ($\Delta G^{\#}$ = 8.3 *vs* $\Delta G^{\#}$ = 10.4 kcal/mol for other carbon) and the energy difference between the two activation barriers is very close to that previously computed for heteroarylation ($\Delta\Delta G^{\#}$ ~ 2.0-2.1 kcal/mol). The coordination of the alkenol at Au is slightly less dissymmetric than for the $(P,N)Au^{2+}$-Ph complex (Δ(Au-C) = 0.253 *vs* 0.364 Å), the contribution of C_{Me} atom in the LUMO of the π-complex remains very important (higher than 80%) and the charge of C_i is still higher than that of C_t (Δq = 0.26 e$^-$), consistent with full regioselectivity for the 5-*exo* cyclization (Figure II-10 & Figure SII-10).
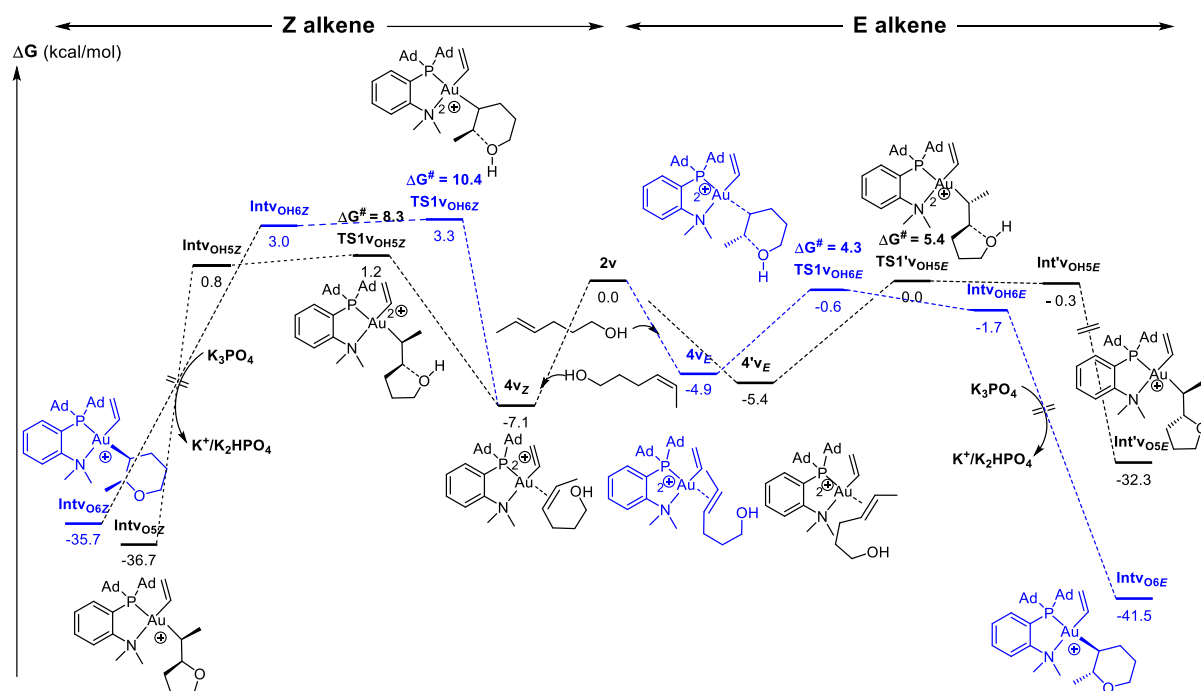
*Figure II-12: Energy profiles (ΔG in kcal/mol) for the cyclization step of the oxy-vinylation reaction involving (P,N)Au²⁺-vinyl gold complex **2v** and Z-4-hexen-1-ol or E-4-hexen-1-ol computed at SMD(DCM)-B3PW91-D3(BJ)/SDD+f(Au), 6-31+G**(other atoms)// B3PW91/SDD+f(Au), 6-31G** (other atoms) level of theory. Formation of 5-exo (black) and 6-endo (blue) products.*

Concerning the *E*-alkene, the analysis of the reaction profile (Figure II-12, right) for the nucleophilic attack of the oxygen atom shows that the most favorable 5-*exo* or 6-*endo* cyclizations come from different π-complexes **4v$_E$** and **4'v$_E$**, which differ from the approach of the alkene to gold (Me pointing up or down, repectively, Figure II-10). The π-complex **4'v$_E$** being more stable than **4v$_E$** (ΔG = 0.5 kcal/mol from **4v$_E$**), this latter is formed preferentially. The 5-*exo* cyclization occurs from this π-intermediate through **TS1'v$_{OH5E}$**. The activation barrier associated to this cyclization is low and equivalent to the decoordination of the alkene from **4'v$_E$** (ΔG = 5.4 kcal/mol). The alkene can then recoordinate to gold in complex **2v** with a different approach, to give **4v$_E$**. From **4v$_E$**, the 6-*endo* cyclization can occur easily with an activation barrrier of $\Delta G^{\#}$ = 4.3 kcal/mol, lower in energy than that computed for the 5-*exo*

process ($\Delta\Delta G^{\#}$ =1.1 kcal/mol). As a result, these two processes are likely to compete. These theoretical results are consistent with the experimental observations and confirm the key role of the π-complex on the regioselectivity of the cyclization. The most stable π-complex (**4'v$_E$**) connects with the 5-*exo* product, while the 6-*endo* product comes from **4v$_E$** and is associated with the lowest activation barrier.[4] In **4v$_E$**, the contribution of C_i and C_{Me} atoms are 30.7% and 69.3%, respectively (Figure II-10 & Figure SII-10) and the charge is higher at C_{Me} than C_i (Δq = 0.19 e$^-$), in line with the dissymmetry of the π-complex (Au-C_i is shorter than Au-C_{Me} in **4v$_E$**) and the formation of the 6-*endo* product. For the other π-complex **4'v$_E$**, the coefficients (19.7% for C_{Me} and 80.3% for C_i) and the charges are consistent with the formation of the 5-membered ring.

Overall, this computational study supports the postulated outer-sphere Au^I/Au^{III} mechanism. The key intermediates are the gold(III) π-complexes. Indeed, the coordination of the alkene to gold governs the regioselectivity (η^1 to η^2 slippage), impacting the contribution of the two carbon atoms in the LUMO as well as their charges. The privileged nucleophilic attack of the oxygen on the C_t (C_{Me}) or C_i atoms, affording respectively 6-*endo* and 5-*exo* cyclizations, is directed by the highest coefficient in the π orbital of the LUMO. Thus, by looking at the geometrical and electronic structures of the π-complex, one could be able to anticipate the regioselectivity, but should be careful when several alkene coordination to gold are possible and can be competitive.

V.   Conclusions and outlook

In summary, the first gold-catalyzed reaction to combine oxidative addition of aryl iodides and π-activation of alkenes has been developed. The transformation is efficient and robust. It works with a broad scope of substrates and gives access to 5-, as well as 6- and 7-membered rings. It is based on a ligand-induced approach, using the (P,N) ligand MeDalphos, that complements and significantly extends the synthetic utility of the oxy- and amino-arylation reactions performed under oxidative/ photoredox conditions. The reaction is compatible and most efficient with electron-rich aryl substrates which otherwise react sluggishly. The (P,N) ligand brings steric shielding to gold and induces synthetically useful levels of diastereoselectivity upon formation of 2,3-disubstituted products (dr 6-10:1), which surpasses that of other gold systems. Also, noteworthy and very unusual is the complete switch in

---

[4] Another isomer **4'$_E$** was also found for the heteroarylation reaction, but it is higher in energy than **4$_E$** and the activation barrier to access 5-*exo* cyclization is higher than the one for the 6-*endo* pathway (Figure SII-5, SI p.95).

regioselectivity from 5-*exo* to 6-*endo* cyclization between the Z and E isomers of internal alkenols.[43]

This unusual switch of regioselectivity was also observed for the reaction of heterovinylation of alkenes. Intrigued by this behavior, a DFT study on the mechanism of the hetero-arylation/vinylation of alkenes was performed. DFT calculations supported the outer-sphere mechanism and allowed to rationalize the regioselectivity. The reaction of alkenols with (P,N)Au^{2+}-Ph/vinyl complex proceeds through 3 steps: *i*) formation of a π-complex resulting from coordination of the C=C double bond to gold, *ii*) nucleophilic addition of the alcohol at the C_i (5-*exo* cyclization) or C_t (C_{Me}) atom (6-*endo* cyclization) of the double bond of the π-complex and formation of a dicationic intermediate, which is easily deprotonated by K_3PO_4, *iii*) C_{sp}^2-C_{sp}^3 reductive elimination, affording the benzyltetrahydrofuran (5-*exo* derivative) or 3-phenylpyrane (6-*endo* derivative). It was shown that the regioselectivity found its origin in the coordination mode of the alkene (η^1 *vs* η^2) to gold. The η^2 coordination mode favors the 6-*endo* cyclization and the η^1 mode the 5-*exo* cyclization.

Following this work, Patil's and Shi's groups described the three-component 1,2-oxyarylation of alkenes using the same (MeDalPhos)AuCl complex (Scheme II-25, top).[44,45] The more challenging 1,2-aminoarylation of alkenes with external amine (Scheme II-25, top) was also achieved with the same complex.[46]
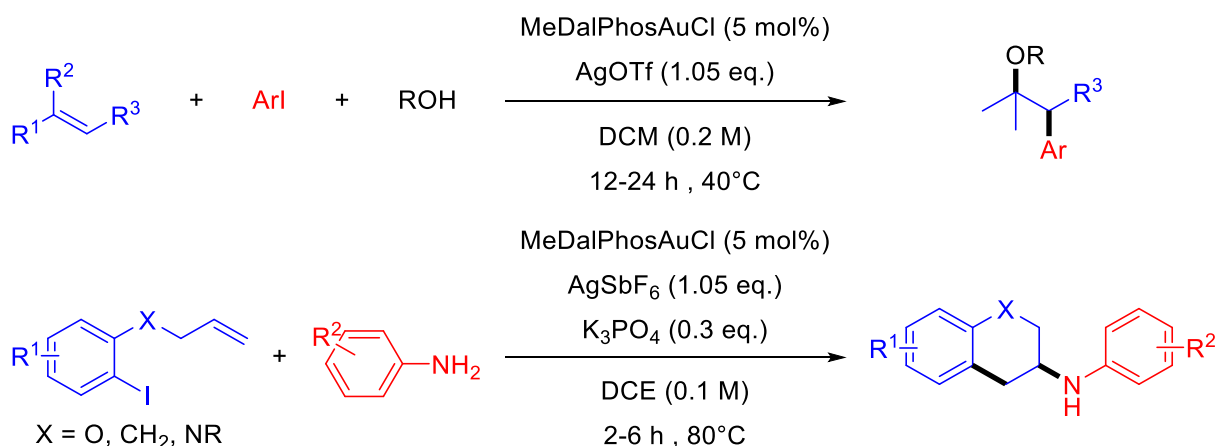
Scheme II-25: Ligand-enabled gold-catalyzed 1,2-difunctionalization of alkenes using external nucleophiles.

The MeDalPhos gold complex is efficient for both the hetero-arylation and hetero-vinylation of alkenes. A competitive experiment, using a substrate bearing both an aryl iodide and a vinyl iodide, was performed and showed a chemoselectivity for vinyl substrates. Taking advantage of this, several polyfunctional tetrahydrofuran products were obtained straightforwardly by sequential hetero-vinylation/arylation (Scheme II-26).[42]
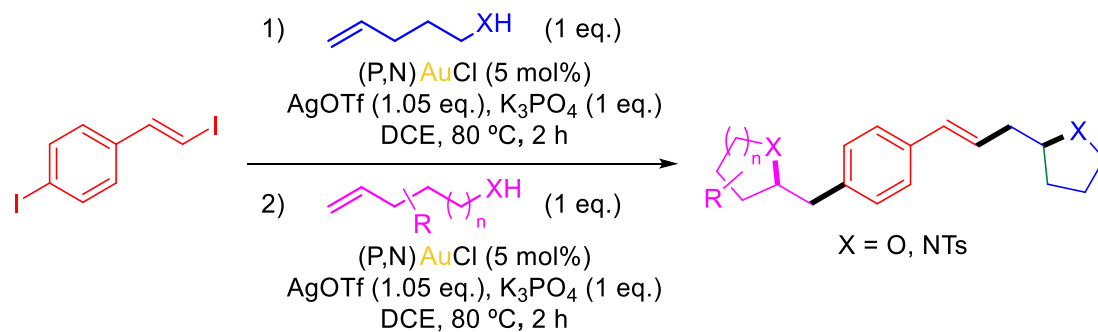
Scheme II-26: Sequential gold-catalyzed hetero-vinylation/arylation transformations of the bifunctional substrate.

No enantioselective gold-catalyzed 1,2-difunctionalization of alkenes is known yet and future work will try to fill this gap. Owing to the unique efficiency of the MeDalPhos gold complex, one could envision a chiral version of this ligand. To this end, our group, teamed up with the Lacour's group, who has expertise on Tröger's bases,[47] designed and synthesized a new bis (P,N) chiral ligand (Scheme II-27). After coordination to gold, the oxidative addition of aryl/vinyl halides should be tested, and if successful catalytic heteroarylation and heterovinylation of alkenes could be envisioned.
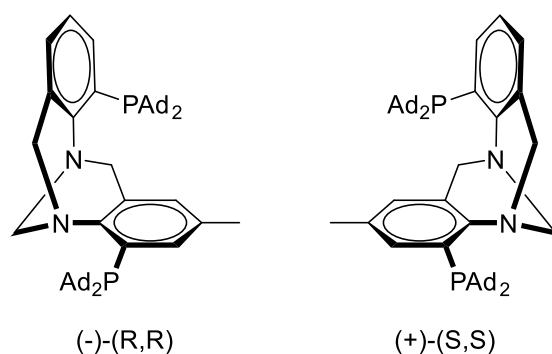
Scheme II-27: Achiral (P,N) ligand based on Tröger's base.

VI.   Experimental procedures and analytical data
1. Oxidative addition of phenyl iodide to gold in the presence of additives
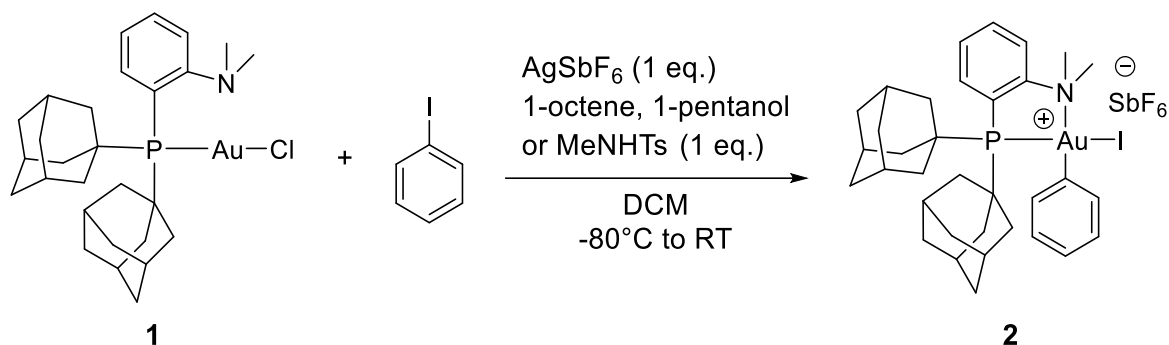
1   **2**

In a glovebox, a screw-cap NMR tube was charged with silver hexafluoroantimonate (8.0 mg, 0.023 mmol) in dichloromethane (0.2 mL). Complex **1** (15 mg, 0.023 mmol) was transferred into a small glass vial and dissolved in dichloromethane (0.4 mL), phenyl iodide (2.6 µL, 0.023 mmol) and the additive (1-octene, 1-pentanol or *N*-tosylmethylamine, 0.023 mmol) were added. The prepared solution was loaded into a plastic syringe equipped with stainless steel needle. The syringe was closed by blocking the needle with a septum. Outside the glovebox, the NMR tube was cooled down to -80°C (acetone/N_2 cold bath). At this temperature, the prepared solution was added. The tube was gently shaken and allowed to warm to rt. The formation of the gold(III) was confirmed by $^{31}P\{^1H\}$ NMR spectroscopy.

2. Stoichiometric reaction from gold(III)

Complex **2** was prepared according to the reported procedure.[22]

2   **Ia**   **3**
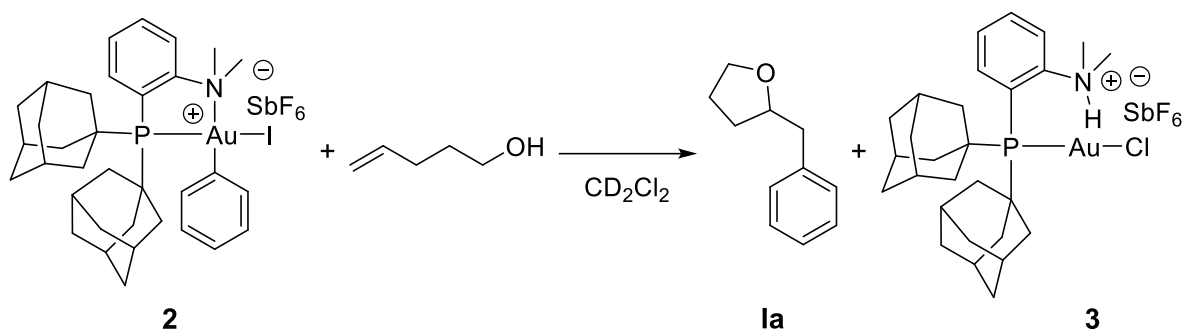
In a glovebox, a screw-cap NMR tube was charged with complex **2** (23.3 mg, 0.023 mmol) dissolved in dichloromethane-d_2 (0.5 mL). The 4-penten-1-ol (2.4 µL, 0.023 mmol) was added to the solution. The tube was gently shaken and monitored by $^{31}P\{^1H\}$ and ^1H NMR spectroscopy.

2-benzyltetrahydrofuran (Ia): Analytical data are consistent with those previously reported[5]:
^1H NMR (300 MHz, CDCl$_3$): δ 7.26-7.12 (m, 5H), 4.05-3.97 (m, 1H), 3.88-3.81 (m, 1H), 3.72-3.65 (m, 1H), 2.87 (dd, J_{HH} = 13.5, 6.5 Hz, 1H), 2.69 (dd, J_{HH} = 13.5, 6.5 Hz, 1H), 1.92-1.73 (m, 3H), 1.56-1.45 (m, 1H).

3. Gold-catalyzed oxy-arylation of alkenes
3.1 Synthesis of substrates

2,2-dimethylpent-4-en-1-ol (**4a**)[48], 2,2-diphenyl-4-penten-1-ol (**4b**)[49], 3-phenylpent-4-en-1-ol (**4c**)[5], 2-benzylpent-4-en-1-ol (**4d**)[5], 1-decen-5-ol (**4e**)[5], 1-but-3-enylcyclohexanol (**4f**)[50], 2-allylcyclohexanol (**4g**)[51], 2,2-dimethyl-5-hexen-1-ol (**4j**)[52], heptenol (**4k**)[53] and 2,2-diallylpropane-1,3-diol (**4l**)[49] were prepared according to reported procedures.
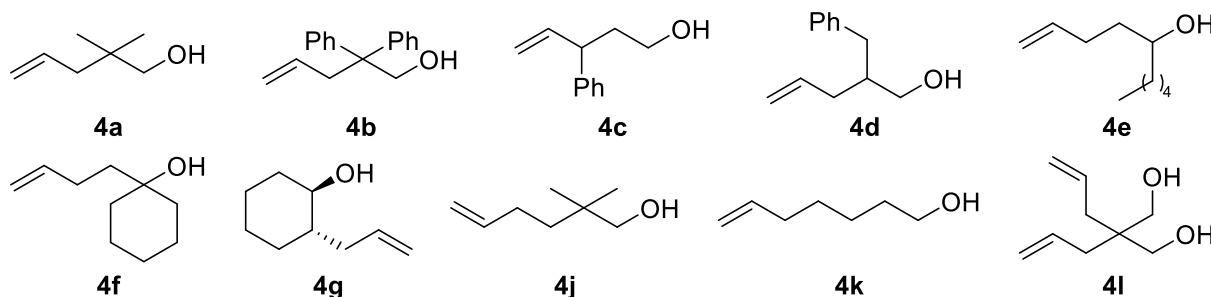
4-methyl-4-penten-1-ol (**4m**):
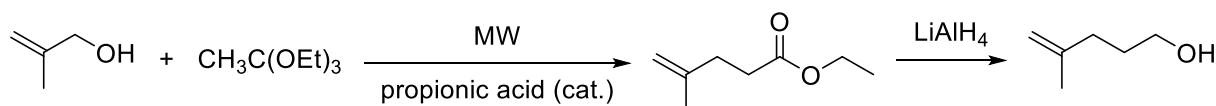
<u>Preparation adapted from Hamashima *et al.*</u>[54] A mixture of 2-methallyl alcohol (6.93 mmoles, 500 mg), ethyl orthoacetate (4 mL) and a drop of propanoic acid was irradiated under microwave (200 W, 190°C) during 10 min. The mixture was dissolved in EtOAc (30 mL) and stired vigorously with HCl 2N (30 mL) for 2h. The organic phase was washed with water, brine and dried over sodium sulfate. The crude was purified by flash chromatography (petroleum/EtOAc 95/5) to yield a clear oil (64%).
The ester was reduced by LiAlH$_4$ in THF. The excess of LiAlH$_4$ was hydrolyzed by NaOH and water. The crude was purified by flash chromatography (petroleum/EtOAc 70/30) to yield colorless oil (84%). Analytical data are consistent with those previously reported.[55]

3.2 General procedure for the gold-catalyzed oxy-arylation of alkenes
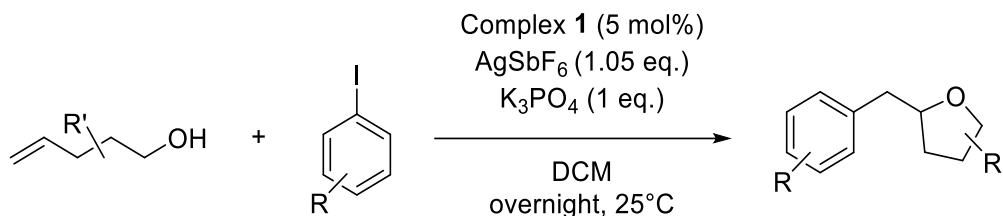
In a glovebox, a dry Schlenk equipped with a magnetic stirrer bar was charged with silver hexafluoroantimonate (143 mg, 0.42 mmol) and potassium phosphate tribasic (85 mg, 0.40 mmol) in DCM (0.4 mL). Complex **1** (13 mg, 0.02 mmol) was transferred into a small glass vial and dissolved in solvent (0.6 mL). The aryl iodide (0.4 mmol, 1 eq.), the functionalized alkene (0.4 mmol, 1 eq.) and dibenzylether (internal standard, 0.1 mmol, 20 µL) were added to the

gold complex solution. This solution was loaded into a plastic syringe equipped with stainless steel needle. The syringe was closed by blocking the needle with a septum. Outside the glovebox, the prepared solution was added to the Schlenk under agitation. The reaction mixture was then stirred at 25°C. The reaction was monitored by NMR spectroscopy by taking an aliquot of the crude reaction mixture. To isolate the product, silver salts were removed by filtration and the sample was purified by column chromatography.
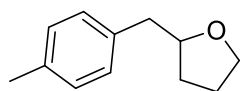
2-(4-methyl-benzyl)tetrahydrofuran (Ib): Analytical data are consistent with those previously reported[14]: **^{1}H NMR** (300 MHz, CDCl$_3$): 7.15-7.07 (m, 4H), 4.09-3.98 (m, 1H), 3.94-3.85 (m, 1H), 3.78-3.68 (m, 1H), 2.89 (dd, J_{HH} = 13.5, 6.4 Hz, 1H), 2.71 (dd, J_{HH} = 13.5, 6.6 Hz, 1H), 2.32 (s, 3H), 1.98-1.79 (m, 3H), 1.62-1.49 (m, 1H).
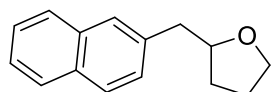
2-(2-naphtalenyl-methyl)tetrahydrofuran (Ic): Analytical data are consistent with those previously reported[1]: **^{1}H NMR** (300 MHz, CDCl$_3$): δ 7.83-7.75 (m, 3H), 7.67 (s, 1H), 7.52-7.38 (m, 3H), 4.23-4.12 (m, 1H), 3.97-3.87 (m, 1H), 3.80-3.71 (m, 1H), 3.09 (dd, J_{HH} = 13.6, 6.4 Hz, 1H), 2.92 (dd, J_{HH} = 13.6, 6.5 Hz, 1H), 2.01-1.83 (m, 3H), 1.68-1.55 (m, 1H).
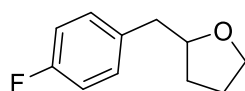
2-(4-fluoro-benzyl)tetrahydrofuran (Id): Analytical data are consistent with those previously reported[14]: **^{1}H NMR** (300 MHz, CDCl$_3$): δ 7.23-7.14 (m, 2H), 7.03-6.92 (m, 2H), 4.09-3.98 (m, 1H), 3.93-3.84 (m, 1H), 3.78-3.69 (m, 1H), 2.86 (dd, J_{HH} = 13.8, 6.7 Hz, 1H), 2.74 (dd, J_{HH} = 13.8, 6.0 Hz, 1H), 2.00-1.80 (m, 3H), 1.58-1.49 (m, 1H).
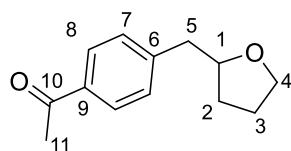
2-(4-acetyl-benzyl)tetrahydrofuran (Ie): The pure product was obtained after column chromatography **(**Pentane/Ethyl Acetate: 8/2) as a colorless oil (66 mg, 70%). **^{1}H NMR** (500 MHz, CDCl$_3$): δ 7.90-7.85 (m, 2H, H$_8$), 7.4-7.29 (m, 2H, H$_7$), 4.11-4.03 (m, 1H, H$_1$), 3.90-3.84 (m, 1H, H$_4$), 3.75-3.69 (m, 1H, H'$_4$), 2.92 (dd, J_{HH} = 13.7, 7.0 Hz, 1H, H$_5$), 2.82 (dd, J_{HH} = 13.7, 5.7 Hz, 1H, H'$_5$), 2.56 (s, 3H, H$_{11}$), 1.98-1.90 (m,1H, H$_2$), 1.89-1.81 (m, 2H, H$_3$), 1.59-1.49 (m, 1H, H'$_2$). **^{13}C NMR** (126 MHz, CDCl$_3$): δ 198.0 (C$_{10}$), 144.9 (C$_6$), 135.4 (C$_9$), 129.5 (C$_7$), 128.5 (C$_8$), 79.6 (C$_1$), 68.1 (C$_4$), 42.0 (C$_5$), 31.2 (C$_2$), 26.6 (C$_{11}$), 25.7 (C$_3$). **EI-MS:** Calculated for C$_{13}$H$_{16}$O$_2$: 204.12. Found: 204.02
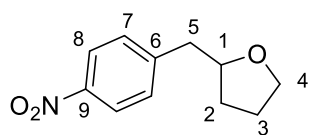
2-(4-nitro-benzyl)tetrahydrofuran (If): The pure product was obtained after column chromatography **(**Pentane/Ethyl Acetate: 8/2) as a colorless oil (57 mg, 80%). **^{1}H NMR** (400 MHz, CDCl$_3$): δ 8.18-8.12 (m, 2H, H$_8$), 7.43-7.37 (m, 2H, H$_7$), 4.13-4.05 (m, 1H, H$_1$), 3.93-3.84 (m, 1H, H$_4$), 3.79-3.69 (m, 1H, H'$_4$), 2.94 (dd, J_{HH} = 13.8, 6.8 Hz, 1H, H$_5$), 2.90 (dd, J_{HH} = 13.8, 5.7 Hz, 1H, H'$_5$), 2.04-1.95 (m,1H, H$_2$), 1.92-1.83 (m, 2H, H$_3$), 1.62-1.49 (m, 1H, H'$_2$). **^{13}C NMR** (100 MHz, CDCl$_3$): δ 147.1 (C$_6$), 145.7 (C$_9$), 130.2 (C$_7$), 123.6 (C$_8$), 79.2 (C$_1$), 68.2 (C$_4$), 41.8 (C$_5$), 31.3 (C$_2$), 25.7 (C$_3$). **EI-MS:** Calculated for C$_{11}$H$_{13}$NO$_3$: 207.09. Found: 206.93.
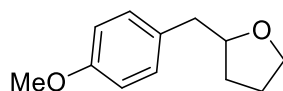
2-(4-methoxy-benzyl)tetrahydrofuran (Ig): The pure product was obtained after column chromatography **(**Pentane/Ethyl Acetate: 8/2) as a colorless oil (77 mg, 70%). Analytical data are consistent with those previously reported[56]: **^{1}H NMR** (300 MHz, CDCl$_3$): δ 7.14 (d, J_{HH} = 8.5 Hz, 2H), 6.83 (d,

J_{HH} = 8.5 Hz, 2H), 4.02 (pseudo quin, J_{HH} = 6.8 Hz, 1H), 3.93-3.84 (m, 1H), 3.78 (s, 3H), 3.77-3.68 (m, 1H), 2.86 (dd, J_{HH} = 13.7, 6.4 Hz, 1H), 2.69 (dd, J_{HH} = 13.7, 6.4 Hz, 1H), 1.97-1.77 (m, 3H), 1.60-1.48 (m, 1H).
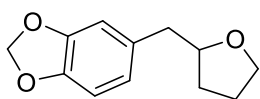

5-(tetrahydrofuran-2-ylmethyl)benzo[1,3]dioxole (Ih): Analytical data are consistent with those previously reported[57]: **^{1}H NMR** (300 MHz, CDCl$_3$): δ 6.78-6.64 (3H, m), 5.92 (2H, s), 4.05-3.94 (1H, m), 3.93-3.84 (1H, m), 3.78-3.69 (1H, m), 2.81 (1H, dd, J_{HH} = 13.8, 6.6 Hz), 2.67 (1H, dd, J_{HH} = 13.5, 6.3 Hz), 1.99-1.79 (3H, m), 1.58-1.49 (1H, m).
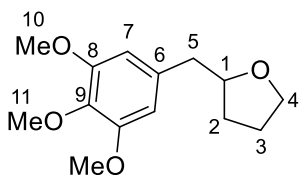
2-(3,4,5-trimethoxy-benzyl)tetrahydrofuran (Ii): **^{1}H NMR** (500 MHz, CDCl$_3$): δ 6.45 (s, 2H, H$_7$), 4.11-4.03 (m, 1H, H$_1$), 3.94-3.88 (m, 1H, H$_4$), 3.85 (s, 6H, H$_{10}$), 3.82 (s, 3H, H$_{11}$), 3.78-3.72 (m, 1H, H'$_4$), 2.83 (dd, J_{HH} = 13.5, 6.5 Hz, 1H, H$_5$), 2.71 (dd, J_{HH} = 13.5, 6.0 Hz, 1H, H'$_5$), 2.00-1.92 (m, 1H, H$_3$), 1.91-1.81 (m, 2H, H$_2$), 1.61-1.52 (m, 1H, H'$_3$). **^{13}C NMR** (126 MHz, CDCl$_3$): δ 153.2 (C$_8$), 136.6 (C$_9$), 135.0 (C$_6$), 106.2 (C$_7$), 80.1 (C$_1$), 68.2 (C$_4$), 61.0 (C$_{11}$), 56.2 (C$_{10}$), 42.5 (C$_5$), 31.3 (C$_3$), 25.8 (C$_2$). **EI-MS:** Calculated for C$_{14}$H$_{20}$O$_4$: 252.14. Found: 252.07.

2-(2-methoxy-benzyl)tetrahydrofuran (Ij): **^{1}H NMR** (400 MHz, CDCl$_3$): δ 7.22-7.16 (m, 2H, H$_{7,9}$), 6.92-6.86 (m, 1H, H$_8$), 6.87-6.82 (m, 1H, H$_{10}$), 4.17-4.09 (m, 1H, H$_1$), 3.94-3.87 (m, 1H, H$_4$), 3.82 (s, 3H, H$_{12}$), 3.77-3.70 (m, 1H, H'$_4$) 2.93 (dd, J_{HH} = 13.2, 6.4 Hz, 1H, H$_5$), 2.77 (dd, J_{HH} = 13.2, 7.2 Hz, 1H, H'$_5$), 1.95-1.77 (m, 3H, H$_{3,2}$), 1.63-1.53 (m, 1H, H'$_2$). **^{13}C NMR** (126 MHz, CDCl$_3$): δ 157.7 (C$_6$ & C$_{11}$), 131.0 (C$_7$), 127.6 (C$_9$), 120.5 (C$_8$), 110.4 (C$_{10}$), 78.9 (C$_1$), 67.9 (C$_4$), 55.4 (C$_{12}$), 36.3 (C$_5$), 31.1 (C$_2$), 25.7 (C$_3$). **EI-MS:** Calculated for C$_{12}$H$_{16}$O$_2$: 192.12. Found: 192.11.
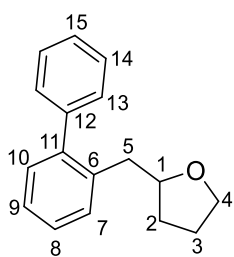
2-(2-phenyl-benzyl)tetrahydrofuran (Ik): The pure product was obtained after column chromatography (Pentane/Ethyl Acetate: 8/2) as a colorless oil (48 mg, 50%). **^{1}H NMR** (400 MHz, CDCl$_3$): δ 7.43-7.37 (m, 3H, H$_{7,14}$), 7.36-7.28 (m, 4H, H$_{10,13,15}$), 7.27-7.23 (m, 1H, H$_9$), 7.22-7.19 (m, 1H, H$_8$), 3.97-3.89 (m, 1H, H$_1$), 3.82-3.74 (m, 1H, H$_4$), 3.69-3.62 (m, 1H, H'$_4$), 2.92 (dd, J_{HH} = 14.0, 7.2 Hz, 1H, H$_5$), 2.76 (dd, J_{HH} = 14.0, 6.4 Hz, 1H, H'$_5$), 1.82-1.70 (m, 3H, H$_{2,3}$), 1.40-1.32 (m, 1H, H'$_2$). **^{13}C NMR** (126 MHz, CDCl$_3$): δ 142.4 (C$_{11}$), 142.0 (C$_{12}$), 136.6 (C$_6$), 130.2 (C$_8$), 130.1 (C$_7$), 129.6 (C$_{13}$), 128.2 (C$_{14}$), 127.5 (C$_{10}$), 126.9 (C$_{15}$), 126.2 (C$_9$), 79.8 (C$_1$), 67.8 (C$_4$), 38.7 (C$_5$), 31.2 (C$_2$), 25.6 (C$_3$). **EI-MS:** Calculated for C$_{17}$H$_{18}$O: 238.14. Found: 238.23.
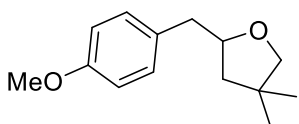
2-(4-methoxy-benzyl)-4-(dimethyl)tetrahydrofuran (IIa): The pure product was obtained after column chromatography (Heptane/Ethyl Acetate: 9/1) as a colorless oil (68 mg, 77%). Analytical data are consistent with those previously reported[58]: **^{1}H NMR** (300 MHz, CDCl$_3$): δ 7.15 (d, J_{HH} = 8.7 Hz, 2H), 6.84 (d, J_{HH} = 8.7 Hz, 2H), 4.20 (m, 1H), 3.78 (s, 3H), 3.54 (m, 2H), 2.89 (m, 1H), 2.70 (m, 1H), 1.73 (m, 1H), 1.43 (m, 1H), 1.09 (s, 3H), 1.07 (s, 3H).
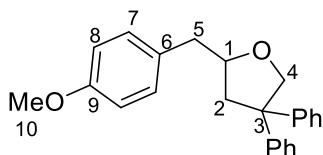
2-(4-methoxy-benzyl)-4-(diphenyl)tetrahydrofuran (IIb): The pure product was obtained after column chromatography (Pentane/Ethyl Acetate: 20/1) as a white solid (80%, 111 mg). **^{1}H NMR** (500 MHz, CDCl$_3$): δ 7.32-7.14 (m, 10H, H_{Ph}), 7.13-7.09 (m, 2H, H_7), 6.84-6.79 (m, 2H, H_8), 4.60 (dd, J_{HH} = 8.8, 1.0 Hz, 1H, H_4), 4.27-4.20 (m, 1H, H_1), 4.15 (d, J_{HH} = 8.8 Hz, 1H, H'_4), 3.78 (s, 3H, H_{10}), 2.91 (dd, J_{HH} = 13.7, 6.5 Hz, 1H, H_5), 2.75 (dd, J_{HH} = 13.7, 6.5 Hz, 1H, H'_5), 2.54 (ddd, J_{HH} = 12.1, 5.8, 1.1 Hz, 1H, H_2), 2.37 (dd, J_{HH} = 12.1, 9.4 Hz, 1H, H'_2). **^{13}C NMR** (126 MHz, CDCl$_3$): δ 158.3 (C_9), 146.3 (C_{Ph}), 146.1 (C_{Ph}), 130.7 (C_6), 130.3 (C_7), 128.5 (CH_{Ph}), 128.4 (CH_{Ph}), 127.3 (CH_{Ph}), 127.2 (CH_{Ph}), 126.5 (CH_{Ph}), 126.3 (CH_{Ph}), 114.0 (C_8), 77.0 (C_4), 76.8 (C_1), 56.1 (C_3), 55.4 (C_{10}), 44.5 (C_2), 41.5 (C_5). **EI-MS:** Calculated for C$_{24}$H$_{24}$O$_2$: 344.18. Found: 344.01.
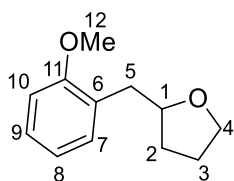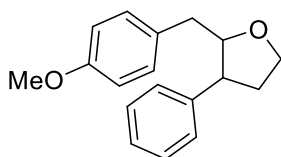

2-(4-methoxy-benzyl)-3-(phenyl)tetrahydrofuran (IIc): Crude dr: 6.1:1. The pure product was obtained after column chromatography (Heptane/Ethyl Acetate: 9/1) as a colorless oil (84 mg, 78%). Analytical data are similar to those previously reported.[5] Data for the major diastereoisomer: **^{1}H NMR** (300 MHz, CDCl$_3$): δ 7.36-7.32 (m, 2H), 7.26-7.20 (m, 3H), 7.14 (d, J_{HH} = 8.7 Hz, 2H), 6.83 (d, J_{HH} = 8.7 Hz, 2H), 4.10-3.95 (m, 3H), 3.78 (s, 3H), 2.98 (m, 1H), 2.88 (dd, J_{HH} = 14.1, 3.6 Hz, 1H), 2.72 (dd, J_{HH} = 14.1, 7.5 Hz, 1H), 2.30-2.41 (m, 1H), 2.04-2.17 (m, 1H). **^{13}C NMR** (75 MHz, CDCl$_3$): δ 157.9, 141.8, 130.8, 130.2, 128.5, 127.6, 126.5, 113.6, 86.6, 67.6, 55.1, 50.1, 38.7, 35.4. Data for the minor diastereoisomer: **^{1}H NMR** (300 MHz, CDCl$_3$): δ 7.36-7.32 (m, 2H), 7.26-7.20 (m, 3H), 6.98 (d, J_{HH} = 8.8 Hz, 2H), 6.80 (d, J_{HH} = 8.8 Hz, 2H), 4.27-4.15 (m, 2H), 3.94-3.85 (m, 1H), 3.77 (s, 3H), 3.36 (m, 1H), 2.43-2.52 (m, 3H), 2.15-2.21 (m, 1H). **^{13}C NMR** (75 MHz, CDCl$_3$): δ 157.8, 142.1, 131.2, 129.8, 128.2, 127.6, 126.3, 113.5, 83.6, 66.9, 55.1, 47.8, 36.6, 33.4. **MS (DCI-NH$_3$):** Calculated for C$_{18}$H$_{24}$NO$_2$$^+$: 286.18; Found: 286.00 (M+NH$_4$$^+$).

2-(4-methoxy-benzyl)-4-(benzyl)tetrahydrofuran (IId): Crude dr: 1.2:1. Data for the major diastereoisomer: **^{1}H NMR** (500 MHz, CDCl$_3$): δ 7.31-7.26 (m, 2H, H_{14}), 7.23-7.17 (m, 1H, H_{15}), 7.17-7.11 (m, 4H, H_7 et H_{13}), 6.86-6.81 (m, 2H, H_8), 4.09-4.02 (m, 1H, H_1), 3.85 (dd, J_{HH} = 8.5, 7.5 Hz, 1H, H_4), 3.79 (s, 3H, H_{10}), 3.58 (dd, J_{HH} = 8.3, 7.3 Hz, 1H, H'_4), 2.91 (dd, J_{HH} = 13.7, 6.4 Hz, 1H, H_5), 2.77-2.61 (m, 3H, H'_5 & H_{11}), 2.59-2.49 (m, 1H, H_3), 1.78-1.67 (m, 1H, H_2), 1.34-1.25 (m, 1H, H'_2). **^{13}C NMR** (126 MHz, CDCl$_3$): δ 158.2 (C_9), 140.8 (C_{12}), 131.0 (C_6), 130.2 (C_7), 128.7 (C_{13}), 128.5 (C_{14}), 126.2 (C_{15}), 113.9 (C_8), 81.0 (C_1), 73.2 (C_4), 55.4 (C_{10}), 41.6 (C_3), 41.4 (C_5), 39.9 (C_{11}), 38.4 (C_2). Data for the minor diastereoisomer: **^{1}H NMR** (500 MHz, CDCl$_3$): δ 7.31-7.26 (m, 2H, H_{14}), 7.23-7.17 (m, 1H, H_{15}), 7.17-7.11 (m, 4H, H_7 et H_{13}), 6.86-6.81 (m, 2H, H_8), 4.21 (pseudo quint, J_{HH} = 6.6 Hz, 1H, H_1), 3.96 (dd, J_{HH} = 8.6, 6.6 Hz, 1H, H_4), 3.79 (s, 3H, H_{10}), 3.47 (dd, J_{HH} = 8.6, 6.6 Hz, 1H, H'_4), 2.83 (dd, J_{HH} = 13.7, 6.6 Hz, 1H, H_5), 2.73-2.61 (m, 3H, H'_5 & H_{11}), 2.59-2.49 (m, 1H, H_3), 1.78-1.67 (m, 2H, H_2). **^{13}C NMR** (126 MHz, CDCl$_3$): δ 158.2 (C_9), 140.9 (C_{12}), 131.0 (C_6), 130.3 (C_7), 128.8 (C_{13}), 128.5 (C_{14}), 126.2 (C_{15}), 113.9 (C_8), 79.7 (C_1), 72.9 (C_4), 55.4 (C_{10}), 41.5 (C_5), 40.6 (C_3), 39.5 (C_{11}), 37.0 (C_2). **EI-MS:** Calculated for C$_{19}$H$_{22}$O$_2$: 282.16. Found: 282.03.

2-(4-methoxy-benzyl)-5-(pentyl)tetrahydrofuran (IIe): Crude dr: 1.5:1. The pure product was obtained after column chromatography (Heptane/Ethyl Acetate: 9/1) as a colorless oil

(71 mg, 81%). Analytical data are similar to those previously reported[5]: **^{1}H NMR** (500 MHz, CDCl$_3$): δ 7.14 (m, 2H), 6.83 (d, 2H), 4.20-4.15 (m, 0.6H, major), 4.06-4.00 (m, 0.4H, minor), 3.91-3.92 (m, 0.4H, minor), 3.80-3.86 (m, 0.6H, major), 3.78 (s, 3H), 2.95-2.88 (dd, J_{HH} = 13.5, 5.7 Hz, 1H), 2.60-2.69 (dd, J_{HH} = 13.5, 6.9 Hz, 1H), 2.00-1.78 (m, 2H), 1.62-1.32 (m, 10H), 0.91 (m, 3H). **^{13}C NMR** (126 MHz, CDCl$_3$): δ 157.9, 130.9, 130.2, 128.3, 127.7, 113.5, 80.0, 79.6, 79.4, 79.0, 55.1, 41.4, 41.2, 36.1, 36.0, 31.9, 31.4, 30.9, 25.9, 22.6, 14.0.
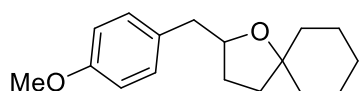
2-(4-methoxy-benzyl)-1-oxaspiro[4.5]decane (IIf): Analytical data are similar to those previously reported[5]: **^{1}H NMR** (300 MHz, CDCl$_3$): δ 7.14 (d, J_{HH} = 8.7 Hz, 2H), 6.82 (d, J_{HH} = 8.7 Hz, 2H), 4.17-4.06 (m, 1H), 3.79 (s, 3H), 2.92 (dd, J_{HH} = 13.5, 5.1 Hz, 1H), 2.62 (dd, J_{HH} = 13.5, 7.5 Hz, 1H), 1.90-1.31 (m, 14H). **EI-MS:** Calculated for C$_{17}$H$_{24}$O$_2$: 260.18. Found: 260.02.
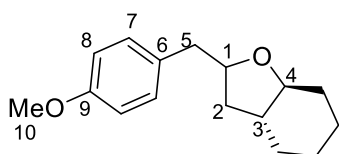
2-(4-methoxy-benzyl)-octahydrobenzofuran (IIg): Crude dr: 1.7:1. After purification by column chromatography (Pentane/Ethyl Acetate : 9/1) dr: 1:1. Data for the major diastereoisomer: **^{1}H NMR** (500 MHz, CDCl$_3$): δ 7.14 (d, J_{HH} = 8.7 Hz, 2H, H$_7$), 6.82 (d, J_{HH} = 8.7 Hz, 2H, H$_8$), 4.24-4.18 (m, 1H, H$_1$), 3.78 (s, 3H, H$_{10}$), 3.03 (pseudo td, J_{HH} = 10.4, 3.7 Hz, 1H, H$_4$), 2.87 (dd, J_{HH} = 13.6, 5.5 Hz, 1H, H$_5$), 2.64 (dd, J_{HH} = 13.6, 7.4 Hz, 1H, H'$_5$), 2.13-2.07 (m, 1H, H$_{cycle}$), 1.89-1.84 (m, 1H, H$_{cycle}$), 1.82-1.77 (m, 1H, H$_{cycle}$), 1.74 (ddd, J_{HH} = 11.8, 7.3, 2.8 Hz, 1H, H$_2$), 1.69-1.65 (m, 1H, H$_{cycle}$), 1.54 (pseudo td, J_{HH} = 11.8, 9.1 Hz, 1H, H'$_2$), 1.38-1.11 (m, 4H, H$_{cycle}$ et H$_3$), 1.08-0.98 (m, 1H, H$_{cycle}$). **^{13}C NMR** (126 MHz, CDCl$_3$): δ 158.1 (C$_9$), 131.0 (C$_6$), 130.4 (C$_7$), 113.8 (C$_8$), 83.9 (C$_4$), 78.5 (C$_1$), 55.4 (C$_{10}$), 44.2 (C$_3$), 42.2 (C$_5$), 35.4 (C$_2$), 31.6 (C$_{cycle}$), 29.2 (C$_{cycle}$), 25.9 (C$_{cycle}$), 24.5 (C$_{cycle}$). Data for the minor diastereoisomer: **^{1}H NMR** (500 MHz, CDCl$_3$): δ 7.14 (d, J_{HH} = 8.7 Hz, 2H, H$_7$), 6.82 (d, J_{HH} = 8.7 Hz, 2H, H$_8$), 4.28-4.21 (m, 1H, H$_1$), 3.78 (s, 3H, H$_{10}$), 3.12 (pseudo td, J_{HH} = 10.4, 3.7 Hz, 1H, H$_4$), 2.94 (dd, J_{HH} = 13.6, 6.1 Hz, 1H, H$_5$), 2.69 (dd, J_{HH} = 13.6, 7.0 Hz, 1H, H'$_5$), 2.13-2.07 (m, 1H, H$_{cycle}$), 2.01-1.95 (m, 1H, H$_2$), 1.89-1.84 (m, 1H, H$_{cycle}$), 1.82-1.77 (m, 1H, H$_{cycle}$), 1.69-1.65 (m, 1H, H$_{cycle}$), 1.47-1.37 (m, 1H, H$_3$), 1.38-1.11 (m, 4H, H$_{cycle}$ et H'$_2$), 1.11-1.02 (m, 1H, H$_{cycle}$). **^{13}C NMR** (126 MHz, CDCl$_3$): δ 158.1 (C$_9$), 131.0 (C$_6$), 130.4 (C$_7$), 113.8 (C$_8$), 82.6 (C$_4$), 79.4 (C$_1$), 55.4 (C$_{10}$), 46.3 (C$_3$), 42.1 (C$_5$), 37.8 (C$_2$), 31.6 (C$_{cycle}$), 29.2 (C$_{cycle}$), 25.9 (C$_{cycle}$), 24.5 (C$_{cycle}$). **EI-MS:** Calculated for C$_{16}$H$_{22}$O$_2$: 246.16. Found: 246.04.
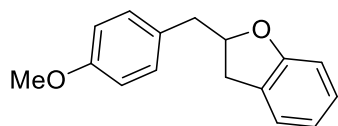
2-(4-methoxy-benzyl)-octahydrobenzofuran (IIh): Analytical data are consistent with those previously reported[59]: **^{1}H NMR** (300 MHz, CDCl$_3$): δ 7.20 (d, J_{HH} = 8.7 Hz, 2H), 7.16-7.07 (m, 2H), 6.87 (d, J_{HH} = 8.7 Hz, 2H), 6.84-6.76 (m, 2H), 5.03-4.91 (m, 1H), 3.80 (s, 3H), 3.21 (dd, J_{HH} = 15.6, 8.9 Hz, 1H), 3.13 (dd, J_{HH} = 13.9, 6.8 Hz, 1H), 2.95 (dd, J_{HH} = 15.6, 7.5 Hz, 1H), 2.88 (dd, J_{HH} = 13.9, 6.7 Hz, 1H).
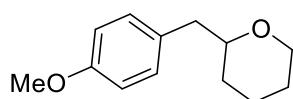
2-(4-methoxy-benzyl)tetrahydropyran (IIi): The pure product was obtained after column chromatography (Pentane/Dichloromethane: 1/1) as a colorless oil (55 mg, 66%). Analytical data are consistent with those previously reported[60]: **^{1}H NMR** (300 MHz, CDCl$_3$): δ 7.16-7.09 (d, J_{HH} = 8.7 Hz, 2H), 6.86-6.79 (d, J_{HH} = 8.7 Hz, 2H), 4.02-3.93 (m, 1H), 3.79 (s, 3H), 3.49-3.35 (m, 2H), 2.82 (dd, J_{HH} = 13.6, 6.6 Hz, 1H), 2.58 (dd, J_{HH} = 13.6, 6.3 Hz, 1H), 1.86-1.75 (m, 1H), 1.62-1.23 (m, 5H).
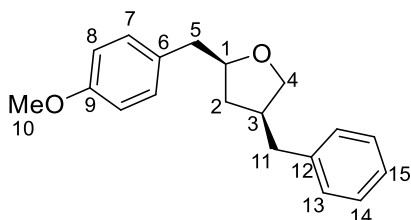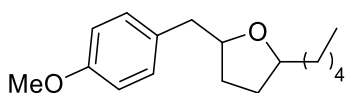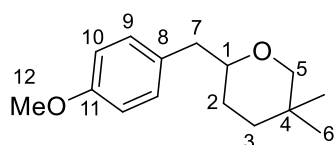
2-(4-methoxy-benzyl))-4-(dimethyl)tetrahydropyran (IIj): The pure product was obtained after column chromatography (Pentane/Dichloromethane: 1/1) as a colorless oil (55 mg, 59%). **^{1}H NMR** (400 MHz, CDCl$_3$): δ 7.16-7.10 (m, 2H, H$_9$), 6.85-6.79 (m, 2H, H$_{10}$), 3.78 (s, 3H, H$_{12}$), 3.45 (dd, J_{HH} = 11.1, 2.5 Hz, 1H, H$_5$), 3.40-3.31 (m, 1H, H$_1$), 3.14 (dd, J_{HH} = 11.1, 0.6 Hz, 1H, H'$_5$), 2.86 (dd, J_{HH} = 13.8, 6.2 Hz, 1H, H$_7$), 2.62 (dd, J_{HH} = 13.8, 6.7 Hz, 1H, H'$_7$), 1.51-1.36 (m, 3H, H$_3$ et H$_2$), 1.32-1.23 (m, 1H, H'$_3$), 1.01 (s, 3H, H$_6$), 0.78 (s, 3H, H'$_6$). **^{13}C NMR** (100 MHz, CDCl$_3$): δ 158.1 (C$_{11}$), 131.1 (C$_8$), 130.4 (C$_9$), 113.8 (C$_{10}$), 79.2 (C$_1$), 78.6 (C$_5$), 55.4 (C$_{12}$), 42.0 (C$_7$), 36.9 (C$_3$), 30.1 (C$_4$), 27.8 (C$_2$), 27.4 (C$_6$), 23.6 (C'$_6$). **EI-MS:** Calculated for C$_{15}$H$_{22}$O$_2$: 234.16. Found: 234.03.
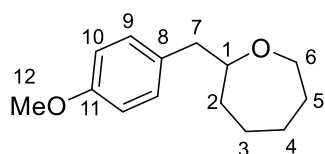
2-(4-methoxy-benzyl)oxepane (IIk): The pure product was obtained after column chromatography (Pentane/Ethyl Acetate: 8/2) as a colorless oil (62 mg, 50%). **^{1}H NMR** (500 MHz, CDCl$_3$): δ 7.15-7.10 (d, J_{HH} = 8.7 Hz, 2H, H$_9$), 6.85-6.80 (d, J_{HH} = 8.7 Hz, 2H, H$_{10}$), 3.85-3.75 (m, 1H, H$_6$), 3.79 (s, 3H, H$_{12}$), 3.68-3.61 (m, 1H, H$_1$), 3.51-3.44 (m, 1H, H'$_6$), 2.78 (dd, J_{HH} = 7.0, 13.5 Hz, 1H, H$_7$), 2.58 (dd, J_{HH} = 6.0, 13.5 Hz, 1H, H'$_7$), 1.79-1.67 (m, 3H, H$_2$ & H$_3$ & H$_5$), 1.67-1.55 (m, 2H, H$_4$ & H'$_5$), 1.53-1.41 (m, 2H, H'$_2$ & H'$_3$). **^{13}C NMR** (126 MHz, CDCl$_3$): δ 158.0 (C$_{11}$), 131.8 (C$_8$), 130.3 (C$_9$), 113.7 (C$_{10}$), 80.9 (C$_1$), 68.5 (C$_6$), 55.4 (C$_{12}$), 42.4 (C$_7$), 35.3 (C$_2$), 31.2 (C$_5$), 26.9 (C$_4$), 25.9 (C$_3$). **EI-MS:** Calculated for C$_{14}$H$_{20}$O$_2$: 220.15. Found: 220.15.
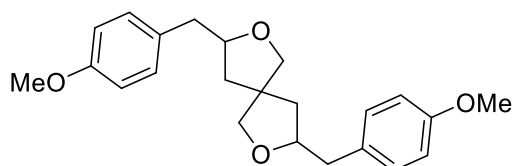
3,8-di-(4-methoxy-benzyl)-2,7-dioxaspiro[4.4] nonane, (III): The pure product was obtained after column chromatography (Heptane/Ethyl Acetate : 9/1) as a colorless oil (62 mg, 42%). **^{1}H NMR** (300 MHz, CDCl$_3$): δ 7.17-7.10 (m, 2H), 6.86-6.80 (m, 2H), 4.15-4.06 (m, 1H), 3.78 (m, 3H), 3.81-3.79 (m, 0.5H), 3.73-3.65 (m, 1H), 3.57-3.49 (m, 0.5H), 2.91-2.89 (m, 1H), 2.75-2.68 (m, 1H), 2.00-1.87 (m, 1H), 1.68-1.51 (m, 1H). **^{13}C NMR** (75 MHz, CDCl$_3$): δ 158.3, 130.6, 130.5, 130.3, 130.3, 114.0, 80.4, 80.3, 80.2, 77.7, 77.5, 77.3, 76.8, 55.4, 51.3, 51.28, 51.0, 42.8, 42.7, 42.3, 41.5, 41.3, 41.2, 41.2. **HRMS:** Calculated for C$_{23}$H$_{29}$O$_4$: 369.2066. Found: 369.2077.
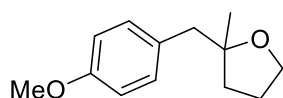
2-Methyl-2-(4-methoxy-benzyl)tetrahydrofuran (IIm): Analytical data are similar to those previously reported[14]: **^{1}H NMR** (300 MHz, CDCl$_3$): δ 7.15 (d, J_{HH} = 8.8 Hz, 2H), 6.82 (d, J_{HH} = 8.7 Hz, 2H), 3.85-3.74 (m, 2H), 3.79 (s, 3H), 2.73 (s, 2H), 1.93-1.55 (m, 4H), 1.17 (s, 3H). **^{13}C NMR** (75 MHz, CDCl$_3$): δ 158.0, 131.3, 130.7, 113.3, 82.9, 67.4, 55.2, 46.0, 36.1, 26.3, 26.0.

The stereochemistry of **IIn,IIp**[61–63] and **IIo, IIq**[5] was assigned by comparison with known related compounds.
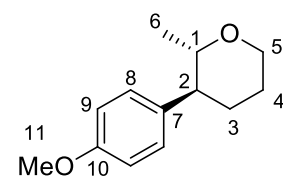
(±)-(R,R)-2-methyl, 3-(4-methoxy-phenyl)-tetrahydropyran (IIn): **^{1}H NMR** (500 MHz, CDCl$_3$): δ 7.08 (d, J_{HH} = 8.5 Hz, 2H, H$_8$), 6.84 (d, J_{HH} = 8.5 Hz, 2H, H$_9$), 4.07-4.01 (m, 1H, H$_5$), 3.79 (s, 3H, H$_{11}$), 3.55 (td, J_{HH} = 11.5, 2.5 Hz, 1H, H$_5$), 3.48 (dq, J_{HH} = 10.0, 6.0 Hz, 1H, H$_1$), 2.38-2.31 (m, 1H, H$_2$), 1.96-1.89 (m, 1H, H$_3$), 1.82-1.63 (m, 3H, H'$_3$ et H$_4$), 0.97 (d, J_{HH} = 6.0 Hz, 3H, H$_6$). **^{13}C NMR** (126 MHz, CDCl$_3$): δ 158.3 (C$_{10}$), 136.1 (C$_7$), 128.7

(C$_8$), 114.0 (C$_9$), 78.6 (C$_1$), 68.6 (C$_5$), 55.4 (C$_{11}$), 49.8 (C$_2$), 32.5 (C$_3$), 26.8 (C$_4$), 20.2 (C$_6$). **EI-MS:** Calculated for C$_{13}$H$_{18}$O$_2$: 206.13. Found: 205.98.
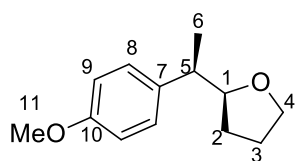
(±)-(R,S)-2-(1-(4-methoxyphenyl)ethyl)-tetrahydrofuran (IIo): **¹H NMR** (400 MHz, CDCl$_3$): δ 7.20-7.14 (m, 2H, H$_8$), 6.87-6.82 (m, 2H, H$_9$), 3.97-3.88 (m, 1H, H$_1$), 3.82-3.75 (m, 1H, H$_4$), 3.78 (s, 3H, H$_{11}$), 3.72-3.65 (m, 1H, H'$_4$), 2.76 (app quint, J$_{HH}$ = 7.2 Hz, 1H, H$_5$), 2.00-1.90 (m, 1H, H$_2$), 1.88-1.77 (m, 2H, H$_3$), 1.61-1.50 (m, 1H, H'$_2$), 1.24 (d, J$_{HH}$ = 7.2 Hz, 3H, H$_6$). **¹³C NMR** (100 MHz, CDCl$_3$): δ 158.1 (C$_{10}$), 136.9 (C$_7$), 128.8 (C$_8$), 113.8 (C$_9$), 84.0 (C$_1$), 68.3 (C$_4$), 55.4 (C$_{11}$), 44.1 (C$_5$), 29.7 (C$_2$), 26.0 (C$_3$), 18.4 (C$_6$). **EI-MS:** Calculated for C$_{13}$H$_{18}$O$_2$: 206.13. Found: 206.08.
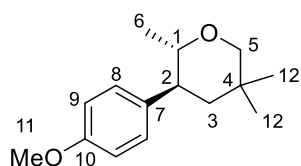
(±)-(R,R)-2,4,4-tri-methyl, 3-(4-methoxy-phenyl)-tetrahydropyran (IIp): **¹H NMR** (400 MHz, CDCl$_3$): δ 7.08 (d, J$_{HH}$ = 8.8 Hz, 2H, H$_8$), 6.83 (d, J$_{HH}$ = 8.8 Hz, 2H, H$_9$), 3.79 (s, 3H, H$_{11}$), 3.53 (dd, J$_{HH}$ = 11.1 Hz, 2.6 Hz, 1H, H$_5$), 3.38 (dq, J$_{HH}$ = 10.0, 6.1 Hz, 1H, H$_1$), 3.30 (dd, J$_{HH}$ = 11.1, 0.5 Hz, 1H, H'$_5$), 2.55 (ddd, J$_{HH}$ = 12.4, 10.0, 4.0 Hz, 1H, H$_2$), 1.65-1.49 (m, 2H, H$_3$), 1.13 (s, 3H, H$_{12}$), 1.01 (d, J$_{HH}$ = 6.1 Hz, 3H, H$_6$), 0.86 (s, 3H, H'$_{12}$). **¹³C NMR** (100 MHz, CDCl$_3$): δ 158.3 (C$_{10}$), 135.7 (C$_7$), 128.8 (C$_8$), 114.0 (C$_9$), 78.8 (C$_1$), 78.4 (C$_5$), 55.4 (C$_{11}$), 46.0 (C$_3$), 45.9 (C$_2$), 31.3 (C$_4$), 27.3 (C$_{12}$), 24.1 (C'$_{12}$), 19.8 (C$_6$).
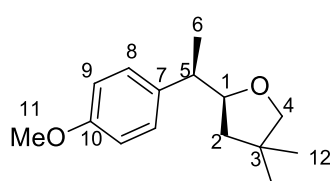
(±)-(R,S)-2-(1-(4-methoxyphenyl)ethyl)-4-(dimethyl)tetrahydrofuran (IIq): **¹H NMR** (400 MHz, CDCl$_3$): δ 7.11 (d, J$_{HH}$ = 8.8 Hz, 2H, H$_8$), 6.83 (d, J$_{HH}$ = 8.8 Hz, 2H, H$_9$), 4.08-4.00 (m, 1H, H$_1$), 3.79 (s, 3H, H$_{11}$), 3.50-3.46 (m, 2H, H$_4$), 2.72-2.65 (app quint, J$_{HH}$ = 7.0 Hz, 1H, H$_5$), 1.44 (dd, J$_{HH}$ = 12.4, 6.5 Hz, 1H, H$_2$), 1.34-1.28 (m, 1H, H'$_2$), 1.33 (d, J$_{HH}$ = 7.0 Hz, 3H, H$_6$), 1.02 (s, 3H, H$_{12}$), 1.01 (s, 3H, H'$_{12}$). **¹³C NMR** (100 MHz, CDCl$_3$): δ 158.3 (C$_{10}$), 135.7 (C$_7$), 128.8 (C$_8$), 113.8 (C$_9$), 84.5 (C$_1$), 80.4 (C$_4$), 55.4 (C$_{11}$), 45.6 (C$_2$), 45.2 (C$_5$), 31.3 (C$_3$), 26.7 (C$_{12}$), 26.6 (C'$_{12}$), 19.1 (C$_6$).

4. Catalytic oxy-arylation under air with reagent-grade chemicals
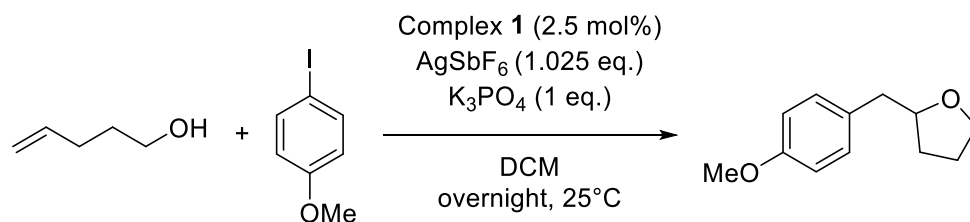
Under air, a Schlenk equipped with a magnetic stirrer bar was charged with silver hexafluoroantimonate (240 mg, 0.82 mmol) and potassium phosphate tribasic (170 mg, 0.80 mmol) in DCM (0.8 mL, reagent grade from commercial bottle, not degassed or dried). Complex **1** (13 mg, 0.02 mmol) was transferred into a small glass vial and dissolved in DCM (1.2 mL). 4-Iodoanisole (187 mg, 0.80 mmol, 1 eq.), 4-penten-1-ol (83 μL, 0.80 mmol, 1 eq.) and internal standard dibenzylether (0.2 mmol, 39 μL) were added to the gold complex solution. This solution was added to the Schlenk under agitation. The reaction mixture was then stirred at 25°C. The reaction was monitored by NMR spectroscopy by taking an aliquot of the crude reaction mixture (NMR yield: 94%).

5. Catalytic oxy-arylation of alkene: scale-up
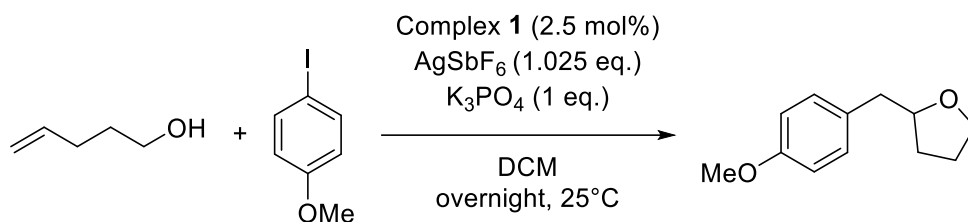
In a glovebox, a dry Schlenk equipped with a magnetic stirrer bar was charged with silver hexafluoroantimonate (1.752 g, 5.1 mmol) and potassium phosphate tribasic (1.061 mg, 5.0 mmol) in DCM (5 mL). Complex **1** (82 mg, 0.1 mmol) was transferred into a small glass vial and dissolved in DCM (7.5 mL). 4-Iodoanisole (5.0 mmol, 1 eq.), 4-penten-1-ol (5.0 mmol, 1 eq.) and internal standard dibenzylether (1.2 mmol, 0.25 mL) were added to the gold complex solution. This solution was loaded into a plastic syringe equipped with stainless steel needle. The syringe was closed by blocking the needle with a septum. Outside the glovebox, the prepared solution was added to the Schlenk under agitation. The reaction mixture was then stirred at 25°C. The reaction was monitored by NMR spectroscopy by taking an aliquot of the crude reaction mixture (NMR yield: 96%). Silver salt was filtrated and the product was purified through column chromatography (pentane/ethyl acetate: 8/2). The product was obtained as a colorless oil (672 mg, 3.5 mmol, 70%).

6. Gold-catalyzed amino-arylation of alkenes
6.1 Synthesis of substrate

N-(2,2-dimethyl-4-penten-1-yl)-4-methyl-benzenesulfonamide (**5b**)[64], *N*-(3-phenyl-4-penten-1-yl)- 4-methyl benzenesulfonamide (**5c**)[65], *N*-[1-(3-buten-1-yl)hexyl]-4-methyl-benzenesulfonamide (**5d**)[5] and *N*-[(4-methylphenyl)sulfonyl]-4-pentenamide (**5e**)[66] , 3-phenyl-n-tosylpent-4-enamide (**5f**)[66] were prepared according to reported procedures.
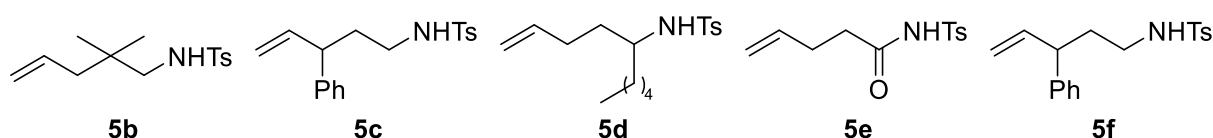
N-tosyl pent-4-enyl amine (5a):
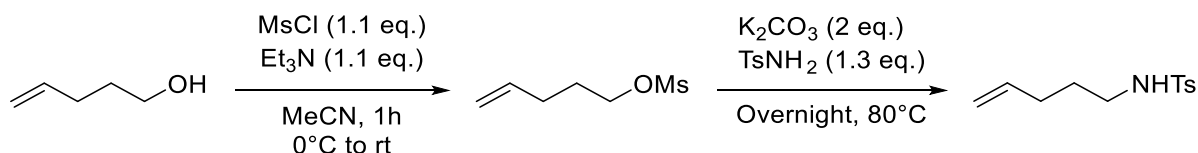
To a solution of 4-penten-1-ol (1.5 mL, 14.5 mmol) in MeCN (15 mL) were added MsCl (1.24 mL, 16.0 mmol, 1.1 eq) and Et₃N (2.16 mL, 16.0 mmol, 1.1 eq) successively at 0°C. The mixture was allowed to warm to room temperature. After 1 h, K₂CO₃ (4.0 g, 29 mmol, 2 eq) and TsNH₂ (3.20 g, 19 mmol, 1.1 eq) were added, and then the mixture was heated to 80°C overnight. The solution was filtrated and the solvent was removed under reduced pressure.

The residue was purified through flash chromatography with petroleum ether/ethyl acetate (9:1). The product was obtained as a yellow oil (1.49 g, 6.2 mmol, 43%). Analytical data are consistent with those previously reported:[5] **¹H NMR** (300 MHz, CDCl₃): δ 7.78-7.71 (m, 2H), 7.33-7.28 (m, 2H), 5.78-5.63 (m, 1H), 5.02-4.92 (m, 2H), 4.41 (bs, 1H), 2.95 (q, J_{HH} = 6.8 Hz, 2H), 2.43 (s, 3H), 2.09-1.99 (m, 2H), 1.62-1.50 (m, 2H).

6.2 General procedure for the gold-catalyzed amino-arylation of alkenes
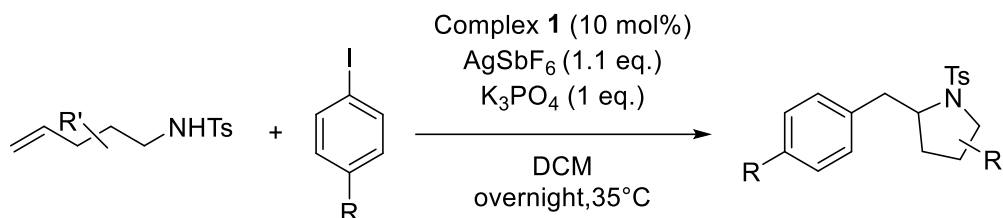
In a glovebox, a dry Schlenk equipped with a magnetic stirrer bar was charged with silver hexafluoroantimonate (150 mg, 0.44 mmol) and potassium phosphate tribasic (85 mg, 0.40 mmol) in solvent (0.4 mL). Complex **1** (26 mg, 0.04 mmol) was transferred into a small glass vial and dissolved in solvent (0.6 mL). Aryl iodide (0.40 mmol, 1 eq.), functionalized alkene (0.40 mmol, 1 eq.) and internal standard dibenzylether (0.10 mmol, 20 μL) were added to the gold complex solution. This solution was loaded into a plastic syringe equipped with stainless steel needle. The syringe was closed by blocking the needle with a septum. Outside the glovebox, the prepared solution was added to the Schlenk under agitation. The reaction mixture was then stirred at 35°C. The reaction was monitored by NMR spectroscopy by taking an aliquot of the crude reaction mixture. To isolate the product, silver salts were removed by filtration and the sample was purified by column chromatography.
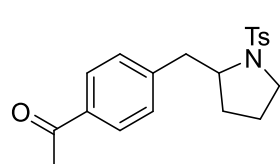
2-(4-acetyl-benzyl)-1-(toluene-4-sulfonyl)pyrrolidine (IIIa): Analytical data are consistent with those previously reported[5]: **¹H NMR** (300 MHz, CDCl₃): δ 7.90 (d, J_{HH} = 8.3 Hz, 2H), 7.75 (d, J_{HH} = 8.3 Hz, 2H), 7.39-7.28 (m, 4H), 3.88-3.79 (m, 1H), 3.41-3.34 (m, 1H), 3.27 (dd, J_{HH} = 13.3, 3.6 Hz, 1H), 3.18-3.08 (m, 1H), 2.88 (dd, J_{HH} = 13.3, 9.1 Hz, 1H), 2.60 (s, 3H), 2.43 (s, 3H), 1.65-1.54 (m, 2H), 1.51-1.43 (m, 2H).
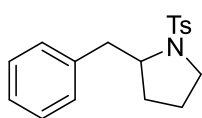
2-Benzyl-1-(toluene-4-sulfonyl)pyrrolidine (IIIb): Analytical data are consistent with those previously reported[5]: **¹H NMR** (300 MHz, CDCl₃): δ 7.70 (d, J_{HH} = 8.1 Hz, 2H), 7.27-7.12 (m, 7H), 3.80-3.69 (m, 1H), 3.39-3.27 (m, 1H), 3.18 (dd, J_{HH} = 13.3, 3.4 Hz, 1H), 3.12-3.00 (m, 1H), 2.70 (dd, J_{HH} = 13.3, 9.6 Hz, 1H), 2.35 (s, 3H), 1.65-1.48 (m, 2H), 1.45-1.27 (m, 2H).
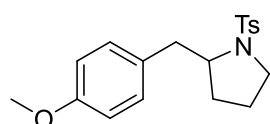
2-(4-methoxy-benzyl)-1-(toluene-4-sulfonyl)pyrrolidine (IIIc): Analytical data are consistent with those previously reported[65]: **¹H NMR** (300 MHz, CDCl₃): δ 7.75 (d, J_{HH} = 8.2 Hz, 2H), 7.31 (d, J_{HH} = 8.2 Hz, 2H), 7.16 (d, J_{HH} = 8.5 Hz, 2H), 6.84 (d, J_{HH} = 8.5 Hz, 2H), 3.80-3.73 (m, 1H), 3.79 (s, 3H), 3.42-3.33 (m, 1H), 3.19-3.07 (m, 2H), 2.72 (dd, J_{HH} = 13.5, 9.6 Hz, 1H), 2.42 (s, 3H), 1.66-1.56 (m, 2H), 1.49-1.36 (m, 2H).
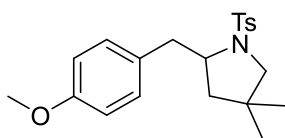
2-(4-methoxy-benzyl)-4,4-dimethyl-1-(toluene-4-sulfonyl)pyrrolidine (IIId): The pure product was obtained after column chromatography **(**Petroleum ether/DCM: 8/2**)** as a colorless oil (96 mg, 64%). Analytical data are consistent with those previously reported [67]: **^{1}H NMR** (300 MHz, CDCl$_3$): δ 7.78 (d, J_{HH} = 8.4 Hz, 2H), 7.32 (d, J_{HH} = 8.4 Hz, 2H), 7.14 (d, J_{HH} = 8.6 Hz, 2H), 6.83 (d, J_{HH} = 8.6 Hz, 2H), 3.78 (s, 3H), 3.75-3.70 (m, 1H), 3.44-3.49 (m, 1H), 3.07-3.14 (m, 2H), 2.71-2.78 (m, 1H), 2.42 (s, 3H), 1.49-1.46 (m, 2H), 0.97 (s, 3H), 0.44 (s, 3H).
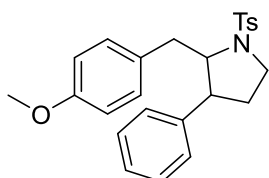
2-(4-methoxy-benzyl)-3-phenyl-1-(toluene-4-sulfonyl)pyrrolidine (IIIe): Crude dr: 10.1:1. The pure product was obtained after column chromatography **(**Petroleum ether/Ethyl acetate: 7/3**)** as a colorless oil (98 mg, 58%). Analytical data are similar to those previously reported.[65] Data for the major diastereoisomer: **^{1}H NMR** (300 MHz, CDCl$_3$): δ 7.78 (m, 2H), 7.32 (m, 2H), 7.28 (m, 2H), 7.06-7.12 (m, 3H), 6.87 (m, 2H), 6.61 (m, 2H), 3.90-3.86 (m, 1H), 3.80 (s, 3H), 3.59-3.51 (m, 1H), 3.26-3.93 (m, 4H), 2.47 (s, 3H), 1.89-1.77 (m, 1H), 1.51-1.39 (m, 1H). **^{13}C NMR** (75 MHz, CDCl$_3$): δ 158.1, 143.4, 141.6, 134.8, 131.2, 129.6, 129.2, 128.4, 127.34, 126.9, 126.3, 113.6, 68.0, 55.1, 49.0, 47.9, 39.4, 32.2, 21.4. **HRMS**: Calculated for C$_{25}$H$_{28}$NO$_3$S: 422.1790. Found: 422.1799.
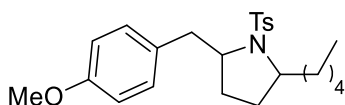
2-(4-methoxy-benzyl)-5-pentyl-1-(toluene-4-sulfonyl)pyrrolidine (IIIf): Crude dr: 1:1. The pure product was obtained after column chromatography **(**Petroleum ether/DCM: 8/2**)** as a colorless oil (101 mg, 61%). Analytical data are similar to those previously reported.[5] Data for the mixture of diastereoisomers: **^{1}H NMR** (300 MHz, CDCl$_3$): δ 7.80 (d, J_{HH} = 8.5 Hz, 2H), 7.73 (d, J_{HH} = 8.5 Hz, 2H), 7.31-7.26 (m, 4H), 7.16 (d, J_{HH} = 8.5 Hz, 2H), 7.09 (d, J_{HH} = 8.5 Hz, 2H), 6.82 (m, 4H), 4.02 (m, 1H), 3.85 (m, 1H), 3.79 (s, 6H), 3.74 (m, 1H), 3.54 (m, 1H), 3.32 (dd, J_{HH} = 13.2, 3.3 Hz, 1H), 3.16 (dd, J_{HH} = 13.5, 3.3 Hz, 1H), 2.42 (m, 1H), 2.41 (m, 6H), 1.90-1.12 (m, 25H), 0.83-0.91 (m, 6H). **^{13}C NMR** (75 MHz, CDCl$_3$): δ 158.2, 158.1, 143.1, 142.6, 139.9, 135.0, 130.9, 130.7, 130.4, 130.3, 129.5, 129.4, 127.5, 126.9, 113.8, 113.6, 62.9, 62.3, 62.1, 61.0, 55.2, 42.0, 39.3, 36.7, 33.7, 31.7, 31.6, 29.4, 28.5, 27.5, 27.1, 26.0, 25.9, 22.5, 21.5, 21.4, 14.0, 13.9. **MS (DCI-NH$_3$):** Calculated for C$_{24}$H$_{34}$NO$_3$S$^+$: 416.30; Found: 416.00 (M+H$^+$).
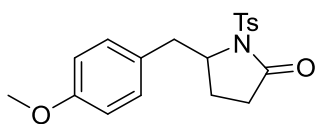
5-(4-methoxy-benzyl)-1-(toluene-4-sulfonyl)-2-pyrrolidinone (IIIg): The pure product was obtained after column chromatography **(**pentane/DCM: 7/3**)** as a colorless waxy oil (68 mg, 47%). **^{1}H NMR** (400 MHz, CD$_3$OD, 213K): δ 7.74 (d, J_{HH} = 7.9 Hz, 2H), 7.70 (d, J_{HH} = 7.8 Hz, 2H), 7.40 (d, J_{HH} = 8.0 Hz, 2H), 7.30 (d, J_{HH} = 8.0 Hz, 2H), 7.13 (d, J_{HH} = 8.0 Hz, 2H), 7.02 (d, J_{HH} = 8.5 Hz, 2H), 6.86 (d, J_{HH} = 8.2 Hz, 2H), 6.80 (d, J_{HH} = 8.3 Hz, 2H), 5.00 (m, 1H), 4.88 (m, 1H), 3.79 (s, 3H), 3.75 (s, 3H), 3.05-2.85 (m, 6H), 2.69 (m, 1H), 2.45 (s, 3H), 2.41 (s, 3H), 2.24 (m, 3H), 2.00-1.89 (m, 2H). **^{13}C NMR** (101 MHz, CD$_3$OD, 213K): δ 183.9, 178.6, 160.0, 159.9, 145.2, 145.2, 139.4, 138.7, 131.8, 131.7, 130.7, 130.3, 129.2, 128.9, 128.9, 128.0, 114.7, 114.7, 91.9, 87.0, 55.5, 55.4, 40.3, 40.3, 33.4, 31.5, 28.3, 27.3, 24.1, 21.6. Broad signals are observed in CDCl$_3$. The resolution is better in CD$_3$OD at 213K, two conformers in ~1:1 ratio are distinguished. **MS (DCI/CH$_4$):** Calculated for C$_{19}$H$_{22}$NO$_4$S$^+$: 360.13. Found: 360.00.
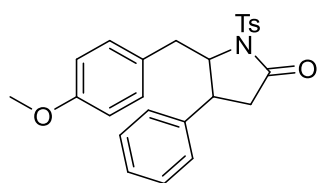
5-(4-methoxy-benzyl)-4-phenyl-1-(toluene-4-sulfonyl)-2-pyrrolidinone (IIIh): Crude dr: 1.5:1. **^{1}H NMR** (400 MHz, CD$_3$OD, 213 K): δ 7.77 (m, 1H), 7.69 (m, 1H), 7.42-7.25 (m, 7H), 7.07 (m, 2H), 6.90 (m, 1H), 6.78 (m, 1H), 4.93 (m, 0.6H), 4.82 (m, 0.4H), 3.80-3.73 (m, 3H), 3.60 (m, 1H), 3.44 (m, 1.2H), 3.09 (m, 0.7H), 2.98-2.79 (m, 2.8H), 2.45-2.41(m, 3H). **^{13}C NMR** (101 MHz, CD$_3$OD, 213 K): δ 180.6, 175.5, 158.6, 158.5, 143.9, 143.9, 138.2, 138.0, 137.5, 137.3, 129.4, 129.2, 129.0, 128.8, 128.7, 127.9, 127.8, 127.6, 127.5, 126.7, 125.8, 113.2, 95.1, 90.9, 87.8, 56.9, 54.1, 54.0, 40.2, 38.6, 37.2, 37.0. **MS (DCI/CH$_4$):** Calculated for C$_{25}$H$_{26}$NO$_4$S$^+$: 336.15. Found: 336.16.

6.3 Synthesis of Anysomycin's analogue
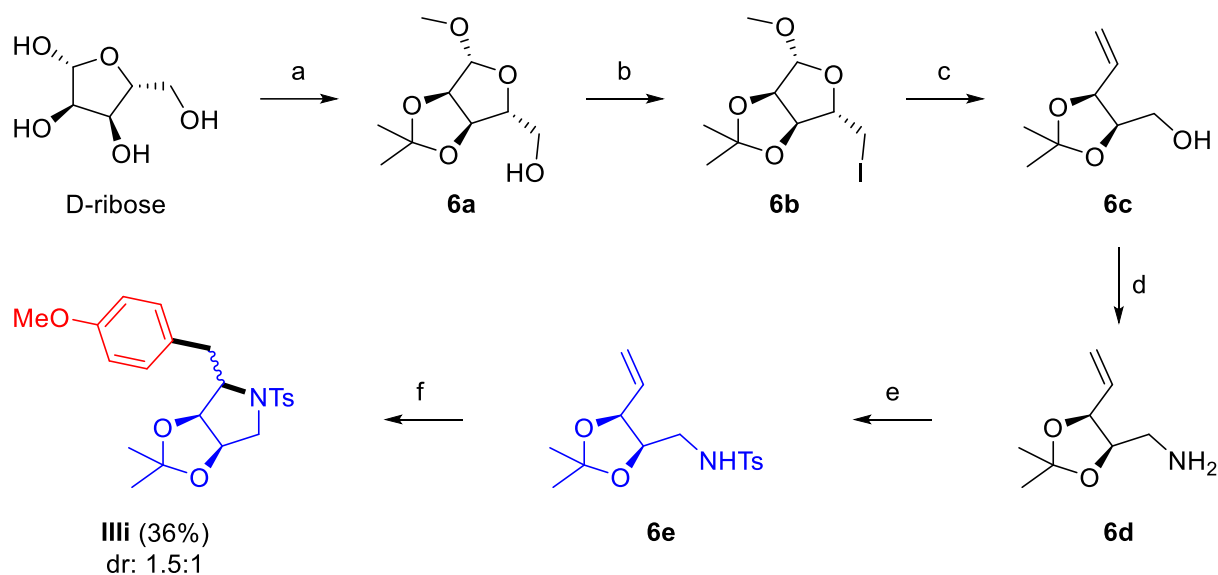
Step a: In a round bottom flask, D-Ribose (7.5 g, 50 mmol) was dissolved in acetone (30 mL) and methanol (30 mL). 0.5 mL of sulfuric acid was added and the solution was heated to 40°C for 20 h. The reaction was quenched with NaHCO$_3$. The solution was filtered and solvent was evaporated under *vacuum* to obtain a viscous oil. THF was added, and the insoluble were filtered off. The product **6a** was obtained as a colorless oil (9.54 g, 46.5 mmol, 93%).

Step b: In a round bottom flask, **6a** (9.54 g, 46.5 mmol) was dissolved in THF (200 mL). Triphenylphosphine (18.4 g, 70.2 mmol, 1.5 eq.) and imidazole (6.36 g, 93.4 mmol, 2 eq.) were added. At 0°C, iodine was added portion wise until the brown coloration remained. The reaction mixture was stirred overnight at rt. The solution was filtered and solvent was evaporated under *vacuum*. After purification by column chromatography (petroleum ether/ethyl acetate: 80/20), product **6b** was obtained as a colorless oil (10.55 g, 33.5 mmol, 72%).

Step c: 13 g of Zn was activated with 12 mL of ClSiMe$_3$ in 180 mL of Et$_2$O, stirring for 1h30. Solvent was removed under *vacuum* and Zn was redissolved in 120 mL of EtOH. Product **6b** (5.6 g, 17.8 mmol) was dissolved in 50 mL of EtOH and added to the previous solution. The reaction was stirred for 1 h at 80°C, filtered on celite and the solvent was removed carefully (the aldehyde is volatile).

To a solution of aldehyde in EtOH (25 mL), NaBH$_4$ (812 mg, 21.4 mmol, 1.2 eq.) was added dropwise at 0°C. The reaction was stirred for 1h when going back to room temperature.

Solvent was removed under *vacuum* and then 45 mL of water was added. Product was extracted with ethyl acetate. The organic phases were washed with brine and dried over Na_2SO_4. The product **6c** was obtained after column chromatography (petroleum ether/ethyl acetate: 70/30) as a colorless oil (901 mg, 5.7 mmol, 32%).

Step d: In a Schlenk, compound **6c** (901 mg, 5.7 mmol), triphenylphosphine (1.8 g, 6.8 mmol, 1.2 eq.), phthalimide (839 mg, 5.7 mmol, 1 eq.) were dissolved in 25 mL of anhydrous THF. DIAD (1.3 mL, 6.8 mmol, 1.2 eq.) was added dropwise. The reaction mixture was stirred at rt for 2 h under inert atmosphere. Solvent was evaporated under vacuum and after purification by column chromatography (petroleum ether/ethyl acetate: 70/30), the phthalimide compound was obtained as a yellow solid (1.3 g, 4.5 mmol, 80%).

In a round bottom flask, the phthalimide compound (510 mg, 1.8 mmol) was dissolved in methanol (20 mL) and hydrazine monohydrate was added (0.15 mL, 3.1 mmol, 1.7 eq.). The reaction was heated at 60°C for 4 h. When going back to rt, a white solid was formed which was dissolved by adding a solution of KOH (141 mg, 2.5 mmol) in methanol (3 mL). The resulting solution was concentrated and product was extracted with DCM. The combine organic layers were washed with brine and dried over Na_2SO_4. Solvent was removed under *vacuum* and the product **6d** was obtained as a yellow oil (163 mg, 1.04 mmol, 60%).

Step e: In a round bottom flask, amine **6d** (113 mg, 0.72 mmol) and tosyl chloride (137 mg, 0.72 mmol, 1 eq.) were dissolved in DCM (4 mL). Triethylamine (0.15 mL, 1.08 mmol, 1.5 eq.) was added and the reaction mixture was stirred overnight at rt. Reaction mixture was diluted with 5 mL of H_2O and extracted with Et_2O. The combine organic layers were washed with brine and dried over Na_2SO_4. Pure product was obtained after column chromatography (Pentane/Ethyl acetate: 90/10) as a white solid (190 mg, 0.61 mmol, 84%).

Step f: General procedure for the gold-catalyzed amino-arylation of alkenes
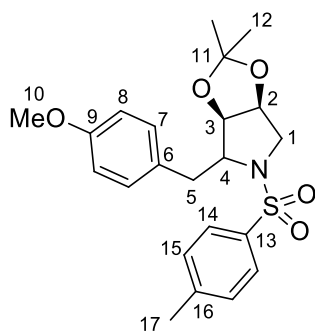
Anysomicin's analogue (IIIi): Crude dr: 1.5 :1. The pure product was obtained after column chromatography (pentane/DCM: 7/3) as a colorless oil (44 mg, 36%). Data for the major diastereoisomer: **^{1}H NMR** (500 MHz, $CDCl_3$): δ 7.76 (d, J_{HH} =7.7 Hz, 2H, H_{14}), 7.19 (d, J_{HH} = 8.5 Hz, 2H, H_7), 7.28 (d, J_{HH} = 7.7 Hz, 2H, H_{15}), 6.85 (d, J_{HH} = 8.5 Hz, 2H, H_8), 4.43 (d, J_{HH} = 5.5 Hz, 1H, H_3), 4.30 (app td, J_{HH} = 5.5, 1.5 Hz, 1H, H_2), 4.19 (dd, J_{HH} = 8.0, 4.0 Hz, 1H, H_4), 3.80 (s, 3H, H_{10}), 3.42 (dd, J_{HH} = 12.5, 2.0 Hz, 1H, H_1), 3.30 (dd, J_{HH} = 12.5, 5.5 Hz, 1H, H_1), 3.00-2.93 (m, 1H, H_5), 2.88 (dd, J_{HH} = 14.0, 8.0 Hz, 1H, H_5), 2.40 (s, 3H, H_{17}), 1.10 (s, 3H, H_{12}), 0.83 (s, 3H, H'$_{12}$). **^{13}C NMR** (126 MHz, $CDCl_3$): δ 158.7 (C_9), 143.4 (C_{16}), 136.7 (C_{13}), 130.8 (C_7), 129.6 (C_{15}), 128.8 (C_6), 127.6 (C_{14}), 114.3 (C_8), 111.6 (C_{11}), 83.5 (C_3), 79.1 (C_2), 67.1 (C_4), 55.4 (C_{10}), 53.9 (C_1), 38.7 (C_5), 21.6 (C_{17}), 25.9 (C'$_{12}$), 24.6 (C_{12}). Data for the minor diastereoisomer: **^{1}H NMR** (500 MHz, $CDCl_3$): δ 7.74 (d, J_{HH} = 7.7 Hz, 2H, H_{14}), 7.35 (d, J_{HH} = 7.7 Hz, 2H, H_{15}), 7.19 (d, J_{HH} = 8.5 Hz, 2H, H_7), 6.81 (d, J_{HH} = 8.5 Hz, 2H, H_8), 4.41 (app td, J_{HH} = 6.0, 1.7 Hz, 1H, H_2), 4.27 (dd, J_{HH} = 6.5, 5.0 Hz, 1H, H_3), 3.78 (s, 3H, H_{10}), 3.68 (dd, J_{HH} = 11.5, 2.0 Hz, 1H, H_1), 3.42 (dd, J_{HH} = 13.0, 2.0 Hz, 1H, H_5), 3.08 (dd, J_{HH} = 13.5, 11.0 Hz, 1H, H_5), 3.00 (dd, J_{HH} = 12.0, 6.0 Hz, 1H, H_1), 3.98-2.93 (m, 1H, H_4), 2.45 (s, 3H, H_{17}), 1.58 (s, 3H, H_{12}), 1.27 (s, 3H, H'$_{12}$). **^{13}C NMR** (126 MHz, $CDCl_3$): δ 158.3 (C_9), 144.1 (C_{16}), 133.2 (C_{13}), 130.7 (C_7), 130.3 (C_6), 129.9 (C_{15}), 128.0 (C_{14}), 113.8 (C_8), 112.3 (C_{11}), 80.2 (C_3), 76.0 (C_2), 66.0 (C_4), 55.4 (C_1), 55.4 (C_{10}), 33.3

(C$_5$), 21.7 (C$_{17}$), 26.8 (C$_{12}$), 25.5 (C'$_{12}$). **MS (DCI/NH$_3$):** Calculated for C$_{22}$H$_{27}$NO$_5$S$^+$: 418.2. Found: 418.2.

7. Control experiment for no cyclization at gold(I)
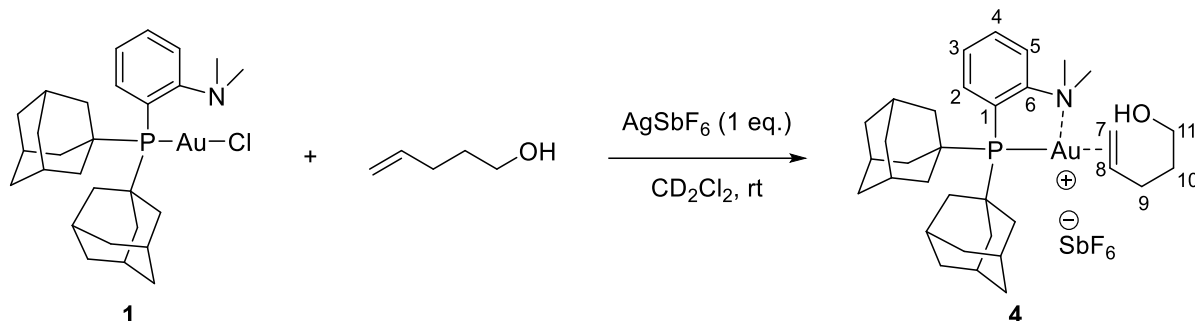
In a glovebox, a screw-cap NMR tube was charged with silver hexafluoroantimonate (8.0 mg, 0.023 mmol) in dichloromethane-d$_2$ (0.2 mL). Complex **1** (15 mg, 0.023 mmol) was transferred into a small glass vial and dissolved in dichloromethane-d$_2$ (0.4 mL). The 4-penten-1-ol (2.4 µL, 0.023 mmol) was added to the gold solution. The prepared solution was loaded into a plastic syringe equipped with stainless steel needle. The syringe was closed by blocking the needle with a septum. Outside the glovebox, the NMR tube was cooled down to -80°C. At this temperature, the prepared solution was added. The tube was gently shaken and allowed to warm to rt. The reaction was monitored by ^{31}P{^{1}H} NMR spectroscopy.

Complex 4: ^{1}**H NMR** (500 MHz, CD$_2$Cl$_2$): δ 7.80 (t, J$_{HH}$ = 4.6 Hz, 1H, H$_5$), 7.73 (t, J$_{HH}$ = 3.1Hz, 2H, H$_3$ & H$_4$), 7.54-7.47 (m, 1H, H$_2$), 5.84-5.56 (m, 1H, H$_8$), 3.96 (dd, J$_{HH}$ = 8.7, 5.8 Hz, 1H, H$_7$), 3.83 (dd, J$_{HH}$ = 14.7, 5.8 Hz, 1H, H'$_7$), 3.77 (q, J$_{HH}$ = 3.8 Hz, 2H, H$_{11}$), 3.03 (s, 3H, N(CH$_3$)$_2$), 2.99 (s, 3H, N(CH$_3$)$_2$), 2.70-2.62 (m, 1H H$_9$), 2.30-2.23 (m, 1H, H'$_9$), 2.17-2.00 (m, 12H, H$_{Ad}$), 1.92 (bs, 7H, H$_{Ad}$ & H$_{10}$), 1.77-1.65 (m, 13H, H$_{Ad}$ & H'$_{10}$). ^{31}P{^{1}H} **NMR** (162 MHz, CD$_2$Cl$_2$): δ 58.0 (s). ^{13}**C NMR** (126 MHz, CD$_2$Cl$_2$): δ 158.4 (d, J$_{CP}$ = 9.6 Hz, C$_6$), 136.4 (s, C$_5$), 134.5 (d, J$_{CP}$ = 1.2 Hz, C$_4$), 128.1 (d, J$_{CP}$ = 5.7 Hz, C$_2$), 125.2 (d, J$_{CP}$ = 42.0 Hz, C$_1$), 124.8 (d, J$_{CP}$ = 4.4 Hz, C$_3$), 108.6 (s, C$_8$), 75.2 (d, J$_{CP}$ = 18.0 Hz, C$_7$), 62.5 (s, C$_{11}$), 52.4 (s, N(CH$_3$)$_2$), 42.1 (d, J$_{CP}$ = 27.1 Hz, C$_{qtAd}$), 41.1 (t, J$_{CP}$ = 19.1 Hz, CH$_{2Ad}$), 36.4 (s, CH$_{2Ad}$), 33.3 (s, C$_{10}$), 31.9 (s, C$_9$), 28.9 (bs, C$_{HAd}$).

8. Catalytic oxy-arylation catalyzed by gold(III) complex
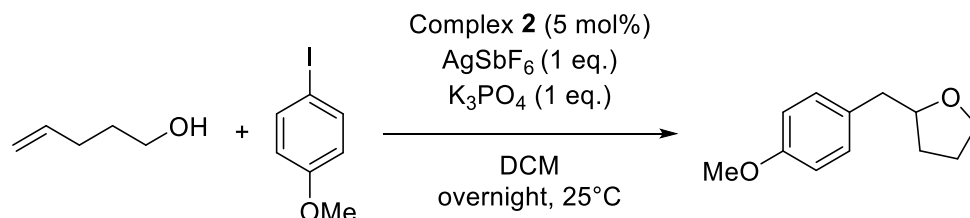
In a glovebox, a dry Schlenk equipped with a magnetic stirrer bar was charged with silver hexafluoroantimonate (62 mg, 0.18 mmol) and potassium phosphate tribasic (38 mg, 0.18 mmol) in dichloromethane (0.2 mL). Complex **2** (10 mg, 0.01 mmol) was transferred into a small glass vial and dissolved in solvent (0.3 mL). The aryl iodide (41 mg, 0.17 mmol, 0.95

eq.), the functionalized alkene (16 µL, 0.18 mmol, 1 eq.) and dibenzylether (internal standard, 0.04 mmol, 8 µL) were added to the gold complex solution. This solution was loaded into a plastic syringe equipped with stainless steel needle. The syringe was closed by blocking the needle with a septum. Outside the glovebox, the prepared solution was added to the Schlenk under agitation. The reaction mixture was then stirred at 25°C. The reaction was monitored by NMR spectroscopy by taking an aliquot of the crude reaction mixture. The oxy-arylation product was obtained in >95% yield after overnight, exactly as in the case of the catalytic run starting from the gold(I) complex **1**.

9. Deuterium-labelling study

9.1 Synthesis of substrates

The syntheses of the D-labeled substrates was adapted from those reported by Zhang *et al.*[68]

4-Methyl-*N*-pent-4-enylbenzenesulfonamide (E)-5a-d:
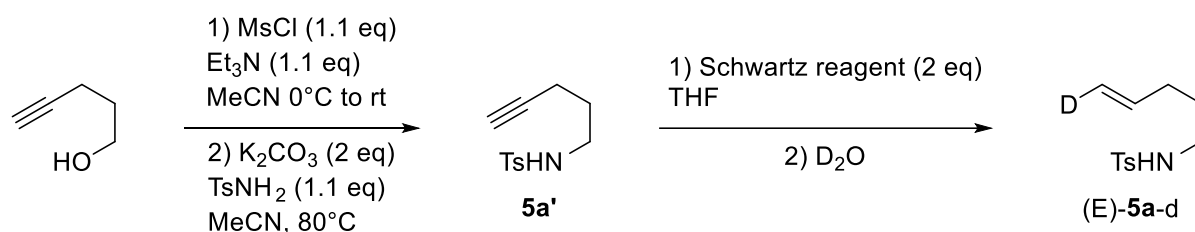
To a solution of 4-pentyn-1-ol (1.85 mL, 20 mmol) in MeCN (20 mL) was added MsCl (1.70 mL, 22 mmol, 1.1 eq.) and Et_3N (2.97 mL, 22 mmol, 1.1 eq.) successively at 0°C. The mixture was allowed to warm to room temperature. After 1 h, K_2CO_3 (5.53 g, 40 mmol, 2 eq.) and $TsNH_2$ (3.77 g, 22 mmol, 1.1 eq.) were added, and then the mixture was heated to 80°C overnight. The solution was filtrated and the solvent was removed under reduced pressure and the residue was purified through flash chromatography with petroleum ether/ethyl acetate (9:1). The product was obtained as a yellow oil (2.59 g, 10.9 mmol, 54%).[69]

In a glovebox, a dry Schlenk equipped with a magnetic stirrer bar was charged with LiH (300 mg, 37.5 mmol). Outside the glove box, under argon, a solution of Et_3B in THF (1 M) was added (25 mL) and the solution was stirred overnight. To $ZrCp_2Cl_2$ (2.92 g, 10 mmol) in THF (60 mL) at 0 ºC was added slowly a solution of $LiEt_3BH$ (1M in THF, 10 mL, 10 mmol) under argon. The resulting suspension was stirred for 1 h at room temperature, followed by addition of a solution of **5a'** (1.19 g, 5 mmol) in THF (7 mL). The mixture was stirred for 1 h at room temperature, followed by addition of D_2O (5 mL). After stirring for 1 h, the reaction mixture was poured into 50 mL of saturated aqueous $NaHCO_3$ and extracted with diethyl ether (3x 80 mL). The combined organic layers were washed with brine, dried over $MgSO_4$ and solvent was removed under *vacuum*. The residue was purified through silica gel flash column chromatography (eluent: hexanes: ethyl acetate = 5:1) to give only compound (E)-**5a**-d with 98% deuteration (738 mg, 3.1 mmol, 61%). Analytical data are consistent with those previously reported[68]: **¹H NMR** (300 MHz, $CDCl_3$): δ 7.77-7.71 (m, 2H), 7.33-7.29 (m, 2H), 5.76-5.64 (m, 1H), 4.95 (dt, J_{HH} = 17.1, 1.5 Hz, 1H), 4.39 (bs, 1H), 2.95 (q, J_{HH} = 6.7 Hz, 2H), 2.43 (s, 3H), 2.09-1.99 (m, 2H), 1.62-1.50 (m, 2H).

4-Methyl-*N*-pent-4-enylbenzenesulfonamide (Z)-5a-d:
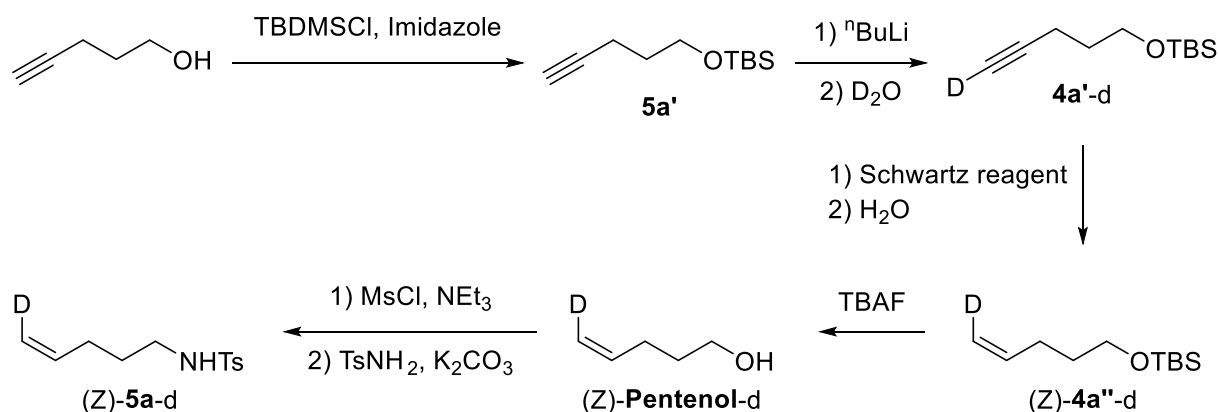
To a solution of imidazole (2.0 g, 30 mmol) and 4-pentyn-1-ol (1.8 mL, 20 mmol) in DCM (20 mL) was added TBSCl (2.70 g, 17.8 mmol) under argon at 0°C. The reaction was warmed to RT and stirred for 1 h. Then the solution was filtered through a plug of silica and washed with EtOAc. The solvent was removed under vacuum and the product **4a'** was obtained as a colorless oil (3.97 g, 20 mmol, 100%).[70]

To a solution of **4a'** (3.97 g, 20 mmol) in anhydrous THF (20 mL) was added dropwise at -78°C a solution of ^{n}BuLi in hexanes (17 mL, 1.36 M, 24 mmol, 1,2 eq.) After stirring for 30min at -78°C, the mixture is brought to 0°C and allowed to stir an additional 20min. At this point, the reaction is quenched by slow addition of D_2O (1.8 mL, 100 mmol, 5.0 eq.). The resulting mixture is allowed to stir for 4h, then directly dried over Na_2SO_4 and passed through a pad of SiO_2, rinsing with Et_2O. Solvent was removed under vacuum and the product **4a'-d** was obtained as a colorless oil (3.57 g, 18 mmol, 89%).[71]

To $ZrCp_2Cl_2$ (10.4 g, 35.5 mmol) in THF (170 mL) at 0 °C was added slowly a solution of $LiEt_3BH$ (1M in THF, 35.5 mL, 35.5 mmol) under argon. The resulting suspension was stirred for 1 h at room temperature, followed by addition of a solution of **4a'-d** (3.57 g, 17.7 mmol) in THF (60 mL). The mixture was stirred for 1 h at room temperature, followed by addition of H_2O (25 mL). After stirring for 1 h, the reaction mixture was poured into saturated aqueous $NaHCO_3$ and extracted with diethyl ether. The combined organic layer was washed with brine, dried over $MgSO_4$. After filtration and concentration, the residue was purified through silica gel flash column chromatography (eluent: hexanes: ethyl acetate = 10:1) to give compound (*Z*)-**4a''-d** (1.33 g, 6.5 mmol) in 37% yield.

To a solution of (*Z*)-**4a''-d** (1.56 g, 7.67 mmol) in anhydrous THF (8 mL) was added dropwise a TBAF solution in THF (19.2 mL, 1 M, 19.2 mmol, 2.5 eq.) at 0°C. After addition, the mixture was allowed to stir at room temperature for 5h. Then the reaction mixture was poured into 15 mL of brine and the organics are extracted with Et_2O (3x 15mL). Combined organics are then dried over Na_2SO_4 and concentrated under *vacuum* (0.79 g, 9.1 mmol). The product was used in the next step without further purification.

To a solution of deuterated (*Z*)-**Pentenol**-d (0.3 g, 3.4 mmol) in MeCN (5 mL) was added MsCl (0.29 mL, 3.8 mmol, 1.1 eq.) and Et_3N (0.1 mL, 3.8 mmol, 1.1 eq.) successively at 0°C. The mixture was allowed to warm to room temperature. After 1 h, K_2CO_3 (940 mg, 6.8 mmol, 2 eq.)

and TsNH$_2$ (650 mg, 3.8 mmol, 1.1 eq.) were added, and then the mixture was heated to 80°C overnight. The solution was filtrated and the solvent was removed under reduced pressure and the residue was purified through flash chromatography with petroleum ether/ethyl acetate (9:1). The only product (Z)-**5a**-d was obtained with 97% deuteration as a yellow oil (0.2 g, 0.83 mmol). Analytical data are consistent with those previously reported[68]: **¹H NMR** (300 MHz, CDCl$_3$): δ 7.77-7.71 (m, 2H), 7.33-7.28 (m, 2H), 5.75-5.64 (m, 1H), 4.94 (d, 1H, J = 10.2 Hz), 4.44 (bs, 1H), 2.95 (dd, 2H, J = 6.6, 13.2 Hz), 2.43 (s, 3H), 2.09-1.99 (m, 2H), 1.62-1.50 (m, 2H).

9.2 General procedure for the gold-catalyzed amino-arylation of alkenes
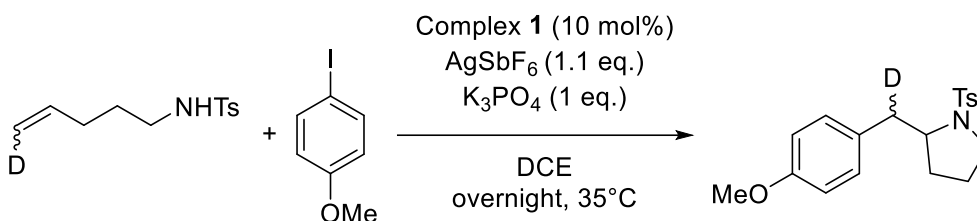
In a glovebox, a dry Schlenk equipped with a magnetic stirrer bar was charged with silver hexafluoroantimonate (150 mg, 0.44 mmol) and potassium phosphate tribasic (85 mg, 0.40 mmol) in DCE (0.4 mL). Complex **1** (26 mg, 0.04 mmol) was transferred into a small glass vial and dissolved in DCE (0.6 mL). 4-iodoanisole (0.40 mmol, 1 eq.) and functionalized deuterated alkene (0.40 mmol, 1 eq.) were added to the gold complex solution. This solution was loaded into a plastic syringe equipped with stainless steel needle. The syringe was closed by blocking the needle with a septum. Outside the glovebox, the prepared solution was added to the Schlenk under agitation. The reaction mixture was then stirred at 35°C. Silver salt was filtrated and the product was purified by column chromatography (pentane/ethyl acetate:9/1).
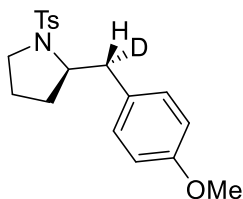
Compound **IIIj** was obtained in 73% yield (dr 4:1). **¹H NMR** (400 MHz, DMSO-d$_6$): δ 7.77-7.72 (m, 2H), 7.46-7.40 (m, 2H), 7.18-7.13 (m, 2H), 6.89-6.84 (m, 2H), 3.72 (s, 3H), 3.68-3.61 (m, 1H), 3.27-3.21 (m, 1H), 3.10-3.02 (m, 1H), 2.65 (d, J$_{HH}$ = 9.6 Hz, 1H), 2.39 (s, 3H), 1.66-1.46 (m, 2H), 1.38-1.22 (m, 2H).
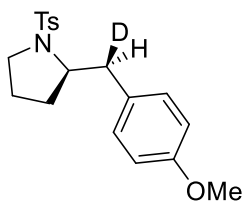
Compound **IIIk** was obtained in 78% yield (dr 4:1). **¹H NMR** (400 MHz, DMSO-d$_6$): δ 7.77-7.72 (m, 2H), 7.45-7.40 (m, 2H), 7.18-7.12 (m, 2H), 6.89-6.84 (m, 2H), 3.72 (s, 3H), 3.68-3.61 (m, 1H), 3.29-3.20 (m, 1H), 3.10-3.02 (m, 1H), 2.96 (d, J$_{HH}$ = 3.6 Hz, 1H), 2.39 (s, 3H), 1.65-1.45 (m, 2H), 1.38-1.21 (m, 2H).

VII.   Computational details

All optimizations were performed using the Gaussian 16 package[5] and the B3PW91 hybrid functional[6] on the real systems. All stationary points involved were fully optimized in gas phase. The gold atom was described with the relativistic electron core potential SDD and associated basis set, augmented by a set of f-orbital polarization functions.[7] The 6-31G** basis set was employed for all other atoms. Frequency calculations were undertaken to confirm the nature of the stationary points, yielding one imaginary frequency for transition states (TS), corresponding to the expected process, and all of them positive for minima. The connectivity of the transition states and their adjacent *minima* was confirmed by intrinsic reaction coordinate (IRC) calculations.[8]

To have a better accuracy on the Gibbs free energies, the energy profiles were computed at SMD(DCM)-B3PW91-D3(BJ)/SDD+f(Au), 6-31+G**(other atoms)// B3PW91/SDD+f(Au), 6-31G** (other atoms) level of theory. Dispersion effects have been included with D3 correction of Grimme with Becke-Johnson damping (DFT-*D3(BJ)*)[9] and solvent effects were considered (Dichloromethane : DCM) by means of the universal Solvation Model based on solute electron Density (SMD).[10]

The geometrical structures were plotted with the Chemcraft 1.8[11] program. For the key unoccupied molecular orbital (LUMO) of the π-complexes, the atomic orbital compositions of each MO (%) have been computed thanks to Multiwfn 3.6 package.[12]

The atomic *charge* distribution in terms of *NPA charges has been computed by using NBO analysis*[13] (NBO, 5.9 version).[14]

[5] Gaussian 16, Revision B.01, M. J. Frisch, G. W. Trucks, H. B. Schlegel, G. E. Scuseria, M. A. Robb, J. R. Cheeseman, G. Scalmani, V. Barone, G. A. Petersson, H. Nakatsuji, X. Li, M. Caricato, A. V. Marenich, J. Bloino, B. G. Janesko, R. Gomperts, B. Mennucci, H. P. Hratchian, J. V. Ortiz, A. F. Izmaylov, J. L. Sonnenberg, D. Williams-Young, F. Ding, F. Lipparini, F. Egidi, J. Goings, B. Peng, A. Petrone, T. Henderson, D. Ranasinghe, V. G. Zakrzewski, J. Gao, N. Rega, G. Zheng, W. Liang, M. Hada, M. Ehara, K. Toyota, R. Fukuda, J. Hasegawa, M. Ishida, T. Nakajima, Y. Honda, O. Kitao, H. Nakai, T. Vreven, K. Throssell, J. A. Montgomery, Jr., J. E. Peralta, F. Ogliaro, M. J. Bearpark, J. J. Heyd, E. N. Brothers, K. N. Kudin, V. N. Staroverov, T. A. Keith, R. Kobayashi, J. Normand, K. Raghavachari, A. P. Rendell, J. C. Burant, S. S. Iyengar, J. Tomasi, M. Cossi, J. M. Millam, M. Klene, C. Adamo, R. Cammi, J. W. Ochterski, R. L. Martin, K. Morokuma, O. Farkas, J. B. Foresman, and D. J. Fox, Gaussian, Inc., Wallingford CT, 2016.
[6] (a) A. D. Becke *J. Chem. Phys.* **1993**, *98*, 5648-5652. (b) J. P. Perdew, in *Electronic Structure of Solids '91*, Ed. P. Ziesche and H. Eschrig, Akademie Verlag, Berlin, **1991**, 11.
[7] A. W. Ehlers, M. Biihme, S. Dapprich, A. Gobbi, A. Hijllwarth, V. Jonas, K. F. Kiihler, R. Stegmann, A. Veldkamp, G. Frenking, *Chem. Phys. Letters*, **1993**, *208*, 111.
[8] (a) K. Fukui, Acc. Chem. Res., **1981**, *14*, 363.(b) H. P. Hratchian, H. B. Schlegel, in *Theory and Applications of Computational Chemistry: The First 40 Years*, Ed. C. E. Dykstra, G. Frenking, K. S. Kim, G. Scuseria, Elsevier, Amsterdam, **2005**, 195.
[9] (a) S. Grimme, J. Antony, S. Ehrlich, H. Krieg, Journal of Chemical Physics, **2010**, *132*, 154104. (b) S. Grimme, S. Ehrlich, L. Goerigk, *J. Comp. Chem.*, **2011**, *32*, 1456.
[10] Marenich, A. V.; Cramer, C. J.; Truhlar, D. G. *J. Phys. Chem. B* **2009**, *113*, 6378.
[11] Chemcraft - graphical software for visualization of quantum chemistry computations. https://www.chemcraftprog.com
[12] Tian Lu, Feiwu Chen, *J. Comput. Chem.*, **2012**, *33*, 580.
[13] a) E. Reed; L. A. Curtiss; F. Weinhold, *Chem. Rev.* **1988**, *88*, 899; b) J. P. Foster; F. Weinhold, *J.Am. Chem. Soc.* **1980**, *102*, 7211; c) A. E. Reed; F. Weinhold, *J. Chem. Phys.* **1985**, *83*, 1736.
[14] E. D. Glendening, J, K. Badenhoop, A. E. Reed, J. E. Carpenter, J. A. Bohmann, C. M. Morales, F. Weinhold, Theoretical Chemistry Institute, University of Wisconsin, Madison, **2001**.

TS1$_{OH5}$

TS1$_{OH6}$

TS1$_{OH5Z}$

TS1$_{OH6Z}$
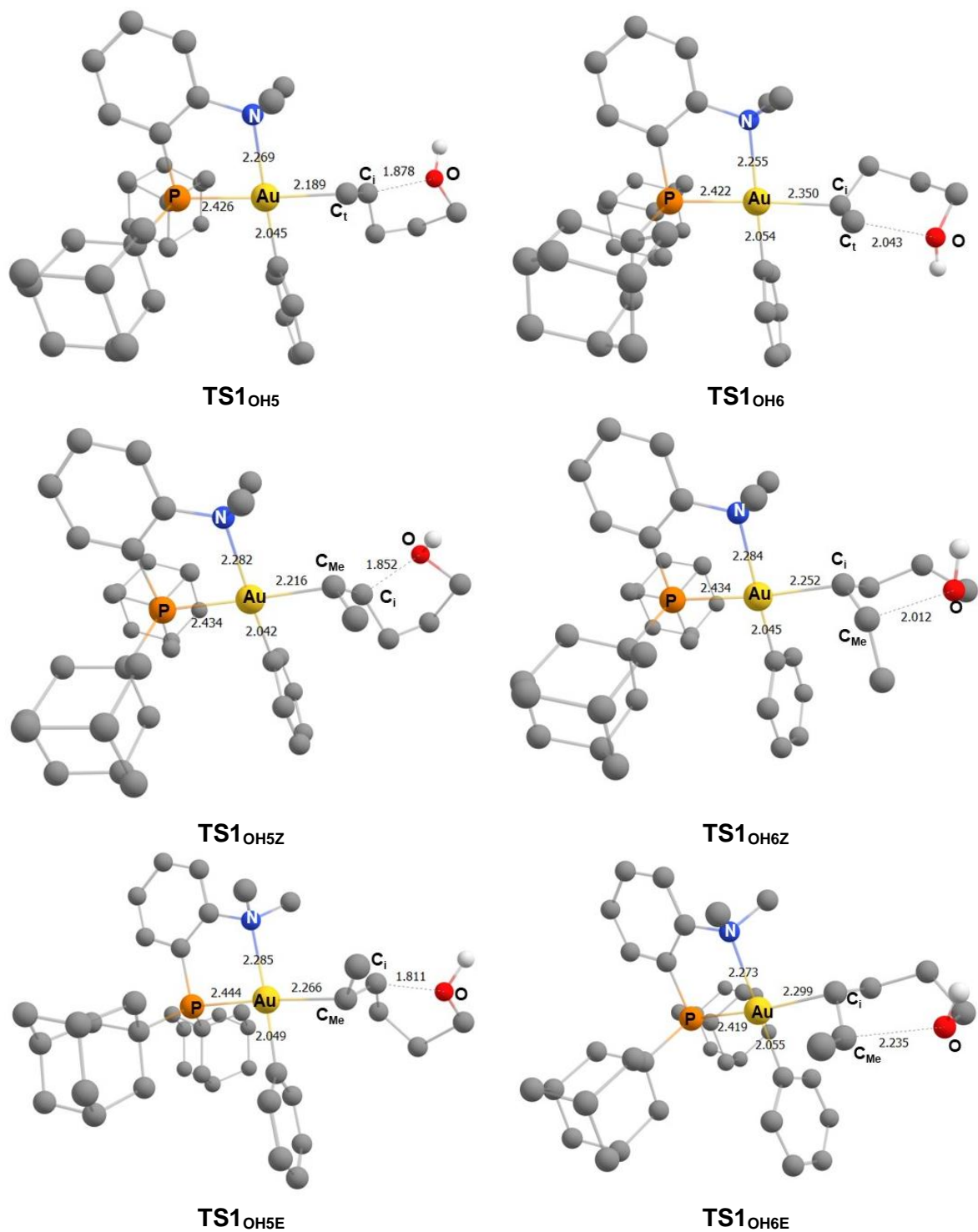
TS1$_{OH5E}$

TS1$_{OH6E}$

*Figure SII-1: Geometrical features of the transition states associated to the 5-exo (**TS1$_{OH5}$**) and 6-endo (**TS1$_{OH6}$**) cyclization step for the reaction between complex **2** and the 3 alkenols. Main distances in Å.*

Int$_{OH5}$

Int$_{OH6}$

Int$_{OH5Z}$

Int$_{OH6Z}$
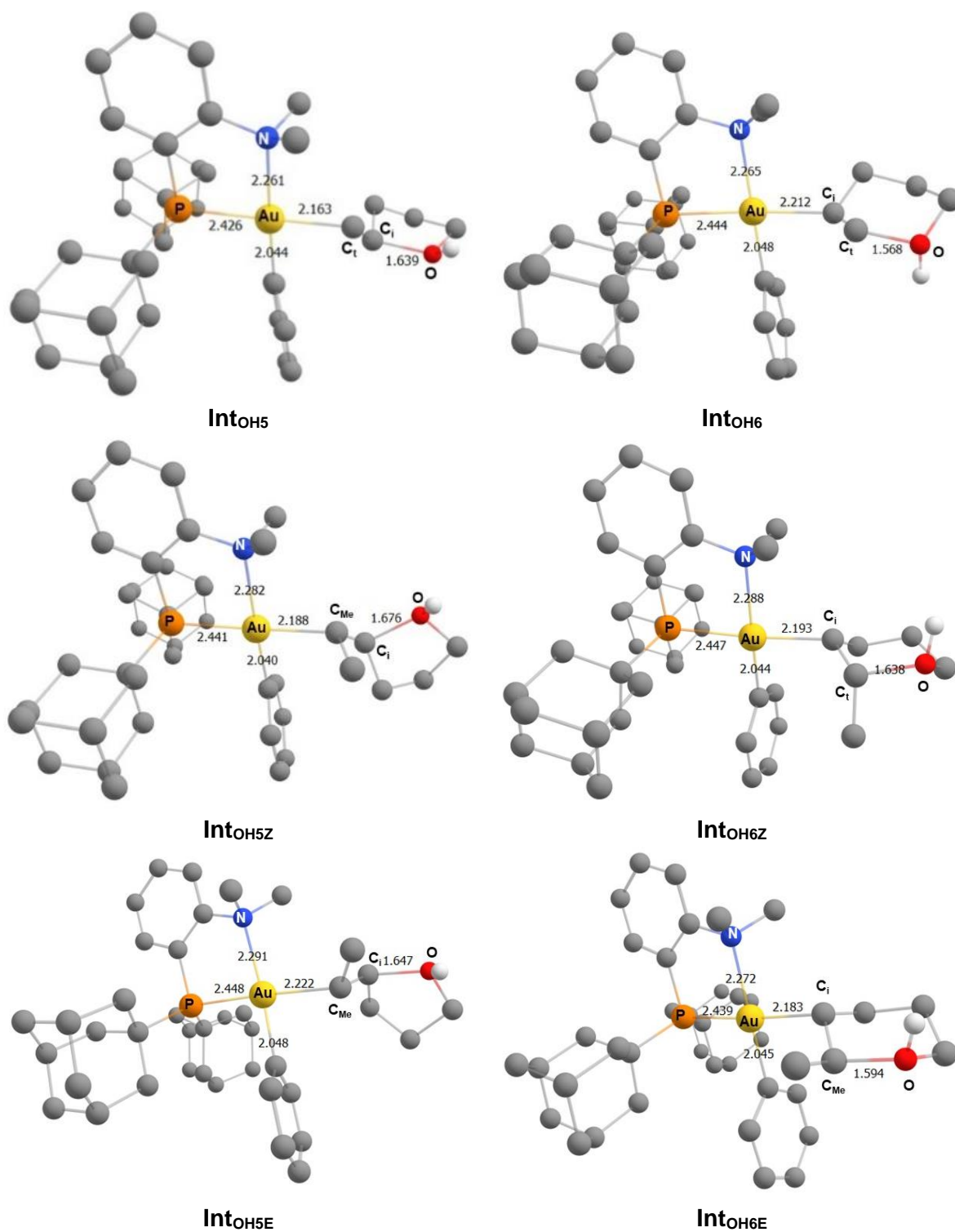
Int$_{OH5E}$

Int$_{OH6E}$

*Figure SII-2: Geometrical features of the intermediate associated to the 5-exo (**Int$_{OH5}$**) and 6-endo (**Int$_{OH6}$**) cyclization for the reaction between complex **2** and the 3 alkenols. Main distances in Å.*

TS2$_{O5}$

TS2$_{O6}$

P$_{O5}$

P$_{O6}$
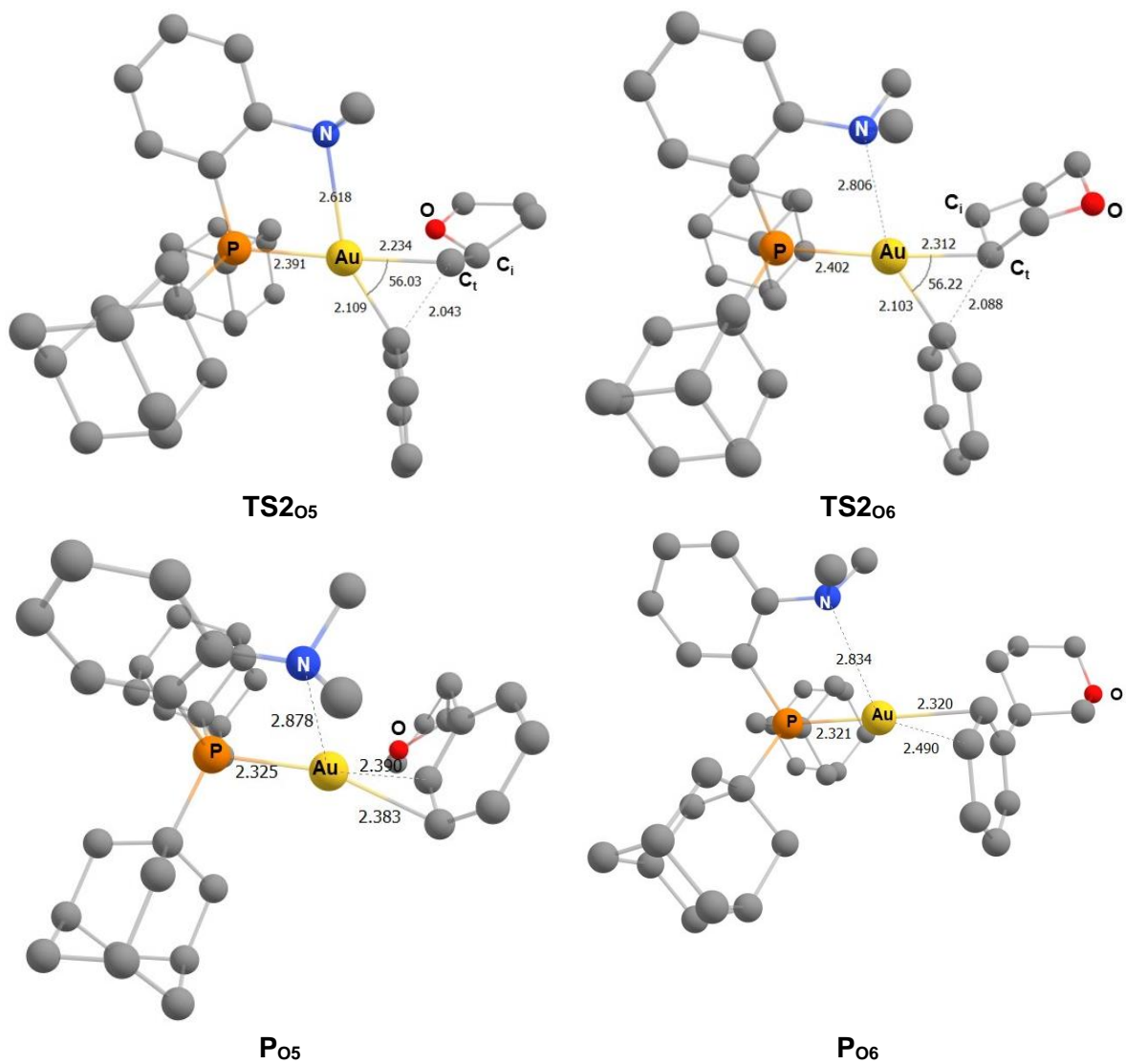
*Figure SII-3: Geometrical features of the TS associated to the reductive elimination 5-exo (**Int$_{OH5}$**) and 6-endo (**Int$_{OH6}$**) and final product the reaction between complex **2** and 4-penten-1-ol. Main distances in Å and angle in °.*
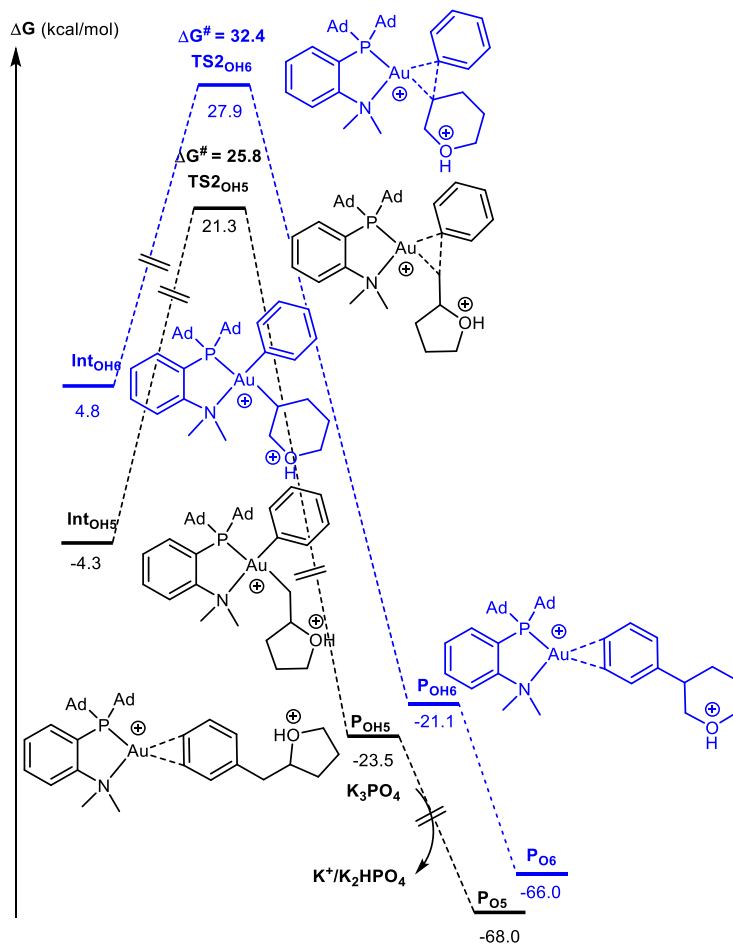
Figure SII-4: Energy profiles (ΔG in kcal/mol) for the reductive elimination from Int$_{OH5}$ and Int$_{OH6}$ computed at SMD(DCM)-B3PW91-D3(BJ)/SDD+f(Au), 6-31+G**(other atoms)// B3PW91/SDD+f(Au), 6-31G** (other atoms) level of theory. Formation of 5-exo (black) and 6-endo (blue) products. K$_3$PO$_4$ comes in after the reductive elimination step.
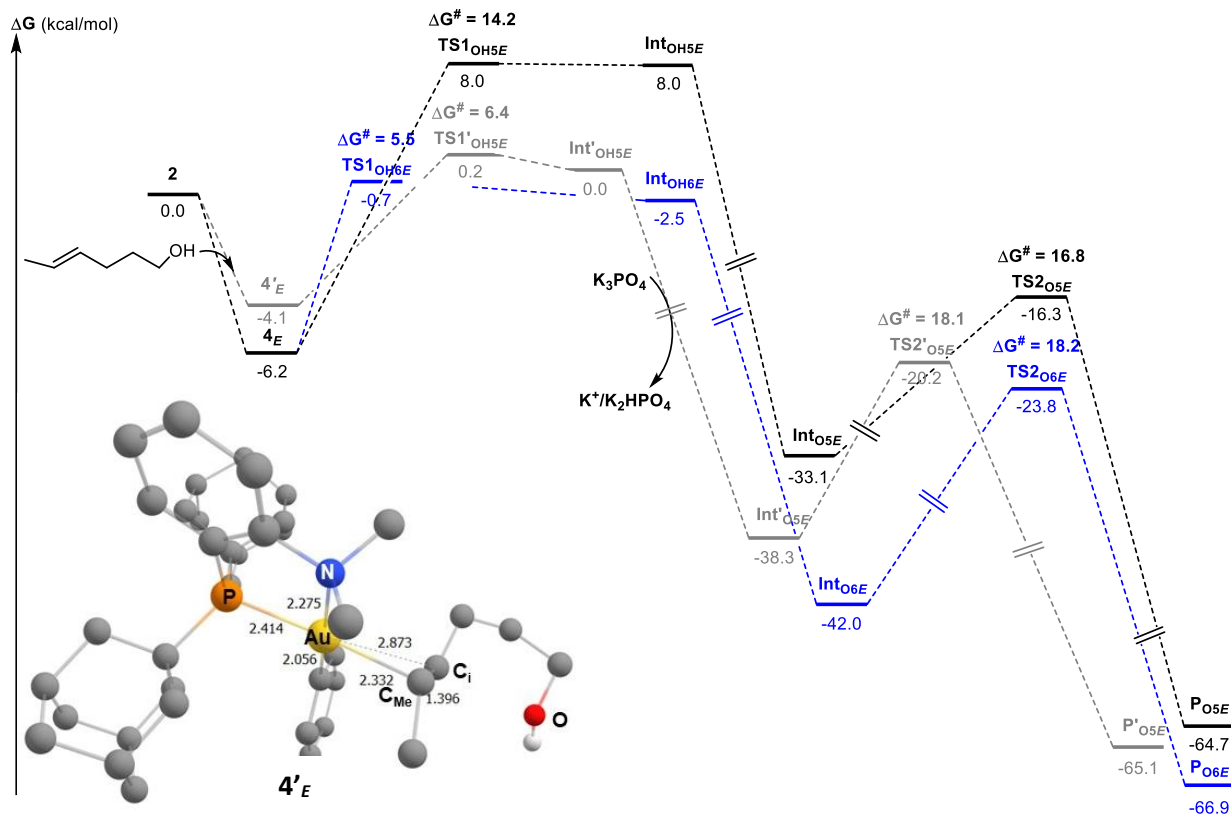
*Figure SII-5: Energy profiles (ΔG in kcal/mol) for the oxy-arylation reaction involving (P,N)Au^{2+}-Ph gold complex **2** and the E-4-hexen-1-ol, computed at SMD(DCM)-B3PW91-D3(BJ)/SDD+f(Au), 6-31+G**(other atoms)//B3PW91/SDD+ f(Au), 6-31G** (other atoms) level of theory and in the presence of K$_3$PO$_4$. Formation of 5-exo (black and grey) and 6-endo (blue) products. The K$_3$PO$_4$, K$_2$HPO$_4$ and K$^+$ molecules are included in order to ensure the correct energetic balance in all the reaction steps. Two π-complexes, which differ from orientation of the alkenol to gold, are involved **4$_E$** (black) and **4'$_E$** (grey). Geometrical structure and main distances in Å for complex **4'$_E$**.*
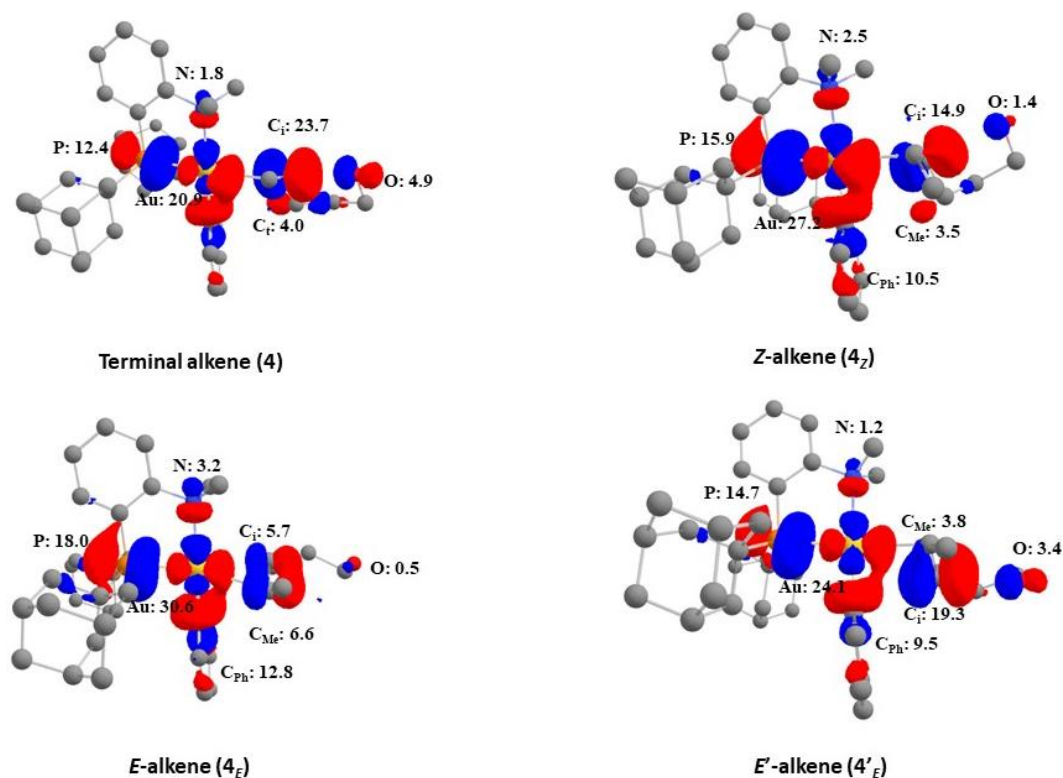
Figure SII-6: Plot of the LUMO (cutoff :0.04) for the π-complexes 4 and 4$_{Z/E/E'}$ associated to the oxy-arylation cyclization with the 3 alkenols. Participation of each atom (in %) for the main atoms.

4v
ΔG = 0 kcal/mol
Vinyl substituent directed toward the CH$_2$
group side (C$_t$ atom) of the alkenol

4v^B
ΔG = 0.6 kcal/mol
Vinyl substituent directed toward the alkyl
chain side (C$_i$ atom) of the alkenol
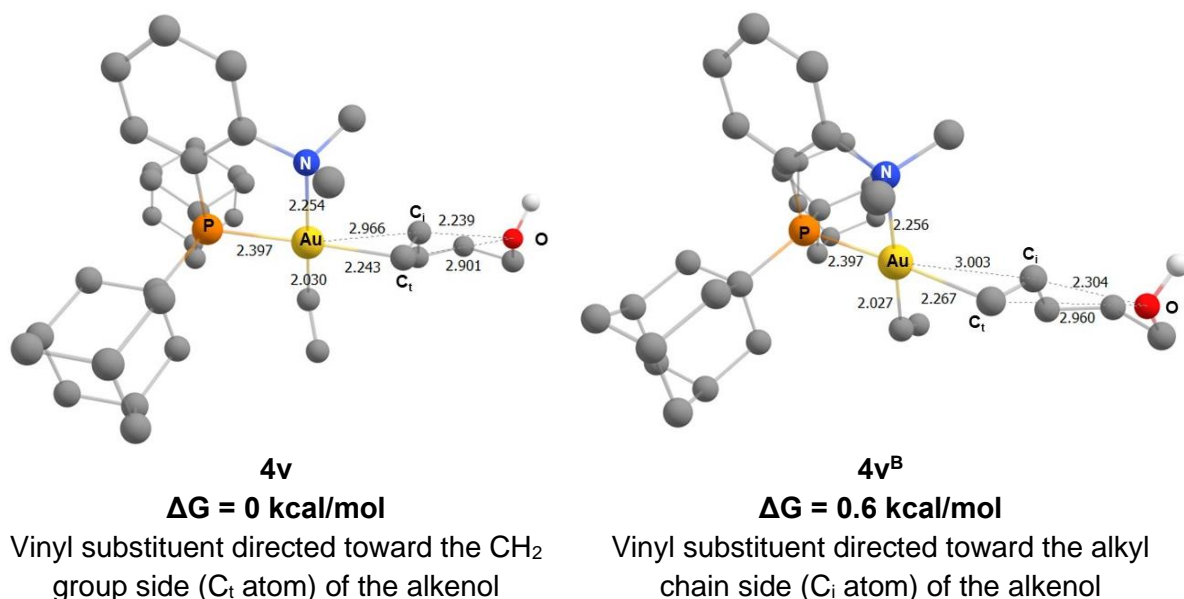
*Figure SII-7: Geometrical structures of the two π-complexes (**4v** and **4v^B**) associated to the coordination of 4-penten-1-ol on the (P,N)Au^{2+}-vinyl catalyst (2v), computed at B3PW91/SDD+f(Au), 6-31G** (other atoms) level of theory. Relative stability (ΔG) in kcal/mol calculated at SMD (DCM)-B3PW91-D3(BJ)/SDD+f(Au),6-31+G**//B3PW91/SDD+f(Au), 6-31G** (other atoms) level.*
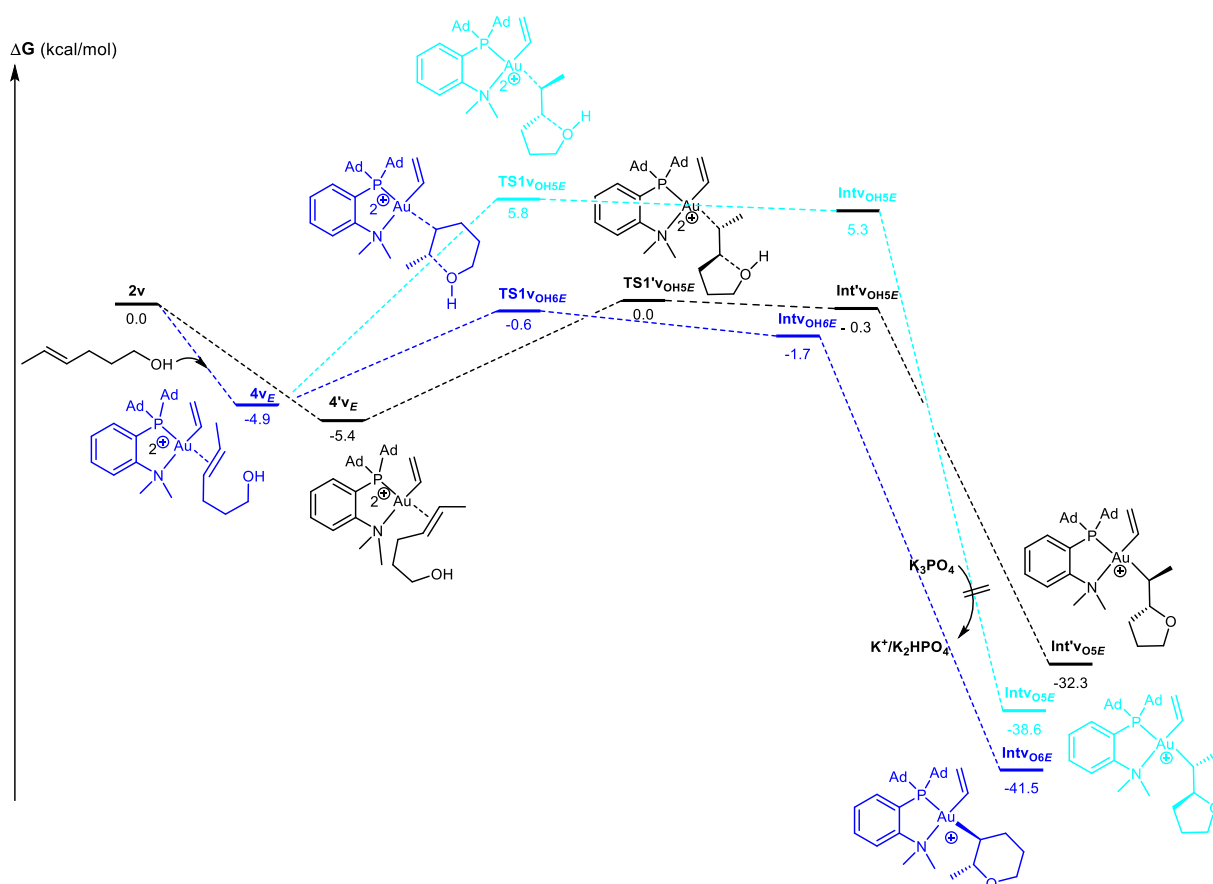
*Figure SII-8: Energy profiles (ΔG in kcal/mol) for the cyclization step of the oxy-vinylation reaction (orientation 1 from **4v$_E$** and **4'v$_E$**) involving (P,N)Au^{2+}-vinyl gold complex **2v** and **E**-4-hexen-1-ol computed at SMD(DCM)-B3PW91-D3(BJ)/SDD+f(Au, 6-31+G**(other atoms)//B3PW91/ SDD+f(Au), 6-31G** (other atoms) level of theory. Formation of 5-exo (blue and turquoise) and 6-endo (black) products.*

TS1v_OH5

TS1v_OH6

TS1v_OH5Z

TS1v_OH6Z
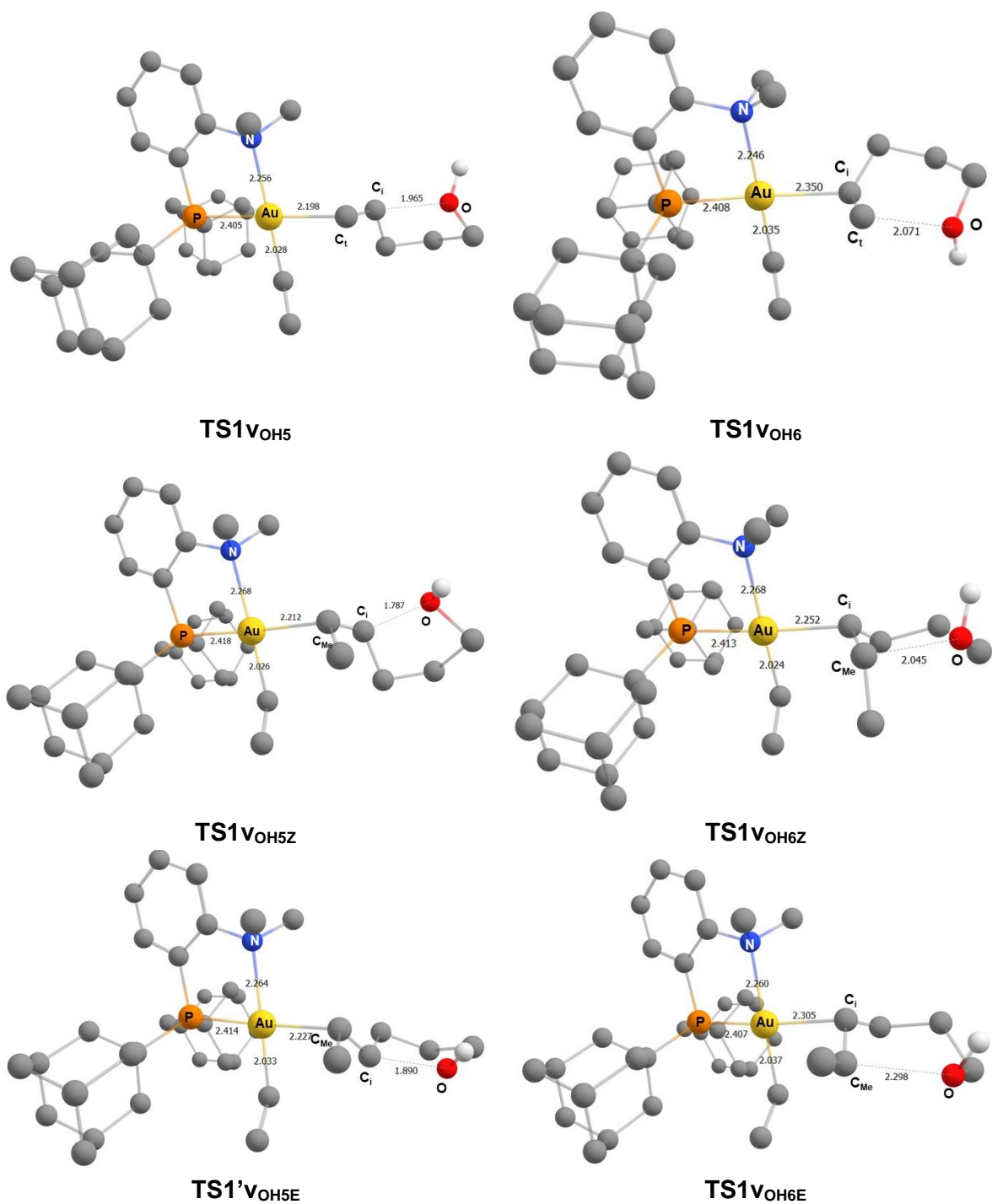
TS1'v_OH5E

TS1v_OH6E

Figure SII-9: Geometrical features of the transition states associated to the 5-exo (TS1v_OH5) and 6-endo (TS1v_OH6) cyclization step for the reaction between complex 2 and the 3 alkenols. Main distances in Å.
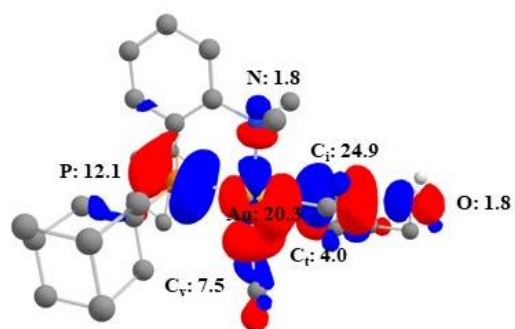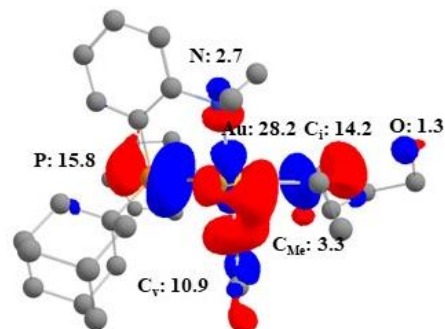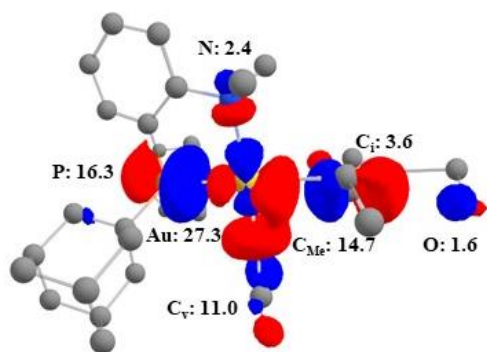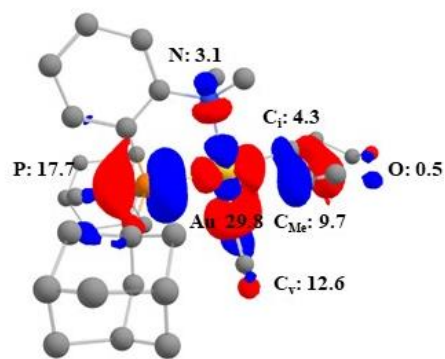
*Figure SII-10: Plot of the LUMO (cutoff :0.04) for the π-complexes **4v_Z**, **4v_E** and **4v_E'** associated to the 6-endo and 5-exo cyclizations for the oxy-vinylation of Z/E-alkenol substrates. Participation of each atom (in %) for the main atoms.*

VIII. References

[1] J. P. Wolfe, M. A. Rossi, *J. Am. Chem. Soc.* **2004**, *126*, 1620–1621.

[2] M. B. Hay, A. R. Hardin, J. P. Wolfe, *J. Org. Chem.* **2005**, *70*, 3099–3107.

[3] J. E. Ney, J. P. Wolfe, *Angew. Chem. Int. Ed.* **2004**, *43*, 3605–3608.

[4] M. B. Hay, J. P. Wolfe, *J. Am. Chem. Soc.* **2005**, *127*, 16468–16476.

[5] G. Zhang, L. Cui, Y. Wang, L. Zhang, *J. Am. Chem. Soc.* **2010**, *132*, 1474–1475.

[6] W. E. Brenzovich, D. Benitez, A. D. Lackner, H. P. Shunatona, E. Tkatchouk, W. A. Goddard, F. D. Toste, *Angew. Chem. Int. Ed.* **2010**, *49*, 5519–5522.

[7] C. Cazorla, E. Métay, B. Andrioletti, M. Lemaire, *Tetrahedron Lett.* **2009**, *50*, 3936–3938.

[8] E. Tkatchouk, N. P. Mankad, D. Benitez, W. A. Goddard, F. D. Toste, *J. Am. Chem. Soc.* **2011**, *133*, 14293–14300.

[9] A. D. Melhado, W. E. Brenzovich, A. D. Lackner, F. D. Toste, *J Am Chem Soc* **2010**, *132*, 8885–8887.

[10]W. E. Brenzovich, J.-F. Brazeau, F. D. Toste, *Org. Lett.* **2010**, *12*, 4728–4731.

[11]L. T. Ball, M. Green, G. C. Lloyd-Jones, C. A. Russell, *Org. Lett.* **2010**, *12*, 4724–4727.

[12]L. T. Ball, G. C. Lloyd-Jones, C. A. Russell, *Chem. – Eur. J.* **2012**, *18*, 2931–2937.

[13]M. J. Harper, E. J. Emmett, J. F. Bower, C. A. Russell, *J. Am. Chem. Soc.* **2017**, *139*, 12386–12389.

[14]B. Sahoo, M. N. Hopkinson, F. Glorius, *J Am Chem Soc* **2013**, *135*, 5505–5508.

[15]X. Shu, M. Zhang, Y. He, H. Frei, F. D. Toste, *J. Am. Chem. Soc.* **2014**, *136*, 5844–5847.

[16]Q. Zhang, Z.-Q. Zhang, Y. Fu, H.-Z. Yu, *ACS Catal.* **2016**, *6*, 798–808.

[17]B. Dong, H. Peng, S. E. Motika, X. Shi, *Chem. – Eur. J.* **2017**, *23*, 11093–11099.

[18]M. N. Hopkinson, B. Sahoo, F. Glorius, *Adv. Synth. Catal.* **2014**, *356*, 2794–2800.

[19]C. C. Chintawar, A. K. Yadav, N. T. Patil, *Angew. Chem. Int. Ed.* **2020**, *59*, 11808–11813.

[20]M. Navarro, A. Toledo, S. Mallet-Ladeira, E. D. S. Carrizo, K. Miqueu, D. Bourissou, *Chem. Sci.* **2020**, *11*, 2750–2758.

[21]M. Navarro, A. Toledo, M. Joost, A. Amgoune, S. Mallet-Ladeira, D. Bourissou, *Chem. Commun.* **2019**, *55*, 7974–7977.

[22]A. Zeineddine, L. Estévez, S. Mallet-Ladeira, K. Miqueu, A. Amgoune, D. Bourissou, *Nat. Commun.* **2017**, *8*, 565.

[23]D.-P. Yang, H.-F. Ji, G.-Y. Tang, W. Ren, H.-Y. Zhang, *Molecules* **2007**, *12*, 878–884.

[24]A. Flores, M. J. Camarasa, M. J. Pérez-Pérez, A. San-Félix, J. Balzarini, E. Quesada, *Org. Biomol. Chem.* **2014**, *12*, 5278–5294.

[25]J. S. Nakhla, J. W. Kampf, J. P. Wolfe, *J. Am. Chem. Soc.* **2006**, *128*, 2893–2901.

[26]M. B. Bertrand, J. D. Neukom, J. P. Wolfe, *J. Org. Chem.* **2008**, *73*, 8851–8860.

[27] J. P. Wolfe, in *Synth. Heterocycles Met.-Catalyzed React. Gener. One More Carbon-Heteroat. Bonds* (Ed.: J.P. Wolfe), Springer, Berlin, Heidelberg, **2013**, pp. 1–37.

[28] Y. Wei, M. Shi, *ACS Catal.* **2016**, *6*, 2515–2524.

[29] B. Alcaide, P. Almendros, T. M. del Campo, I. Fernández, *Chem. Commun.* **2011**, *47*, 9054–9056.

[30] S. Ajay, A. K. Shaw, *Synthesis* **2018**, *50*, 17–34.

[31] H. Wang, Y. Pan, Q. Tang, W. Zou, H. Shao, *Chin. Chem. Lett.* **2018**, *29*, 73–75.

[32] A. Fan, G. K. Chuah, S. Jaenicke, *Carbohydr. Res.* **2019**, *472*, 103–114.

[33] V. W. Bhoyare, A. G. Tathe, A. Das, C. C. Chintawar, N. T. Patil, *Chem. Soc. Rev.* **2021**, *50*, 10422–10450.

[34] J. Rodriguez, A. Zeineddine, E. D. S. Carrizo, K. Miqueu, N. Saffon-Merceron, A. Amgoune, D. Bourissou, *Chem. Sci.* **2019**, *10*, 7183–7192.

[35] J. Rodriguez, N. Adet, N. Saffon-Merceron, D. Bourissou, *Chem. Commun.* **2019**, *56*, 94–97.

[36] M. O. Akram, A. Das, I. Chakrabarty, N. T. Patil, *Org. Lett.* **2019**, *21*, 8101–8105.

[37] M. Rovira, L. Jašíková, E. Andris, F. Acuña-Parés, M. Soler, I. Güell, M.-Z. Wang, L. Gómez, J. M. Luis, J. Roithová, X. Ribas, *Chem. Commun.* **2017**, *53*, 8786–8789.

[38] S. Komiya, A. Shibue, *Organometallics* **1985**, *4*, 684–687.

[39] M. S. Winston, W. J. Wolf, F. D. Toste, *J. Am. Chem. Soc.* **2014**, *136*, 7777–7782.

[40] A. Couce-Rios, A. Lledós, I. Fernández, G. Ujaque, *ACS Catal.* **2019**, *9*, 848–858.

[41] A. Couce-Rios, A. Lledós, G. Ujaque, *Chem. – Eur. J.* **2016**, *22*, 9311–9320.

[42] J. Rodriguez, A. Tabey, S. Mallet-Ladeira, D. Bourissou, *Chem. Sci.* **2021**, *12*, 7706–7712.

[43] M. Rigoulet, O. Thillaye du Boullay, A. Amgoune, D. Bourissou, *Angew. Chem. Int. Ed.* **2020**, *59*, 16625–16630.

[44] S. Zhang, C. Wang, X. Ye, X. Shi, *Angew. Chem. Int. Ed.* **2020**, *59*, 20470–20474.

[45] A. G. Tathe, C. C. Chintawar, V. W. Bhoyare, N. T. Patil, *Chem. Commun.* **2020**, *56*, 9304–9307.

[46] A. G. Tathe, Urvashi, A. K. Yadav, C. C. Chintawar, N. T. Patil, *ACS Catal.* **2021**, 4576–4582.

[47] S. Sergeyev, *Helv. Chim. Acta* **2009**, *92*, 415–444.

[48] C. Brenninger, A. Pöthig, T. Bach, *Angew. Chem. Int. Ed.* **2017**, *56*, 4337–4341.

[49] S. Fujita, M. Abe, M. Shibuya, Y. Yamamoto, *Org. Lett.* **2015**, *17*, 3822–3825.

[50] Y.-S. Hon, Y.-W. Liu, C.-H. Hsieh, *Tetrahedron* **2004**, *60*, 4837–4860.

[51] S. Nicolai, J. Waser, *Org. Lett.* **2011**, *13*, 6324–6327.

[52] J. Escudero, V. Bellosta, J. Cossy, *Angew. Chem. Int. Ed.* **2018**, *57*, 574–578.

[53] A. Verma, S. Jana, C. D. Prasad, A. Yadav, S. Kumar, *Chem. Commun.* **2016**, *52*, 4179–4182.

[54] H. Egami, S. Tamaoki, M. Abe, N. Ohneda, T. Yoshimura, T. Okamoto, H. Odajima, N. Mase, K. Takeda, Y. Hamashima, *Org. Process Res. Dev.* **2018**, *22*, 1029–1033.

[55] A. Fernández-Mateos, P. Herrero Teijón, L. Mateos Burón, R. Rabanedo Clemente, R. Rubio González, *J. Org. Chem.* **2007**, *72*, 9973–9982.

[56] S. Protti, D. Dondi, M. Fagnoni, A. Albini, *Eur. J. Org. Chem.* **2008**, *2008*, 2240–2247.

[57] N. Hoffmann, J.-P. Pete, *J. Org. Chem.* **1997**, *62*, 6952–6960.

[58] D. S. Hamilton, D. A. Nicewicz, *J. Am. Chem. Soc.* **2012**, *134*, 18577–18580.

[59] J. T. Hutt, J. P. Wolfe, *Org. Chem. Front.* **2016**, *3*, 1314–1318.

[60] N. Fleury-Brégeot, M. Presset, F. Beaumard, V. Colombel, D. Oehlrich, F. Rombouts, G. A. Molander, *J. Org. Chem.* **2012**, *77*, 10399–10408.

[61] A. I. Perrott, H. J. P. D. Lijser, D. r. Arnold, *Can. J. Chem.* **1997**, *75*, 384–397.

[62] B. B. Snider, R. Cordova, R. T. Price, *J. Org. Chem.* **1982**, *47*, 3643–3646.

[63] M. Suginome, T. Iwanami, Y. Ito, *J. Org. Chem.* **1998**, *63*, 6096–6097.

[64] Z. Zhang, X. Tang, C. S. Thomoson, W. R. Dolbier, *Org. Lett.* **2015**, *17*, 3528–3531.

[65] L. J. Peterson, J. P. Wolfe, *Adv. Synth. Catal.* **2015**, *357*, 2339–2344.

[66] S. Nicolai, C. Piemontesi, J. Waser, *Angew. Chem. Int. Ed.* **2011**, *50*, 4680–4683.

[67] T. M. Nguyen, D. A. Nicewicz, *J. Am. Chem. Soc.* **2013**, *135*, 9588–9591.

[68] G. Zhang, L. Cui, Y. Wang, L. Zhang, *J Am Chem Soc* **2010**, *132*, 1474–1475.

[69] X. Wang, Z. Yao, S. Dong, F. Wei, H. Wang, Z. Xu, *Org. Lett.* **2013**, *15*, 2234–2237.

[70] J. T. R. Liddon, M. J. James, A. K. Clarke, P. O'Brien, R. J. K. Taylor, W. P. Unsworth, *Chem. – Eur. J.* **2016**, *22*, 8777–8780.

[71] X. Liu, T. M. Deaton, F. Haeffner, J. P. Morken, *Angew. Chem. Int. Ed.* **2017**, *56*, 11485–11489.

Chapter 3

Hydrogen bonding to gold: first evidence, bonding analysis & exploration of structural variations

I.   Hydrogen bonding

According to IUPAC definition, "the hydrogen bond is an attractive interaction between a hydrogen atom from a molecule or a molecular fragment D-H in which D is more electronegative than H, and an atom A or a group of atoms in the same or a different molecule, in which there is evidence of bond formation". It is part of the 3-center-4-electron (3c-4e) bonding, the three centers being the D, H and A atoms and the four electrons the two from the D-H bond and the two from the lone pair of A atom. It can be depicted as D-H···A, where the three dots symbolize the interaction. The DHA angle is usually close to linearity (180°) and the length of the D-H bond usually increases on hydrogen bond formation leading to a red shift in the infrared D-H stretching frequency. Moreover, characteristic NMR signature is the pronounced deshielding for H. Depending on the nature of D and A, the energy of a hydrogen bond lies in the range 2 to 15 kcal/mol.[1]

Hydrogen bonds are ubiquitous and play a major role in chemistry. Indeed, without hydrogen bonding, the boiling point of water would be -100°C, showing their influence on physical properties. Moreover, on the structural aspect, hydrogen bonds are responsible for the helix organization of DNA, one of the major factors for its stability. The classical hydrogen bond acceptors are nitrogen, oxygen, halogen, sulfur and phosphorus, but since several decades, transition metals have also been recognized as such.[2–4]

1. Hydrogen bonding with transition metals

One of the first examples, in which platinum was supposed to act as an hydrogen bond acceptor was described in 1987 by Koetzle and Orpen.[5] The neutron diffraction analysis of crystals of *cis*-platin derivatives **III-A** showed a large NHPt bond angle (167.1(9)°) and a close intermolecular H···Pt distance (2.262(11) Å), typical for 3c-4e interactions (Figure III-1, left). NMR data for the amine protons of **III-A** could not be obtained, so they turned their attention to a similar compound **III-B** for which the X-ray structure showed close Pt···H contact too (2.318(22) Å). ^{1}H NMR study in $CDCl_3$ indicated a downfield shift of the resonance assigned to the interacting hydrogen (δ 11.0 ppm), with respect to the free ligand (δ 9.0 ppm), characteristic of participation in hydrogen bonding (Figure III-1, middle).[6]

The same tendency has been observed by van Koeten's group for different platinum complexes of type **III-C** (Figure III-1, right). ^{1}H NMR data of the proton involved in Pt···H-N interaction range from δ 16.0 to 11.5 ppm and non negligible $^1J_{PtH}$ coupling constants (from 66 to 180 Hz) argue in favor of an attractive interaction. Furthermore, a red shift by 600 cm^{-1} compared to the free ligand is observed for the υ_{NH} vibration showing the weakening of the N-H bond.[7]
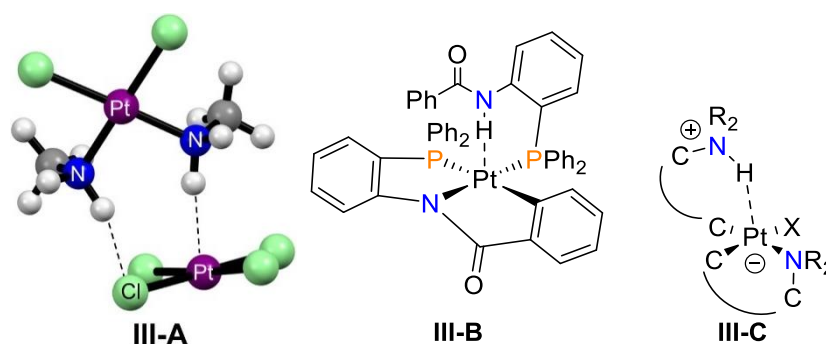
Figure III-1: Structure of complexes involving platinum as hydrogen bond acceptor.

Since the 1990s, M···H-X interactions have been unambiguously authenticated both intra- and intermolecularly with various hydrogen bond donor moieties (ammoniums, amides, water…) and have been extended to other electron-rich transition metals (Os, Ru, Co…).[2–4] These interactions have been characterized by NMR analysis (downfield shift of H involved and coupling constant with metals) as well as IR spectroscopy (important red shift). Complexes showing such interaction can be seen as intermediates in proton transfer to form hydridic structure as studied by Brammer with cobalt complexes (Figure III-2).[8]

H···M	3.00 Å	2.63(1) Å		1.55 Å
CO_{eq}-Co-CO_{eq}	109.5°	112.4(1)°		117.3°
CO_{eq}-Co-CO_{ax}	109.5°	106.3(1)°		99.7(3)°
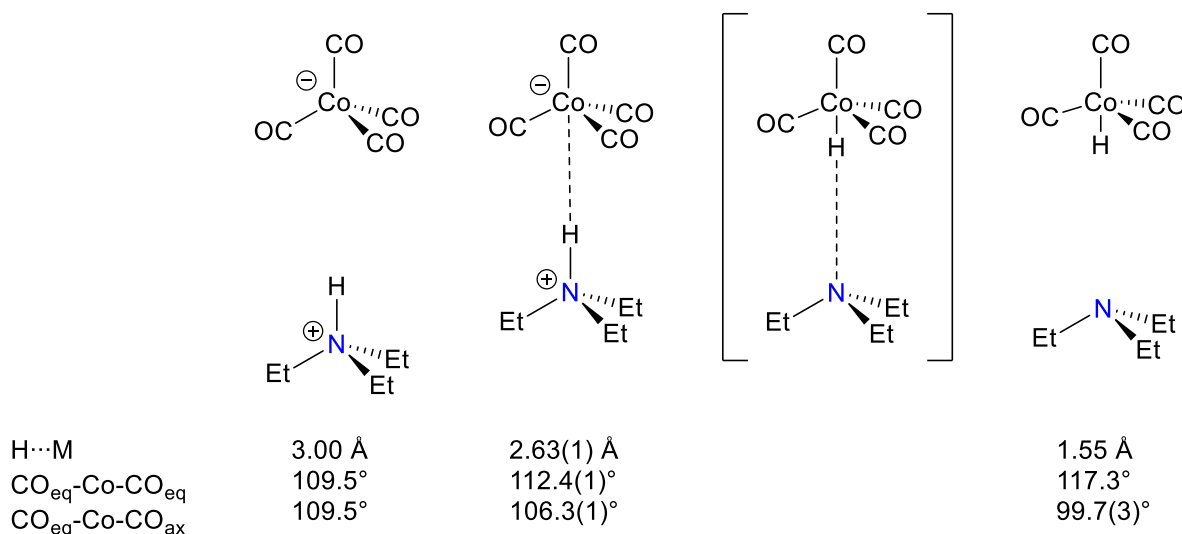
Figure III-2: Postulated pathway for the protonation of $Co(CO)_4^-$ involving complex with Co···H-N interaction as intermediate. Pertinent geometric data

Surprisingly, the case of gold as a proton acceptor remains an open question. Firstly, gold is the most electronegative among all metals making it a candidate of choice to accept hydrogen bond. Secondly, the possibility for gold to act as Lewis base has been already demonstrated. Indeed, the synthesis of gold complexes deriving from (P,B) and (P,Al) ligands allows the characterization of Au → Al/B interactions. The presence of the Au → Lewis acid interactions has been unambiguously evidenced by analytical data (XRD, NMR) and computational means (NBO): the Lewis acid moiety coordinates as a σ-acceptor Z-type ligand,

with Au acting as Lewis base (Scheme III-1).[9–11] Nevertheless, despite intense experimental and theoretical research in the last decades, gold as a proton acceptor is still a matter of debate.
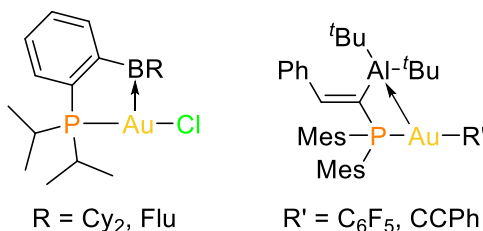
Scheme III-1: Gold complexes deriving from ambiphilic (P,B) and (P,Al) ligands showing Au → Lewis acid interaction.

2. Hydrogen bonding in gold chemistry

The story of gold as proton acceptor goes back to the beginning of 2005 with the work of Kryachko reporting computational evidence of the propensity of a triangular gold cluster to behave as a proton acceptor with O-H or N-H group.[12,13] One year later, Jansen prepared and characterized by X-ray diffraction an ammonia complex of the auride ion Au⁻. The presence of Au⋯H-N hydrogen bonding was inferred based on the relatively short Au⋯H distance and wide AuHN bond angle (2.58(1) Å and 158(1)°) agreeing well with the previous calculations.[14] Since then a number of Au(I) and Au(III) complexes have been reported to display relatively short Au⋯H distances in the solid state (2.3-3.0 Å).[15] However, as emphasized by Schmidbaur *et al.*, the observed Au⋯H contacts are likely to result from other factors than hydrogen bonding, such as electrostatic interactions, crystal packing, conformational restrictions… and their attractive nature has not yet been substantiated.[15–17]

Recent theoretical studies combining geometry optimizations and bonding analyses have examined and supported the possible existence of Au⋯H-X hydrogen bonding in Au(I) molecular complexes, stimulating and providing guidelines for forthcoming experimental studies. Esterhuysen *et al.* investigated extensively the interaction between the Au(I) atom of dimethylaurate [Me-Au-Me]⁻ (DMA) and different neutral H-bond donors (HF, HCN, H_2O, HCCH, NH_3, CH_4).[18,19] All of the optimized geometries of DMA with the H-bond donors show close Au⋯H contacts (2.22-2.92 Å) and almost linear Au⋯H-X skeletons (151.3-179.2°). To confirm the formation of hydrogen bonds, Atom-in-Molecules (AIM) analyses have been performed. The observation of Atomic Interaction Lines (AIL) connecting the Au and H atoms accompanying by a Bond Critical Point (BCP) attests the interaction between the two atoms and the properties of the BCP (density, Laplacian and total local energy) are characteristic of

attractive hydrogen bonding. The BCP must verify the following conditions: for the electron density $0.01 < \rho_{AuH} < 0.04$ e.bohr^{-3} and for the Laplacian of ρ $0.04 < \nabla^2\rho_{AuH} < 0.12$ e.bohr^{-5}.[20] Except with methane, all the other adducts with H-bond donors present BCP between Au and H atoms and fulfill the criteria defined for hydrogen bonds (ρ_{AuH} = 0.013-0.028 e.bohr^{-3} and $\nabla^2\rho_{AuH}$ = 0.037-0.051 e.bohr^{-5}). To complete, they performed Non-Covalent Interaction (NCI) analysis, an alternative method also derived from the electron density[21–23] and visualize the NCI plot. The sign of λ_2 (second eigenvalue of the electron density Hessian matrix) can be utilized to distinguish bonding ($\lambda_2 < 0$) and non-bonding ($\lambda_2 > 0$) interactions. All DMA and hydrogen bond donor adducts show an attractive interaction (Figure III-3), as evidence by the negative value of sign $(\lambda_2)\rho$. They also calculated the influence of relativistic effects on the DMA/HF adducts. When they are omitted, the H-bond disappears. This is coherent with the increase of electronegativity and destabilization of the 5d orbitals induced by relativistic effects. With them, the energy of the HOMO of gold being increased, the energy separation between the occupied d_{Au} and vacant σ^*_{FH} is reduced and so the Au$\cdots$H-F interaction is favored.[24,25]
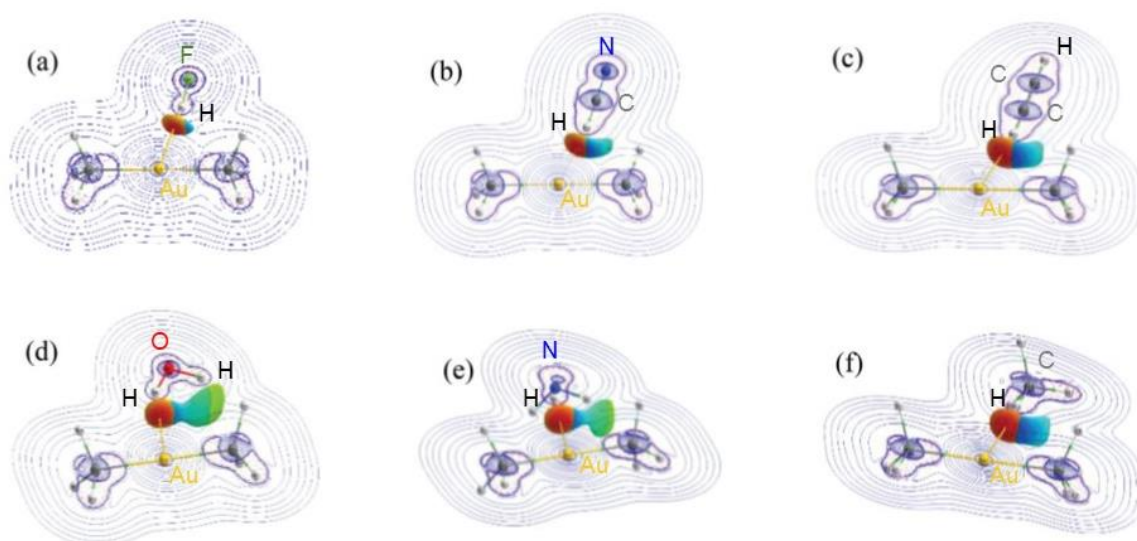
Figure III-3: Two-dimensional contour plots of $\nabla^2\rho_b(ea_0^{-5})$ with the NCI plot included of DMA/H-donors adducts with ^{a}HF, ^{b}HCN, ^{c}HCCH, ^{d}H$_2$O, ^{e}NH$_3$ and ^{f}CH$_4$ calculated at the MP2/aug-cc-pVTZ-pp level of theory. Red and yellow indicates a negative sign(λ_2)ρ value (attractive interactions), green indicates a sign(λ_2)*ρ value of zero and blue shows the regions that have a positive sign(λ_2)*ρ value (repulsive interactions).[19]*

Berger and Monkowius computationally investigated Au$\cdots$H-N bonding on the gold(I) complex **III-D.** Their design has three advantages: 1) due to the torsional degree of freedom of the phenyl pyridine moiety, no geometry constraints are imposed, 2) the gold bears a high negative partial charge thanks to the electron donating nature of the ligand, and 3) the complex should be easily synthesized.[26] A geometry optimization of **III-D** showed two *minima*: **III-Da** with the N-H bond pointing toward gold and **III-Db** by rotation of the C-C bond of the phenylpyridine, 7.5 kcal/mol higher in energy (Figure III-4). From a structural point of view, the

N-H bond is elongated in **III-Da** compared to **III-Db** (1.043 Å *vs* 1.030 Å) and the Au⋯H distance of 2.060 Å is below the sum of the van der Waals radii[27] (Table III-1).

*Figure III-4: Chemdraw structure and optimized geometries of the different forms of the complex **III-D** at the SCS-MP2/ECP level of theory. Relative energies (ΔE) in kcal/mol.*

	III-Da	**III-Db**
N-H	1.043	1.030
Au⋯H	2.060	/
NHAu	141.4	/
υ_{NH} (cm^{-1})	3006.4	3581.6
$\Delta\upsilon_{NH}$ with [ppyH]$^+$	-560.4	-14.8

*Table III-1: Key geometric features (distances in Å, angles in °) and spectroscopic data (IR) for the two conformers **III-D**.*

To confirm the presence of the hydrogen bonding, they compare the spectroscopic properties. In **III-Da** the calculated stretching frequency υ_{NH} is 3006.4 cm^{-1}, which is red-shifted by more than 500 cm^{-1} relative to the one of phenylpryridinium cation [ppyH]$^+$ or of **III-Db** (Table III-1). This shows the weakening of the N-H bond and confirmed the attractive nature of the Au⋯H interaction. Finally, they studied the influence of relativistic effects: without them, the gold hydrogen bonding, if existing, is much less important. The relativistic effects of gold play a major role in its ability to engage in H-bonding.

On the experimental part, Konishi's group reported in 2017 a diphosphine-ligated Au$_6$ clusters with short Au⋯H contacts and large AuHC bond angles (2.60-2.66 Å and 162.0-171.0°, X-ray data with the H atoms located at calculated positions, Figure III-5). Moreover, the corresponding ^{1}H and ^{13}C NMR signals of the atoms involved are observed at really low field (δ 11.57 ppm and 143.3 ppm compared to 7.20 ppm and 137-129 ppm). Therefore, they postulated that the interaction between the Au and the H atoms should have hydrogen-bond character.[28] Nevertheless, identifying the precise location of H atoms in close proximity of a heavy element as gold by XRD is intrinsically challenging[29] and it is well known that close proximity of hydrogen with transition metals compounds may influence the ^{1}H NMR shifts.[30,31] To determine whether this close contact was indeed an interaction or it resulted from geometric

factor, L. Estévez performed some DFT calculations. After geometry optimization fitting well with the X-Ray data, she turned her attention to AIM analysis that revealed BCPs between Au and H with ρ_{AuH} and $\nabla^2\rho_{AuH}$ in typical range for hydrogen bonding. Moreover, NBO analysis showed some donor-acceptor stabilizing interaction from gold to σ^*_{CH}. By changing, the phenyl substituent on phosphorus by methyl or hydrogen, she showed that the main geometrical features and AIM data remained similar. She concluded that the close contact is a hydrogen bonding to gold that might be facilitated by chelation but not enforced by geometry.[32]
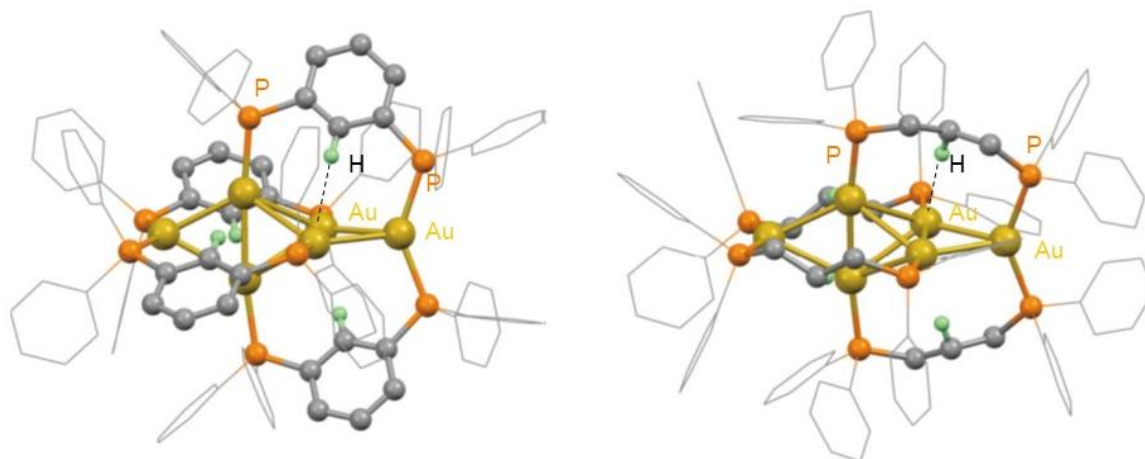
Figure III-5: X-ray crystal structure of the hexagold clusters bearing m-phenylene (left) or trimethylene (right) diphosphine ligands.

This overview of experimental and computational results about gold involved in hydrogen bonding as proton acceptor shows that it is theoretically plausible to observe such a hydrogen bonding but so far, there is no experimental compelling evidence.[15,18,26,28] Indeed, none of the described structures satisfied all of the following conditions to conventional hydrogen bond A···H-D:

(i)   there exists clear evidence that this bond specifically involves a hydrogen atom bonded or bridged to A predominantly along the bond direction D-H;

(ii)   the A-H bond elongates relative to that in the unbonded moiety;

(iii)   the hydrogen bond separation d(H···A) defined as the distance between the bridging proton and the proton acceptor A is shorter than the sum of van der Waals radii of H and A;

(iv)   the stretching vibrational mode υ_{DH} undergoes a red shift with respect to that in the isolated D-H group;

(v)   Proton nuclear magnetic resonance (^{1}H NMR) chemical shifts in the D-H···A hydrogen bond is shifted downfield compared to the free D-H moiety.

One challenge that must be overcome to establish and authenticate hydrogen bonding in gold complexes is that the inherently weak Au⋯H-X interaction must be favored over other competitive bonding situations such as intermolecular Au⋯Au aurophilic interactions[33] and/or hydrogen bonding of the H-X moiety with electron-rich sites surrounding the metal (ligand, solvent…).[34] The following chapter will provide experimental evidence for Au⋯H-X interaction that satisfied all the common features (i)-(v) for conventional hydrogen bond and the presence of such interaction and the nature of the bonding will be analyzed by DFT/NBO, AIM and NCI calculations.

II. Evidence for hydrogen bonding in MeDalPhos gold(I) complex

1. Synthesis and characterization of the cationic MeDalPhos gold complex

Due to the hemilabile character of its ligand and the basic nature of the nitrogen center, the MeDalPhos gold complex **1** was chosen as a first candidate to form and authenticate hydrogen bonding to gold(I). Addition of 1 equivalent of trifluoromethane sulfonic acid (HOTf) to the MeDalPhos gold complex **1** immediately leads to a new complex **3** according to ^{31}P NMR spectroscopy (Scheme III-2). ^{1}H NMR unambiguously indicates protonation of the nitrogen atom: a broad N-H signal appears at δ 10.9 ppm while the N(CH$_3$)$_2$ signal is shifted to low field by about 1 ppm and resonates as a doublet with a $^3J_{HH}$ coupling constant of 5.0 Hz.

Of note, complex **3** can also be prepared by protonating the (P,N) ligand prior to coordination to gold. Upon addition of HOTf, the phosphorus atom, not the nitrogen, is protonated, and the P-H phosphonium salt **5** is obtained. Diagnostic NMR features are the low-field shift of the ^{31}P NMR signal (δ 17.5 ppm), the large $^1J_{PH}$ coupling constant (485.3 Hz) and the absence of low-field shift of the N(CH$_3$)$_2$ ^{1}H NMR signal. The structure has been confirmed by growing crystals in a dichloromethane/pentane solution at -30°C and analyzing them by X-ray diffraction (for detailed crystallographic data, see SI p.157). Despite the protonation of phosphorus, compound **5** reacts rapidly with AuCl(SMe$_2$) to give complex **3**. The proton shifts from phosphorus to nitrogen and the phosphorus atom coordinates to gold, displacing the SMe$_2$ ligand.
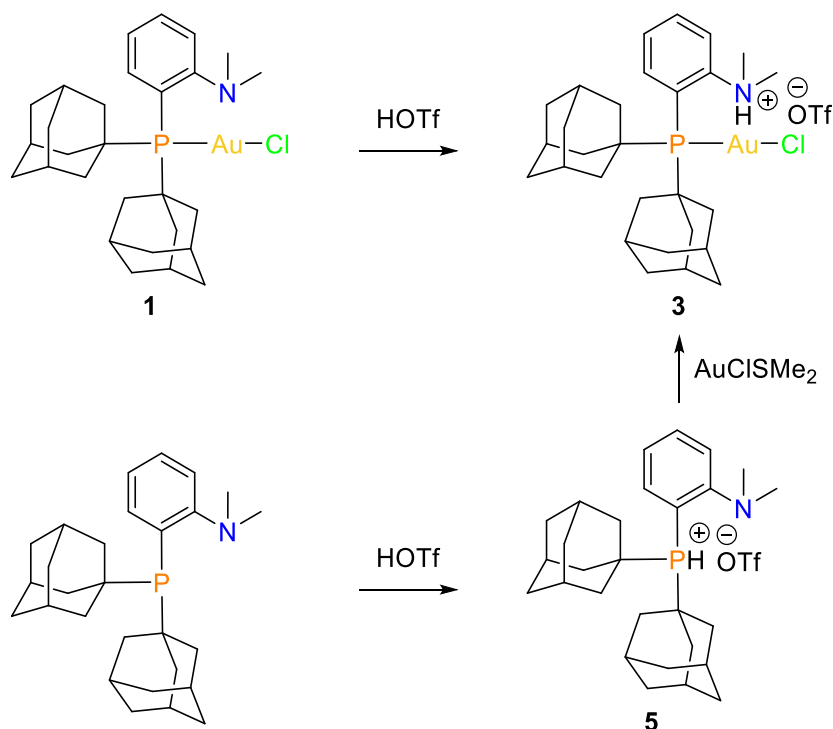
Scheme III-2: Synthesis (two routes) of the (P,NH+) gold(I) complex derived from MeDalPhos.

DFT calculations confirm that protonation of the phosphorus atom of **5** is slightly more favored thermodynamically ($\Delta G_{PH \rightarrow NH}$ = 1.6 kcal/mol) than that of the nitrogen atom. The activation barrier for the proton shift from phosphorus to nitrogen is fairly accessible at room temperature ($\Delta G^{\neq}_{PH \rightarrow NH}$ = 7.7 kcal/mol) (Figure III-6) allowing coordination of phosphorus to gold.
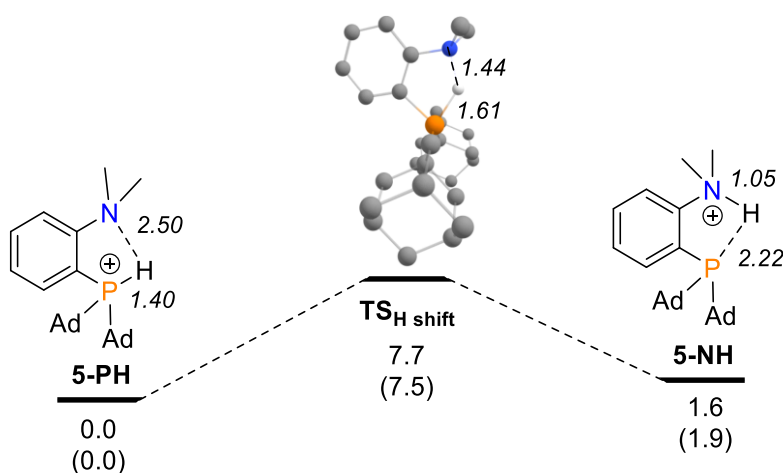
*Figure III-6: Optimized geometries of the different forms of the protonated ligand **5** at the SMD(DCM)-B3PW91/6-31G** level of theory, without taking into account the TfO- counteranion. Protonation of P (**5-PH**) or N (**5-NH**), and associated transition state for the proton transfer. Distances in Å and relative energies in kcal/mol (ΔG values and ΔE values into brackets).*

Crystals of **3** were grown from a dichloromethane/pentane solution at -30°C and analyzed by X-ray diffraction (Figure III-7). The H atom at N was located in the difference Fourier map and refined freely. There is no interaction between the acidic proton at N and the TfO-

counteranion (shortest distance > 4.4 Å), compound **3** adopts a separated ion-pair structure. The N-H bond points towards Au and the N-H···Au skeleton is close to linear (165(2)°). The Au···H distance (2.24(3) Å) is well within the sum of van der Waals radii (2.86 Å)[27] and falls in the very low range of those previously reported.[15] As pointed out previously, short N-H···Au contacts are not indicative of attractive interactions and the associated metrical parameters should be considered with caution.[29]
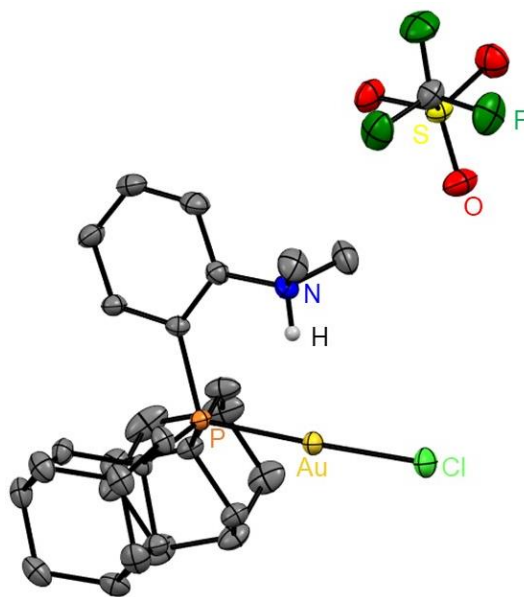
*Figure III-7: X-ray structure of the (P,NH+) gold(I) complex **3** derived from MeDalPhos. Thermal ellipsoids are drawn at 50% probability, hydrogen atoms, except that on nitrogen, are omitted for clarity. Selected bond lengths (Å) and bond angles (°): P-Au 2.270(1), Au-Cl 2.283(1), Au···H 2.24(3), PAuCl 176.98(2), NHAu 165(2).*

Multi-nuclear NMR confirms the general connectivity and according to 2D [1]H-^{1}H NOESY experiments, complex **3** adopts in solution the same conformation than in the solid state (the adamantyl groups at P and the methyl groups at N show correlations with the adjacent H atoms of the *ortho*-phenylene spacer, circle spots on Figure III-8). The very high ^{1}H NMR chemical shift of the N-H proton (δ 10.9 ppm) is typical of H-bonding.[2,3,35] Spin-spin coupling has also been inferred as a characteristic of H-bonding M···H-X interactions, although such couplings have been measured only very rarely. The $^1J_{NH}$ coupling in complex **3** was determined precisely at natural ^{15}N abundance *via* a ^{1}H-^{15}N HSQC experiment using homonuclear band selective (HOBS) detection scheme (SI p.154 for details). The obtained value (69.7 Hz) is very close to that reported by Pregosin and van Koeten for Pt(II) complexes featuring an intramolecularly hydrogen-bonded NMe_2H^+ moiety (**III-C** described in Figure III-1).[7,36]

As seen for platinum complexes and assessed theoretically, infrared spectroscopy is a useful analytical tool to probe hydrogen-bonding interactions. No characteristic band was detected for the N-H stretch of **3**. Considering it may be masked by the C-H stretches, the deuterium-labeled complex **3-D** was prepared using DOTf. A N-D band appeared at 2124 cm⁻

[1] in the IR spectrum, corresponding to a N-H stretch at about 3000 cm^{-1}. This is 500 cm^{-1} lower than typical wavenumbers for free N-H (ammonium) oscillators. This shift confirms the presence of Au···H-N bonding in solution and provides direct spectroscopic evidence for such H-bonding.
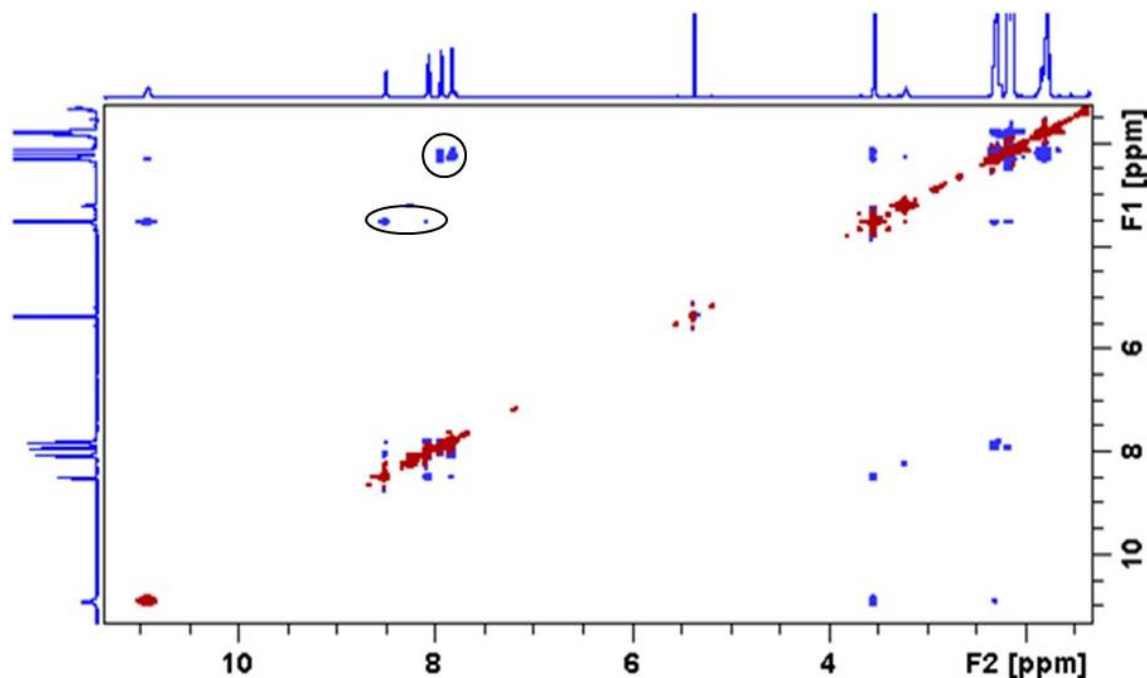
*Figure III-8: NOESY ^1H-^1H NMR spectrum of **3** in CD$_2$Cl$_2$ (mixing time = 1s). Positive and negative levels are plotted in red and blue, respectively.*

To probe the chemical influence of the Au···H-N interaction in complex **3**, the possibility of proton transfer was then examined. Mixing the neutral gold(I) complex **1** with its protonated form **3** in solution give two well-resolved ^{31}P NMR signals at room temperature (Figure III-9), indicating slow, if any, proton transfer and chemical exchange between **1** and **3** at the NMR timescale.

Cross-peaks in ^{31}P/^{31}P EXSY experiments indicate that there is some chemical exchange, but it is slow at the NMR time-scale, no coalescence and even no broadening of the NMR signals being observed upon heating at 45°C (Figure III-9 & Figure III-10). The gold complex **3** behaves very differently from the corresponding anilinium salt PhNMe$_2$H,OTf for which proton exchange between the base and acid forms is fast by NMR at room temperature and even at low temperature (down to -70°C, a unique set of ^1H NMR signals is observed for the two species).
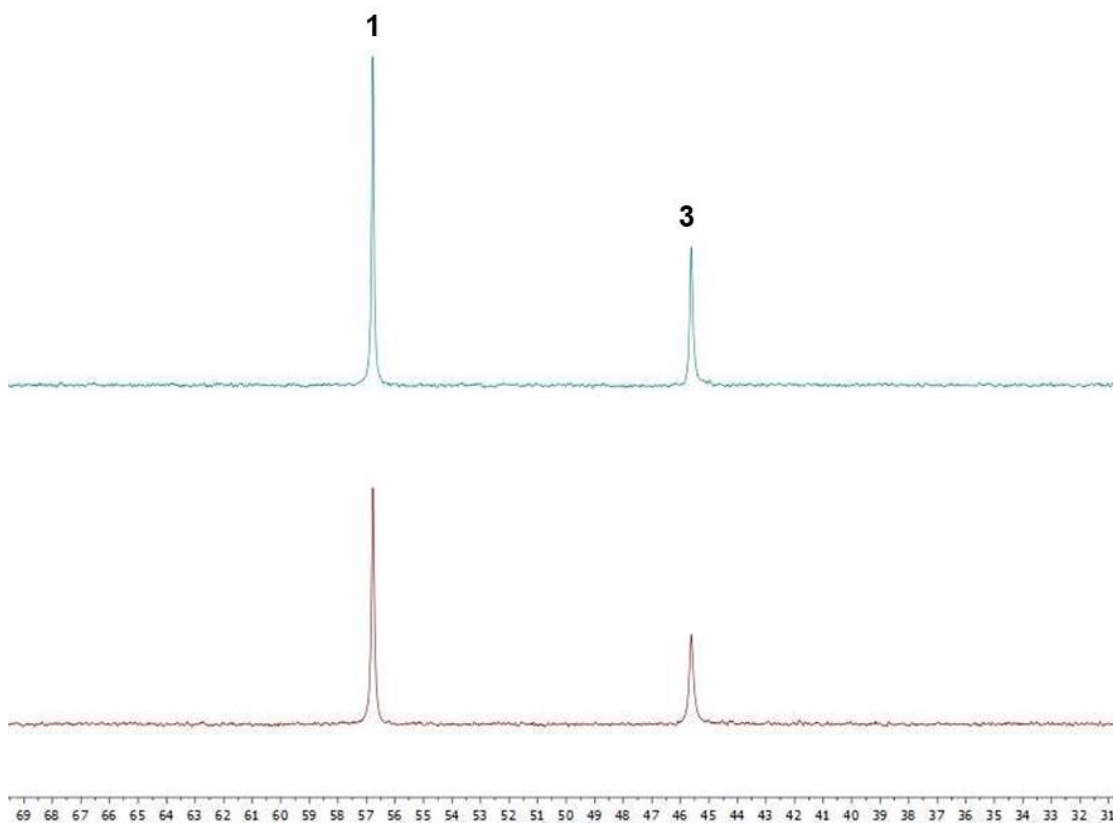
*Figure III-9: ^{31}P NMR spectra of a 2:1 mixture of **1** and **3** in CD$_2$Cl$_2$ at 25°C (blue) and 45°C (red).*
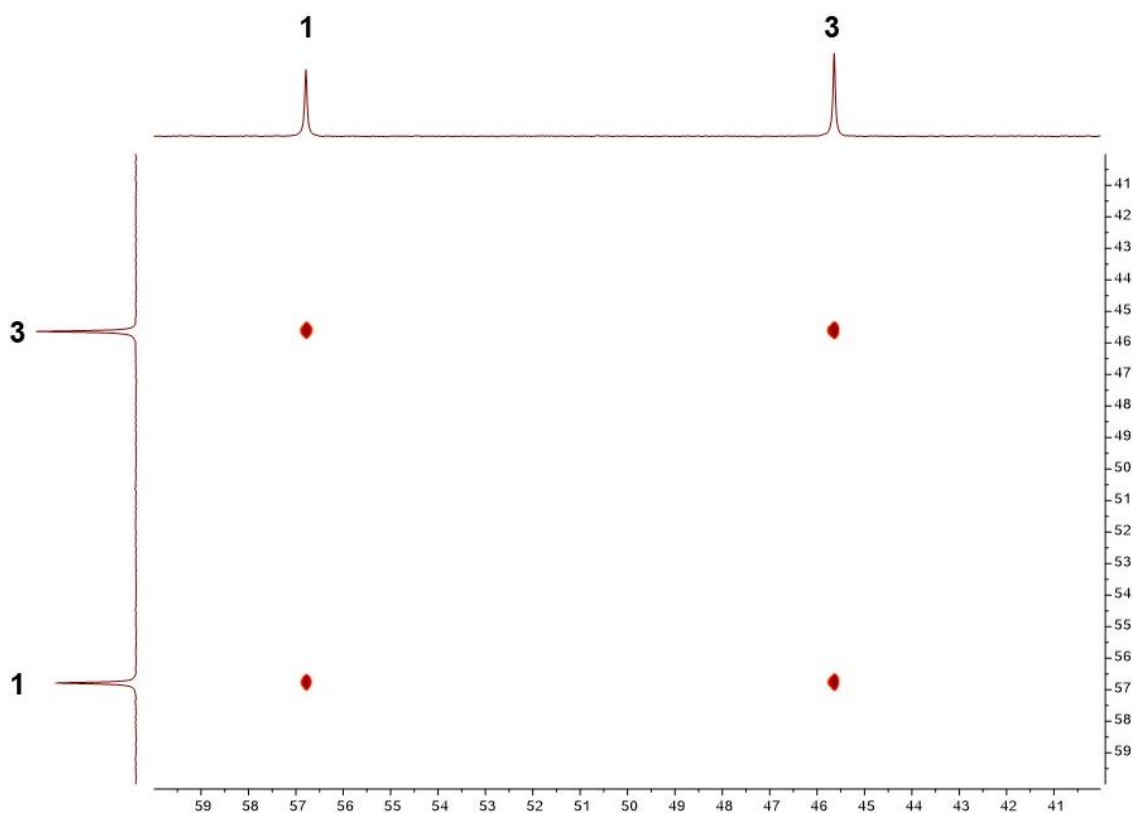
*Figure III-10: EXSY ^{31}P-^{31}P NMR spectrum of a 1:1 mixture of **1** and **3** in CD$_2$Cl$_2$ at 25°C (mixing time = 50 ms).*

2. Computational studies on the cationic MeDalPhos gold complex

A comprehensive theoretical study was performed to analyze the bonding situation in the gold complex **3.** The main objective of these quantum chemical calculations was to establish unambiguously the presence of an attractive N-H⋯Au interaction and to precise its nature.

First, optimization of the structure of complex **3** with different functionals have been carried out to determine the most suitable one (SI p.161). B3PW91 functional has been chosen over other hybrid (PBE0 or B3LYP), GGA (BP86) or meta GGA (TPSS) functionals since the theoretical value for N-H stretching fits best with experimental one. For weak interactions, dispersion effects are generally non-negligible. The influence of dispersion (B3PW91-D3(BJ)) has been studied and showed almost no difference in the Au⋯H and N-H distances or stretching, so it was not taken into account for ease of calculations. Finally, the B3PW91/SDD+f(Au),6-31G**(other atoms) level of theory was used and solvent effects (CH_2Cl_2) were taken into account by means of the universal continuum solvation model, based on density, SMD (see SI for computational details).

2.1 Geometry optimization and spectroscopic data

Calculations were first carried out on the naked cation since the X-ray structure showed that complex **3** adopts an ion-pair structure. Several *minima* **3a-d'** were located on the Potential Energy Surface (PES) (Figure III-11 & Table III-2).

	3a	**3b**	**3c**	**3d**	**3d'**
P-Au	2.303	2.304	2.305	2.295	2.428
Au-Cl	2.338	2.344	2.339	2.382	2.321
N-H	1.046	1.024	1.025	/	/
Au⋯H	2.134	/	/	1.544	1.582
PAuCl	178.5	176.5	178.1	176.5	101.5
NHAu	174.2	/	/	/	/
υ_{NH} (cm^{-1})	3032.3	3457.3	3445.9	/	/
$\Delta\upsilon_{NH}$ with HNMe$_2$Ph$^+$	-443.3	-18.3	-29.7	/	/
υ_{ND} (cm^{-1})	2089.4	2544.5	2489.2	/	/
δ ^{1}H NMR (NH, ppm)	11.94	5.64	6.31	/	/

Table III-2: Key geometric features (distances in Å, angles in °) and spectroscopic data (IR and NMR) for the five conformers 3a-d'.
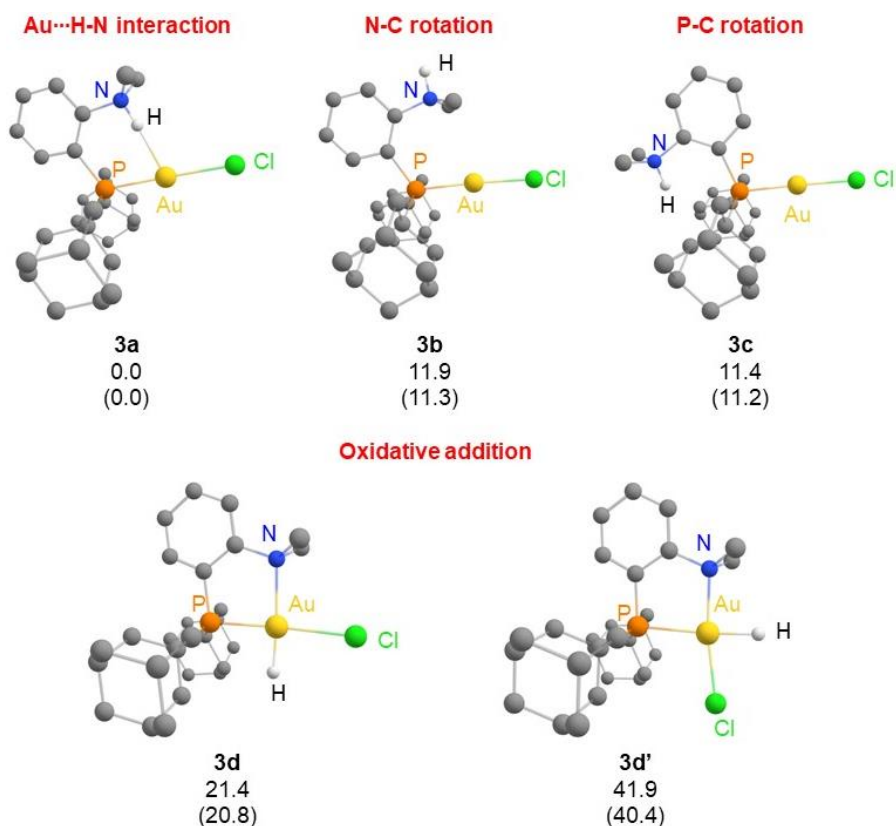
*Figure III-11: Energy minima located on the potential energy surface of complex **3**, without OTf counteranion. Relative energies in kcal/mol (ΔG values, with ΔE values into brackets).*

The ground state structure **3a** parallels that observed by X-ray diffraction, with the N-H bond pointing towards Au. Two other *minima* **3b** and **3c** correspond to conformers associated with rotations around the C_{Ph}-N and C_{Ph}-P bonds. Two other local *minima* are the square-planar gold(III) hydrides **3d** and **3d'** resulting from oxidative addition of the N-H bond to gold (H *cis* or *trans* to P). In **3a**, the H atom at N enters the coordination sphere of gold (Au⋯H = 2.134 Å) with a quasi-linear N-H⋯Au arrangement (174.2°), in line with that expected for hydrogen bonding. Comparison of the metrical data shows that the N-H bond is noticeably elongated upon interaction with gold (1.046 Å in **3a** *vs* 1.024-1.025 Å in **3b-c**). The conformers **3b** and **3c** are located 11 to 12 kcal/mol higher in energy than **3a**, suggesting some stabilization of **3a** thanks to N-H⋯Au interaction. However, the energy difference between the forms with or without interaction may overestimate the strength of the Au⋯H-N interaction. Indeed, other parameters like the steric hindrance of the methyl groups near the gold center (**3b**) or the adamantyl groups near the NH bond (**3c**), can increase the energies of other isomers upon rotation. The gold(III) hydrides **3d** and **3d'** are even higher in energy, about 21 and 42 kcal/mol respectively above **3a**.

Inclusion of TfO⁻ in the calculations induces only small changes in the optimized geometries, indicating that the counteranion has little influence (Figure III-12 & Table III-3). The difference in energy between conformers is reduced compared to calculations without counteranion due to the involvement of a stabilizing N-H···O hydrogen bonding with OTf. Moreover, a new conformer **3a'_OTf** with similar geometry as **3a_OTf** but including hydrogen bonding with the counteranion and not the gold has been found. Anyway, the ground state is still the form with the Au···H-N interaction, also showing that the hydrogen bonding to gold is preferred over the interaction with the counteranion.
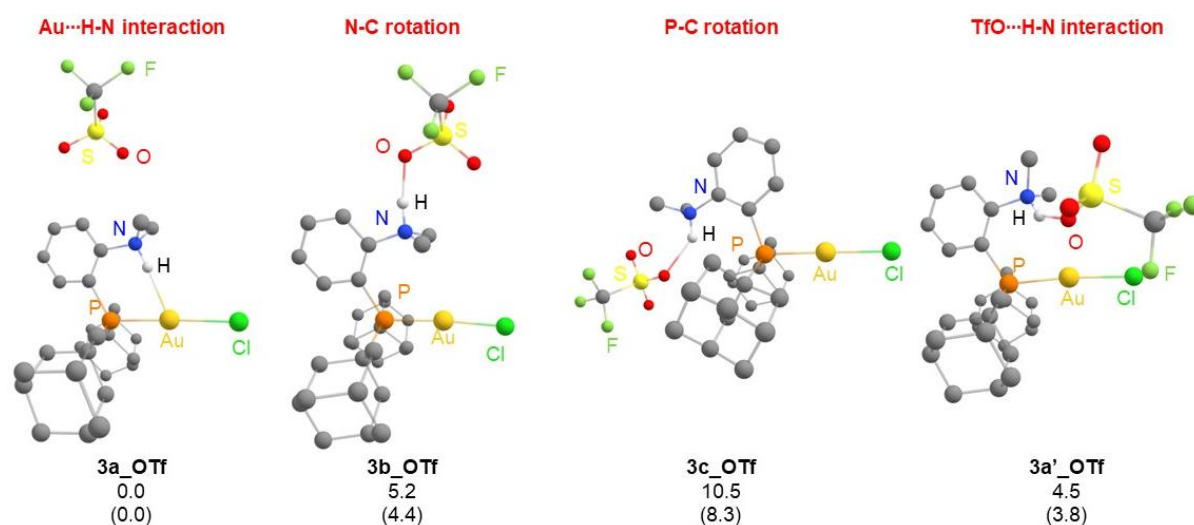
*Figure III-12: Optimized geometries of the different forms of the cationic complex **3**, taking into account the TfO⁻ counteranion. Relative energies in kcal/mol (ΔG values, with ΔE values into brackets).*

	3a_OTf	**3b_OTf**	**3c_OTf**	**3a'_OTf**
P-Au	2.301	2.303	2.325	2.294
Au-Cl	2.343	2.344	2.344	2.347
N-H	1.043	1.056	1.034	1.038
Au···H	2.161	/	/	2.658
H-O$_{Tf}$	2.288	1.670	2.008	2.018
PAuCl	177.3	175.2	178.1	171.4
NHAu	172.8	/	/	127.9

*Table III-3: Key geometric features (distances in Å, angles in °) for the four conformers **3a-c_OTf** and **3a'_OTf**.*

The ¹H NMR chemical shifts and IR stretching frequencies computed for the three gold(I) conformers **3a-c** corroborate the experimental assignment and confirm the presence of a N-H···Au hydrogen bond interaction in **3a** (Table III-2). Upon interaction with gold, the ¹H NMR resonance signal for the N-H moiety is predicted to shift from δ 5.6-6.3 ppm for **3b,c** to δ 11.9 ppm for **3a**, in good agreement with the signal observed at δ 10.9 ppm experimentally. The N-H stretches computed for **3b** and **3c** are very similar to that of the anilinium PhNMe₂H⁺ (~ 3500 cm⁻¹), while that of **3a** is about 500 cm⁻¹ red-shifted, indicating substantial weakening of the N-H bond upon interaction with gold.[26,37] For completeness, the N-D stretch for the deuterium-

labeled **3a-D** was also computed (2089 cm^{-1}). The obtained value matches quite well with that determined experimentally (2124 cm^{-1}).

To assess the impact of relativistic effects, known to profoundly influence the properties of gold,[18,19,24–26,38] optimizations were performed with ADF on **3a** at the COSMO(DCM)-BP86/TZ2P level of theory with and without ZORA effect, and compared with Gaussian 09 calculations at B3PW91 or BP86/SDD+f(Au),6-31G**(other atoms) level (Table III-4).

	Gaussian		ADF		
	B3PW91[a]	BP86[a]	BP86[b]	ZORA (relativistic scalar)-BP86[c]	ZORA (spin orbit)-BP86[d]
P-Au	2.303	2.307	2.529	2.297	2.294
Au-Cl	2.338	2.348	2.461	2.317	2.314
N-H	1.046	1.065	1.049	1.063	1.060
Au···H	2.134	2.101	2.277	2.078	2.099
PAuCl	178.5	178.4	176.5	178.5	178.3
NHAu	174.2	178.8	174.2	174.9	175.8

*Table III-4: Investigations of the relativistic effects on the geometry of complex 3 in its form 3a, with Au···H-N contact. Distances in Å and bond angles in °. [a]Gaussian 09, optimization in solvent with SMD model (DCM) using SDD+f(Au)/6- 31G** basis set, [b]ADF 2017, optimization in solvent using COSMO (DCM) model with TZ2P basis set without taking into account relativistic effects, [c]ADF 2017 optimization in solvent using COSMO (DCM) model with TZ2P basis set and by taking into account relativistic effects using ZORA with scalar correction, [d]ADF 2017 optimization in solvent using COSMO (DCM) model with TZ2P basis set and by taking into account relativistic effects using ZORA with spin-orbit coupling.*

The geometrical structures computed for **3a** using Gaussian 09 program with the two functionals, B3PW91 and BP86, are very similar. These structures are also similar close to that obtained upon optimization using the ADF program with BP86 functional taking into account zero-order regular approximation (ZORA). When relativistic effects were not taken into account for the geometry optimization (calculations carried out without ZORA) the N-H bond departs from Au and strengthens, reflecting their importance in the structure of **3a**. In turn, this shows that the N-H···Au interaction is assisted by chelation but not imposed geometrically in **3a**.

2.2 Bonding Analysis

The bonding situation in **3a** was then analyzed using various methods. Natural Bond Orbital (NBO) analysis (Table III-5) substantiates the weakening of the N-H bond upon interaction with gold. The Wiberg Bond Index (WBI) of the N-H bond decreases from 0.71-0.73 in **3b,c** to 0.61 in **3a**, while the WBI for the Au···H interaction in **3a** is small but non-negligible (0.124). In the meantime, the computed Natural Population Analysis (NPA) charges show some charge transfer from the metal fragment to the ammonium moiety: the charge for the

PAuCl fragment increases from 0.65-0.71 in **3b,c** to 0.76 in **3a**, while the charge for the NMe$_2$H fragment decreases from 0.66-0.68 in **3b,c** to 0.61 in **3a**. This charge transfer is also apparent from the electrostatic potential (ESP) maps. Side views of **3a** and **3b** are displayed in Figure III-13, left. The ammonium moiety is located in a positive (blue) area in both cases, but when H-bonded to gold, its charge is reduced and the surface is lighter.

	3a	**3b**	**3c**	**3a_OTf**	**6a**
ΔE(2) (kcal/mol)	12.8	/	/	12.3	8.9
NLMO	95.9% Au	97.7% Au	97.6% Au	96.6% Au	97.1% Au
d$_{Au}$	0.7% N			0.6% N	0.4% N
	2.5% H			2.0% H	1.5% H
pop (d$_{Au}$)	1.92	1.95	1.95	1.93	1.94
pop (σ*$_{NH}$)	0.12	0.02	0.03	0.10	0.09
WBI (Au···H)	0.12	/	/	0.10	0.08
WBI (N-H)	0.61	0.73	0.71	0.65	0.64
NPA charges					
q$_{NR2H}$	0.605	0.656	0.675	0.595	1.274
q$_{PAuCl}$	0.765	0.713	0.651	0.754	0.720

*Table III-5: NBO analyses for complexes **3** and **6**. Stabilizing energy ΔE(2) and percentage of main atoms in the NLMO accounting for the d$_{Au}$ → σ*$_{NH}$ donor-acceptor interaction. Populations of the occupied d$_{Au}$ and vacant σ*$_{NH}$ NBO orbitals involved in the Au···H-N interaction. Wiberg Bond indexes (WBI) between Au and H, N and H. NPA charges of the NR$_2$H and PAuCl fragments (q$_X$).*

Besides this electrostatic component, the NBO analysis revealed some orbital contribution to the N-H···Au interaction. A weak donor-acceptor interaction (delocalization energy ΔE(2) = 12.8 kcal/mol) between an occupied d$_{Au}$ orbital and the σ*$_{NH}$ orbital was found at the second-order perturbation theory (Figure III-13, right). This picture is consistent with a 3c-4e interaction, as inferred for H-bonded complexes and as opposed to the 3c-2e interaction involved in agostic complexes.[2,39]
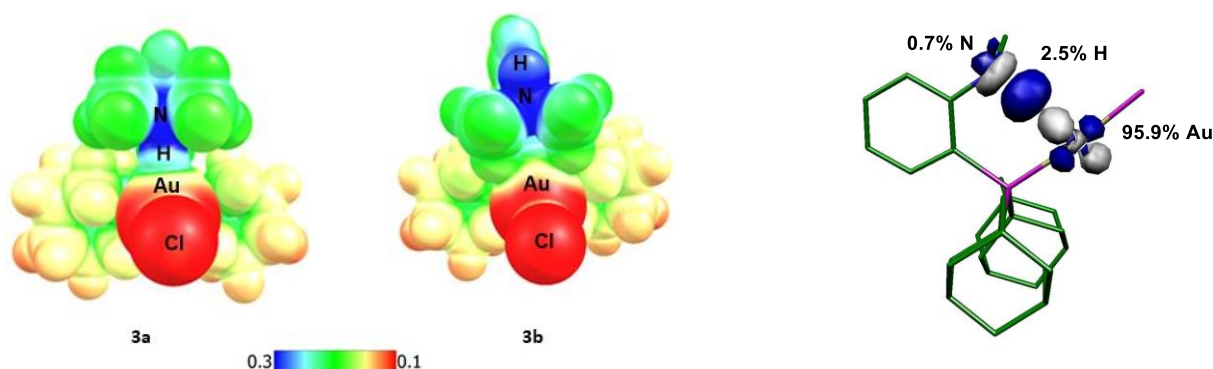
*Figure III-13: Left: Electrostatic potential maps for **3a** and **3b** plotted over the range 0.1 (red) to 0.3 au (blue). The isosurfaces are drawn at 0.002 e.au^{-3}. Right: Superposition of the donor and acceptor NBO orbitals (cutoff = 0.08) involved in the N-H···Au interaction. Participation of each atom in percent in the associated NLMO.*

AIM analysis was then performed. The electron density at the N-H BCP is smaller for **3a** than for the two conformers **3b,c** (ρ = 0.319 *vs* 0.343 e.bohr^{-3}), in line with the bond weakening delineated by IR and NBO. In addition, the ground state structure shows a BCP between the Au and H atoms with ρ_{AuH} = 0.039 e.bohr^{-3} and $\nabla^2\rho_{AuH}$ = 0.068 e.bohr^{-5} (Figure III-14, left for the Laplacian of the electron density map). The ρ_{AuH} value is in the upper limit of the range defined for hydrogen bonding interaction.[20]
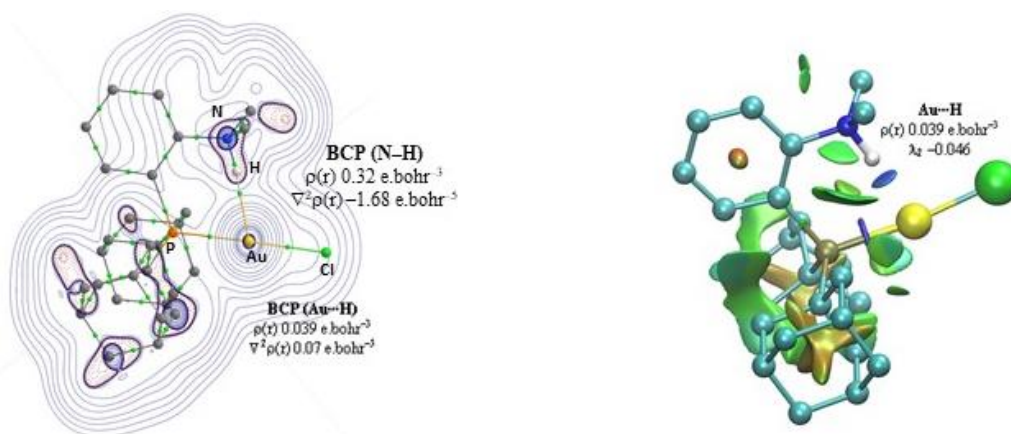
*Figure III-14: Left: Contour plot of the Laplacian distribution $\nabla^2\rho(r_c)$ for **3a** with relevant bond paths and bond critical points (green spheres). Hydrogen atoms have been omitted for clarity except that on the nitrogen atom. Right: NCI plot for **3a**. Gradient isosurface (s = 0.5 au) colored according to a BGR scheme over the range of -0.05 < sign (λ_2)ρ < 0.05 au). Blue indicates strong attraction, green indicates very weak interaction, and red indicates strong repulsion.*

This picture is corroborated by the NCI plot (Figure III-14, right). The negative value of λ_2 between Au and H is indicative of attractive non-covalent interaction and consistent with N-H⋯Au hydrogen bonding.[22]

This detailed analysis thus provides compelling evidence for the presence of N-H⋯Au hydrogen bonding in **3a**. The computational methods and obtained results complete each other and are all consistent with a 3c-4e attractive interaction.

III. Not a unique case: other examples of gold hydrogen bonding

To complete the study and generalize the bonding situation to other gold complexes, an analogue of **3** was studied. The cationic MorDalPhos gold complex **6,** with a morpholine instead of dimethylamine group, was prepared and characterized by multi-nuclear NMR spectroscopy. The proton at N resonates at low field in ^{1}H NMR (δ 11.4 ppm). Exchange of the TfO$^-$ counteranion for the tetraarylborate BAr$^F_4$ enabled the growth of crystals suitable for X-ray diffraction analysis. As apparent from the X-ray structure (Figure III-15), complex **6** adopts

the same conformation as **3**. The N-H bond points towards Au (with a quasi-linear N-H⋯Au arrangement, 174(6)°) and the H⋯Au distance is quite short (2.27(2) Å).
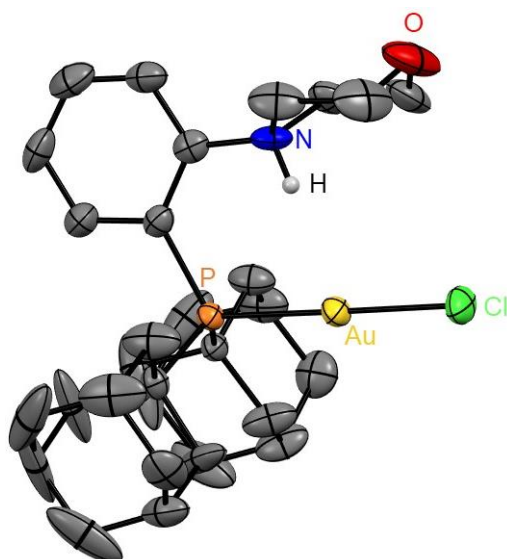
*Figure III-15: X-ray structure of the (P,NH⁺) gold(I) complex **6** derived from MorDalPhos. Thermal ellipsoids are drawn at 50% probability, counteranion BAr$^F_4$ and hydrogen atoms, except that on nitrogen, are omitted for clarity. Selected bond lengths (Å) and bond angles (°): P-Au 2.272(2), Au-Cl 2.287(2), Au⋯H 2.28(5), PAuCl 177.88(8), NHAu 174(6).*

DFT calculations (Figure III-16 & Table III-6) support further the analogy between **3** and **6**. The ground state structure of the MorDalPhos complex **6** is that observed experimentally. Its geometric and spectroscopic features are very similar to those of **3**.

Bonding analysis indicates the presence of Au⋯H-N hydrogen bonding, whose magnitude is slightly weaker than for the MeDalPhos complex **3** according to NBO and AIM analyses (see for comparison the numerical values of the WBI, NPA charges, second-order NBO delocalization energies, electron density at BCPs, Table III-5).
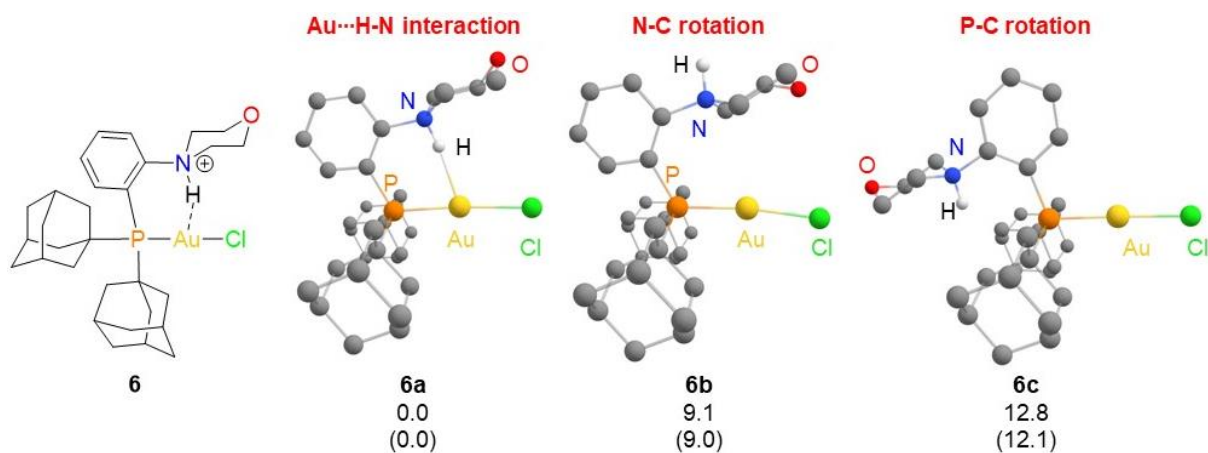
*Figure III-16: Optimized geometries of the different forms of the cationic complex **6**, without taking into account the counteranion. Relative energies in kcal/mol (ΔG values, with ΔE values into brackets).*

	6a	6b	6c
P-Au	2.298	2.302	2.308
Au-Cl	2.338	2.343	2.339
N-H	1.045	1.028	1.026
Au···H	2.218	/	/
PAuCl	175.1	172.5	178.2
NHAu	170.1	/	/
υ_{NH} (cm^{-1})	3078.4	3406.4	3489.9
$\Delta\upsilon_{NH}$[a]	-365.3	-37.4	46.1
δ ^{1}H NMR (NH, ppm)	11.23	5.04	5.81

*Table III-6: Key geometric features (distances in Å, angles in °) and spectroscopic data (IR and NMR) computed for the three conformers **6a-c**. [a]difference with HNmorpholine$^+$*

Not only the amino group but also the co-ligand can be modified, as substantiated later on by Bochmann's group.[40] They prepared the dicationic complex **3_W** featuring two hydrides bridging W and Au (Scheme III-3).
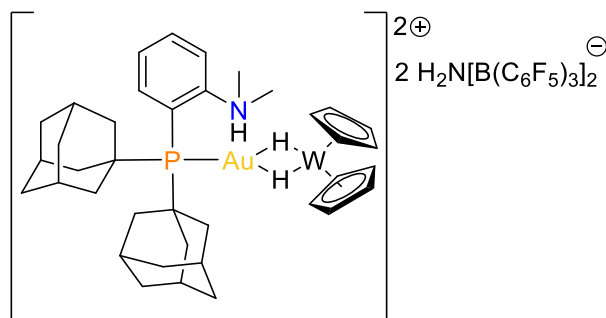
*Scheme III-3: Chemdraw structure of (P,NH$^+$) complex **3_W**.*

X-ray data showed that the (P,N) ligand adopts the same conformation as in **3** and on the ^{1}H NMR spectrum a downfield shift signal at δ 12.4 ppm was observed. On the DFT-optimized structure a short Au···H distance (2.114 Å) can be observed and the attractive nature of the interaction was confirmed by AIM and NBO analyses (delocalization energy for the donor-acceptor interaction $d_{Au} \to \sigma^*_{NH}$, ΔE(2) = 13.4 kcal/mol).

Simultaneous to our characterization of the (P,NH$^+$) gold(I) complexes, Straka *et al.* reported evidence for very similar Au···H-N hydrogen bonding in cationic gold(I) complex **III-E** featuring an NHC ligand.[41] The complex **III-E** was characterized in the gas phase by helium-tagging infrared photodissociation (IRPD) spectroscopy. A red-field shift of about 500 cm^{-1} was observed both for the N-H and N-D vibrational bands demonstrating experimentally the presence of Au···H-N hydrogen bonding. All isolation and/or characterization attempts in condensed phase led to decomposition of the gold(I)-carbene species.

Their DFT calculations (Figure III-17 & Table III-7) support further the attractive nature of this hydrogen bond. The ground state structure of the complex **III-Ea** shows Au⋯H-N interaction with short Au⋯H contact (2.165 Å), a large AuHN bond angle (169.0°) and an elongated N-H bond (1.045 *vs* 1.018 Å). Another conformer **III-Eb** with rotation around the C_{CH2}-N bond was found 11.0 kcal/mol higher in energy. Bonding analysis shows $d_{Au} \rightarrow \sigma^*_{NH}$ donor-acceptor interaction with a delocalization energy of 13.0 kcal/mol as well as a BCP between the gold and the hydrogen atom (ρ_{AuH} = 0.033 e.bohr^{-3} and a positive Laplacian of 0.08 e.bohr^{-5}). These data confirm the presence of an attractive Au⋯H-N hydrogen bonding.
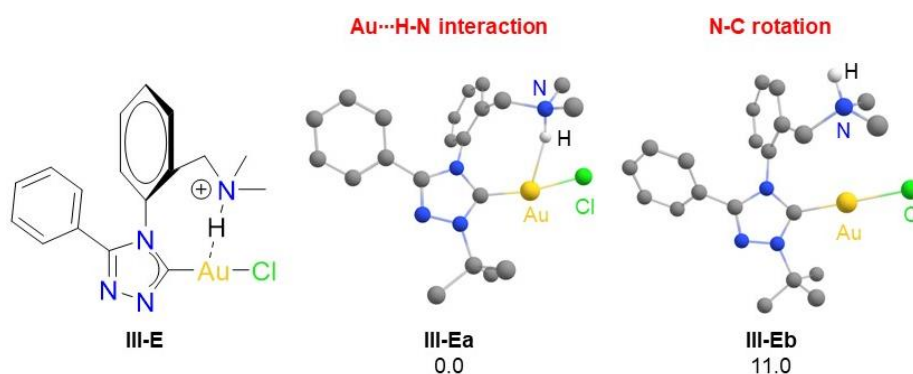
Figure III-17: Optimized geometries of the different forms of the cationic complex **III-E** at the PBE0-D3/def2-TZVPP level of theory, without taking into account the counteranion. Relative energy (ΔE) in kcal/mol.

	III-Ea	**III-Eb**
C-Au	1.988	1.989
Au-Cl	2.273	2.271
N-H	1.045	1.018
Au⋯H	2.165	/
CAuCl	169.0	173.4
NHAu	159.2	/
δ ^{1}H NMR (NH, ppm)	10.6	5.8
ΔE(2)^a (kcal/mol)	13.0	/

Table III-7: Key geometric features (distances in Å, angles in °) and spectroscopic data (NMR) computed for the two conformers of **III-E**. Stabilizing energy ΔE(2) for the $d_{Au} \rightarrow \sigma^*_{NH}$ donor-acceptor interaction.

Another gold(I) complex susceptible to display Au⋯H hydrogen bonding was identified from recent literature and we analyzed it computationally. Complex **III-F** was characterized by NMR and considered, but ruled out, as intermediate in the formation of a pincer Au(III) hydride complex.[42] According to the optimized geometries (Figure III-18, left), the H atom at N enters the coordination sphere of Au, with computed H⋯Au distance of 2.216 Å. NBO and AIM analyses do support the presence of some H-type bonding (delocalization energy of 3.8 kcal/mol and BCP between the gold and the hydrogen atom with ρ_{AuH} = 0.034 e.bohr^{-3} and a positive Laplacian of 0.112 e.bohr^{-5}), albeit substantially weaker than those observed in the (P,NH$^+$) gold complexes derived from the Me/MorDalPhos ligands.
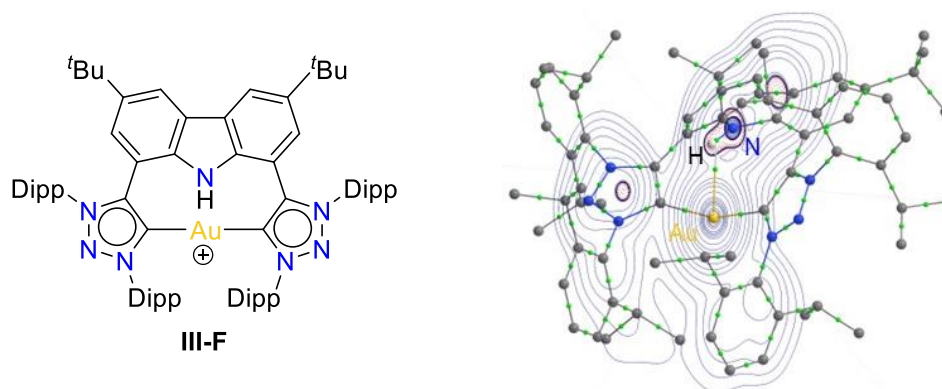
*Figure III-18: ChemDraw structure and contour plot of the Laplacian distribution $\nabla^2\rho(r_c)$ of the gold(I) complexes **III-F**.*

Previous examples are dealing with R_3NH^+ donor groups, which enhance the protic character of the hydrogen. Recently, Gabbaï and co-workers studied H-bonds to gold with a neutral OH group.[43] They synthesized two gold(I) complexes with NHC ligands bearing either a carbinol or a silanol moiety (Figure III-19). X-ray data showed structures with the hydroxyl group pointing toward gold (hydrogen atoms involved were refined isotropically). The downfield shift resonance of the hydroxyl group in ^1H NMR as well as the red-field shift observed in IR spectroscopy confirmed the presence of hydrogen bonds.

Also typical features of H-bonding were observed in the optimized structures: the ground state is the one where O-H is pointing toward gold, there is short Au···H contact (2.293 Å for carbinol and 2.494 Å for silanol) and elongated O-H bonds compared to other isomers without interaction (0.974 Å and 0.969 Å *vs* 0.965 Å and 0.961 Å for carbinol and silanol respectively). AIM analyses exhibit BCP between Au and H for each structure with $\rho = 0.026$ e.bohr^{-3} for carbinol or 0.017 e.bohr^{-3} for silanol, in the range expected for hydrogen bonding interaction. NBO analyses show multiple $d_{Au} \rightarrow \sigma^*_{OH}$ interactions with a total energy of 10.6 kcal/mol for carbinol and 5.0 kcal/mol for silanol. DFT calculations have been performed as the same level of theory as our compounds, suggesting that these O-H···Au interactions are weaker than the N^+-H···Au interactions.
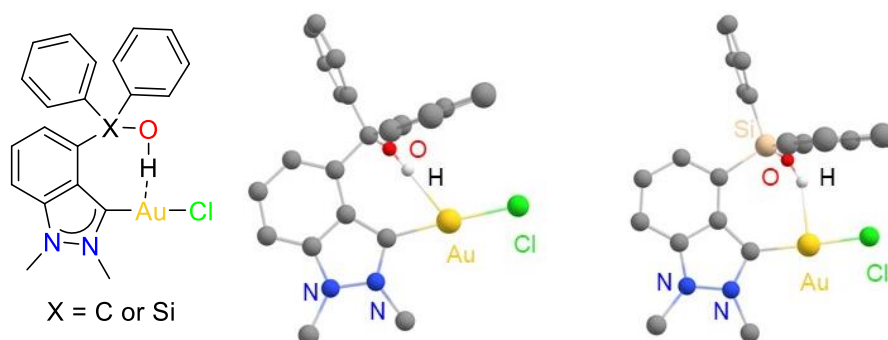
Figure III-19: Optimized structures of carbinol and silanol gold(I) complexes described by Gabbaï's group.

X-H···Au used to be considered as elusive and their existence was a matter of debate.[43,44] Within less than five years, the situation has changed completely. As described in this part, strong, convincing and consistent evidences for the existence of several X-H···Au interactions have been obtained.

IV.   Possible variants: *In silico* study and first experimental clue

In view of the growing interest in the structure presenting hydrogen bonding to gold, we performed a computational study aiming at investigating the influence of different parameters (Scheme III-4). Do they favor the establishment of hydrogen bonding to gold? How much do they stabilize this interaction? This *in silico* study intended to provide guidelines for further experimental work.

H-bond donors

Ligands

Scheme III-4: Targeted complexes presenting hydrogen bonding to gold.

This work was initiated by Dr. E.Daiann Sosa Carrizo from the team of Dr. Karinne Miqueu. I then took it over and studied the different models discussed below. All calculations were performed using the Gaussian 09 package at the B3PW91/SDD+f(Au),6-31G**(other atoms) level of theory. Solvent effects (CH$_2$Cl$_2$) were taken into account by means of the universal continuum solvation SMD model. For each model, the following analyses have been performed: optimization of geometry, NBO and AIM analyses, calculations υ_{XH} stretching mode

and NMR chemical shift. The reference for relative energies is always the isomer displaying Au⋯H- N interaction. To simplify the discussion and since elongation of the X-H bond, NMR and IR data are similar for the isomers with rotation around the X-C or P-C bond, only one isomer will be mentioned.

First, the nature of the donor of H bond was investigated. The same ligand has been kept (the phosphorus bears two adamantyl and one phenyl groups) and hydroxyl (**7**), sulfonamide (**8**) and phosphonium (**9**) have been tested as donors (Figure III-20 & Table III-8). This way the existence and strength of the bond will only depend on the nature of the H-bond donor.

The alcohol complex **7** presents all the features of a hydrogen bonding to gold: elongation of the OH bond (0.013 Å), large OHAu bond angle (167.7°), red shift of the OH frequency (309 cm^{-1}), downfield shift in NMR ($\Delta\delta$ = 3.98 ppm) and a BCP between Au and H atoms with ρ_{AuH} = 0.033 e.bohr^{-3} and $\nabla^2\rho_{AuH}$ = 0.067 e.bohr^{-5} in the range for such interaction. The rotation around the CO bond do not suffer steric hindrance, so the difference of energy (ΔG = 2.3 kcal/mol) between the two conformers may provide a measure for the strength of the hydrogen bonding. This value is relatively similar to the one found by Gabbai and co-workers (ΔG = 3.2 kcal/mol).

The sulfonamide complex **8** also presents a short Au⋯H contact. The elongation is only 0.008 Å, but this value is in the same range than that obtained by Gabbai and co-workers in the silanol complex observed experimentally. Other parameters (red shift of the υ_{NH} bond by 215 cm^{-1}, downfield shift in NMR and BCP with ρ_{AuH} = 0.029 e.bohr^{-3}) are in favor of the attractive hydrogen bonding interaction. Here, the energy difference between the ground state and the isomer with rotation around the CN bond is important (31.9 kcal/mol) showing that it does not always give an accurate estimation of the strength for the hydrogen bonding.

The same statement can be made for the phosphonium complex **9**. Despite a small PHAu bond angle (138.7°), all the other parameters go in favor of the hydrogen bonding.

Whatever the donor moiety, it seems possible to observe hydrogen bonding to gold. The strength of the hydrogen bonding follows the polarity of the X-H bond. The stronger one seems to be formed with ammonium moiety (complex **3**) following by the alcohol complex **7**. The smallest ones are observed with sulfonamide and phosphonium.

Figure III-20: Optimized geometries of the different forms of the cationic complex **7**, **8** and **9**. Relative energies in kcal/mol (ΔG values, with ΔE values into brackets).

	Alcohol		Sulfonamide		Phosphonium	
	7a	**7b**	**8a**	**8b**	**9a**	**9b**
Au···H (Å)	2.181	/	2.255	/	2.233	/
X-H (Å)	0.982	0.969	1.029	1.021	1.409	1.398
XHAu (°)	167.7	/	157.05	/	138.7	/
υ_{XH} (cm^{-1})	3475.5	3784.0	3310.7	3525.4	2431.3	2589.8
δ ^{1}H NMR (NH, ppm)	8.63	4.65	10.04	5.73	12.34	5.71
ΔE(2) (kcal/mol)	8.7	/	5.4	/	5.6	/
ρ_{AuH} (e.bohr^{-3})	0.033	/	0.029	/	0.034	/

Table III-8: Key geometric features, spectroscopic (NMR and IR), NBO and AIM data for complexes **7**, **8** and **9**. Stabilizing energy ΔE(2) and percentage of main atoms in the NLMO accounting for the $d_{Au} \rightarrow \sigma^*_{XH}$ donor-acceptor interaction.

To assess the strength of the bond, the complex bearing the NMeH$_2$$^+$ (**10**) instead of the NMe$_2$H$^+$ (**3**) was considered. The two hydrogens can be involved in the bonding with gold and the energy of exchange between the 2 hydrogens may give an estimation for the strength of the bond (Scheme III-5). Moreover, the ^{1}H NMR signals of the two protons differing, a kinetic measurement may allow to determine experimentally the barrier of rotation and so the energy of the hydrogen bonding.[45]
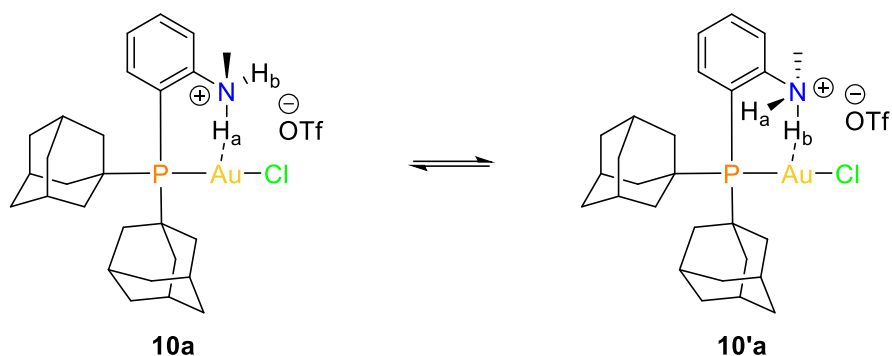
Scheme III-5: Reaction of exchange of the proton involved in the Au···H-N interaction.

DFT calculations proved that the ground state (**10a/10a'**) is the geometry where only one H is in interaction with gold. The data are similar to complex **3** (Table III-9): elongation of the N-H bond of 0.019 Å, donor-acceptor interaction with delocalization energy $\Delta E(2)$ = 12.8 kcal/mol between an occupied d_{Au} orbital and the σ^*_{NH} orbital and a BCP between Au and H with ρ_{AuH} = 0.038 e.bohr^{-3} and $\nabla^2\rho_{AuH}$ = 0.066 e.bohr^{-5}. Another isomer with the 2 H directed toward gold (**10b**) has been localized on the PES but the Au···H distances (> 2.6 Å) are too long and the NHAu bond angles (< 110°) far from 180° to consider a hydrogen bonding. The latest is 3.5 kcal/mol higher in energy than the ground state. A transition state has been found between **10a/10'a** and **10b**, associated to the exchange of proton involved in the Au···H-N interaction, with an activation barrier of 4.0 kcal/mol (Figure III-21). This barrier, which allows us to estimate more accurately the energy of the hydrogen bonding (3.5-4.0 kcal/mol), is probably too weak to be determined by NMR experiments.

	10a		**10b**
	N-H in interaction	Free N-H	
Au···H (Å)	2.151	/	2.651/2.626
X-H (Å)	1.045	1.026	1.029/1.029
NHAu (°)	166.3	/	107.3/109.0
υ_{NH} (cm^{-1})	3062.0	3472.7	3427.5/3389.8
δ ^{1}H NMR (XH, ppm)	12.21	4.98	7.30/7.15
$\Delta E(2)$ (kcal/mol)	12.8	/	/
NLMO % Au	96.0	/	/
% N	0.7	/	/
% H	2.4	/	/
ρ_{AuH} (e.bohr^{-3})	0.038	/	/
$\nabla^2\rho_{AuH}$ (e.bohr^{-5})	0.066	/	/

*Table III-9: Key geometric features, spectroscopic (IR and NMR), NBO and AIM data for complexes **10**. Stabilizing energy ΔE(2) and percentage of main atoms in the NLMO accounting for the $d_{Au} \rightarrow \sigma^*_{NH}$ donor-acceptor interaction.*

d(H_a-Au) = 2.515 Å
d(H_b-Au) = 2.850 Å
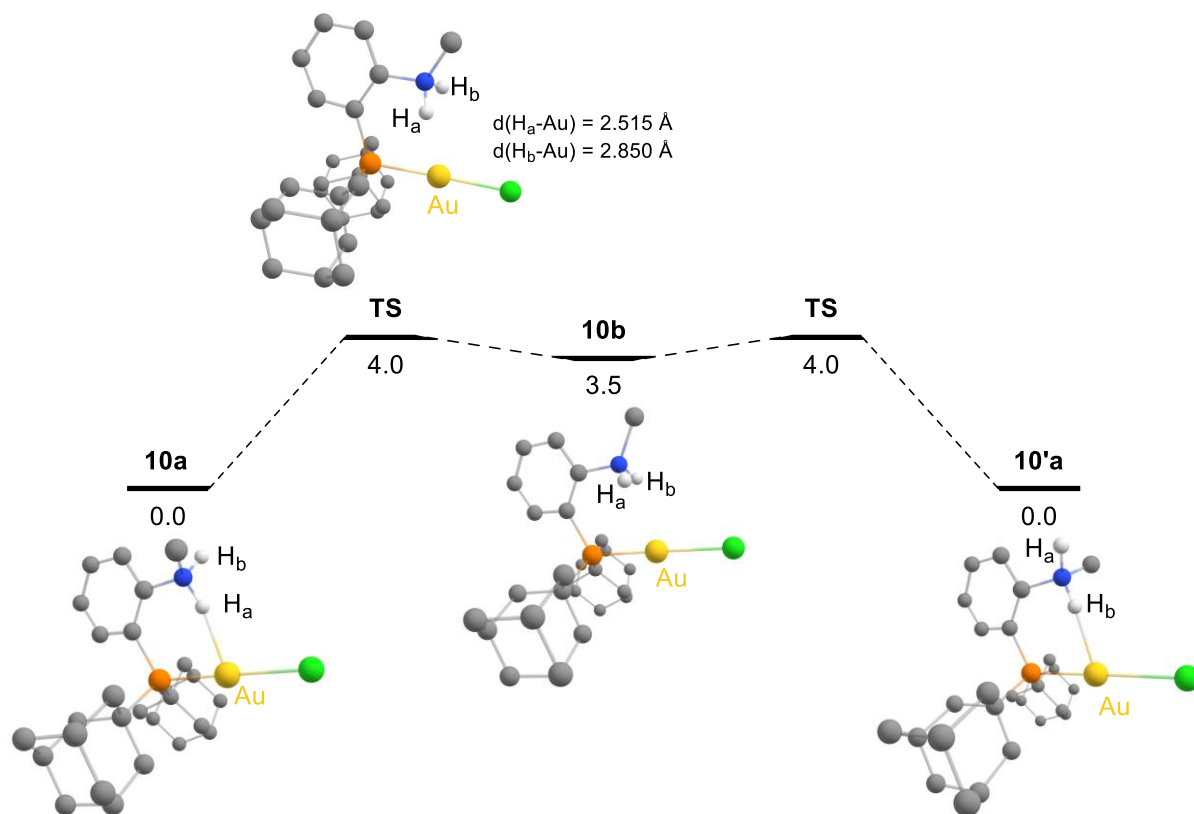
*Figure III-21: Optimized geometries of the different forms of the cationic complex **10**. Exchange of proton involved in the Au···H-N interaction. Relative Gibbs energies (ΔG) in kcal/mol.*

Then, the influence of the substituents on the phosphorus was investigated. Recently, the di-*tert*-butyl-substituted aminophosphine (P,N) gold complex has been proven to efficiently undergo oxidative addition of aryl iodides and was used in S-cysteine arylation.[46,47] Behaving as the MeDalPhos gold complex, we wondered if it was the same regarding hydrogen bonding (Figure III-22 & Table III-10).

*Figure III-22: Optimized geometries of the different forms of the cationic complex **11**. Relative energies in kcal/mol (ΔG values, with ΔE values into brackets).*

	11a	**11b**
Au···H (Å)	2.142	/
X-H (Å)	1.045	1.025
NHAu (°)	172.7	/
υ_{NH} (cm^{-1})	3036.6	3463.5
δ ^{1}H NMR (NH, ppm)	11.72	5.65
ΔE(2) (kcal/mol)	11.4	/
NLMO % Au	96.0	/
% N	0.6	
% H	2.3	
NPA charges q_{NR2H}	0.617	0.667
q_{PAuCl}	0.722	0.673
ρ_{AuH} (e.bohr^{-3})	0.039	/
$\nabla^2\rho_{AuH}$ (e.bohr^{-5})	0.068	/

*Table III-10: Key geometric features, spectroscopic (IR and NMR), NBO and AIM data for complexes **11** and its isomer (rotation around the C-N bond). Stabilizing energy ΔE(2) and percentage of main atoms in the NLMO accounting for the $d_{Au} \rightarrow \sigma^*_{NH}$ donor-acceptor interaction.*

There are no noticeable changes compared to MeDalPhos ligand: the elongation of the N-H bond, the υ_{NH} vibration and the ^{1}H NMR signal are almost identical. The Au···H distance being longer for *tert*-butyl (2.142 Å) than for adamantyl (2.134 Å), the rotation barrier around the C-N bond is smaller (9.4 kcal/mol *vs* 11.9 kcal/mol) and the orbital contribution in the Au···H interaction is less important (ΔE(2) = 11.4 kcal/mol *vs* 12.8 kcal/mol), but the charge transfer from the metal fragment to the ammonium moiety is similar. The existence of the Au···H-N interaction is also confirmed by the presence of a BCP between Au and H atoms with similar value as the MeDalPhos gold complex.

Next, the phenyl spacer was exchanged by a Naphthyl one (**12**). The Au···H-N interaction will induce the formation of a 7 membered cycle instead of 6 in the MeDalPhos gold complex. Three different *minima* were found on the PES (Figure III-23 & Table III-11).
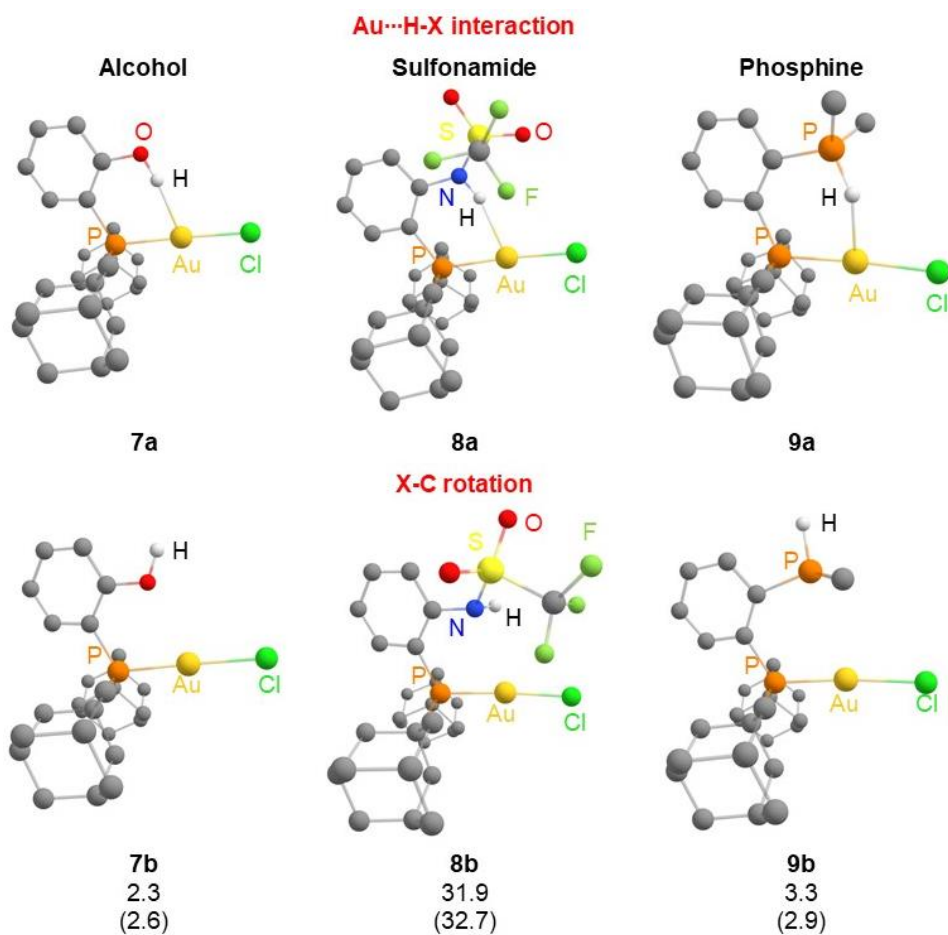

*Figure III-23 : Optimized geometry of the different forms of the cationic complex **12**. Relative energies in kcal/mol (ΔG values, with ΔE values into brackets).*

	12a	**12b**	**12c**
Au⋯H (Å)	2.149	/	/
N-H (Å)	1.041	1.024	1.024
NHAu (°)	153.5	/	/
υ_{NH} (cm^{-1})	3066.1	3467.9	3481.3
δ ^{1}H NMR (NH, ppm)	11.92	5.88	7.61
ΔE(2) (kcal/mol)	10.5	/	/
NLMO %Au	96.2	/	/
%N	0.6		
%H	2.0		
ρ_{AuH} (e.bohr^{-3})	0.041	/	/

*Table III-11: Key geometric features, spectroscopic (IR, NMR), NBO and AIM data for complexes **12**. Stabilizing energy ΔE(2) and percentage of main atoms in the NLMO accounting for the Au⋯H-N interaction.*

Again, the most stable isomer is the one involving N-H⋯Au interaction (**12a**). The Au⋯H distance is very close to that obtained with NMe$_2$H$^+$ substituent and *o*-phenylene linker (2.149 Å *vs* 2.134 Å), but the NHAu bond angle is smaller (153.5° *vs* 174.2° in **3**), likely because of geometric constraints. In line with the Au⋯H distance, the stabilizing interaction (ΔE(2)) computed at the second order perturbation theory level is slightly weaker than that computed for MeDalPhos (10.5 kcal/mol *vs* 12.5 kcal/mol).

To compare the influence of the ligand, a NHC complex (**13**) was examined. It bears exactly the same donor moiety as the MeDalPhos (NMe$_2$H), the ring size is kept (6-membered ring) but with only C or N that are smaller atoms than P. One main difference is the rigidity of the framework that reduced the degree of freedom (only the N-C rotation is possible, Figure III-24).


*Figure III-24: Optimized geometries of the different forms of the cationic complex **13**. Relative energies in kcal/mol (ΔG values, with ΔE values into brackets).*

	13a	**13b**
ΔG isomers (kcal/mol)		8.4
Au···H (Å)	2.177	/
N-H (Å)	1.045	1.025
NHAu (°)	162.1	/
υ_{NH} (cm^{-1})	3021.8	3451.6
δ ^{1}H NMR (NH, ppm)	12.47	5.89
ΔE(2) (kcal/mol)	12.6	/
NLMO % Au	95.6	/
% N	0.7	/
% H	2.8	/
NPA charges q_{NMe2H}	0.652	0.678
ρ_{AuH} (e.bohr^{-3})	0.036	/
$\nabla^2\rho_{AuH}$ (e.bohr^{-5})	0.064	/

*Table III-12: Key geometric features, spectroscopic (IR and NMR), NBO and AIM data for complexes **14**. Stabilizing energy ΔE(2) and percentage of main atoms in the NLMO accounting for the Au···H-N interaction.*

Once again, the ground state is the one with N-H pointing toward gold with all data being in favor of a hydrogen bonding interaction (Table III-12). Despite a slightly longer Au···H distance and smaller NHAu bond angle in **13** (2.177 Å and 162.1°) compared to **3** (2.143 Å and 174.2°), the elongation of the N-H bond is similar (0.020 Å) and so the shift observed in infra-red is analogous (430 cm^{-1}), meaning that the strength of the hydrogen bonding for both complexes should be identical. The other conformer (rotation around the CN bond) is 8.4 kcal/mol higher in energy. This difference in energy is smaller than the one observed for complex **3** in line with the increase distance between Au and N.

The orbital contributions to the N-H···Au interaction are almost the same for the two complexes **13** and **3** (ΔE(2) = 12.6-12.8 kcal/mol and NLMOs display 95.6-95.9%Au, 0.7%N and 2.8-2.5%H) whereas the electrostatic participation is weaker for the NHC complex. When looking at the difference of NPA charges at the NMe$_2$H moiety, from the isomer with interaction to the isomer without one, a decrease of charge can be observed for both complexes but with a smaller impact for **13** (NPA charge transfer in **13**: 0.026 whereas it is 0.051 for **3**).

Some experimental work went to orient the *in silico* study. Having in hand the 8-(diphenylphosphino)quinoline, a protonation test was performed. Addition of 1 equivalent of HOTf to this gold complex immediately led to a new complex **14** according to ^{31}P NMR spectroscopy and ^{1}H NMR (a broad signal appears at δ 11.5 ppm confirming the presence of NH). Crystals of **14** were grown from a dichloromethane/pentane solution at -30°C and analyzed by X-ray diffraction (Figure III-25, left). The H atom at N was located in the difference Fourier map and refined freely. The N-H bond is directed toward the TfO⁻ counteranion: the NHO bond angle is large (160(5)°) and the O···H distance (2.14(5) Å) is well within the sum of van der Waals radii.[27]

To circumvent this issue an exchange of the TfO counteranion for the BAr$^F_4$ was done and new crystals of **14_BAr$^F_4$** were grown from a toluene/pentane solution at -30°C and analyzed by X-ray diffraction (Figure III-25, right). Once again, no N-H interaction toward gold is observed, instead an intermolecular interaction between an N-H from one complex and the Cl of another complex was formed (and *vice versa*). Contrary to the gas phase, interferences of the environment (other molecules, counteranion…) cannot be neglected in the condensed phase. Chlorine at gold was exchanged by a methyl substituent that prevents intermolecular hydrogen bonding. The new gold complex was treated with H(Et$_2$O)BAr$^F_4$ (and not HOTf, to avoid hydrogen bonding with the counteranion), but the desired product was not obtained. The Au-CH$_3$ bond was protonated, as apparent from the characteristic singlet associated with CH$_4$ in ^{1}H NMR (even at low temperature). Cleavage of the Au-CH$_3$ bond instead of nitrogen protonation is surprising since Au-C$_{sp}$^{3} bonds were shown to be quite reluctant to protonolysis.[48] The experiment should be tested with a less acidic compound, the difficulty being to find one with an inert counteranion toward hydrogen bonding.
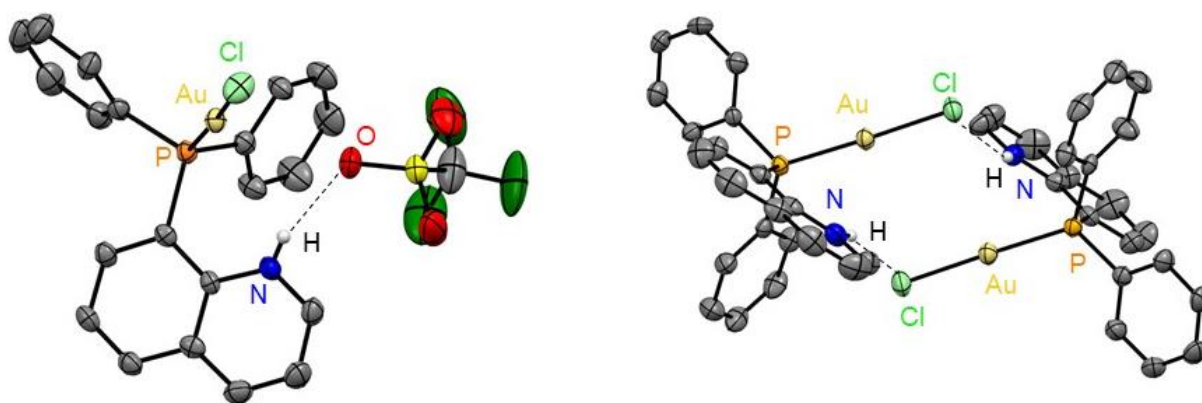
*Figure III-25: X-ray structures of the (P,NH+) gold(I) complex **14** derived from 8-(Diphenylphosphino)quinoline with OTf (left) and BAr$^F_4$ (right) as counte anion. Thermal ellipsoids are drawn at 50% probability, hydrogen atoms, except that on nitrogen, and Bar$^F_4$ counteranion are omitted for clarity.*

After these experimental observations, we wondered if the DFT calculations, despite the treatment of isolated species and the absence of counteranion, also suggest the absence of hydrogen bonding to gold. Even if a *minimum* was found with N-H···Au interaction, it is not the ground state. Indeed, by rotation around the P-C bond (PAuCC : 48.9°), another isomer without interaction can be identified and it is lower in energy by 2.0 kcal/mol (Figure III-26 & Table III-13).
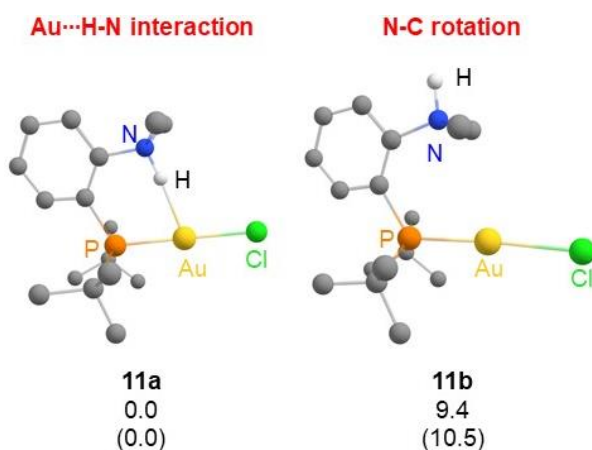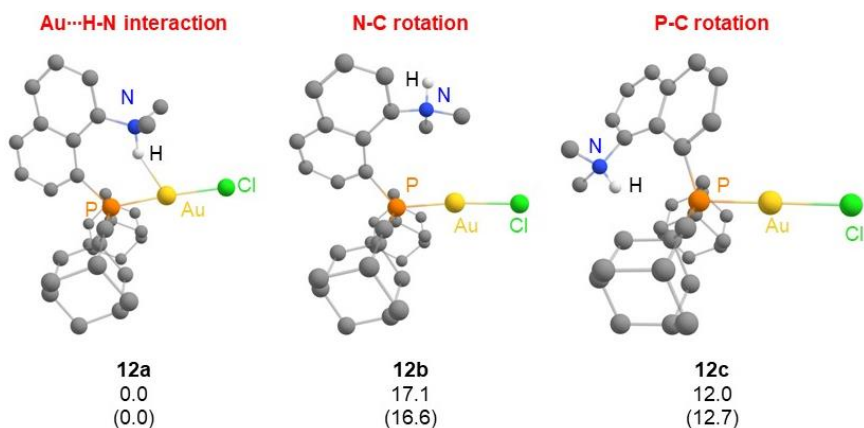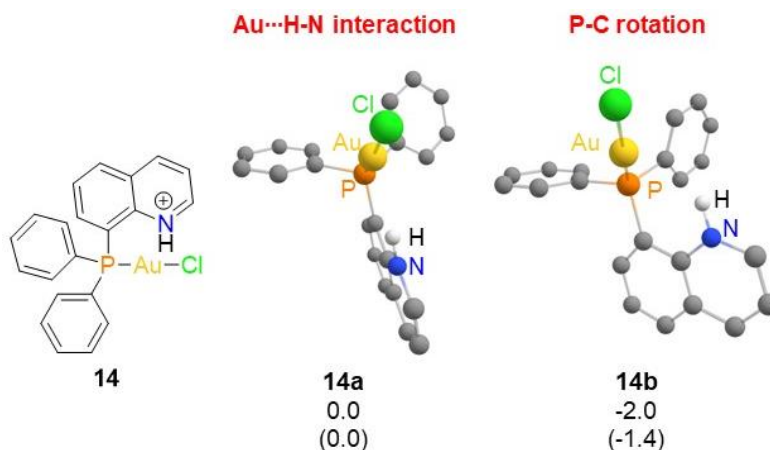
Figure III-26: Chemdraw structure and optimized geometries of the different forms of the cationic complex **14**. Relative energies in kcal/mol (ΔG values, with ΔE values into brackets).

	14a	**14b**
Au⋯H (Å)	2.288	2.592
X-H (Å)	1.030	1.022
NHAu (°)	160.5	138.8
AuPCC (°)	0.0	48.9
υ_{NH} (cm^{-1})	3300.9	3461.7
ΔE(2) (kcal/mol)	5.8	/
NLMO % Au	96.7	/
% N	0.4	/
% H	1.3	/
ρ_{AuH} (e.bohr^{-3})	0.029	/

Table III-13: Key geometric features, spectroscopic (IR) and NBO data for complexes **14**. Stabilizing energy ΔE(2) and percentage of main atoms in the NLMO accounting for the Au⋯H-N interaction.

The conformational control induced by the steric hindrance of adamantyl or *tert*-butyl group preorganized the ligand, notably the orientation of the N-H bond toward gold. At this point, we can wonder to which extent this conformational control favors hydrogen bonding to gold. To assess this point, the 2-(diphenylphosphino)-*N*,*N*-dimethyl-gold chloride complex was studied computationally. Despite the careful inspection of the PES, no *minimum* with a short Au⋯H distance (≈ 2.1-2.2 Å) and AuPCC dihedral angle near to 0° was found. This suggests that the absence of conformational control induced a weakening of the strength of the hydrogen bonding interaction compared to other complexes. The ground state (**15a**) presents an AuPCC dihedral angle of 44.4° similar to the angle found for the isomer **14b** and an Au⋯H distance of 2.431 Å, distance longer than those previously computed (Figure III-27 & Table III-14). Another *minimum* was found by rotation of the N-C bond (**15b**), 9.5 kcal/mol higher in energy than **15a**. In **15a**, an elongation of the N-H bond is observed compared to the isomer **15b** associated with the rotation around the N-C bond (0.01 Å), as well as a red-field shift of the υ_{NH} vibration (205 cm^{-1}) and a downfield shift on ^{1}H NMR (3.87 ppm), but these variations are reduced compared to previous complexes. Also, a small donor-acceptor interaction (ΔE(2) = 4.5

kcal/mol) and a BCP between Au and H are detected but with values in the lower limit of the range defined from hydrogen bonding interaction (ρ_{AuH} = 0.024 e.bohr^{-3} and $\nabla^2\rho_{AuH}$ = 0.048 e.bohr^{-5}).
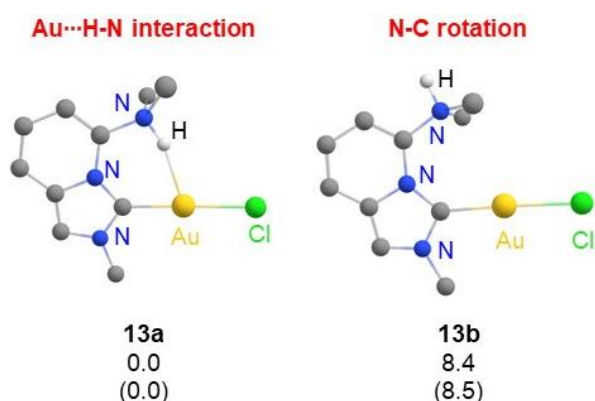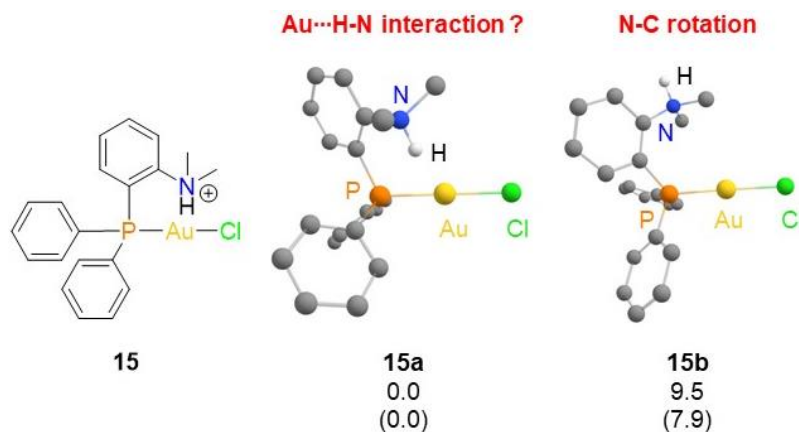

Figure III-27: Chemdraw structure and optimized geometries of the different forms of the cationic complex 15. Relative energies in kcal/mol (ΔG values, with ΔE values into brackets).

	15a	**15b**
Au⋯H (Å)	2.431	/
X-H (Å)	1.035	1.025
NHAu (°)	153.7	/
AuPCC (°)	44.4	45.4
υ_{NH} (cm^{-1})	3257.3	3462.3
δ ^{1}H NMR (NH, ppm)	9.47	5.60
ΔE(2) (kcal/mol)	4.5	/
NLMO % Au	96.4	/
% N	0.5	
% H	1.6	
ρ_{AuH} (e.bohr^{-3})	0.024	/
$\nabla^2\rho_{AuH}$ (e.bohr^{-5})	0.048	/

Table III-14: Key geometric features, spectroscopic (IR and NMR) and NBO data for complexes 15. Stabilizing energy ΔE(2) and percentage of main atoms in the NLMO accounting for the Au⋯H-N interaction.

The conformational control seems to significantly influence the hydrogen bonding to gold. Preventing P-C rotation, the Au⋯H-N interaction is stronger and there is no competition with intermolecular hydrogen bonding to co-ligand.

To favor the pyridinium-gold interaction, adamantyl substituents can be used instead of phenyl, but we faced problem in the synthesis of the corresponding ligand and thus, we turned our attention to a rigid NHC ligand. The gold complex, containing an NHC ligand bearing a pyridine derivative, synthesized by Monkowius and co-workers[49] seems to be a good candidate. The ligand being rigid, no rotation is possible. We optimized the structure of the protonated complex and showed that it has characteristics of hydrogen bonding: elongation of

the N-H bond of 0.010 Å compared to the free ligand, red-field shift for υ_{NH} ($\Delta\upsilon_{NH}$ = 235 cm^{-1}), a non-negligible donor-acceptor interaction ($\Delta E(2)$ = 9.0 kcal/mol) and a BCP between Au and H atoms with ρ_{AuH} and $\nabla^2\rho_{AuH}$ values in the typical range for hydrogen bonding. The geometric constraints induced by the rigidity of the ligand decrease the NHAu bond angle for **16** compared to the NHC gold complex **13** (148.1 *vs* 162.1° respectively) and might be responsible for the weaker NH bond interaction observed for **16**.
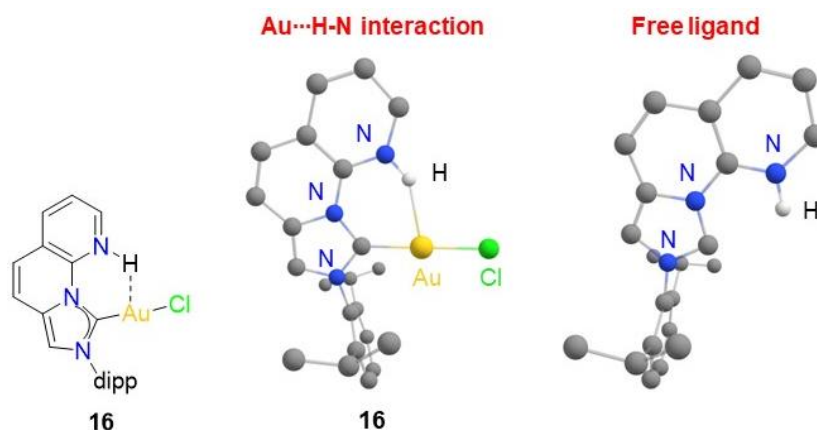
Figure III-28: Chemdraw structure and optimized geometries of the complex **16** and its free ligand.

	16	Ligand
Au⋯H	2.269	/
N-H	1.034	1.024
NHAu	148.1	/
υ_{NH} (cm^{-1})	3240.9	3475.5
δ ^{1}H NMR (NH, ppm)	15.89	12.76
$\Delta E(2)$ (kcal/mol)	9.0	/
NLMO % Au	96.5	/
% N	0.6	
% H	1.9	
ρ_{AuH} (e.bohr^{-3})	0.029	/
$\nabla^2\rho_{AuH}$ (e.bohr^{-5})	0.059	/

*Table III-15: Key geometric features, spectroscopic (IR and NMR) and NBO data for complex **16** and free ligand. Stabilizing energy $\Delta E(2)$ and percentage of main atoms in the NLMO accounting for the Au⋯H-N interaction.*

V.   Conclusions and outlook

Thanks to the MeDalPhos ligand, the complex **3** featuring a close contact between the gold(I) center and the proximal NH⁺ ammonium moiety has been prepared. The N-H⋯Au interaction verifies all the common features for hydrogen bond: (i) the XRD shows that the N-H bond is pointing towards Au, (ii) the N-H bond is elongated compared to isomer without interaction, (iii) the Au⋯H bond is smaller than the sum of van der Waals radii, (iv) the υ_{NH} undergoes a red-field shift and (v) ^{1}H NMR chemical signal is shifted downfield.

Thorough DFT analyses of the Au⋯H-N interaction have provided compelling evidence for 3-center-4-electron attractive interaction with gold acting as a proton acceptor. The hydrogen bond results from the electrostatic and the donor-acceptor orbital interactions. Similar situations have been authenticated in other gold(I) complexes, demonstrating that **3** is not a unique case.[44,50]

Several new models have been analyzed computationally and the most promising one will be synthesized to answer the following questions: what is the influence of the donor moiety (with complex **7, 8** and **9**)? What is the impact of the ligand (NHC complex **13** will be directly compared to complex **3**)? Does gold can engage in hydrogen bonding with pyridinium (complex **16**)? The *in silico* study has shown that a conformational control is needed to favor the weak hydrogen bonding to gold over other competitive bonding situations.

Having substantiated the existence of hydrogen bonding in gold(I) complexes, the same question can be raised for gold(III) complexes. Gold(III) complexes usually adopt square planar geometry, allowing a hydrogen bond to approach perpendicular to the plane. The HOMO is the $d_z{}^2$, ideally orientated for the formation of Au⋯H-X interactions. Nonetheless, gold(III) being less electron rich that gold(I), the interaction should be weaker.

Thanks to the use of chelating bis-carbanionic biphenylyl ligand, Bochmann's group synthesized two gold complexes **III-G** and **III-H** (Scheme III-6) containing a pyridinium moiety and an aurate(III). In the X-ray structure of **III-G**, the N-H bond points away from the gold center ruling out any possible hydrogen bonding. For **III-H**, a short Au⋯H contact can be observed, but no evidence for hydrogen bonding to gold(III) was reported. DFT calculations, based on the WBI, concluded that if hydrogen bonds exist in gold(III) complexes, there are considerably weaker than those involving gold(I) center.[51]

Menjón's group prepared organogold(III) compounds $(CF_3)_3Au(hq)$ **III-I** (Scheme III-6).[52] Despite many attempts, X-ray data showed only the solvates **III-I**.OEt$_2$ or **III-I**.OH$_2$ complexes with the OH interacting with the O of the solvent. Geometry optimization at the DFT/M06 level of theory were performed and the ground state was found to be the isomer with the OH group pointing away from the gold center (despite the absence of water or ether). Moreover, the

rotamer with the OH pointing toward gold is not a *minimum* and is located 4.5 kcal/mol higher in energy than the ground state. In this case, the Au···H-O interaction is repulsive. By analysis of the electronic structure, they shown that the d_z^2 orbital is considerably lowered in energy. Thus, this molecular orbital is no more suited for axial interaction with a protic hydrogen limiting the role of Au(III) as a hydrogen bond acceptor.
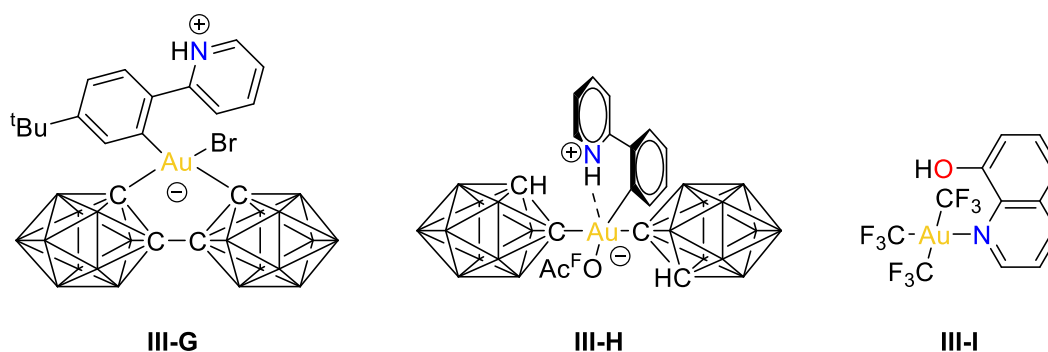
Scheme III-6 : Chemdraw structure of gold(III) complexes **III-G**, **III-H** and **III-I** described in literature.

As for gold, several close Ag···H contact has been described,[12,53,54] but no compelling evidence for hydrogen bonding involving silver as acceptor has been given. Silver has isotopes active in NMR, which give a new probe to assess the existence of the hydrogen bonding.

Straka performed DFT calculations substituted the gold atom by silver in their NHC complex **III-E**. Instead of the Ag···H-N interaction, they observed the Cl···H-N bond.[41]

When exchanging gold by silver in the MeDalPhos complex, the DFT optimization gave the structure involving Ag···H-N interaction as a ground state (Figure III-29 & Table III-16). Whereas the interaction seems weaker (smaller NH elongation, smaller NMR downfield shift and smaller IR red-shift, Table III-16), it could be possible to observe it.

		3_Ag_a	3_Ag_b
Au···H (Å)		2.234	/
X-H (Å)		1.037	1.025
NHAu (°)		178.3	/
υ_{NH} (cm^{-1})		3205.3	3459.8
δ ^{1}H NMR (NH, ppm)		10.20	5.57
ΔE(2) (kcal/mol)		5.7	/
NLMO	% Ag	97.5	
	% N	0.4	
	% H	1.3	
ρ_{AuH} (e.bohr^{-3})		0.027	/

Table III-16: Key geometric features, spectroscopic (IR and NMR) and NBO data for complexes **3_Ag**. Stabilizing energy ΔE(2) and percentage of main atoms in the NLMO accounting for the Au···H-N interaction.

Ag···H-N interaction   C-N rotation
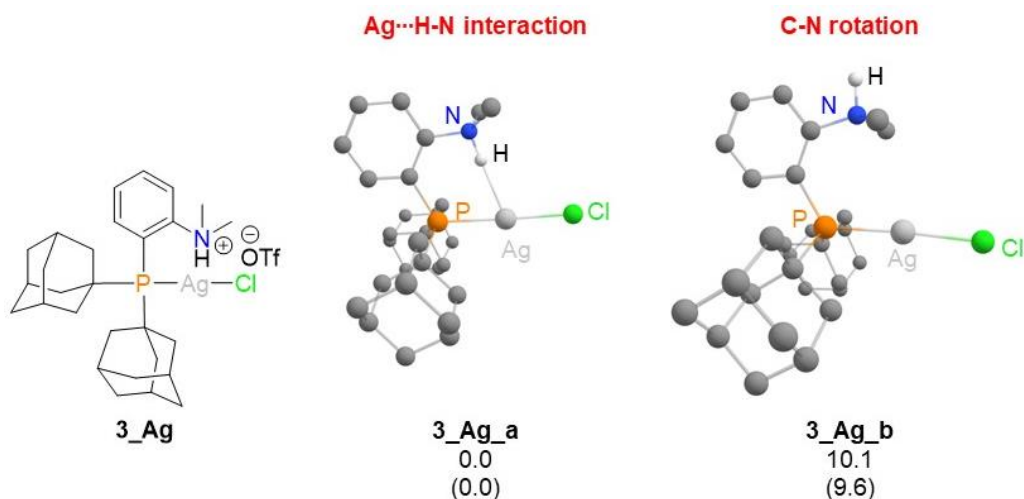
*Figure III-29 : Chemdraw structure and optimized geometry of **3_Ag**.*

So, the MeDalPhosAgCl complex **1_Ag** was synthesized by mixing MeDalPhos ligand with one equivalent of AgCl. The ^{31}P NMR spectrum showed two doublets at δ 39.4 (J_{AgP} = 601.8, 695.1 Hz) characteristic of silver compounds. The protonation of **1_Ag** with HOTf at room temperature led to the protonation of the phosphorus and release of the AgCl salt according to ^{31}P NMR and the formation of a precipitate. This was not observed with gold since the bond dissociation energy of P-Au is stronger than the P-Ag one. When the reaction was performed at -80°C, two new doublets can be observed at δ 25.3 ppm (J_{AgP} = 525.0, 609.1 Hz) but overtime (even keeping at low temperature) the phosphonium is formed (Figure III-30). The reaction was performed in non-deuterated solvent (due to the use of a solution of HOTf in DCM), so no ^{1}H NMR has been registered. Despite many attempts, only small amount of the new product was obtained (maximum: 31%). The product **3_Ag** was too unstable to be fully characterized and to analyze in detail (Ag NMR and IR) the Ag···H-N interaction.
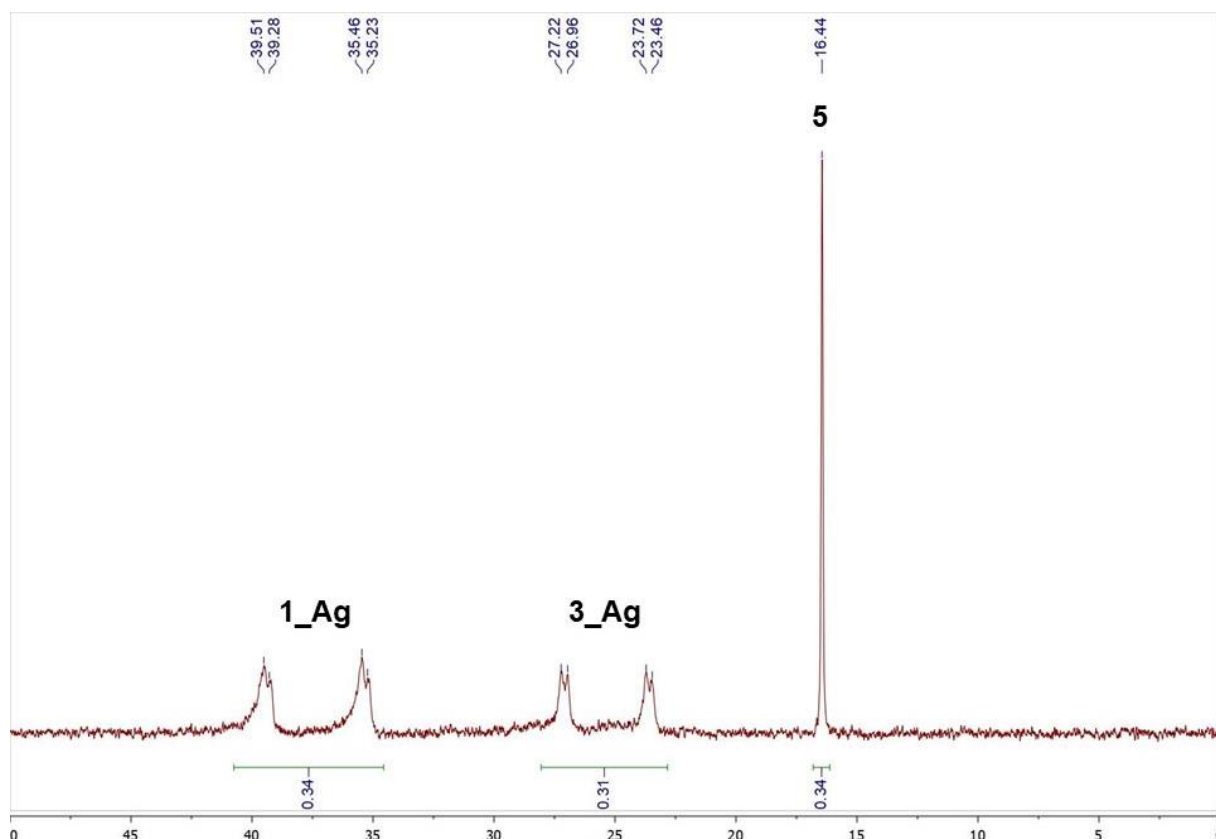
*Figure III-30: ^{31}P NMR spectrum of the reaction between **1_Ag** and HOTf.*

Due to the weakness of the Ag-P bond, we turned our attention toward NHC ligand. According to DFT calculations, the N-H···Ag interaction may also be observable for the NHC complex **14_Ag** (Table III-17). This complex will be synthesized too, and the presence of the hydrogen bonding to silver will be investigated.

	14_Ag
Au···H (Å)	2.248
X-H (Å)	1.039
NHAu (°)	165.0
υ_{NH} (cm^{-1})	3213.1
δ ^1H NMR (NH, ppm)	10.75
ΔE(2) (kcal/mol)	6.5
NLMO % Ag	97.2
% N	0.5
% H	1.7
ρ_{AuH} (e.bohr^{-3})	0.026
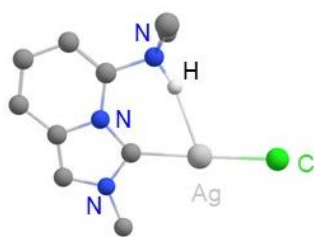
*Table III-17: Optimized geometry and key geometric features, spectroscopic (IR and NMR), NBO and AIM data for silver complex **14_Ag**. Stabilizing energy ΔE(2) and percentage of main atoms in the NLMO accounting for the Ag···H-N interaction.*

151

VI. Experimental procedures and analytical data
1. Synthesis of the cationic gold MeDalPhos complex 3
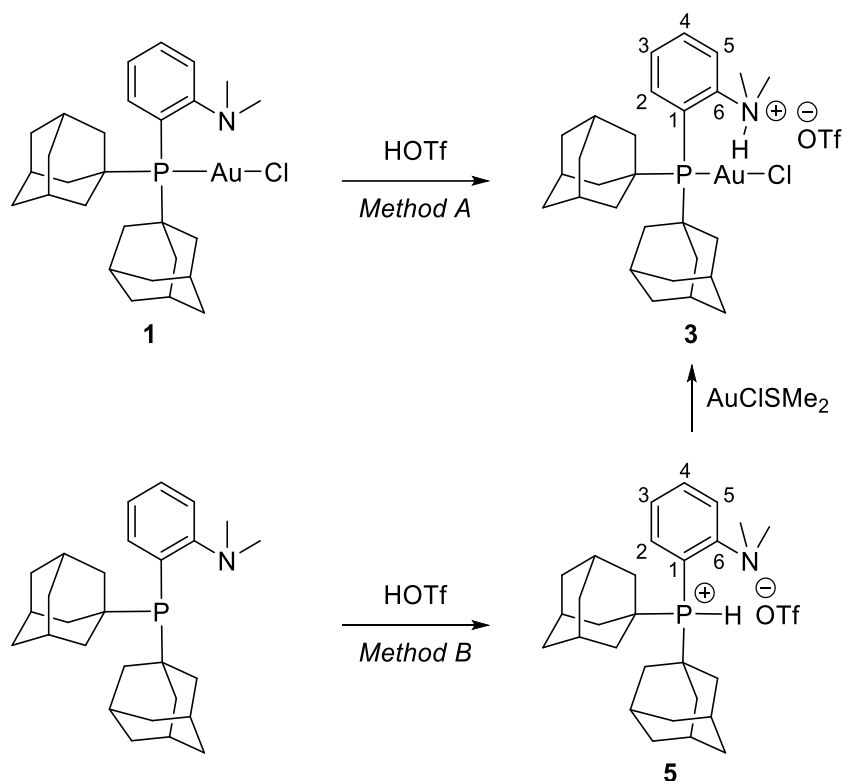
Method A (gold first): In a glovebox, a dried Schlenk was charged with complex **1** (30 mg, 0.046 mmol) in dichloromethane (1 mL). Outside the glovebox, the Schlenk was cooled to -80°C (Acetone/N_2 cold bath) and 0.17 mL dichloromethane solution of trifluoromethane sulfonic acid (0.28 M, 0.046 mmol) was added dropwise. The Schlenk was allowed to warm to room temperature and the reaction mixture was stirred for 1 hour. The product was precipitated by addition of pentane (5 mL). The gold complex **3** was obtained as a white powder (31 mg, 85%) after filtration and drying under *vacuum*. Crystals suitable for XRD analysis were obtained from a dichloromethane/pentane solution at -30°C.

^{31}**P{^{1}H} NMR** (162 MHz, CD_2Cl_2): δ 45.6 (s). ^{1}**H NMR** (500 MHz, CD_2Cl_2): δ 10.88 (bs, 1H, NH), 8.43-8.36 (m, 1H, H_5), 8.06-8.00 (pseudo t, 1H, H_4), 7.93-7.87 (pseudo t, 1H, H_2), 7.83-7.77 (pseudo t, 1H, H_3), 3.48 (d, J_{HH} = 5.0 Hz, 6H, N(CH$_3$)$_2$), 2.33-2.05 (m, 18H, H_{Ad}), 1.74 (s, 12H, H_{Ad}). ^{13}**C NMR** (126 MHz, CD_2Cl_2): δ 146.6 (d, $^2J_{CP}$ = 3.5 Hz, C_6), 136.4 (d, $^4J_{CP}$ = 1.8 Hz, C_4), 136.2 (d, $^2J_{CP}$ = 1.4 Hz, C_2), 131.0 (d, $^3J_{CP}$ = 6.5 Hz, C_3), 124.8 (d, $^3J_{CP}$ = 3.9 Hz, C_5), 115.2 (d, J_{CP} = 36.9 Hz, C_1), 48.6 (s, N(CH$_3$)$_2$), 45.3 (d, J_{CP} = 21.0 Hz, C_{qtAd}), 42.9 (s, CH$_{2Ad}$), 36.1 (d, $^2J_{CP}$ = 1.6 Hz, CH$_{2Ad}$), 29.1 (d, $^3J_{CP}$ = 10.2 Hz, CH$_{Ad}$). ^{19}**F{^{1}H} NMR** (282 MHz, CD_2Cl_2): δ - 78.99 (s). ^{15}**N NMR** (51 MHz, CD_2Cl_2): δ 49.1 (d, J_{PN} = 7.1 Hz, J_{H-N} = 69.5 Hz). **MALDI:** calculated for [M$^+$] = $C_{28}H_{41}NClPAu^+$: 654.2331. Found: 654.2506. **Elemental Analysis**: calculated for $C_{29}H_{41}NClF_3O_3AuPS$: C 43.32, H 5.14, N 1.74. Found: C 43.56, H 4.92, N 1.72. **Mp:** 208°C (decomposition)

Method B (proton first): In a glovebox, a dried Schlenk was charged with MeDalPhos (80 mg, 0.19 mmol) in dichloromethane (4 mL). Outside the glovebox, the Schlenk was cooled to -80°C (Acetone/N_2 cold bath) and 0.7 mL of dichloromethane solution of trifluoromethane sulfonic acid (0.28 M, 0.19 mmol) was added dropwise. The Schlenk was allowed to warm to room temperature and the reaction mixture was stirred for 1 hour. The product was precipitated by addition of pentane (5 mL). The protonated ligand was obtained as a white powder (80 mg, 74%) after filtration and drying under *vacuum*. Crystals suitable for XRD analysis were obtained from a dichloromethane/pentane solution at -30°C.

^{31}P NMR (121 MHz, CD_2Cl_2): δ 17.6 (d, J_{PH} = 485.3 Hz). **^{1}H NMR** (500 MHz, CD_2Cl_2): δ 7.83-7.78 (m, 1H, H_4), 7.66-7.64 (m, 1H, H_2), 7.63-7.60 (m, 1H, H_5), 7.52-7.46 (m, 1H, H_3), 6.80 (d, J_{PH} = 485.3 Hz, 1H, PH), 2.70 (s, 6H, N(CH$_3$)$_2$), 2.22-2.05 (m, 18H, H_{Ad}), 1.84-1.76 (m, 12H, H_{Ad}). **^{13}C NMR** (126 MHz, CD_2Cl_2): δ 160.4 (s, C_6), 136.5 (d, $^4J_{CP}$ = 2.3 Hz, C_4), 133.7 (d, $^2J_{CP}$ = 8.0 Hz, C_2), 126.7 (d, $^3J_{CP}$ = 11.5 Hz, C_3), 125.3 (d, $^3J_{CP}$ = 6.3 Hz, C_5), 111.5 (d, J_{CP} = 74.7 Hz, C_1), 46.5 (s, N(CH$_3$)$_2$), 39.4 (d, $^2J_{CP}$ = 3.2 Hz, CH_{2Ad}), 39.3 (d, J_{CP} = 32 Hz, C_{qtAd}), 35.8 (d, $^4J_{CP}$ = 1.8 Hz, CH_{2Ad}), 28.7 (d, $^3J_{CP}$ = 9.9 Hz, CH_{Ad}). **^{19}F NMR** (282 MHz, CD_2Cl_2): δ -78.86 (s). **HRMS (ESI+):** calculated for [L^+] = $C_{28}H_{41}NP^+$: 422.2979. Found: 422.2977. **Elemental Analysis:** calculated for $C_{29}H_{41}F_3NO_3PS$: C 60.93, H 7.23, N 2.45. Found: C 59.05, H 6.92, N 2.30. **Mp:** 216°C

In a glovebox, a dried Schlenk was charged with phosphonium **5** (40 mg, 0.07 mmol) and AuCl(SMe$_2$) (21 mg, 0.07 mmol) in dichloromethane (1.5 mL). The reaction mixture was stirred for 1 hour. The product was precipitated by addition of pentane (5 mL). The gold complex **3** was obtained as a white powder (46 mg, 80%) after filtration and drying under *vacuum*.

2. Synthesis of the cationic gold MeDalPhos complex 3_D

In a glovebox, a screw cap NMR tube was charged with complex **1** (10 mg, 0.015 mmol) and dichloromethane (0.6 mL). DOTf (1.3 µL, 0.015 mmol) was carefully added. The tube was gently shaken. ^{31}P and ^{1}H NMR analyses show the formation of the desired complex **3_D** with 93% deuteration of the ammonium moiety. The crude mixture was diluted with dichloromethane and directly analyzed by IR.

1 + DOTf →[CH$_2$Cl$_2$] **3-D**
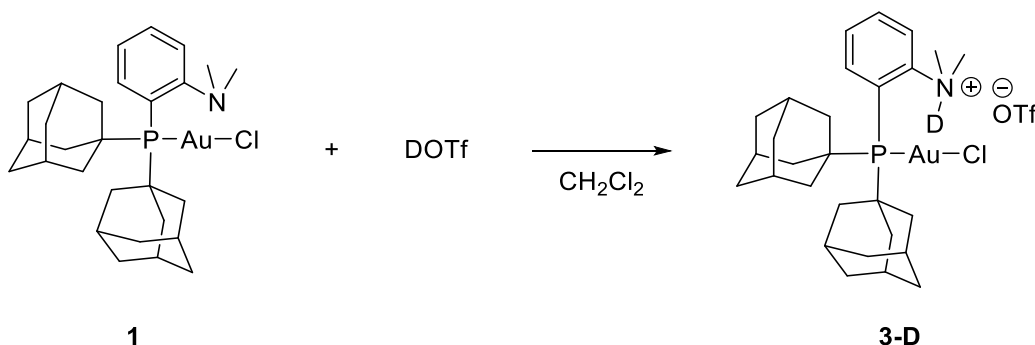
^{31}P{^{1}H} NMR (121 MHz, CH_2Cl_2): δ 45.7 (s, **2-D**), 45.6 (s, **2**) **IR:** ν(N-D) = 2124 cm^{-1}.

3. HSQC ^{1}H-^{15}N NMR spectrum of 3
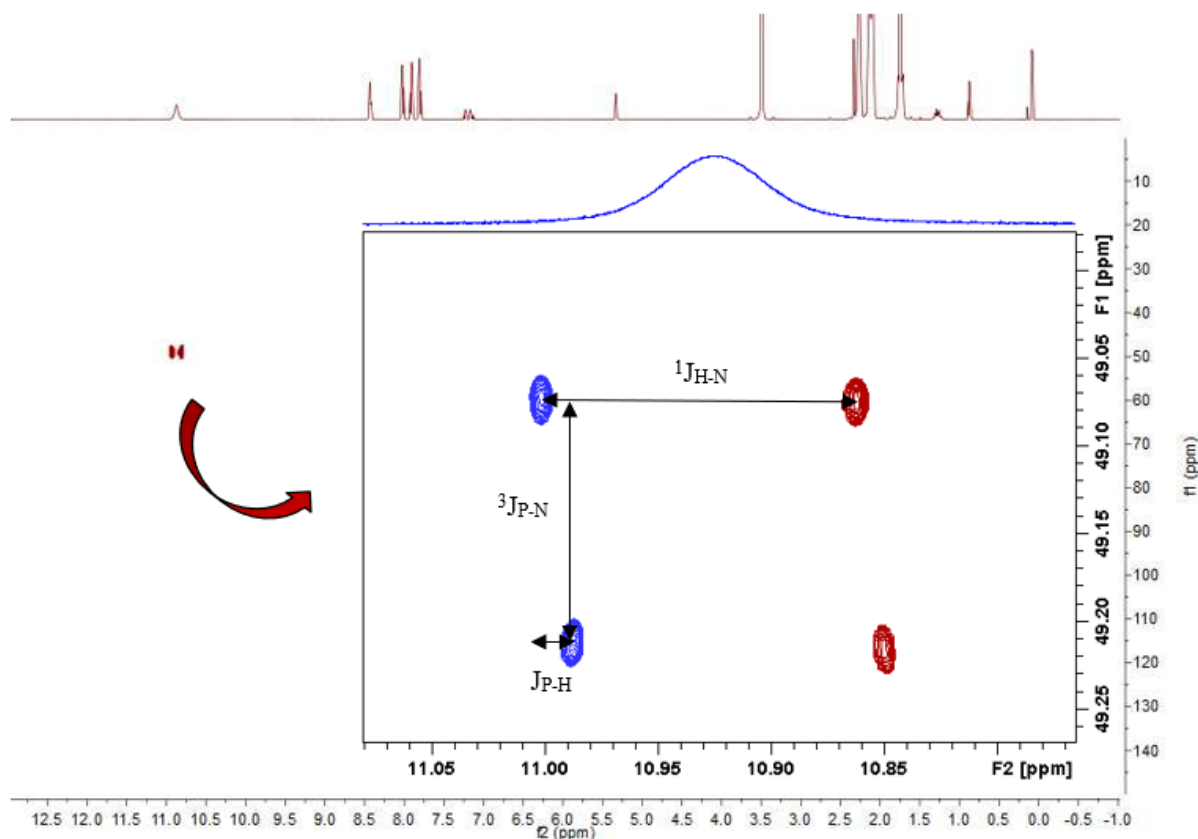
Figure SIII-1: No refocused HSQC ^{1}H-^{15}N NMR spectrum of (3) in CD$_2$Cl$_2$. HOBS observation scheme has been used. To determine ^{1}J$_{HN}$, no ^{15}N decoupling has been applied during acquisition. High resolution is achieved in the indirect dimension because of ^{15}N small spectral width (1 ppm).[1]

4. Synthesis of the cationic gold MorDalPhos complex 6 and 8-(Diphenylphosphino)quinoline gold complex 15

8-(Diphenylphosphino)quinoline gold chloride complex was prepared according to reported procedure.[2]

8-(Diphenylphosphino)quinoline gold methyl complex:
In a glovebox, a dried Schlenk was charged with gold complex (70 mg, 0.12 mmol) in THF (1 mL). Outside the glovebox, the Schlenk was cooled to -78°C (Acetone/N$_2$ cold bath) and 0.32 mL toluene solution of dimethyl zinc (2.0 M, 0.64 mmol, 5 eq.) was added dropwise. The reaction mixture was stirred for 4 hours. The Schlenk was allowed to warm to -20°C. The product was precipitated by addition of cold pentane (2 x 5 mL). The product was obtained as a brown powder (36 mg, 0.07 mmol, 57%).

---

[1] a) L. Castañar, P. Nolis, A. Virgili, T. Parella, *Chem. – Eur. J.* **2013**, *19*, 17283. b) L. Castañar, J. Saurí, P. Nolis, A. Virgili, T. Parella, *J. Magn. Reson.* **2014**, *238*, 63. c) N. Marcó, A. Fredi, T. Parella, *Chem. Commun.* **2015**, *51*, 3262.
[2] L. Huang, F. Rominger, M. Rudolph, A. S. K. Hashmi, *Chem. Commun.* **2016**, *52*, 6435.

^{31}**P{^{1}H} NMR** (121 MHz, CDCl$_3$): δ 45.2 (s). **^{1}H NMR** (300 MHz, CDCl$_3$): δ 8.85 (m, 1H), 8.17 (d, J_{HH} = 8.3 Hz, 1H), 7.93 (d, J_{HH} = 8.3 Hz), 7.63-7.35 (m, 12H), 7.22-7.15 (m, 1H), 0.50 (d, J_{HH} = 8.1 Hz).

Protonation:

Counteranion OTf: In a glovebox, a dried Schlenk was charged with gold complex (0.07 mmol) in dichloromethane (1 mL). Outside the glovebox, the Schlenk was cooled to -80°C (Acetone/N$_2$ cold bath) and 0.25 mL dichloromethane solution of trifluoromethane sulfonic acid (0.28 M, 0.07 mmol, 1 eq.) was added dropwise. The Schlenk was allowed to warm to room temperature and the reaction mixture was stirred for 1 hour. The product was precipitated by addition of pentane (8 mL).

Counteranion BAr$^F_4$: Synthesis of H(Et$_2$O)$_2$BAr$^F_4$ (BAr$^F_4$ = B(3,5-(F$_3$C)$_2$C$_6$H$_3$)$_4$)
Under argon, a solution of NaBAr$^F_4$ (1.00 g, 1.13 mmol) in diethyl ether (3 mL) was transferred *via* cannula to a 100 mL Schlenk containing a solution of HCl in diethyl ether (2 M, 3 mL, 6 mmol) at -30°C. The solution was stirred for 4 hours. After filtration, the solvent was evaporated under *vacuum*. The solid was triturated in cold pentane. The product was obtained as a white powder (710 mg, 62%) after filtration and drying under *vacuum*. Analytical data are consistent with those previously reported.[3]

^{1}H NMR (300 MHz, CD$_2$Cl$_2$): δ 11.44 (bs, 1H, H), 7.72 (s, 8H, H$_{BArF4,ortho}$), 7.58 (s, 4H, H$_{BArF4,para}$), 3.75 (q, 8H, CH$_2$), 1.27 (t, 12H, CH$_3$)

In a glovebox, a dried Schlenk was charged with gold complex (0.06 mmol) and dichloromethane (1 mL). Another dried Schlenk was charged with H(Et$_2$O)$_2$BAr$^F_4$ (61 mg, 0.06 mmol) and dichloromethane (1 mL). Outside the glovebox, both Schlenk were cooled to -80°C (Acetone/N$_2$ cold bath) and the solution of H(Et$_2$O)$_2$BAr$^F_4$ was added to the solution of gold complex *via* a cannula. The Schlenk was rinsed with 1 mL of dichloromethane. The reaction mixture was allowed to warm to room temperature and stirred for 1 hour. The product was precipitated by addition of pentane (8 mL).
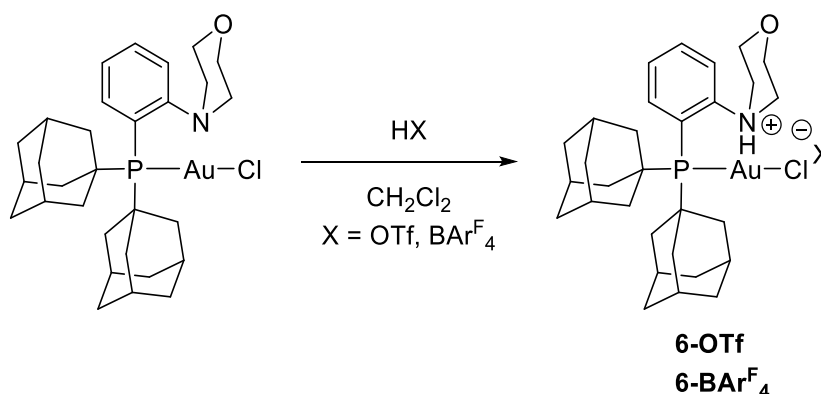
6-OTf
6-BAr$^F_4$

The gold complex **6-OTf** was obtained as a white powder (37 mg, 62%) after filtration and drying under *vacuum*.

---

[3] M. Brookhart, B. Grant, A. F. Volpe, *Organometallics* **1992**, *11*, 3920.

³¹P{¹H} NMR (202 MHz, CD₂Cl₂): δ 44.4 (s). **¹H NMR** (500 MHz, CD₂Cl₂): δ 11.02 (s, 1H, NH), 8.33-8.28 (m, 1H, H₂), 8.09-8.04 (m, 1H, H₄), 7.96-7.91 (m, 1H, H₃), 7.86-7.81 (m, 1H, H₅), 4.69-4.61 (m, 2H, H₈), 4.31-4.23 (m, 4H, H'₈, H₇), 3.53-3.48 (m, 2H, H'₇), 2.30-2.24 (m, 6H, H_Ad), 2.18-2.09 (m, 12H, H_Ad), 1.79-1.71 (m, 12H, H_Ad).

The gold complex **6-BAr^F₄** was obtained as a white powder (77 mg, 82%) after filtration and drying under *vacuum*. Crystals suitable for XRD analysis were obtained from a dichloromethane/pentane solution at -30°C.

³¹P{¹H} NMR (202 MHz, CD₂Cl₂): δ 44.3 (s). **¹H NMR** (500 MHz, CD₂Cl₂): δ 11.37 (s, 1H, NH), 8.00-7.96 (m, 1H, H₂), 7.95-7.91 (m, 1H, H₄), 7.85-7.80 (m, 1H, H₃), 7.72 (s, 8H, o-H_BArF4), 7.71-7.67 (m, 1H, H₅), 7.56 (s, 4H, p-H_BArF4), 4.75-4.68 (m, 2H, H₈), 4.29-4.24 (m, 2H, H'₈), 3.90-3.82 (m, 2H, H₇), 3.55-3.51 (m, 2H, H'₇), 2.27-2.24 (m, 6H, H_Ad), 2.13-2.09 (m, 12H, H_Ad), 1.80-1.70 (m, 12H, H_Ad). **¹³C NMR** (126 MHz, CD₂Cl₂): δ 162.2 (q, J_{CB} = 49.9 Hz, C_BArF4), 143.9 (d, $^2J_{CP}$ = 3.5 Hz, C₆), 136.7 (d, $^2J_{CP}$ = 1.6 Hz, C₂), 135.6 (d, $^4J_{CP}$ = 1.7 Hz, C₄), 134.7 (s, o-C_BArF4), 131.2 (d, $^3J_{CP}$ = 6.6 Hz, C₃), 128.3 (qq, $^2J_{CF}$ = 31.6 Hz, $^4J_{CF}$ = 2.8 Hz, m-C_BArF4), 124.6 (q, J_{CF} = 272.2 Hz, CF₃), 123.3 (d, $^3J_{CP}$ = 3.9 Hz, C₅), 117.9 (sept, $^3J_{CF}$ = 4.1 Hz, p-C_BArF4), 116.0 (d, $^2J_{CP}$ = 34.7 Hz, C₁), 63.7 (s, C₈), 57.7 (s, C₇), 45.4 (d, $^2J_{CP}$ = 19.9 Hz, C_qtAd), 42.7 (s, CH₂_Ad), 35.6 (d, $^2J_{CP}$ = 1.2 Hz, CH₂_Ad), 28.7 (d, $^2J_{CP}$ = 9.7 Hz, CH_Ad). **¹⁵N NMR** (51 MHz, CD₂Cl₂): δ 60.0 ppm (d, J_{PN} = 7.1 Hz, J_{HN} = 68.3 Hz). **¹⁹F{¹H} NMR** (470 MHz, CD₂Cl₂): δ -62.85 (s). **¹¹B{¹H} NMR** (96 Hz, CD₂Cl₂): δ -6.6 ppm (s). **MALDI:** calculated for [M⁺] = C₃₀H₄₃NOPClAu⁺: 696.2436. Found: 696.2870. **Elemental Analysis:** calculated for C₃₁H₄₃AuClF₃NO₄PS: C 44.00, H 5.12, N 1.66. Found: C 43.08, H 4.84, N 1.56. **Mp:** 190°C (decomposition).

The gold complex **14-OTf** was obtained as a white powder after filtration and drying under *vacuum*. Crystals suitable for XRD analysis were obtained from a dichloromethane/pentane solution at -30°C.

³¹P{¹H} NMR (202 MHz, CD₂Cl₂): δ 19.7 (s). **¹H NMR** (500 MHz, CD₂Cl₂): δ 13.22 (bs, 1H, NH), 9.58 (dd, J_{HH} = 5.6, 1.5 Hz, 1H), 9.24 (d, J_{HH} = 8.5 HZ, 1H), 8.52 (dt, J_{HH} = 8.3, 1.2 Hz, 1H), 8.21 (dd, J_{HH} = 8.3, 5.5 Hz, 1H), 7.95-7.90 (m, 1H), 7.70-7.53 (m, 11H). **¹³C NMR** (126 MHz, CD₂Cl₂): δ 149.8, 148.2, 142.3 (d, J_{CP} = 4.5 Hz), 138.0 (d, J_{CP} = 7.0 Hz), 135.6 (d, J_{CP} = 17.5 Hz), 134.7 (d, J_{CP} = 2.0 Hz), 134.6 (d, J_{CP} = 2.1 Hz), 133.9 (d, J_{CP} = 2.6 Hz), 132.7 (d, J_{CP} = 10.7 Hz), 130.9 (d, J_{CP} = 5.3 Hz), 130.5 (d, J_{CP} = 12.6 Hz), 130.4 (d, J_{CP} = 8.9 Hz), 130.2, 129.9 (d, J_{CP} = 12.8 Hz), 125.1 (d, J_{CP} = 64.9 Hz), 124.8, 124.0, 123.0 (d, J_{CP} = 52.5 Hz), 122.2, 119.7, 117.1 (d, J_{CP} = 8.8 Hz). **¹⁹F{¹H} NMR** (470 MHz, CD₂Cl₂): δ -78.56 (s).

The gold complex **14-BAr^F₄** was obtained as a white powder after filtration and drying under *vacuum*. Crystals suitable for XRD analysis were obtained from a toluene/pentane solution at -30°C.

5. Synthesis of the cationic MeDalPhos silver complex 3_Ag

MeDalPhos silver chloride complex 1_Ag:
In a glovebox, a dried Schlenk was charged with MeDalPhos (40 mg, 0.09 mmol) and AgCl (14 mg, 0.09 mmol) in DCM (2 mL). The reaction mixture was stirred for 1 hour. The product was precipitated by addition of pentane. The product was obtained as a grey powder (50 mg, 0.088 mmol, 99%).

^{31}P{^{1}H} NMR (121 MHz, CD$_2$Cl$_2$): δ 39.4 (2d, J$_{AgP}$ = 694.8, 602.1 Hz). ^{1}H NMR (300 MHz, CD$_2$Cl$_2$): δ 7.82-7.76 (m, 1H, H$_5$), 8.61-7.51 (m, 2H, H$_4$ & H$_2$), 7.35-7.27 (m, 1H, H$_3$), 2.67 (s, 6H, N(CH$_3$)$_2$), 2.13-2.05 (m, 6H, H$_{Ad}$), 1.98-1.89 (m, 12H, H$_{Ad}$), 1.70 (s, 12H, H$_{Ad}$).

Protonation:

In a glovebox, an NMR tube was charges with silver complex (30 mg, 0.05 mmol) in dichloromethane (0.06 mL). Outside the glovebox, the NMR tube was cooled to -80°C (Acetone/N$_2$ cold bath) and 0.19 mL dichloromethane solution of trifluoromethane sulfonic acid (0.26 M, 0.05 mmol, 1 eq.) was added dropwise.

6. Selected Crystallographic Data

The N-bound and P-bound H atoms were located in a difference Fourier maps and refined freely for **2** and **5**. For **6-BAr$^F_4$**, the standard N-H distance was fixed.

CCDC 1868951 (**3**), 1868952 (**5**) and 1868953 (**6-BAr$^F_4$**) contain the supplementary crystallographic data for this paper. These data can be obtained free of charge from The Cambridge Crystallographic Data Centre.

ID	(**3**)	(**5**)
formula	C$_{28}$H$_{41}$AuClNP, CF$_3$O$_3$S, CH$_2$Cl$_2$	C$_{28}$H$_{41}$NP, CF$_3$O$_3$S, CH$_2$Cl$_2$
M_r	889.00	656.58
crystal system	orthorhombic	orthorhombic
space group	$Pbca$	$Pna2_1$
a (Å)	16.2991 (11)	20.1177 (11)
b (Å)	14.3181 (11)	10.9433 (6)
c (Å)	28.507 (2)	14.4201 (10)
α (°)	90	90
β (°)	90	90
γ (°)	90	90
V (Å^3)	6652.7 (8)	3174.6 (3)
Z	8	4
ρ_{calc} (g cm^{-3})	1.775	1.374
μ (mm^{-1})	4.824	0.371
F(000)	3536	1384
crystal size (mm^3)	0.180 x 0.160 x 0.140	0.200 x 0.060 x 0.060
T/K	193 (2)	193 (2)
measd reflns	234119	25042
Unique reflns (Rint)	10598 (0.0417)	5538 (0.0619)
reflns used for refinement	10598	5538
refined parameters	394	376
GOF on F^2	1.079	1.067
R$_1$^{a} [I>2σ(I)]	0.0250	0.0508
wR$_2$^{b} [all data]	0.0564	0.1363

Table SIII-1: Crystal Data, Data Collection, and Structure Refinement. ^{a}R$_1$ = Σ||F$_o$| - |F$_c$||/ Σ |F$_o$|, ^{b}wR$_2$ = [Σ[w(F$_o$^{2} - F$_c$^{2})^2] / Σ [w(F$_o$^{2})^2]]$^{1/2}$.
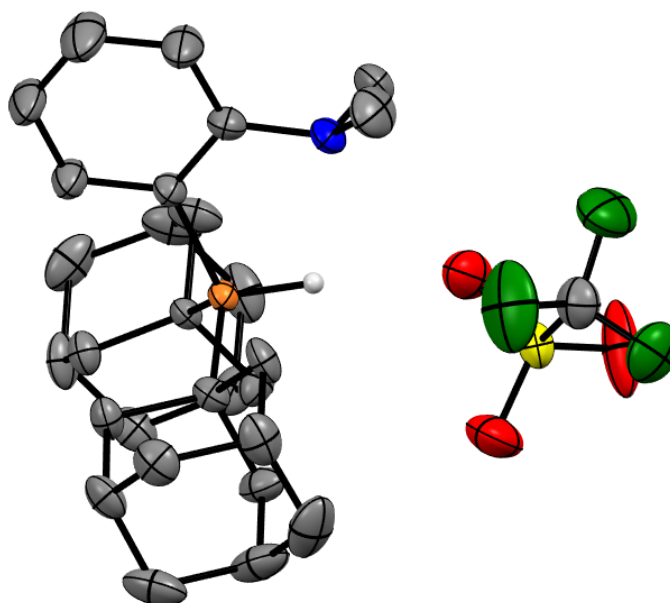
*Figure SIII-2: X-ray structure of the (PH$^+$,N) **4** derived from MeDalPhos. Thermal ellipsoids are drawn at 50% probability. Hydrogen atoms, except that on phosphorus are omitted for clarity. Selected bond lengths (Å): P-H 1.28(6), NH 2.60(6).*

ID	(6-BAr$^F_4$)	(14-OTf)	(14-BAr$^F_4$)
formula	C$_{30}$H$_{43}$AuClNOP, C$_{32}$H$_{12}$BF$_{24}$, CH$_2$Cl$_2$	C$_{21}$H$_{17}$AuClNP, CF$_3$O$_3$S, CH$_2$Cl$_2$	C$_{21}$H$_{17}$AuClNP, C$_{32}$H$_{12}$BF$_{24}$, 2 C$_7$H$_8$
M_r	1645.20	780.74	1594.23
crystal system	monoclinic	monoclinic	orthorhombic
space group	$P2_1/c$	$C2/c$	$Pca2_1$
a (Å)	10.0805 (8)	28.114 (3)	39.987(4)
b (Å)	30.253 (3)	11.1242 (10)	12.7338 (11)
c (Å)	21.381 (2)	16.9436 (14)	25.477 (2)
α (°)	90	90	90
β (°)	97.816 (4)	93.457 (5)	90
γ (°)	90	90	90
V (Å^3)	6459.9 (10)	5289.4 (8)	12972 (2)
Z	4	8	8
ρ_{calc} (g cm^{-3})	1.692	1.961	1.633
μ (mm^{-1})	2.539	6.053	2.445
$F(000)$	3264	3008	6288
crystal size (mm^3)	0.140 x 0.060 x 0.040	0.080 x 0.060 x 0.020	0.380 x 0.200 x 0.150
T/K	193 (2)	193 (2)	193 (2)
measd reflns	68767	50304	302661
Unique reflns (Rint)	13005 (0.0993)	7487 (0.0799)	30734 (0.0822)
reflns used for refinement	13005	7487	30734
refined parameters	1000	329	2260
GOF on F^2	1.038	1.078	1.032
R$_1$[a] [I>2σ(I)]	0.0629	0.0371	0.0342
wR$_2$[b] [all data]	0.1646	0.0705	0.0661

Table SIII-2: Crystal Data, Data Collection, and Structure Refinement. [a]$R_1 = \Sigma||F_o| - |F_c||/\Sigma |F_o|$, [b]$wR_2 = [\Sigma[w(F_o{}^2 - F_c{}^2)^2] / \Sigma [w(F_o{}^2)^2]]^{1/2}$.

VII. Computational details

All calculations were performed using the Gaussian 09 package[4] and the B3PW91 hybrid functional[5] on the real experimental systems. The gold atom was described with the relativistic electron core potential SDD and associated basis set,[6] augmented by a set of f-orbital polarization functions.[7] The 6-31G** basis set were employed for all other atoms.[8]

Optimizations were carried out in solvent (DCM: CH_2Cl_2) by means of the universal continuum solvation SMD model.[9] Frequency calculations were undertaken to confirm the nature of the stationary points, yielding one imaginary frequency for transition states (TS) corresponding to the expected process, exchange of proton involved in the Au···H-N interaction) and all of them positive for *minima*, as well as for determination of υ_{XH} stretching mode (in cm^{-1}). The connectivity of the transition states and their adjacent *minima* was confirmed by intrinsic reaction coordinate (IRC)[10] calculations.

In order to gain more insight into the hydrogen bonding to gold, different approaches were used:

i) Natural Bond Orbital analyses – NBO[11] – were performed with NBO, 5.9 version.[12] Stabilizing interactions ($\Delta E(2)$ in kcal/mol), determined at second order perturbation theory, have been computed to analyze $d_{Au} \rightarrow \sigma^*_{XH}$ interaction. Natural Localized Molecular Orbitals (NLMO) associated to this interaction have also been determined. The population of the d(Au) orbital involved in the hydrogen bonding and the σ^*_{XH} NBO orbital have been examined as well as Wiberg bond indexes (WBI). NPA (Natural Population Analysis) charges have been computed to analyze the charge transfer (CT) between gold fragment and ligand.

---

[4] Gaussian 09, M. J. Frisch, G. W. Trucks, H. B. Schlegel, G. E. Scuseria, M. A. Robb, J. R. Cheeseman, G. Scalmani, V. Barone, B. Mennucci, G. A. Petersson, H. Nakatsuji, M. Caricato, X. Li, H. P. Hratchian, A. F. Izmaylov, J. Bloino, G. Zheng, J. L. Sonnenberg, M. Hada, M. Ehara, K. Toyota, R. Fukuda, J. Hasegawa, M. Ishida, T. Nakajima, Y. Honda, O. Kitao, H. Nakai, T. Vreven, J. A. Montgomery, Jr., J. E. Peralta, F. Ogliaro, M. Bearpark, J. J. Heyd, E. Brothers, K. N. Kudin, V. N. Staroverov, T. Keith, R. Kobayashi, J. Normand, K. Raghavachari, A. Rendell, J. C. Burant, S. S. Iyengar, J. Tomasi, M. Cossi, N. Rega, J. M. Millam, M. Klene, J. E. Knox, J. B. Cross, V. Bakken, C. Adamo, J. Jaramillo, R. Gomperts, R. E. Stratmann, O. Yazyev, A. J. Austin, R. Cammi, C. Pomelli, J. W. Ochterski, R. L. Martin, K. Morokuma, V. G. Zakrzewski, G. A. Voth, P. Salvador, J. J. Dannenberg, S. Dapprich, A. D. Daniels, O. Farkas, J. B. Foresman, J. V. Ortiz, J. Cioslowski, and D. J. Fox, Gaussian, Inc., Wallingford CT, **2009**.

[5] a) A. D. Becke, *Phys. Rev.* **1988**, *A38*, 3098-3100; b) A. D. Becke *J. Chem. Phys.* **1993**, *98*, 5648; b) J. P. Perdew, in *Electronic Structure of Solids '91*, Ed. P. Ziesche and H. Eschrig, Akademie Verlag, Berlin, **1991**, 11.;

[6] a) D. Andrae, U. Häussermann, M. Dolg, H. Stoll, H. Preuss, *Theor. Chim. Acta* **1990**, *77*, 123; b) M. Dolg, *Modern Methods and Algorithm of Quantum Chemistry, Vol. 1* (Ed.: J. Grotendorst), John von Neuman Institute for Computing, Jülich (Germany), **2000**, 479.

[7] A. W. Ehlers, M. Biihme, S. Dapprich, A. Gobbi, A. Hijllwarth, V. Jonas, K. F. Kiihler, R. Stegmann, A. Veldkamp, G. Frenking, *Chem. Phys. Letters* **1993**, *208*, 111.

[8] P. C. Hariharan, J. A. Pople, *Theor. Chim. Acta* **1973**, *28*, 213.

[9] A. V. Marenich, C. J. Cramer, D. G. Truhlar, *J. Phys. Chem. B* **2009**, *113*, 6378.

[10] a) K. Fukui, *Acc. Chem. Res.*, **1981**, *14*, 363. b) H. P. Hratchian, H. B. Schlegel, in *Theory and Applications of Computational Chemistry: The First 40 Years*, Ed. C. E. Dykstra, G. Frenking, K. S. Kim, G. Scuseria, Elsevier, Amsterdam, **2005**, 195.

[11] a) E. Reed, L. A. Curtiss, F. Weinhold, *Chem. Rev.* **1988**, *88*, 899; b) J. P. Foster, F. Weinhold, *J. Am. Chem. Soc.* **1980**, *102*, 7211; c) A. E. Reed, F. Weinhold, *J. Chem. Phys.* **1985**, *83*, 1736.

[12] NBO 5.0 program, E. D. Glendening, J. K. Badenhoop, A. E. Reed, J. E. Carpenter, J. A. Bohmann, C. M. Morales, F. Weinhold, Theoretical Chemistry Institute, University of Wisconsin, Madison, **2001**.

ii) Atoms-In Molecules analysis (QTAIM analysis)[13] was performed using AIMAll software.[14] The density ρ_r was determined for the Bond Critical Points (BCP) associated to the Au $\rightarrow$ NH interactions. Laplacian of the density $\nabla^2\rho_r$ indicates the regions where the density ρ_r is depleted or concentrated. In covalent bonding (also referred to as "open-shell" or "sharing" interactions), $\nabla^2\rho_r$ is negative, while positive values are observed for interactions showing closed-shell (e.g, ionic, Van-der-Waals, or hydrogen).

iii) Non Covalent Interaction calculations (NCI)[15] were also used to analyze the bonding situation of the different gold complexes. NCIPLOT were drawn with VMD software.[16]

^{1}H NMR chemical shifts were evaluated by employing the direct implementation of the Gauge Including Atomic Orbitals (GIAO),[17] with the IGLOII[18] basis set on H, C, P, and N atoms, using as reference the corresponding SiMe$_4$ shielding constant calculated at the same level of theory.

In order to analyze the impact of the relativistic effects on the geometrical parameters of complex **3**, structural optimization and frequency calculations were performed with the ADF-2017[19] program developed by Baerends *et al.* BP86 functional[20] was used. The MOs were expanded in a large uncontracted set of Slater-type orbitals (STOs) containing diffuse functions, TZ2P.[21] Auxiliary sets of s, p, d, f, and g STOs were used to fit the molecular densities and to represent the Coulomb and exchange potentials accurately in each SCF cycle. Scalar relativistic effects or spin-orbit coupling effects were incorporated by applying the ZORA to the Dirac equation.[22] Finally, the solvent effect was considered using Conductor like Screening Model (COSMO) of solvation implemented in ADF.[23]

[13] a) R. F. W. Bader, *Chem. Rev.* **1991**, *91*, 893; b) R. F. W. Bader, *Acc. Chem. Res.* **1985**, *18*, 9.

[14] AIMAll (Version 10.10.11), Todd A. Keith, **2010** (aim.tkgristmill.com).

[15] a) E. R. Johnson, S. Keinan, P. Mori-Sanchez, J. Contreras-Garcia, A. J. Cohen, W. Yang, *J. Am. Chem. Soc.* **2010**, *132*, 6498-6506; b) J. Contreras-Garcia, E. R. Johnson, S. Keinan, R. Chaudret, J. P. Piquemal, D. N. Beratan, W.Yang. *J. Chem. Theory Comput.* **2011**, *7*, 625-632.

[16] W. Humphrey, A. Dalke, K. Schulten, "VMD - Visual Molecular Dynamics", *J. Molec. Graphics* **1996**, *14*, 33-38. http://www.ks.uiuc.edu/Research/vmd/

[17] a) F. London, *J. Phys. Radium* **1937**, *8*, 397-409; b) R. McWeeny, *Phys. Rev.* **1962**, *126*, 1028-1034; c) R. Ditchfield, *Mol. Phys.* **1974**, *27*, 789-807; d) K. Wolinski, J. F. Hilton, Pulay, P. *J. Am. Chem. Soc.* **1990**, *112*, 8251-8260; e) J. R. Cheeseman, G. W. Trucks, T. A. Keith, Frisch, M. J. *J. Chem. Phys.* **1996**, *104*, 5497-5509.

[18] W. Kutzelnigg, U. Fleischer, M. Schindler, *The IGLO-Method: Ab Initio Calculation and Interpretation of NMR Chemical Shifts and Magnetic Susceptibilities*, Springer-Verlag, Heidelberg, **1990**, vol. 23.

[19] E. J. Baerends, T. Ziegler, J. Autschbach, D. Bashford, A. Bérces, F.M. Bickelhaupt, C. Bo, P.M. Boerrigter, L. Cavallo, D.P. Chong, L. Deng, R.M. Dickson, D.E. Ellis, M. van Faassen, L. Fan, T.H. Fischer, C. Fonseca Guerra, M. Franchini, A. Ghysels, A. Giammona, S.J.A. van Gisbergen, A.W. Götz, J.A. Groeneveld, O.V. Gritsenko, M. Grüning, S. Gusarov, F.E. Harris, P. van den Hoek, C.R. Jacob, H. Jacobsen, L. Jensen, J.W. Kaminski, G. van Kessel, F. Kootstra, A. Kovalenko, M.V. Krykunov, E. van Lenthe, D.A. McCormack, A. Michalak, M. Mitoraj, S.M. Morton, J. Neugebauer, V.P. Nicu, L. Noodleman, V.P. Osinga, S. Patchkovskii, M. Pavanello, P.H.T. Philipsen, D. Post, C.C. Pye, W. Ravenek, J.I. Rodríguez, P. Ros, P.R.T. Schipper, H. van Schoot, G. Schreckenbach, J.S. Seldenthuis, M. Seth, J.G. Snijders, M. Solà, M. Swart, D. Swerhone, G. te Velde, P. Vernooijs, L. Versluis, L. Visscher, O. Visser, F. Wang, T.A. Wesolowski, E.M. van Wezenbeek, G. Wiesenekker, S.K. Wolff, T.K. Woo, A.L. Yakovle, ADF2017, SCM, Theoretical Chemistry, Vrije Universiteit, Amsterdam, The Netherlands,http://www.scm.com.

[20] J. P. Perdew, *Phys. Rev. B* **1986**, *33*, 8822–8824.

[21] F. Weigend, R. Ahlrichs, *Phys. Chem. Chem. Phys.* **2005**, *7*, 3297–3305.

[22] E. van Lenthe, E. J. Baerends, J. G. Snijders, *J. Chem. Phys.* **1994**, *101*, 9783–9792.

[23] a) A. Klamt, *J. Phys. Chem.* **1995**, *99*, 2224–2235. b) A. Klamt, G. Schüürmann, *J. Chem. Soc. Perkin Trans. 2* **1993**, 799–805.

Choice of functional: The optimized geometry of **3** has been calculated in gas phase with different functionals: hybrid (B3PW91,[5] PBE0,[24] B3LYP[5,25]), GGA (BP86[20]), meta-GGA (TPSS[26]). The influence of dispersion has been tested using B3PW91-D3(BJ).[27]

	B3PW91	PBE0	B3LYP	BP86	TPSS	B3PW91-D3(BJ)
N-H (Å)	1.058	1.056	1.053	1.080	1.069	1.058
Au⋯H (Å)	2.021	2.013	2.051	1.999	2.022	1.979
NHAu (°)	176.23	173.38	173.65	174.40	172.94	171.62
PAuCl (°)	174.16	173.03	173.95	175.56	174.58	171.57
υ_{NH} (cm^{-1})	2836.5	2876.3	2885.8	2575.2	2680.2	2836.7

*Table SIII-3: Comparison of structural and spectroscopic (IR) parameters of complex **3** using different functionals.*

[24] C. Adamo and V. Barone, *J. Chem. Phys.*, **1999**, *110,* 6158-6169.

[25] C. Lee, W. Yang, R. G. Parr, *Phys. Rev*. **1988**, *B37*, 785-789.

[26] J. M. Tao, J. P. Perdew, V. N. Staroverov, and G. E. Scuseria, *Phys. Rev. Lett.*, **2003**, *91*, 146401-1-146401-4.

[27] a) S. Grimme, J. Antony, S. Ehrlich, H. Krieg, *J. Chem. Phys.*, **2010**, *132*, 154104-1-154104-19. b) S. Grimme, S. Ehrlich, L. Goerigk, *J. Comp. Chem*., **2011**, *32*, 1456-1465.

VIII.   References

[1]   K. Szalewicz, in *Encycl. Phys. Sci. Technol. Third Ed.* (Ed.: R.A. Meyers), Academic Press, New York, **2003**, pp. 505–538.

[2]   L. Brammer, *Dalton Trans.* **2003**, 3145–3157.

[3]   A. Martín, *J. Chem. Educ.* **1999**, *76*, 578–583.

[4]   L. M. Epstein, E. S. Shubina, *Coord. Chem. Rev.* **2002**, *231*, 165–181.

[5]   L. Brammer, J. M. Charnock, P. L. Goggin, R. J. Goodfellow, T. F. Koetzle, A. G. Orpen, *J. Chem. Soc. Chem. Commun.* **1987**, *0*, 443–445.

[6]   L. Brammer, J. M. Charnock, P. L. Goggin, R. J. Goodfellow, A. G. Orpen, T. F. Koetzle, *J. Chem. Soc. Dalton Trans.* **1991**, 1789–1798.

[7]   I. C. M. Wehman-Ooyevaar, D. M. Grove, H. Kooijman, P. Van der Sluis, A. L. Spek, G. Van Koten, *J. Am. Chem. Soc.* **1992**, *114*, 9916–9924.

[8]   L. Brammer, J. C. Mareque Rivas, C. D. Spilling, *J. Organomet. Chem.* **2000**, *609*, 36–43.

[9]   S. Bontemps, G. Bouhadir, K. Miqueu, D. Bourissou, *J. Am. Chem. Soc.* **2006**, *128*, 12056–12057.

[10] A. Amgoune, D. Bourissou, *Chem. Commun.* **2010**, *47*, 859–871.

[11] M. Devillard, E. Nicolas, A. W. Ehlers, J. Backs, S. Mallet-Ladeira, G. Bouhadir, J. C. Slootweg, W. Uhl, D. Bourissou, *Chem. – Eur. J.* **2015**, *21*, 74–79.

[12] E. S. Kryachko, F. Remacle, *Chem. Phys. Lett.* **2005**, *404*, 142–149.

[13] E. S. Kryachko, *J. Mol. Struct.* **2008**, *880*, 23–30.

[14] H. Nuss, M. Jansen, *Angew. Chem. Int. Ed.* **2006**, *45*, 4369–4371.

[15] H. Schmidbaur, H. G. Raubenheimer, L. Dobrzańska, *Chem. Soc. Rev.* **2013**, *43*, 345–380.

[16] L. M. Scherf, S. A. Baer, F. Kraus, S. M. Bawaked, H. Schmidbaur, *Inorg. Chem.* **2013**, *52*, 2157–2161.

[17] F. Kraus, H. Schmidbaur, S. S. Al-juaid, *Inorg. Chem.* **2013**, *52*, 9669–9674.

[18] F. Groenewald, J. Dillen, H. G. Raubenheimer, C. Esterhuysen, *Angew. Chem. Int. Ed.* **2016**, *55*, 1694–1698.

[19] F. Groenewald, H. G. Raubenheimer, J. Dillen, C. Esterhuysen, *Dalton Trans.* **2017**, *46*, 4960–4967.

[20] W. Nakanishi, S. Hayashi, K. Narahara, *J. Phys. Chem. A* **2008**, *112*, 13593–13599.

[21] J. Contreras-García, E. R. Johnson, S. Keinan, R. Chaudret, J.-P. Piquemal, D. N. Beratan, W. Yang, *J. Chem. Theory Comput.* **2011**, *7*, 625–632.

[22] E. R. Johnson, S. Keinan, P. Mori-Sánchez, J. Contreras-García, A. J. Cohen, W. Yang, *J. Am. Chem. Soc.* **2010**, *132*, 6498–6506.

[23] J. Contreras-García, W. Yang, E. R. Johnson, *J. Phys. Chem. A* **2011**, *115*, 12983–12990.

[24] P. Schwerdtfeger, *Heteroat. Chem.* **2002**, *13*, 578–584.

[25] D. J. Gorin, F. D. Toste, *Nature* **2007**, *446*, 395–403.

[26] R. J. F. Berger, J. Schoiber, U. Monkowius, *Inorg Chem* **2017**, *56*, 956–961.

[27] S. S. Batsanov, *Inorg. Mater.* **2001**, *37*, 871–885.

[28] M. A. Bakar, M. Sugiuchi, M. Iwasaki, Y. Shichibu, K. Konishi, *Nat. Commun.* **2017**, *8*, 576.

[29] M. Lusi, L. J. Barbour, *Cryst. Growth Des.* **2011**, *11*, 5515–5521.

[30] M. Brookhart, M. L. H. Green, G. Parkin, *Proc. Natl. Acad. Sci.* **2007**, *104*, 6908–6914.

[31] J. Vícha, C. Foroutan-Nejad, M. Straka, *Nat. Commun.* **2019**, *10*, 1643.

[32] L. Estévez, *Dalton Trans.* **2020**, *49*, 4797–4804.

[33] H. Schmidbaur, A. Schier, *Chem. Soc. Rev.* **2011**, *41*, 370–412.

[34] S. Sen, F. P. Gabbaï, *Chem. Commun.* **2017**, *53*, 13356–13358.

[35] Y. Zhang, J. C. Lewis, R. G. Bergman, J. A. Ellman, E. Oldfield, *Organometallics* **2006**, *25*, 3515–3519.

[36] P. S. Pregosin, H. Rüegger, F. Wombacher, G. Van Koten, D. M. Grove, I. C. M. Wehman-Ooyevaar, *Magn. Reson. Chem.* **1992**, *30*, 548–551.

[37] E. Andris, P. C. Andrikopoulos, J. Schulz, J. Turek, A. Růžička, J. Roithová, L. Rulíšek, *J. Am. Chem. Soc.* **2018**, *140*, 2316–2325.

[38] P. Jerabek, L. Vondung, P. Schwerdtfeger, *Chem. – Eur. J.* **2018**, *24*, 6047–6051.

[39] W. Yao, O. Eisenstein, R. H. Crabtree, *Inorganica Chim. Acta* **1997**, *254*, 105–111.

[40] L. Rocchigiani, W. T. Klooster, S. J. Coles, D. L. Hughes, P. Hrobárik, M. Bochmann, *Chem. – Eur. J.* **2020**, *26*, 8267–8280.

[41] M. Straka, E. Andris, J. Vícha, A. Růžička, J. Roithová, L. Rulíšek, *Angew. Chem. Int. Ed.* **2019**, *58*, 2011–2016.

[42] G. Kleinhans, M. M. Hansmann, G. Guisado-Barrios, D. C. Liles, G. Bertrand, D. I. Bezuidenhout, *J. Am. Chem. Soc.* **2016**, *138*, 15873–15876.

[43] G. Park, F. P. Gabbaï, *J. Am. Chem. Soc.* **2021**, *143*, 12494–12498.

[44] H. Schmidbaur, *Angew. Chem. Int. Ed.* **2019**, *58*, 5806–5809.

[45] F. P. Gasparro, N. H. Kolodny, *J. Chem. Educ.* **1977**, *54*, 258.

[46] A. Genoux, M. Biedrzycki, E. Merino, E. Rivera-Chao, A. Linden, C. Nevado, *Angew. Chem. Int. Ed.* **2021**, *60*, 4164–4168.

[47] J. M. Stauber, A. L. Rheingold, A. M. Spokoyny, *Inorg. Chem.* **2021**, *60*, 5054–5062.

[48] K. E. Roth, S. A. Blum, *Organometallics* **2010**, *29*, 1712–1716.

[49] M. Kriechbaum, M. List, R. J. F. Berger, M. Patzschke, U. Monkowius, *Chem. – Eur. J.* **2012**, *18*, 5506–5509.

[50] M. Rigoulet, S. Massou, E. D. S. Carrizo, S. Mallet-Ladeira, A. Amgoune, K. Miqueu, D. Bourissou, *Proc. Natl. Acad. Sci.* **2019**, *116*, 46–51.

[51] I. Chambrier, D. L. Hughes, R. J. Jeans, A. J. Welch, P. H. M. Budzelaar, M. Bochmann, *Chem. – Eur. J.* **2020**, *26*, 939–947.

[52] A. Pérez-Bitrián, M. Baya, J. M. Casas, A. Martín, B. Menjón, *Dalton Trans.* **2021**, *50*, 5465–5472.

[53] G. Rodríguez-López, P. Montes-Tolentino, T. O. Villaseñor-Granados, A. Flores-Parra, *J. Organomet. Chem.* **2017**, *848*, 166–174.

[54] C.-S. Liu, P.-Q. Chen, E.-C. Yang, J.-L. Tian, X.-H. Bu, Z.-M. Li, H.-W. Sun, Z. Lin, *Inorg. Chem.* **2006**, *45*, 5812–5821.

Chapter 4

Isolation of reactive α-CF$_3$ gold(I) carbene complexes

The presence of fluorine atoms in organic compounds have effects on their physical, chemical and biological properties (electronic, lipophilic, steric, conformational…).[1] There is thus considerable interest in developing efficient methods for the selective introduction of fluorinated groups into organic compounds. In this context, the trifluoromethyl group occupies a forefront position. It is present in a wide range of biologically active molecules (Scheme IV-1).

Antifungal agent
Agrochemical use

FXR modulator
Pharmaceutical activity
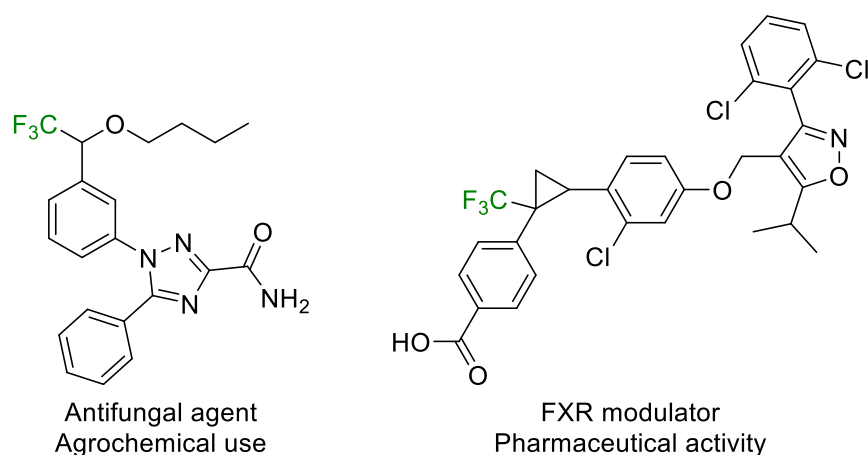
Scheme IV-1: Molecules of medicinal interest bearing CF₃ substituent.

Thanks to the strong electron-withdrawing nature of the CF_3 group (Hammett constant $\sigma_p = 0.54$), α-trifluoromethyl diazoalkanes are relatively stable and represent very powerful synthons to introduce CF_3 motifs into molecules. Upon N_2 release, they can form metal carbenes with a variety of transition metals, giving way to a large panel of reactions (Scheme IV-2).

Cyclopropanation

Insertion reaction
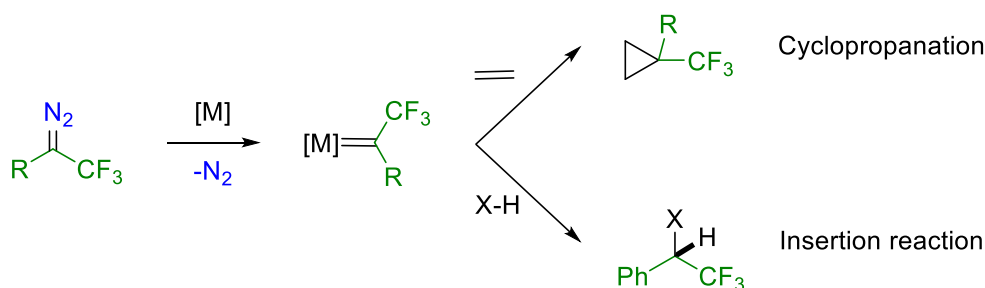
Scheme IV-2: Formation of σ-CF₃ carbene complexes from trifluoromethyl diazoalkanes and representative carbene transfer reactions.

This chapter starts by a brief state-of-the-art on α-CF₃ carbene complexes, their synthetic developments as well as the synthesis and characterization of stable species. The study of α-CF₃ gold(I) carbene complexes is then presented, from their synthesis/characterization, to the analysis of their bonding situation and reactivity studies under stoichiometric and catalytic conditions.

I. Transition metal complexes of α-CF₃ carbenes

1. Synthetic aspect of trifluorocarbenes

1.1 Cyclopropanation

Metal catalyzed cyclopropanation using trifluorodiazoethane was described in 2006 by Simonneaux's group. Using iron or ruthenium porphyrins complexes and different styrene derivatives, trifluoromethylphenyl cyclopropanes were synthesized with high diastereoselectivity (>94%) and moderate enantioselectivity (17-69%) but low yield (24-52%, Scheme IV-3, top).[2] To achieve higher enantioselectivity, Davies and co-workers turned their attention towards donor/acceptor-substituted carbenoids. These ones are more stable than those lacking a donor group and have a reduced electrophilic character allowing higher selectivity. Using chiral Rh[II] catalysts, reactions between donor-acceptor diazo compounds and styrene derivatives give access to cyclopropanes with good yields (61-76%), with high diastereoselectivities (>94%) and high enantiomeric excesses (88-98% ee, Scheme IV-3, bottom). As usual for donor/acceptor carbenoids, the major cyclopropane formed has the aryl group *cis* to the alkene substituent (structure determined by $^{19}F\{^{1}H\}$ HOESY NMR).[3] Shortly after, Komarov and Mykhailiuk expanded the scope of this reaction to other alkenes like dihydropyran, enol ether, cyclohexene or cyclic enamide using $Rh_2(OAc)_4$ or CuCl as catalyst.[4,5] Later on, Carreira and co-workers showed that this methodology could also be applied to dienes and enynes using iron catalyst[6] and highly enantioselectivity could be obtained on styrene derivatives with chiral salen-based Co[II]-catalyst.[7]
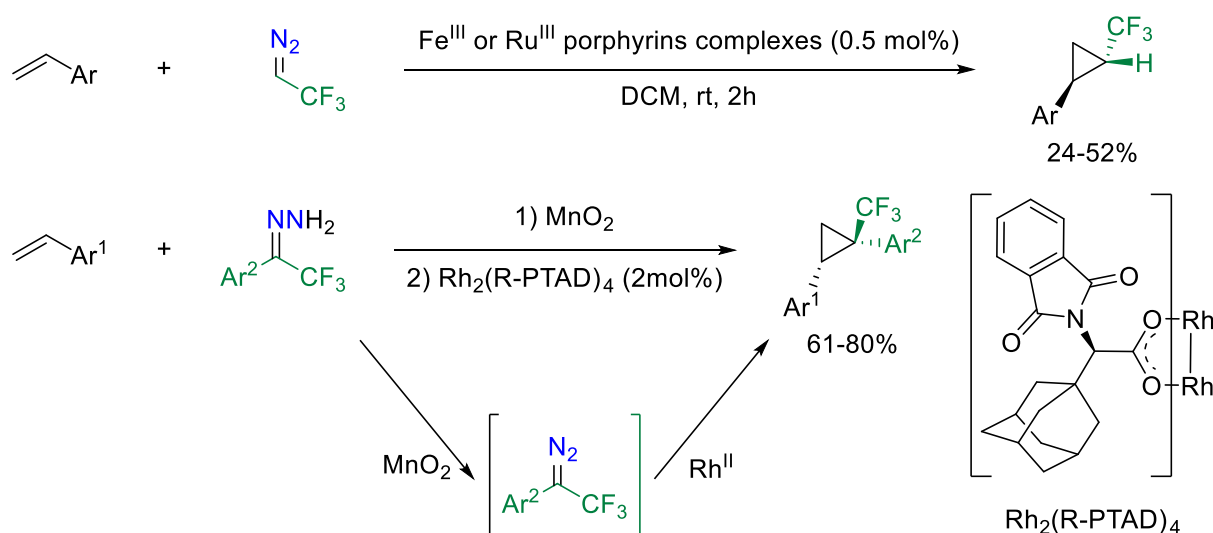
Scheme IV-3: Cyclopropanation of styrene derivatives with trifluoromethyl diazo compounds. Top: Iron-catalyzed reaction reported by Simonneaux and co-workers. Bottom: Rhodium-catalyzed reaction reported by Davies and co-workers.

Concerning trifluoromethylated cyclopropene compounds, a straightforward thermal synthesis was described by Valdès and co-workers, using tosylhydrazone (decomposed to diazo thanks to a base) and alkyne, without the need for any catalyst.[8] To induce asymmetric transformations, some metal catalysts were used for cyclopropenation reactions.[9]
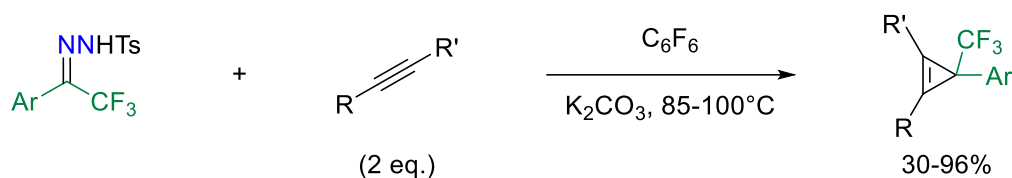
Scheme IV-4: Reaction of trifluoromethylated tosylhydrazone with alkynes.

1.2 Insertion reaction

Insertion reactions are another very important application of carbene complexes. They represent an elegant and efficient synthesis of highly functionalized molecules (with a trifluoromethyl group and other heteroatoms for example). The introduction of a 2,2,2-trifluoroethyl group on the amino group of anilines was reported by Wang and co-workers in 2015, using a catalytic amount of AgSbF$_6$. When using amide derivatives, the expected N-H insertion products were not observed, and instead, *O*-trifluoroethylation occurred. To note, AgSbF$_6$ do not catalyze the cyclopropanation of styrene with CF$_3$CHN$_2$. Based on this experimental observation, they proposed, for the insertion reaction, that the silver carbene is formed after the formation of the Nucleophile-Ag interaction, followed by migratory insertion of the carbene into this Nu-Ag bond (Scheme IV-5).[10]
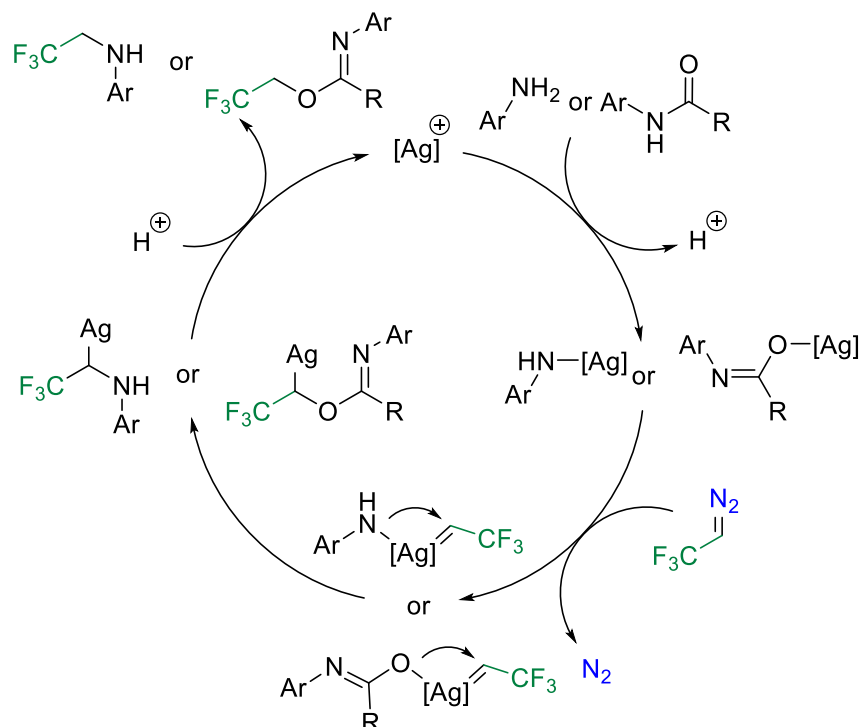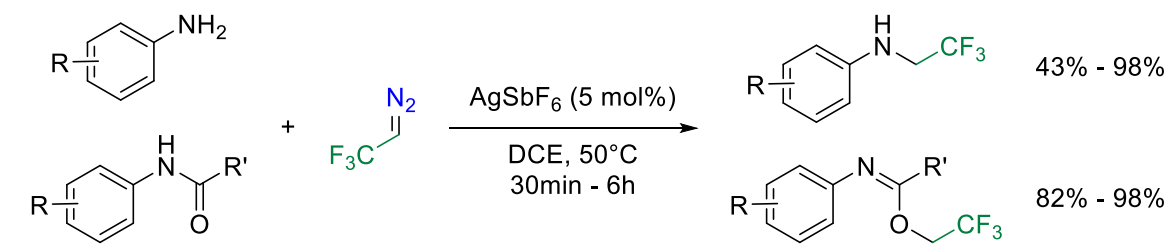
Scheme IV-5: Silver(I) catalyzed trifluoroethylation of anilines and amides. Postulated reaction mechanism.

This catalytic system was applied exclusively to amines and amides. In 2016, Gouverneur and co-workers reported that not only N-H but also B-H, Si-H, S-H and P-H insertion reactions of trifluorodiazoethane are possible under Cu^I catalysis. They further extend the scope toward push-pull diazo compounds (Scheme IV-6). Thanks to competition experiments (the same catalyst being used for all these insertion reactions), an order of reactivity has been determined: N-H > S-H > B-H > Si-H > P-H. This ranking can serve as a predictive tool for insertion when substrates possess two or more heteroatom-hydrogen functionalities and can be complementary to other metal catalysts.[11]
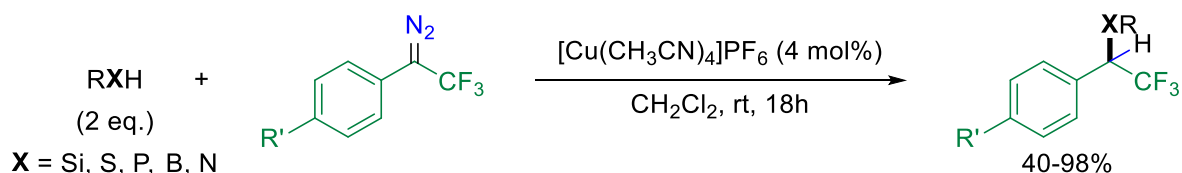
Scheme IV-6: Copper-catalyzed insertion of trifluorodiazo compounds into heteroatom-H bonds.

By adding a chiral ligand (Spirobox), the asymmetric version of the Si-H insertion reaction can be achieved. In order to further develop the applicability of this method to numerous silane compounds, Ollevier's group modified the chiral ligand and used an easily

available diimine ligand. Mechanistic studies based on KIE experiments and DFT calculations indicates that the insertion takes place in a concerted manner on the carbene center.[12]

Switching from copper to rhodium catalyst, the insertion reactions was further extended to Sn-H bonds.[13]
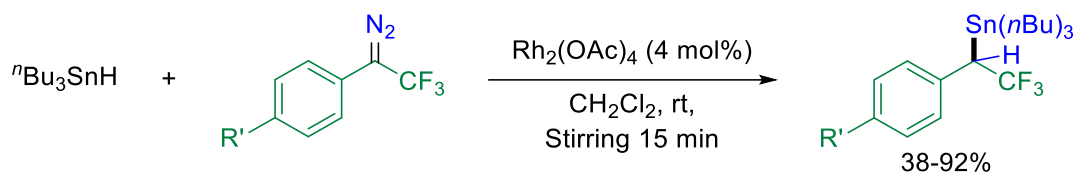
Scheme IV-7: Rhodium-catalyzed insertion of trifluorodiazo compounds into Sn-H bonds.

1.3 C-H activation

In parallel to previously described X-H insertions, Ma and co-workers reported in 2012 insertion reactions into C_{sp}-H bonds. Trifluoroethylation of alkynes can be easily achieved under mild conditions employing CuI as catalyst and CF_3CHN_2 (Scheme IV-8). Trifluoroethylated alkynes can be further transformed (hydrogenation, cyclopropanation, oxidation…) allowing the synthesis of more functionalized trifluoromethylated products.[14]
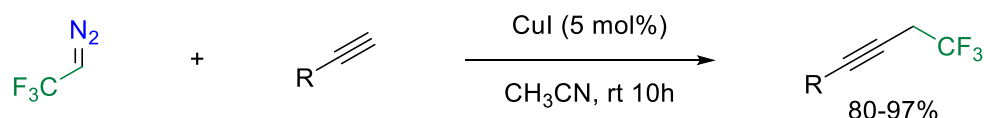
Scheme IV-8: Copper-catalyzed trifluoroethylation of terminal alkynes with CF_3CHN_2.

Due to the presence of indoles and their derivatives (including fluorinated one) in many bioactive substances, there was a growing interest for the synthesis of such compounds. In this context, insertion of CF_3 moiety through CH activation represents one of the most attractive and straight forward tools. First, Osipov and co-workers investigated in 2014 the reaction between trifluoro diazopropionate and indoles with copper catalysts. Despite the need for high reaction temperatures for the activation of this stabilized diazoester, good regioselectivity was obtained for the C3 position of indoles.[15] Then, Koenig's group reported in 2020 a Pd-catalyzed reaction of fluorinated diazoalkanes with indole heterocycles. They did not observe insertion products (at C3 or C2 positions) but either the cyclopropanation product or the gem-difluroro olefin depending on the indoles used (Scheme IV-9).[16]
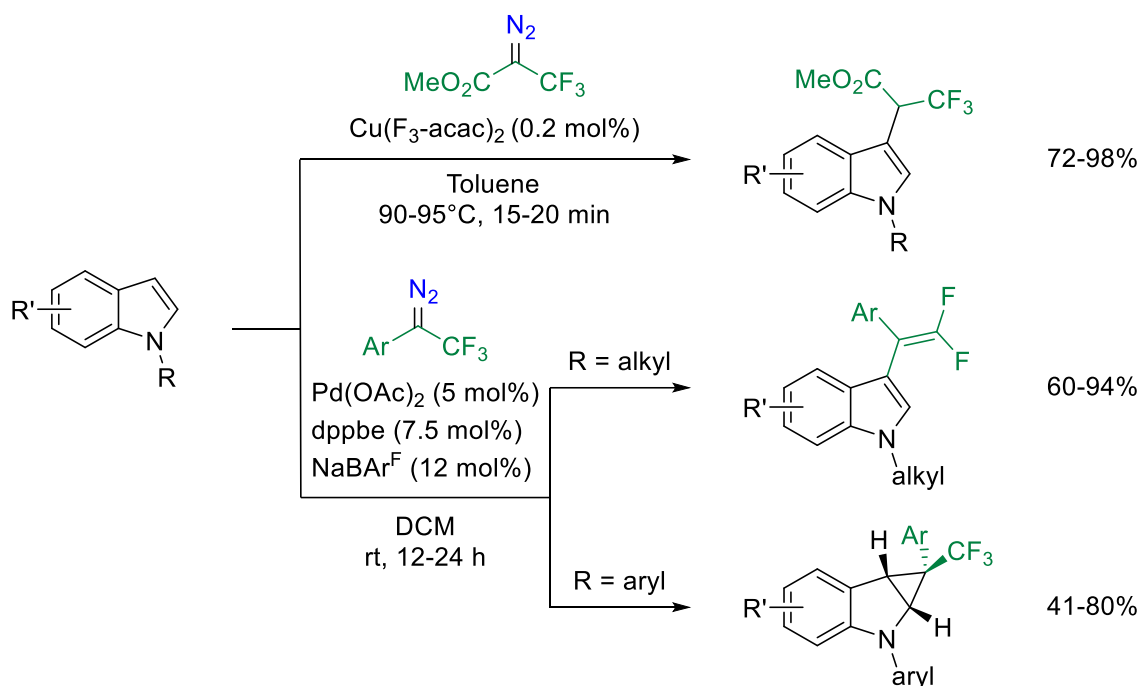
Scheme IV-9: Palladium or copper-catalyzed reaction of fluorinated diazoalkane with indole heterocycles.

In all cases, the mechanism is proposed to go through a palladium carbene complex. After nucleophilic addition of the indole, two pathways are possible: with alkylindoles, a β-fluoride elimination is suggested to access the *gem*-difluoro olefins, whereas under identical reaction conditions, the cyclopropane product is obtained with arylindoles through stepwise cyclization. The trifluoromethylated product, observed by Osparov's group, could be obtained by 1,2 proton shift (Scheme IV-10).

The gem-difluoro olefination reactions, starting from trifluorodiazo compounds was further extended to aniline, indoline and tetrahydroquinoline derivatives using CuI as catalyst.[17]
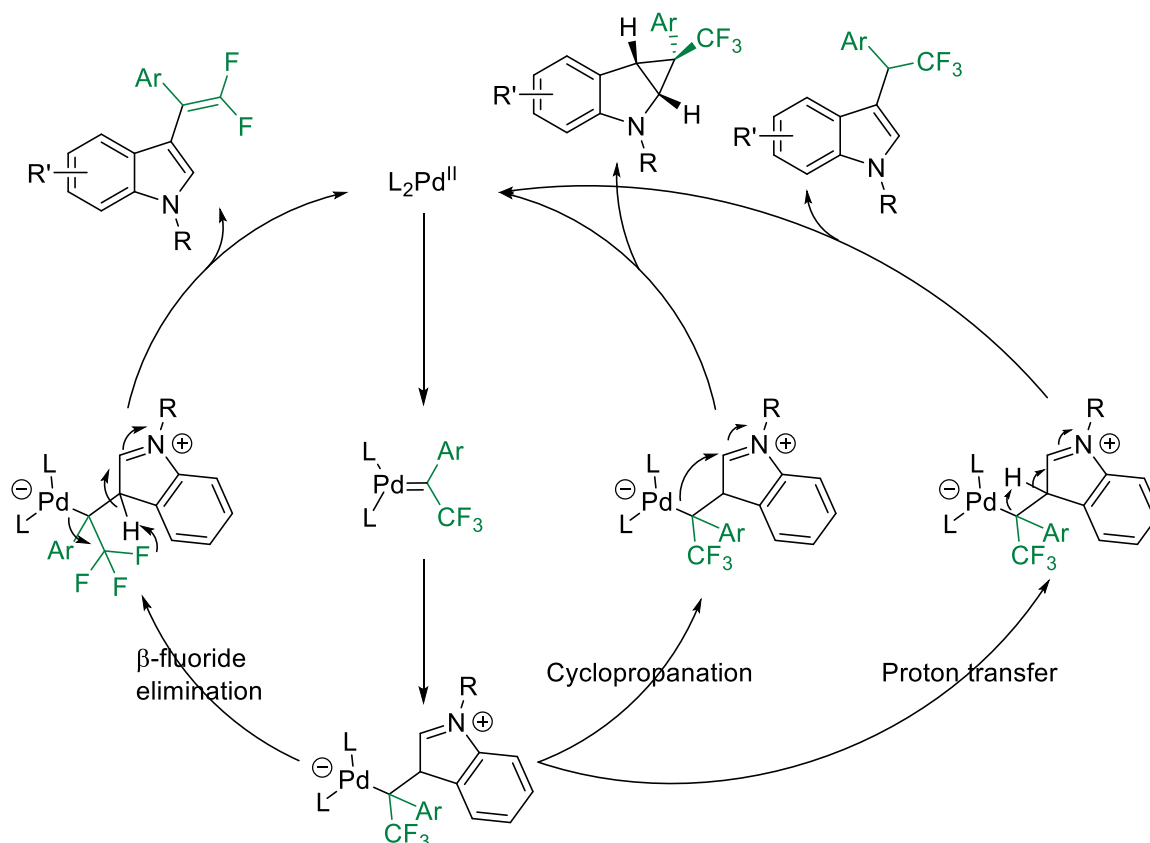
Scheme IV-10: Hypothesized reaction mechanisms for Pd-catalyzed reaction of fluorinated diazoalkane with indole heterocycles.

Concerning gold, only two isolated examples involving α-CF₃ species were found in the literature. The C-H functionalization of phenothiazine[18] or carbazole[19] with phenyl trifluoromethyl diazomethane catalyzed by (phosphite)AuCl/AgSbF₆ was described by Koenig and co-workers. With the phenothiazine, the product of mono C-H functionalization is major, with a small amount of double C-H insertion, whereas with carbazole, the latter is the only product (Scheme IV-11).

This overview showed that carbene transfer reactions from fluorinated diazoalkanes give access to a large panel of highly functionalized molecules: cyclopropanes, small molecules with other heteroatoms, indole derivatives… Several metals catalyze these transformations and the reaction outcome strongly depends on the substrates and catalysts used.
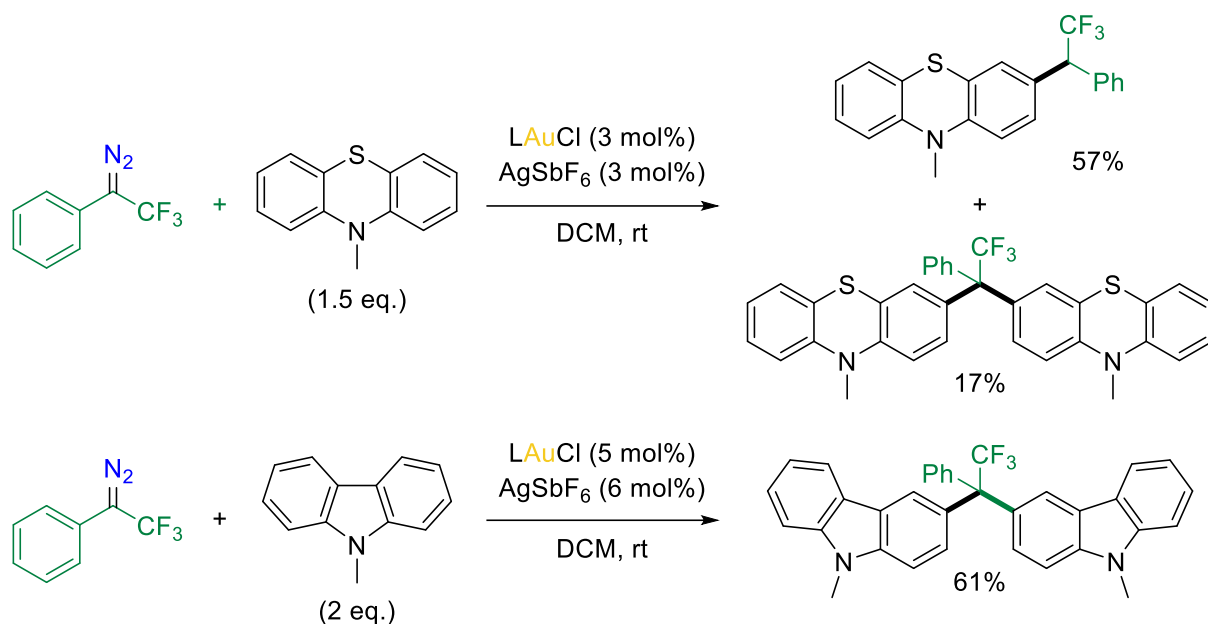
Scheme IV-11: C-H functionalization of phenothiazine (top) and carbazole (bottom) catalyzed by LAuCl/AgSbF₆ (L = tris(2,4-di-tert-butylphenyl)phosphite).

2. Isolated and characterized fluorinated carbenes

For all reactions described, the carbene complex was postulated as intermediate but never isolated or characterized *in situ*. Nevertheless, few examples of carbenes, bearing trifluoromethyl substituents have been characterized.

Fischer carbene complexes are generally synthesized by means of nucleophilic addition to one of the CO ligands of hexacarbonyltungsten. The same strategy, with a CF_3 anion (generated from trimethyl(trifluoromethyl)silane and fluoride), was applied to obtain a methoxytrifluorocarbene (Scheme IV-12).[20] A downfield shift signal on ^{13}C NMR spectrum (δ 295.9 ppm) is observed, characteristic of a Fischer carbene. Further reaction with an amine gives access to a new carbene where the OMe has been substituted by the NEt_2 group. A downfield shift signal is still observed but at a lower value (δ 238.4 ppm) and the W=C bond is elongated (2.276(6) Å *vs* 2.086(17) Å for OMe). Indeed, the strong N → C_{carb} π-donation, reduces the W=C bond order. The reaction of the methoxy(trifluromethyl)carbene complex with the CF_3 anion was investigated. This latest coordinates to the C_{carb} atom, not to tungsten, showing that this species acts as an electrophile and it is indeed a Fischer carbene.
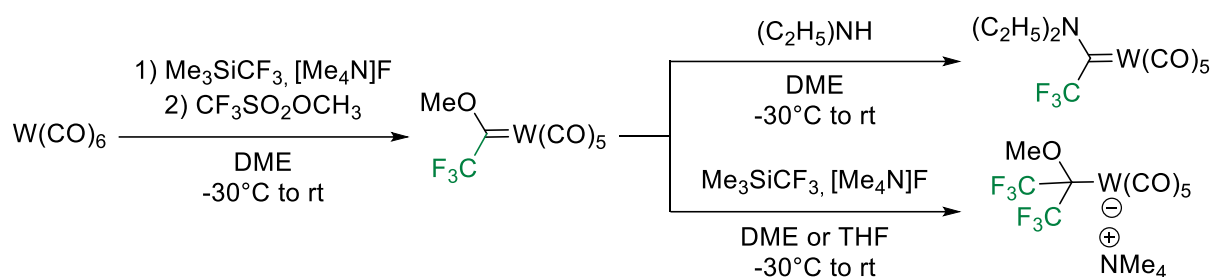
Scheme IV-12: Synthesis of α-CF₃ tungsten carbene complexes and its reactivity as a Fischer carbene

Several examples of Schrock-type fluoro(trifluoromethyl) carbenes have also been described with Cobalt,[21,22] Iridium[23,24] or Nickel.[25] Most of them were obtained by reductive method (action of KC_8 or Na) on perfluoroalkyl complexes and showed nucleophilic reactivity. To confirm the Schrock-type reactivity, HCl was added on the iridium carbene complex and HBr on Cobalt carbene complex. Each time, the protonation occurred at the carbene center (Scheme IV-13, top). With the aim of synthesizing hydrofluoroalkenes or perfluoropolymers *via* olefin metathesis or polymerization, the triflurocarbene complexes were reacted with tetrafluoroethylene (TFE). The metallacyclobutane resulting from [2+2] cycloaddition was formed but unfortunately, no chain growth was observed. In the best cases, a small amount of metathesis product was obtained (Scheme IV-13, bottom).
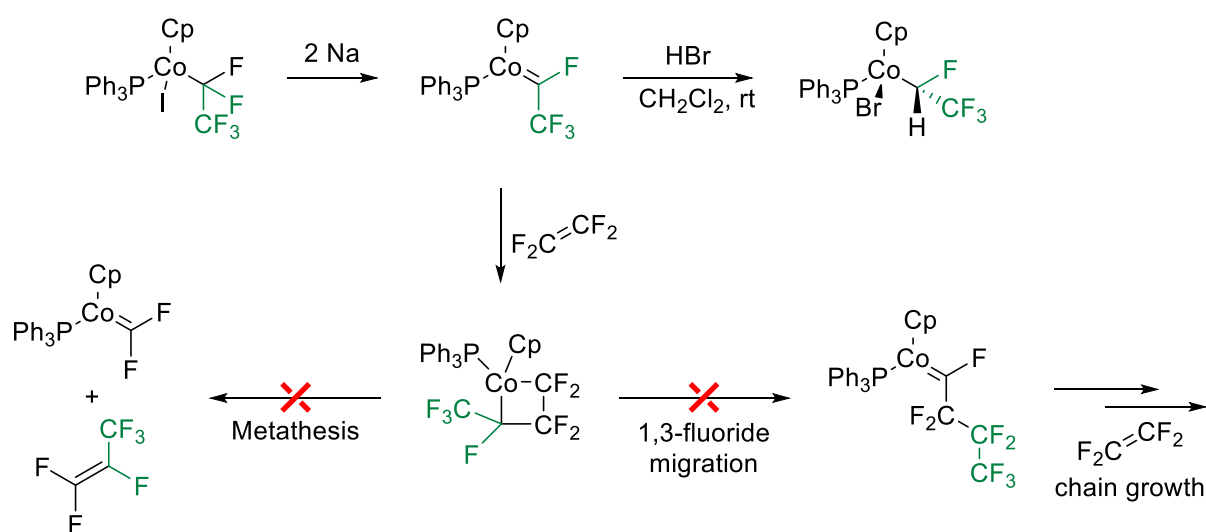
Scheme IV-13: Synthesis and reactivity of a fluoro(trifluoromethyl) Cobalt carbene complex.

The bonding analysis[1] of the carbene cobalt complex indicates donor-acceptor interaction between the metal and carbene fragments: σ-donation from the highest occupied fragment orbital (HOFO) on the carbene to the lowest unoccupied fragment orbital (LUFO) of $CpCo(PPh_3)$ and π-back-donation from the HOFO of $CpCo(PPh_3)$ to the LUFO of the carbene ligand. The strong HOFO → carbene LUFO is also apparent from the net charge of the carbene ligand (-0.104 e).[21]

---

[1] DFT computations performed at the PBE/TZVP level of theory

Only one example was synthesized by decomposition of an α-CF₃ substituted diazo compound in 2008. Reaction between the Ru(TPP)(CO) and trifluoromethylphenyl diazomethane leads to the formation of the ruthenium carbene complex characterized by XRD. X-ray structure shows a short Ru=C bond (1.838(2) Å) and a phenyl ring perpendicular to the carbene plane, meaning that no π-delocalization is involved for the stabilization of the species (Scheme IV-14).[26] The Ru(TPP) platform is reminiscent of the catalyst used by Simonneaux's group for the cyclopropanation with trifluorodiazoethane.[2] Neverthless, no reaction was described with this well-defined and isolated complex to confirm that it does exhibit the typical cyclopropanation reactivity of transient carbenes.
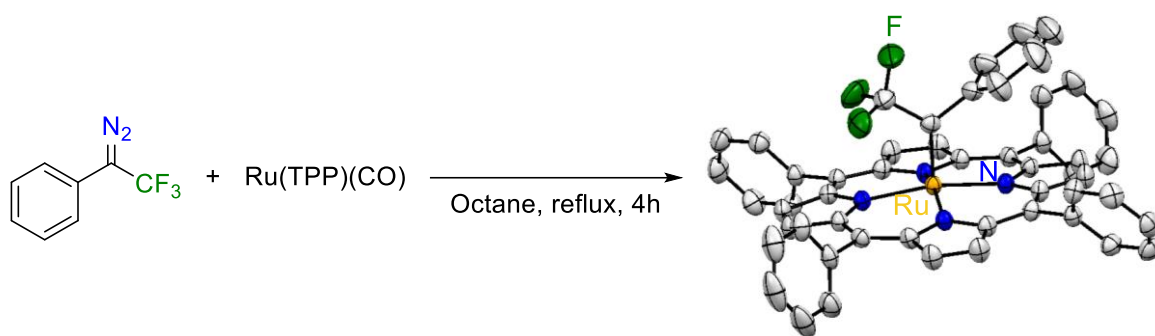
Scheme IV-14: Synthesis of α-CF₃ ruthenium carbene complex via decomposition of diazo compound. XRD structure.

From all the trifluoromethyl carbene complexes presented in this part, no catalytic reaction was reported raising the question if the transient carbene complexes postulated in the cyclopropanation reaction or X-H insertion reaction are really active species. For this reason, the synthesis of trifluoromethyl complexes, the study of their reactivity in stoichiometric reaction and their generation *in situ* for catalytic reaction are of high interest.

II.   Synthesis and characterization of α-CF₃ gold(I) carbenes
1. Synthesis, spectroscopic and structural characterization

As mention in Chapter 1, the (P,P) ligand allowed the stabilization and characterization of the reactive α-oxo gold carbene, this is why this ligand was tried first for the synthesis, isolation and characterization of α-CF₃ gold carbene. One equivalent of biphenyl trifluoromethyl diazomethane was added at -80°C to the tricoordinate pseudo-cationic complex (P,P)AuNTf₂ **17** in dichloromethane (Scheme IV-15). Small bubbles of dinitrogen immediately evolved and the solution turned deep blue. After quick work up at -40°C, the formed species was spectroscopically characterized. The ^{31}P{^{1}H} NMR signal (Figure IV-1, left) appears at very similar chemical shift than the gold precursor (δ 137.8 and 138.2 ppm, respectively), but as a quartet instead of a singlet. The quartet multiplicity results from PF coupling, as unambiguously established by the presence of a triplet signal in the ^{19}F NMR spectrum with similar coupling

(22.2 Hz). These patterns suggest the formation the desired $(P,P)Au=C(CF_3)(biphenyl)^+$ complex **18-Ph**, something that was definitely confirmed by ^{13}C NMR spectroscopy. The ^{19}F-decoupled spectrum (Figure IV-1, right top) shows a diagnostic signal at δ 269.8 ppm. In line with the blue color, a strong absorption is found at 623 nm in UV-vis spectroscopy. Carbene **18-Ph** proved to be moderately stable at room temperature, about 30% decomposition being observed after 24 hours in DCM. The *para*-substituent at the phenyl ring was then changed for OMe and CF_3 to assess the impact of electron-donating/withdrawing groups. In both cases, the corresponding carbene complexes **18-OMe** and **18-CF₃** were formed (Scheme IV-15), and NMR data in line with those of **18-Ph** were obtained (SI p.190). Some features deserve comment: *i*) the diagnostic ^{13}C NMR signal barely shifts (from δ 269.8 to 265.8 ppm), *ii*) the $^3J_{PC}$ and $^4J_{PF}$ coupling constants decrease in the series *p*-CF₃ > *p*-Ph > *p*-OMe (from 109.0 to 79.5 Hz for $^3J_{PC}$, and from 32.1 to 14.0 Hz for $^4J_{PF}$), the carbene becomes less electron-deficient and the Au=C bond order/double bond character decreases (see Structure and bonding analysis, p. 180), *iii*) the carbene **18-CF₃** displays a long-range $^8J_{PF}$ coupling of 10.8 Hz, as apparent in the ^{31}P and ^{19}F NMR spectra. It is also worth noting that if the carbene complex **18-OMe** survives for a few hours at room temperature, as **18-Ph**, **18-CF₃** is much less stable. All attempts to work it up at room or low temperature resulted in complete degradation. It was thus characterized *in situ* at low temperature.
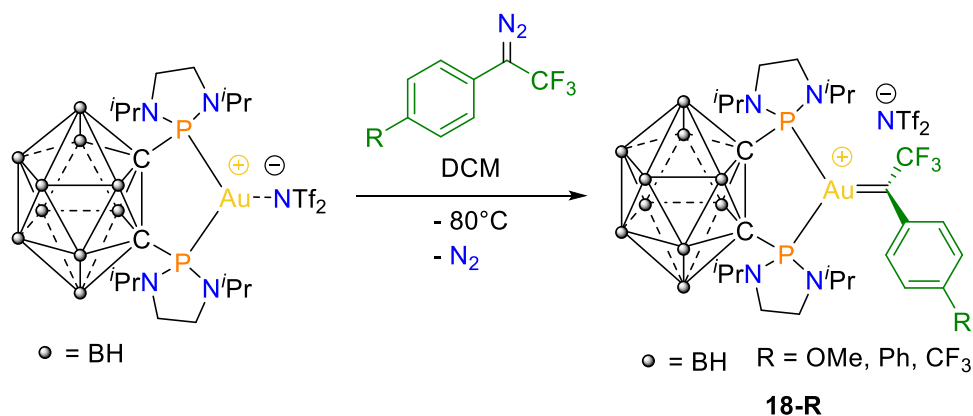
Scheme IV-15: Formation of the gold(I) trifluoromethyl carbenes **18-R** by diazo decomposition.

Efforts were then made to obtain crystallographic data to know more about the structure of the obtained carbene. Gratifyingly, crystals suitable for XRD analysis were obtained by slow diffusion of pentane on a dichloromethane solution of **18-Ph** at 4°C (Figure IV-1, right bottom). The asymmetric unit contains two molecules of very similar geometries (Table SIV- 2, SI p.197) For sake of simplicity, the key features of only one will be discussed here. Accordingly, the carbene complex adopts an ion pair structure. The DPCb ligand symmetrically chelates gold with Au-P bond lengths of 2.347(1)/2.348(1) Å and a PAuP bite angle of 90.59(4)°. The carbene center is in perfectly planar environment (as apparent from the sum of bond angles of

360.0°) and it is oriented perpendicularly to the PAuP coordination plane (the mean planes around Au and C_{carb} make an angle of 89.76°). This orientation minimizes steric repulsions between the carbene and phosphorus substituents, it also maximizes the d(Au) to $2p^{\pi}(C_{carb})$ back-donation. The Au=C bond distance (1.971(2) Å) is in the lower range of those reported for gold(I) carbene complexes.[2] The carbene center is also stabilized by π-donation from the biphenyl substituent, as indicated by their coplanar arrangement (the mean plane of the phenyl ring bonded to C_{carb} is rotated by only 2.5° from the carbene coordination plane) and from the relatively short C_{carb}-C_{ipso} bond length (1.444(6) Å).
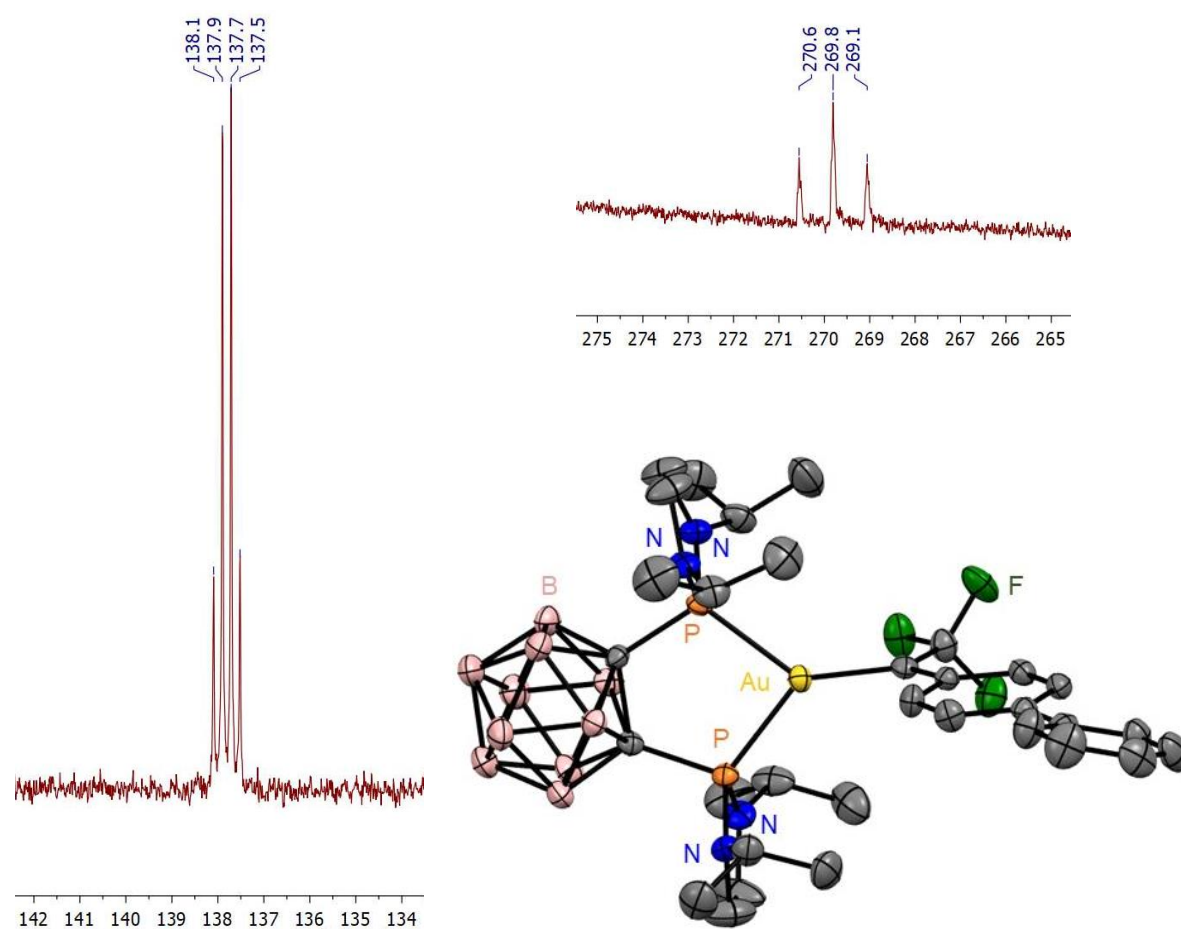
*Figure IV-1: Diagnostic ³¹P (left) and ¹³C{¹⁹F} NMR (right) signals for **18-Ph**; molecular structure of **18-Ph**. Thermal ellipsoids drawn at 50% probability, hydrogen atoms, counter anion and disordered atoms are omitted. Selected bond lengths (Å), and bond angles (°): Au-C_{carb} 1.971(2), Au-P1 2.347(1), Au-P2 2.348(1), C_{carb}-C_{Ar} 1.444(6), C_{carb}-CF_3 1.500(6), P1AuP2 90.59(4), P1AuC_{carb} 135.7(1), P2AuC_{Carb} 133.7(1).*

---

[2] A Cambridge Chemical Database search gave 13 relevant entries, the Au=C bond length ranges from 1.961 to 2.068 Å, the average value is 2.024 Å.

Since the (P,N) gold complex is widely used in catalysis, we also tried the synthesis of the α-CF$_3$ gold carbene with the (P,N) ligand. In a screw cap NMR tube, a solution of (P,N)AuCl **1** and biphenyl trifluoromethyl diazomethane (1 eq.) was added over a suspension of AgSbF$_6$ (1 eq.) at -80°C. The solution rapidly turned deep pink. The ^{31}P{^{1}H} NMR spectra, performed at room temperature, showed a main peak at δ 46.4 ppm (q, $^{4}J_{PF}$ = 6.1 Hz). Unfortunately, the complex decomposed during the acquisition and neither the ^{1}H or ^{19}F NMR spectra were exploitable. All attempts to reproduce this experiment and characterized further the ensuing complex by low temperature NMR failed.

When trying other methods to synthesize the (P,N) gold carbene, we noted that α-CF$_3$ aryl diazo compounds can be decomposed by halide scavengers (silver or sodium salts and GaCl$_3$) in less than 1 hour. The absence of these compounds during the synthesis of the carbene complex or the study of its reactivity is crucial to avoid side reaction, and confirm that gold is indeed the active species.

First, we used the same strategy as the (P,P) ligand (Scheme IV-16, top). Abstraction of chloride by a silver salt, filtration over a pad of celite to remove silver compounds and then addition of the diazo substrate at low temperature. Unfortunately, the carbene complex was not observed spectroscopically. With AgPF$_6$, the abstraction of Cl is not clear, so no further reaction was tested. With AgSbF$_6$, the cationic (P,N)AuSbF$_6$ species is not stable, and probably decomposition of the gold compound occurs before the addition of diazo derivatives. With AgNTf$_2$, a stable (P,N)AuNTf$_2$ complex is obtained, but reaction with α-CF$_3$ aryl diazo substrate leads to dimerization of the latter. No carbene was detected even at low temperature.

Secondly, the reaction from a stable π-complex was investigated (Scheme IV-16, middle). Indeed, as shown in Chap 1. II.1., the (P,N) ligand allowed the stabilization of gold π-complex with styrene.[27] We thought, that adding an excess of α-CF$_3$ aryl diazo compounds on this complex, the cyclopropanation can occur and then the carbene can be formed. Unfortunately, when 2 equivalents of diazo compounds was added over a solution of gold π-complex in DCM at -80°C, only a small amount of cyclopropanation is formed (6%), and mainly dimerization of the diazo compounds is observed. At the end of the reaction (no more diazo compound), the resting state is the π-complex of gold.

Last attempts were made by the insertion of the diazo into the Au-Cl bond under thermal or photochemical conditions, based on the recent work from Echavarren's group (Scheme IV-16, bottom).[28] Photochemical reaction leads to only small conversion of the (P,N)AuCl precursor. Heating to 80°C, some conversion (30% maximum) to the new complex was observed, but separation with the starting material was not possible (decomposition on silica or alumina, co-precipitation, attempts of crystallization failed). This strategy was dropped out too.

179

Despite many trials, it was not possible to isolate or characterize *in situ* the (P,N) gold carbene complex.
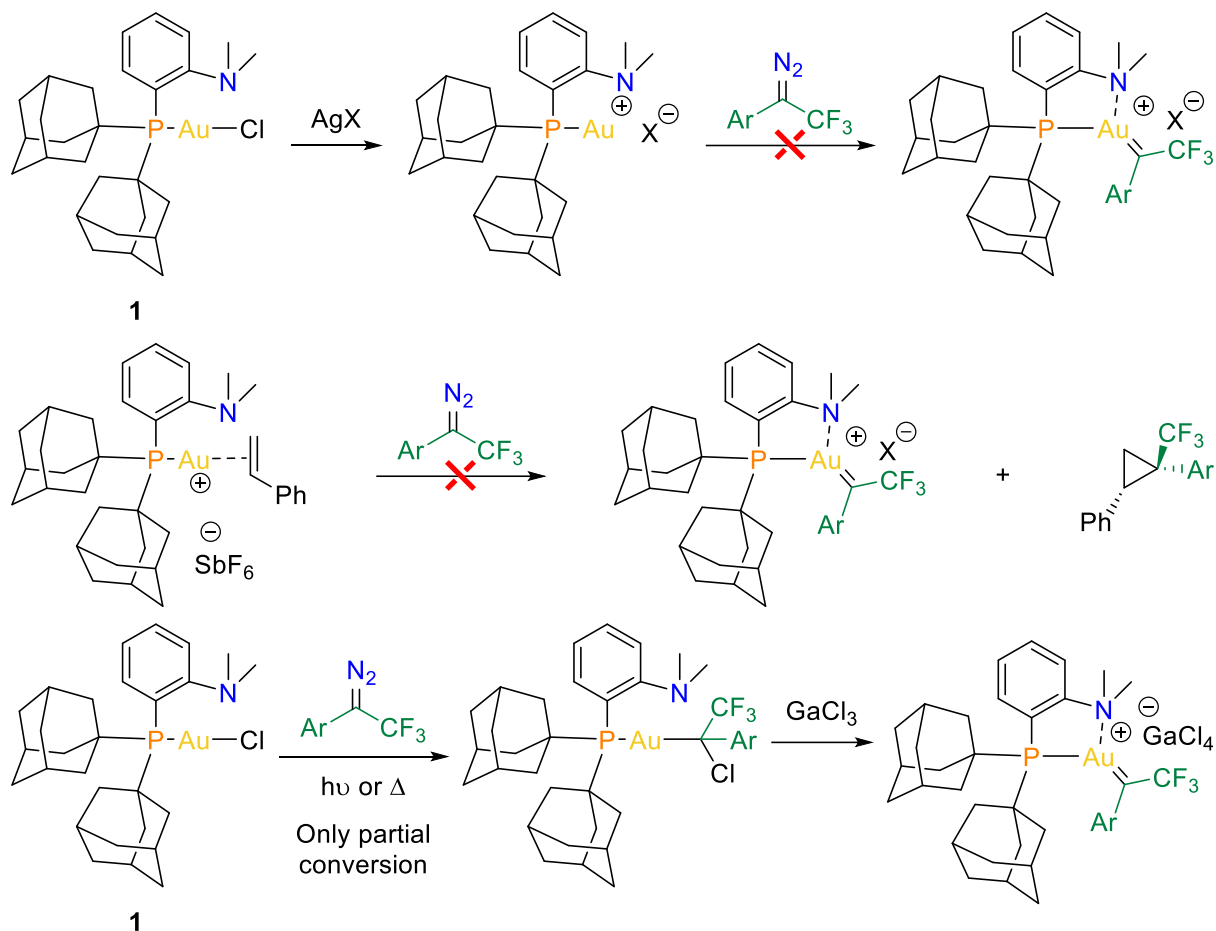
Scheme IV-16: Envisioned strategies to synthesis the (P,N) gold carbene complex.

2. Structure and bonding analysis

To gain more insight into the bonding situation and stabilization mode of the α-CF₃ gold(I) carbenes **18**, DFT calculations (B3PW91/SDD+f(Au), 6-31G** (other atoms)) were performed. The geometry optimized for **18-Ph** matches well that determined crystallographically with deviations of less than 0.08 Å and 2.2° in the key bond distances and angles (Table SIV-3, SI p.199). The carbenes **18-OMe** and **18-CF₃** were also computed, showing similar structures than **18-Ph**. The small variations found in the Au=C/C_{carb}-C_{ipso} bond lengths and associated Wiberg bond indexes (WBI) are in line with the electron bias induced by the *para* substituent, *ie* stronger arene-to-C_{carb} π-donation and weaker Au-to-C_{carb} back-donation from **18-CF₃** to **18-Ph**, and **18-OMe** (Table IV-1). The NMR data for **18-CF₃**, **18-Ph** and **18-OMe** were also calculated. The trends observed experimentally for the $^2J_{PC}$ and $^4J_{PF}$ couplings were nicely reproduced (Table SIV-3, SI p.199). The bonding situation was then assessed in detail *via* NBO and CDA analyses (Table IV-1). The C_{carb}-to-Au charge transfer (CT) is slightly negative

for the three carbenes, a little more for the electron-deprived carbene **18-CF₃** (-0.25 e⁻) than for the electron-enriched one **18-OMe** (-0.10 e⁻). CT values close to zero suggest that overall the C_{carb}-to-Au donation and Au-to-C_{carb} back-donation roughly compensate each other. The donation/back-donation ratio (d/b), as estimated by CDA, falls in the 1.8-2.2 range (slightly lower for the electron-deprived carbene **18-CF₃**, slightly higher for the electron-enriched carbene **18-OMe**), indicating that C_{carb}-to-Au donation prevails, but Au-to-C_{carb} back-donation is significant.

	18-OMe	18-Ph	18-CF₃
	Geometric parameters		
Au=C_{carb} (Å)	1.987	1.982	1.971
C_{carb}-C_{ipso} (Å)	1.423	1.429	1.442
PAuP (°)	89.81	89.88	89.79
	NBO Analysis		
WBI (Au=C)	0.677	0.687	0.710
WBI (C_{carb}-C_{ipso})	1.312	1.289	1.234
CT (e)	-0.10	-0.14	-0.25
d_{xz}(Au)→C_{carb} back-donation %C_{carb} in NLMO d_{xz}(Au)	7.3%	9.7%	15.5%
$\pi_{C=Caryl}$→C_{carb} donation %C_{carb} in NLMO $\pi_{C=Caryl}$	24.2%	16.3%	10.1%
	CDA Analysis		
d/b ratio	2.16	2.09	1.86

*Table IV-1: Data computed for the gold(I) α-CF₃ carbene complexes **18-Ph**, **18-OMe** and **18-CF₃** at the B3PW91/SDD+f(Au),6-31G**(other atoms) level of theory: selected bond lengths/angles, Wiberg bond indexes (WBI) for Au-C_{carb} and C_{carb}-C_{ipso} bonds, charge transfer (CT) from the carbene to the (P,P)Au⁺ fragment, NLMO associated with the aryl-to-C_{carb} π-donation and Au-to-C_{carb} back-donation (contribution of C_{carb}), donation/back-donation (d/b) ratio as estimated by CDA.*

Inspection of the molecular orbitals provides useful insight. The HOMO is centered on gold and is associated with an in-plane d orbital in bonding combination with $2p^\pi(C_{carb})$ orbital. Reciprocally, the LUMO is centered on the carbene center and corresponds to the $2p^\pi(C_{carb})$ vacant orbital in antibonding combination with d(Au) orbital (Figure IV-2, top & Figure SIV-2). In addition, the π-system of the aryl substituent is involved in these frontier orbitals, in line with π-donation from the biphenyl substituent to the carbene center. This description is confirmed by referring to the Natural Localized Molecular Orbitals (NLMO). The Au-to-C_{carb} back-donation and aryl-to-C_{carb} π-donation are apparent from the contributions of $2p^\pi(C_{carb})$ in the d(Au)-centered and π-aryl orbitals (Figure IV-2, bottom). Both interactions stabilize the carbene by filling partially its vacant orbital. The strength of the two interactions mildly evolves in the **18-CF₃**, **18-Ph**, **18-OMe** series. As expected from the electron-withdrawing/releasing effect of the *para* substituent, the C_{carb} contribution is the largest in the d(Au) NLMO for **18-CF₃**, while for **18-OMe**, it is in the π(arene) NLMO (Table IV-1). Of note, the energy gap between the HOMO/LUMO frontier orbitals is relatively small (2.34 eV from DFT and 1.95 eV from TD-DFT,

Figure SIV-2, SI p.201). Consistently, TD-DFT calculations, taking into account solvent effect (DCM) by SMD model, predict a low-energy symmetry-allowed electronic transition at 634 nm (HOMO → LUMO) that nicely matches the absorption band found experimentally at 619 nm.
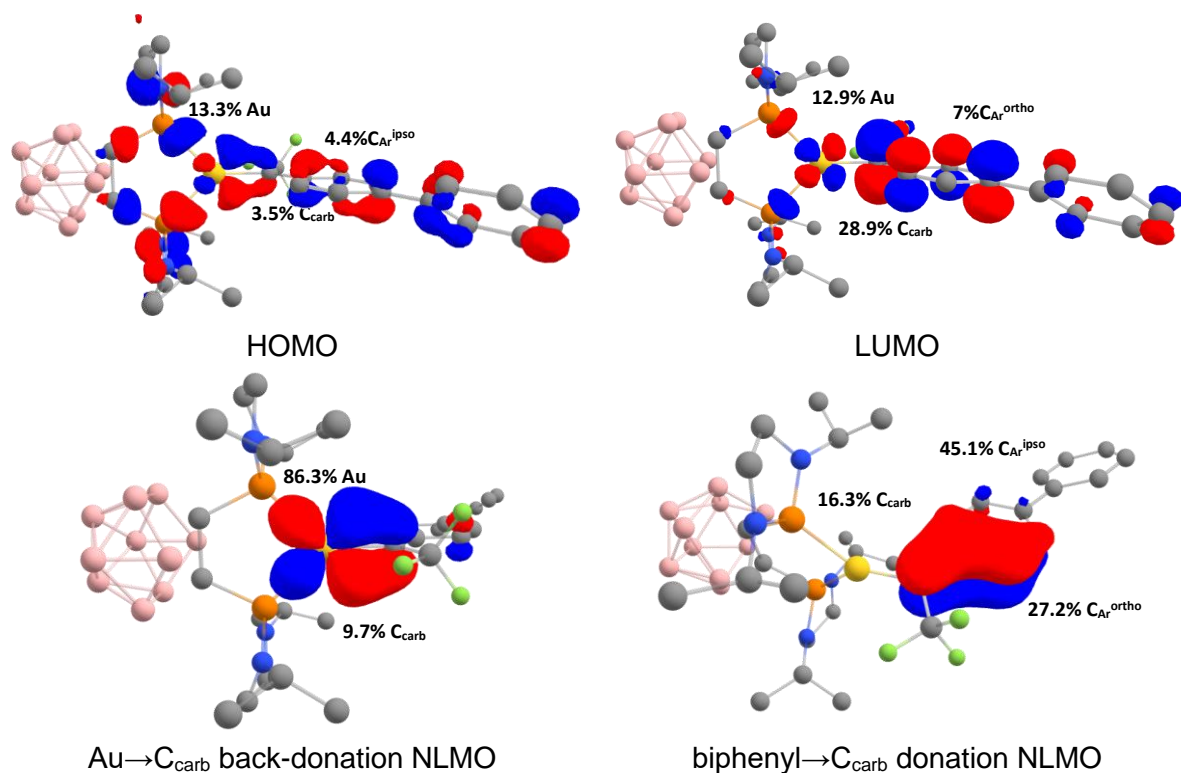
*Figure IV-2: HOMO, LUMO and NLMO (cutoff : 0.04) associated with the arene-to-C_{carb} π-donation and Au-to-C_{carb} back-donation computed for the gold(I) α-CF₃ carbene complex **18-Ph** at the B3PW91/SDD+f(Au),6-31G**(other atoms) level of theory. Contribution of the main atoms (in %) in the frontier orbitals and NLMO.*

To assess further the stabilization effect and relative importance of the arene-to-C_{carb} π-donation and Au-to-C_{carb} back-donation the "dynamics" of the parent α-CF₃ gold(I) carbene **18-H** was analyzed. No transition state was located for the rotation around the Au=C bond.[3] The rotation around the C_{carb}-C_{ipso} bond turned to be possible (Figure IV-3). Forcing the phenyl group to be perpendicular to the carbene center costs *ca* 10 kcal/mol (**TS_rot Ph**). It induces some shortening of the Au=C_{carb} bond length (from 1.975 to 1.934 Å). In the absence of π-donation from the phenyl substituent, Au-to-C_{carb} back-donation is further enhanced in **TS_rot Ph**, as apparent from the more negative C_{carb}-to-Au CT (-0.34 *vs* -0.20 e in **18-H**), an increase of the $2p^{\pi}(C_{carb})$ contribution in the d(Au) NLMO (17.6 vs 15.5% in **18-H**) and a decrease of d/b ratio. To assess further the role of the bidentate ligand and its influence on the back-donation, we looked for a TS associated to the dissociation of one P atoms from gold. Unfortunately, for the moment, it was not located on the PES.

---

[3] Rotational barriers of 18-27 kcal/mol were computed for [Co]=CF(CF₃)[21] and [Ir]=CF(CF₂CF₃)[23] complexes.
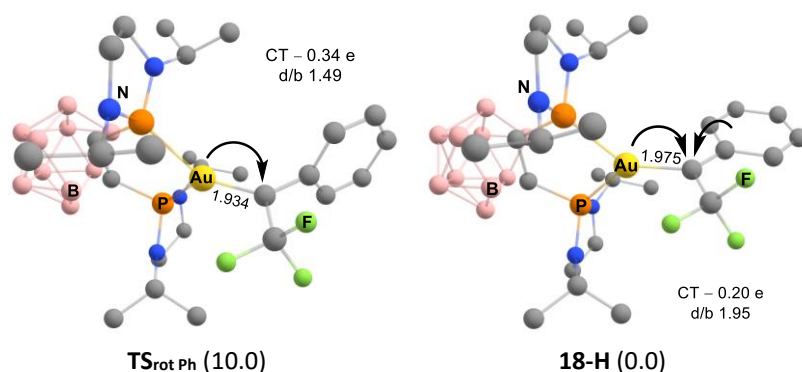
*Figure IV-3: Optimized geometry of the parent α-CF₃ gold(I) carbene **18-H** and transition state associated with the rotation of the phenyl ring (**TS$_{rot\,Ph}$**) at the B3PW91/SDD+f(Au),6-31G**(other atoms) level of theory. Charge transfer (CT) and d/b ratio. In parenthesis, activation barrier, in kcal/mol, computed from **18-H**.*

III. Reactivity of α-CF₃ gold(I) carbenes

1. Electrophilic carbene

First of all, the electrophilic behavior of the new synthesized complex was verified. Upon addition of pyridine (1 eq.) at -40°C, the blue color characteristic of **18-Ph** rapidly vanished, indicating rapid reaction. After work-up, the carbene-pyridine adduct **19** was isolated in 70% yield as a pale-yellow solid (Scheme IV-17). The NMR data are diagnostic for the addition of pyridine to the carbene center, not to gold. The ^{13}C NMR signal at 270.9 ppm for the carbene center is shifted by more than 170 ppm and now appears at δ 98.4 ppm (q, $^2J_{CF}$ = 38.0 Hz). The ^{1}H NMR signals for the H$_{ortho}$ atoms of pyridine are significantly deshielded at δ 8.98 ppm, while the $^4J_{PF}$ coupling constant decreases to 5.8 Hz upon coordination of the Lewis base. Since all our attempts to crystallographically characterize **19** failed, we prepared the analogous 4-dimethylamino-pyridine (DMAP) adduct **19'**. Gratifyingly, crystals suitable for XRD analysis could be obtained in this case, unambiguously confirming the addition of the N-Lewis base to the carbene center (Scheme IV-17, bottom). The pyridine N atom of DMAP is tightly coordinated to the former carbene center (N-C 1.499(5) Å) which is now in tetrahedral environment. Of note, only one of the P atoms is coordinated to gold which adopts a quasi-linear dicoordinate geometry (P-Au-C 167.81(11)°). The coordination of the Lewis base reduces the electrophilicity of the carbene center and gold atom. Combined with higher steric shielding, this prevents the two P atoms of the DPCb ligand to chelate gold. It is likely that the gold fragment swings in between the two phosphorus atoms, as previously observed in the (P,P)AuCl precursor.[29] The reactions of **18-Ph** with pyridine and DMAP substantiates its C-centered electrophilic behavior, in line with a Fischer-type carbene complex.
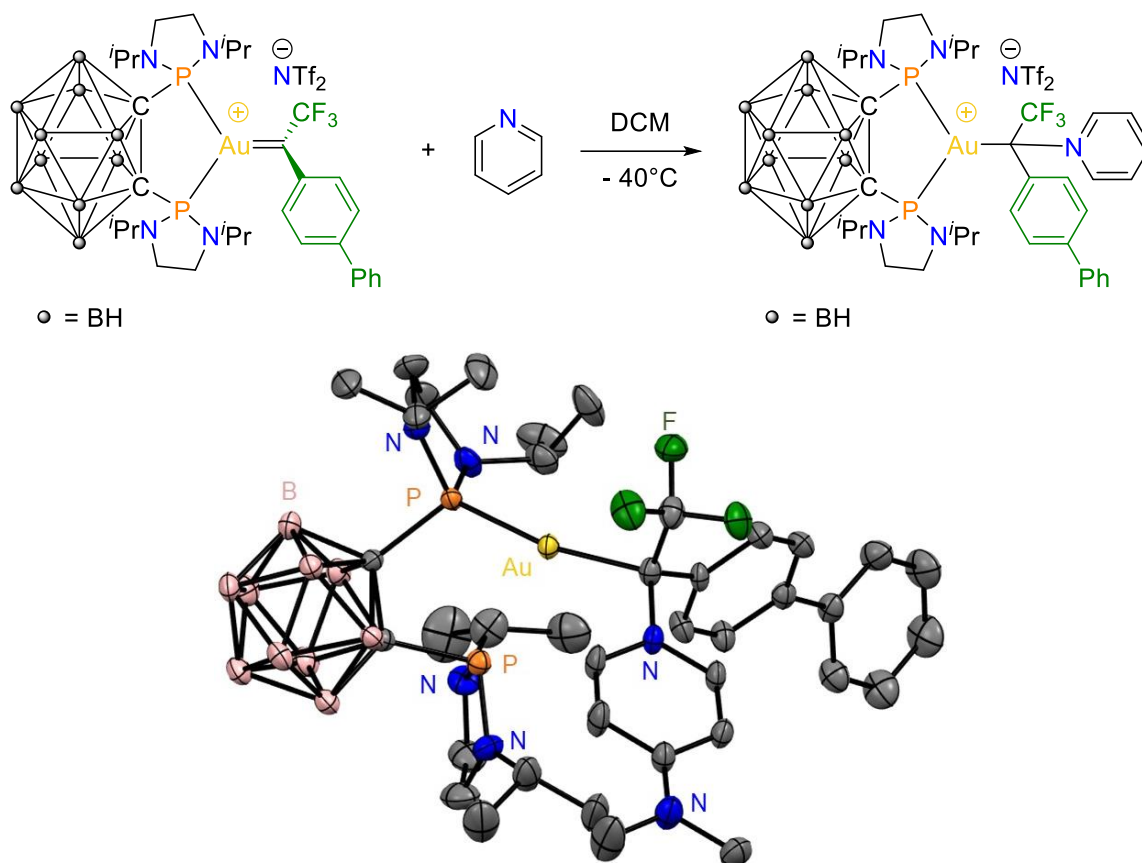
*Scheme IV-17: Reaction of the α-CF₃ gold(I) carbene **18-Ph** with pyridine ; molecular structure of the DMAP adduct. Thermal ellipsoids drawn at 50% probability, hydrogen atoms, counter anion and disordered atoms are omitted. Selected bond lengths (Å), and bond angles (°): Au-C$_{carb}$ 2.108(4), Au-P1 2.254(1), Au-P2 3.606(1), C$_{carb}$-C$_{Ar}$ 1.530(5), C$_{carb}$-CF₃ 1.521(5), C$_{carb}$-N 1.499(5), P1AuP2 68.14(3), P1AuC$_{carb}$ 167.8(1), P2AuC$_{Carb}$ 116.9(1).*

2. Stoichiometric reactions

The next step was to investigate the reactivity of this α-CF₃ gold carbene. For easiness of handling, the reactions were performed with **18-Ph**. First of all, the cyclopropanation was studied. When a solution of styrene (2 eq.) and 4,4'-difluorobiphenyl (internal standard, IS) was added over a solution of **18-Ph** at -40°C, the blue color of **18-Ph** disappeared over 1 hour. The NMR data unambiguously showed the formation of the cyclopropane (quantitatively) with high diastereoselectivity. The cyclopropane product has the biphenyl group *cis* to the phenyl group from styrene, which is typical for donor/acceptor carbenoids.[3] This configuration was first deduced from {¹H, ¹⁹F} HOESY NMR (correlation peaks were observed between the fluor atoms and the protons of the cyclopropane ring), and then definitively confirmed by XRD analysis. Moreover, no gold decomposition is observed during the reaction and the resting state is the π-complex (Scheme IV-18). This result seems promising for future catalytic reaction.
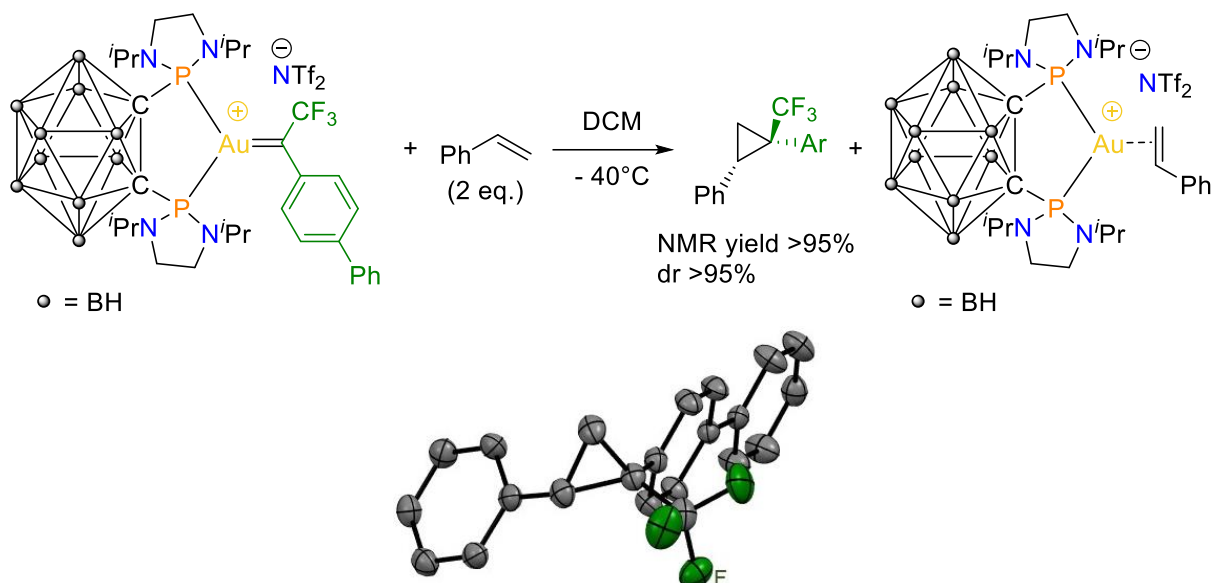
*Scheme IV-18: Reactivity of **18-Ph** with styrene and molecular structure of the ensuing cyclopropane (bottom) showing the syn relationship of the phenyl and biphenyl moieties (thermal ellipsoids drawn at 50% probability, hydrogen atoms are omitted).*

Reactivity of **18-Ph** was also tested toward Si-H insertion. When **18-Ph** reacts with 1 equivalent of SiHMe₂Ph and 4,4'-difluorobiphenyl (IS), the product of Si-H insertion is formed in 94% NMR yield (NMR data are consistent with those previously reported[11]). Some gold decomposition was observed (black precipitate) and the resting state of the complex is a new species showing ^{31}P NMR signal at 148.3 ppm whose structure could not be determined.
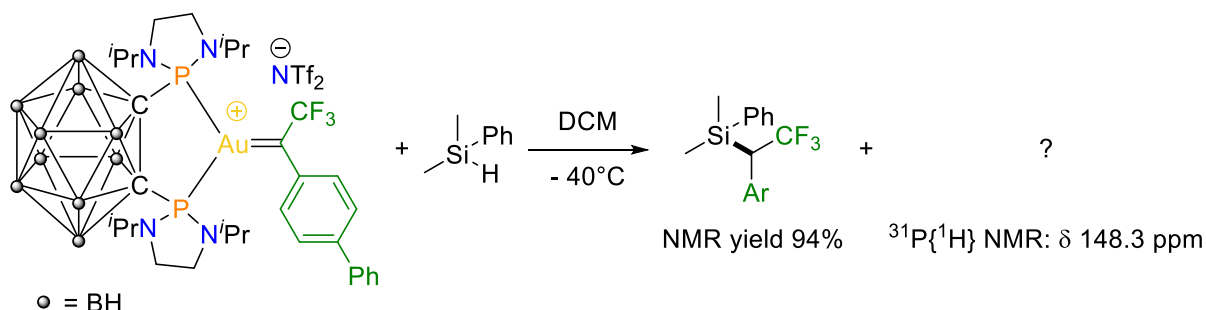
*Scheme IV-19: Reactivity of **18-Ph** with silane.*

Reactions of indoles with donor/acceptor diazo compounds catalyzed by Pd(OAc)₂ described in part 1.3, give access to *gem*-difluoro olefins or cyclopropane products depending on the indoles used. It could be interesting, if the reactivity of the newly synthesized carbene is complementary to these previous reactions, meaning if the CH insertion product could be obtained. So, **18-Ph** was reacted with 1 equivalent of different indoles. With the simplest indole, the product of C3 insertion is obtained in 75% NMR yield after 3 hours as deduced from ^{19}F NMR and ^{1}H NMR and traces of *gem*-difluoro olefins are detected (≈ 1%). With *N*-Methylindole, the product of C3 insertion is obtained as well in 70% NMR yield after 3 hours with a larger amount of *gem*-difluoro olefins (15%). Finally, with *N*-Phenylindole, only 23% NMR yield of the C3 insertion product was obtained after 24 hours. In all the reactions, no more carbene

complex is detected after 10 min and an unknown intermediate is formed. This latter slowly evolves to the formation of the C3 products in the case of indole and *N*-Methyl indole, and remains the main product for *N*-Phenylindole. Unfortunately, this intermediate was not characterized, since any attempts to isolate it, led to decomposition. To note, in all cases, no well-defined complex was detected at the end of the reaction.
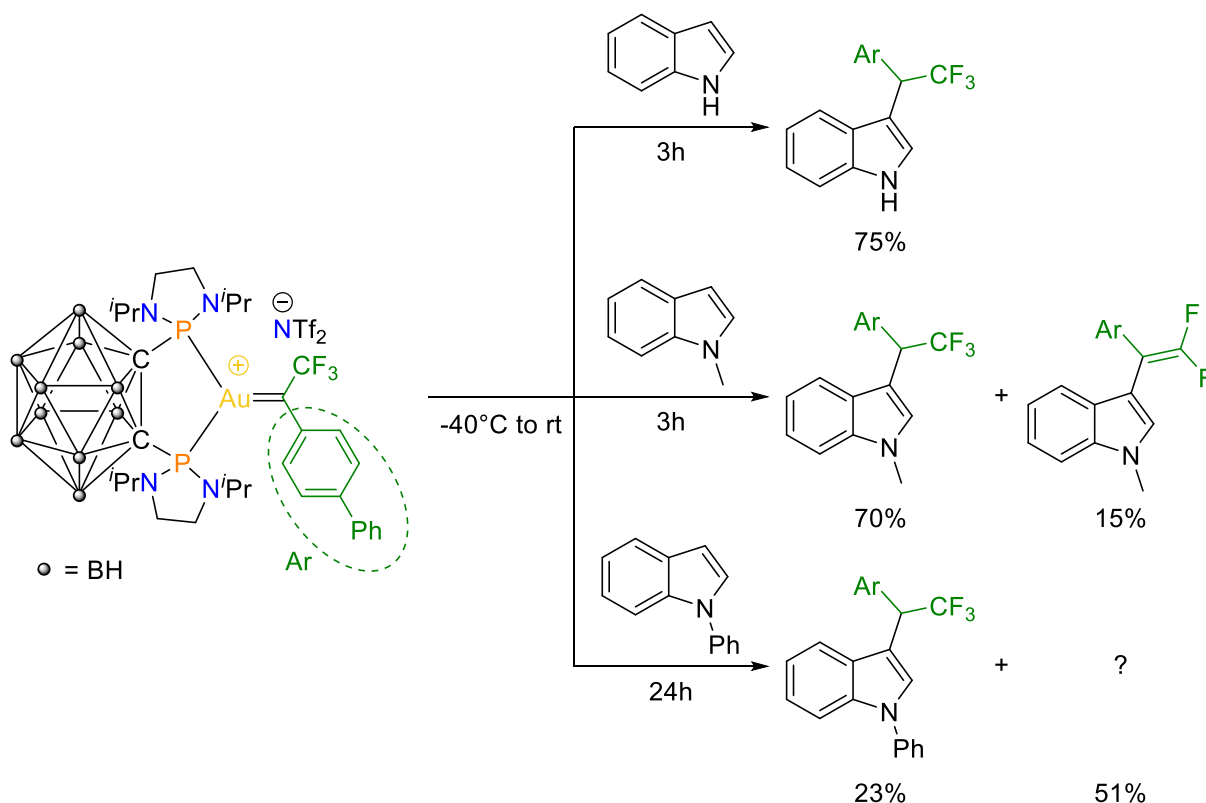
*Scheme IV-20: Reactivity of **18-Ph** with indole derivatives (NMR yields determined by $^{19}F\{^{1}H\}$ NMR using 4,4'-difluorobiphenyl as internal standard).*

3. Toward catalysis

In the light of the stoichiometric results, we then turned our attention toward catalysis. Is it possible to generate the carbene *in situ* and performed some catalytic reactions?

First, cyclopropanation was tested, since no degradation of the gold compounds was observed and the desired product was formed quantitatively. When mixing, biphenyl trifluoromethyl diazomethane with styrene, and catalytic amount of (P,P)AuNTf₂ (5 mol% freshly prepared from (P,P)AuI and AgNTf₂), the cyclopropane product was obtained in 67% NMR yield (38% isolated yield). As for the stoichiometric reaction, only one diastereoisomer was obtained.

Then a more challenging substrate was envisioned, indene, for which competition between cyclopropanation and CH insertion is possible. Same conditions as styrene were employed, and after 24 hours, the cyclopropane product was obtained in 56% NMR yield (39%

isolated yield) and 2 products of CH insertion were observed (13% yield), but not attributed. The cyclopropanation is fully diastereoselective, only the product presenting the indane moiety and the aryl of the diazo compound in *syn* position is obtained according to {¹H, ¹⁹F} HOESY NMR.
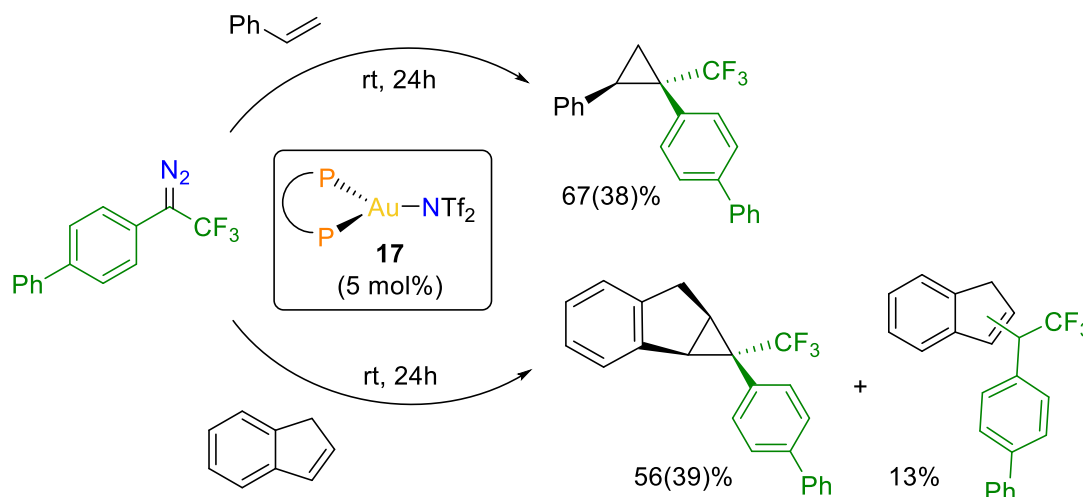
Scheme IV-21: Gold-catalyzed cyclopropanation reactions from the α-CF₃ diazo derivative (NMR yields determined by ¹⁹F{¹H} NMR using 4,4'-difluorobiphenyl as internal standard, isolated yields in parentheses).

Concerning Si-H insertion, no turnover was possible. Using 5 mol% of complex, no product was detected. Increasing the catalytic amount to 10mol%, 10% of the Si-H insertion product was obtained. Looking at the reaction media, we saw that the resting state was the unknown species showing an $^{31}P\{^{1}H\}$ NMR signal at δ 148.3 ppm, already observed in stoichiometric reaction. To note, this species is also obtained by mixing $(P,P)AuNTf_2$ with $SiHMe_2Ph$. Some black precipitate is observed during the process, which may suggest gold decomposition. Our investigation stopped here since no catalytic turnover can be achieved.

The selectivity for C3 insertion observed when mixing **18-Ph** and indoles prompted us to investigate the catalytic version of this reaction. Unfortunately, when mixing biphenyl trifluoromethyl diazomethane and indole derivatives with catalytic amount of $(P,P)AuNTf_2$ no selectivity was observed. Several products of CH insertion were observed (at least 3, not all of them were assigned). An optimization of the reaction conditions has been performed: ratio of compounds, increase of catalytic loading, temperature, order and rate of addition, but in the best case the C3 insertion product was obtained in 30% NMR yield with at least 2 other CH insertion products (20% NMR yield each).

This different outcome observed for the catalytic reaction from the diazo compound, compared to the stoichiometric reaction from the preformed carbene complex, can be explained by the involvement of a different active species. One possibility is the diazo / gold adduct (Scheme IV-22), prior to the release of N_2 and formation of the carbene. The diazo /

gold adduct may indeed lead to carbene transfer but *via* different pathways resulting in different chemoselectivity than the carbene complex. As such, having in hands carbene complexes enable to study their innate reactivity and confirm or infirm their participation in catalytic transformations. It is worth noting that α-oxo gold carbene complexes have also been questioned as the true reactive species in catalytic transformations starting from alkynes and pyridine oxides.[30]
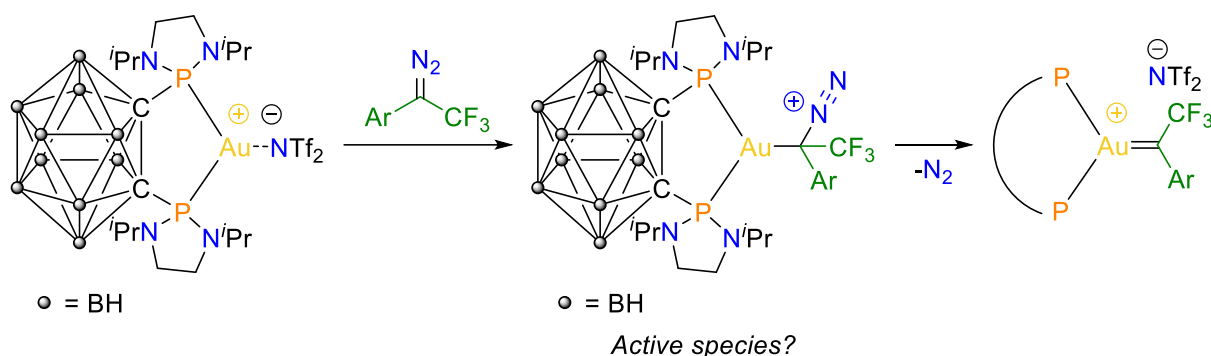
Scheme IV-22: Possible pathway for the synthesis of α-CF₃ gold carbene.

The overview of literature showed that there was no insertion reaction into O-H bond, this is why (P,P)AuNTf₂ **17** (5 mol%) was reacted with diazo compound and different alcohols (1 eq.). To our delight, the product of O-H insertion was obtained in 2 hours: 76% NMR yield with EtOH and 54% NMR yield with ^{i}PrOH.
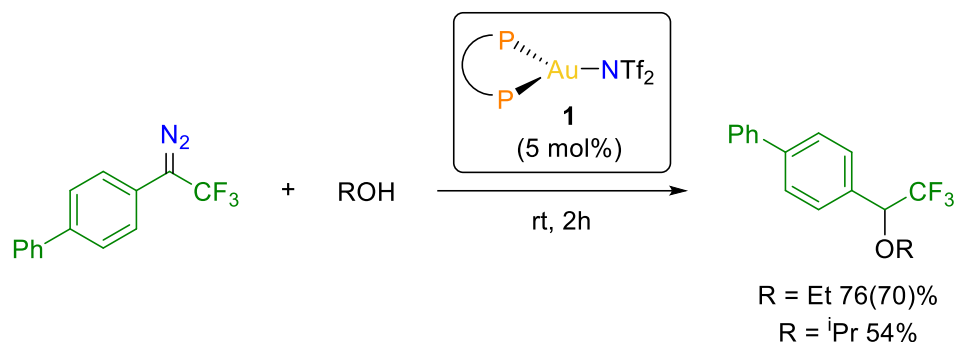
Scheme IV-23: Gold-catalyzed O-H insertion reactions from the α-CF₃ diazo derivative (NMR yields determined by ^{19}F NMR using 4,4'-difluorobiphenyl as internal standard, isolated yields in parentheses).

IV.   Conclusions and outlook

Thanks to the use of DCPb ligand, three α-CF$_3$ gold carbene complexes have been experimentally authenticated for the first time. The carbene center is both stabilized by Au→C$_{carbene}$ back-donation and aryl→C$_{carbene}$ donation as shown by XRD analysis and DFT calculations. Despite many attempts, no α-CF$_3$ gold carbenes were isolated or even characterized using the (P,N) hemilabile ligand.

The newly isolated carbene **18-Ph** participates in several catalytic reactions (cyclopropanation, O-H insertion). Despite good results in stoichiometric reaction, the catalytic version for the C-H insertion of indoles and the Si-H insertion could not be achieved.

The (P,P) ligand was proven to be efficient for the stabilization of highly reactive double bond,[31] thanks to its ability to enhance back-donation at gold. Is it possible to go further and stabilize Au≡C bond? To date, no complex of this type has been characterized. Some examples of M≡C triple bond exist with W, Mo, Fe or Ru,[32] but no example with later transition metals. Two synthetic pathways can be envisioned and are currently under study in the team: i) deprotonation of mono-substituted carbene complexes (Scheme IV-24, top) or ii) transmetalation of a diazo compound on gold and N$_2$ release (Scheme IV-24, bottom).
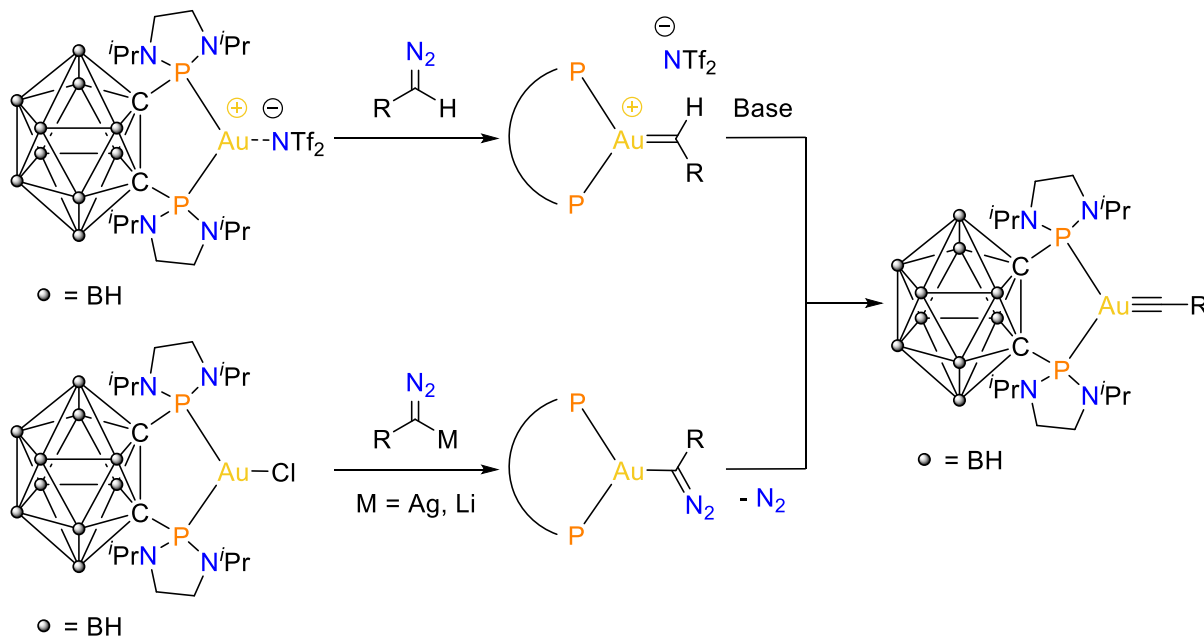
Scheme IV-24: Different synthetic pathways to access gold carbyne complexes

V. Experimental procedures and analytical data

1. Synthesis of gold complexes

$\circ$ = BH $\circ$ = BH
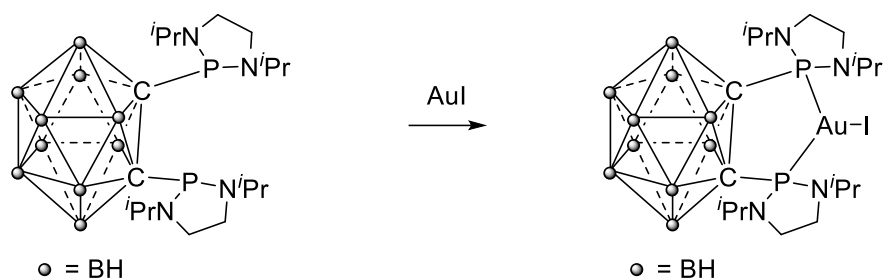
Prepared in a similar way than the gold Cl one,[33] with AuI instead of (DMS)AuCl.
$^{31}P\{^1H\}$ **NMR** (121 MHz, CDCl₃): δ 141.0 (s).

2. Synthesis of diazo compounds
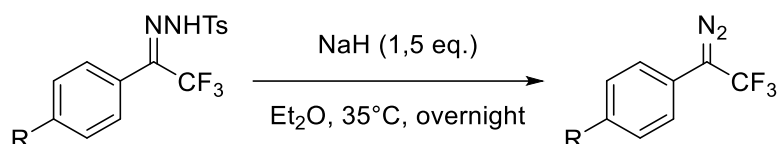
In a Schlenk flask, under argon, hydrazone was dissolved in Et₂O (0.3 M). A solution of NaH in Et₂O (0.3 M) was added stepwise over the solution of hydrazone. The reaction mixture was stirred overnight at 35°C. The solution was filtrate and the product was purified by silica gel chromatography (passivated with Et₃N, eluent: pentane). CAUTION: diazo compounds are presumed to be toxic and potentially explosive and should be handled with care, in a fume hood.

Data of 1-(1-Diazo-2,2,2-trifluoroethyl)-4-methoxybenzene, 4-(1-Diazo-2,2,2-trifluoroethyl)-1,1'-biphenyl and 1-(1-Diazo-2,2,2-trifluoroethyl)-4-trifluoromethylbenzene are consistent with literature.[34]

3. Synthesis of the α-CF₃ gold carbene

$\circ$ = BH $\circ$ = BH **17** $\circ$ = BH **18-R**
                                                    R = OMe, Ph, CF₃
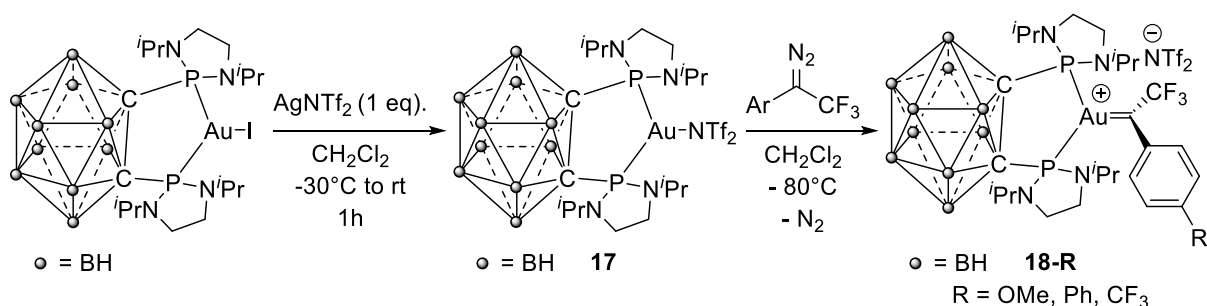
A solution of **1** (326 mg, 0.40 mmol) in dichloromethane (8 mL) was added to a dispersion of AgNTf₂ (155 mg, 0.40 mmol, 1.0 eq) in dichloromethane (4 mL) at -20°C and stirred for 1 hour under protection from light while slowly warming up to room temperature.

Compound 17: ^{31}**P{**^{1}**H} NMR** (121 MHz, CD$_2$Cl$_3$): δ 138.2 (s)

The reaction mixture was filtered over a pad of celite to give a clear yellow filtrate. A solution of diazo (0.40 mmol, 1.0 eq) in dichloromethane (2 mL) was added to the previous solution at -80°C. At -40°C, solvent was partially evaporated (do not dry completely) under vacuum. The product was precipitate by addition of pentane. Solution was removed by filtrating cannula. The product was dissolved in toluene (partially soluble) and precipitate by addition of pentane. Solution was removed by filtrating cannula and the product was dried under vacuum to give the desired product.
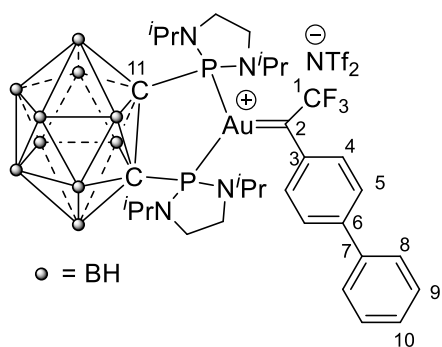
α-CF$_3$ gold(I) carbene 18-Ph: The pure product was obtained as a dark blue powder (428 mg, 89%). ^{31}**P{**^{1}**H} NMR** (121 MHz, CDCl$_3$, 298 K): δ 137.8 (q, ^{4}J$_{PF}$ = 23.2 Hz). ^{1}**H NMR** (500 MHz, CD$_2$Cl$_2$, 243 K): δ 8.00-7.88 (m, 2H, H$_5$), 7.88-7.82 (m, 2H, H$_4$), 7.81-7.78 (d, J$_{HH}$ = 7.1 Hz, 2H, H$_8$), 7.55-7.49 (m, 3H, H$_9$ & H$_{10}$), 3.72-3.60 (m, 4H, C*H*(CH$_3$)$_2$), 3.39-3.23 (m, 8H, N(C*H$_2$*)$_2$N), 3.01-1.70 (bs, 10H, BH), 1.36 (d, 6H, J$_{HH}$ = 6.5 Hz, CH(C*H$_3$*)$_2$), 1.34 (d, 6H, J$_{HH}$ = 6.6 Hz, CH(C*H$_3$*)$_2$), 1.19 (d, J$_{HH}$ = 6.5 Hz, 6H, CH(C*H$_3$*)$_2$), 1.04 (d, J$_{HH}$ = 6.6 Hz, 6H, CH(C*H$_3$*)$_2$). ^{13}**C{**^{1}**H}**

NMR (126 MHz, CD$_2$Cl$_2$, 243K): δ 269.8 (qt, ^{2}J$_{CF}$ = 34.9 Hz, ^{3}J$_{CP}$ = 94.4 Hz, C$_2$), 150.6 (t, J$_{PC}$ = 12.8 Hz, C$_6$), 143.6 (m, C$_3$), 138.1 (t, J$_{PC}$ = 6.1 Hz, C$_7$), 130.6 (s, C$_{10}$), 129.6 (s, C$_8$ & C$_9$), 128.3 (t, J$_{PC}$ = 9.5 Hz, C$_4$), 127.7 (t, J$_{PC}$ = 3.7 Hz, C$_5$), 119.8 (q, ^{1}J$_{CF}$ = 321.1 Hz, NTf$_2$), 90.2 (t, ^{1}J$_{PC}$ = 25.8 Hz, C$_{11}$), 50.5 (*pseudo* q, J$_{CP}$ = 8.7 Hz, *C*H(CH$_3$)$_2$), 42.6 (s, N(*C*H$_2$)$_2$N), 42.2 (s, N(*C*H$_2$)$_2$N), 21.6 (s, CH(*C*H$_3$)$_2$), 21.5 (s, CH(*C*H$_3$)$_2$), 21.2 (s, CH(*C*H$_3$)$_2$), 19.9 (s, CH(*C*H$_3$)$_2$). ^{19}**F NMR** (282 MHz, CDCl$_3$): δ -54.8 (t, ^{4}J$_{PF}$ = 23.2 Hz, CF$_3$), -79.7 (s, NTf$_2$). ^{11}**B{**^{1}**H} NMR** (96 Hz, CD$_2$Cl$_2$): -2.5, -10.1, -16.9. **(ESI+):** calculated for [M]+ = C$_{32}$H$_{55}$B$_{10}$N$_4$P$_2$F$_3$Au^{+}: 920.4510. Found: 920.4500.

Due to the coupling with F and P and its localization in the middle of aromatics carbon, C$_1$ was not attributed.

Crystals suitable for XRD analysis were obtained by slow diffusion of pentane into a concentrated solution of **18-Ph** in DCM at 4°C.
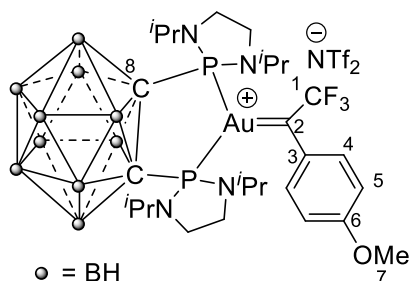
α-CF$_3$ gold(I) carbene 18-OMe: The pure product was obtained as a dark blue powder (240 mg, 52%). ^{31}**P{**^{1}**H} NMR** (121 MHz, CDCl$_3$): δ 142.1 (q, ^{4}J$_{PF}$ = 14.0 Hz). ^{1}**H NMR** (500 MHz, CD$_2$Cl$_2$): δ 7.90 (dq, J$_{HH}$ = 9.1 Hz, ^{5}J$_{HF}$ = 5.0 Hz, 2H, H$_4$), 7.20 (d, J$_{HH}$ = 9.1 Hz, 2H, H$_5$), 4.07 (t, J$_{HH}$ = 1.4 Hz, H$_7$), 3.74-3.61 (m, 4H, C*H*(CH$_3$)$_2$), 3.36-3.33 (m, 8H, N(C*H$_2$*)$_2$N), 3.18-1.71 (bs, 10H, H$_{BH}$), 1.38-1.32 (m, 12H, CH(C*H$_3$*)$_2$), 1.19 (d, J$_{HH}$ = 6.5 Hz, 6H, CH(C*H$_3$*)$_2$), 1.04 (d, J$_{HH}$ = 6.5 Hz, 6H, CH(C*H$_3$*)$_2$). ^{13}**C{**^{1}**H} NMR** (126 MHz, CD$_2$Cl$_2$):

δ 268.5 (qt, ^{2}J$_{CF}$ = 37.2 Hz, ^{2}J$_{CP}$ = 79.5 Hz, C$_2$), 171.3 (t, J$_{CP}$ = 9.9 Hz, C$_4$), 140.0 (qt, J$_{CP}$ = 13.3 Hz, J$_{CF}$ = 5.6 Hz, C$_3$), 129.5 (qt, , J$_{CP}$ = 8.3 Hz, J$_{CF}$ = 278.1 Hz, C$_1$), 120.4 (q, ^{1}J$_{CF}$ = 321.4 Hz, NTf$_2$), 117.3 (t, J$_{CP}$ = 5.9 Hz, C$_5$), 115.1 (s,C$_6$), 92.5 (t, J$_{CP}$ = 26.5 Hz, C$_8$), 58.0 (s, C$_7$), 51.0 (t, J$_{CP}$ = 8.1 Hz, *C*H(CH$_3$)$_2$), 50.9 (t, J$_{CP}$ = 8.1 Hz, *C*H(CH$_3$)$_2$), 43.1 (s, N(*C*H$_2$)$_2$N), 42.7 (s,

N(CH_2)$_2$N), 21.9 (s, CH(CH_3)$_2$), 21.4 (s, CH(CH_3)$_2$), 20.2 (s, CH(CH_3)$_2$), 19.0 (s, CH(CH_3)$_2$). **¹⁹F NMR** (282 MHz, CDCl₃): δ -53.9 (t, $^4J_{PF}$ = 14.3 Hz, CF₃), -78.5 (s, NTf₂). **HRMS (ESI+):** calculated for [M]+ = $C_{27}H_{53}B_{10}N_4P_2OF_3Au^+$: 874.4300. Found: 874.4297.
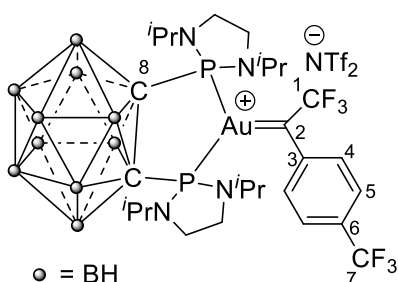
α-CF₃ gold(I) carbene 18-CF₃: Any work up of the carbene lead to decomposition. The product was characterized directly after addition of diazo, that give a deep purple color of the solution. **³¹P{¹H} NMR** (121 MHz, CD₂Cl₂, 298 K): δ 132.8 (qq, $^4J_{PF}$ = 32.1 Hz, $^8J_{PF}$ = 10.8 Hz). **¹H NMR** (400 MHz, CD₂Cl₂, 213 K): δ 7.80-7.73 (m, 4H, H$_{Ar}$), 3.70-3.54 (m, 4H, C*H*(CH₃)₂), 3.40-3.17 (m, 8H, N(C*H*₂)₂N), 2.96-1.65 (bs, 10H, H$_{BH}$), 1.31 (pseudo t, J_{HH} = 6.9 Hz, 12H, CH(C*H*₃)₂), 1.14 (d, J_{HH} = 6.5Hz, 6H, CH(C*H*₃)₂), 0.97 (d, J_{HH} = 6.4 Hz, 6H, CH(C*H*₃)₂). **¹³C{¹H, ¹⁹F} NMR** (100 MHz, CD₂Cl₂, 213 K): δ 265.8 (t, J_{CP} = 109.0 Hz, C₂), 145.2 (t, J_{CP} = 24.1 Hz, C₃), 134.7 (t, J_{CP} = 13.5 Hz, C₅), 132.4 (t, J_{CP} = 14.1 Hz, C₄), 129.1 (t, J_{CP} = 17.5 Hz, C₁), 126.3 (t, J_{CP} = 10.7 Hz, C₆), 123.0 (t, J_{CP} = 5.9 Hz, C₇), 119.3 (s, NTf₂), 87.7 (t, $^1J_{PC}$ = 25.9 Hz, C₈), 50.1 (t, J_{CP} = 6.8 Hz, C*H*(CH₃)₂), 50.0 (t, J_{CP} = 7.1 Hz, C*H*(CH₃)₂), 42.1 (s, N(CH₂)₂N), 41.7 (s, N(CH₂)₂N), 21.5 (s, CH(CH₃)₂). 21.0 (s, CH(CH₃)₂). 20.4 (s, CH(CH₃)₂), 19.6 (s, CH(CH₃)₂). **¹⁹F{¹H} NMR** (282 MHz, CD₂Cl₂, 213 K): δ -54.5 (t, $^4J_{PF}$ = 32.1 Hz, CF₃), -64.2 (t, $^8J_{PF}$ = 10.8 Hz, CF₃), -79.4 (s, NTf₂). **¹¹B {¹H} NMR** (96 MHz, CD₂Cl₂, 298 K): -2.4, -6.8, -10.9, -16.9. **HRMS (ESI+):** calculated for [M]+ = $C_{27}H_{50}B_{10}N_4P_2F_6Au^+$: 912.4068. Found: 912.4077.

4. Reactivity with nucleophilic reagent

To a solution of **18-Ph** (36 mg, 0.03 mmol) in dichloromethane (1.5 mL) was added a solution of base (0.06 mmol) in DCM (0.5 mL) at -40°C. The reaction mixture was stirred for 1 h while slowly warming up to room temperature. Solvent was removed under vacuum and the solid was washed twice with pentane. After drying under vacuum the Carbene/pyridine adduct was obtained as a pale-yellow solid (27 mg, 0.021, 70%).
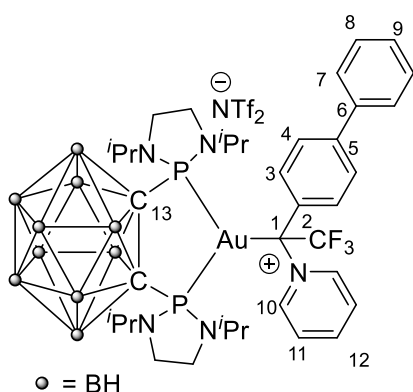
Compound 19: ³¹P{¹H} NMR (202 MHz, CDCl₃): δ 127.6 (q, $^4J_{PF}$ = 5.8 Hz). **¹H NMR** (500 MHz, CDCl₃): δ 8.98 (d, J_{HH} = 6.2 Hz, 2H, H₁₀), 8.65 (t, J_{HH} = 7.7 Hz, 1H, H₁₂), 8.14 (t, J_{HH} = 7.1 Hz, 2H, H₁₁), 7.65 (d, J_{HH} = 8.5 Hz, 2H, H₄), 7.57 (d, J_{HH} = 7.5 Hz, 2H, H₇), 7.47 (t, J_{HH} = 7.7 Hz, 2H, H₈), 7.41-7.33 (m, 3H, H₃ & H₉), 3.69-3.57 (m, 4H, C*H*(CH₃)₂), 3.28-3.16 (m, 8H, N(C*H*₂)₂N), 2.96-1.65 (bs, 10H, H$_{BH}$), 1.22 (d, J_{HH} = 6.6 Hz, 6H, CH(C*H*₃)₂), 1.17 (d, J_{HH} = 6.6 Hz, 6H, CH(C*H*₃)₂), 1.08 (d, J_{HH} = 6.6 Hz, 6H, CH(C*H*₃)₂), 1.05 (d, J_{HH} = 6.5 Hz, 6H, CH(C*H*₃)₂). **¹³C{¹H} NMR** (126 MHz, CDCl₃): δ 148.1 (s, C₁₂), 147.8 (s, C₁₀), 141.2 (s, C₅), 139.5 (s, C₆), 135.9 (s, C₂), 129.2 (s, C₈), 128.6 (s, C₁₁), 128.5 (s, C₄), 128.2 (s, C₉), 127.9 (s, C₃), 127.6 (q, $^1J_{CF}$ = 279.3 Hz, CF₃), 127.1 (s, C₇), 120.0 (q, $^1J_{CF}$ = 321.4 Hz, NTf₂), 98.4 (q, $^2J_{CF}$ = 38.0 Hz, J$_{PC}$ not observed, C₁), 90.4 (t, J_{PC} = 32.2 Hz, C₁₃), 50.3 (t, J_{CP} = 12.5 Hz, C*H*(CH₃)₂), 50.0 (t, J_{CP} = 12.5 Hz, C*H*(CH₃)₂), 42.9 (s, N(CH₂)₂N), 42.8 (s, N(CH₂)₂N), 21.8 (t, J_{CP} = 3.1 Hz, CH(CH₃)₂), 21.7 (t, J_{CP} = 3.1 Hz, CH(CH₃)₂), 21.2 (s,

CH(CH_3)$_2$), 20.7 (s, CH(CH_3)$_2$). **¹⁹F{¹H} NMR** (470 MHz, CD$_2$Cl$_2$, 213 K): δ -62.6 (bs, CF$_3$), -78.7 (s, NTf$_2$). **¹¹B {¹H} NMR** (160 MHz, CDCl$_3$): -1.3, -6.1, -10.0.

Compound 19': **³¹P{¹H} NMR** (202 MHz, CDCl$_3$): δ 125.9 (q, ⁴J_{PF} = 5.3 Hz). **¹H NMR** (500 MHz, CDCl$_3$): δ 8.21 (d, J_{HH} = 7.7 Hz, 2H), 7.60-7.52 (m, 4H), 7.49-7.33 (m, 4H), 7.27-7.20 (m, 2H), 6.82 (d, J_{HH} = 7.7 Hz, 2H), 3.78-3.59 (m, 4H, CH(CH$_3$)$_2$), 3.28-3.19 (m, 8H, N(CH_2)$_2$N), 3.29 (s, 6H, N(CH$_3$)$_2$), 2.96-1.65 (bs, 10H, H$_{BH}$), 1.27 (d, J_{HH} = 6.7 Hz, 6H, CH(CH_3)$_2$), 1.18 (d, J_{HH} = 6.6 Hz, 6H, CH(CH_3)$_2$), 1.20 (d, J_{HH} = 6.4 Hz, 6H, CH(CH_3)$_2$), 1.03 (d, J_{HH} = 6.5 Hz, 6H, CH(CH_3)$_2$). **¹⁹F{¹H} NMR** (470 MHz, CDCl$_3$, 213 K): δ -62.6 (bs, CF$_3$), -78.7 (s, NTf$_2$).

Crystals of carbene/DMAP adduct **19'** were grown from a dichloromethane/pentane solution at -30°C.

5. Stoichiometric reaction

With styrene: To a solution of **18-Ph** (28 mg, 0.023 mmol) in CDCl$_3$ (0.5 mL) was added a solution of styrene (5.3 µL, 0.046 mmol, 2 eq.) and 4,4'-difluorobiphenyl (2 mg, 0.011 mmol, 0.5 eq.) in CDCl$_3$ (0.1 mL) at -40°C and stirred manually when going back to room temperature. After 1h, the formation of one diastereoisomer of the cyclopropane (*cis* position of biphenyl of carbene and phenyl of styrene) is quantitative (>95%) according to ¹⁹F{¹H} NMR.

With silane: To a solution of **18-Ph** (28 mg, 0.023 mmol) in CDCl$_3$ (0.5 mL) was added a solution of SiHMe$_2$Ph (3.5 µL, 0.023 mmol, 1 eq.) and 4,4'-difluorobiphenyl (2 mg, 0.011 mmol, 0.5 eq.) in CDCl$_3$ (0.1 mL) at -40°C and stirred manually when going back to room temperature.

(1-([1,1'-biphenyl]-4-yl)-2,2,2-trifluoroethyl)dimethyl(phenyl)silane: 94% NMR yield. **¹H NMR** (300 MHz, CDCl$_3$): δ 7.71-7.31 (m, 14H), 7.06 (d, J_{HH} = 7.9 Hz, 2H), 3.15 (q, ³J_{HF} = 12.9 Hz, 1H), 0.48 (s, 3H), 0.39 (s, 3H). **¹⁹F NMR** (282 MHz, CDCl$_3$): δ -56.5 (d, ³J_{HF} = 12.9 Hz). **EI-MS:** Calculated for C$_{22}$H$_{21}$F$_3$Si: 370.14. Found: 370.07.

With indoles: To a solution of **18-Ph** (28 mg, 0.023 mmol) in CDCl$_3$ (0.5 mL) was added a solution of indole derivative (1 eq.) and 4,4'-difluorobiphenyl (2 mg, 0.011 mmol, 0.5 eq.) in CDCl$_3$ (0.1 mL) at -40°C and stirred manually when going back to room temperature.

3-(1-([1,1'-biphenyl]-4-yl)-2,2,2-trifluoroethyl)-1-methyl-1H-indole: 70% NMR yield after 3h. The product was not isolated. Characteristic data: **¹H NMR** (300 MHz, CDCl$_3$): δ 5.03 (q, ³J_{HF} = 9.6 Hz, 1H), 3.82 (s, 3H). **¹⁹F NMR** (282 MHz, CDCl$_3$): δ -67.3 (d, ³J_{HF} = 9.6 Hz). **EI-MS:** Calculated for C$_{23}$H$_{18}$F$_3$N: 365.14. Found: 365.27.

3-(1-([1,1'-biphenyl]-4-yl)-2,2,2-trifluoroethyl)-1H-indole: 75% NMR yield after 3h. The product was not isolated. Characteristic data: **^{1}H NMR** (300 MHz, CDCl$_3$): δ 5.04 (q, $^3J_{HF}$ = 9.4 Hz, 1H).**^{19}F NMR** (282 MHz, CDCl$_3$): δ -67.3 (d, $^3J_{HF}$ = 9.4 Hz). **EI-MS:** Calculated for C$_{22}$H$_{16}$F$_3$N: 351.12. Found: 351.27.

6. Catalytic reaction

A solution of (P,P)AuI (8.1 mg, 0.01 mmol) in DCM (0.4 mL) was added to a dispersion of AgNTf$_2$ (3.8 mg, 0.01 mmol) in DCM (0.2 mL) at -20°C and stirred for 1h while slowly warming up to room temperature. The reaction mixture was filtered over a pad of celite to give a clear yellow solution.

In a glovebox, a flame dried Schlenk equipped with a magnetic stirrer bar was charged with diazo compound (52.4 mg mg, 0.2 mmol) and styrene, indene or alcohol (0.2 mmol, 2 eq.) or fluorene (0.6 mmol, 3 eq.) in DCM (0.4 mL). Outside the glovebox, the yellow solution was added to the Schlenk and the reaction was stirred for the appropriate amount of time. The yield was determined by ^{19}F{^{1}H} NMR spectroscopy using 4,4'-difluorobiphenyl as internal standard.

With styrene and indene: reactions were stirred for 24 h under static vacuum.

2-(4-Phenylbenzenyl)-1-(trifluoromethyl)cyclopropyl)benzene: 67% NMR yield. The pure product was obtained after column chromatography **(**Petroleum ether/Toluene : 9/1) as a white powder (25,5 mg, 38%). **^{1}H NMR** (500 MHz, CDCl$_3$): δ 7.55-7.52 (m, 2H, H$_{11}$), 7.43-7.39 (m, 4H, H$_7$ & H$_{10}$), 7.36-7.31 (m, 1H, H$_{12}$), 7.24-7.20 (m, 2H, H$_6$), 7.13-7.09 (m, 3H, H$_{15}$ & H$_{16}$), 6.96-6.82 (m, 2H, H$_{14}$), 2.89 (dd, J$_{HH}$ = 9.7, 6.0 Hz, 1H, H$_2$), 1.93 (dd, J$_{HH}$ = 9.7, 6.0 Hz, 1H, H$_3$), 1.73 (pseudo t, J$_{HH}$ = 6.0 Hz, 1H, H'$_3$). **^{13}C$_{jmod}$**
NMR (126 MHz, CDCl$_3$): δ 141.0 (C$_8$), 140.5 (C$_9$), 135.7 (C$_{13}$), 133.0 (C$_6$), 130.7 (C$_5$), 128.9 (C$_7$), 128.1 (C$_{14}$), 128.0 (C$_{15}$), 127.6 (C$_{12}$), 127.2 (C$_{11}$), 126.8 (C$_{10}$), 126.7 (C$_{16}$), 125.9 (q, $^1J_{CF}$ = 274,2 Hz, C$_4$), 35.6 (q, $^2J_{CF}$ = 32.7 Hz, C$_1$), 25.9 (q, $^3J_{CF}$ = 2.5 Hz, C$_2$), 14.9 (q, $^3J_{CF}$ = 2.5 Hz, C$_3$). **^{19}F NMR** (376 MHz, CDCl$_3$): -69.7 ppm (s). The diastereoselectivity has been confirmed by {^{1}H, ^{19}F} HOESY NMR. **EI-MS:** Calculated for C$_{22}$H$_{17}$F$_3$: 338.13. Found: 338.15.
Crystals were grown by slow evaporation of DCM.
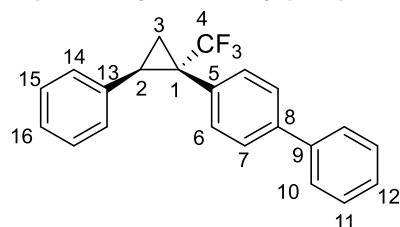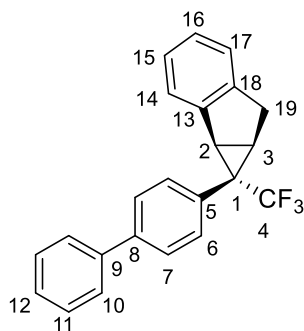
56% NMR yield. The pure product was obtained after column chromatography **(**Petroleum ether/Toluene : 9/1) as a white powder (27,1 mg, 39%). **¹H NMR** (400 MHz, CDCl₃): δ 7.50-7.45 (m, 2H, H_{11}), 7.42 (d, J_{HH} = 7.6 Hz, 1H, H_{14}), 7.40-7.26 (m, 5H, H_7 & H_{10} & H_{12}), 7.16-7.07 (m, 3H, H_{15} & H_6), 6.92 (td, J_{HH} = 7.6, 1.2 Hz, 1H, H_{16}), 6.75 (d, J_{HH} = 7.6 Hz, 1H, H_{17}), 3.33 (d, J_{HH} = 6.8 Hz, 1H, H_2), 3.25 (dd, J_{HH} = 17.6, 6.8 Hz, 1H, H_{19}), 2.83 (d, J_{HH} = 17.6 Hz, 1H, H'_{19}), 2.65 (pseudo t, J_{HH} = 6.8 Hz, 1H, H_3). **¹³C_jmod NMR** (101 MHz, CDCl₃): δ 142.3 (C_{18}), 140.6 (C_{13} & C_8), 140.4 (C_9), 133.4 (C_6), 128.8 (C_{10}), 128.0 (C_5), 127.4 (C_{12}), 127.1 (C_{11}), 126.7 (C_{16}), 126.5 (C_{15}), 126.4 (C_7), 125.9 (q, $^1J_{CF}$ = 274,4 Hz, C_4), 125.1 (C_{14}), 124.6 (C_{17}), 36.7 (q, $^2J_{CF}$ = 31.2 Hz, C_1), 33.8 (q, $^3J_{CF}$ = 3.0 Hz, C_2), 32.7 (C_{19}), 25.4 (q, $^3J_{CF}$ = 2.7 Hz, C_3). **¹⁹F NMR** (376 MHz, CDCl₃): -68.6 ppm (s). The diastereoselectivity has been confirmed by {¹H, ¹⁹F} HOESY NMR. **EI-MS:** Calculated for $C_{23}H_{17}F_3$: 350.13. Found: 350.27.
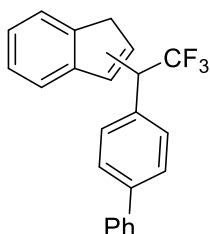
13% NMR yield. **¹H NMR** (300 MHz, CDCl₃): Characteristic data: δ 4.71 (q, $^3J_{HF}$ = 10.1 Hz, 1H, 3%), 4.52 (q, $^3J_{HF}$ = 9.4 Hz, 1H, 10%). **¹⁹F NMR** (282 MHz, CDCl₃): δ -65.7 (d, $^3J_{HF}$ = 10.1 Hz, 3%), -66.6 (d, $^3J_{HF}$ = 9.4 Hz, 10%).

With alcohol: Reactions were stirred for 2 h under flux of argon.
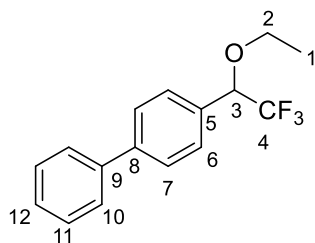
1-phenyl-4-(1-ethoxy-2,2,2-trifluoro-ethyl)benzene (10): 76% NMR yield The pure product was obtained after column chromatography **(**Petroleum ether/Ethyl Acetate : 95/5) as an oil (39 mg, 70%). **¹H NMR** (300 MHz, CDCl₃): δ 7.67-7.59 (m, 4H, H_7 & H_{11}), 7.53 (d, J_{HH} = 8.0 Hz, 2H, H_6), 7.43 (m, 2H, H_{10}), 7.41-7.35 (m, 1H, H_{12}), 4.67 (q, $^3J_{HF}$ = 6.6 Hz, 1H, H_3), 3.63 (q, J_{HH} = 7.0 Hz, 2H, H_2), 1.29 (t, J_{HH} = 7.0 Hz, 3H, H_1). **¹³C_jmod NMR** (75 MHz, CDCl₃): δ 142.5 (C_8), 140.6 (C_9), 132.3 (C_5), 129.0 (C_{10}), 128.7 (C_6), 127.8 (C_{12}), 127.4 (C_{11}), 127.3 (C_7), 124.3 (q, $^1J_{CF}$ = 281,8 Hz, C_4), 79.6 (q, $^2J_{CF}$ = 31.0 Hz, C_3), 66.4 (C_2), 15.2 (C_1). **¹⁹F NMR** (282 MHz, CDCl₃): -76.5 ppm (d, $^3J_{HF}$ = 6.6 Hz). **EI-MS:** Calculated for $C_{23}H_{17}F_3$: 280.11. Found: 280.27.
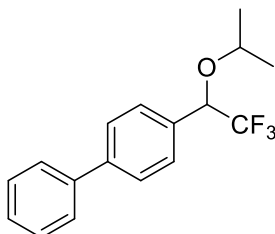
1-phenyl-4-(1-isopropoxy-2,2,2-trifluoro-ethyl)benzene (10'): NMR yield: 54%. Analytical data are consistent with those previously reported:[35] **¹H NMR** (300 MHz, CDCl₃): δ 7.63-7.30 (m, 9H), 4.72 (q, J = 6.8 Hz, 1H), 3.73 (hept, J = 6.0 Hz, 1H), 1.24 (d, J = 6.1 Hz, 3H), 1.17 (d, J = 6.2 Hz, 3H). **¹⁹F NMR** (282 MHz, CDCl₃): -76.8 ppm (d, $^3J_{HF}$ = 6.8 Hz).

7. Selected Crystallographic Data

Crystallographic data were collected at low temperature (193(2) K) on a Bruker-AXS APEX II Quazar diffractometer equipped with a 30W air-cooled microfocus or on a Bruker-AXS PHOTON100 D8 VENTURE diffractometer, using MoK$_\alpha$ radiation (λ = 0.71073 Å). Phi- and omega-scans were used. An empirical absorption correction was performed with SADABS.[4] The structures were solved by direct intrinsic phasing method (SHELXT),[5] and refined using the least-squares method on F^2.[6] All H atoms on carbon atoms were refined isotropically at calculated positions using a riding model.

ID	18-Ph	19'	Cyclopropane
formula	2($C_{32}H_{55}AuB_{10}F_3N_4P_2$), 2($C_2F_6NO_4S_2$), CH_2Cl_2	$C_{39}H_{65}AuB_{10}F_3N_6P_2$, $C_2F_6NO_4S_2$	$C_{22}H_{17}F_3$
M_r	2484.85	1322.13	338.35
crystal system	Triclinic	Monoclinic	Orthorhombic
space group	P-1	Cc	$P2_12_12_1$
a (Å)	12.9747 (7)	11.5655 (7)	5.7542 (8)
b (Å)	19.5323 (11)	23.5016 (15)	16.803 (2)
c (Å)	20.5359 (11)	21.3348 (12)	17.010 (2)
α (°)	89.793 (2)	90	90
β (°)	87.456 (2)	97.358 (2)	90
γ (°)	80.079 (2)	90	90
V (Å^3)	5121.4 (5)	5751.2 (6)	1644.7 (4)
Z	2	4	4
ρ_{calc} (g cm^{-3})	1.611	1.527	1.366
μ (mm^{-1})	3.144	2.761	0.102
F(000)	2476	2656	704.0
crystal size (mm^3)	0.180 x 0.120 x 0.080	0.200 x 0.040 x 0.040	0.140 x 0.080 x 0.060
T/K	193 (2)	193 (2)	193 (2)
measd reflns	124878	108721	5064
Unique reflns (Rint)	17950 (0.0587)	22126 (0.0527)	3966 (0.0434)
reflns used for refinement	17950	22126	3966
refined parameters	1250	695	226
GOF on F^2	1.049	1.039	1.039
R_1[a] [I>2σ(I)]	0.0320	0.0327	0.0434
wR_2[b] [all data]	0.0766	0.0655	0.1300

Table SIV-1: Crystal Data, Data Collection, and Structure Refinement. [a]$R_1 = \Sigma||F_o| - |F_c||/\Sigma|F_o|$, [b]$wR_2 = [\Sigma[w(F_o^2 - F_c^2)^2] / \Sigma[w(F_o^2)^2]]^{1/2}$.

[4] Bruker, *SADABS*, Bruker AXS Inc., Madison, Wisconsin, USA.

[5] G. M. Sheldrick *Acta Cryst.* **2015**, A71, 3–8.

[6] G. M. Sheldrick *Acta Cryst.* **2015**, C71, 3–8.

	Unit 1	Unit 2
Au-C	1.971(2)	1.971(4)
P-Au	2.347(1)/2.348(1)	2.361(1)/2.355(1)
C-C$_{1aryl}$	1.444(6)	1.439(6)
C-CF$_3$	1.500(6)	1.496(6)
PAuC	135.7(1)/133.7(1)	134.5(1)/135.9(1)
PAuP	90.59(4)	89.58(4)
C$_{3aryl}$-C$_{1aryl}$-C-Au	0.6(5)	-3.4(6)

*Table SIV- 2: Key geometric feature of the two independent molecules of the crystal structure of **18-Ph**.*

VI.   Computational details

All calculations were performed using the Gaussian 09 package[7] and the B3PW91 hybrid functional[8] on the real experimental systems. The gold atom was described with the relativistic electron core potential SDD and associated basis set,[9] augmented by a set of f-orbital polarization functions.[10] The 6-31G** basis set were employed for all other atoms.[11] Frequency calculations were undertaken to confirm the nature of the stationary points, yielding zero imaginary frequency for *minima*, yielding one imaginary frequency for transition states (TS), corresponding to the expected process. The connectivity of the transition states and their adjacent *minima* was confirmed by intrinsic reaction coordinate (IRC)[12] calculations. All the geometrical structures were plotted with Chemcraft program.[13] For the frontier orbitals, the atomic orbital compositions of each MO (%) have been computed thanks to Multiwfn 3.6 package.[14]

[7] Gaussian 09, M. J. Frisch, G. W. Trucks, H. B. Schlegel, G. E. Scuseria, M. A. Robb, J. R. Cheeseman, G. Scalmani, V. Barone, B. Mennucci, G. A. Petersson, H. Nakatsuji, M. Caricato, X. Li, H. P. Hratchian, A. F. Izmaylov, J. Bloino, G. Zheng, J. L. Sonnenberg, M. Hada, M. Ehara, K. Toyota, R. Fukuda, J. Hasegawa, M. Ishida, T. Nakajima, Y. Honda, O. Kitao, H. Nakai, T. Vreven, J. A. Montgomery, Jr., J. E. Peralta, F. Ogliaro, M. Bearpark, J. J. Heyd, E. Brothers, K. N. Kudin, V. N. Staroverov, T. Keith, R. Kobayashi, J. Normand, K. Raghavachari, A. Rendell, J. C. Burant, S. S. Iyengar, J. Tomasi, M. Cossi, N. Rega, J. M. Millam, M. Klene, J. E. Knox, J. B. Cross, V. Bakken, C. Adamo, J. Jaramillo, R. Gomperts, R. E. Stratmann, O. Yazyev, A. J. Austin, R. Cammi, C. Pomelli, J. W. Ochterski, R. L. Martin, K. Morokuma, V. G. Zakrzewski, G. A. Voth, P. Salvador, J. J. Dannenberg, S. Dapprich, A. D. Daniels, O. Farkas, J. B. Foresman, J. V. Ortiz, J. Cioslowski, and D. J. Fox, Gaussian, Inc., Wallingford CT, **2009**.

[8] a) A. D. Becke, *Phys. Rev.* **1988**, *A38*, 3098-3100; b) A. D. Becke *J. Chem. Phys.* **1993**, *98*, 5648; b) J. P. Perdew, in *Electronic Structure of Solids '91*, Ed. P. Ziesche and H. Eschrig, Akademie Verlag, Berlin, **1991**, 11.

[9] a) D. Andrae, U. Häussermann, M. Dolg, H. Stoll, H. Preuss, *Theor. Chim. Acta* **1990**, *77*, 123; b) M. Dolg, *Modern Methods and Algorithm of Quantum Chemistry, Vol. 1* (Ed.: J. Grotendorst), John von Neuman Institute for Computing, Jülich (Germany), **2000**, 479.

[10] A. W. Ehlers, M. Biihme, S. Dapprich, A. Gobbi, A. Hijllwarth, V. Jonas, K. F. Kiihler, R. Stegmann, A. Veldkamp, G. Frenking, *Chem. Phys. Letters* **1993**, *208*, 111.

[11] P. C. Hariharan, J. A. Pople, *Theor. Chim. Acta* **1973**, *28*, 213.

[12] a) K. Fukui, *Acc. Chem. Res.*, **1981**, *14*, 363; b) H. P. Hratchian, H. B. Schlegel, in *Theory and Applications of Computational Chemistry: The First 40 Years*, Ed. C. E. Dykstra, G. Frenking, K. S. Kim, G. Scuseria, Elsevier, Amsterdam, **2005**, 195.

[13] Chemcraft graphical software for visualization of quantum chemistry computations. https://www.chemcraftprog.com

[14] T. Lu, F. Chen, *J. Comput. Chem.*, **2012**, *33*, 580.

The bonding situation in all systems was studied using Natural Bond Orbital[15] analyses (NBO, 7.0 version).[16] Charge transfer between the carbene and the metallic fragment has been calculated using atomic NPA charges. The Natural Localized Molecular Orbitals (NLMO) associated to the interactions involving the vacant of the carbene, *i.e.* the d$_{xz}$(Au)→2p$^\pi$(C$_{carbene}$) and π$_{C=Caryl}$→2p$^\pi$(C$_{carbene}$) interactions, have been analyzed. NLMO plot associated to the Au→C back-donation was drawn (cutoff : 0.04) with Chemcraft program.[13]

For each system, a charge decomposition analysis (CDA) was carried out with the CDA 2.2 program developed by G. Frenking.[17] The orbital contributions to the charge distributions are divided into four parts: *i)* the mixing of the occupied orbitals of the ligand (carbene) and the unoccupied MOs of the metal fragment (P,P)Au$^+$ (Ligand→Au donation *d*), *ii)* the mixing of the unoccupied orbitals of the ligand and the occupied MOs of the metal fragment (Ligand←Au back-donation *b*), *iii)* the mixing of the occupied orbitals of the ligand and the occupied orbitals of the metal fragment (Ligand↔Au repulsive polarization *r*), and *(iv)* the mixing of the unoccupied orbitals of the ligand and the unoccupied orbitals of the metal fragment (residual term Δ).

The absorption spectrum was calculated at SMD(DCM)/B3PW91/SDD+f(Au), 6-31G**(other atoms)// B3PW91/SDD+f(Au), 6-31G**(other atoms) level by using time-dependent density functional theory (TD-DFT)[18] method on the geometry of the ground-state. Solvents effects (DCM : dichloromethane) was included by means of the universal Solvation Model based on Density (SMD).[19]

For the NMR calculations of the carbene gold complexes, the ^{13}C$_{carbene}$ NMR chemical shift (δ in ppm) and J_{PC} and J_{PF} coupling constants (in Hertz) were computed by employing the direct implementation of the Gauge Including Atomic Orbitals (GIAO),[20] with the IGLOII[21] basis set on B, C, H, N, F and P atoms and using as reference SiMe$_4$, optimized at the same level of theory.

[15] a) E. Reed, L. A. Curtiss, F. Weinhold, *Chem. Rev.* **1988**, *88*, 899; b) J. P. Foster, F. Weinhold, *J. Am. Chem. Soc.* **1980**, *102*, 7211; c) A. E. Reed, F. Weinhold, *J. Chem. Phys.* **1985**, *83*, 1736.

[16] NBO 7.0 program, E. D. Glendening, J. K. Badenhoop, A. E. Reed, J. E. Carpenter, J. A. Bohmann, C. M. Morales, P. Karafiloglou, C. R. Landis, and F. Weinhold, Theoretical Chemistry Institute, University of Wisconsin, Madison, **2018**.

[17] S. Dapprich, G. Frenking, *J. Phys. Chem.* **1995**, *99*, 9352.

[18] a) R. Bauernschmitt, R. Ahlrichs, Chem. Phys. Lett. **1996**, *256*, 454; b) M. E. Casida, C. Jamorski, K. C. Casida, D. R. Salahub, J. Chem. Phys. **1998**, *108*, 4439; c) R.E. Stratmann, G.E.Scuseria, M. J. Frisch, J. Chem. Phys. **1998**, *109*, 8218.

[19] Marenich, A. V.; Cramer, C. J.; Truhlar, D. G. *J. Phys. Chem. B* **2009**, *113*, 6378.

[20] a) F. London, *J. Phys. Radium* **1937**, *8*, 397; b) R. McWeeny, *Phys. Rev.* **1962**, *126*, 1028; c) R. Ditchfield, *Mol. Phys.* **1974**, *27*, 789; d) K. Wolinski, J. F. Hilton, P. Pulay, *J. Am. Chem. Soc.* **1990**, *112*, 8251; e) J. R. Cheeseman, G. W. Trucks, T. A. Keith, M. J. Frisch, *J. Chem. Phys.* **1996**, *104*, 5497.

[21] W. Kutzelnigg, U. Fleischer, M. Schindler, *The IGLO-Method: Ab Initio Calculation and Interpretation of NMR Chemical Shifts and Magnetic Susceptibilities*, Springer-Verlag, Heidelberg, **1990**, vol. 23.
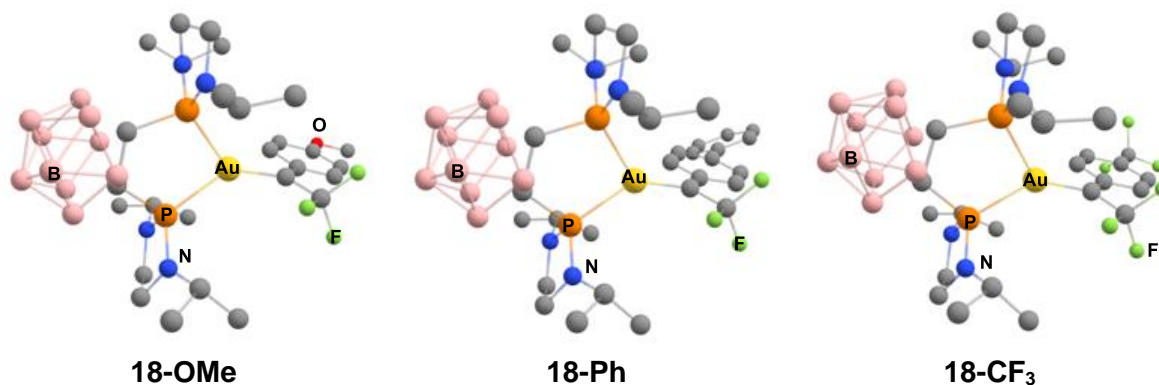
18-OMe   **18-Ph**   **18-CF₃**

	18-OMe	**18-Ph**		**18-CF₃**
	Geometrical parameters			
	DFT	**DFT**	**X-Ray**	**DFT**
Au-C	1.987	1.982	1.971(2)	1.971
P-Au	2.420/2.422	2.418/2.418	2.347(1)/2.348(1)	2.408/2.412
C-C$_{ar}^{ipso}$	1.423	1.429	1.444(6)	1.442
C-CF₃	1.515	1.515	1.500(6)	1.514
PAuC	133.5/136.6	135.9/134.2	135.7(1)/133.7(1)	134.4/134.7
PAuP	89.81	89.88	90.59(4)	89.79
C$_{ar}^{ortho}$-C$_{ar}^{ipso}$-C-Au	3.8	-0.9	0.6(5)	-1.7
	NMR Data			
	DFT[a]			
δ ^{13}C (C$_{Carb}$, ppm)	271.4	276.9		284.2
$^2J_{PC}$ (Hz)	92.5	100.4		135.3
$^4J_{PF}$ (Hz)	16.9	21.2		39.1
$^8J_{PF}$ (Hz)				14.7
	Experimental			
δ ^{13}C (C$_{Carb}$, ppm)	268.5	270.9		265.8
$^2J_{PC}$ (Hz)	79.5	94.4		109.0
$^4J_{PF}$ (Hz)	14.0	23.2		32.1
$^8J_{PF}$ (Hz)				10.8

*Table SIV-3: Main geometrical parameters (distance in Å, bond angles and bond dihedral angles in °) and NMR data (^{13}C$_{carb}$ chemical shifts δ in ppm and J$_{PC}$, J$_{PF}$ coupling constants in Hz) for the complexes **18-OMe**, **18-Ph** and **18-CF₃** calculated at the B3PW91/SDD+f(Au), 6-31G**(other atoms) level of theory. [a]NMR calculations carried out at GIAO-B3PW91/IGLO(II) for H, B, C, N, F, P atoms and SDD+f for Au.*

	18-OMe	18-Ph	18-CF₃
	NBO Analysis		
WBI (Au-C)	0.677	0.687	0.710
WBI (C-C$_{Ar}$)	1.312	1.289	1.234
CT	-0.10	-0.14	-0.25
d$_{xz}$(Au) → 2p^π(C) interaction	87.8% Au	86.3% Au	82.5% Au
	7.3% C$_{Carb}$	9.7% C$_{Carb}$	15.5% C$_{Carb}$
NLMO d$_{xz}$(Au)	1.0% C$_{ar}$	1.7% C$_{ar}$	0.4% C$_{ar}$
	1.0% C$_{ar}$	0.4% C$_{ar}$	0.2% C$_{ar}$
π$_{C=Caryl}$ → 2p^π(C) interaction	24.2% C$_{carb}$	16.3% C$_{carb}$	10.1% C$_{carb}$
	49.3% C$_{ar}$	45.1% C$_{ar}$	45.8% C$_{ar}$
NLMO π$_{C=Caryl}$	8.5% C$_{ar}$	27.2% C$_{ar}$	29.2% C$_{ar}$
	7.7% C$_{ar}$		
	CDA Analysis		
CR$_2$ → AuL$_2$ donation (d)	0.414	0.409	0.394
Au → CR$_2$ back-donation (b)	0.191	0.195	0.211
d/b ratio	2.16	2.09	1.86
Au ↔ C repulsion	-0.379	-0.396	-0.397
Residue term (Δ)	-0.017	-0.015	-0.012

*Table SIV-4: Bonding situation for complexes **18-OMe**, **18-Ph** and **18-CF₃** calculated at the B3PW91/SDD+f(Au),6-31G**(other atoms) level of theory. Wiberg Bond indexes (WBI) for Au-C$_{carbene}$ and C$_{carbene}$-C$_{Ar}$. Charge transfer (CT) from carbene to gold fragment accounting for NBO calculation. Contributions of main atoms (in percent) in the NLMO associated to d$_{xz}$(Au) and π$_{C=Caryl}$ orbitals. CDA analysis for the different complexes.*
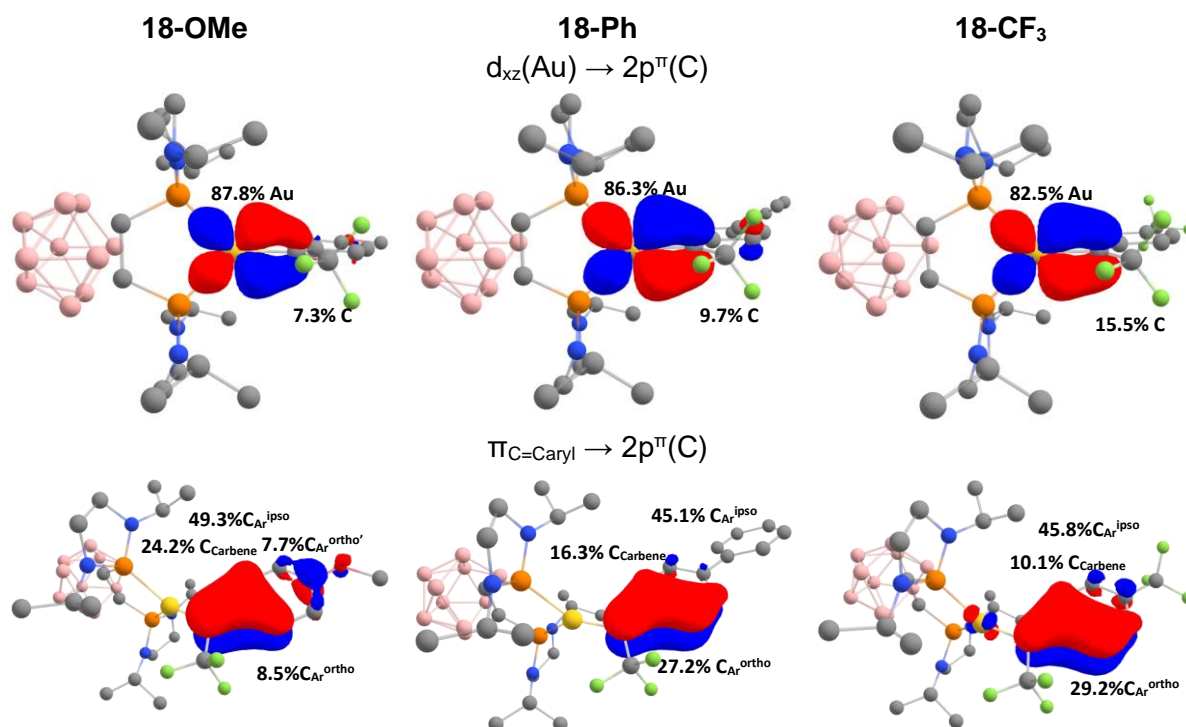
*Figure SIV-1: Plot of the NLMO (cutoff : 0.04) associated to the back-donation Au→C$_{carbene}$ (d$_{xz}$(Au) → 2p^π(C)) and the delocalization of the aryl group on the vacant of the carbene (π$_{C=Caryl}$ → 2p^π(C)) for complexes **18-OMe**, **18-Ph** and **18-CF₃**. Contribution of gold and C$_{carbene}$ atoms in percent.*
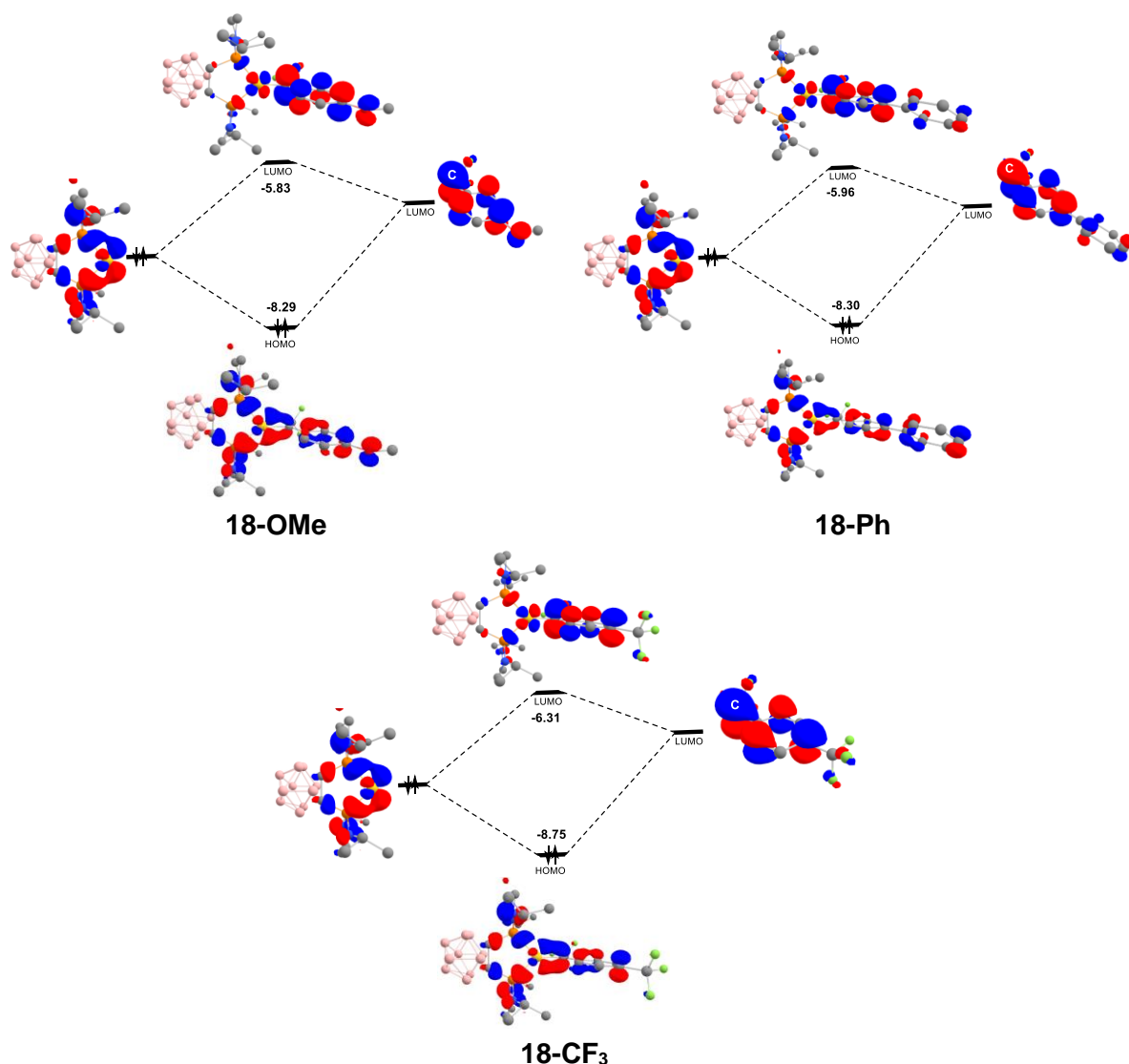
18-OMe

18-Ph

18-CF₃

*Figure SIV-2: Molecular diagrams corresponding to interaction between d_{xz}(Au) and $2p^\pi$(C) orbitals for each complex **18-OMe**, **18-Ph** and **18-CF₃**. Plot of the HOMO and LUMO and their energy levels for the α-CF₃ gold carbene complexes.*

For all complexes, the plot of the frontier orbitals evidences interaction of the $2p^\pi(C_{carb})$ orbital with both the metal and the aryl substituent. The energy gap between the frontier orbitals is relatively small in all cases: 2.34 eV for **18-Ph**, 2.46 eV for **18-OMe** and 2.44 eV for **18-CF₃**.

Excited state	λ (nm)	Transition energy (eV)	f	Electronic transitions[a]
1	634.8	1.95	1.13	HOMO→LUMO
2	517.0	2.40	0.01	HOMO -1 → LUMO
3	504.2	2.46	0.01	HOMO -2 → LUMO
4	463.7	2.67	0.03	HOMO -4 → LUMO (59.8%)
				HOMO -6 → LUMO (40.2%)
5	406.6	3.05	0.26	HOMO -3 →LUMO (86.7%)
				HOMO -6 → LUMO (13.3%)
6	399.89	3.10	0.08	HOMO -6 → LUMO (51.7%)
				HOMO -4 → LUMO (35.8%)
				HOMO -3 → LUMO (12.5%)

*Table SIV-5:. TD-DFT calculations for complex **18-Ph**: absorption wavelengths λ (in nm) and transition energies (in eV) corresponding to the main π → π* absorptions for the 6 first excited states, oscillator strength f, electronic transitions associated. [a]With HOMO-1 and HOMO-2 centered on phosphorus ligand; HOMO-3, HOMO-4 and HOMO-6 centered on π_{aryl}.*
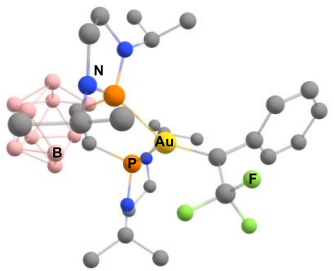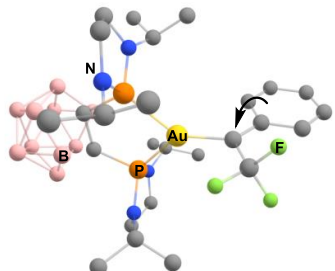
	TS$_{rot\ Ph}$	18-H
ΔG$^{\#}$	10.0	0.0
Geometrical parameters		
Au-C	1.934	1.975
P-Au	2.393/2.399	2.412/2.413
C-C$_{ipso}$	1.476	1.438
C-CF$_3$	1.511	1.516
PAuC	135.41/134.93	135.91/134.27
PAuP	89.58	89.77
C$_{ipso}$- C$_{ortho}$-C-Au	91.46	3.52
NBO Analysis		
WBI (Au-C)	0.786	0.705
WBI (C-C$_{ipso}$)	1.056	1.251
CT	-0.34	-0.20
d$_{xz}$(Au) → 2p$^{\pi}$(C) interaction	81.0% Au	83.2% Au
	17.6% C$_{Carbene}$	14.8% C$_{Carbene}$
NLMO d$_{xz}$(Au)	0.1% C$_{Ar}$	0.3% C$_{Ar}$
	0.1% C$_{Ar}$	0.2% C$_{Ar}$
π$_{C=Caryl}$ → 2p$^{\pi}$(C) interaction	0.3% C$_{carbene}$	10.6% C$_{carbene}$
	42.5% C$_{Ar}$	50.0% C$_{Ar}$
NLMO π$_{C=Caryl}$	40.1% C$_{Ar}$	30.2% C$_{Ar}$
CDA Analysis		
CR$_2$ → AuL$_2$ donation (d)	0.387	0.403
Au → CR$_2$ back-donation (b)	0.260	0.207
d/b ratio	1.49	1.95
Au ↔ C repulsion	-0.393	-0.392
Residue term (Δ)	-0.007	-0.015

*Table SIV-6: Main geometrical parameters and bonding situation for complexes **18-H** and transition states associated to rotation of phenyl ring (**TS$_{rot\ Ph}$**) and dissociation of one phosphine (**TS$_{dissoc\ P}$**) calculated at the B3PW91/SDD+f(Au),6-31G**(other atoms) level of theory. Distances are given in angstroms, bond angles and bond dihedral angles in degrees. Charge transfer (CT) from carbene to gold fragment accounting for NBO calculation. Contribution of main atoms (in percent) in the NLMO associated to d$_{xz}$(Au) and π$_{C=Caryl}$. CDA analysis.*

VII. References

[1] D. O'Hagan, D. B. Harper, *J. Fluor. Chem.* **1999**, *100*, 127–133.

[2] P. L. Maux, S. Juillard, G. Simonneaux, *Synthesis* **2006**, *2006*, 1701–1704.

[3] J. R. Denton, D. Sukumaran, H. M. L. Davies, *Org. Lett.* **2007**, *9*, 2625–2628.

[4] O. S. Artamonov, E. Y. Slobodyanyuk, D. M. Volochnyuk, I. V. Komarov, A. A. Tolmachev, P. K. Mykhailiuk, *Eur. J. Org. Chem.* **2014**, *2014*, 3592–3598.

[5] P. K. Mykhailiuk, S. Afonin, A. S. Ulrich, I. V. Komarov, *Synthesis* **2008**, *2008*, 1757–1760.

[6] B. Morandi, J. Cheang, E. M. Carreira, *Org. Lett.* **2011**, *13*, 3080–3081.

[7] B. Morandi, B. Mariampillai, E. M. Carreira, *Angew. Chem. Int. Ed.* **2011**, *50*, 1101–1104.

[8] R. Barroso, A. Jiménez, M. C. Pérez-Aguilar, M.-P. Cabal, C. Valdés, *Chem. Commun.* **2016**, *52*, 3677–3680.

[9] U. P. N. Tran, R. Hommelsheim, Z. Yang, C. Empel, K. J. Hock, T. V. Nguyen, R. M. Koenigs, *Chem. – Eur. J.* **2020**, *26*, 1254–1257.

[10] H. Luo, G. Wu, Y. Zhang, J. Wang, *Angew. Chem. Int. Ed.* **2015**, *54*, 14503–14507.

[11] S. Hyde, J. Veliks, B. Liégault, D. Grassi, M. Taillefer, V. Gouverneur, *Angew. Chem. Int. Ed.* **2016**, *55*, 3785–3789.

[12] V. Carreras, C. Besnard, V. Gandon, T. Ollevier, *Org. Lett.* **2019**, *21*, 9094–9098.

[13] S. Hyde, J. Veliks, D. M. H. Ascough, R. Szpera, R. S. Paton, V. Gouverneur, *Tetrahedron* **2019**, *75*, 17–25.

[14] C.-B. Liu, W. Meng, F. Li, S. Wang, J. Nie, J.-A. Ma, *Angew. Chem. Int. Ed.* **2012**, *51*, 6227–6230.

[15] I. E. Tsyshchuk, D. V. Vorobyeva, A. S. Peregudov, S. N. Osipov, *Eur. J. Org. Chem.* **2014**, *2014*, 2480–2486.

[16] Z. Yang, M. Möller, R. M. Koenigs, *Angew. Chem. Int. Ed.* **2020**, *59*, 5572–5576.

[17] Z. Yang, C. Pei, R. M. Koenigs, *Org. Lett.* **2020**, *22*, 7234–7238.

[18] S. Jana, C. Empel, C. Pei, T. Vinh Nguyen, R. M. Koenigs, *Adv. Synth. Catal.* **2020**, *362*, 5721–5727.

[19] S. Jana, C. Empel, T. V. Nguyen, R. M. Koenigs, *Chem. – Eur. J.* **2021**, *27*, 2628–2632.

[20] W. Tyrra, Y. L. Yagupolskii, N. V. Kirij, E. B. Rusanov, S. Kremer, D. Naumann, *Eur. J. Inorg. Chem.* **2011**, *2011*, 1961–1966.

[21] D. J. Harrison, S. I. Gorelsky, G. M. Lee, I. Korobkov, R. T. Baker, *Organometallics* **2013**, *32*, 12–15.

[22] D. J. Harrison, G. M. Lee, M. C. Leclerc, I. Korobkov, R. T. Baker, *J. Am. Chem. Soc.* **2013**, *135*, 18296–18299.

[23] J. Yuan, C. J. Bourgeois, A. L. Rheingold, R. P. Hughes, *Dalton Trans.* **2015**, *44*, 19528–19542.

[24] R. P. Hughes, R. B. Laritchev, J. Yuan, J. A. Golen, A. N. Rucker, A. L. Rheingold, *J. Am. Chem. Soc.* **2005**, *127*, 15020–15021.

[25] D. J. Harrison, A. L. Daniels, J. Guan, B. M. Gabidullin, M. B. Hall, R. T. Baker, *Angew. Chem. Int. Ed.* **2018**, *57*, 5772–5776.

[26] H. Yuge, N. Arakawa, S. Wada, T. K. Miyamoto, *Acta Crystallogr. Sect. E Struct. Rep. Online* **2008**, *64*, m1110–m1110.

[27] M. Navarro, A. Toledo, M. Joost, A. Amgoune, S. Mallet-Ladeira, D. Bourissou, *Chem. Commun.* **2019**, *55*, 7974–7977.

[28] C. García-Morales, X.-L. Pei, J. M. Sarria Toro, A. M. Echavarren, *Angew. Chem. Int. Ed.* **2019**, *58*, 3957–3961.

[29] M. Joost, Synthesis and Original Reactivity of Copper and Gold Complexes, Thesis, Université Paul Sabatier - Toulouse III, **2015**.

[30] J. Schulz, L. Jašíková, A. Škríba, J. Roithová, *J. Am. Chem. Soc.* **2014**, *136*, 11513–11523.

[31] A. Zeineddine, F. Rekhroukh, E. D. Sosa Carrizo, S. Mallet-Ladeira, K. Miqueu, A. Amgoune, D. Bourissou, *Angew. Chem. Int. Ed.* **2018**, *57*, 1306–1310.

[32] J. W. Herndon, *Coord. Chem. Rev.* **2012**, *256*, 1281–1376.

[33] M. Joost, L. Estévez, S. Mallet-Ladeira, K. Miqueu, A. Amgoune, D. Bourissou, *Angew. Chem. Int. Ed.* **2014**, *53*, 14512–14516.

[34] E. Emer, J. Twilton, M. Tredwell, S. Calderwood, T. L. Collier, B. Liégault, M. Taillefer, V. Gouverneur, *Org. Lett.* **2014**, *16*, 6004–6007.

[35] C. Kuang, X. Zhou, Q. Xie, C. Ni, Y. Gu, J. Hu, *Org. Lett.* **2020**, *22*, 8670–8675.

General conclusion & Perspectives

Gold chemistry has been a hot topic in the last years. The design of novel ligands, notably bidentate ones, allowed the synthesis of original gold compounds, which were considered elusive so far, and the development of novel reactivities. This PhD work falls within this topic. Our objective was to expand our knowledge in gold chemistry by a joint experimental/computational approach.

With the aim to develop new gold catalyzed reactions, we envisioned that the oxidative addition at gold, previously shown feasible by the group thanks to the use of the (P,N) hemilabile ligand,[1] could be merged with π-activation. Indeed, gold complexes are known for a long time to be efficient to activate CC multiple bonds. To study this new reactivity, we turned our attention to the heteroarylation of alkenes. This reaction, catalyzed by the MeDalPhos gold complex, works for a broad scope of substrates (*Scheme V-1*) and is particularly efficient for electron-rich aryl substrates, which is complementary to other systems (Pd-promoted or Au-based catalysis under oxidative or photoredox conditions).
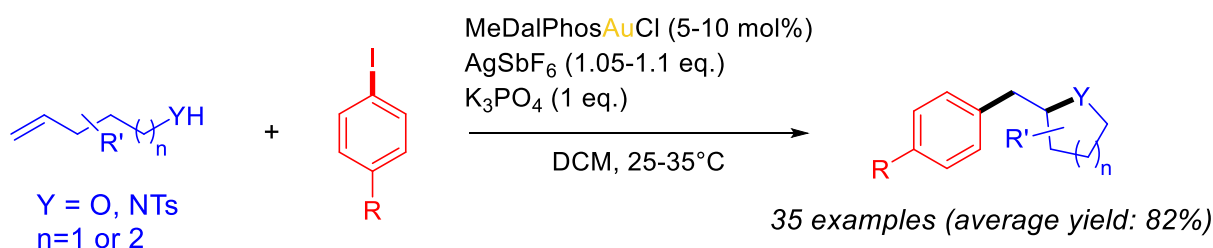
Scheme V-1: Heteroarylation of alkenes catalyzed by MeDalPhosAuCl.

Thanks to experimental studies, combining NMR monitoring and D-labelling, we came up with the following mechanism proposal: oxidative addition at gold, nucleophilic attack on a π-activating alkene, and then release of the product by reductive elimination. This catalytic cycle was further supported by DFT calculations. Noteworthy is the unusual switch of regioslectivity observed for internal alkenes. Indeed, whereas terminal alkenols and *Z*-alkenols undergo the 5-*exo* cyclization to access benzyltetrahydrofuran derivatives, *E*-alkenols reacts through 6-*endo* process and give phenylpyran products. Analyses of the geometry, the LUMO and NPA charges of the π-complexes showed that this switch of regioselectivity correlates with the bonding mode of the C=C bond (η^2 to η^1 slippage). η^1-coordination in this key intermediate promotes the 5-*exo* cyclization while η^2-coordination favors 6-*endo* cyclization (Scheme V-2).
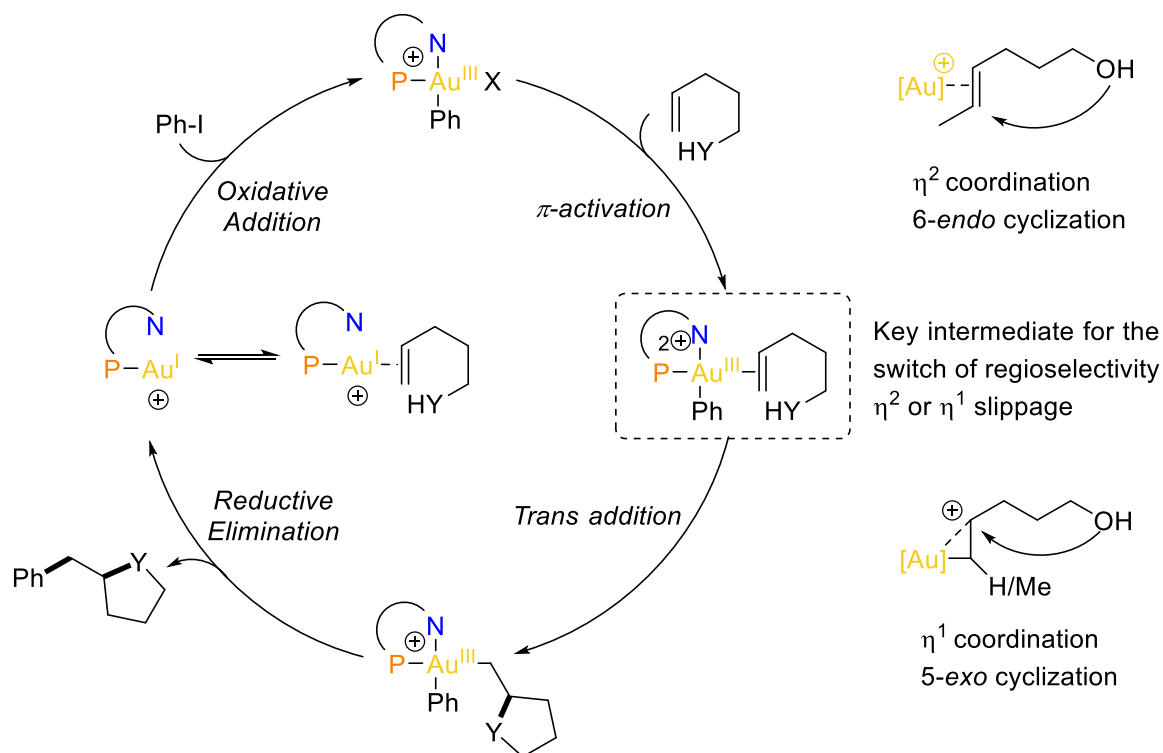
Scheme V-2: Mechanism of the heteroarylation of alkene highlighting the key intermediate for the regioselectivity of the cyclization (5-exo vs 6-endo).

During the mechanistic studies, a new complex presenting a N-H bond pointing towards gold was identified. Intriguing by this unusual situation, further analyses were performed. NMR and especially IR spectroscopies identified a N-H···Au hydrogen bonding which was further confirmed by DFT calculations, NBO and AIM analyses (Scheme V-3, left). This newly identified interaction fills the gap highlighted by Schmidbaur in 2014.[2] An *in silico* study, performed on new models potentially presenting X-H···Au or X-H···Ag hydrogen bonding, showed that this peculiar bonding situation should also be observable with other ligands and even with silver. This provides guideline for future experimental work, the most promising models (phenol and NHC ligand in a first place, Scheme V-3, left) will be synthesized and characterized.
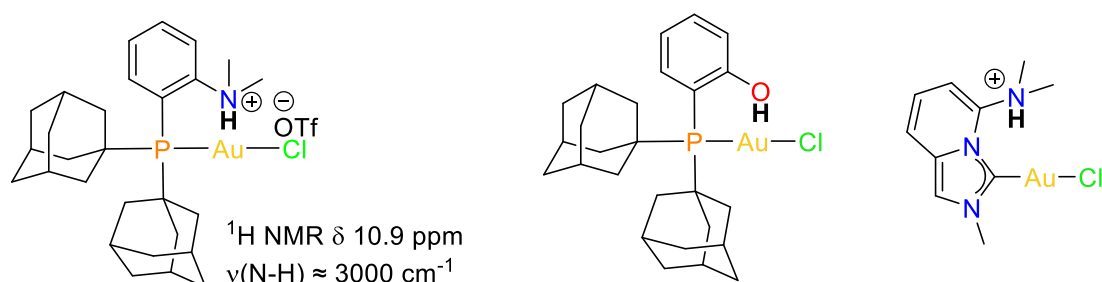
Scheme V-3: Complexes presenting hydrogen bonding to gold. Left: Protonated MeDalPhos gold complex already fully characterized (XRD, NMR & IR spectroscopies, DFT calculations, NBO & AIM analyses). Right: Targeted complexes for future experimental work.

Taking advantage of the enhanced back-donation at gold induced by the chelating DCPb ligand,[3] a new type of carbene complex was isolated, α-CF$_3$ gold(I) carbene. Three such compounds were characterized experimentally (XRD, MS, UV-Vis and Multi-nuclear NMR) and analyzed computationally (DFT calculations, NBO and AIM). They showed Fischer-type structure and reactivity. They do participate in catalytic cyclopropanation and O-H insertion reactions (*Scheme V-4*).
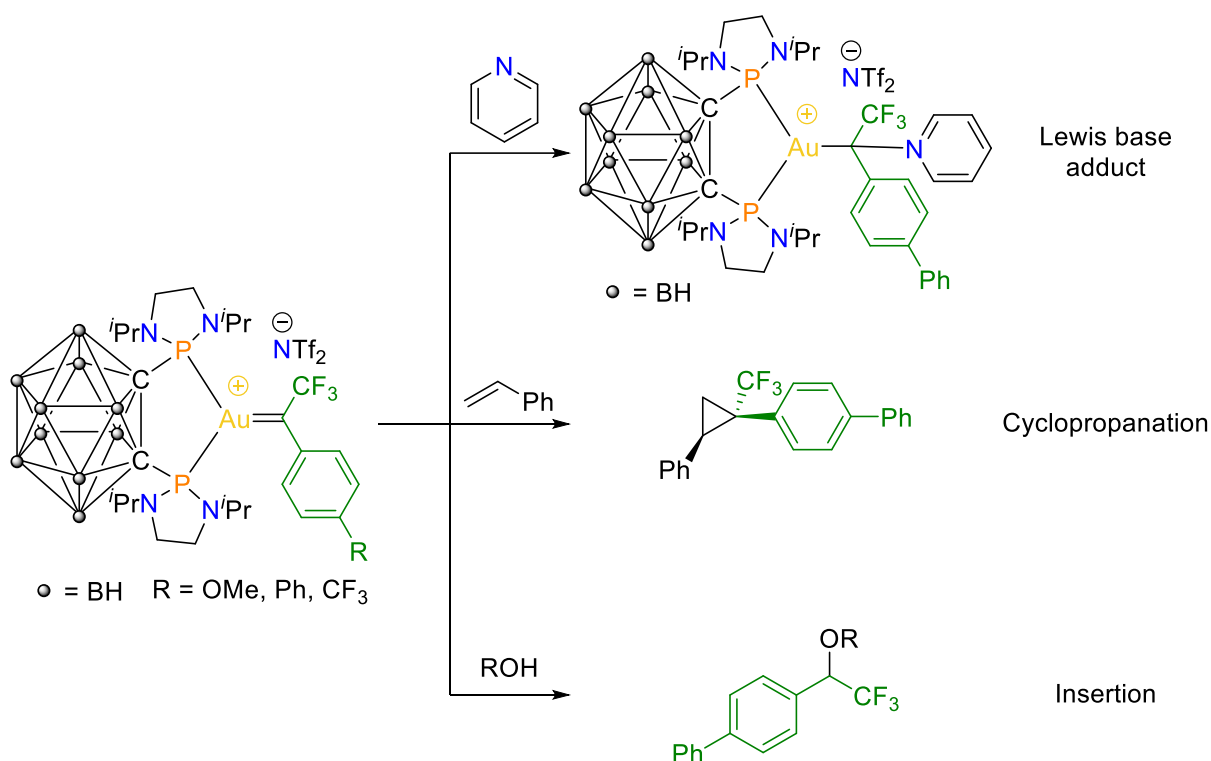
Scheme V-4: Characterized α-CF$_3$ gold carbene complexes and the reactivity of the biphenyl substituted one.

An underexplored area in gold chemistry is the preparation, characterization and application of super high-valent Au^V complexes. The large number and variety of well-defined gold(III) complexes, notably expanded thanks to the use of multidentate ligands, strongly encourage the quest for higher oxidation states.

The interest of complexes in high oxidation states is twofold: 1) they help to enhance and expand our basic knowledge, and 2) they may serve as oxidants for many important processes (oxidation of CO to CO$_2$, selective functionalization of C-H bonds…). Thus, the synthesis and characterization of well-defined complexes in high oxidation state, as well as their use in catalysis, have attracted considerable attention over the past few years.

Group 10 metal complexes in the +IV oxidation state (isoelectronic to Au(V) complexes) have been authenticated recently.[4] The use of multidentate ligands was crucial to synthesize and stabilize such species. For example, Sanford and co-workers showed that Ni^{II} can be oxidized to Ni^{IV} using the S-TDTT oxidant, and to enhance the stability of Ni^{IV} complex,

tridentate ligand were used. The Ni[IV] complex **V-A** bearing tris(2-pyridil)methane ligand was isolated and characterized by NMR spectroscopy and XRD analysis (Scheme V-5, top). To reduce the electrophilicity of this complex, and thus improve its reactivity, they changed the ligand to the trispyrazolylborate, providing a neutral Ni[IV] complex **V-B**. Selective Csp^3-heteroatom (O, S and N) coupling reaction was achieved in this case (Scheme V-5, bottom).[5]

X = OAc, OPh, SPh, NMeMes
> 98% conversion by ^{1}H NMR
78-94% isolated yield
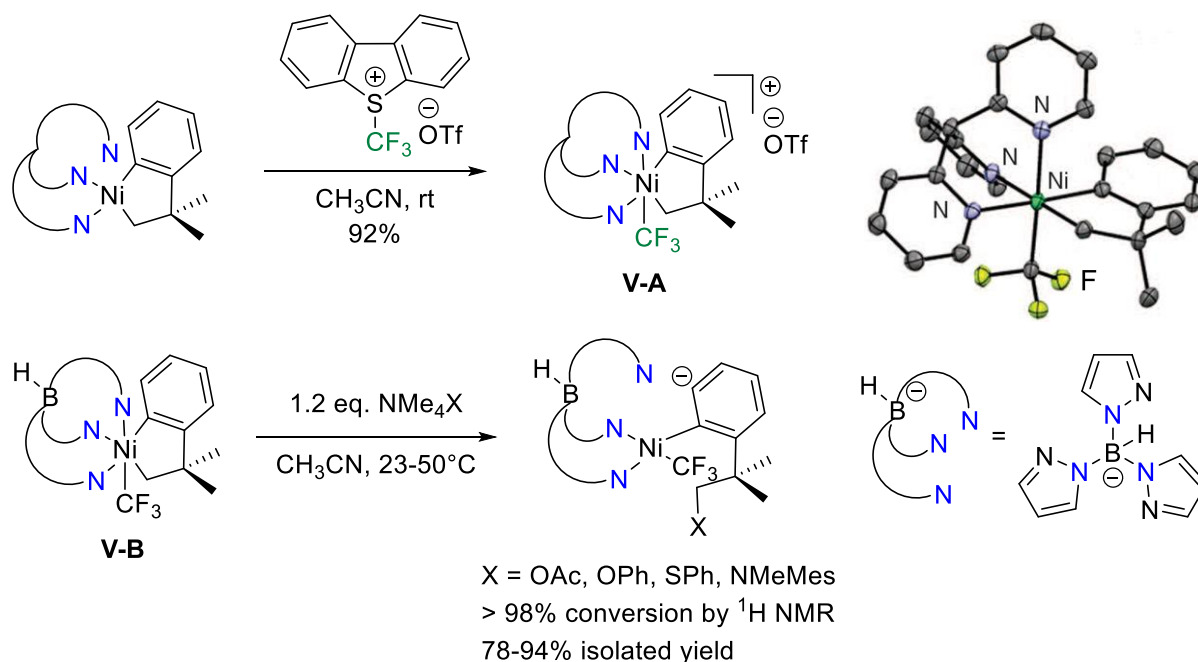
Scheme V-5: Use of tridentate ligand to access Ni[IV] complexes. Synthesis and molecular structure of V-A (top). Selective Csp^3-heteroatom (O, S and N) bond formation from V-B (bottom)

Concerning palladium, the Ritter's group designed a catalyst bearing an ancillary ligand (*o*-phenanthroline) that favors Pd[II] to Pd[IV] oxidation and stabilizes the high oxidation state. Reaction of the Pd[II] complex **V-C** with Selectfluor yielded the Pd[IV]-F complex, which further reacted with arenes to give the fluorinated product (Scheme V-6). They showed that the Pd[IV] complexes can be generated *in situ* and participate in catalytic fluorination.[6]
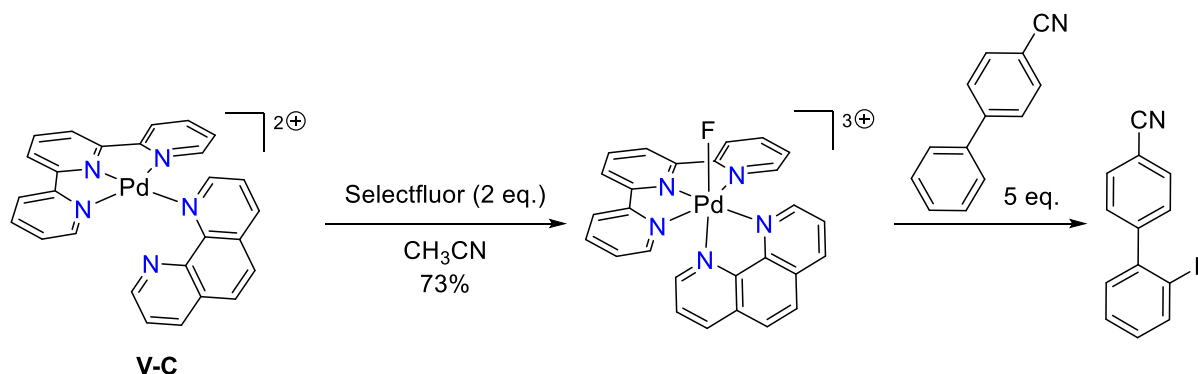
Scheme V-6: Oxidation of Pd[II] complex to Pd[IV] assisted by the presence of the o-phenanthroline and reactivity with arene.

To date, the +V state for gold is limited to AuF_5 and some AuF_6^- salts.[7] The recent progress on isoelectronic group 10 complexes increases the interest for Au^V complexes featuring an organic ligand. The structure of the Au^V complexes and the nature of the ancillary ligand will have to be carefully adjusted to impart stability. From a synthetic viewpoint, the targeted Au^V complexes could be accessed from Au^{III} precursors that would be oxidized by a F^+ (or CF_3^+) transfer agent. A joint experimental/computational approach will be particularly useful for this project. The experience gained by the group from the previous DFT studies has shown that B3PW91 is a good functional to describe gold complexes. An *in silico* study will be first performed, with this functional, to identify the different types of ligands and complexes suitable for Au^V chemistry. DFT calculations will tell if the targeted complexes are thermodynamically accessible, and particular focus will be put on the reductive elimination into Au^{III} species. Molecular orbital and NBO analyses, notably looking at d orbitals occupancy and atomic charges, will give information on the oxidation state of the gold center and the nature of the newly form Au-F (Au-CF_3) bond. After identification of the best candidates, synthetic work will be engaged and different characterization and analyses performed. If possible, single XRD will be done to confirm the structure of the complexes. NMR spectroscopies will also represent a very powerful tool. ^{19}F NMR will be informative for the fluoro (and trifluoromethyl) Au^V complexes. If N-based ligands are used, ^{15}N NMR can be exploited to assess the coordination of the N atom.[8] With the experience in DFT calculations and the utilities available at the LHFA, the gold(V) project will be further developed in the team.

The large panel of multidentate ligands available were showed to be useful for the gold chemistry: from the stabilization induced by the formation of cyclometalated complexes, to the improved properties achieved thanks to chelating ligands and the development of Au^I/Au^{III} catalysis induced by hemilabile ligands. The field of gold chemistry have been largely expanded and future work, using these different ligands or new ones, designed on purpose, are very promising.

References

[1]   A. Zeineddine, L. Estévez, S. Mallet-Ladeira, K. Miqueu, A. Amgoune, D. Bourissou, *Nat. Commun.* **2017**, *8*, 565.

[2]   H. Schmidbaur, H. G. Raubenheimer, L. Dobrzańska, *Chem. Soc. Rev.* **2013**, *43*, 345–380.

[3]   M. Joost, L. Estévez, S. Mallet-Ladeira, K. Miqueu, A. Amgoune, D. Bourissou, *Angew. Chem. Int. Ed.* **2014**, *53*, 14512–14516.

[4]   B. Zhang, X. Yan, S. Guo, *Chem. – Eur. J.* **2020**, *26*, 9430–9444.

[5]   N. M. Camasso, M. S. Sanford, *Science* **2015**, *347*, 1218–1220.

[6]   K. Yamamoto, J. Li, J. A. O. Garber, J. D. Rolfes, G. B. Boursalian, J. C. Borghs, C. Genicot, J. Jacq, M. van Gastel, F. Neese, T. Ritter, *Nature* **2018**, *554*, 511–514.

[7]   F. Mohr, *Gold Bull.* **2004**, *37*, 164–169.

[8]   H. Andersson, A.-C. C. Carlsson, B. Nekoueishahraki, U. Brath, M. Erdélyi, in *Annu. Rep. NMR Spectrosc.* (Ed.: G.A. Webb), Academic Press, **2015**, pp. 73–210.

Résumé en Français

I.   Introduction

L'or n'est pas seulement utilisé en bijouterie, c'est également un métal particulier du tableau périodique. Contrairement aux autres métaux, l'étude de l'élément or est très récente et ses premières utilisations en catalyse datent des années 70.[1] Les quantités de catalyseurs nécessaires pour atteindre de bon rendement étant élevé l'or a été considéré comme « catalytiquement mort » en 1995.[2] Ce point de vue a totalement changé en 1998, quand Teles a rapporté une catégorie de catalyseur [L-Au+] (où L est un ligand phosphine, phosphite ou un arsine) efficace pour l'addition d'alcool sur les alcynes (Schéma 1).[3] Inspiré par ces travaux, les propriétés carbophiles de l'or ont été largement explorées pour développer de nouvelles réactions catalysées par l'or, notamment pour la synthèse de molécules hautement fonctionnalisées.[4–6]
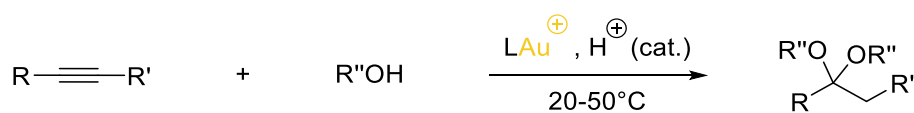
L = phosphine, phosphite ou arsine

Schéma 1 : Addition nucléophile d'alcools sur les alcynes catalysée par l'or.

Pour étendre la chimie de l'or au-delà de la π-activation, la conception de ligands appropriés, notamment les ligands bidentes, a été nécessaire. Le second site de coordination modifie les propriétés de l'or et contrôle sa réactivité. Grâce à l'utilisation de ligands bifonctionnels, des réactions élémentaires avec l'or ont été mise en évidence (addition oxydante, insertion migratoire…), ouvrant la voie vers de nouveaux cycles catalytiques Au^I/Au^{III}. De plus, des intermédiaires clés ont pu être isolés et caractérisés (complexes π, carbènes…) permettant d'éclaircir les mécanismes mises en jeux. Les effets des ligands bidentes ont été scrupuleusement analysés pour comprendre les facteurs clés gouvernant la réactivité des complexes d'or et élargir leur champ d'application.[7,8]

L'objectif de ce travail de thèse est d'étendre la réactivité de l'or et d'augmenter la variété des complexes accessibles, utilisant des ligands « sur mesure » qui impactent fortement les propriétés de l'or en termes de liaison et de comportement chimique. La synthèse et la caractérisation de complexes originaux ainsi que le développement de nouvelles réactivités se sont accompagnés d'études théoriques pour la compréhension des propriétés électroniques et l'étude des mécanismes mis en jeu.

II. Fusionner le comportement redox de l'or et l'activation π : vers une hétéroarylation d'alcène catalytique

Les complexes d'or sont extrêmement puissants pour activer les liaisons π et les développements synthétiques associés sont nombreux. La faculté des ligands hémilabiles (P,N) à favoriser l'addition oxydante d'halogénures d'aryle à l'or,[9,10] nous a incité à essayer de combiner cette étape élémentaire et l'activation π dans une transformation catalytique Au[I]/Au[III]. A cet égard, les réactions d'oxy- et d'amino-arylation des alcènes avec les acides boroniques arylé ou les sels d'aryle diazonium représentent de très beaux exemples de catalyse redox à l'or dans des conditions oxydantes[11] et photoredox,[12] respectivement.

1. Optimisations des conditions de réactions catalytiques

Après avoir démontré que l'addition oxydante était compatible avec la présence d'alcène ou de groupement OH ou NHTs, la faisabilité de la réaction catalytique a été démontré utilisant 10 mol% du complexes d'or(I) (P,N), 1,1 équivalent de $AgSbF_6$ et 1 équivalent de base K_3PO_4. Dans le dichlorométhane, le produit d'oxy-arylation a été obtenu avec un rendement de 82 % après 4 heures à température ambiante (Tableau 1, entrée 1). A ce stade, quelques expériences de contrôle ont été mises en place : 1) la réaction sans complexe d'or n'a donné aucun produit (Tableau 1, entrée 2) confirmant le rôle de l'or comme catalyseur, 2) la réaction avec seulement 10 mol% d'$AgSbF_6$ (Tableau 1, entrée 3) n'a fourni aucun composé d'oxy-arylation montrant la nécessité de plus d'un équivalent d'abstracteur d'halogène. Sur la base de ce résultat prometteur, les paramètres de réaction (solvant, additif, abstracteur d'halogène, ratio des substrats, quantité de base) ont été modifiés (Tableau 1, Schéma 2). Finalement, les conditions optimisées suivantes ont été déterminées : K_3PO_4 (1 eq.), DCM, 25°C, $AgSbF_6$ (1.1 eq.), 1:1 iodobenzene/4-penten-1-ol.
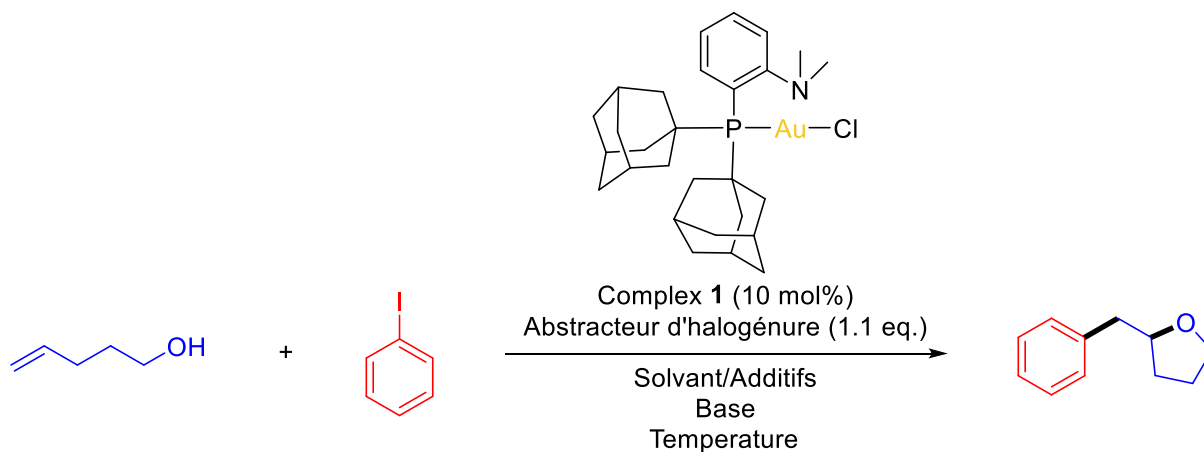

Schéma 2 : Optimisation des conditions de réaction catalytique (solvant, quantité de base, abstracteur d'halogéne, température, ratio des substrats).

Entrée	Solvant	Iodobenzene:4-penten-1-ol	Sel d'argent	Rendement[a]
1	DCM	1:1	$AgSbF_6$	82%
2[b]	DCM	1:1	$AgSbF_6$	0%
3[c]	DCM	1:1	$AgSbF_6$	0%
4	DCE	1:1	$AgSbF_6$	80%
5[d]	DCB	1:1	$AgSbF_6$	63%
6	DCM/MeOH (50:1)	1:1	$AgSbF_6$	15%
7	DCM/CHCl$_3$ (50:1)	1:1	$AgSbF_6$	40%
8	DCM/DMF (50:1)	1:1	$AgSbF_6$	0%
9	DCM/DMSO (50:1)	1:1	$AgSbF_6$	0%
10[e]	DCM	1:1	$AgSbF_6$	54%
11	DCM	1:5	$AgSbF_6$	31%
12	DCM	5:1	$AgSbF_6$	77%
13	DCM	1:1	AgOTf	11%
14	DCM	1:1	$AgNTf_2$	32%

*Tableau 1 : Optimisation des conditions de réaction catalytique (solvant, quantité de base, abstracteur d'halogène, température, ratio des substrats) [a]Rendement GC-MS après 4 h de réaction avec 10 mol% de complexe **1**, 1.1 eq d'abastracteur d'halogène et une concentration de 0.1 M en substrat limitant, utilisant le n-dodecane comme standard interne. [b]Sans complexe d'or. [c]10 mol% de $AgSbF_6$. [d]Réaction réalisé à 50°C, rendement GC-MS après 2h [e]2 eq. de K_3PO_4.*
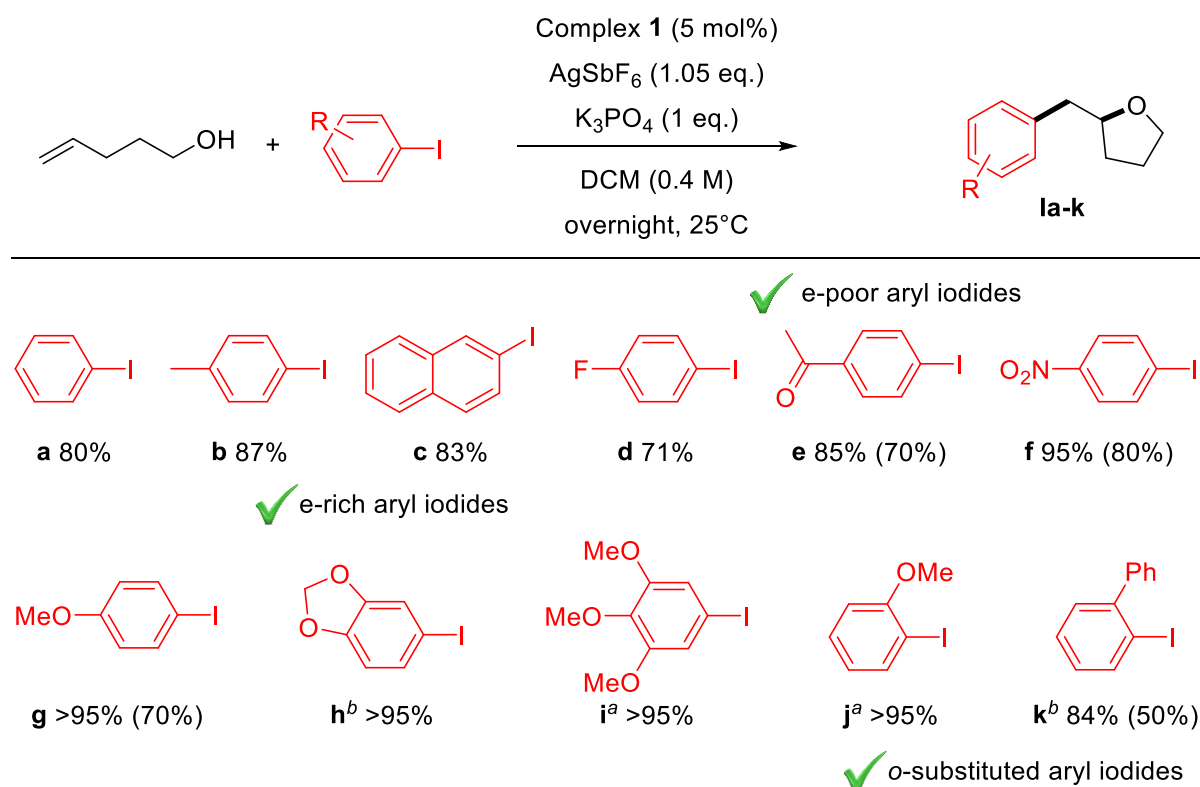
Ensuite, la charge catalytique a été réduite à 5 mol% de complexe **1** (1,05 d'$AgSbF_6$) entraînant une diminution du rendement de 82 % à 57 %. En augmentant la concentration à 0.4 M (au lieu de 0.1 M), un rendement de 80% est obtenu.

2. Portée de la réaction

Tout d'abord, la compatibilité des iodures d'aryle a été évaluée (Schéma 3). L'oxy-arylation du 4-penten-1-ol fonctionne bien avec divers iodobenzènes (avec un rendement moyen de 90 % sur 10 substrats) ainsi que le 2-iodonaphtalène (rendement 83 %). Elle tolère les groupes électro-attracteurs (*p*-COCH$_3$, *p*-NO$_2$) ainsi que les *ortho*-substituants (*o*-OCH$_3$, *o*-Ph). La réaction fonctionne en fait mieux avec des substrats riches en électrons, comme illustré par la préparation à haut rendement (> 95 %) des produits tétrahydrofuranes **Ig-j**.

Ensuite, les alcénols ont été explorée (Schéma 4). L'oxy-arylation tolère des substitutions aryle et alkyle sur toutes les positions du squelette entre les groupes alcène et alcool (produit **IIa-f**). Des tétrahydrofuranes fusionnés avec des cycles cyclohexane et benzénique (produits **IIg,h**) peuvent également être obtenus efficacement. Pour les substrats tri-substitués, une bonne diastéréosélectivité a été observée (jusqu'à 6,1:1 pour le tétrahydrofurane 2,3-disubstitué **IIc**). La double oxy-arylation de substrats tétrafonctionnels est également possible, donnant un accès direct aux produits spirocycliques tels que **IIi**. Les alcénols gem-disubstitués sont des substrats appropriés, permettant la formation de centres quaternaires (produit **IIj**), bien qu'ils nécessitent un chauffage doux (35°C) et que le rendement associé soit plus faible. Dans tous les cas, la cyclisation est entièrement régiosélective et se déroule exclusivement

de façon 5-*exo*. Remarquablement, il est également possible d'allonger l'attache pour obtenir des cycles > à 5 membres plus difficiles à synthétiser. Les cyclisations se déroulent à 35°C avec le 5-hexen-1-ol ainsi que le 6-heptene-1-ol pour donner les produits correspondants de pyrane et d'oxépane **IIk,l** et **IIm**, respectivement, avec des rendements élevés. Les alcénols internes sont également des substrats appropriés, comme l'atteste l'oxy-arylation des 4-hexen-1-ols. Les deux isomères *E* et *Z* réagissent et, dans chaque cas, un seul produit résultant de l'addition trans (**IIn** et **IIo**, respectivement) est obtenu. Le plus notable est le changement complet de régiosélectivité entre les deux isomères. Le substrat *Z* le plus réactif subit la cyclisation 5-*exo* «normale», tandis que le substrat *E* réagit *via* un processus 6-*endo* pour donner un cycle pyrane (les structures ont été attribuées sans équivoque sur la base des expériences de RMN ^{1}H-^{13}C HSQC/HMBC et de la comparaison avec composés apparentés connus). Le comportement du complexe d'or (P,N) contraste fortement avec celui observé par Glorius et *al.*, combinant or et catalyse photoredox : la cyclisation 5-*exo* s'est produite quelle que soit la stéréochimie de l'alcénol interne utilisé comme substrat.[12]

Schéma 3 : Réaction d'oxy-arylation des alcènes catalysée à l'or, compatibilité des iodures d'aryle. Rendements déterminés par RMN ^{1}H utilisant le dibenzyl ether comme standard interne (rendement isolé) ^{a}35°C. ^{b}35°C, 10 mol% Au.

Complex **1** (5 mol%)

AgSbF$_6$ (1.05 eq.)

K$_3$PO$_4$ (1 eq.)

DCM (0.4 M)

overnight, 25°C

X = O or NTs

IIa-o
IIIa-d

IIa X = O, R = Me 80% (77%)
IIb X = O, R = Ph 87% (80%)
IIIa[b] X = NTs, R = H 89%
IIIb[b] X = NTs, R = Me 80% (64%)

IIc X = O 79% (78%)
dr 6.1:1
IIIc[b] X = NTs 74% (58%)
dr 10.1:1

IId 85%
dr 1.2:1

IIe X = O 83% (81%)
dr 1.5:1
IIId[b] X = NTs 83% (61%)
dr 1:1

IIf[a] 70%

IIh 95%

IIg 95%
dr 1.7:1

IIi[b] 86% (42%)

IIj[a] 50%

IIk[a] R = H >95% (66%)
III[a] R = Me >95% (84%)

IIm[b] 83% (50%)

IIn[b] 57%, dr > 20:1
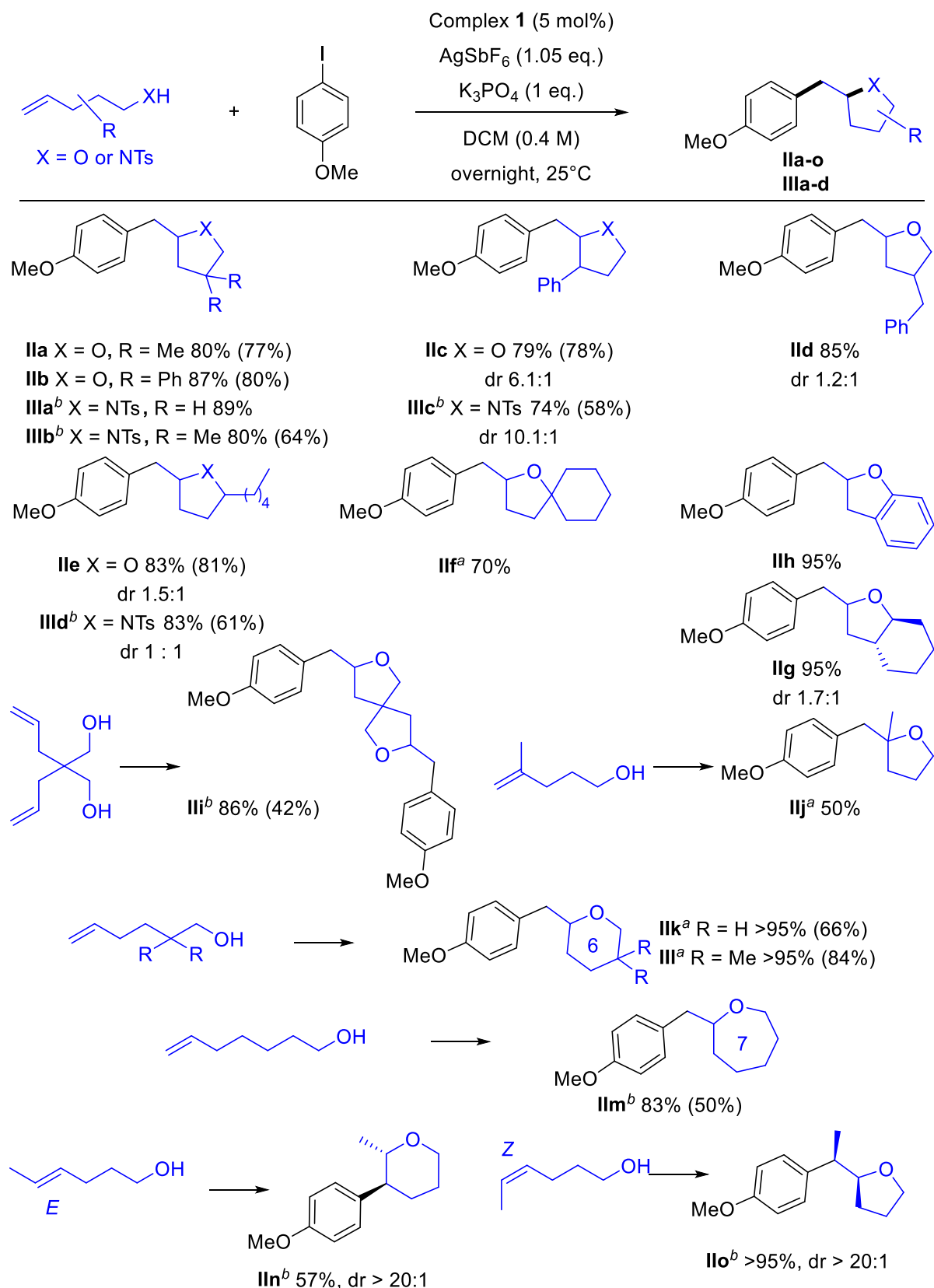
IIo[b] >95%, dr > 20:1

Schéma 4 : Réaction d'oxy-/amino-arylation des alcènes catalysée à l'or, portée des hydroxo ou amino alcènes. Rendements déterminés par RMN ^{1}H utilisant le dibenzyl ether comme standard interne (rendement isolé) ^{a}35°C. ^{b}35°C, 10 mol% Au.

La séquence d'addition oxydante/activation π se déroule également bien pour les réactions d'amino-arylation augmentant la charge catalytique à 10 mol% et élevant légèrement la température à 35°C (Schéma 4). Les alcènes comportant une *N*-tosyl amine sont facilement convertis en pyrrolidines arylées correspondantes **IIIa-d** : les substituants sont tolérés sur toutes les positions du squelette.

3. Etude mécanistique

Basé sur des analyses RMN ^{31}P *in situ* et sur des études de marquage au deutérium, le mécanisme suivant a été proposé (Schéma 5) : l'espèce active [(MeDalPhos)Au$^+$] est en équilibre avec le complexe π-alcène correspondant. Le cycle catalytique commence par l'addition oxydante de l'iodure d'aryle à l'or, puis la coordination η^2 de l'alcène à l'or(III) favorise la cyclisation par addition nucléophile de l'alcool ou de l'amine. Enfin, l'élimination réductrice à l'or induit le couplage C_{sp}^2-C_{sp}^3 et régénérere l'espèce active [(MeDalPhos)Au$^+$].

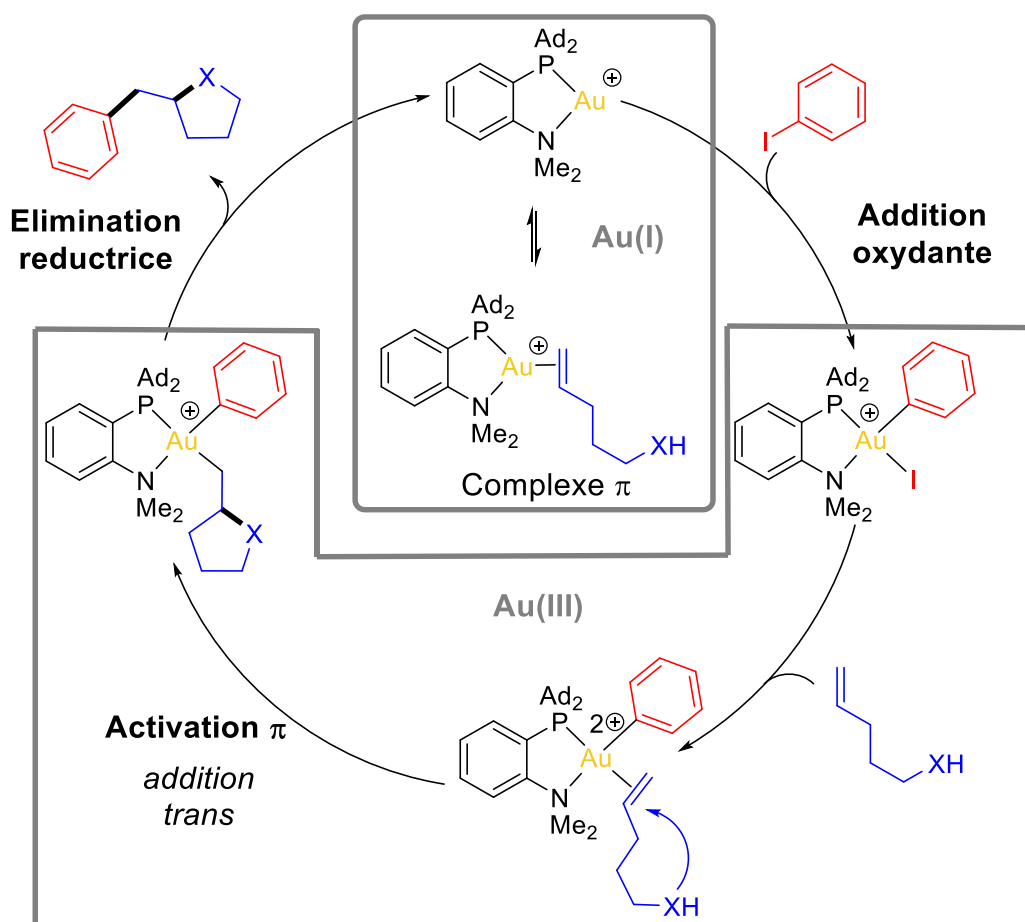*Schéma 5 : Cycle catalytique proposé pour les réactions d'oxy-/amino-arylation des alcènes avec le complexe (MeDalPhos)AuCl.*

Ce mécanisme est supporté par une étude DFT (Figure 1) effectuée sur le système réel cationique $(P,N)Au^{2+}$-Ph au niveau de théorie SMD(DCM)B3PW91-D3(BJ)/SDD+f(Au), 6-31+G** (autres atomes)//B3PW91/ SDD+f(Au), 6-31G** (autres atomes).
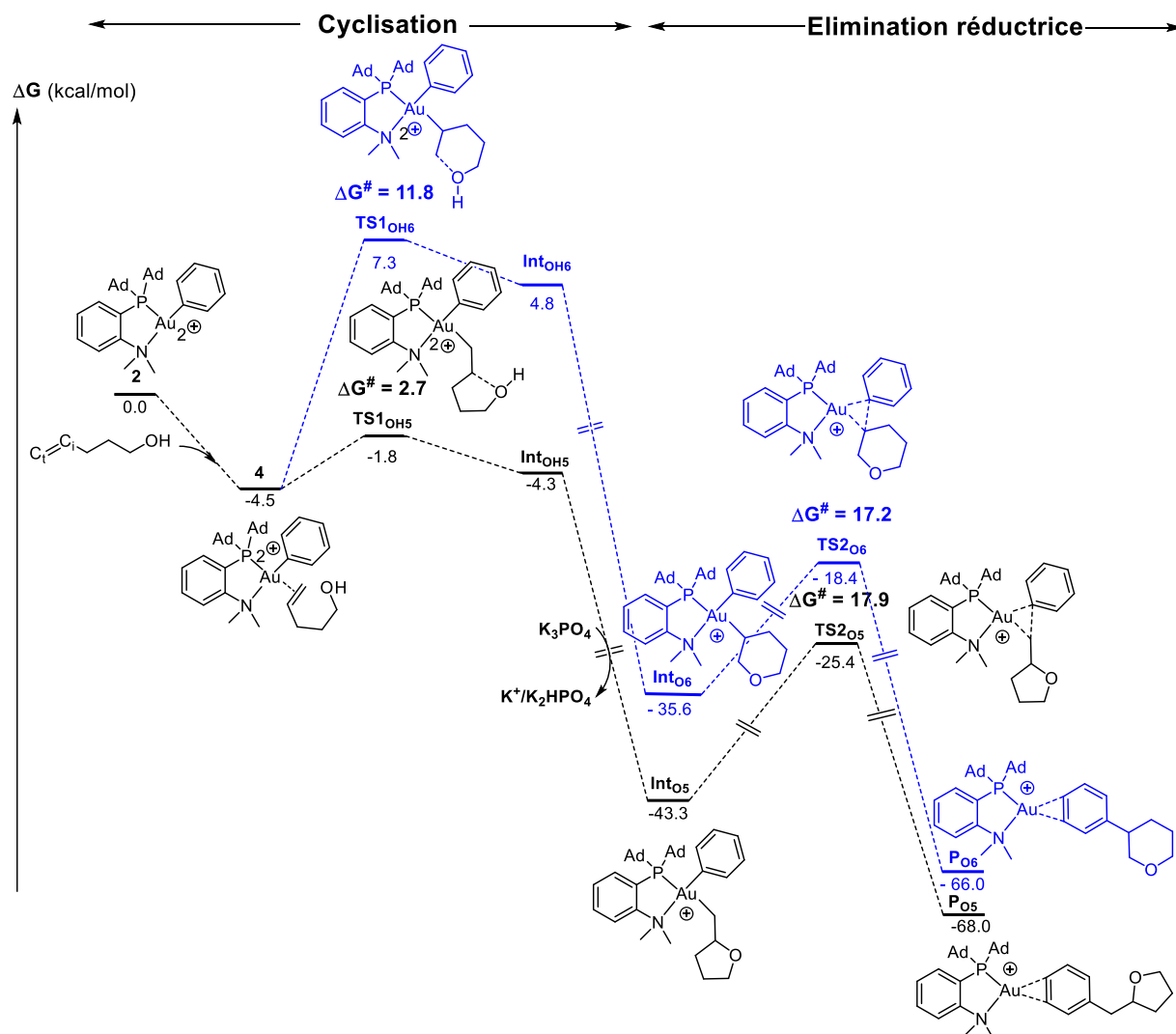
Figure 1 : Profil d'énergie (ΔG en kcal/mol) pour la réaction d'oxy-arylation impliquant le complexe $(P,N)Au^{2+}$-Ph et le 4-penten-1-ol calculé au niveau de théorie SMD(DCM)-B3PW91-D3(BJ)/SDD+f(Au), 6-31+G**(autres atomes)//B3PW91/SDD+f(Au), 6-31G** (autres atomes) et en présence de K_3PO_4. Formation du produit de 5-exo (noir) et 6-endo (bleu). Les molécules de K_3PO_4, K_2HPO_4 et K^+ sont incluses pour assurer la balance énergétique sur toutes les étapes de la réaction.

Un profil similaire a été calculé pour l'alcène interne *Z* justifiant la formation unique du produit de 5-*exo* cyclisation. Pour l'alcène *E*, l'état de transition pour la cyclisation 6-*endo* est inférieur en énergie à celui pour la cyclisation 5-*exo* rationalisant la formation unique du produit 6-*endo*.

III. Liaisons hydrogènes à l'or

Les liaisons hydrogènes impliquant des métaux de transition comme accepteurs de protons ont attiré une attention considérable au cours des trois dernières décennies. Outre leur intérêt fondamental en termes de liaison chimique, elles sont également pertinentes pour plusieurs transformations organométalliques (comme la formation d'hydrures métalliques par protonation). Contrairement aux autres métaux de transition,[13] il n'y a jusqu'à présent aucune preuve univoque de liaison hydrogène à l'or. Un certain nombre de contacts proches Au⋯H ont été reportés pour des structures cristallines des aurides, des complexes d'or(I) ou d'or(III), mais aucune preuve spectroscopique d'interactions attractives Au⋯H en solution n'a été reportée.[14] Cependant, des études théoriques sur des composés modèles suggèrent que la liaison hydrogène à l'or est en effet possible pour des aurides[15,16] ou pour des complexes d'or(I).[17]

1. Synthèse et caractérisation du complexe cationique d'or MeDalPhos

Sur la base des développements récents de la chimie de l'or, nous avons pensé que les ligands (P,N) tels que les *ortho*-amino phénylphosphines (DalPhos) peuvent être de bons candidats et donner accès à des complexes présentant des liaisons hydrogènes. En raison de son caractère basique, le centre azoté donne l'opportunité de former un ammonium avec une liaison protonique N-H à proximité à l'or(I). Comme indiqué ici, cette stratégie s'est avérée fructueuse et nous a permis de former et d'authentifier un complexe d'or(I) présentant une liaison hydrogène.

L'ajout de 1 équivalent d'acide trifluorométhane sulfonique (HOTf) au complexe d'or MeDalPhos **1** conduit immédiatement à un nouveau complexe **3** (Schéma 6) d'après la spectroscopie RMN $^{31}P\{^{1}H\}$. La RMN ^{1}H indique sans ambiguïté la protonation de l'atome d'azote : un large signal N-H apparaît à δ 10,9 ppm tandis que le signal $N(CH_3)_2$ est décalé vers le champ bas d'environ 1 ppm et résonne comme un doublet avec une constante de couplage $^{3}J_{HH}$ de 5,0 Hz. Des cristaux de **3** ont été analysés par diffraction des rayons X (Schéma 6). La liaison N-H pointe vers Au et le squelette N-H⋯Au est presque linéaire (165(2)°). La distance Au⋯H (2,24 (3) Å) est bien comprise dans la somme des rayons de van der Waals (2,86)[18] et se situe dans la limite basse de celles précédemment rapportées.[14] La RMN multinucléaire confirme la connectivité générale et selon les expériences 2D ^{1}H-^{1}H NOESY, le complexe **3** adopte en solution la même conformation qu'à l'état solide. Le déplacement chimique RMN ^{1}H très élevé du proton NH est typique de la liaison H.[13] La spectroscopie infrarouge est un outil analytique utile pour sonder les interactions de liaison hydrogène. Aucune bande caractéristique n'a été détectée pour la vibration N-H de **3**.

Considérant qu'elle peut être masquée par celles des C-H, le complexe **3-D** marqué au deutérium a été préparé en utilisant DOTf. Une bande N-D est apparue à 2124 cm^{-1} sur le spectre IR, correspondant à un étirement N-H à environ 3000 cm^{-1}. C'est 500 cm^{-1} de moins que les nombres d'onde typiques des oscillateurs N-H (ammonium) libres. Cette différence confirme la présence de liaisons Au···H-N en solution et fournit une preuve spectroscopique directe d'une telle liaison H.

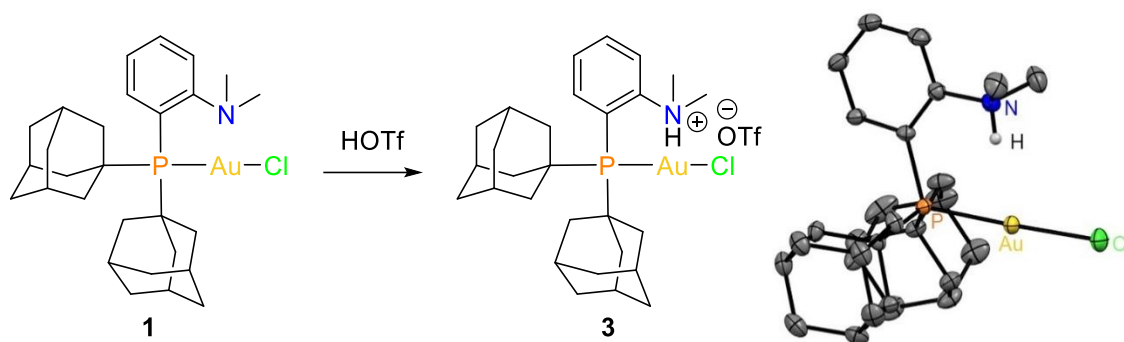*Schéma 6 : Synthèse et structure Rayon X du complexe d'or(I) (P,NH⁺) dérivé du MeDalPhos. Longueur (Å) et angle (°) de liaisons sélectionnés : P-Au 2.270(1), Au-Cl 2.283(1), Au···H 2.24(3), PAuCl 176.98(2), NHAu 165(2).*

2. Etude computationnelle du complexe cationique d'or avec ligand (P,N)

Une étude théorique complète a été réalisée pour analyser la liaison dans le complexe d'or **3**. L'objectif principal de ces calculs de chimie quantique était d'établir sans ambiguïté la présence d'une interaction N-H···Au attractive et d'en préciser la nature.

Les calculs ont été effectués sur le cation nu puisque la structure rayons X a montré que le complexe **3** adopte une structure de paires d'ions. Plusieurs *minima* **3a-c** ont été localisés sur la surface d'énergie potentielle (PES) (Tableau 2 & Figure 2).
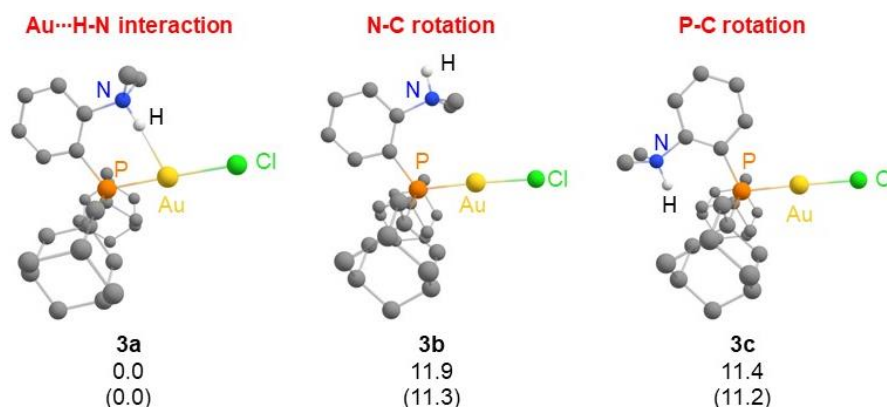

*Figure 2 : Minima d'énergie localisés sur la surface d'énergie potentielle du complexe **3**, sans contre-ion OTf. Energies relatives en kcal/mol (ΔG et ΔE entre parenthèse).*

	3a	3b	3c
P-Au	2.303	2.304	2.305
Au-Cl	2.338	2.344	2.339
N-H	1.046	1.024	1.025
Au···H	2.134	/	/
PAuCl	178.5	176.5	178.1
NHAu	174.2	/	/
υ_{NH} (cm^{-1})	3032.3	3457.3	3445.9
υ_{ND} (cm^{-1})	2089.4	2544.5	2489.2
δ ^{1}H NMR (NH, ppm)	11.94	5.64	6.31
Analyses NBO			
ΔE(2) (kcal/mol)	12.8	/	/
NLMO	95.9% Au	97.7% Au	97.6% Au
d_{Au}	0.7% N		
	2.5% H		
WBI (Au···H)	0.12	/	/
WBI (N-H)	0.61	0.73	0.71
Charges NPA			
q_{NR2H}	0.605	0.656	0.675
q_{PAuCl}	0.765	0.713	0.651

*Tableau 2 : Paramètres géométriques clés (distances en Å, angles en °), données spectroscopiques (IR et RMN) et analyses NBO pour les 3 conformères **3a-c**. Energie stabilisante ΔE(2) et pourcentage des principaux atomes intervenant dans la NLMO de l'intéraction donneur-accepteur $d_{Au} \rightarrow \sigma^*_{NH}$. Indices de Wiberg (WBI) entre Au et H, N et H. Charges NPA des fragments NMe$_2$H et PAuCl (q_X).*

La structure de l'état fondamental **3a** est similaire à celle observée par diffraction des rayons X, la liaison N-H pointant vers Au. Deux autres *minima* **3b** et **3c** correspondent à des conformères associés à des rotations autour des liaisons C_{Ph}-N et C_{Ph}-P. Pour **3a**, l'atome H lié à N entre dans la sphère de coordination de l'or (Au···H = 2.134 Å) avec un arrangement quasi-linéaire N-H···Au (174,2°), conforme à celui attendu pour les liaisons hydrogènes. La comparaison des données métriques montre que la liaison N-H est sensiblement allongée lors de l'interaction avec l'or (1,046 pour **3a** *vs* 1,024-1,025 pour **3b-c**). Les conformères **3b** et **3c** sont 11 à 12 kcal/mol plus élevés en énergie que **3a**, suggérant une certaine stabilisation de **3a** grâce à l'interaction N-H···Au.

Les déplacements chimiques RMN ^{1}H et les fréquences d'étirement IR calculés pour les trois conformères d'or(I) **3a-c** (Tableau 2) sont en accord avec les observations expérimentales et confirment la présence d'une interaction de type liaison hydrogène N-H···Au dans **3a**. Les étirements NH calculés pour **3b** et **3c** sont très similaires, tandis que celui de **3a** est décalé vers le rouge d' environ 500 cm^{-1}, indiquant un affaiblissement substantiel de la liaison N-H lors de l'interaction avec l'or.[17] Pour être complet, l'étirement N-D pour le **3a-D** marqué au deutérium a également été calculé (2089 cm^{-1}). La valeur obtenue correspond assez bien à celle déterminée expérimentalement (2124 cm^{-1}).

La nature de la liaison dans **3a** a ensuite été analysée à l'aide de différentes méthodes. L'analyse NBO (Tableau 2) confirme l'affaiblissement de la liaison N-H lors de l'interaction avec l'or. L'indice de liaison de Wiberg (WBI) de la liaison N-H diminue de 0,71-0,73 en **3b,c** à 0,61 en **3a**, tandis que le WBI pour l'interaction Au⋯H en **3a** est petit mais non négligeable (0,124). Les charges calculées par analyse de la population naturelle (NPA) montrent un certain transfert de charge du fragment métallique vers le fragment ammonium : la charge du fragment PAuCl passe de 0,65-0,71 en **3b,c** à 0,76 en **3a**, tandis que la charge pour le fragment NMe_2H passe de 0,66-0,68 en **3b,c** à 0,61 en **3a**. Ce transfert de charge est également apparent à partir des cartes de potentiel électrostatique (Figure 3, gauche). La fraction ammonium est située dans une zone positive (bleue) dans les deux cas, mais lorsqu'elle est liée à l'or, sa charge est réduite et la surface est plus claire.

Outre cette composante électrostatique, l'analyse NBO a révélé une certaine contribution orbitale à l'interaction N-H⋯Au. Une faible interaction donneur-accepteur (énergie de délocalisation $\Delta E(2)$ = 12,8 kcal/mol) entre une orbitale d_{Au} occupée et l'orbitale σ^*_{NH} a été trouvée par la théorie des perturbations de second ordre (Figure 3, à droite). Cette image est cohérente avec une interaction 3c-4e, telle que déduite pour les complexes à liaison H et par opposition à l'interaction 3c-2e impliquée dans les complexes agostiques.[19]
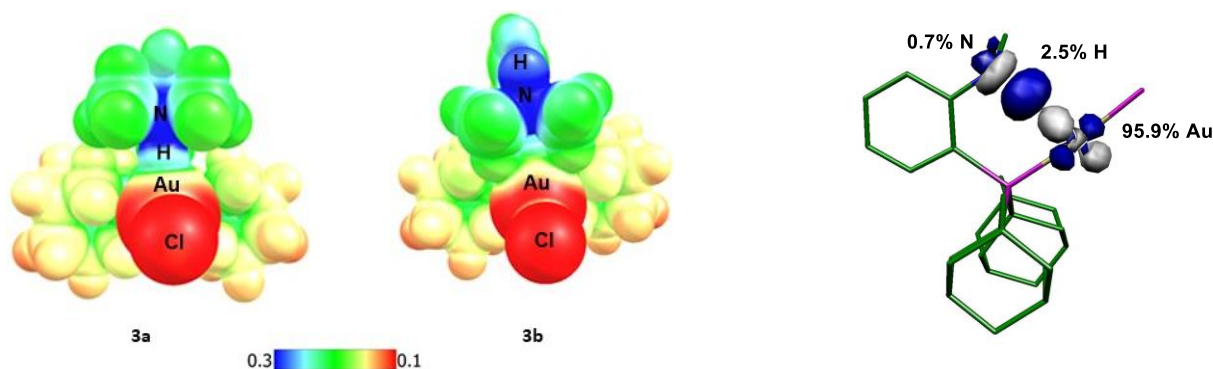

*Figure 3 : Gauche : Cartes de potentiel électrostatique pour **3a** et **3b** tracée sur la gamme 0,1 (rouge) jusqu'à 0,3 (bleu). Les isosurfaces sont dessinés à 0,002 e.au⁻³. Droite : Superposition des obitales NBO donneur et accepteur (seuil = 0,08) impliquées dans l'intéraction N-H⋯Au. Participation de chaque atome en pourcentage dans la NLMO associées.*

Une analyse AIM a ensuite été réalisée. La densité électronique au BCP de la liaison N-H est plus faible pour **3a** que pour les deux conformères **3b,c** (ρ = 0,319 vs 0,343 e.bohr^{-3}), cohérent avec l'affaiblissement de liaison déterminé par IR et NBO. De plus, la structure de l'état fondamental montre un BCP entre les atomes Au et H avec ρ_{AuH} = 0,039 e.bohr^{-3} et $\nabla^2\rho_{AuH}$ = 0,068 e.bohr^{-5} (Figure 4). La valeur ρ_{AuH} se situe dans la limite supérieure de la plage définie pour les interactions de type liaison hydrogène.[20]
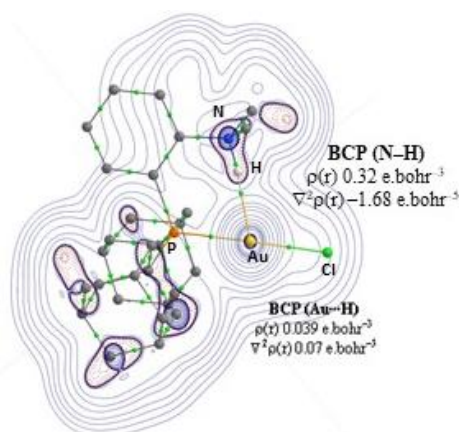

*Figure 4 : Tracé du contour de la distribution Laplacienne $\nabla^2\rho(r_c)$ pour **3a** avec les chemins et les points critiques de liaisons (sphères vertes). Les atomes d'hydrogènes sont omis pour plus de claret, sauf celui de l'atome d'azote.*

Grâce au ligand MeDalPhos, le complexe **3** présentant un contact proche entre le centre or(I) et l'ammonium NH$^+$ a été préparé. L'interaction N-H···Au vérifie toutes les caractéristiques d'une interaction de type liaison hydrogène. De plus, une analyse computationnelle détaillée fournit des preuves convaincantes de la présence d'une liaisons hydrogène N-H···Au dans **3**. Les méthodes de calcul et les résultats obtenus se complètent et sont tous cohérents avec une interaction attractive 3c-4e.

IV. Isolation d'espèces réactives de complexes carbéniques α-CF₃ d'or

La présence d'atomes de fluor dans les composés organiques a des effets sur leurs propriétés physiques, chimiques et biologiques (électroniques, lipophiles, stériques, conformationnelles…).[21] Il existe donc un intérêt considérable pour le développement de méthodes efficaces pour l'introduction sélective de groupes fluorés dans des composés organiques. Dans ce contexte, le groupe trifluorométhyle occupe une place de choix. Il est présent dans une large gamme de molécules biologiquement actives.

Grâce à la forte nature électroattractive du groupement CF₃ (constante de Hammett σ_p = 0,54), les diazoalcanes trifluorométhylés sont relativement stables et représentent des synthons très intéressant pour introduire des motifs CF₃ dans des molécules. Lors de la libération de N₂, ils peuvent former des carbènes métalliques avec une variété de métaux de transition, donnant lieu à un large panel de réactions.

1. Synthèse et caractérisation de carbènes α-CF₃ d'or

Le carborane diphosphine ligand (DPCb) a permis la stabilisation et la caractérisation du carbène α-oxo d'or,[22] c'est pourquoi ce ligand a été utilisé pour la synthèse, l'isolement et la caractérisation du carbène α-CF₃ d'or. Un équivalent de diazométhane biphénylé trifluorométhylé a été ajouté à -80°C au complexe pseudo-cationique tricoordinné (P,P)AuNTf₂ **17** dans du dichlorométhane (Schéma 7). De petites bulles de diazote sont immédiatement apparues et la solution est devenue bleu foncé. Après un traitement rapide à -40°C, l'espèce formée a été caractérisée par spectroscopie. Le signal RMN ³¹P{¹H} apparaît à un déplacement chimique très similaire de celui du précurseur d'or (δ 137,8 et 138,2 ppm, respectivement), mais sous la forme d'un quartet au lieu d'un singulet. La multiplicité du quartet résulte du couplage PF, comme établi sans ambiguïté par la présence d'un signal triplet dans le spectre RMN ¹⁹F avec un couplage similaire (22,2 Hz). Ces motifs suggèrent la formation du complexe souhaité (P,P)Au=C(CF₃)(biphényl)⁺ **18-Ph**, ce qui a été définitivement confirmé par la spectroscopie RMN ¹³C. Le spectre découplé ¹⁹F montre un signal diagnostic à δ 269,8 ppm. En accord avec la couleur bleue, une forte absorption est trouvée à 619 nm en spectroscopie UV-Vis. Le carbène **18-Ph** s'est avéré modérément stable à température ambiante, une décomposition d'environ 30 % étant observée après 24 heures dans le DCM. Le substituant *para* au niveau du cycle phényle a ensuite été remplacé par OMe et CF₃ afin d'évaluer l'impact des groupes électro-donneurs/attracteurs. Dans les deux cas, les complexes carbéniques correspondants **18-OMe** et **18-CF₃** se sont formés (Schéma 7), et des données RMN cohérentes avec celles du **18-Ph** ont été obtenues. Certaines caractéristiques méritent

d'être commentées : i) le signal diagnostic RMN ^{13}C se déplace très peu (de δ 269,8 à 265,8 ppm), ii) les constantes de couplage $^{3}J_{PC}$ et $^{4}J_{PF}$ diminuent dans la série *p*-CF$_3$ > *p*-Ph > *p*-OMe (de 109,0 à 79,5 Hz pour le $^{3}J_{PC}$, et de 32,1 à 14,0 Hz pour le $^{4}J_{PF}$), le carbène devient moins déficient en électrons et l'ordre de liaison Au=C diminue, iii) le carbène **18-CF₃** affiche un couplage $^{8}J_{PF}$ longue portée de 10,8 Hz. Il est également intéressant de noter que si le complexe carbène **18-OMe** survit quelques heures à température ambiante, comme le **18-Ph**, le **18-CF₃** est beaucoup moins stable. Toutes les tentatives de traitement à température ambiante ou à basse température ont entraîné une dégradation complète. Il a ainsi été caractérisé *in situ* à basse température.
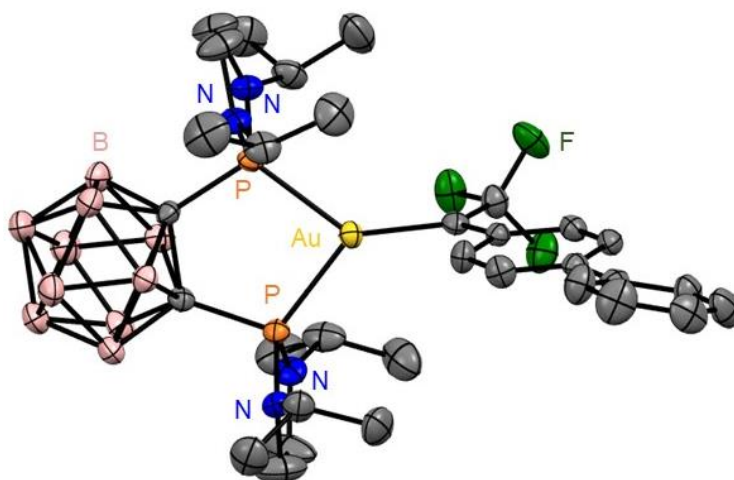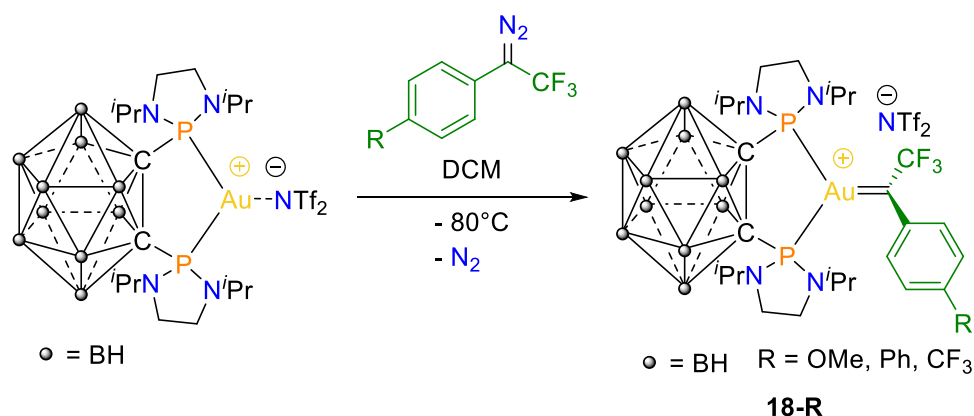

*Schéma 7 : Synthèse des carbènes d'or trifluorométhylés d'or **18-R** par décomposition de diazo. Rayon X du complexe d'or carbéniques **18-Ph**. Longueur (Å) et angle (°) de liaisons sélectionnés : Au-C$_{carb}$ 1.971(2), Au-P1 2.347(1), Au-P2 2.348(1), C$_{carb}$-C$_{Ar}$ 1.444(6), C$_{carb}$-CF$_3$ 1.500(6), P1AuP2 90.59(4), P1AuC$_{carb}$ 135.7(1), P2AuC$_{Carb}$ 133.7(1).*

Des efforts ont ensuite été portés sur l'obtention de données cristallographiques afin d'en savoir plus sur la structure du carbène obtenu. Des cristaux exploitable pour l'analyse DRX ont été obtenus par diffusion lente de pentane sur une solution de dichlorométhane de **18-Ph** à 4°C (Schéma 7). Le complexe de carbène adopte une structure de paires d'ions. Le ligand DPCb chélate symétriquement l'or avec des longueurs de liaison Au-P de 2,347(1)/2,348(1) Å et un angle de morsure PAuP de 90,59(4)°. Le centre carbénique est dans un environnement

parfaitement plan (comme le montre la somme des angles de liaison de 360,0°) et il est orienté perpendiculairement au plan de coordination PAuP (les plans moyens autour de Au et C_{carb} font un angle de 89,76°). Cette orientation minimise les répulsions stériques entre les substituants carbène et phosphore, elle maximise également la rétro-donation de d(Au) à $2p^{\pi}(C_{carb})$. La longueur de liaison Au=C (1,971(2) Å) se situe dans la fourchette inférieure de celles rapportées pour les complexes or(I) carbène. Le centre carbènique est également stabilisé par la donation du substituant biphényle, comme indiqué par leur arrangement coplanaire (le plan moyen du cycle phényle lié à C_{carb} est tourné de seulement 2,5° par rapport au plan de coordination carbène) et par la longueur relativement courte de la liaisons C_{carb}-C_{ipso} (1.444(6) Å).

2. Analyse de structure et de liaison

Pour mieux comprendre la nature de la liaison et le mode de stabilisation des carbènes α-CF_3 d'or(I), des calculs DFT ont été effectués. La géométrie optimisée pour **18-Ph** est similaire à celle déterminée par cristallographie. Les carbènes **18-OMe** et **18-CF₃** ont également été calculés, montrant des structures analogues à celles de **18-Ph**. Les petites variations trouvées dans les longueurs de liaison Au=C/C_{carb}-C_{ipso} et dans les indices de liaison de Wiberg associés (WBI) sont cohérent avec le biais électronique induit par le substituant *para,* c'est-à-dire une plus forte donation de l'aryle vers C_{carb} et une plus faible rétrodonation de Au vers C_{carb} du **18-CF₃** au **18-Ph** et au **18-OMe** (Tableau 3). La liaison Au=C a ensuite été évaluée en détail par des analyses NBO et CDA (Tableau 3). Le transfert de charge (CT) de C_{carb} vers Au est légèrement négatif pour les trois carbènes, un peu plus pour le carbène privé d'électrons **18-CF₃** (-0,25 e⁻) que pour le **18-OMe** enrichi en électrons (-0,10 e⁻). Des valeurs CT proches de zéro suggèrent, dans l'ensemble, que la donation de C_{carb} vers Au et la rétrodonation de Au vers C_{carb} se compensent à peu près l'une l'autre. Le ratio donation/rétrodonation (d/b), tel qu'estimé par le CDA, se situe entre 1,8 et 2,2 (légèrement inférieur pour le carbène **18-CF₃** privé d'électrons, légèrement supérieur pour le carbène **18-OMe** enrichi en électrons), indiquant que le donation C_{carb} vers Au prévaut, mais que la rétrodonation Au vers C_{carb} est importante.

L'inspection des orbitales moléculaires fournit des informations supplémentaires. La HOMO est centrée sur l'or et est associée à une orbitale d en combinaison liante avec l'orbitale $2p^{\pi}(C_{carb})$. Réciproquement, la LUMO est centrée sur le centre carbènique et correspond à l'orbitale vacante $2p^{\pi}(C_{carb})$ en combinaison antiliante avec l'orbitale d(Au) (Figure 5, haut). La rétro-donation Au vers C_{carb} et la donation aryle vers C_{carb} sont également décrites par les contributions de $2p^{\pi}(C_{carb})$ dans les NLMO d(Au) et aryle (Figure 5, en bas). Les deux

interactions stabilisent le carbène en remplissant partiellement son orbitale vacante. La force des deux interactions évolue légèrement dans la série **18-CF₃**, **18-Ph**, **18-OMe**. Comme prévu par l'effet électronique attracteur/donneur du substituant *para*, la contribution de C$_{carb}$ est la plus importante dans le NLMO d(Au) pour le **18-CF₃**, tandis que pour le **18-OMe**, elle est dans le NLMO (arène) (Tableau 3).

	18-OMe	18-Ph	18-CF₃
	Paramètres géométriques		
Au=C$_{carb}$ (Å)	1.987	1.982	1.971
C$_{carb}$-C$_{ipso}$ (Å)	1.423	1.429	1.442
PAuP (°)	89.81	89.88	89.79
	Analyses NBO		
WBI (Au=C)	0.677	0.687	0.710
WBI (C$_{carb}$-C$_{ipso}$)	1.312	1.289	1.234
CT (e)	-0.10	-0.14	-0.25
d$_{xz}$(Au)→C$_{carb}$ rétrodonation %C$_{carb}$ dans la NLMO d$_{xz}$(Au)	7.3 %	9.7 %	15.5 %
π$_{C=Caryl}$→C$_{carb}$ donation %C$_{carb}$ dans la NLMO π$_{C=Caryl}$	24.2 %	16.3 %	10.1 %
	Analyses CDA		
d/b ratio	2.16	2.09	1.86

*Tableau 3 : Données calculées pour les complexes carbéniques α-CF3 d'or(I) **18-Ph**, **18-OMe** et **18-CF₃** au niveau de théorie B3PW91/SDD+f(Au),6-31G**(other atoms) : longueur et angle de liaisons, indices de Wiberg (WBI) pour Au-C$_{carb}$ et C$_{carb}$-C$_{ipso}$, transfert de charge du carbene vers le fragment (P,P)Au⁺, NLMO associée à la donation aryl vers C$_{carb}$ et à la rétrodonation Au vers C$_{carb}$ (contribution du C$_{carb}$), rapport donation/rétrodonation (d/b) estimé par CDA.*

HOMO

LUMO

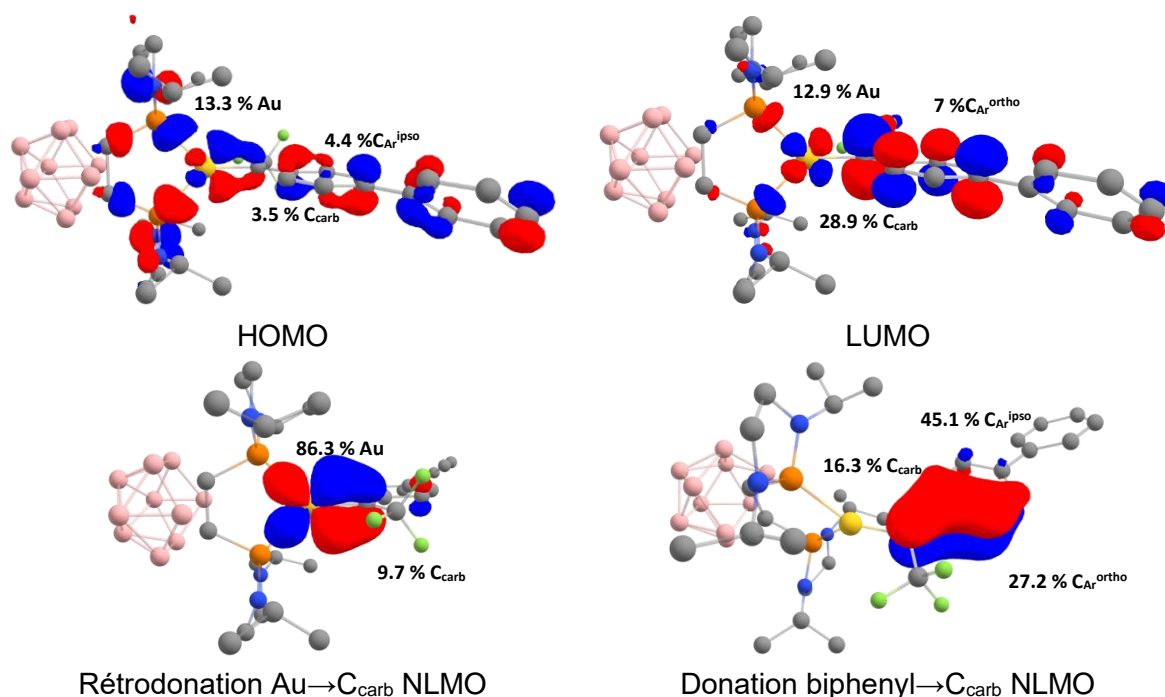Rétrodonation Au→C$_{carb}$ NLMO

Donation biphenyl→C$_{carb}$ NLMO

*Figure 5 : HOMO, LUMO et NLMO (seuil : 0,04) associées à la donation arene vers C$_{carb}$ et la rétrodonation Au vers C$_{carb}$ calculées pour le complexe carbènique α-CF3 d'or(I) **18-Ph** au niveau de théorie B3PW91/SDD+f(Au),6-31G**(other atoms). Contribution des atomes principaux (en %) dans les orbitales frontières et la NLMO.*

3. Réactivité catalytique des carbènes α-CF₃ d'or(I)

Le carbène α-CF₃ d'or(I) a été généré *in situ*, et sa capacité à effectuer des réactions catalytiques a été étudiée. Tout d'abord, la cyclopropanation a été testée. Lors du mélange du diazométhane biphénylé trifluorométhylé avec du styrène et une quantité catalytique de $(P,P)AuNTf_2$ (5 mol%), le produit cyclopropane a été obtenu avec un rendement RMN de 67 % (rendement isolé : 38%) et une diastéréosélectivité élevée. En effet, seul le produit présentant le groupement biphenyle en position *cis* du groupement phényle issu du styrène a été obtenu. Cette configuration a été déduite par analyse RMN {¹H, ¹⁹F} HOESY et confirmée par l'obtention de cristaux analysés en DRX (Schéma 8, top). Ensuite, l'indène, substrat pour lequel la compétition entre la cyclopropanation et l'insertion C-H est possible, a été envisagé. Les mêmes conditions que le styrène ont été utilisées, et après 24 heures, le produit cyclopropane a été obtenu avec un rendement RMN de 56 % (rendement isolé : 39 %) et 2 produits d'insertion CH ont été observés (rendement 13 %), mais non caractérisés (Schéma 8). La cyclopropanation est totalement diastéréosélective, seul le produit présentant le fragment indane et l'aryle du composé diazo en position *syn* est obtenu selon les RMN {¹H, ¹⁹F} HOESY. Ce complexe a aussi prouvé son efficacité pour les réactions d'insertion O-H (Schéma 8, bas).
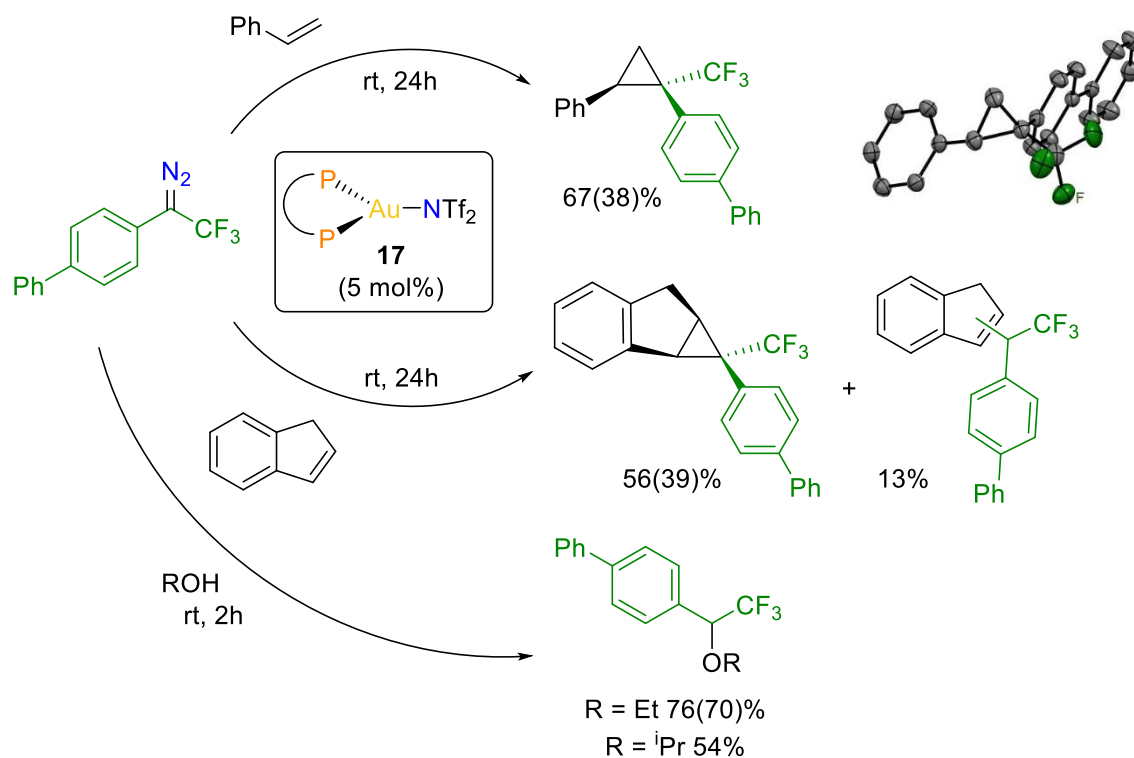

Schéma 8 : Réactions de cyclopropanation et d'insertion O-H catalysées à l'or à parti de dérivés diazo α-CF₃ (rendement RMN déterminés par RMN ¹⁹F{¹H} utilisant le standard interne 4,4'-difluorobiphenyle, rendements isolés entre parenthèses).

231

V. Conclusion

La chimie de l'or a été un sujet brûlant ces dernières années. La conception de nouveaux ligands, notamment bidentes, a permis la synthèse de composés d'or originaux, considérés jusqu'à présent comme inaccessibles, et le développement de nouvelles réactivités. Ce travail de thèse s'inscrit dans cette thématique. Notre objectif était d'élargir nos connaissances en chimie de l'or par une approche conjointe expérimentale/théorique.

Grâce à l'utilisation des ligands MeDalPhos (P, N) ou carborane diphosphine ligand (P,P) de nouvelles réactions catalytiques ont été développées et de nouvelles espèces originales comme les complexes présentant des liaisons hydrogènes à l'or ou les complexes carbéniques α-CF$_3$ ont été isolées.

Par la synthèse de nouveaux ligands « sur mesure », des champs d'applications encore inexplorés peuvent être envisagés, comme la synthèse et la caractérisation de complexes d'or carbyniques présentant une liaison triple Au≡C ou des complexes d'or à des degrés d'oxydation plus élevés (+V).

VI.   Références

[1] G. C. Bond, *Gold Bull.* **1972**, *5*, 11–13.

[2] H. Schmidbaur, *Naturwiss Rundsch* **1995**, *48*, 443–451.

[3] J. H. Teles, S. Brode, M. Chabanas, *Angew. Chem. Int. Ed.* **1998**, *37*, 1415–1418.

[4] N. D. Shapiro, F. D. Toste, *Synlett* **2010**, *2010*, 675–691.

[5] A. S. K. Hashmi, *Gold Bull.* **2004**, *37*, 51–65.

[6] A. S. K. Hashmi, L. Schwarz, J.-H. Choi, T. M. Frost, *Angew. Chem. Int. Ed.* **2000**, *39*, 2285–2288.

[7] M. Joost, A. Amgoune, D. Bourissou, *Angew. Chem. Int. Ed.* **2015**, *54*, 15022–15045.

[8] R. T. Mertens, S. G. Awuah, in *Catal. Met. Complexes Nanomater. Fundam. Appl.*, American Chemical Society, **2019**, pp. 19–55.

[9] A. Zeineddine, L. Estévez, S. Mallet-Ladeira, K. Miqueu, A. Amgoune, D. Bourissou, *Nat. Commun.* **2017**, *8*, 565.

[10] J. Rodriguez, A. Zeineddine, E. D. S. Carrizo, K. Miqueu, N. Saffon-Merceron, A. Amgoune, D. Bourissou, *Chem. Sci.* **2019**, *10*, 7183–7192.

[11] G. Zhang, L. Cui, Y. Wang, L. Zhang, *J. Am. Chem. Soc.* **2010**, *132*, 1474–1475.

[12] B. Sahoo, M. N. Hopkinson, F. Glorius, *J. Am. Chem. Soc.* **2013**, *135*, 5505–5508.

[13] A. Martín, *J. Chem. Educ.* **1999**, *76*, 578.

[14] H. Schmidbaur, H. G. Raubenheimer, L. Dobrzańska, *Chem. Soc. Rev.* **2013**, *43*, 345–380.

[15] F. Groenewald, J. Dillen, H. G. Raubenheimer, C. Esterhuysen, *Angew. Chem. Int. Ed.* **2016**, *55*, 1694–1698.

[16] F. Groenewald, H. G. Raubenheimer, J. Dillen, C. Esterhuysen, *Dalton Trans.* **2017**, *46*, 4960–4967.

[17] R. J. F. Berger, J. Schoiber, U. Monkowius, *Inorg. Chem.* **2017**, *56*, 956–961.

[18] S. S. Batsanov, *Inorg. Mater.* **2001**, *37*, 871–885.

[19] L. Brammer, *Dalton Trans.* **2003**, 3145–3157.

[20] W. Nakanishi, S. Hayashi, K. Narahara, *J. Phys. Chem. A* **2008**, *112*, 13593–13599.

[21] D. O'Hagan, D. B. Harper, *J. Fluor. Chem.* **1999**, *100*, 127–133.

[22] A. Zeineddine, F. Rekhroukh, E. D. Sosa Carrizo, S. Mallet-Ladeira, K. Miqueu, A. Amgoune, D. Bourissou, *Angew. Chem. Int. Ed.* **2018**, *57*, 1306–1310.

Résumé

Cette thèse porte sur l'étude de complexes définis d'or, de la stabilisation de composés originaux à leur utilisation pour de nouvelles transformations. Une approche conjointe expérience/théorie a été employée. De nouveaux complexes d'or ont été synthétisés et caractérisés par différentes techniques spectroscopiques et de diffractométrie. Leurs réactivités, notamment dans des procédés catalytiques, ont été étudiées. Les calculs DFT ont aiguillé le choix des ligands/complexes d'intérêts. Ils ont permis d'analyser la structure électronique des nouvelles espèces isolées et d'élucider les mécanismes mis en jeu.

Une vue d'ensemble de l'utilisation de ligands bidentes pour la chimie de l'or montrant leurs implications dans le développement de cette chimie est présenté dans le premier chapitre. Une comparaison des différents ligands bidentes accessibles rationnalise le choix de deux d'entre eux pour les études présentées par la suite.

Le second chapitre concerne le développement de la réaction d'hétéroarylation des alcènes catalysée par le complexe MeDalPhosAuCl. Cette nouvelle transformation procède *via* un cycle catalytique Au^I/Au^{III} et combine addition oxydante et activation π à l'or. Un mécanisme détaillé est proposé sur la base d'analyses RMN *in situ*, d'étude par marquage au deutérium et de calculs DFT. La réaction a pu être généralisée à un large panel de substrats et un changement inhabituel de régiosélectivité a été observé pour les alcènes internes *cis* ou *trans*.

Le troisième chapitre est dédié à l'isolation et la caractérisation des premiers complexes d'or impliquant des liaisons hydrogènes Au···H-X. Grâce aux ligands hémilabiles (P,N), un contact proche entre l'or et l'hydrogène a été observé par DRX et la présence de la liaison hydrogène N-H···Au a été démontrée sans ambiguïté par spectroscopies RMN et IR. La nature de cette liaison a été méticuleusement analysée par calcul DFT fournissant des arguments en faveur d'une liaison hydrogène, interaction attractive non-covalente. Une étude *in silico* sur de nouveaux modèles, avec des interactions Au···H-X potentielles (X = N, O ou P, variations des ligands ou de l'encombrement stérique) a été réalisée pour donner des directives aux futurs travaux expérimentaux.

Le quatrième chapitre porte sur l'étude de carbènes α-CF$_3$ d'or(I). L'intérêt est double : 1) très peu de carbènes α-CF$_3$ ont été isolés et caractérisés et 2) beaucoup de molécules bioactives ou de matériaux possèdent des substituants CF$_3$ augmentant l'intérêt pour les réactions de trifluorométhylation. Grâce au ligand bis-phosphine *o*-carborane, plusieurs carbènes α-CF$_3$ d'or(I) ont été synthétisés, isolés et complètement caractérisés par spectroscopie RMN multi nucléaire, DRX et spectrométrie de masse. La liaison M=C$_{carbène}$ a été analysée par calculs DFT avec une attention particulière pour la description des orbitales moléculaires et la contribution relative donation/rétrodonation entre le fragment métallique et le carbène. La réactivité de ces nouveaux carbènes d'or vis-à-vis de réactions d'insertion et de cyclopropanation a été étudiée montrant que ces espèces imitent les carbènes α-CF$_3$ transitoires postulés pour d'autres métaux de transition.

Mots clés: Chimie de l'or, Ligands bidentés, Catalyse, Liaison hydrogène, Carbènes α-CF$_3$, Degré d'oxydation

Abstract

The present work deals with the study of defined gold complexes from the stabilization of original compounds to their use for novel transformations. A joint experimental/theoretical approach has been used. New gold complexes were synthesized and characterized by different spectroscopic means and diffractometry. Their reactivities notably in catalytic process were studied. DFT calculations guided for the choice of ligands/complexes of interest. They helped to analyze the electronic bonding of the new isolated species and to elucidate the involved mechanism.

An overview of the use of bidentate ligand in gold chemistry showing their involvement in the expansion of this field is presented in the first chapter. A comparison of the different bidentate ligands available rationalize the choice of two of them for the following studies.

The second chapter concerns the development of hetero-arylation reaction of alkenes catalyzed by the MeDalPhosAuCl complex. This new transformation proceeds *via* Au^I/Au^{III} catalytic cycle and merge oxidative addition and π-activation at gold. A detail mechanism is suggested based on *in situ* NMR analyses, deuterium labelling studies and DFT calculations. The scope of the reaction has been explored for a large number of substrates and an unusual switch of regioselectivity was observed for internal alkenes *cis* or *trans*.

The third chapter is dedicated to the isolation and characterization of the first gold complexes involving Au···H-X hydrogen bonding. Taking advantage of the hemilabile (P,N) ligands, a close contact between gold and hydrogen was observed by XRD and the presence of N-H···Au hydrogen bond was unambiguously demonstrated by NMR and IR spectroscopies. The nature of this bonding was thoroughly analyzed by DFT providing compelling evidence for noncovalent attractive hydrogen-type bonding. An *in silico* study on new models, with potential Au···H-X interaction (X = N, O or P, ligand and steric hindrance modulation) have been performed to provide guidelines for further synthetic work.

The fourth chapter focused on the study of α-CF$_3$ gold(I) carbene complexes. The interest is twofold: 1) very few α-CF$_3$ carbene complexes have been isolated and characterized and 2) many bioactive molecules or materials bear CF$_3$ substituents, increasing the interest for trifluoromethylation reactions. Taking advantage of the *o*-carborane diphosphine ligand, several α-CF$_3$ gold carbene complexes were synthesized, isolated and fully characterized, at low temperature, by means of multinuclear NMR spectroscopy, XRD and mass spectrometry. The M=C$_{carbene}$ bonding situation was analyzed carefully by DFT calculations with particular attention to the description of molecular orbitals and to the relative donation/retrodonation contribution between the metallic fragment and the carbene. The reactivity of this new gold carbene towards insertion reaction and cyclopropanation was studied showing that they mimic transient α-CF$_3$ metal carbene complexes.

Keywords: Gold chemistry, Bidentate ligands, Catalysis, Hydrogen bonding, α-CF$_3$ carbenes, Oxidation state